UNIVERSITY OF NOTTINGHAM

SEMI-RIGID BEHAVIOUR OF CONNECTIONS IN PRECAST CONCRETE STRUCTURES

by

Halil Görgün, B.Sc., M.Sc.

Thesis submitted to the University of Nottingham for the degree of Doctor of Philosophy

DEPARTMENT OF CIVIL ENGINEERING

August 1997

This thesis is dedicated to:

My parents, sisters and brother

ABSTRACT

Multi-storey precast concrete skeletal structures are assembled from individual prefabricated components which are erected on-site using various types of connections. In the current design of these structures, beam-to-column connections are assumed to be pin jointed. This current research work focuses on the flexural behaviour of the beam-to-column connections and their effect on the behaviour of the global precast concrete frame.

The experimental work has involved the determination of moment-rotation relationships for semi-rigid precast concrete connections both in full scale connection tests and smaller isolated joint tests. This has been done using the so called "component method" in which the deformation of various parts of the connection and their interfaces are summated, and compared with results from full scale sub-frame connection tests. The effects of stress redistribution, shear interaction etc. are taken of by linear transformation in the results from the full scale tests, enabling parametric equations to be formulated empirically in order to describe the semi-rigid behaviour. Eight full scale column-beam-slab assemblages were tested to determine the (hogging) moment-rotation behaviour of double (balanced loading) and single sided in-plane connections. Two of the most common types of connection were used, the welded plate and the billet type. Proprietary hollow core slabs were tied to the beams by tensile reinforcing bars, which also provide the in-plane continuity across the joint. The strength of the connections in the double sided tests was at least 0.84 times the predicted moment of resistance of the composite beam and slab. The strength of the single sided connections was limited by the strength of the connection itself, and was

approximately half of that for the double sided connection, even though the connection was identical. The secant stiffness of the connections ranged from 0.7 to 3.9 times the flexural stiffness of the attached beam. When the connections were tested without the floor slabs and tie steel, the reduced strength and stiffness were approximately a third and half respectively. This remarkable contribution of the floor strength and stiffness to the flexural capacity of the joint is currently neglected in the design process for precast concrete frames. Measurements of the extent of damaged zones near to the connection in full scale tests showed that, unlike steel connections, semi-rigid behaviour in precast concrete does not occur at a single nodal position. In general the double sided connections were found to be more suited to a semi-rigid design approach than the single sided ones.

Analytical studies were carried out to determine empirical design equations for column effective length factors β in unbraced and partially braced precast concrete frames. The main variables were the relative flexural stiffness α of the frame members, and the relative linear rotational stiffness K_s of the connection to that of an encastre beam.

The variation of β factors with K_s and α are presented graphically and in the form of design equations similar to those currently used in BS 8110. The change in the response of a structure is greatest when $0 < K_s \leq 1.5$ where β is found to be more sensitive to changes in K_s than α. When $K_s > 2$ the changes in the behaviour are so small that they may be ignored within the usual levels of accuracy associated with stability analysis. This is an important finding because the experiments have found K_s to be generally less than 2 for typical sizes of beam. The results enable designers to

determine β factors for situations currently **not** catered for in design codes of practice, in particular the upper storey of a partially braced frame. A design method is proposed to extend the concrete column design approach in BS 8110 and EC2, whereby the strength and semi-rigid stiffness of the connection enables column bending moments to be distributed to the connected beams. However, the suitability of each type of connection towards a semi-rigid design approach must be related to the stiffness and strength of the frame for which it is a part.

PUBLICATIONS

Part of the results from this study has been published :-

1) **Elliott, K.S., Görgün, H., Virdi, K.S. and Ragupathy, P.** Report to the Precast Concrete Frames Association, on analysis and design of a - 3 storey precast concrete sway frame, Dept. of Civil Eng. Nottingham University & Dept. of Civil Eng. City University, August 1994.

2) **Görgün, H., Elliott, K.S. and Davies, G.** Semi-rigid behaviour of connections in precast concrete structures. Progress Report 1, No. SR 95 029. Dept. of Civil Eng. Nottingham University, September 1994, 82 pp.

3) **Elliott, K.S., Davies, G. and Görgün, H.** Determination of moment-rotation in semi-rigid precast concrete connections using the component method, COST C1 Proceedings of the 2nd. Workshop, Semi-rigid Behaviour of Civil Engineering Structural Connections, Prague, 26-28 October 1994, pp. 31-40.

4) **Görgün, H., Elliott, K.S. and Davies, G.** Semi-rigid behaviour of connections in precast concrete structures. Progress Report 2, No. SR 95 030. Dept. of Civil Eng. Nottingham University, April 1995, 102 pp.

5) **Görgün, H.** Semi-rigid behaviour of connections in precast concrete structures. Dept. of Civil Engineering Report No. SR 96-001, University of Nottingham, February 1996, 344 pp.

6) **Elliott, K.S., Davies, G. and Görgün, H.** Component method validation tests in precast concrete semi-rigid connections, Semi-rigid Structural Connections, Proc. IABSE Colloquium, Vol. 75, Istanbul, September 1996, pp. 299-308.

7) **Elliott, K.S., Davies, G. and Görgün, H.** Effective length factors in precast concrete frames, Semi-rigid Structural Connections, Proc. IABSE Colloquium, Vol. 75, Istanbul, September 1996, pp. 349-358.

8) **Elliott, K.S., Davies, G. and Görgün, H.** Semi-rigid connections in precast concrete frames. Report to EPSRC. Grand No. GR/K17286. Dept. of Civil Eng. Nottingham University, October 1996.

9) **Görgün, H.** An experimental study of the behaviour of double sided welded plate connection in precast concrete frames. Dept. of Civil Engineering Report No SR 97-001, University of Nottingham, January 1997, 160 pp.

10) **Elliott, K.S., Davies, G. and Görgün, H.** Semi-rigid connections in precast concrete frames. FIP Symposium, Johannesburg, 10-12 March 1997.

TABLE OF CONTENTS

CHAPTER 4

RESULTS AND DISCUSSION OF PARAMETRIC STUDY FOR EFFECTIVE LENGTH FACTOR FOR SWAY FRAMES

CHAPTER 5

EXPERIMENTAL PROGRAMME FOR FULL SCALE FRAME CONNECTION TESTS

CHAPTER 6

RESULTS OF FULL SCALE FRAME CONNECTION TESTS

CHAPTER 7

DISCUSSION OF FULL SCALE FRAME CONNECTION TESTS

CHAPTER 8

ISOLATED JOINT TESTS

CHAPTER 9

RESULTS AND DISCUSSION OF COMPONENT METHOD FOR ISOLATED JOINT TESTS

CHAPTER 10

VALIDITY OF COMPONENT METHOD

CHAPTER 11

DESIGN CONSIDERATIONS

CHAPTER 12

CONCLUSIONS AND FUTURE WORK

ACKNOWLEDGEMENTS

The author wishes to acknowledge his sincere gratitude to the following :-

Professor D.A. Nethercot, the Head of the Department of Civil Engineering, the University of Nottingham, for making available department facilities.

Dr. K.S. Elliott and Dr. G. Davies, to whom I would like to express my profound thanks for acting as supervisors to this work, their constant guidance, generous help, continued encouragement and unfailing enthusiasm throughout the process of completing this thesis.

The technicians Michael Bettison, Charles Lambert, Bal Loyla, Geoff Mitchell, Melvyn Ridal and Brian Whitehouse, of the Civil Engineering Laboratory, and the technical staff at the Engineering Faculty Workshop at the University of Nottingham for their skill and technical support with the experimental work.

The Engineering and Physical Sciences Research Council (EPSRC), and the Turkish Government for financial assistance.

Cripps Computing Centre and the Department of Civil Engineering at the University of Nottingham for the local computing facilities.

The staff at the Science Library for their efficient and speedy way in ordering for references.

My colleagues and friends in Nottingham for the good time and moral support.

Finally there are no words to express my love to my parents, sisters and brother in Turkey for their support during the length of the present study and the previous studies (English Courses).

DECLARATION

I declare that this thesis is the result of my own work. No part of this thesis has been submitted to any other University or other educational establishment for a Degree, Diploma or other qualification (except for publication).

(Halil GÖRGÜN)

NOTATION

A cross-sectional area of compression specimens

A_c entire concrete area bh

A_s area of tension reinforcement

b breath of section of beam or column

c flexural stiffness of connection

$\bar{c}$ ratio of stiffness of connection to stiffness of column to which it is attached

cl_c/EI_c

d effective depth

E modulus of elasticity

E_c modulus of elasticity of concrete

E_{ce} effective modulus of elasticity of concrete

E_{ci} modulus of elasticity of infill concrete

E_{cp} modulus of elasticity of precast concrete

E_{cq} dynamic modulus of concrete

E_s modulus of elasticity of steel

e connection eccentricity

F_{cc} force in concrete in compression

F_{st} total tensile yield load in 2T10 reinforcement bars tested

F_t basic tie force

F_t' modified tie force

F_{wt} tensile force in fillet weld

f second order elastic lateral displacement under service load in the case of an unbraced frame, elastic mid-span beam displacement in the case of a braced frame

f_c concrete stress

f_{cu} characteristic cube strength of concrete

f_s steel stress

f_y characteristic strength of reinforcement

g_k characteristic dead load (distributed)

h overall depth of beam or column section

I second moment of area

I_b second moment of area of connected beam

I_c second moment of area of connected column

I_{cr} second moment of area of cracked section

I_u second moment of area of uncracked section

J flexural stiffness of connection (general)

J_c tangent flexural stifness of connection (cracked)

J_e tangent or secant flexural stiffness at intersection with beam-line in final cycle

J_{es} secant flexural stiffness at intersection with beam-line in full cycle

J_{is} initial secant flexural stiffness of connection at M_{cr}

J_s secant flexural stiffness of connection at peak value of each cycle

J_u initial tangent flexural stifness of connection at M_{cr}

J_{us} secant flexural stiffness at M_u

J_{unl} tangent or secant unloading flexural stiffness of connection

K_e effective stiffness of embedded bars

K_s ratio of stiffness of connection to flexural stiffness of beam to which it is attached $Jl/4E_c I$

k ratio of stiffness of connection to flexural stiffness of beam to which it is attached cl/EI

L height of column, anchorage bond length

L_b length of connected beam

L_e effective length of column, effective anchorage length of bars

l span length

l_r greater of distances between centres of columns

M bending moment

M_{add} bending moment due to sway deflections

M_b moment in beam end

M_{beam} predicted ultimate moment capacity of beam

M_c moment in column end

M_{con} strength of connection at face of column

M_{cr} cracked moment of connection

M_e bending moment of connection at intersection with beam-line, connection eccentricity moment

M_h hogging moment

M_i initial bending moment of connection

M_{peak} moment at peak value of each cycle

M_{pred} predicted ultimate moment capacity of connection

M_s sagging moment

M_p plastic moment

M_{plRd} design plastic moment resistance

M_{Rd} design moment resistance

M_u ultimate strength of connection at face of column

M_w bending moment due to frame action in resisting wind loads

n number of interfaces in joint

n_o number of storeys

P bending load, collapse load, shear load, uniaxial compressive load

P_{cr} buckling load

P_E Euler load ($\pi^2 EI/L^2$)

P_s shear force in tie rod

P_y yield load in stability tie bars

p_w design strength of fillet weld

q uniformly distributed load

q_k characteristic imposed load (distributed)

R reaction force at free end of beam due to shear load P, reduction factor

R_b beam rigidity

R_c column rigidity

S_j secant rotational stiffness of connection

T total tensile yield load in 2T25 longitudinal tie bars tested

t infill thickness

x gauge length, depth of stress block

x_{cr} depth to neutral axis (cracked section)

x_u depth to neutral axis (uncracked section)

V shear resistance of connection, pulse velocity

W predicted collapse load for small bending tests

z lever arm

α sum of flexural capacities of columns to beams

α' modified frame stiffness function

α_1 relative stiffnesses of column to lower beam

α_2 relative stiffnesse of column to upper beam

α_e modular ratio

β column effective length factor, bond coefficient

β_u ultimate load criterion

β_f deformation criterion

Δ lateral deflection

δ total deformation in joint, beam mid-span deflection

δ_B compressive deformation

δ_{ci} elastic deformation in in-situ concrete

δ_{cp} elastic deformation in precast concrete

δ_T crack width opening

ε_{av} average axial tensile strain in bars

Φ rotation in end of beam for semi-rigid joint

ϕ relative rotation between beam end and adjacent column, effective bar size

ϕ_{bo} simple beam rotation

ϕ_{cr} relative rotation at cracked moment of connection

ϕ_e relative rotation at intersection with beam-line

ϕ_{end} relative rotation at end of test

ϕ_f relative rotation at final failure

ϕ_{peak} relative rotation at peak value of each cycle

ϕ_u relative rotation at ultimate strength of connection

ϕ_{unl} relative rotation at unloading

γ_f partial safety factor for loads

γ_m partial safety factor for materials

λ normal deformation of precast-in-situ interface across a concrete joint subjected to uniaxial compression or flexure, or both

μ dynamic value for Poisson's ratio 0.25 (assumed)

ρ percentage of transverse reinforcement used within joint, ratio between flexural stiffnesses of beam and column, density

σ uniaxial compressive stress for compression specimens, flexural stress for bending specimens

θ rotation in end of beam or column for rigid joints

CHAPTER 1

INTRODUCTION

1.1 Background

During the past three decades the multi-storey precast concrete structure has developed into an alternative to that of cast in-situ and steel structures. This clearly makes the building market a competitive one.

The present research work focuses on precast concrete structures, where the superstructure is erected from the individual prefabricated components which are made in a factory in a favourable environment and with tight production and quality control. This produces units with high quality performance and appearance. The designer can select from a range of finishes and be able to inspect and accept the units before they leave the factory. Schools, universities and buildings such as hospitals, offices, car parks, hotels are widely being built using precast concrete components. The current market share for precast concrete is about 10% in the UK, 85% in Scandinavia, 70% in the Baltic countries and more than 60% in Northern Continental Europe (Elliott, 1997a).

Precast concrete offers opportunities for speeding the on-site processes of construction, the maximum re-use of mould work and equipment, and for continuity of the processes. There is a reduction in the amount of in-situ concrete required on-site and reduced delays caused by bad weather and seasonal conditions. Precast allows

more accurate programming of the processes of construction and sites using precast concrete structures are typically cleaner. Plate 1.1 shows a typical precast concrete building under construction.

With all the above advantages, the most economic feature in the precast concrete industry is the standardisation of the products. This has a great influence on the cost effectiveness of the industry. In a typical skeletal precast concrete frame, the different precast concrete components are assembled and interconnected using various types of joints. Connections may have to transfer forces such as shear, axial, flexure and torsion between the precast components. The two main types of precast concrete structural frames are:

- unbraced, where the stability is provided by frame action of the beams, columns and floor slabs
- braced, where stability is provided by shear walls, or columns

In both situations the behaviour of the frame in resisting gravity and horizontal load (wind) is influenced greatly by the strength, stiffness and ductility of the connections. The stability of an unbraced structure relies entirely on the foundation moment and shear connection because the frame connections at floor levels are currently designed as pinned. In reality these connections do not behave as pins and therefore the distribution of moments and forces in the frame is not accurately represented in design.

1.2 Strategy of the work

It is therefore important to study the behaviour of these connections together with the effect they have on the overall structure. This thesis mainly concentrates on the flexural behaviour of beam-to-column connections in the internal (double sided two way

connections Figures 1.1(a) and (c)) and external (single sided three way connections Figures 1.1(b) and (d)) beam-to-column joints with and without precast concrete hollow core floor slabs and tie steel. Theoretical work has been supported by experimental testing.

The term "connection" refers to major structural connections between precast components, e.g. welded plate connection. The "joint" includes the connection and where appropriate in-situ concrete, e.g. beam-to-column joint. It is the zone between different adjacent units of a structure.

The purpose of the investigation is to fulfil part of the United Kingdom's obligation as signatory to the COST C1 research initiative. The European Union is sponsoring the co-ordination of the COST C1 research programme, "Semi-Rigid Behaviour of Civil Engineering Structural Connections", whilst leaving individual governments to fund their own national contributions (City, Nottingham and Southampton Universities are the three UK participants in the precast concrete group in this programme).

The stated objectives of the COST precast concrete programme are to extend the test data available, to use computational techniques to extrapolate the data to a full range of geometries and loading conditions, and to standardise the resulting stiffness measurements in the form of moment-rotation curves for inclusion by design consultants in general frame analysis programmes. (The COST Committee have identified Nottingham University as the preferred research contractor for further connection tests, Southampton as the preferred research contractor for the detailed finite element analysis of the connections, and City (London) as the research contractor for testing the general frame analysis).

1.3 Precast concrete beam-to-column connections

In the UK the most popular type of precast concrete connection is known as the "hidden corbel" because the main structural components cannot be seen on completion. This has the advantage of minimising the depth of the connection and protecting all structural steel and rebars in the concreted or grouted joint. The two main variations of the hidden corbel are:

- welded plate and billet beam-to-column connection, Figures 1.1(a) and (b)
- bolted billet beam-to-column connection, Figure 1.1(c) and (d)

A billet is the name given to any projecting steel member, such as solid section, rolled hollow section (RHS) etc. Grade of steel 43 and 50 is used. The space reserved for the site operations immediately beneath the billet is concreted or grouted solid on-site using either concrete containing small sized (6-10 mm) aggregates, or sand-cement grout. Expanding agents (or expansive cements) are used to ensure that no shrinkage cracks allow ingress of reactive substances along the construction joints. The size of the infill depends on the type and the shear capacity of the particular connection, but in the main is 100 to 150 mm x 100 to 200 mm deep. The breadth of the infill may either be equal to the breadth of the beam, or in the case of very wide beams may be equal to the breadth of a pocket. In either case the breadth of the infill will be about 300 mm.

1.4 Properties of beam-to-column connections

1.4.1 Fundamental response

The connections in precast concrete frames are subjected to both clockwise and anti-clockwise bending moments M and this induces the relative rotations ϕ between the beam end and the adjacent column as shown in Figures 1.2(a) to (c).

Connections such as these are known as "semi-rigid". Total frame analysis may therefore be carried out by substituting rigid joint connections with ones of finite strength and rotational stiffness. The relevant properties of connections are strength, stiffness and deformation capacity (ductility). The behaviour may be described in terms of the well known moment-rotation $M-\phi$ data, idealised in Figure 1.2(d), but in the case of precast concrete connections the semi rigidity is due to both material and large deflection effects. There is also a zone of influence beyond the immediate locality of the joint. Previous and new work has shown that this is approximately equal to the cross sectional dimensions of the adjoining beam and column members (Mahdi, 1992). In this context it is very important that the $M-\phi$ characteristics of the connection are tailored to suit the stiffness and strength of the frame.

It is thought that the initial rotational stiffness J_{is} in Figure 1.2(d) of the connection is due mainly to the geometry of the joint, in particular in the manner in which it is constructed and the tolerances made for lack of fit etc. on-site. This is particularly relevant in grouted and bolted joints where slippage may take place at low loads and give an artificially low stiffness. On the other hand the ultimate strength of the connection M_u in Figure 1.2(d) is due mainly to the strength of the critical materials in the joints, i.e. the crushing and shear strength of the concrete and the yield

and tensile strengths of the reinforcements. Finally the ductility of the connection is mainly a function of the ductility of the reinforcement, but geometry plays a large part in this, particularly if the connection is over reinforced. If normative rules are to be developed to classify such connections, the geometric and material effects must be separated and accounted for in any single $M-\phi$ plot, where the general rotational stiffness J of the connection is given by the gradient of the $M-\phi$ curve as shown in Figure 1.2(d).

The usual approach is to express stiffness as a non-dimensional term K_s where

$$K_s = \frac{J}{4E_c I/l} \qquad Eq.1.1$$

i.e. the ratio of the stiffness of the connection to the flexural stiffness of the beam to which it is attached, where E_c is the modulus of elasticity of concrete, I is the second moment of inertia of the beam, and l is the effective span of the beam.

1.4.2 Classification of beam-to-column connections

Depending on which criterion for frame analysis is used, i.e. sway stiffness, column buckling load etc., these connections may fall into one of three classes, namely

- Class 1. rigid with full strength
- Class 2. semi-rigid with full or partial strength
- Class 3. pinned

In the case of precast connections the important classification boundary is the one which separates Classes 2 and 3.

It is well known that the actual response of almost all beam-to-column structural connections is non-linear. The concept of a perfectly rigid or pinned connection is a purely theoretical one but useful to the designer to simplify the calculation of framed structures.

In engineering calculations, some actual beam-to-column connections can yet be considered as pinned or perfectly rigid if their behaviour is such that the bending moment they can carry over is so low, and the relative rotation between the connected beam and column is not large enough, respectively, to significantly influence the overall behaviour of the frame.

Several classification systems for beam-to-column connections in steel frames have so far been proposed in order to determine whether an actual beam-to-column connection can reasonably be considered as pinned or semi-rigid (where the joint flexibility has to be taken into account) or rigid in the frame design stage. Details of these classification systems are given in Chapter 2.

1.4.3 Simplified component method

The definitions used in this work are that the connection moment M_{con} is measured in the joint at the face of the column, and ϕ is the relative rotation of the beam to the column at the same point. Thus assuming that the end of the beam of overall depth h acts as a rigid body, beam end rotations may also be expressed as follows. Refer to Figure 1.2(c):

$$\phi = \frac{\delta_T + \delta_B}{h} \qquad Eq.1.2$$

where δ_T is the crack opening plus other linear displacements in the concrete at the top of the joint, and δ_B is the compressive deformation in the concrete at the bottom of the joint. Thus if δ_T and δ_B can be computed separately for given loading and expressed in terms of material and geometric properties, a simple method to determine ϕ is possible. In this method an "effective modulus of elasticity of concrete E_{ce}" is found by experimentation and the associated strains, and hence deformations δ_B, are determined from the appropriate state of stress. Similarly, in the tension zone an "effective tensile stiffness K_e" is found which relates bond and tensile deformation δ_T to the applied tension forces. Experimental testing has been carried out to measure these values, which may then be validated against the results of full connection assembly tests. These tests are referred to as "interface tests".

1.5 General advantages of using semi-rigid connections

Obviously, the flexural stiffness, bending moment and the deformation capacity (ductility) of semi-rigid beam-to-column connections in any type of structure, either precast, steel or composite, influence greatly the response of the structure as a whole. The general advantages of using semi-rigid connections depend on the type of frame and the usual basis of design. For braced frames this is simple construction, assuming pinned connections, for unbraced frames this is continuous construction, assuming rigid connections.

For braced frames, the effect of semi-rigid connections on beam design can be observed by investigating the behaviour of a single span beam. Figure 1.3(a) shows a

simply supported beam, with a uniformly distributed load, the maximum design bending moment takes place at mid-span of the beam. In Figure 1.3(b) the simple supports have been replaced by fixed supports. Now, the maximum elastic bending moment takes place at the fixed supports, and is two-thirds of the maximum elastic bending moment of the simply supported case.

Figure 1.3(c) shows a beam with semi-rigid end connections. Based on the flexural stiffness of the connection, the maximum elastic bending moment occurs at the supports or at mid-span (assuming the semi-rigid end connections have the same flexural stiffness capacity), but will always be less than that for a simply supported and/or fixed supports beam, and permit a reduction in the beam material. The optimum connections would be those which would allow just enough end rotation to balance end and mid-span moments $\frac{ql^2}{16}$. Semi-rigid connection theory is concerned with this problem and other, similar matters.

Figure 1.4 shows that by an appropriate choice of connection stiffness relative to the beam K_s, the elastic bending moment at the supports can theoretically be made equal to the value at mid-span, hence minimizing the elastic design moment. Of course, there may well be practical difficulties however in providing such a precise flexural stiffness value. Such a solution may not be the optimum. This is because of the additional cost of providing connections with the required flexural stiffness. Figure 1.4 shows that the design moment is significantly reduced even if the stiffness of the connection is only modest. This also means that a small reduction in the stiffness of the connections will have a dramatic effect on the design moment of the beam.

A similar pattern occurs when the elastic mid-span deflection of the beam is considered. The variation in the elastic mid-span deflection of the beam with end conditions and connection stiffness can be seen from Figure 1.5 to Figure 1.6. It has been suggested that reduced beam depth (Anderson, 1993) can economically be obtained by either:

- recognising the inherent stiffness of some types of simple connection, or
- modifying simple connections to a limited extent to provide increased stiffness.

One of the objectives of this study has been to recognise the inherent flexural stiffness and strength of the beam-to-column connections as used in precast concrete structures in the UK and to incorporate this into design procedures rather than to modify the connections.

1.6 Evaluation of semi-rigid connections using beam-line method

For braced frames, the beam-line concept shown in Figure 1.7 provides a convenient method to determine the influence of semi-rigid connections on the behaviour of an elastic beam in one interactive process. This approach in effect combines characterisation of connection response, analysis of internal moments, and evaluation of performance. Using this method, connection characteristics may be tested by being superimposed on the beam-line to determine the corresponding values of end moment, and thereby the beam design moment. Alternatively, the minimum connection stiffness needed to justify a particular beam section can be determined. This approach leads directly to the minimum connection resistance needed to achieve the elastic connection behaviour assumed in the analysis. Full details of the beam-line method are given in Chapter 11.

1.7 Objectives of the work

1) To provide actual moment-rotation characteristics of two types of beam-to-column connections experimentally, incorporated in double and single sided subframes

2) To obtain the moment-rotation characteristics of the connections from smaller isolated joint components tests

3) To study the effects of the flexural stiffness of the connections and frame members on the effective lengths of the columns using linear elastic approach on single storey one bay sway frames

4) To present a method of application of the moment-rotation characteristics of the connections in the analysis and design of multi-storey precast concrete framed structures

These objectives have been realised practically on the basis of the following experimental work:

1) Full scale frame connection tests on:

- welded plate and billet beam-to-column connection
  - (a) Double sided beam-to-column connection (two way connection) Figure 1.1(a) with and without hollow core floor slabs and floor tie steel
  - (b) Single sided beam-to-column connection (three way connection) Figure 1.1(b) with hollow core floor slabs and floor tie steel
- bolted billet beam-to-column connection
  - (a) Double sided beam-to-column connection (two way connection) Figure 1.1(c) with hollow core floor slabs (in-situ concrete only in some tests) and floor tie steel

(b) Single sided beam-to-column connection (three way connection) Figure 1.1(d) with hollow core floor slabs and floor tie steel

2) Interface tests on:

(a) small scale precast-in-situ-precast interfaces in compression and flexure

(b) full scale precast-in-situ-precast interfaces in bond slip and bond failure of rebars in narrow in-situ concrete strips.

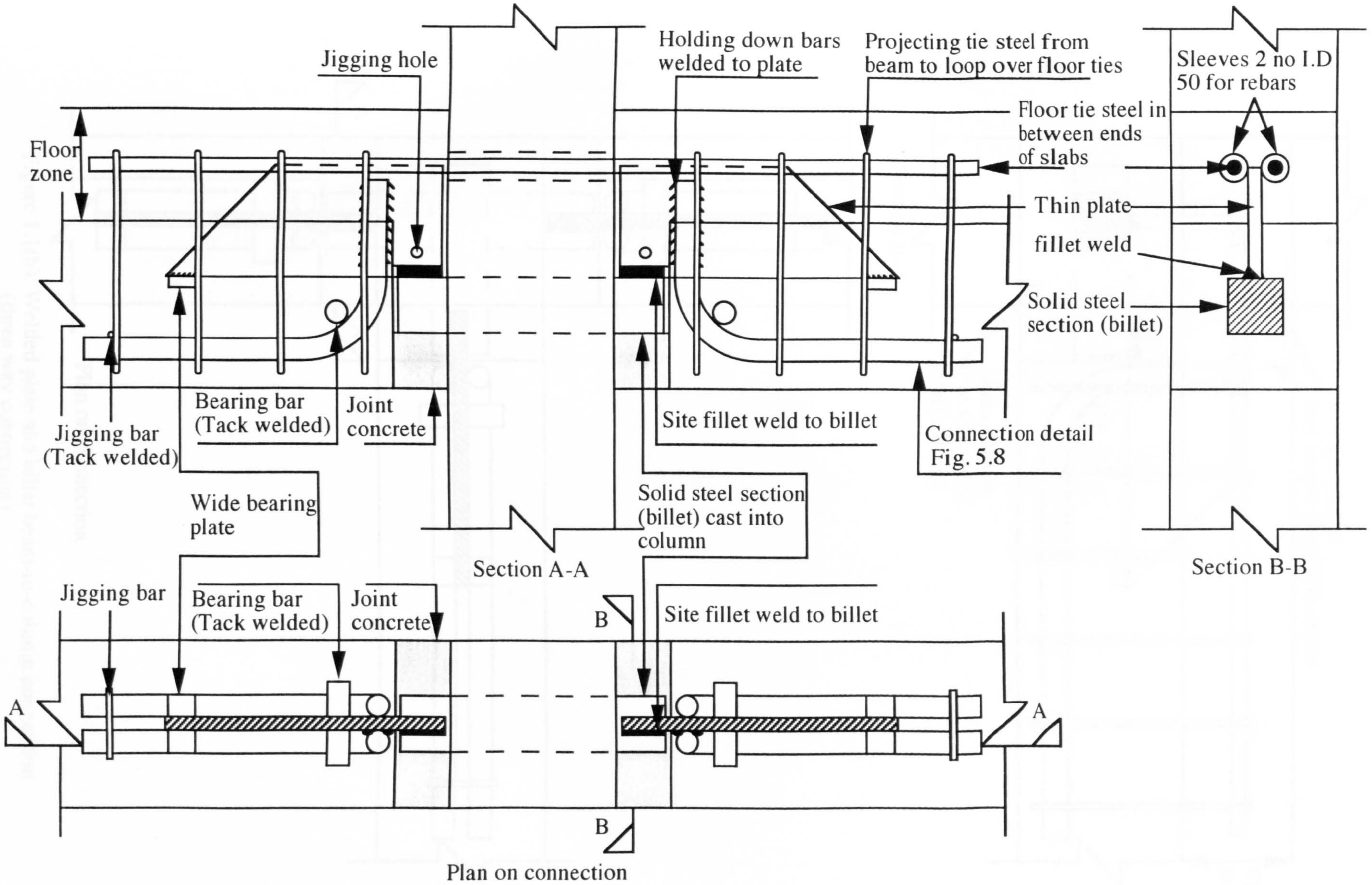

Figure 1.1(a): Welded plate and billet beam-to-column connection (two way connection)

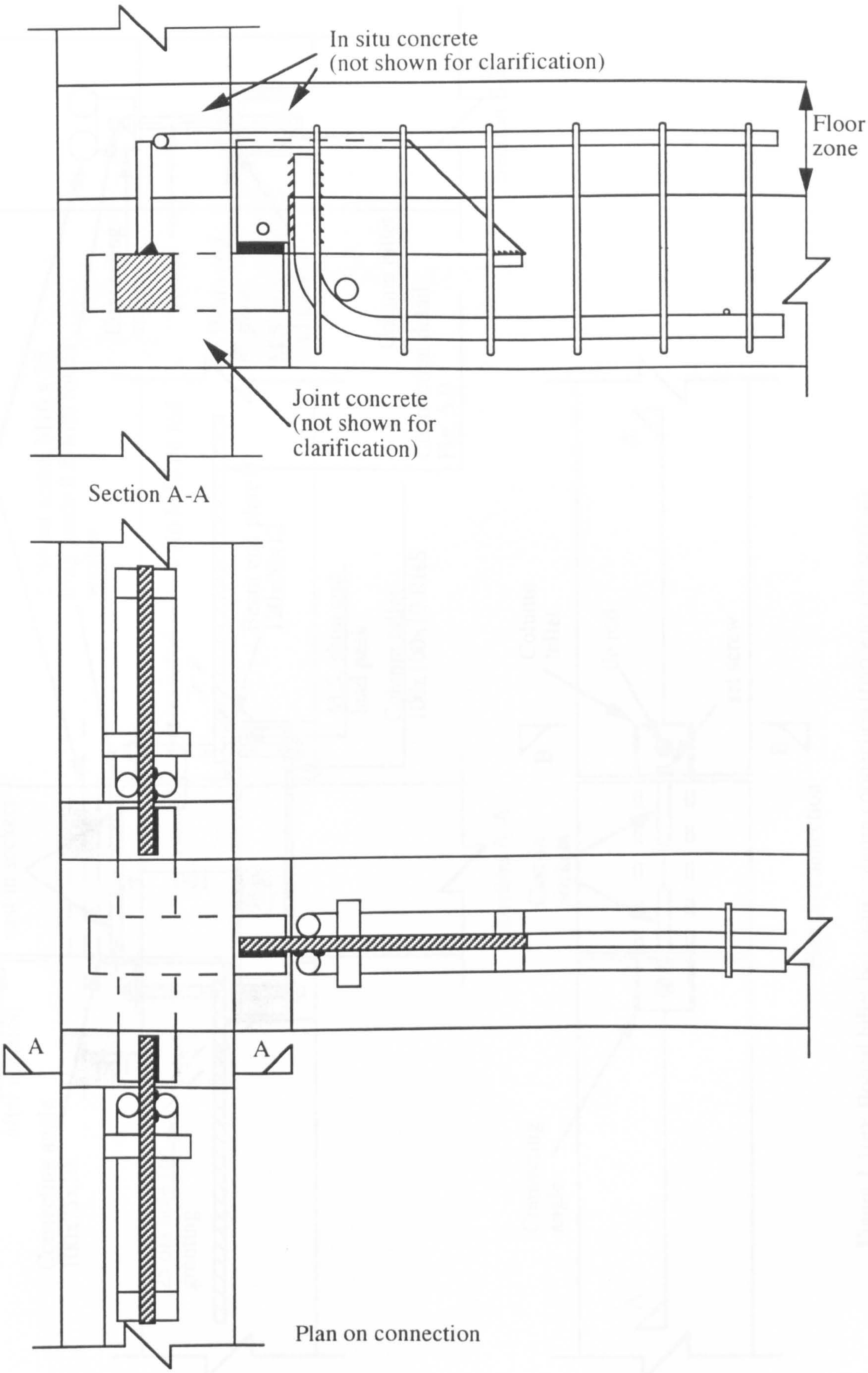

Figure 1.1(b): Welded plate and billet beam-to-column connection (three way connection)

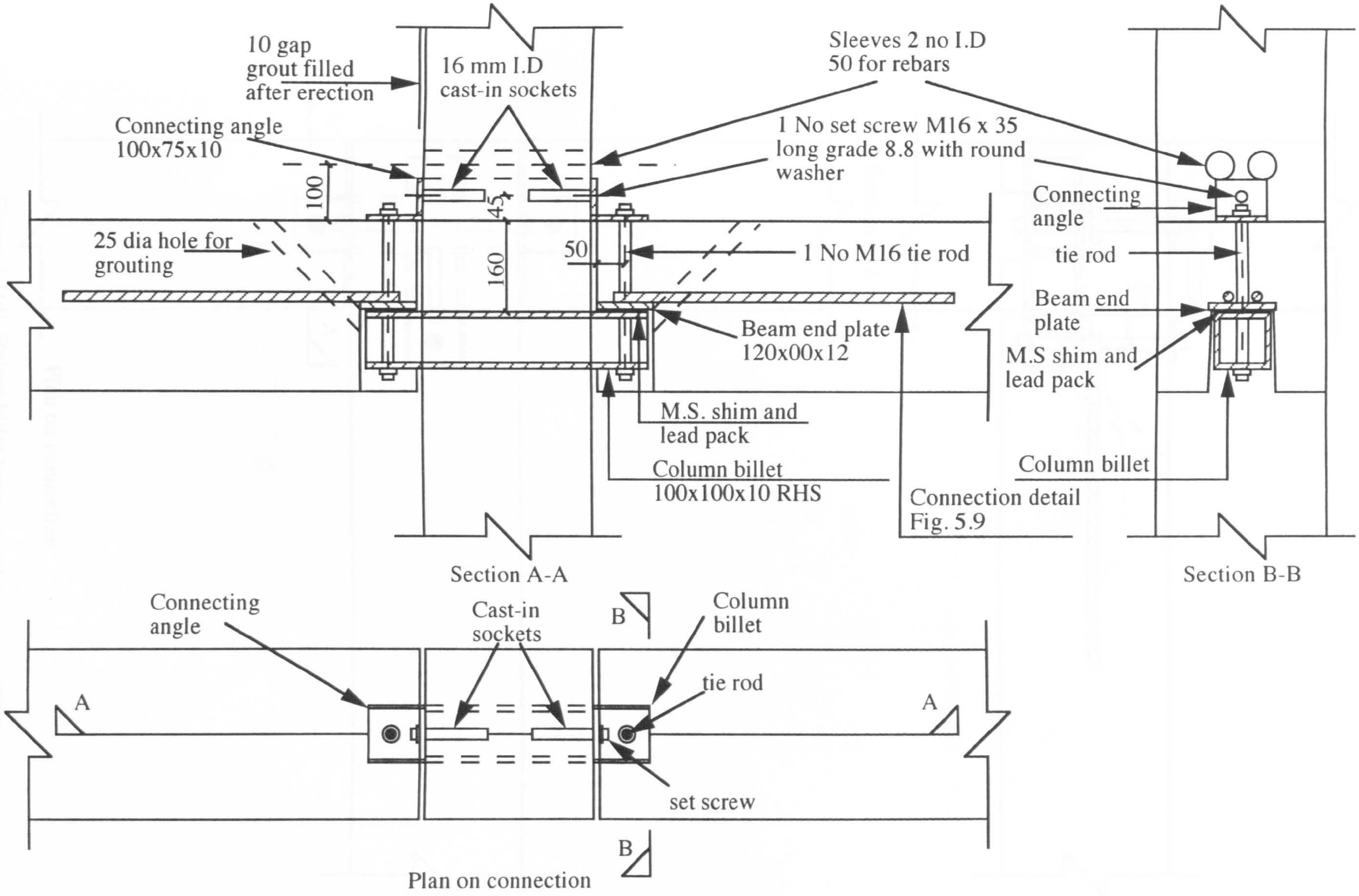

Figure 1.1(c): Bolted billet beam-to-column connection (two way connection)

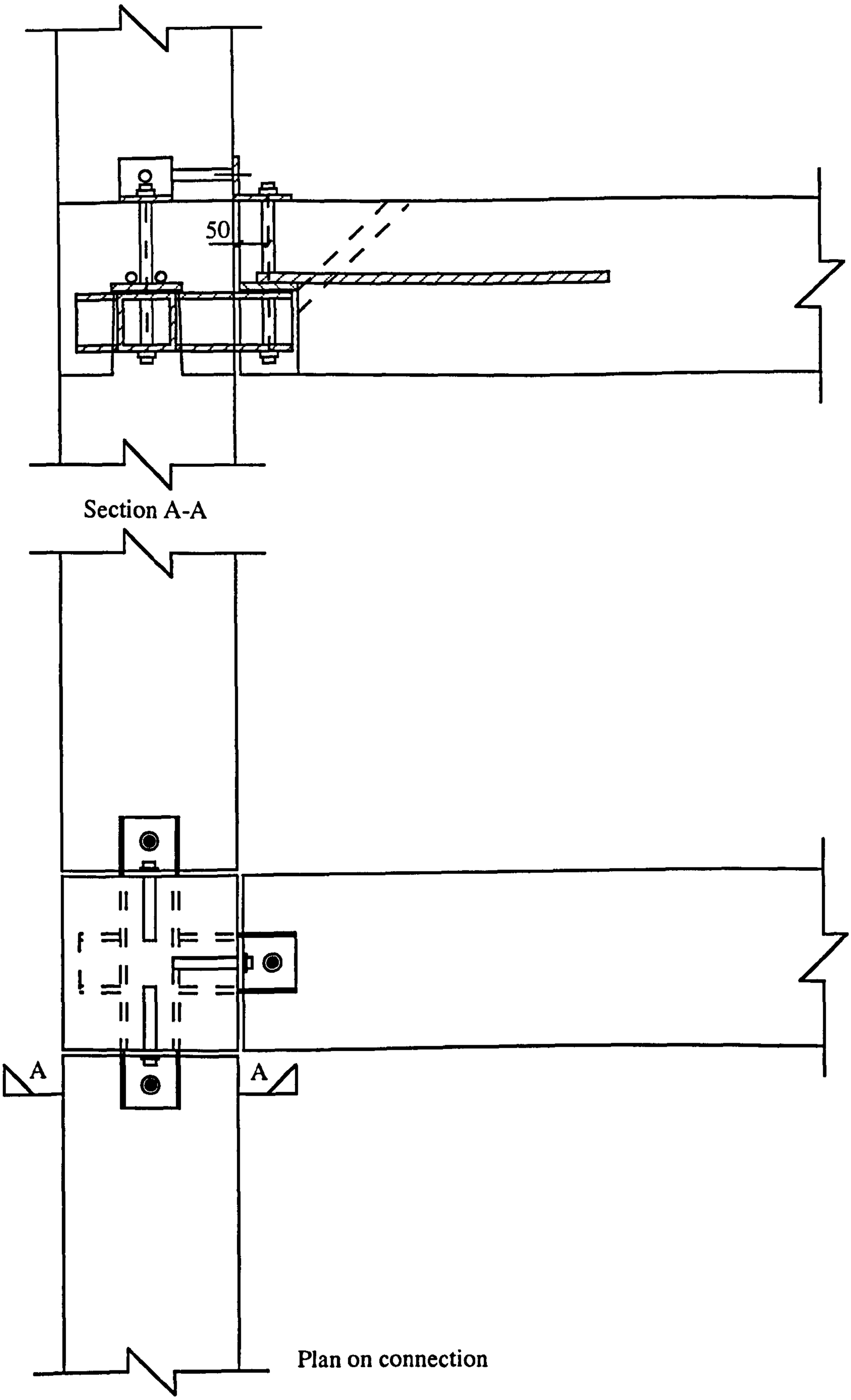

Section A-A

Plan on connection

Figure 1.1(d): Bolted billet beam-to-column connection (three way connection)

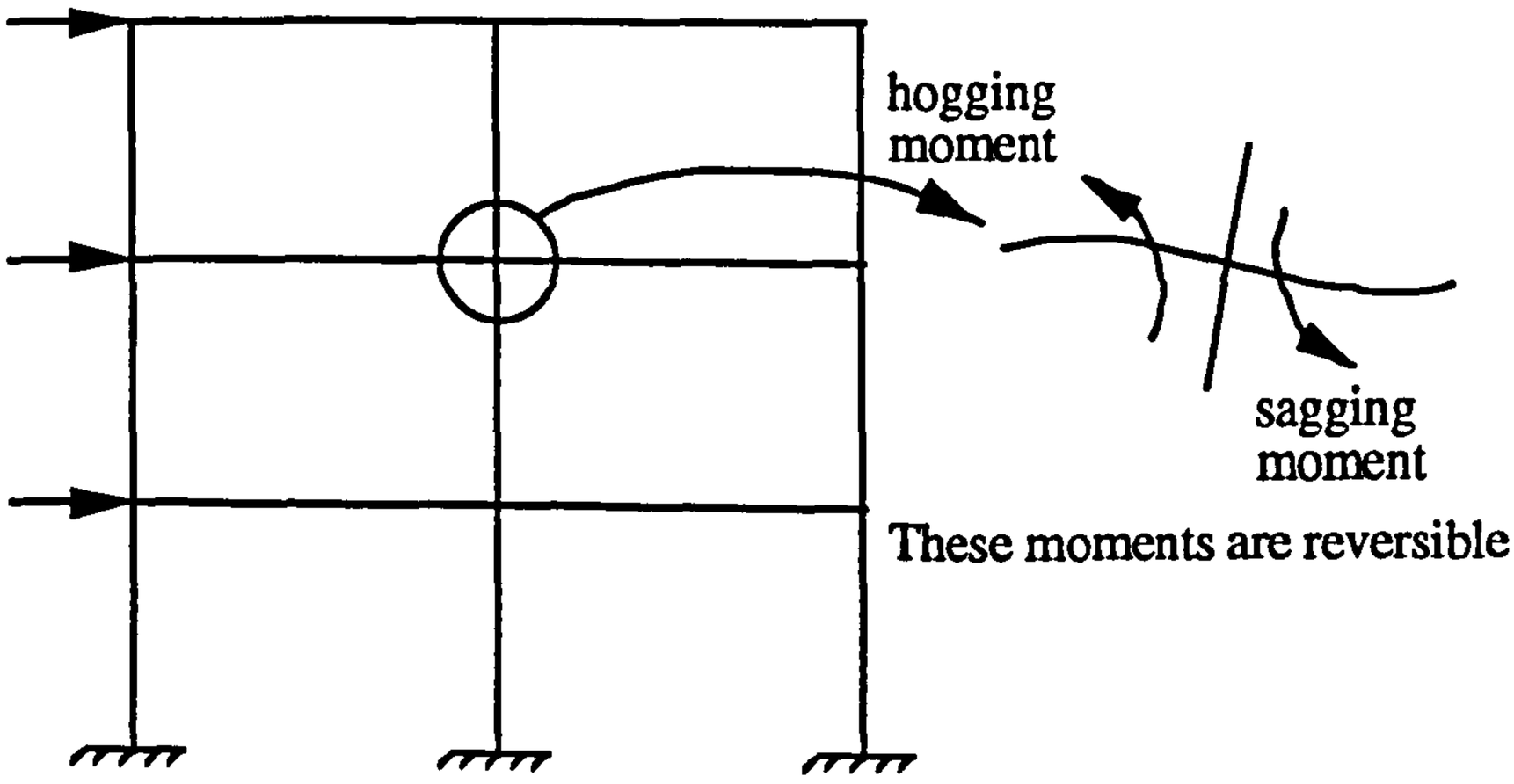

Figure 1.2(a): Sway loading

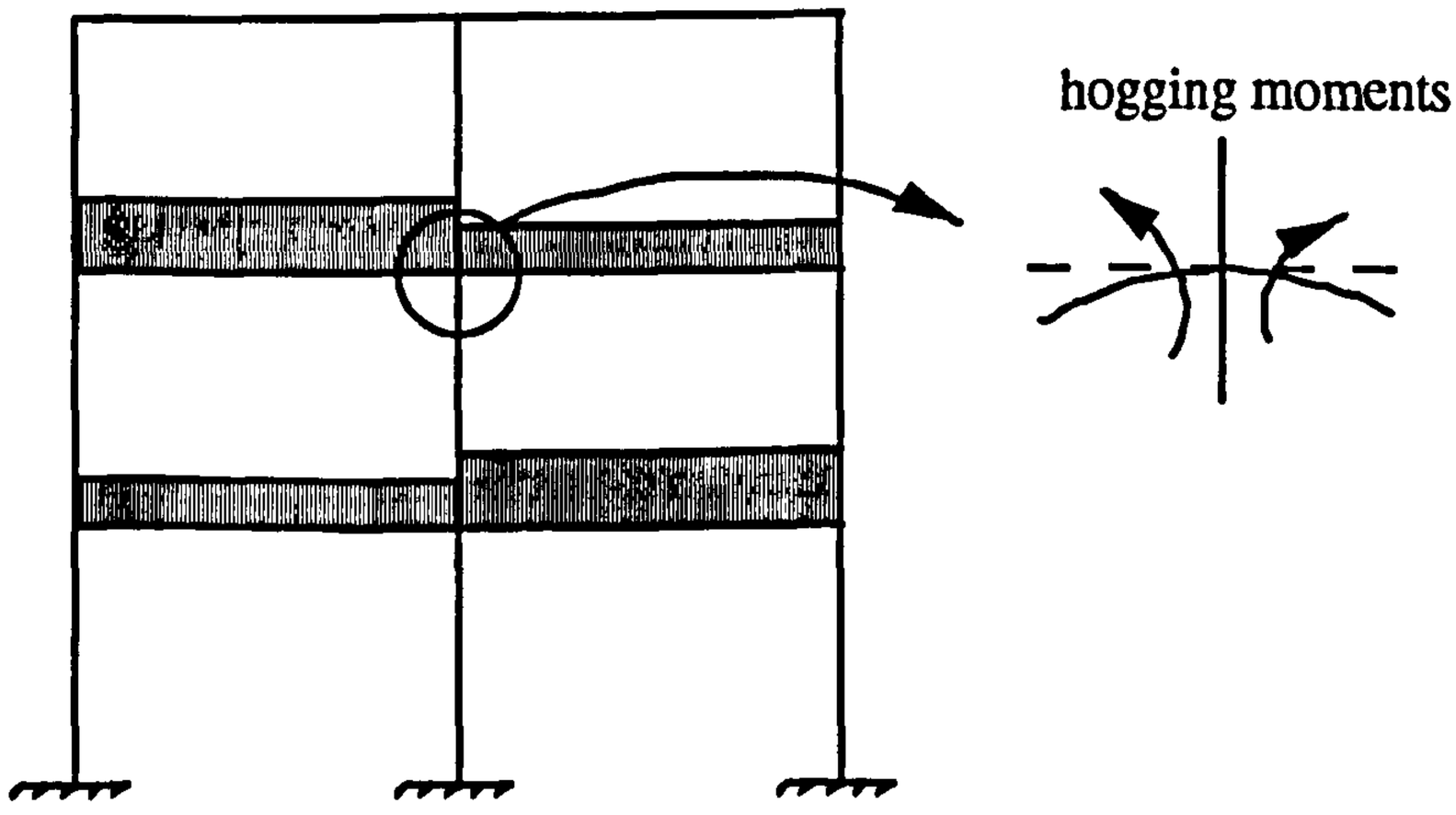

Figure 1.2(b): Gravity loading

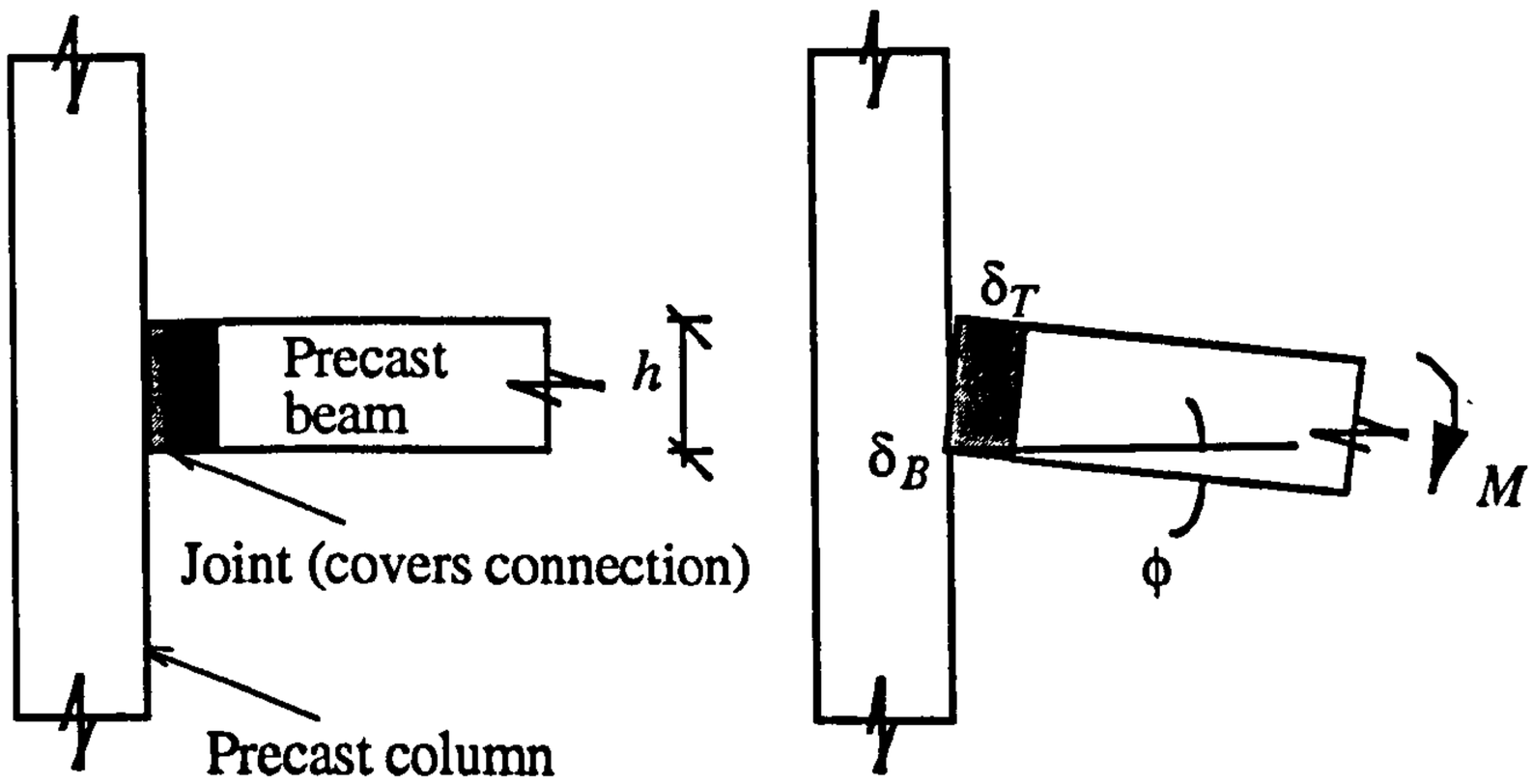

$$\phi = \frac{\delta_T + \delta_B}{h}$$

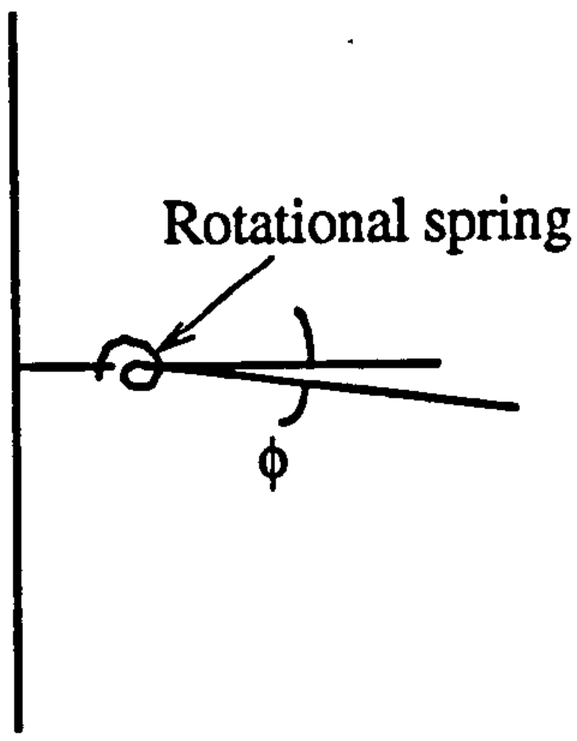

Figure 1.2(c): Simplified definition of joint rotation

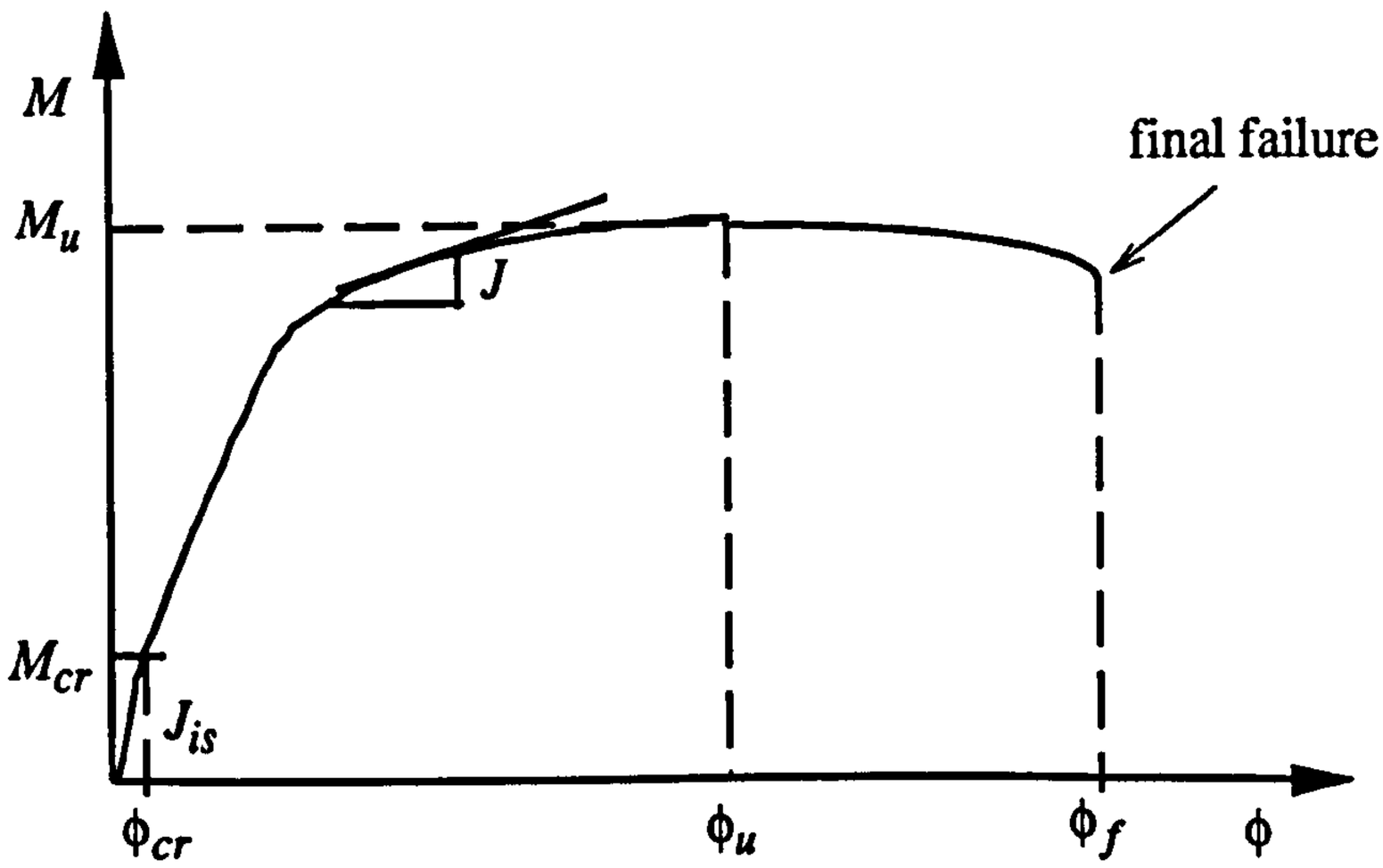

ϕ = relative joint rotation (rad)
J_{is} = initial secant rotational stiffness (kNm/rad)

Figure 1.2(d): Moment-rotation characteristic

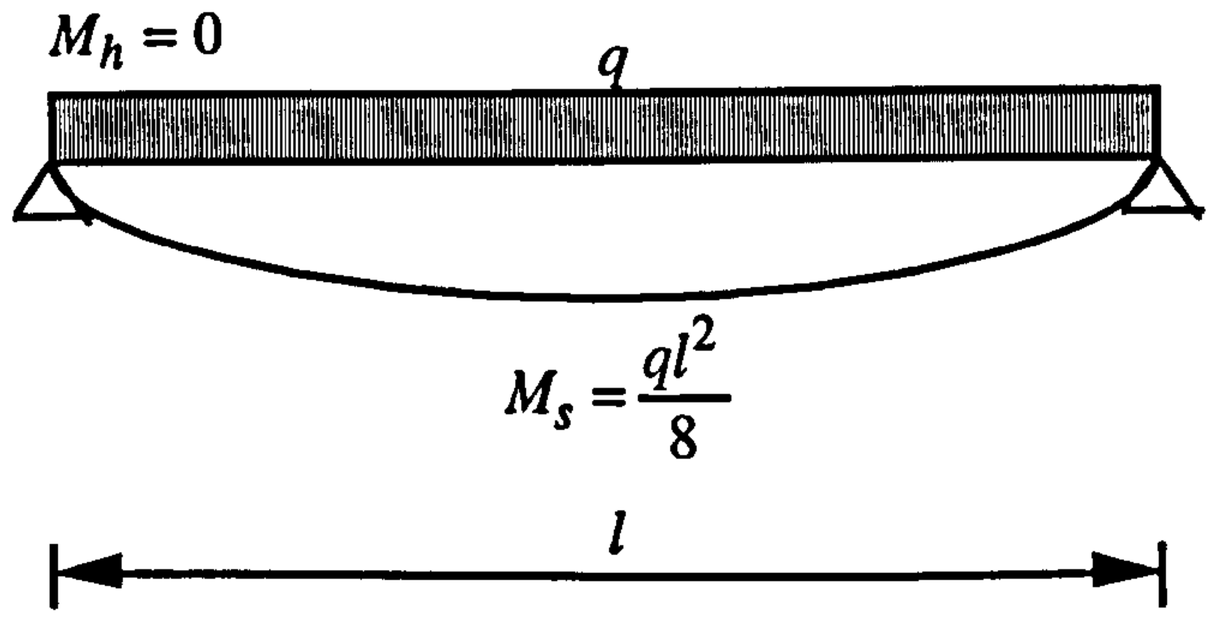

(a) Simply supported

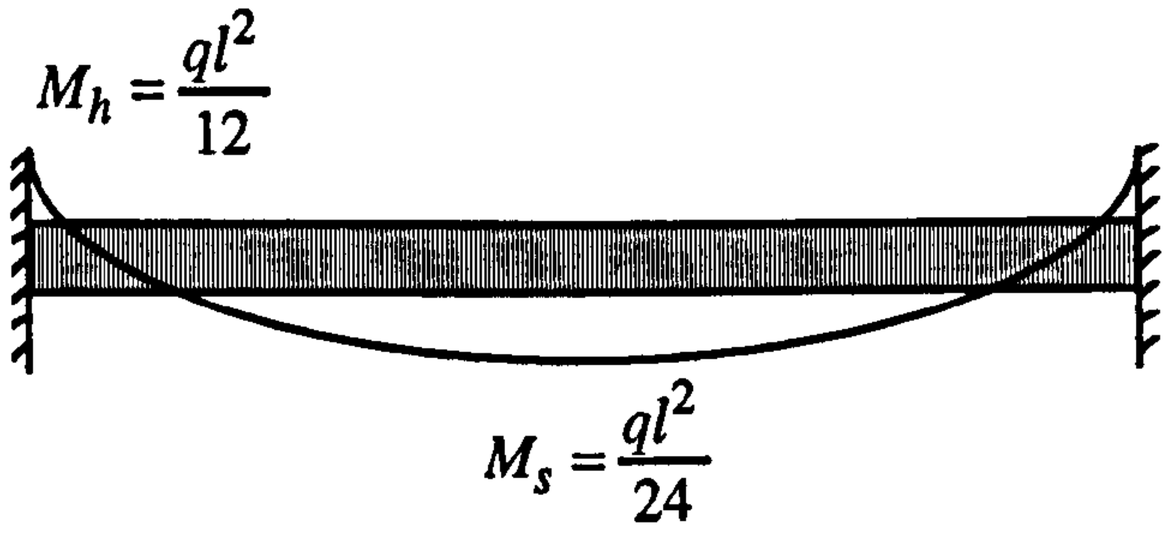

(b) Fixed

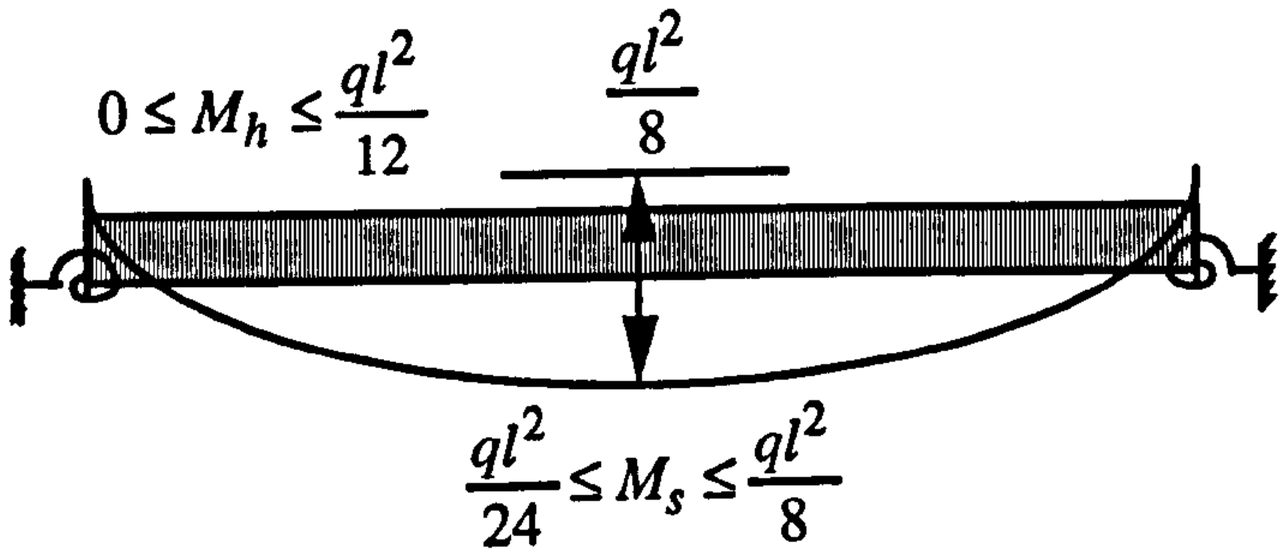

(c) Semi-rigid

Figure 1.3: Beam moments with various end conditions

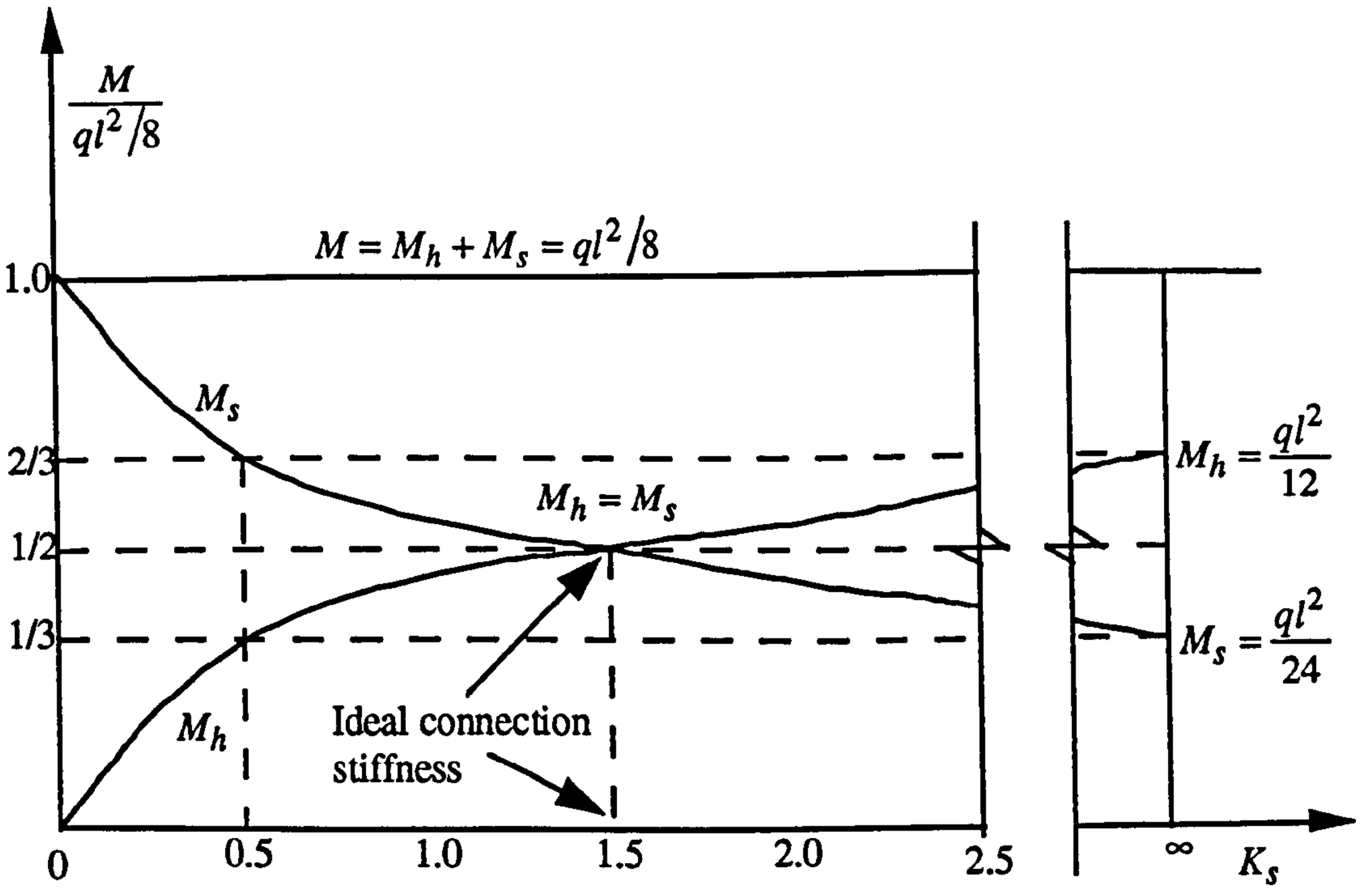

Figure 1.4 : Variation of beam moments with connection stiffness

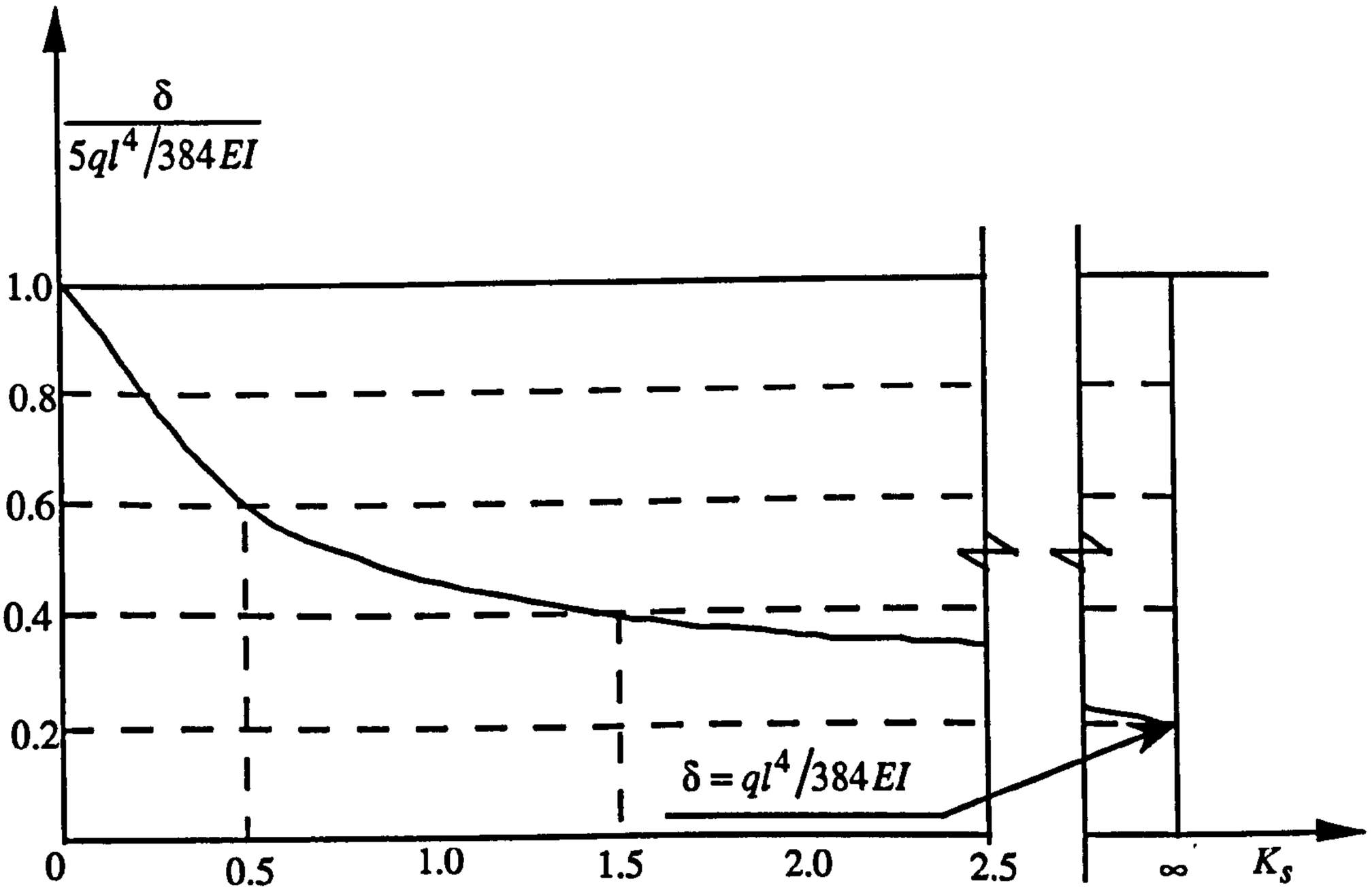

Figure 1.5 : Variation of mid-span deflection with connection stiffness

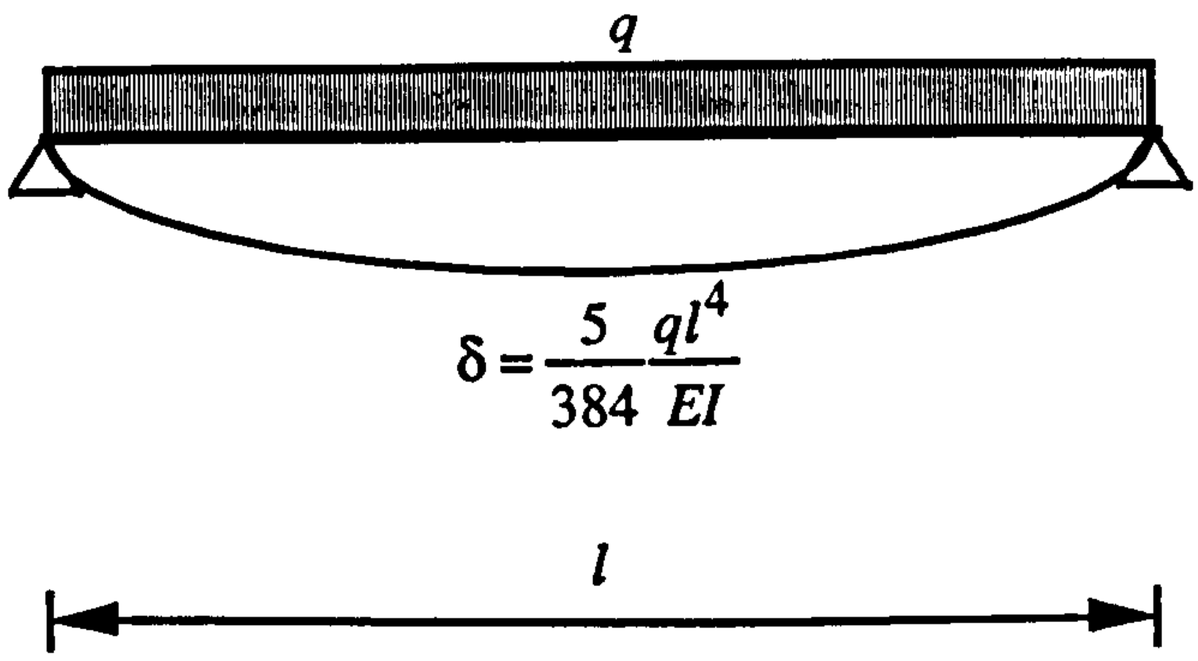

$$\delta = \frac{5}{384}\frac{ql^4}{EI}$$

(a) Simply supported

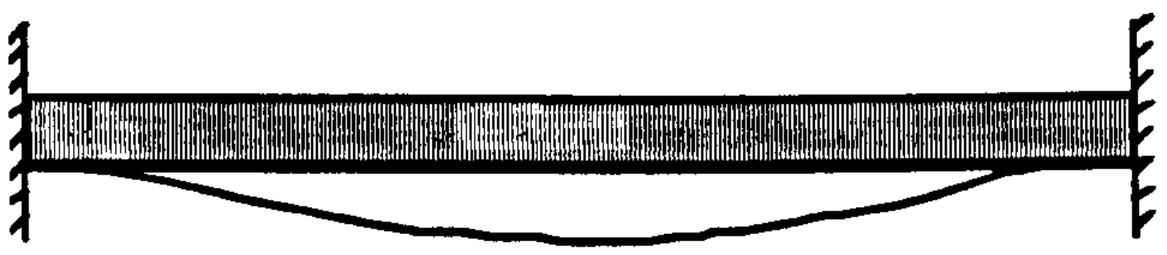

$$\delta = \frac{1}{384}\frac{ql^4}{EI}$$

(b) Fixed

$$\frac{1}{384}\frac{ql^4}{EI} \leq \delta \leq \frac{5}{384}\frac{ql^4}{EI}$$

(c) Semi-rigid

Figure 1.6: Beam deflected profiles with various end conditions

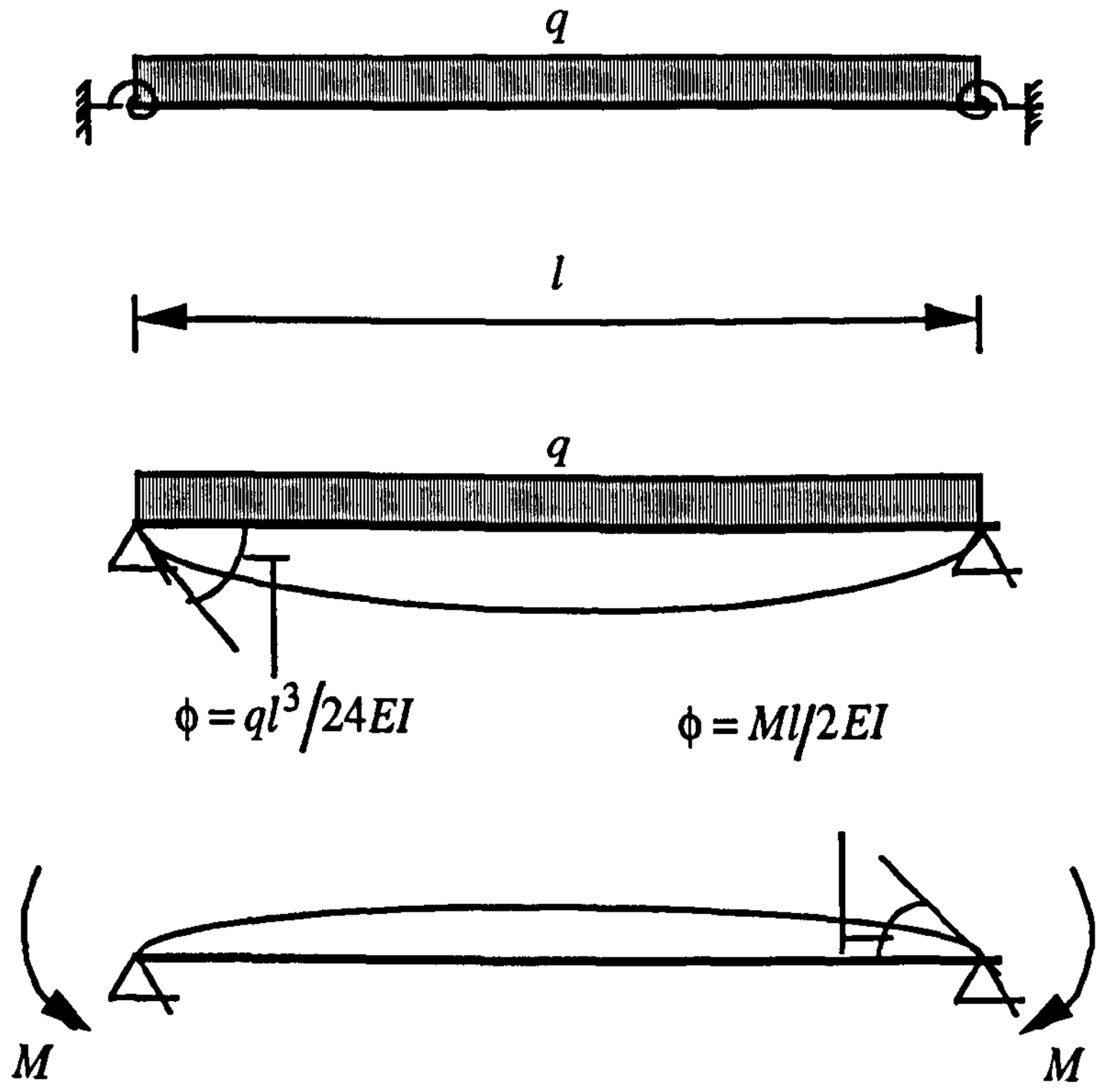

Figure 1.7: Definition of beam-line

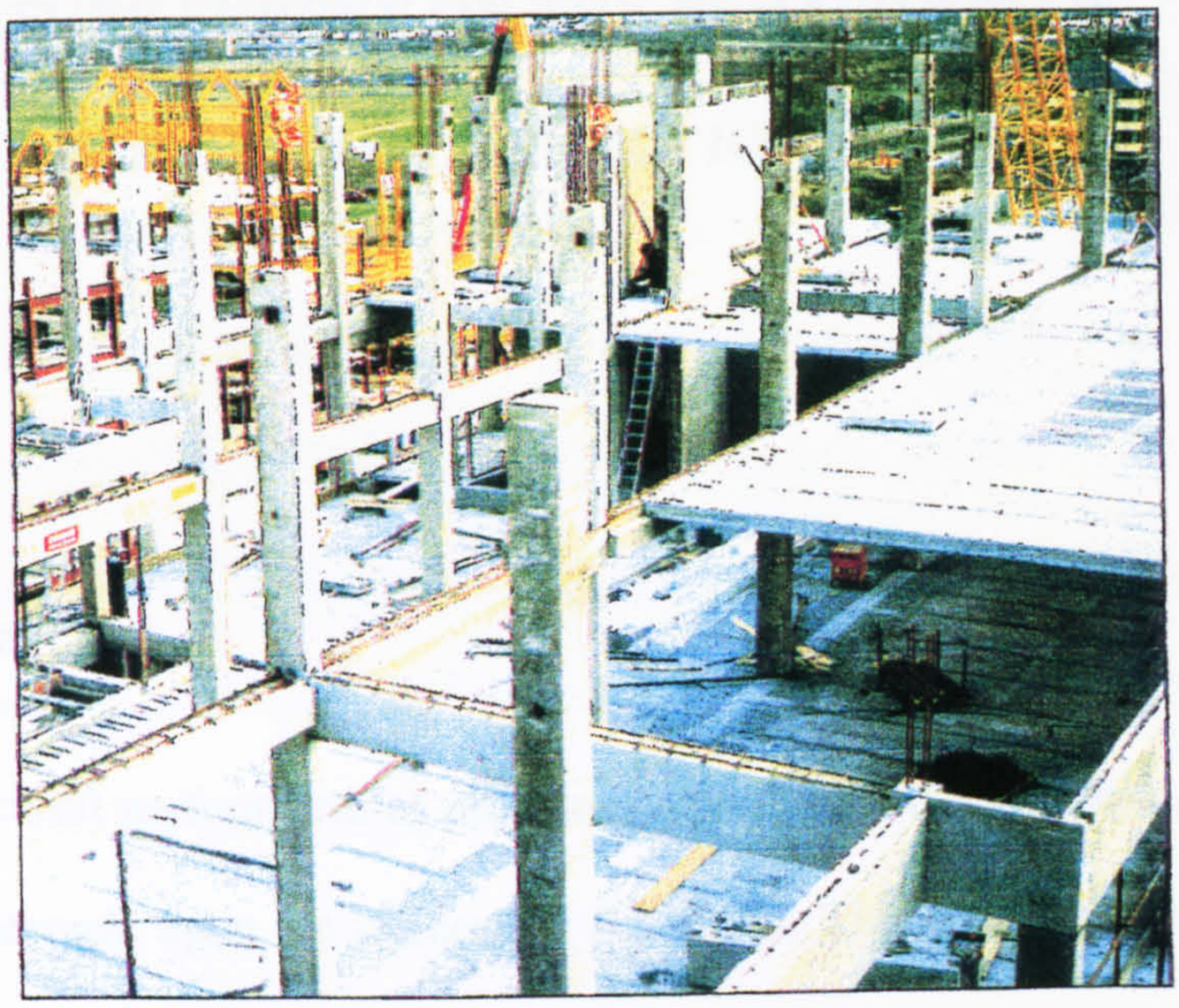

The simplicity of the precast concrete frames

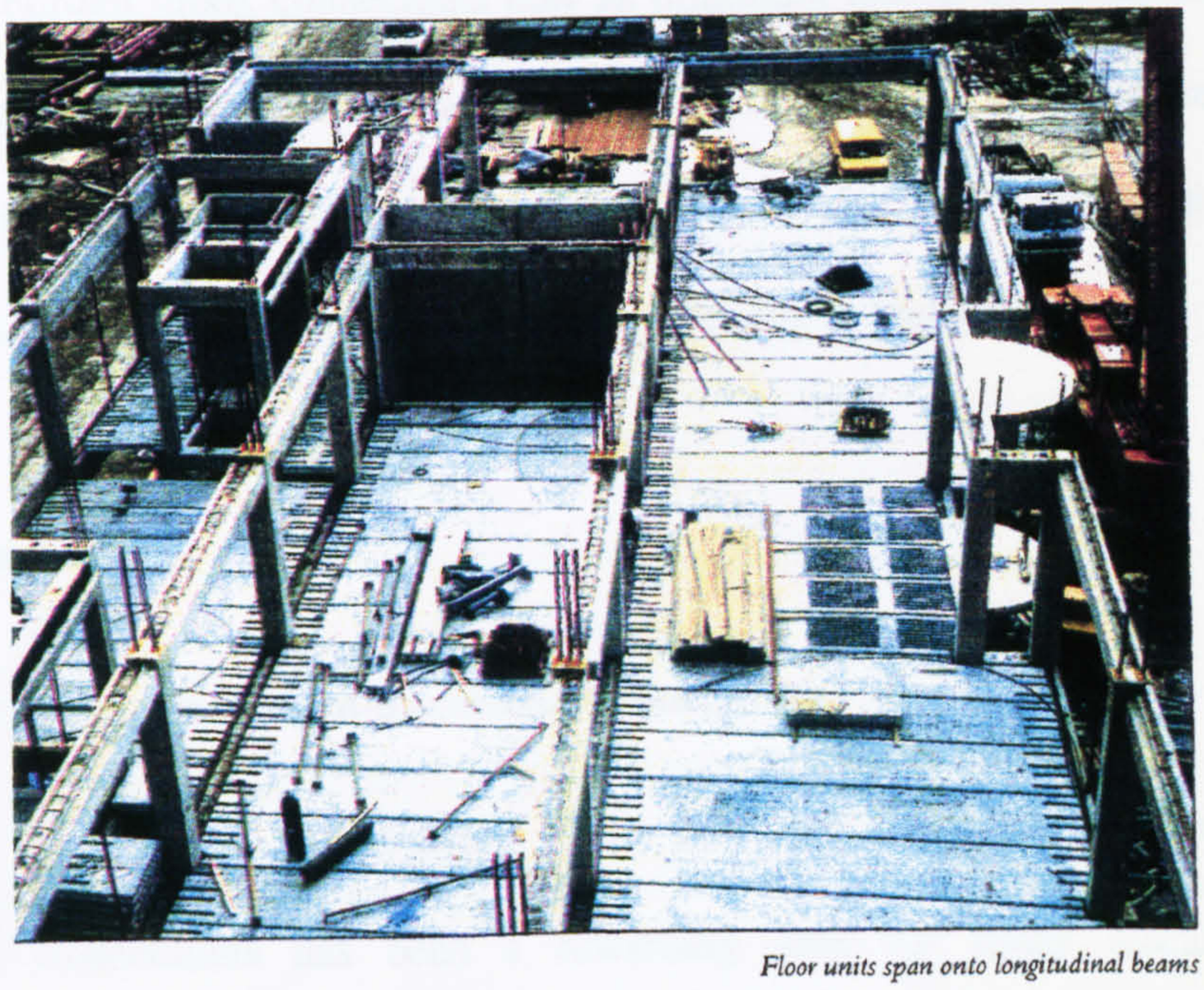

Floor units span onto longitudinal beams

Plate 1.1: A typical precast concrete building under construction

(British Cement Association, 1992)

CHAPTER 2

LITERATURE SURVEY ON THE BEHAVIOUR OF SEMI-RIGID CONNECTIONS

2.1 Introduction

The successful structural performance of precast concrete, in-situ, composite, timber and steel systems depends upon the connection behaviour. The configuration of the connections affects the constructibility, stability, strength, flexibility and residual forces in the structure. Further more, connections play an important role in the dissipation of energy and redistribution of loads as the structure is loaded. This literature review attempts to qualify these statements in the context of beam-to-column and semi-rigid joint behaviour in general, and to precast concrete structures in particular.

2.2 Previous work

2.2.1 Reinforced concrete beam-to-column connections

In the past two decades, the investigation of the behaviour of reinforced concrete beam-to-column connections has been a rewarding area for many researchers especially in the USA.

The first studies on this subject were conducted at the Portland Cement Association Laboratories (Hanson and Conner, 1967; Hanson, 1971). The subject has

also been studied by other investigators in the USA (Lee, 1977), in Canada (Uzumeri and Seckin, 1974) and Japan (Nakata, 1980).

Recommendations for design of beam-to-column joints in monolithic reinforced concrete structures was first published by the ACI-ASCE committee 352 (1976). Some other interesting technical papers (Durrani and Wight, 1985; Ehsani and Wight, 1985) have recently been published dealing with the same subject.

Durrani and Wight (1985) examined the performance of the interior joints which have less transverse reinforcement than required by the draft recommendations of Committee 352. They also investigated the effect of the level of joint shear stress on the strength, stiffness, and energy dissipation of beam-column subassemblages and examined the slippage of beam and column bars through the joint. Three interior beam-to-column subassemblages as shown in Fig. 2.1 were designed and tested under reverse cyclic loading.

The joint shear stress was found to have a significant effect on behaviour at large ductility levels. The joint hoop reinforcement was more effective for lower ductility levels. Guide-lines are suggested to simplify the design of connections. They indicate that a lesser amount of hoop reinforcement could be used without significantly affecting the performance of joints.

Ehsani and Wight (1985) investigated the effect of the flexural strength ratio α, defined as the sum of the flexural capacities of the columns to that of the beam, the percentage of transverse reinforcement used within the joint ρ, and the shear stress in the joint on the behaviour of external reinforced concrete beam-to-column connections subjected to earthquake type loading.

Six exterior in-situ reinforced concrete beam-to-column connections were constructed as shown in Fig. 2.2 and tested. The results were compared with the existing design recommendations. These recommendations prescribe the apportionment of total joint shear to concrete and joint hoops similar to the shear design of flexural members. It is concluded that in some cases where either the flexural strength ratio, the joint shear stress, or the anchorage requirements are significantly more conservative than the limits of the draft recommendations, the present design recommendations could be safely relaxed.

2.2.2 Precast and prestressed concrete beam-to-column connections

Earthquake resistant reinforced concrete buildings require the structure to resist the induced forces in a ductile manner. This demands that the beam-to-column connections be designed as a ductile, moment-resistant connection. This has severely limited the use of precast concrete construction in seismic zones.

Pillai and Kirk (1981) developed a satisfactory ductile, moment-resistant beam-to-column connection to be used in earthquake resistant buildings with precast reinforced concrete construction.

A satisfactory design for such a connection enabled the performance of the connection to be investigated experimentally. A total of eleven tests were conducted on full scale beam-column connections, including two monolithic specimens for purposes of comparison. The type of connection chosen for detailed experimental evaluation is shown in Fig. 2.3.

The test results have indicated that the proposed method of connection developed adequate strength, stiffness, and ductility to be classified as a ductile, moment-resistant connection in the context of seismic design.

Bhatt and Kirk (1985) grouped moment-resisting connections used for joining precast beam to columns into three categories and carried out tests on the third category on an improved version of the joint detail tested by Pillai and Kirk (1981).

Although the joints behaved satisfactorily in terms of ductility, most of the failures took place due to the failure of the weld between the bars and the plate in the column. They improved this position of the joint by increasing the length over which the plate and the bar can be welded.

Results from the tests have shown that it is possible to achieve highly ductile behaviour by using the joint detail adopted.

Stanton et al (1986). In the USA, the PCI Specially Funded Research and Development Programs 1 and 4 (PCI 1/4) focussed on the actual behaviour of commonly used connections. The two programs were combined in order to devote maximum effort to the physical testing of connections in common use. PCI 1/4 consisted of individual tests of eight simple connections, eight moment resisting connections and one moment resisting frame test. The Research Report (Stanton et al, 1986) contains a complete description of the research program, as well as detailed descriptions of the individual tests.

Dolan et al (1987) summarizes the test program, describes the test specimens, and presents the basic findings and conclusions reached during the investigation. The Research Report along with related publications (Pillai and Kirk, 1981; Bhatt and Kirk, 1985; Dolan et al, 1987; Dolan and Pessiki, 1989; Seckin and Fu, 1990) began

to address a void in the technical literature. Currently, there is a shortage of extensive test data describing the behaviour of precast connections. The lack of information is due, in part, to the effort and cost of preparing tests. The PCI report allows the model studies to be compared with tests carried out by these researchers.

Dolan and Pessiki (1989) demonstrated the feasibility of using models for testing precast concrete connections. Model studies have been examined as an alternative for obtaining basic information about the behaviour of precast concrete connections. The advantages of model studies include lower cost, specimens that are more easily manufactured and handled, a significant reduction in applied loading, and a corresponding reduction in test apparatus size. The PCI report allowed model studies to be compared with full scale tests.

Based on a number of considerations, including available materials and available testing frames, a scale of one-quarter was selected for the model studies.

A connection, designated BC-15 in the PCI report "Moment Resistant Connections and Simple Connections" (Stanton et al, 1986) was selected for the model study for three reasons. See Fig. 2.4. First, it is a commonly used connection, thus the data on its behaviour will have widespread application in industry. Second, the connection relies on bond, anchorage, welding and shear friction to develop its strength, thus providing a wide range of modeling parameters. Third, the connection design rationale is identical in the model and the PCI report.

The results have shown that the behaviour characteristics of a welded, monotonically loaded precast concrete connection can be simulated using models. Good agreement has been found between the strength and the normalized moment-rotation response of the model and full scale tests. The agreement has demonstrated

that models can be used to study this type of precast concrete connection behaviour. The effect of poor weld quality and design eccentricities have similar consequences in both the model and the full scale.

CERIB (1990-1991). In Europe, a small number of technical publications and guides on the design of precast wall connections were published, but a lack of information on test data and design models are still missing especially for connections of precast frame structures. The Study and Research Center of the French Precast Industry (CERIB) investigated more deeply in this field. A research programme entitled "Investigation on the behaviour of semi-rigid connections" was divided into two tasks:

- initial classification of connections with respect to their location
- collection of information on tests data and design methods.

Initial studies recognised that there were many connection systems available. A selection of those with the most promise was identified for further development, detailed analysis and testing.

Comair and Dardare (1992) carried out a testing programme on thread-rodded connections with grouted sleeves. It was accepted that this connection system is usually viewed as more economical than other systems used in France.

The model test specimen is a beam-to-column interior connection designated as "BC1" and assumed to be located in the first storey of a three-storey, two-bay moment resisting frame.

The experimental results verified the ductile failure mode of connection BC1. The experimental and calculated values of moments and failure loads are given in Table 2.1.

The moment rotation behaviour of this connection is shown in Fig. 2.5. This has been obtained by deducting from the measured cantilever deflection values the calculated displacement of a beam assuming to be fully fixed at its end.

Based on test data, it has been decided that the elastic moment is roughly estimated to be equal to 20% of the failure moment.

Because the rotation was determined directly from the end deflection of the cantilevers, the relative rotation of the connection should have been separated from the curvature of the cantilevers. Thus Fig. 2.5 does not show the actual relative rotation of the connection.

de Chefdebien and Dardare (1994) have focused on the behaviour of thread rodded beam column connections within the framework of the design of a three storey two bay building.

Five tests were carried out on intermediate and upper level beam column connections with different parameters which is bearing of the beams, filling between beams, and anchorage reinforcement. All beams were 300 mm wide and 500 mm deep with 100 mm in-situ concrete. The concrete grades were 60 MPa for precast members and 25 MPa for cast in-situ part.

The moment-rotation curves are given in Fig. 2.6. Connections bc1, bc2 and bc5 do not include soft elements. The moment-rotation curves are bi-linear. Connections bc3 and bc4 include soft elements. As before, the rotation includes the curvature of the beam.

The initial secant stiffness was calculated before first cracking occurred and secant stiffness was calculated using the beam-line method at the service load, taking

into account the second moment of area, I, of the "T" beam. However, it is not clear whether I is based on the flexurally cracked or uncracked section properties.

Ultimate moments occurred for rotations higher than 0.06 rad, and they have been compared with the ultimate design moments in the beams. The ratio M_{con}/M_{beam} varies from 0.24 to 0.42 for the different tests.

According to the test results, it has been concluded that the continuity moment on intermediate support could easily be increased to a value equal to 30% of the bending moment of a simply supported beam.

Mahdi (1992). Fourteen tests were carried out as shown in Fig. 2.7 and Table 2.2 to evaluate experimentally the degree of semi-rigidity afforded by the most common types of beam-to-column connections used in the precast concrete industry in the U.K. These were the billet, welded plate, corbel and cleat connections, two of these are shown in Fig 1.1.

Results given in Fig. 2.8. (a) and (b) are for the double sided test shown in Fig. 2.7(c) for initially sagging (-ve) and hogging (+ve) moments, respectively. The $M-\phi$ data given in the figures show that relative rotations are in excess of 0.02 radians when the ultimate moments of the connection is reached.

A secant stiffness value J_{es} (see Chapter 11) obtained using the beam-line method, as shown in Fig. 1.7, was used in the stability analysis to determine column buckling load capacities and β (column effective length) factors. The secant stiffness was used because the local tangent stiffness J given by the gradient of the $M-\phi$ curves is changing throughout the loading cycle.

It has been reported that connection moments in the order of -125 kNm to +210 kNm and stiffness values J = 19,000 kNm/radian are sufficient to enable the

frame to resist sway forces and reduce β factors to values which are only 10% greater than for the fully rigid condition. It has been suggested that a partial safety factor increased from 1.5 to 1.6 should therefore be applied to these type of connections to avoid column failures, because damage was extensive in the precast column. The factored moment of 130 kNm is approximately equal to the moment used in the determination of the J_{es} using the beam-line method, and no visual cracking was evident in the column at this bending moment.

It has been observed that all connections possessed some strength and stiffness, but the capacities varied over a wide range, i.e M_{con} from 5 to 210 kNm, and stiffness from 200 to 19,000 kNm/rad. The analytical work showed that the stiffness needed to obtain buckling capacities which differ from fully rigid situation by about 5% is only marginally greater than the flexural stiffness of the beam, i.e. $4EI/l$. Combining the experimental and analytical results it was clear that the welded plate and billet connections would give a precast structure sufficient global stiffness to satisfy serviceability and ultimate limit state criteria, and would lead to a more economical column design, but the cleat and corbel connections would not possess both sufficient strength and stiffness to satisfy these limits and must therefore continue to be classified as pinned.

Virdi and Ragupathy (1992a). The stability behaviour of isolated restrained beam-columns has previously been studied by Virdi (1973, 1976). The method enables an ultimate load analysis of no-sway isolated columns of a variety of cross-section, including material and geometric nonlinearities, following a variety of load paths, as well as allowing variation of cross-section along the length of the column. The method has been extensively verified by tests on composite and reinforced concrete columns.

The above method of analysis of isolated columns of all types has been developed further to include the problem of 3-dimensional frames subjected to side-sway (Virdi and Ragupathy, 1992a). The analysis also applies to no-sway frames and to continuous columns. The analysis takes proper account of the behaviour of flexible connections, such as those encountered in precast frames. The numerical procedure is based on the calculation of the equilibrium deflected shape of the frame and its members for an initially low level of applied external loading. Iterations for obtaining a solution take place in three principal stages: at a section to determine moment curvature relations, along the length of the member to determine the member deflected shape, and at nodal points to ensure equilibrium and compatibility through any flexible or rigid joints. The external forces are increased in steps until, for a given load factor, an equilibrium deflected shape cannot be found. Such a load is taken as the ultimate load of the frame. The theoretical basis of the new technique is described in detail by Virdi and Ragupathy (1992a).

The computer program, labelled SWANSA (SWay And No-Sway Analysis), was developed based on the above method. It has the following options:

1. Linear or non-linear analysis of 3-dimensional precast concrete sway and nonsway frames. Joints can be rigid, pinned or flexible (semi-rigid).

2. Computation of the ultimate load of a single beam-column or continuous beam-column for given external forces, or combination of forces can be increased to reach the ultimate load.

3. The output includes deflections, moments, shear forces, axial forces, strains, and tortions at all member stations and at global nodes.

Virdi and Ragupathy (1992b). They conducted eight tests on precast concrete subframes as shown in Fig. 2.9 to provide data for the validation of computational results. Each subframes consisted of a 6m long continuous column together with a stub length (2 m) of the beam. The dimensions of the test specimens were essentially predetermined in terms of height and overall cross section dimension (300 mm square for the column and 450 x 300 mm for the beam).

The ultimate loads obtained from all the eight experiments are compared with the computed results in Table 2.3, which gives the failure axial load for seven of the subframes tested, and in Table 2.4, which gives the failure moment for Test 7. It can be seen that the correlation for axial loads is within 7%. The correlation for Test 7, in terms of the failure moment is however, not so good.

For illustrative purposes, results for Test CT6, are presented here. It has been reported that results for other tests show similarly good correlation. The connection detail at the beam-column junction for this test is shown in Fig. 2.10. By comparing the slopes of the beam and column at the beam column junction, it has been possible to deduce the moment rotation characteristic of the particular connection. The hogging moment-rotation response obtained for this test is shown in Fig. 2.11.

The Test Program of the Finnish Connections (Tampere, 1995). The main aim of this ongoing project is to examine the semi-rigid behaviour of precast connections used in Finland. The project partially involves full size testing to establish $M-\phi$ curves of various types of connections.

The Finnish test program is divided in two phases. In the first phase the behaviour of connections will be examined (Fig. 2. 12). where three similar tests will be carried out. The tested beam cross section is not rectangular but has flanges to

support slabs. It was selected as being the most common one in Finland. The same kind of structure will be used in both test series to make the comparison of the results simpler. In the second phase the influence of hollow cored floor slabs will be included as shown in Fig. 2.13. In this test series two similar tests will be carried out to examine the single and double sided joints.

The type of connection, called "KP", is shown in Fig. 2.14. The connection behaves rather like a hinge when the joint concrete is not used. The effect of the joint concrete causing the semi-rigid behaviour will be checked, but the grade of the joint concrete has not been mentioned to date.

Mohamed and Jolly (1995) conducted two full-scale test programmes on sleeved bolt connections, shown in Fig. 2.15. Test series A examined the influence of bolt density on overall joint behaviour, e.g. failure mode, ultimate strength and stiffness. Test series B studied the effect of concrete strength and its confinement on the load-carrying capacity of single-bolted joints.

Joint moment stiffness has been characterized by the moment-rotation curve. A moment M has been created at the concrete face due to the eccentricity of the load from the column. This moment, which tends to extend the top bolts, induces the plate rotation ϕ. Values of the $M-\phi$ have been computed, and plotted in Fig. 2.16. These curves show that the number of bolts per joint has an effect on the joint's rotational rigidity.

Loo and Yao (1995) investigated the strength and deformation behaviour of two types of precast reinforced concrete beam-to-column connections. Referred to as Types A and B, these connections have been recommended by the PCI Committee on Connection Details and the Australian Prestressed Concrete Group for use in precast

reinforced concrete building frames. A total of 18 half-scale interior connection models were designed, built, and tested to failure to evaluate their strength and ductility properties under static and unidirectional repeated loading. They include four monolithic models and four each of the precast connection Types A and B static load tests. Details of these connections are given in (Loo and Yao, 1995).

They found that the two types of precast concrete connections performed satisfactorily in that their bending strengths were, without exception, higher than the monolithic connections. In addition, the ductility and energy absorbing capacities of the precast connections, generally, are superior to their monolithic counterparts.

The load deflection curves for some of the specimens are presented in Fig. 2.17. From the results, it was concluded that all the precast models possessed not only greater ductility but also higher stiffness than their monolithic counterparts.

2.2.3 Classification of steel beam-to-column connections

Stiffness boundaries (Zoetemeijer, 1989) investigated the influence of the stiffness of the connections on the stability of the frame. The relationships between loading moments and deformations were given for frequently occurring situations in braced and unbraced frames. These were expressed by considering the situation where rigid connections are multiplied by a reduction factor R, which is a function of k, the ratio between the rotational spring stiffness of the connection and the bending stiffness of the beam. Therefore $k = cl/EI$ where c is the calculated value of the rotational spring stiffness of the connection. The stiffness boundaries were chosen on basis that the Euler buckling load at $k > 25$ deviates by less than 10% from the Euler buckling load at $k = \infty$. It has been concluded that a connection can be considered to be rigid when

the value of k exceeds 25. It has also been concluded that a connection can be considered to be a hinge when the value of k is less than 0.5. The Euler buckling load at $k = 0.5$ deviates by less than 85% of the Euler buckling load at $k = \infty$. When the k value lies between 0.5 and 25, the connection is to be classified as semi - rigid, and flexibility is to be taken into account in calculating the force distribution and the stability of the frame.

Stiffness boundaries (Briquet et al, 1994). As none of classification systems is fully satisfactory, it was decided to dedicate a part of the COST C1 Project to find two new classification boundaries: these boundaries have to be defined in terms of rotation stiffness (rigid, semi-rigid and pinned) and moment capacity (full strength, partial strength and pinned). Therefore as a further step, it should also be tried to eliminate the ductility of the connections (brittle or ductile) in the analysis.

The stiffness boundaries between rigid and semi-rigid have been established for a simple portal frame, braced or unbraced, with rigid or pinned column bases. The comparison of these boundaries allows to determine, in each case, the most determinant ones. They are based on classification criteria defined as ratios β, either between two loads or between two displacements, one calculated for the structure with semi-rigid beam-to-column connections ($\bar{c}$) the other one for the same structure with rigid connections ($\bar{c} = \infty$).

The considered criteria are:

- Ultimate load criterion $\qquad \beta_u = \dfrac{F_u(\bar{c})}{F_u(\bar{c} = \infty)}$

The ultimate load is determined by the Merchant-Rankine formula in the case of an unbraced structure as:

$$F_{cr} = \frac{1}{\left(\frac{1}{F_{pl}} + \frac{1}{F_E}\right)}$$

- Deformation criterion $\beta_f = \frac{f(\overline{c} = \infty)}{f(\overline{c})}$

with f = second order elastic lateral displacement under service load in the case of an unbraced frame:

= elastic mid-span beam displacement in the case of a braced frame.

The joints have been considered as rigid if their influence on the structural frame response is limited to 5% for resistance criteria (β_u = 0.95) or 10% for deformability criteria (β_f = 0.90). All those criteria have been presented by a curve, as shown in Fig. 2.18 where $\rho = R_b / R_c$ = beam / column rigidity.

It has been suggested that in the case of unbraced frames, the most determinant criterion is the one concerning the lateral displacement even if the β values for deformations are less severe (β_f = 0.90) than those relative to ultimate loads (β_u = 0.95).

These boundaries for unbraced structures have been confirmed by calculations performed by means of the non linear FEM software called FINELG on realistic simple portal frames with rigid or pinned column bases.

Another step in the investigation is whether deformation criterion built up for a simple portal frame could be extended to multi-bays, multi-storeys frames. It has been reported that the problem can be solved, in the case of one-storey multi-bays structures, by referring to the so-called "equivalent Grinter frame". Two examples of

one-storey two-bays frames with rigid column bases have been investigated with FINELG and it appeared, as shown in Fig. 2.19, from the study that the same deformation criterion defined here above can be used provided the beam and column rigidity R_b and R_c replaced by the corresponding ones in the equivalent Grinter frame.

Before establishing a classification system for beam-to-column connections, the following work has been programmed:

- stiffness boundary between rigid and semi-rigid domains for multi-storeys unbraced structures;

- stiffness boundary between rigid and semi-rigid fields for braced structures;

- classification according to the resistance for braced or unbraced frames (should be tried for both braced and unbraced frames);

- problem of boundary between semi-rigid and pinned fields.

It has been reported that work on these different topics is in progress, but details have not been given about how it is going to be done.

Beam reference length method (Bjorhovde et al, 1990) has been used to classify connections in terms of strength, stiffness, and ductility, using tests and theoretical data.

The classification system is nondimensional, but is based on connections that can be associated with a certain reference length for the beam component. It has been suggested that this is necessary because in the analysis of the response of frames, it is the angular displacement, i.e. the rotation, of the connection that is needed, rather than the curvature.

The rotation is the essential measure of deformability in the evaluation of the various types of connections, however, in the analysis of the beams, it is the curvature that plays the similar role. This was shown as one of the reasons why it has been decided to use specific beam element length to correlate the connection rotation and the beam slope in the development of the classification criteria. The length of the beam is chosen such that the initial stiffness of the beam matches that of the connection.

Based on evaluations of a large number of test data for a variety of beam-to-column connections as presented by Kishi and Chen (1986) it has been found that a value of the reference length of five times the depth of the beam, that is part of the connection, would be the most appropriate. This length places the connection in the middle of the semi-rigid range. The data confirm that the stiffer the connection, the shorter the equivalent reference length of the beam will be.

To provide the dividing lines between rigid and semi-rigid and between semi-rigid and flexible, reference lengths of $10h$ and $2h$ have been proposed (h = depth of beam). These magnitudes are based on the connection data, obtained from a total of 55 connection data sets.

Based on the data, ultimate moment magnitudes of $0.2M_p$ and $0.7M_p$, respectively, for the flexible to semi-rigid and the semi-rigid to rigid connection strength boundaries have been chosen. For the rigid connections, the ultimate bending moment boundary higher than $0.7M_p$, or perhaps even larger than the full M_p has been chosen. The latter value reflects a design philosophy that aims at having failures occur away from the connection regions.

The nondimensional ductility requirement has been related to the ratio of the ultimate moment capacity of the connection to the fully plastic moment of the beam. It

is found to be approximately inversely proportional to the initial stiffness of the connection. In the other words, the more flexible the connection, the larger the necessary ductility. The ductility region boundary has been simplified on the basis of end-point moment ratios of 0.2 and 0.7, and the initial stiffness connection values of $EI/10h$ and $EI/2h$, respectively. This gives the nondimensional ductility requirement values of 2.7 and 1.2 respectively.

Classification adopted in (Eurocode 3, ENV 1993-1-1:1992 E) based on an Euler instability criterion (Bijaard and Steenhuis, 1991): Generally a connection is assumed to be perfectly rigid, when its flexibility causes a reduction in the axial load carrying capacity of the frame of not more than 5%. Fig. 2.20, (Bijaard and Steenhuis, 1991), illustrates the relationship between the relative rotation stiffness $\bar{c}$ and the ratio between the flexural stiffnesses of the beam and column ρ at a constant ratio between the Euler buckling loads of a frame with semi-rigid connections and rigid ones $\left(\frac{P_{E(\bar{c})}}{P_{E(\bar{c}=\infty)}} = 0.95\right)$. To be able to classify a connection according to this diagram, the moment-rotation relationship of the connection, and the geometry of the column and the beam (cross sections and lengths) are required to obtain ρ. Eurocode 3 uses a simplification by choosing a constant boundary value for the parameter $\bar{c}$ ($\bar{c} = 8$ for unbraced and $\bar{c} = 25$ for braced frames), therefore it is at least not necessary to know the length of the column.

Classification of beam-to-column connections is given for steel connections in steel frames in (Eurocode 3, ENV 1993-1-1:1992 E) as follows (Fig. 2.21):-

Beam-to-column connections may be classified by :-

rotational stiffness

moment resistance

The rotational stiffness of a beam-to-column connection may be classified as:

nominally pinned

semi-rigid

rigid

A beam-to-column connection may be classified as nominally pinned if its rotational stiffness S_j (based on a moment-rotation characteristic representative of its actual anticipated behaviour) satisfies the condition:

$$S_j \leq 0.5EI_b / L_b$$

where S_j is the secant rotational stiffness of the connection

I_b is the second moment of area of the connected beam

L_b is the length of the connected beam

A beam-to-column connection in braced unbraced frames may be considered to be rigid compared to the connected beam if the rising portion of its moment rotation characteristic lies above the solid line on the appropriate diagram in Fig. 2.21.

If the rising portion of its moment rotation characteristic lies below the appropriate line in Fig. 2.21, a beam-to-column connection should be classified as semi-rigid, unless it also satisfies the requirements for a nominally pinned connection.

With respect to the design moment resistance, beam-to-column connections may be classified as

nominally pinned

partial-strength

full-strength

A beam-to-column connection may be classified as nominally pinned if its design moment resistance M_{Rd} is not greater than 0.25 times the design plastic moment resistance of the connected beam M_{plRd} provided that it also has sufficient rotation capacity.

A beam-to-column connection may be classified as full-strength if its design moment resistance $M_{Rd} \geq M_{plRd}$ provided that it also has sufficient rotation capacity.

A beam-to-column connection should be classified as partial strength if its design moment resistance M_{Rd} is less than M_{plRd} (see Fig. 2.21).

Euler instability criterion (Bijaard and Steenhuis, 1991): For the purposes of the standardisation of connections it is desirable to classify a connection without knowing the length of the beam. Bijaard and Steenhuis (1991) published a proposal satisfying this aim. By assuming a specific ratio between the beam length and the beam height ($l/h = 20$ for braced and $l/h = 25$ for unbraced frames), they achieved a classification system independent of the length of the connected beam. Therefore, as a further step, it should also be tried to eliminate the distinction between braced and unbraced systems in the classification process. The following proposal fits this aim.

Proposal Innsbruck (Tschemmernegg, 1993): This proposal is independent of the length of the connected beam and the frame system (braced or unbraced). A boundary curve, which is lying between the two Bijaard proposals has been assumed and has been calculated according to the Eurocode 3 boundaries. The variable relation l/h for braced and unbraced frames according to the Innsbruck proposal, is a quite reasonable, practical range with the advantage of having only one classification-curve, but is only valid for a specific ratio of beam length to height ($l/h = 12$ for braced and

l/h = 37.5 for unbraced frames) up to the elastic behaviour which is present up to at least 2/3 $M_{pl,beam}$. The assumption of Bijaard with constant l/h is also an estimation and leads to different classification-curves for braced and unbraced systems.

Beam-to-column connections in Eurocode 4 (Johnson and Anderson, 1993). Whereas Eurocode 3 gives detailed rules to classify such steelwork connections, Clause 4.10.5 of EC4 extends these to composite connections where the slab reinforcement contributes to the tensile resistance of the connection (i.e. when it resists hogging bending). For this reason, Section 4.10 of EC4 is restricted to braced frames.

To non-dimensionalize the classification limits, the properties of the connection are compared with those of the connected beam. For the composite beams, the design plastic resistance moments are generally different in sagging and hogging bending. Similarly, the flexural rigidity of the beam depends on whether the cracked or uncracked section is considered.

For classification by moment resistance, the appropriate value of the design plastic resistance moment is that of the composite beam's effective section adjacent to the connection. As in Eurocode 3, a connection may then be classified as full-strength or partial-strength, depending on whether the resistance of the connection is greater than or less than the design plastic resistance moment.

For classification by rotational stiffness, clause 4.10.5.2 permits the flexural rigidity of the beam to be taken as the cracked or the uncracked value, consistent with the approach used in global analysis. As the cracked value is lower, it is more likely that a connection will be classified as rigid if this value is used; with this classification, the flexibility of the connection is ignored. This is appropriate, as the cracked approach

is the more accurate model of beam behaviour and therefore greater approximation can be tolerated in the representation of the connection.

No detailed rules are given for the calculation of the three main properties of a composite beam-to-column connection; moment resistance, rotational stiffness and rotation capacity. Methods to predict these properties are not yet sufficiently well established to justify inclusion in Eurocode 4. However, attention is drawn to the use of the rules in Eurocode 3 for steel connections, supplemented by consideration of the slab reinforcement.

2.3 Summary

This literature survey contributes a first step dealing with the knowledge of flexural behaviour of semi-rigid beam-to-column connections in general and to precast concrete structures in particular.

It will enable the performance of the connections to be investigated experimentally. This will allow the test results of the experimental work to be compared with the relevant tests carried out by the researches.

The test results will be non-dimensioned and compared to the classification system used in Eurocode 3 as being the only standard one and yet there is no classification system for precast concrete semi-rigid beam-to-column connections in the literature survey.

Connection	Calculations		Measurements	
Designation	Failure moment kNm	Failure load kN	Failure moment kNm	Failure load kN
BC1	145	96	153	102

Table 2.1: Experimental and calculated values of moments and failure loads

(Comair and Dardare, 1992)

Reference	Connection type	Beam depth (mm)	Subframe type	Loading mode
TB1	Billet	300	Single	Reversible
TB2		300	sided	do
TB3		600	no	do
TB4		600	slab	do
TW1	Welded plate	300		Monotonic
TW2		300		Reversible
TW3		600		do
TW4		600		do
TB5	Billet	300	Double	Reversible
TW5	Welded plate	300	sided	do
TCL5	Cleat	300	no	do
TCO5	Corbel	300	slab	do
TW6	Welded plate	300	Double with slab	Reversible in-plane
TW7		300		Reversible out-of-plane

Table 2.2: Schedule of experimental tests (Mahdi, 1992)

Test No	Experiment	SWANSA	% Error
1	1140.4	1801.0	---
2	1939.1	1818.1	-6.2
3	1862.2	1737.8	-6.7
4	1704.9	1796.5	5.4
5	2042.8	2132.4	4.4
6	2023.6	1899.2	-6.1
8	2038.0	2086.1	2.4

Table 2.3: Experimental and theoretical failure loads (kN) (Virdi and Ragupathy, 1992)

Test No	Experiment	SWANSA	% Error
7	180.1	238.5	32.4

Table 2.4: Experimental and theoretical failure moments (kNm) (Virdi and Ragupathy, 1992)

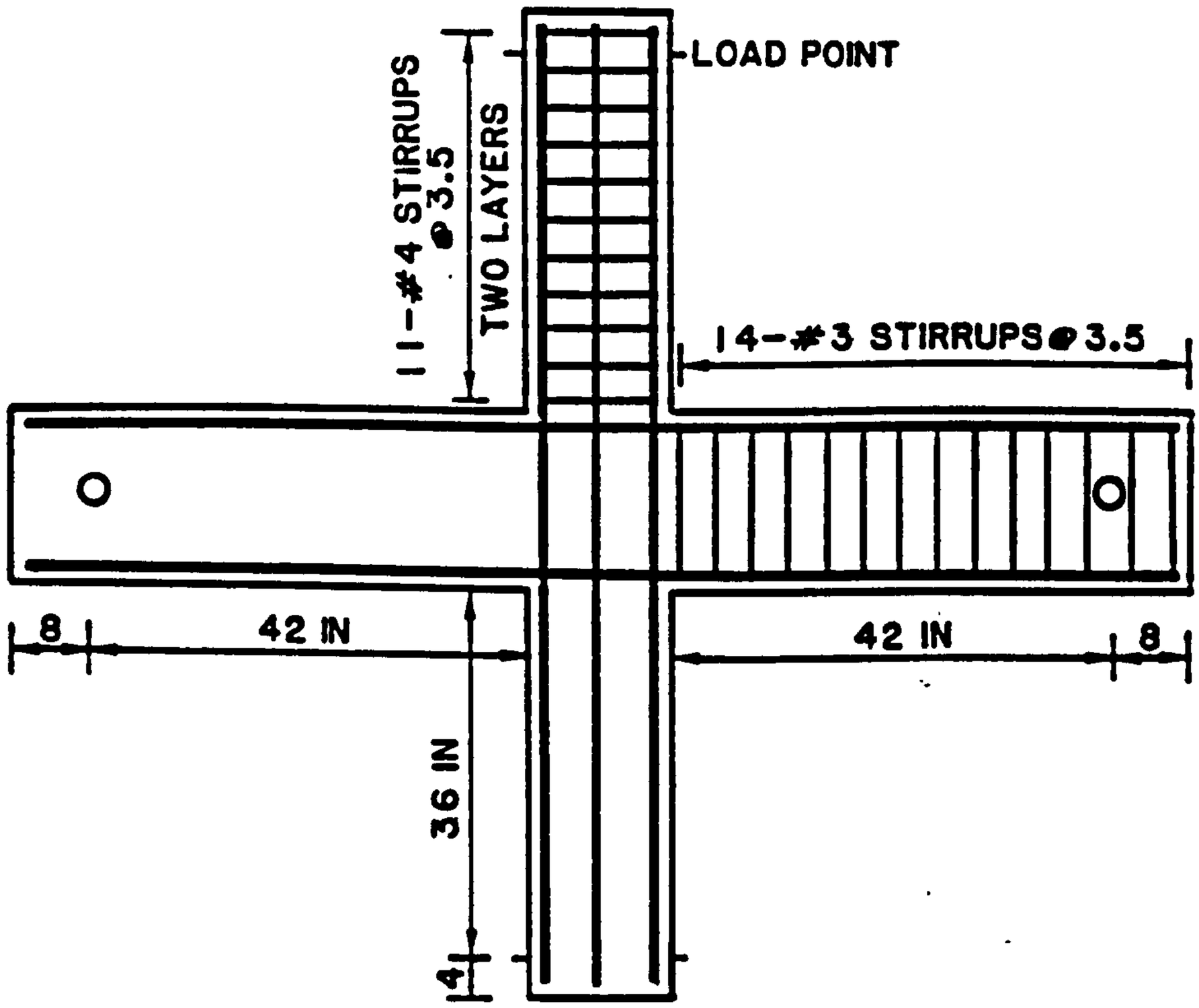

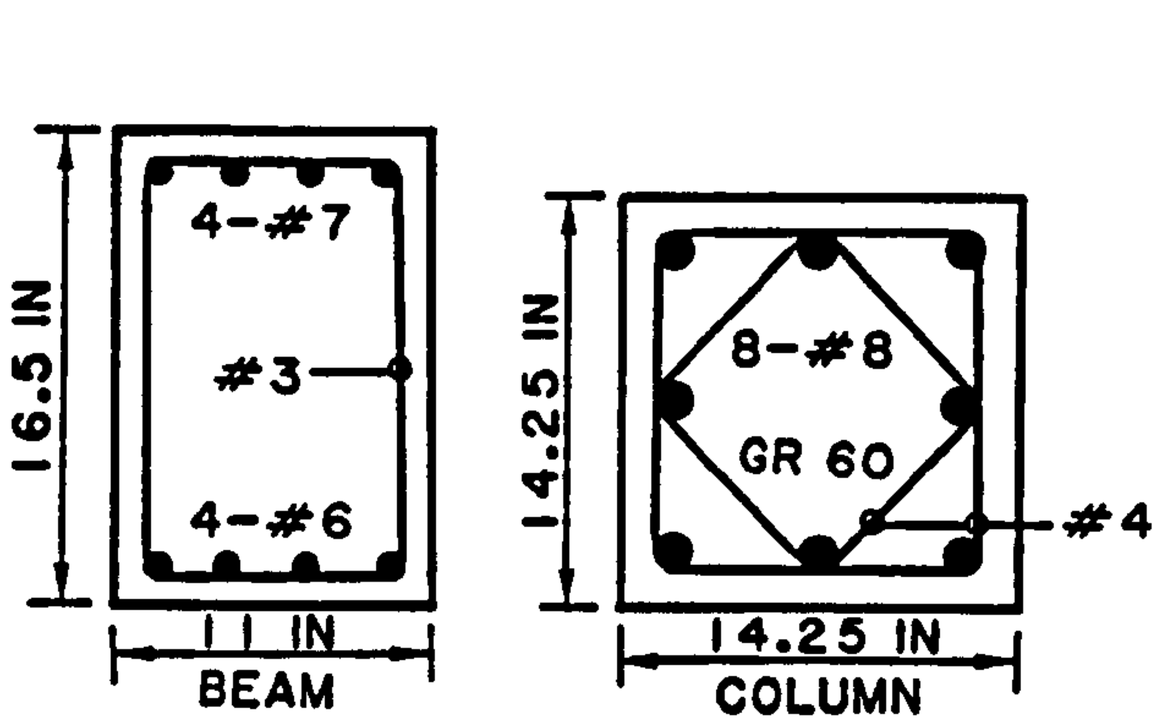

SPECIMENS X1, X2

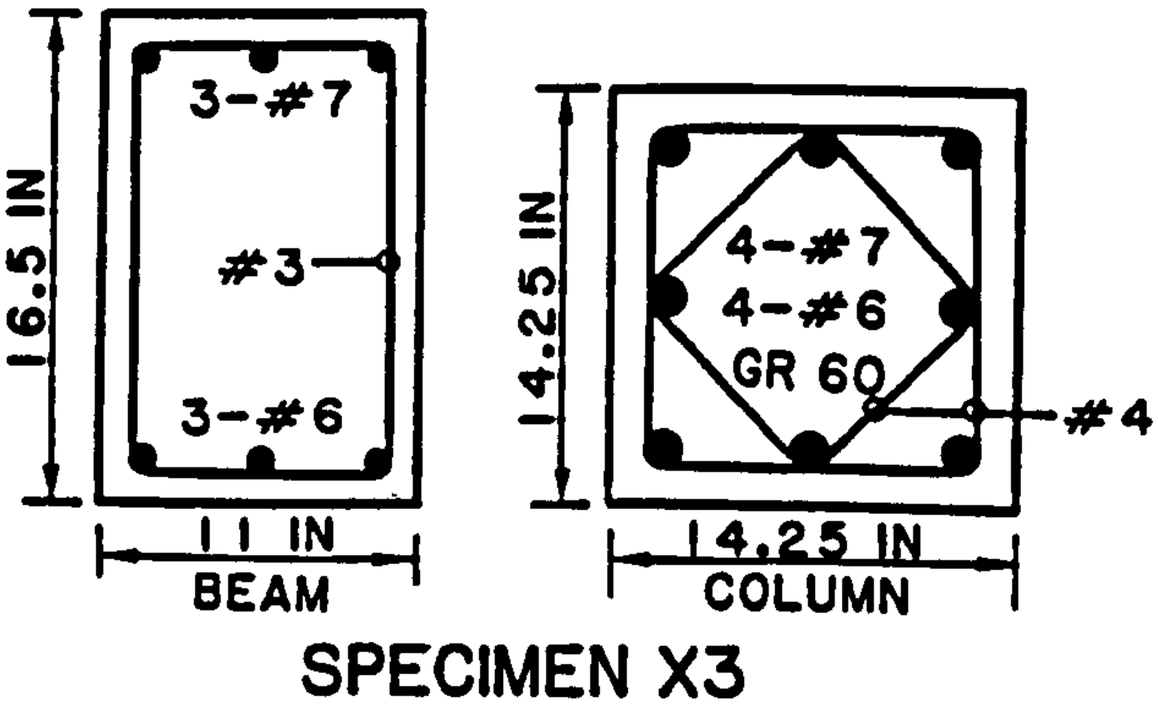

SPECIMEN X3

Figure 2.1: Beam column subassemblage used by Durrani and Wight (1985)

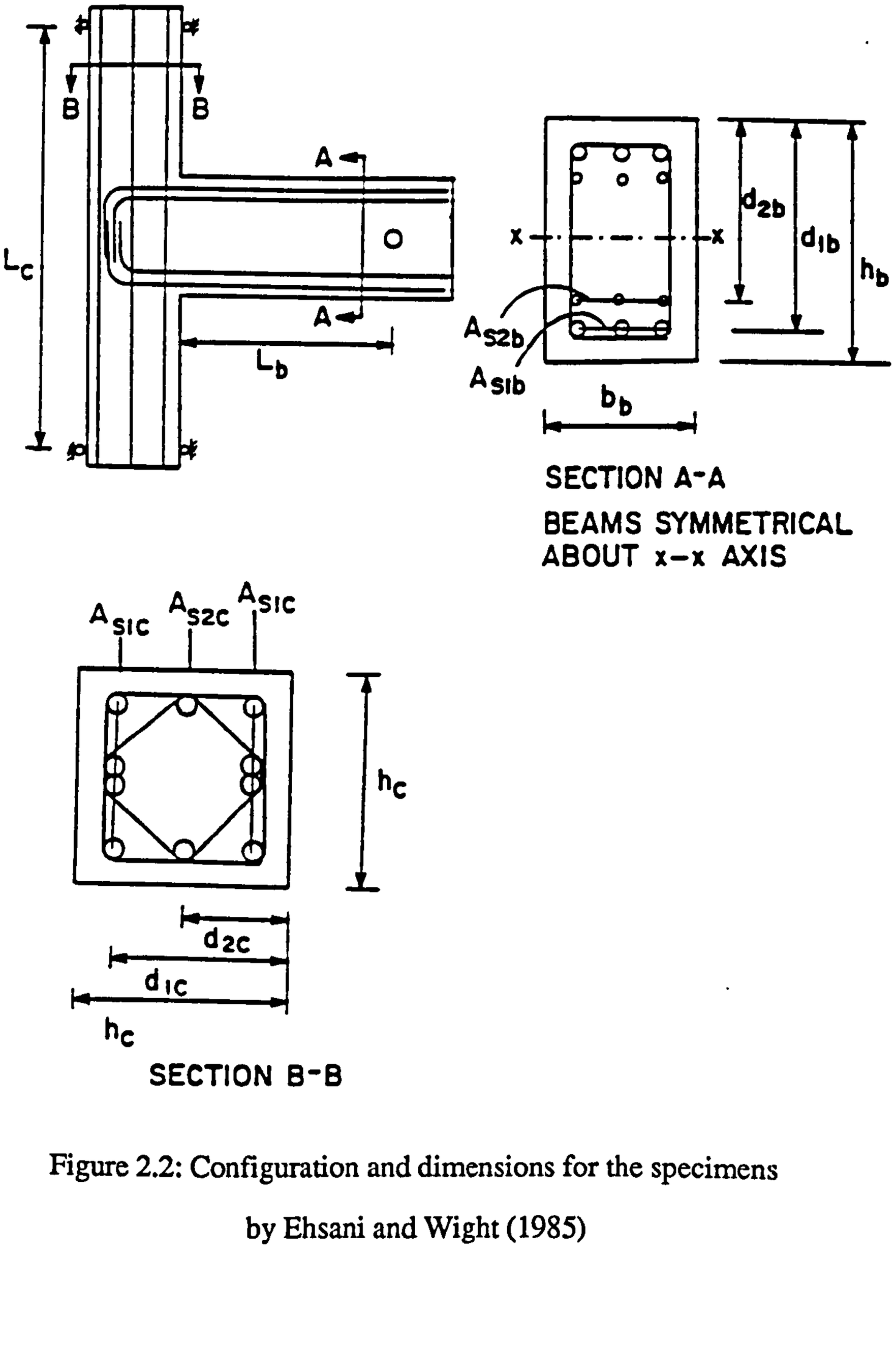

Figure 2.2: Configuration and dimensions for the specimens by Ehsani and Wight (1985)

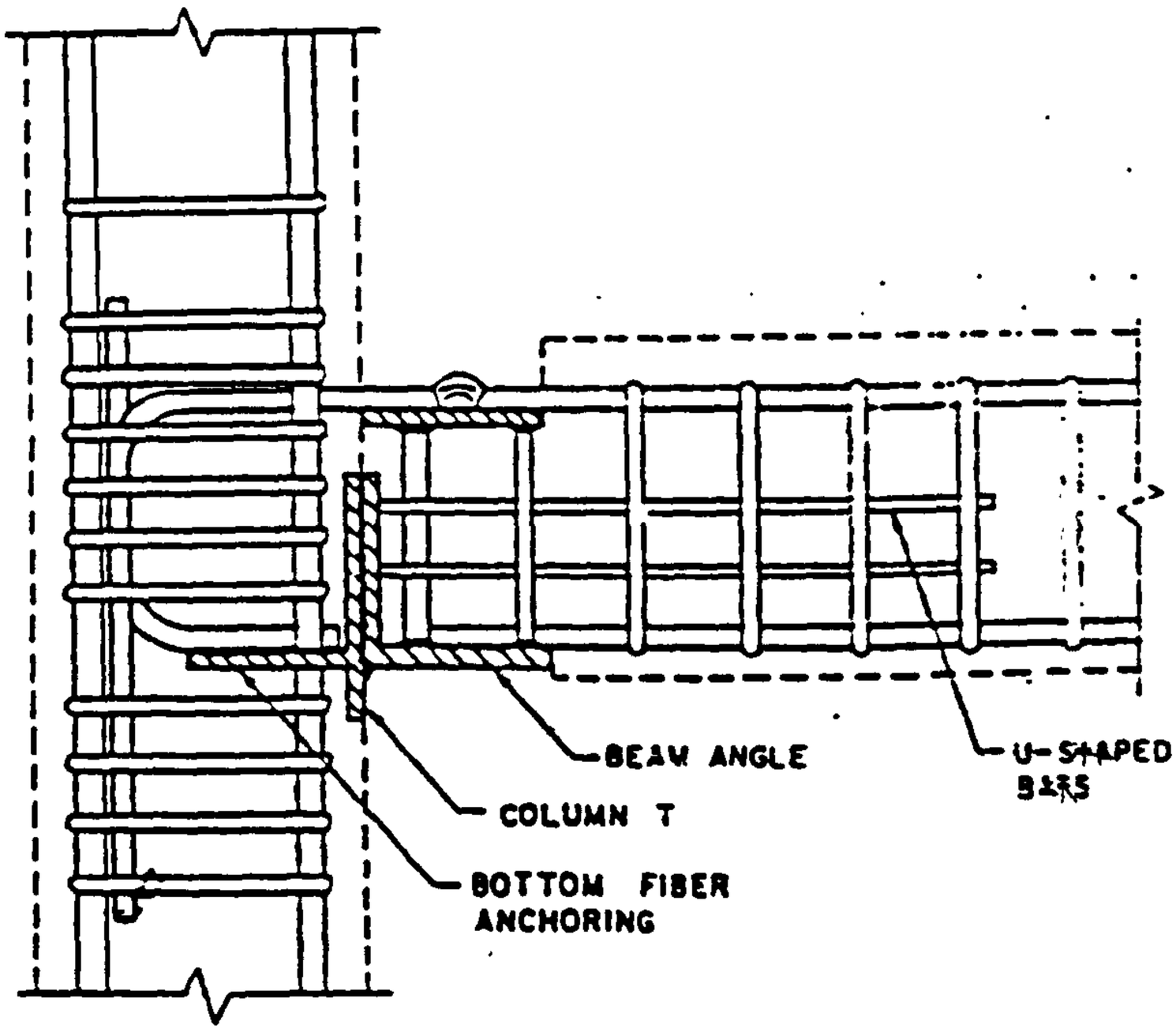

Figure 2.3: Joint detail used by Pillai and Kirk (1981)

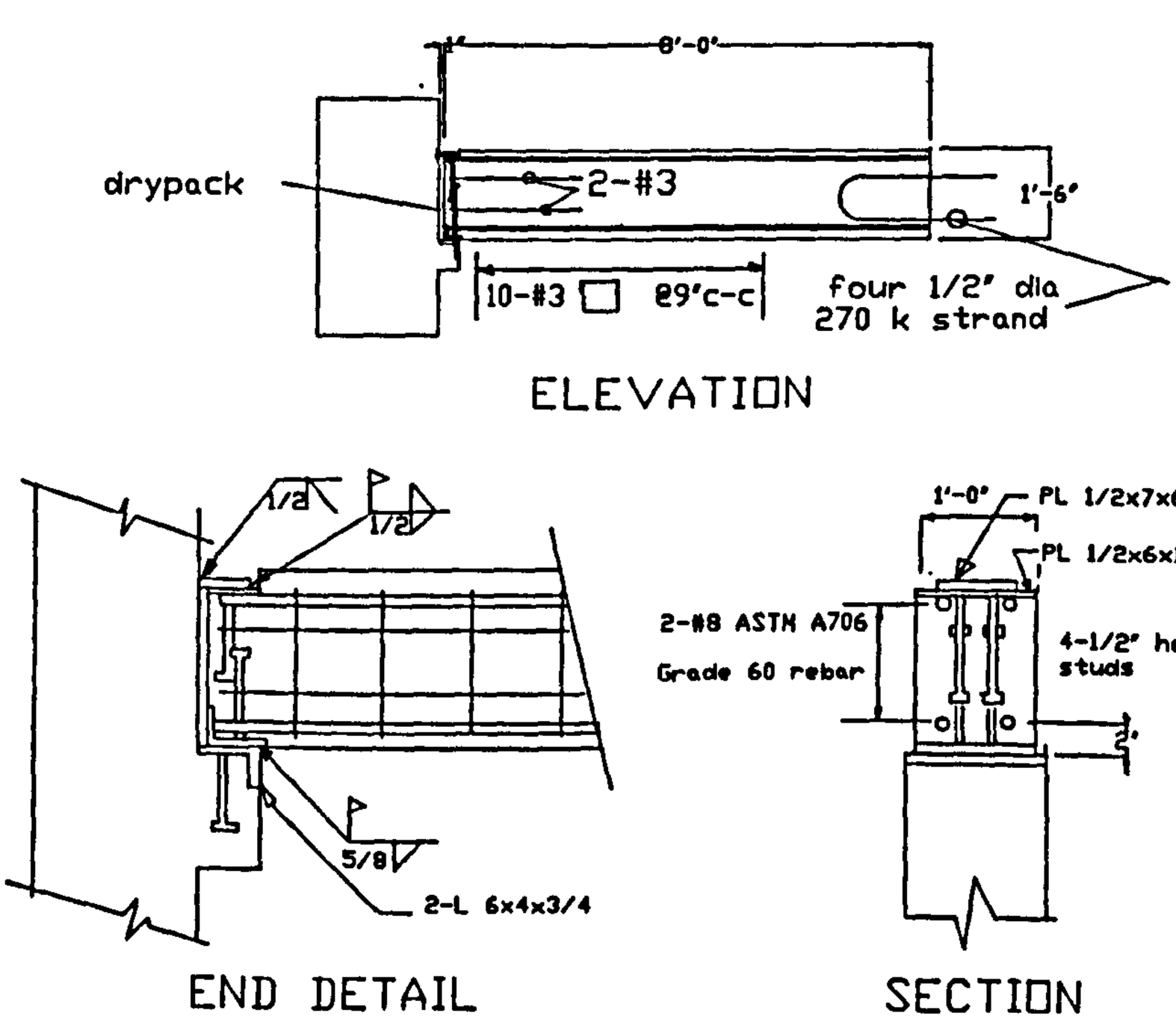

Figure 2.4: The PCI connection BC-15 details

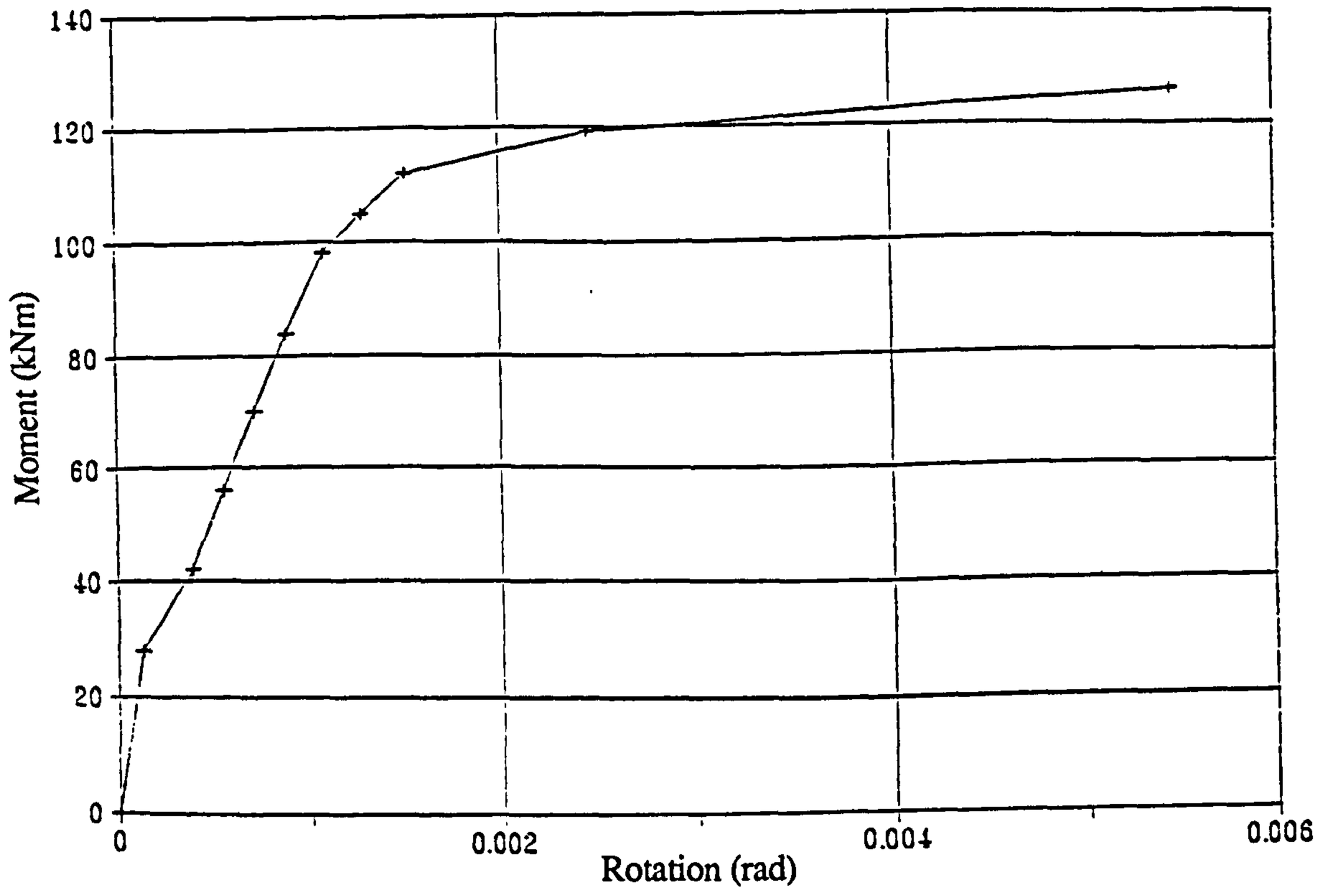

Figure 2.5: Moment-rotation behaviour curve for connection BC1
Comair and Dardare (1992)

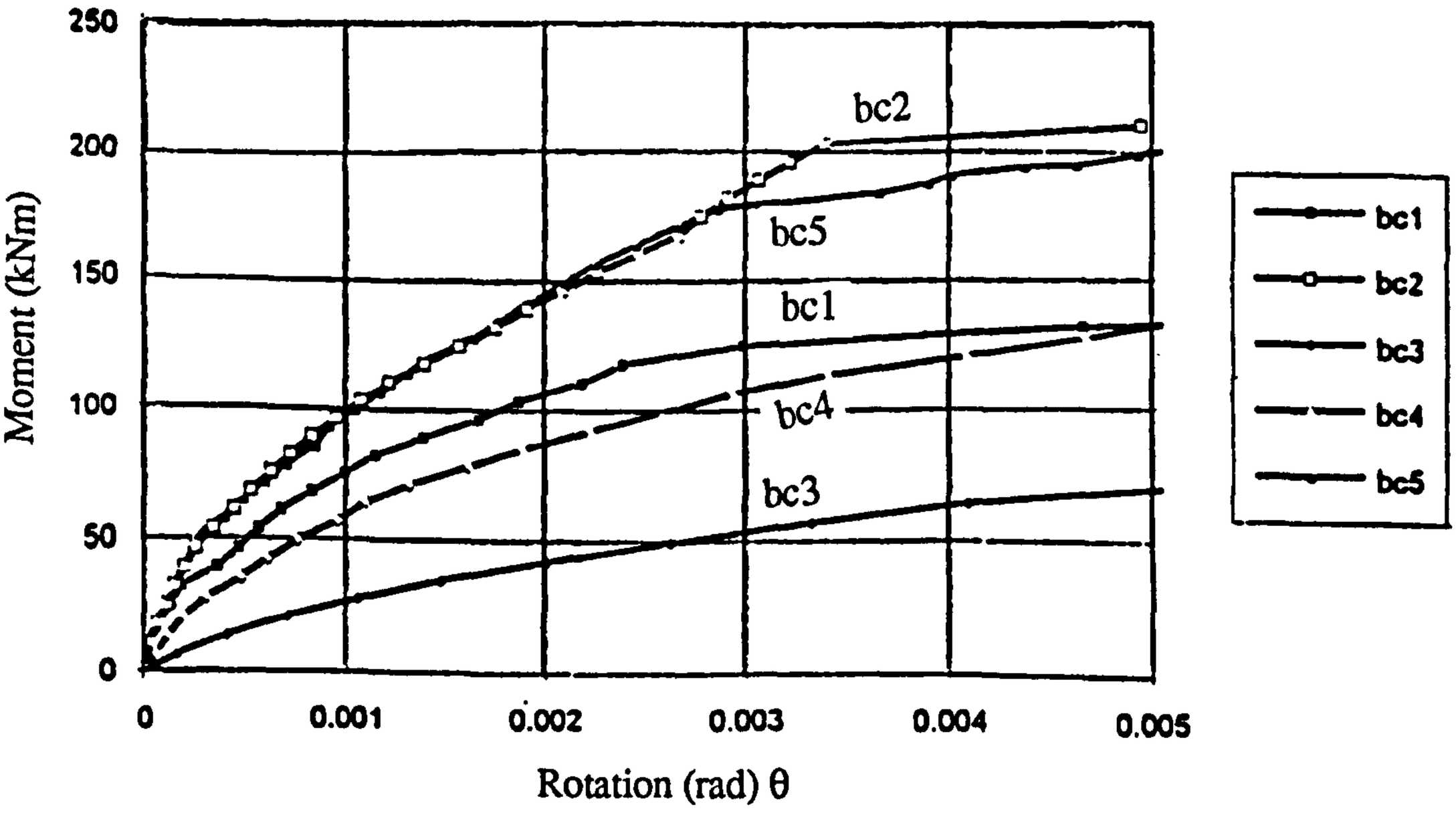

Figure 2.6: Moment-rotation behaviour curves for the tests
de Chefdebien and Dardare (1994)

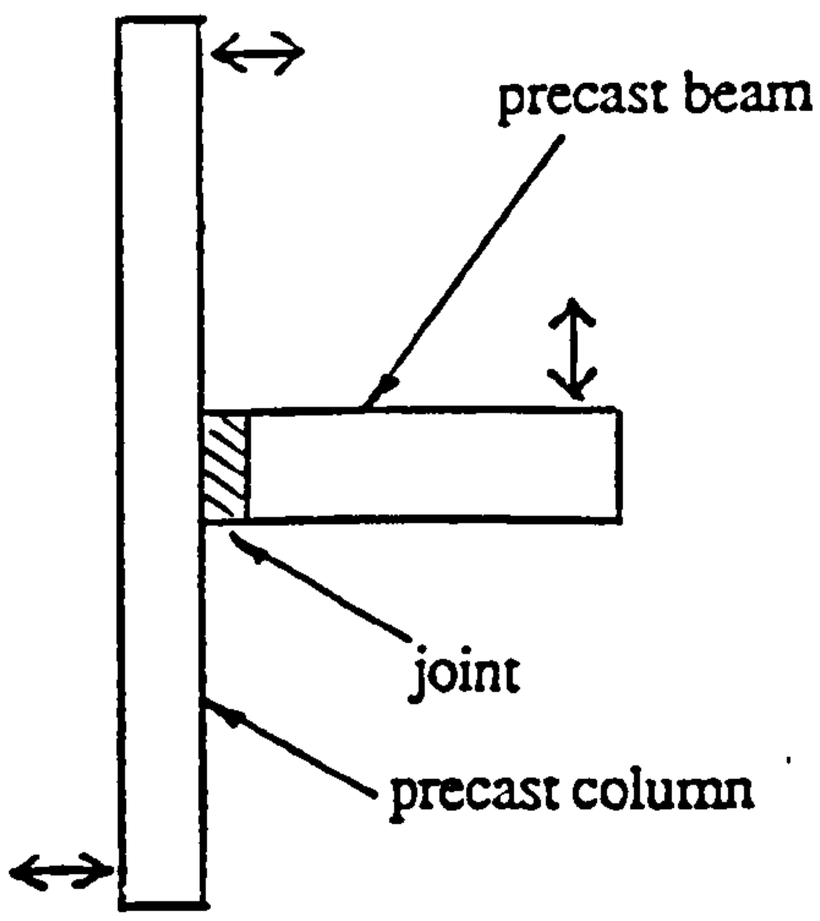

[a] single sided beam-column

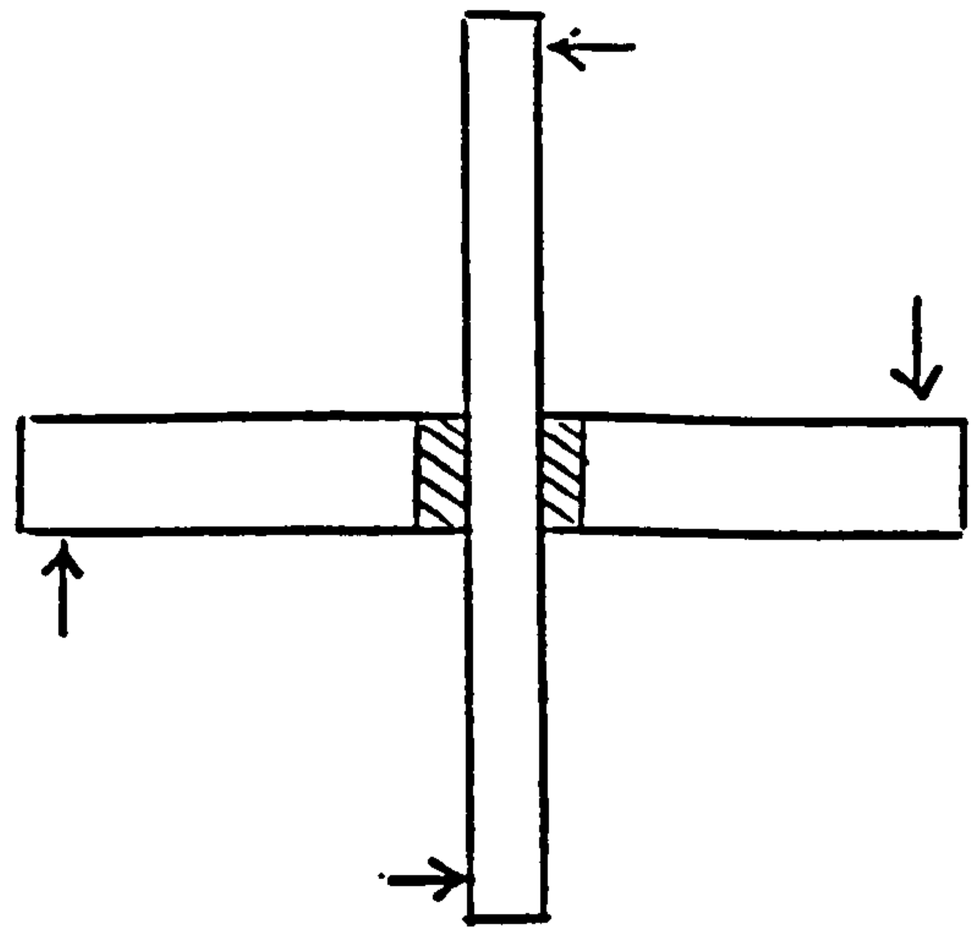

[b] double sided beam-column

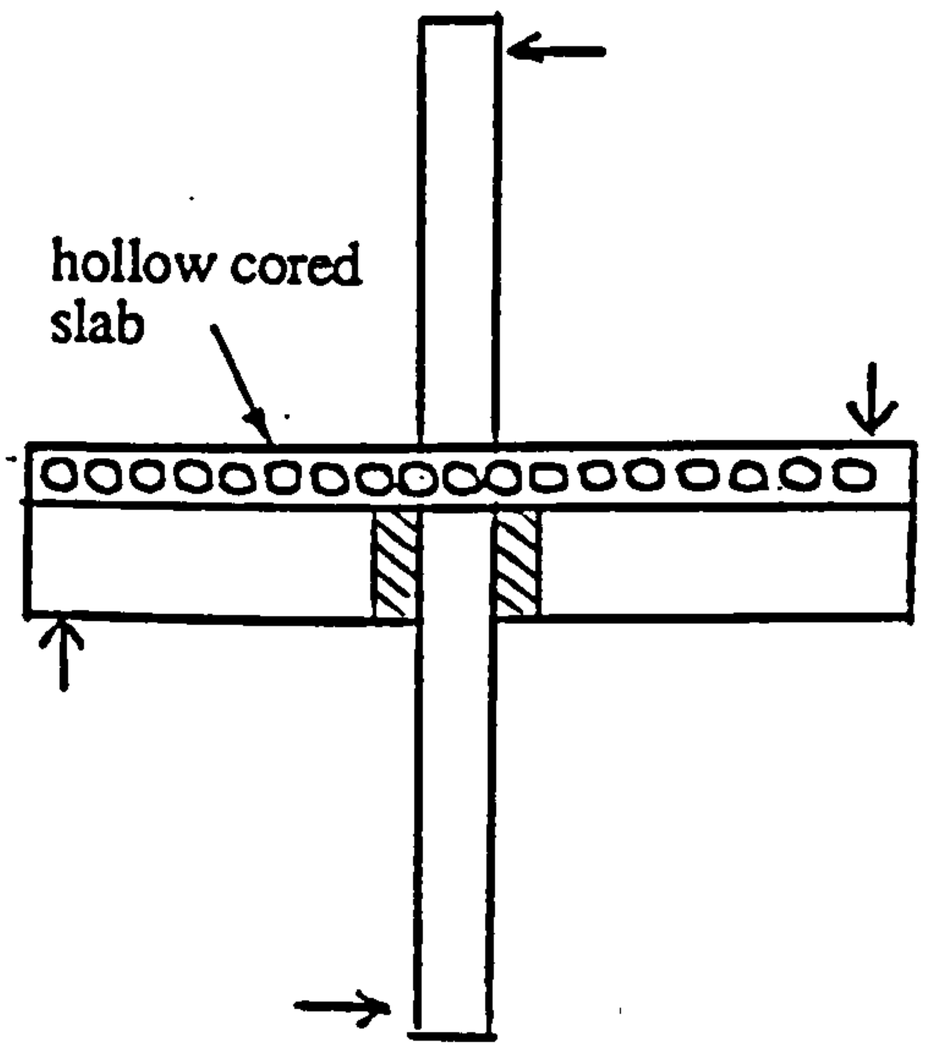

[c] double sided beam-column-slab

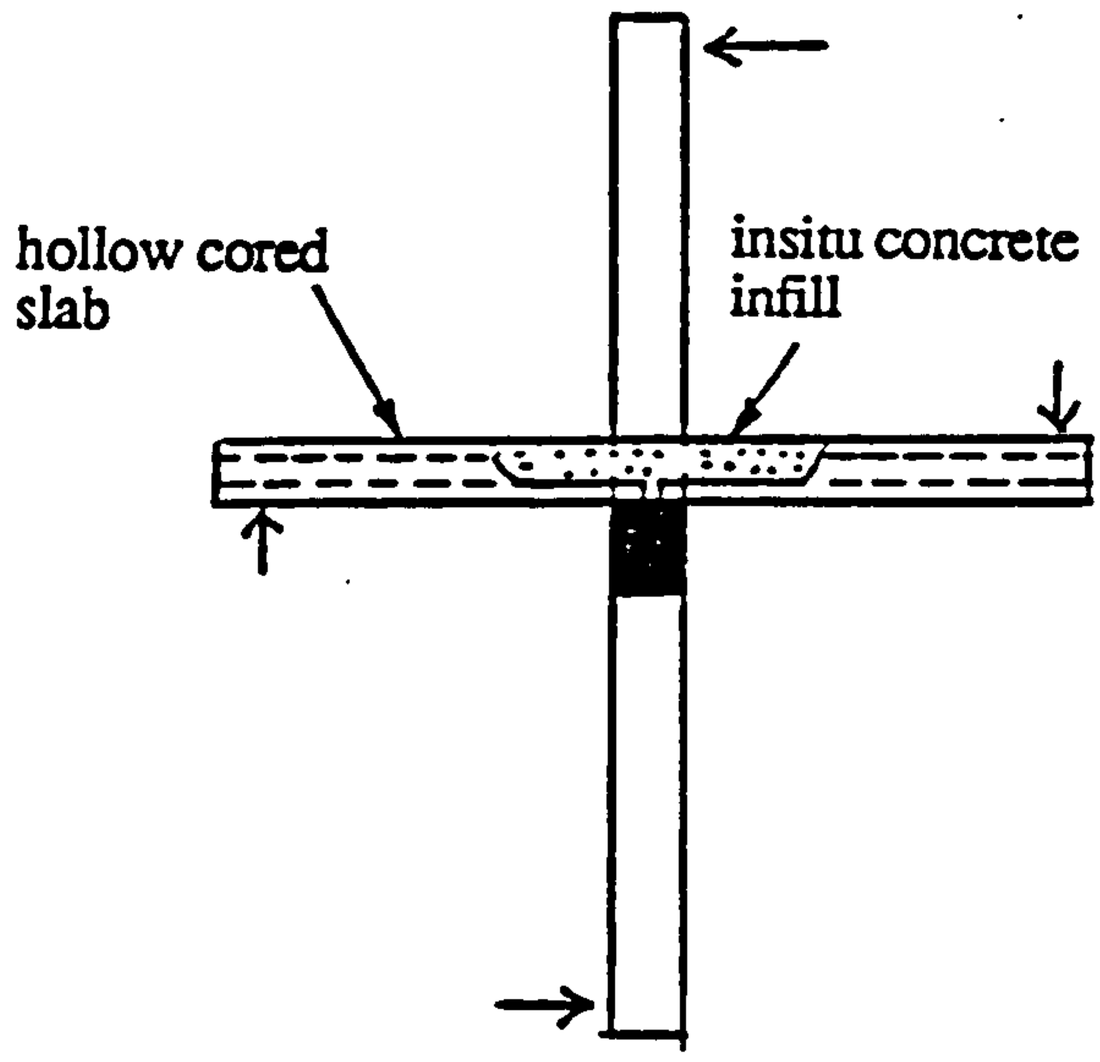

[d] out-of-plane double sided beam-column-slab

Figure 2.7: Test arrangement by Mahdi (1992)

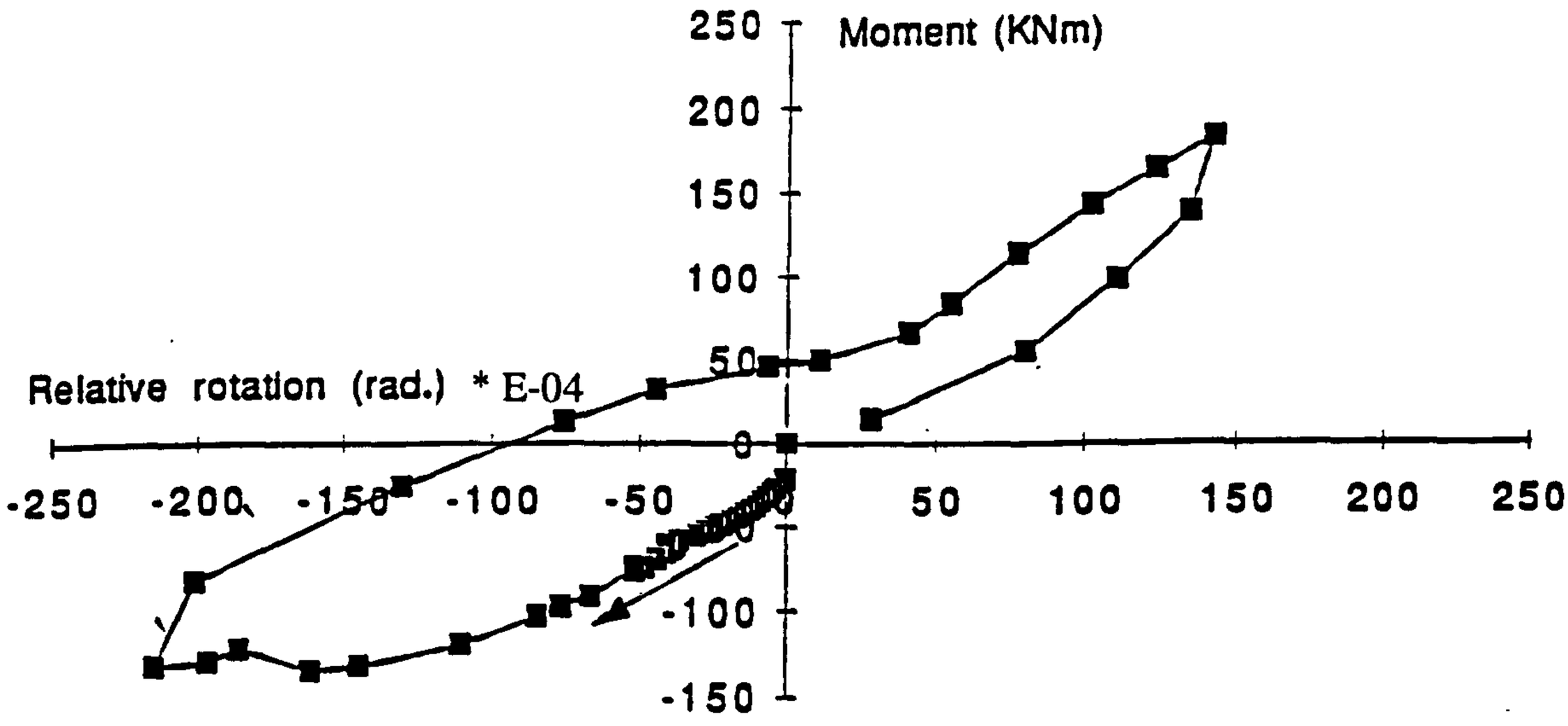

a) Beam 1

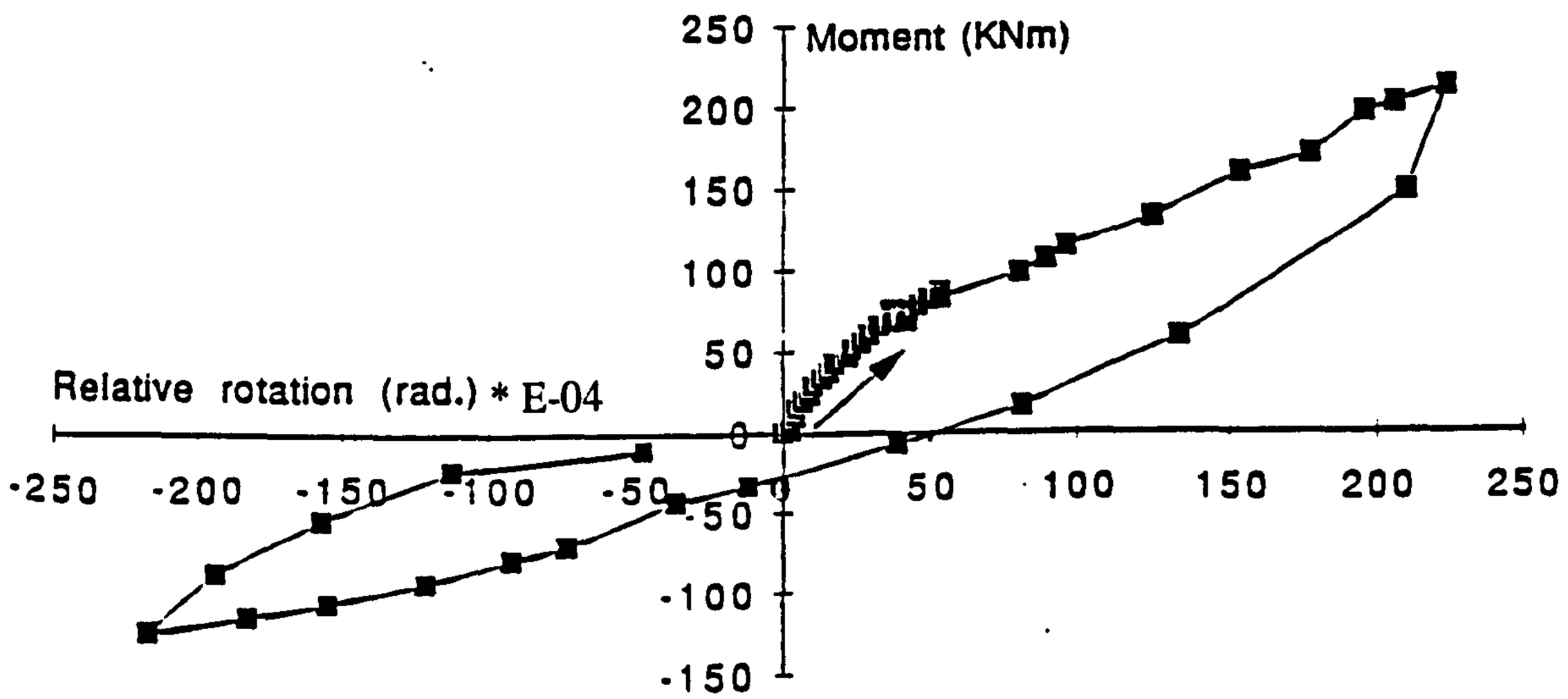

b) Beam 2

Figure 2.8: Moment rotation data for test TW6

Mahdi (1992)

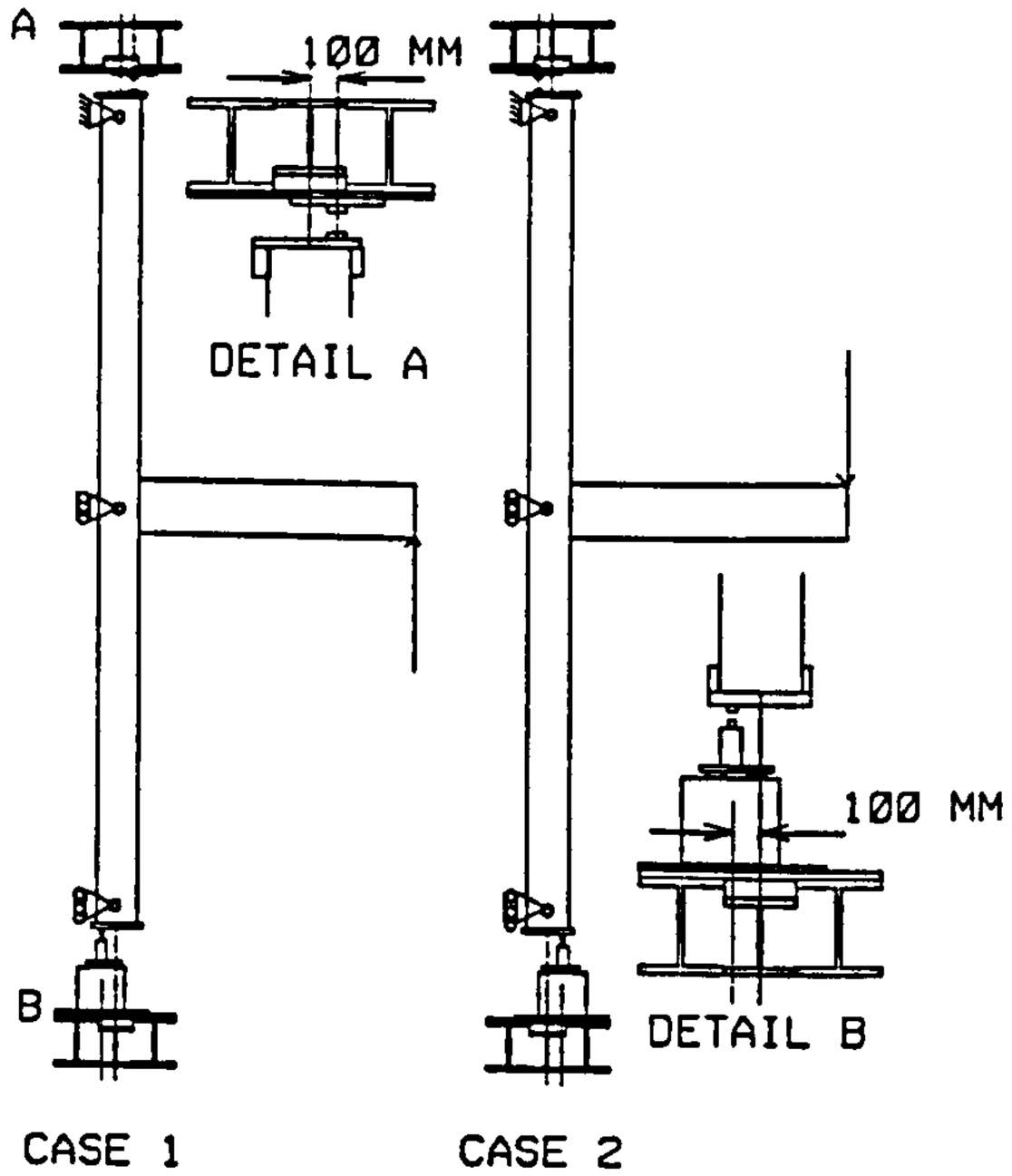

Figure 2.9: Loading cases for subframe tests

Virdi and Ragupathy (1992b)

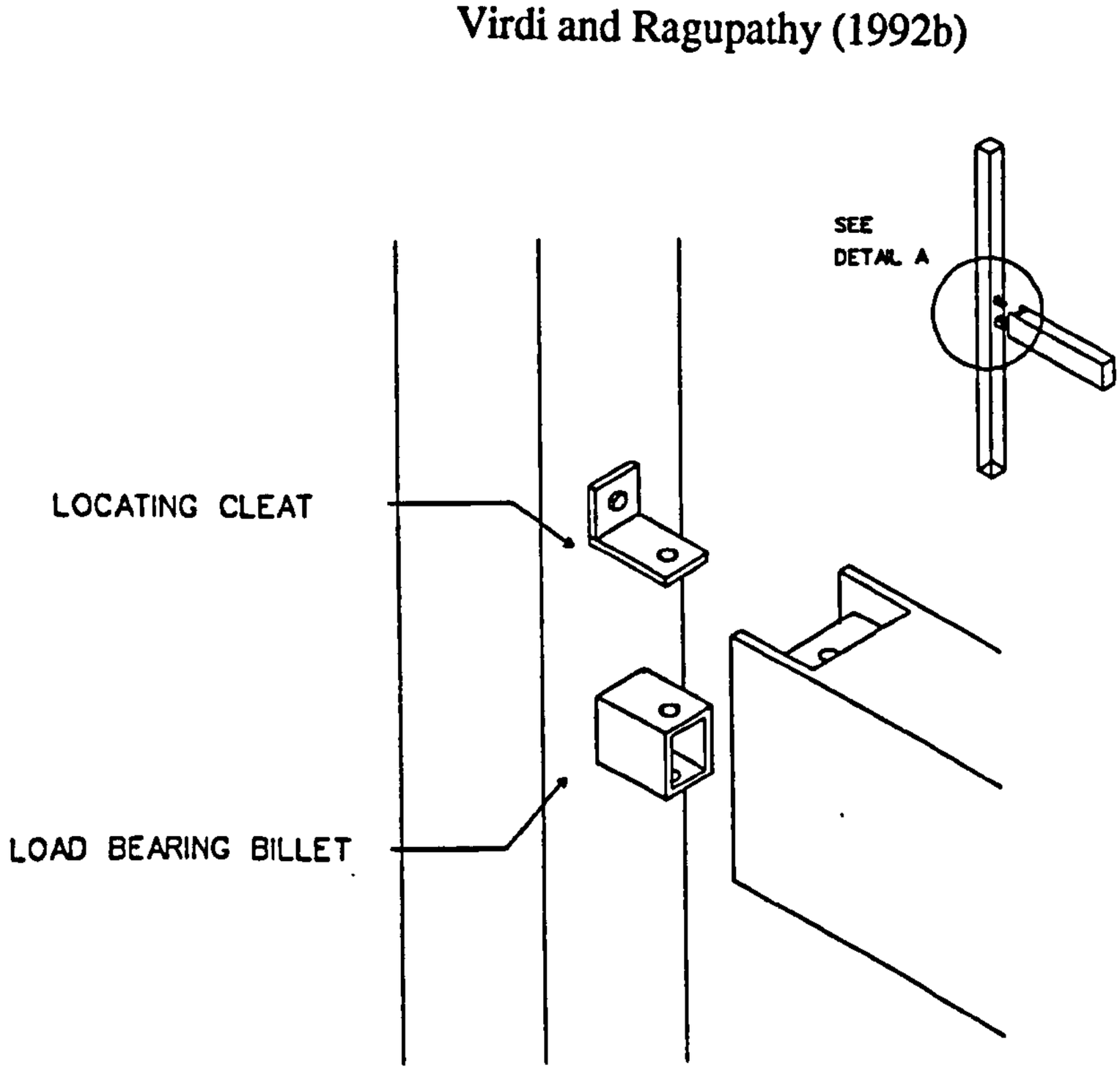

Figure 2.10: Connection details for test CT6

Virdi and Ragupathy (1992b)

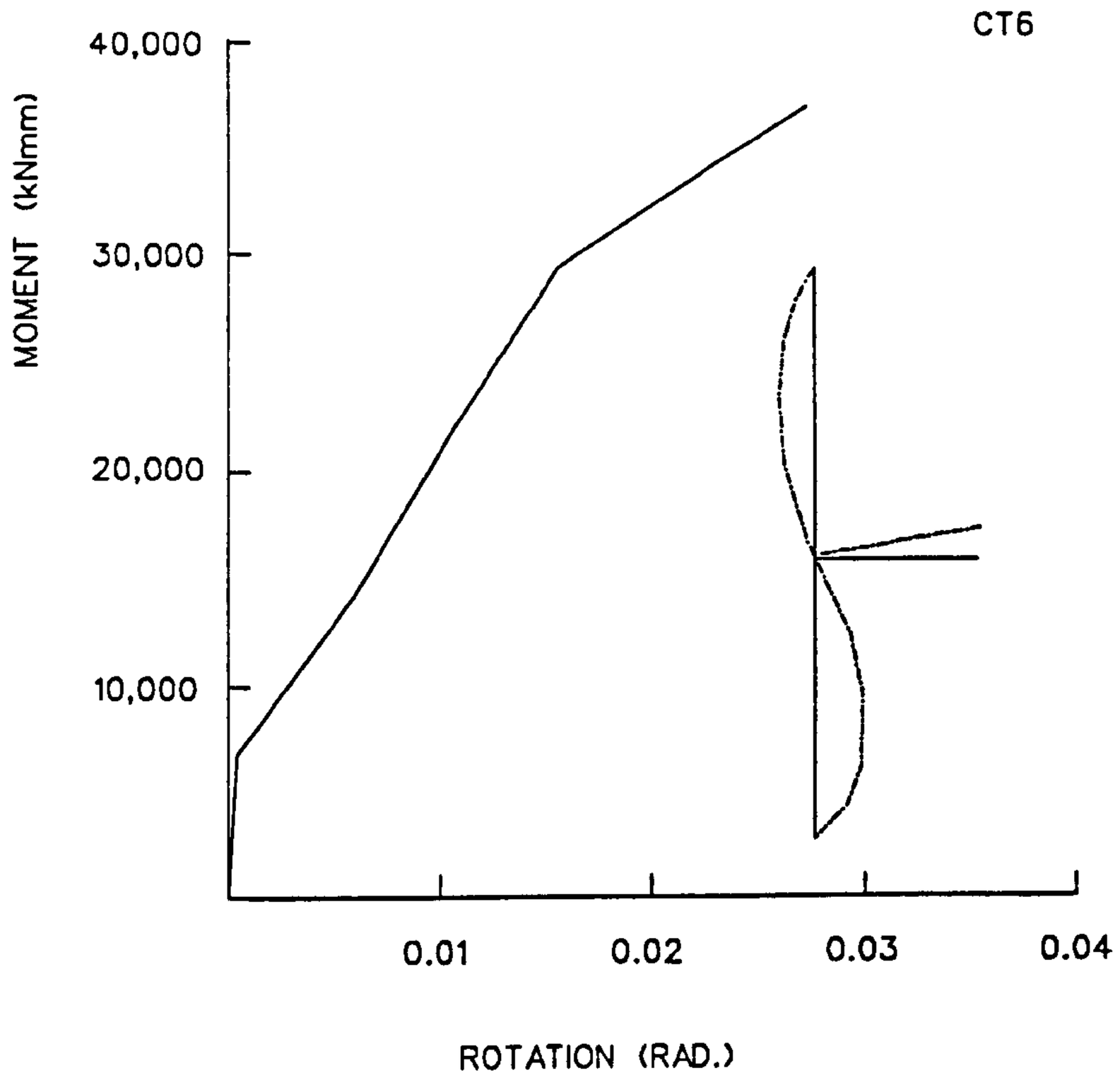

Figure 2.11: Moment-rotation characteristic for the connection used in test CT6

Virdi and Ragupathy (1992b)

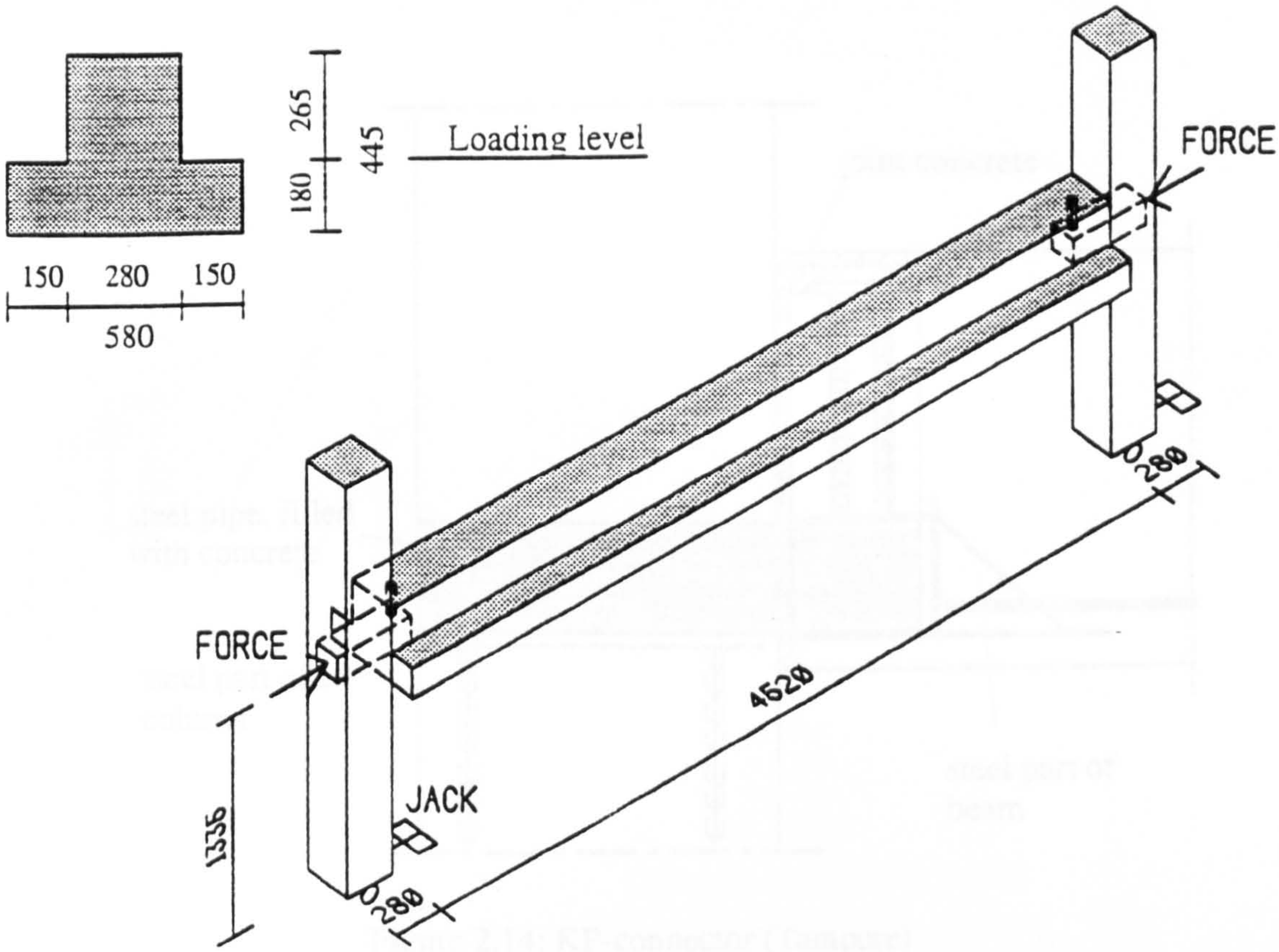

Figure 2.12: Test series 1 (Tampere)

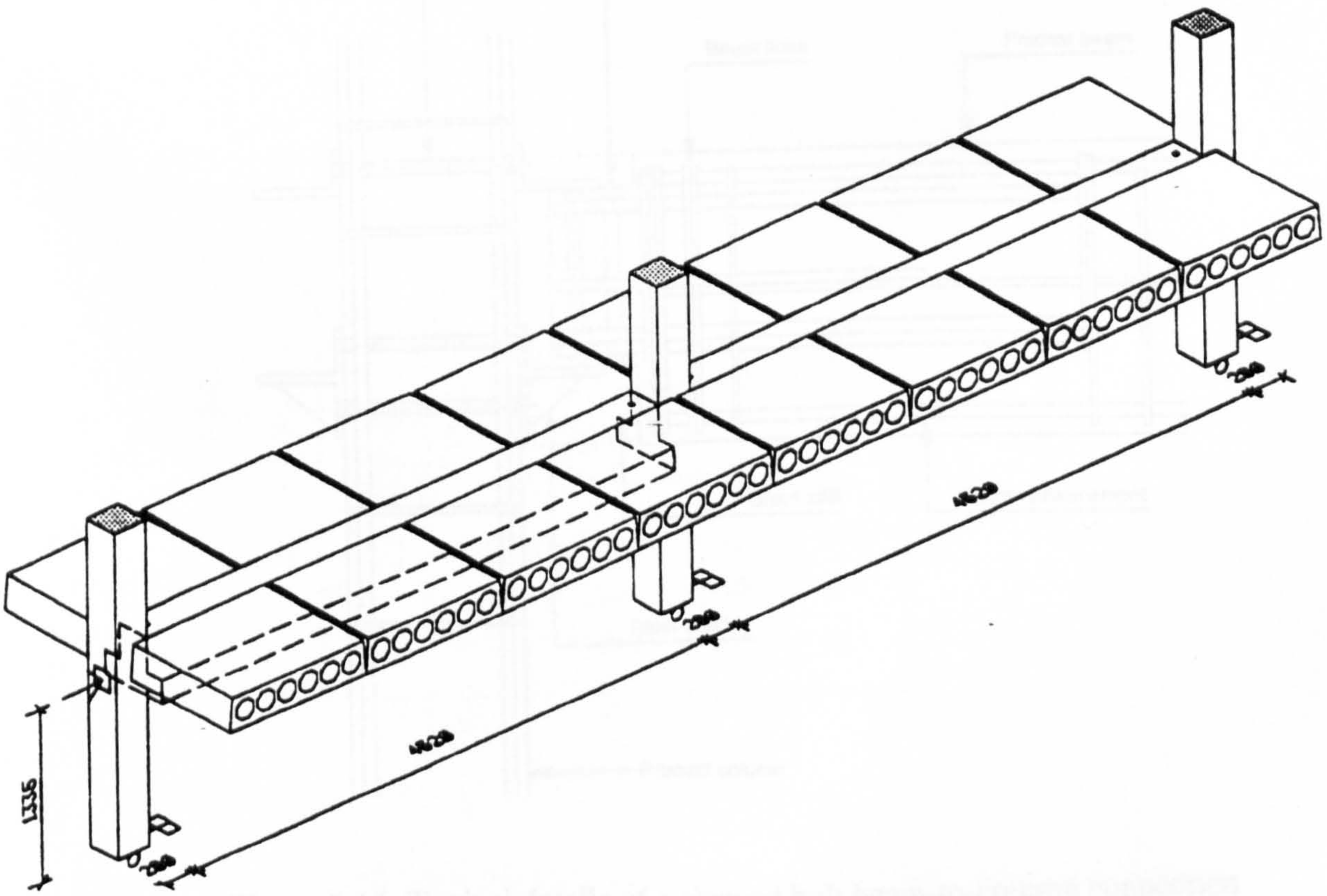

Figure 2.13: Test series 2 (Tampere)

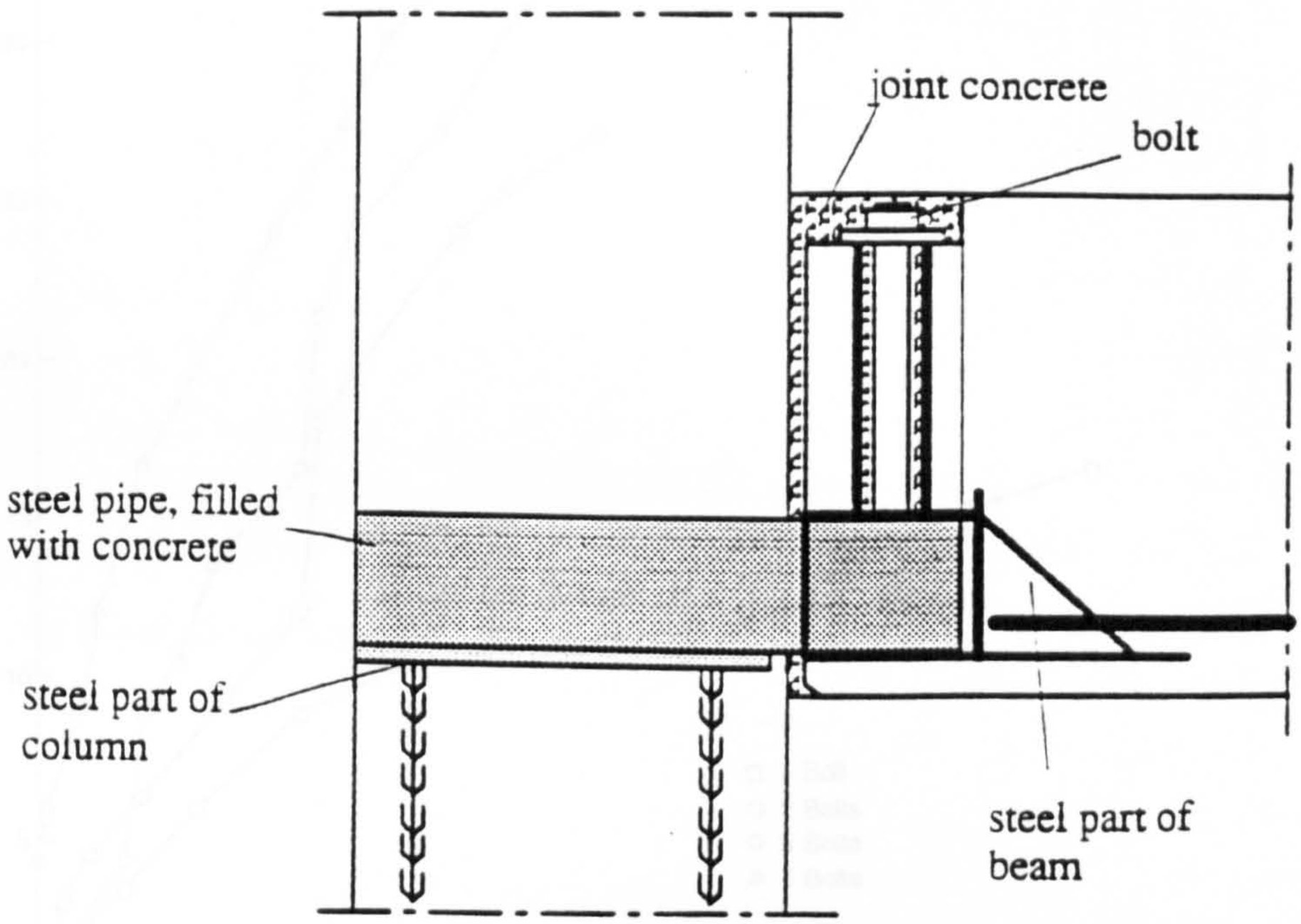

Figure 2.14: KP-connector (Tampere)

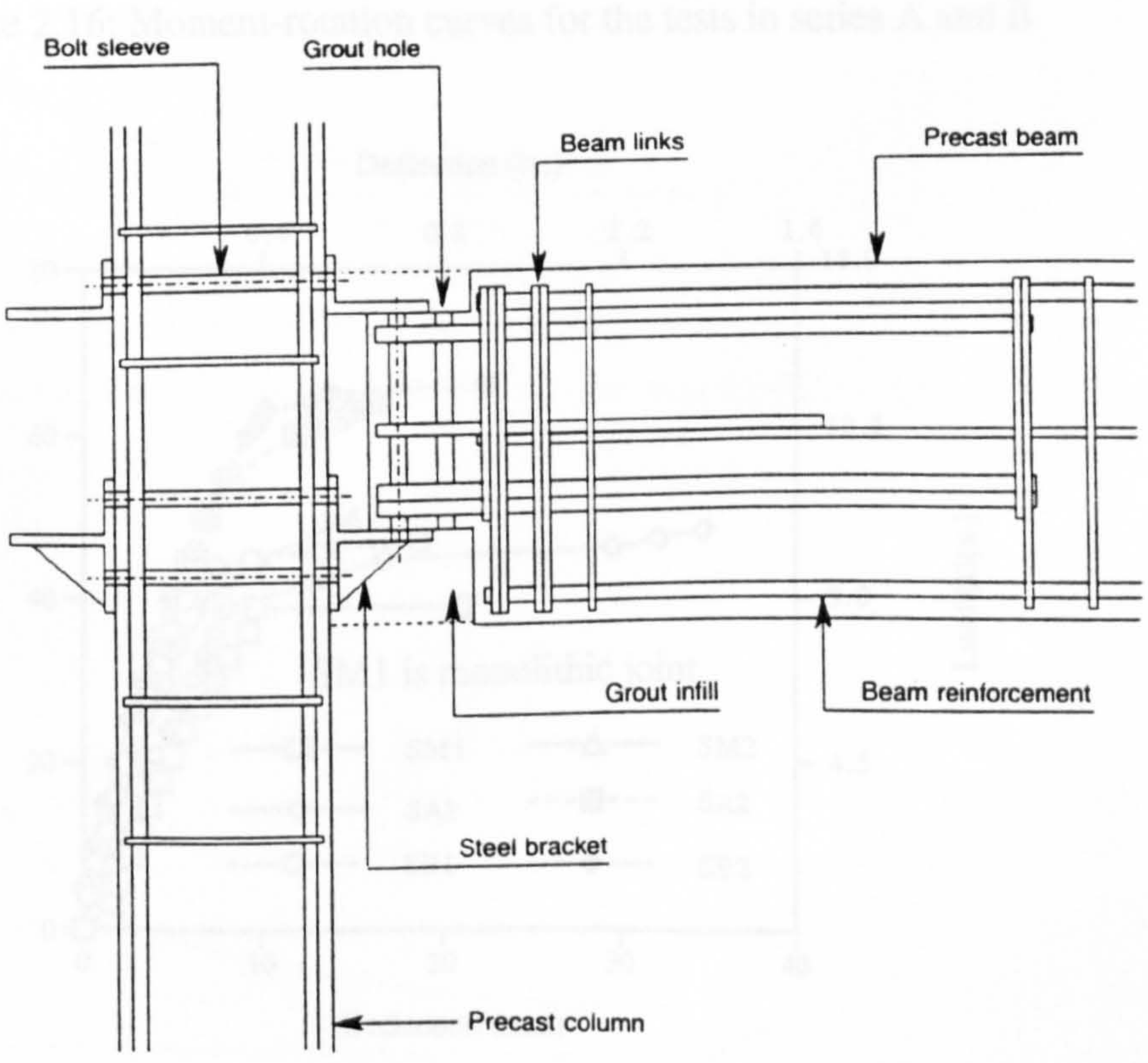

Figure 2.15: Typical details of a sleeved bolt beam-to-column connection

Mohamed and Jolly (1995)

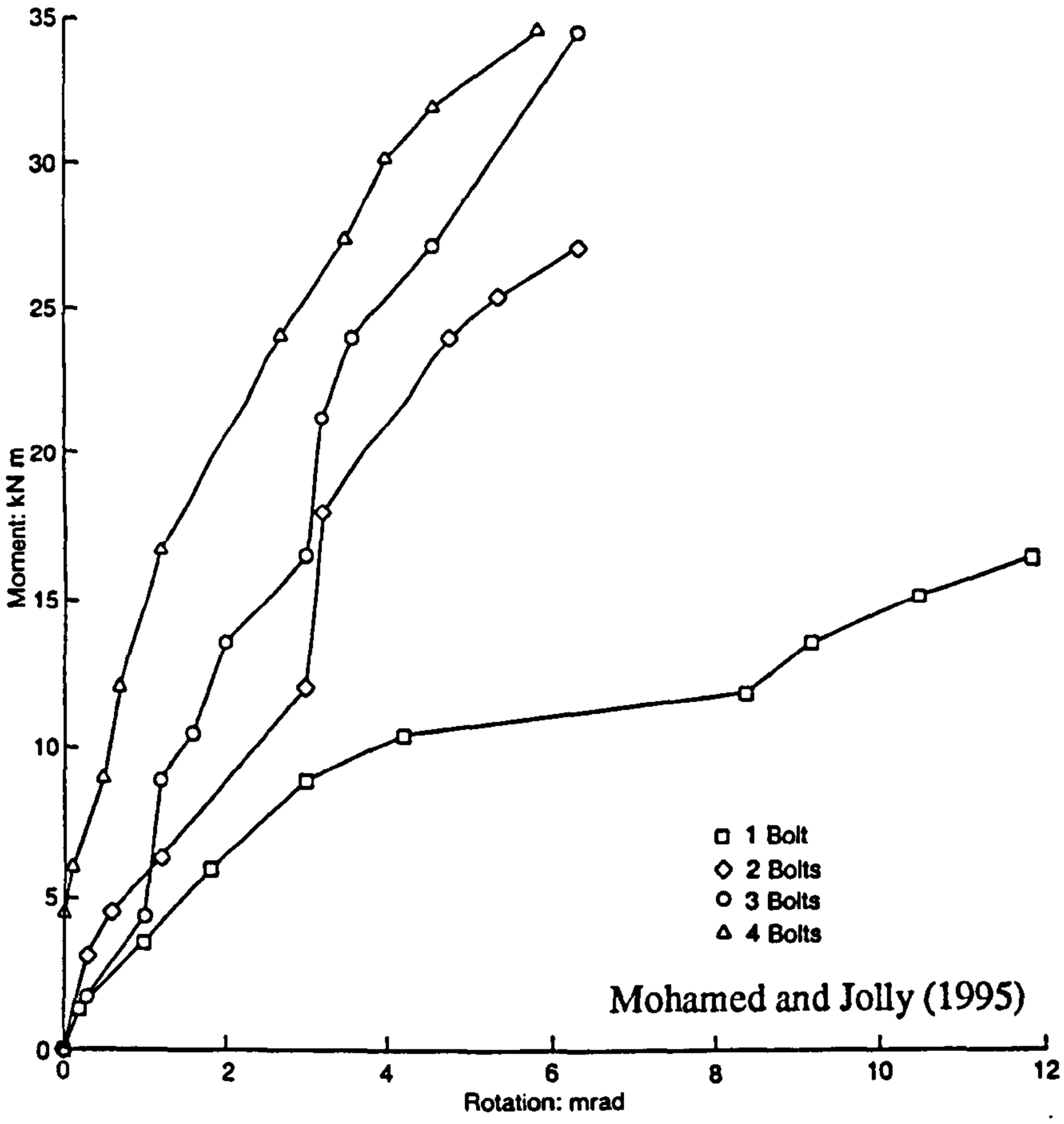

Figure 2.16: Moment-rotation curves for the tests in series A and B

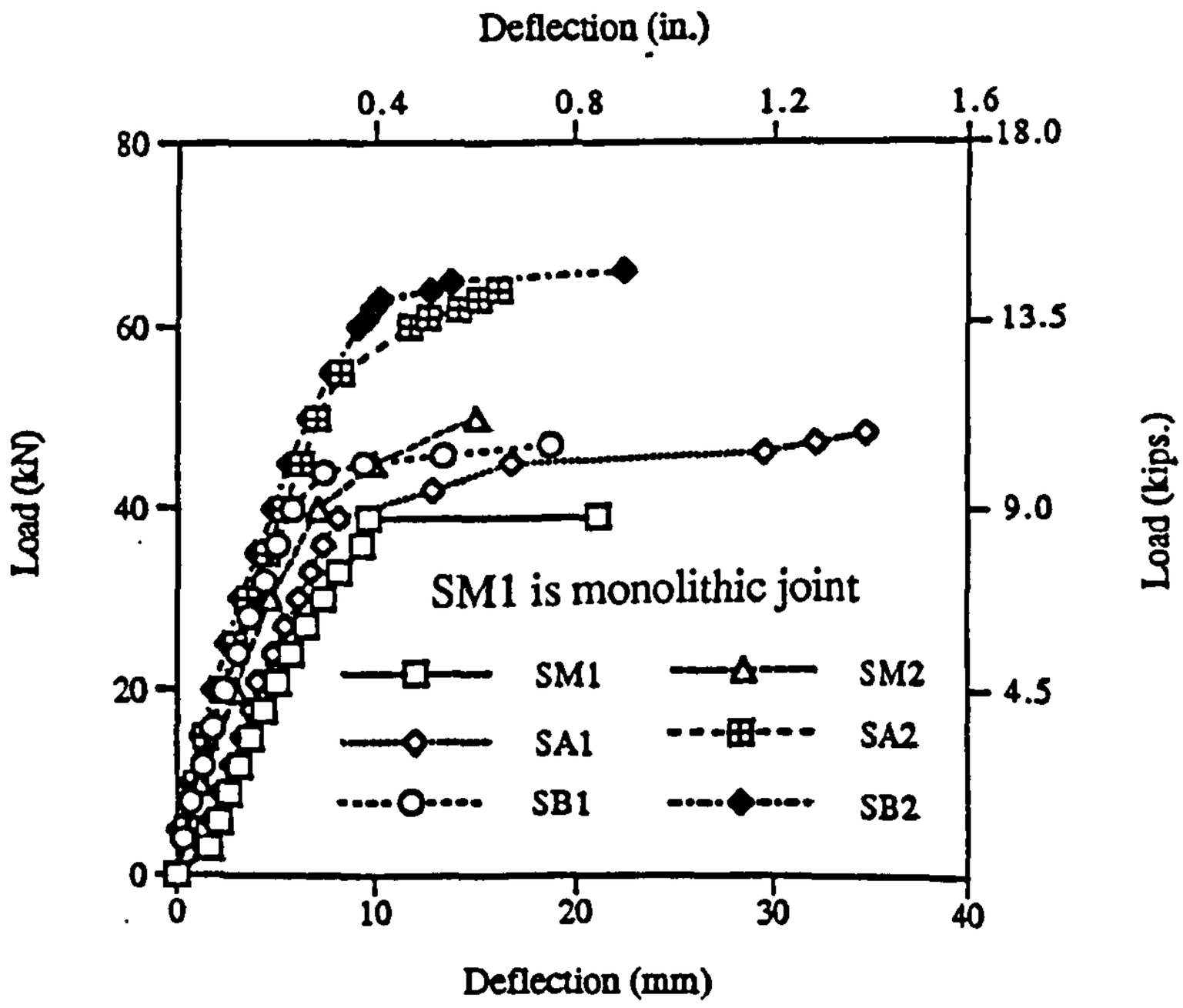

Figure 2.17: Load-deflection curves for Groups 1 and 2 models under static loading

Loo and Yao (1995)

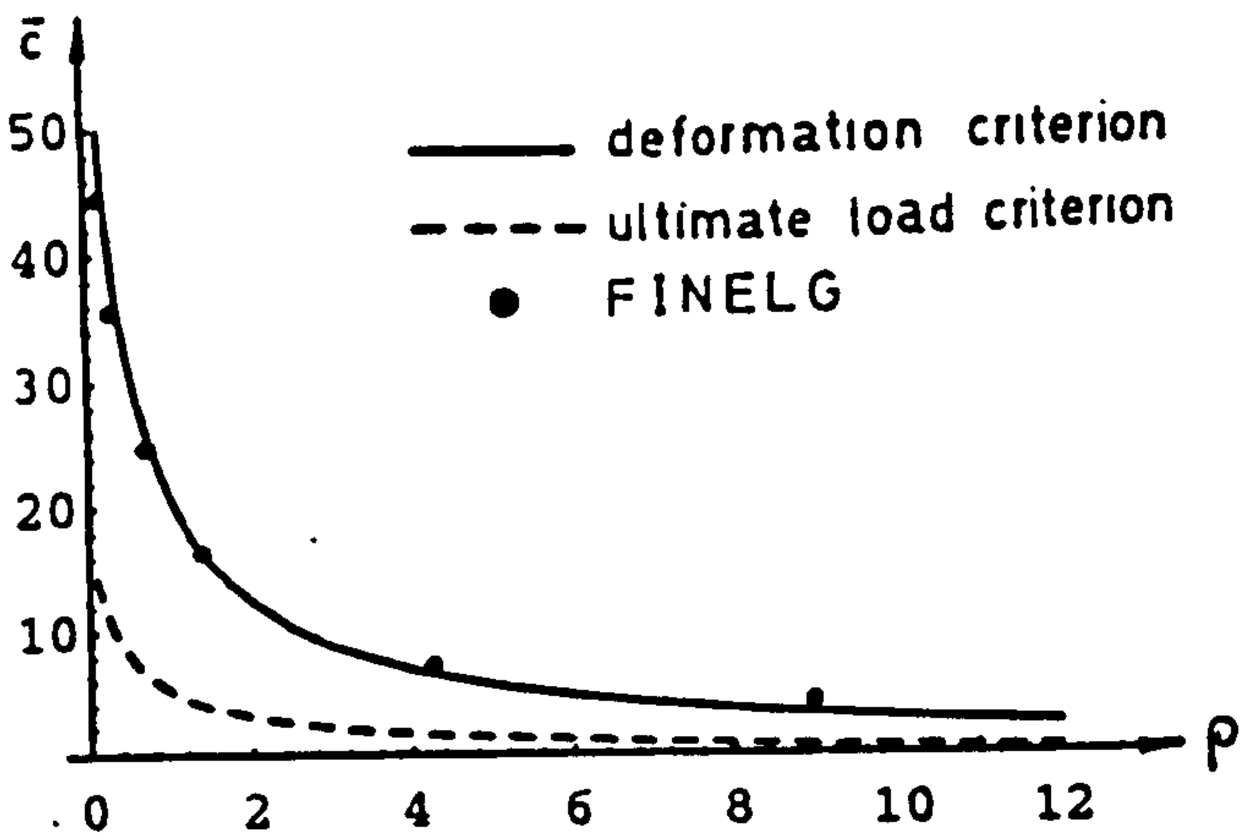

a) Portal frame with rigid column bases

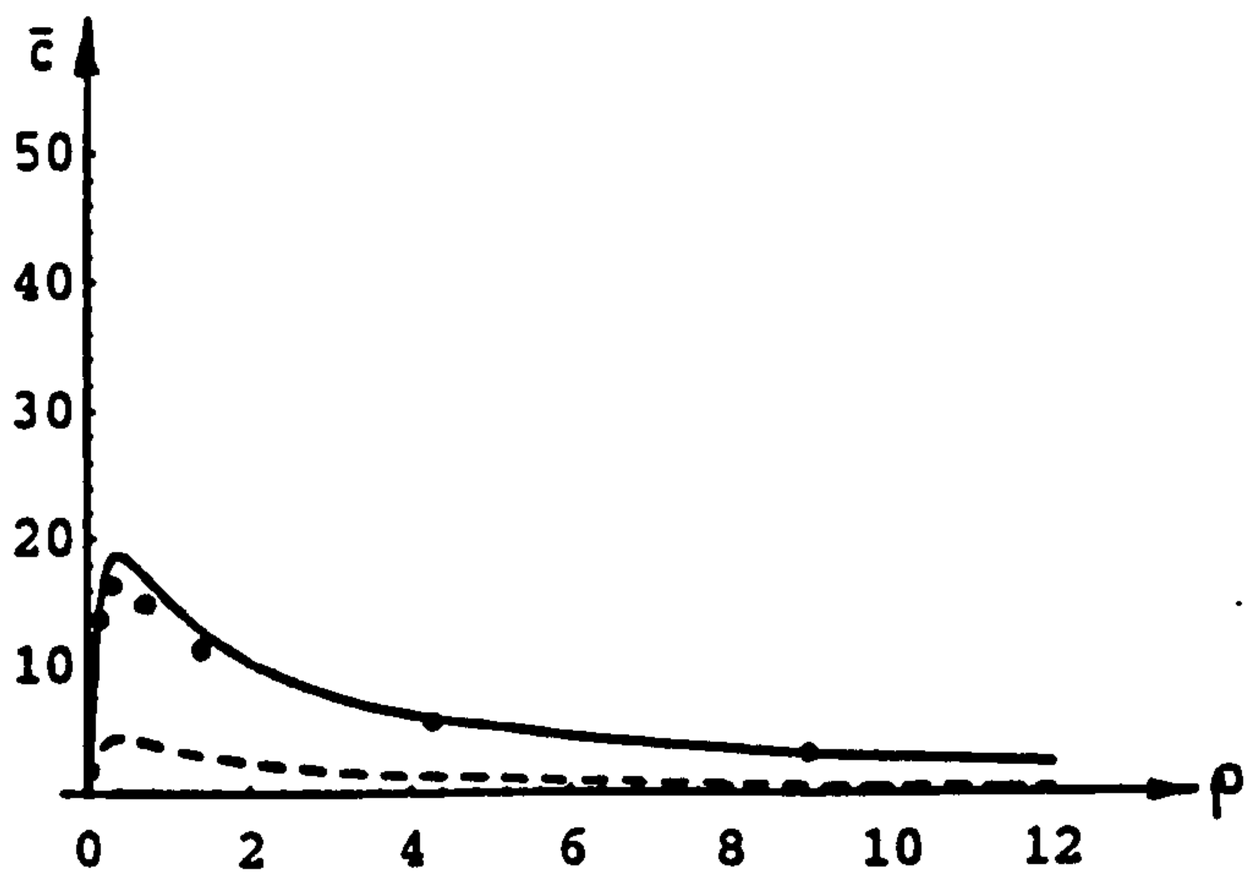

b) Portal frame with pinned column bases

Figure 2.18: Classification criteria and comparison with FINELG Briquet et al (1994)

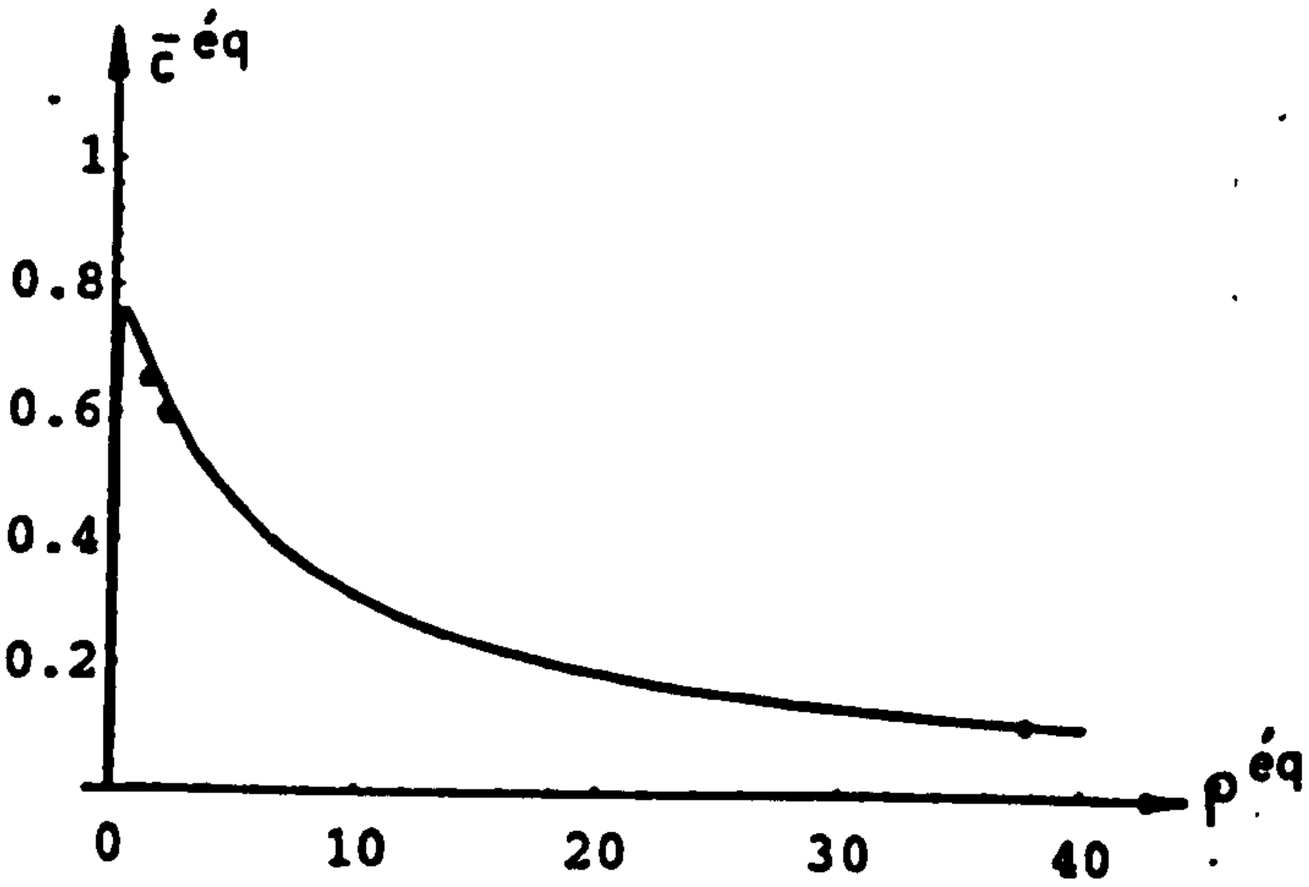

Figure 2.19: Deformation classification criteria and FINELG results for multi-bays frames Briquet et al (1994)

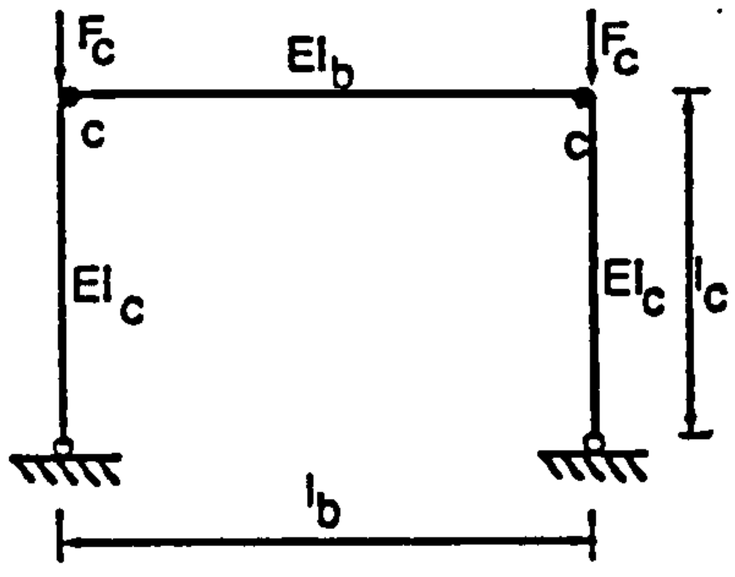

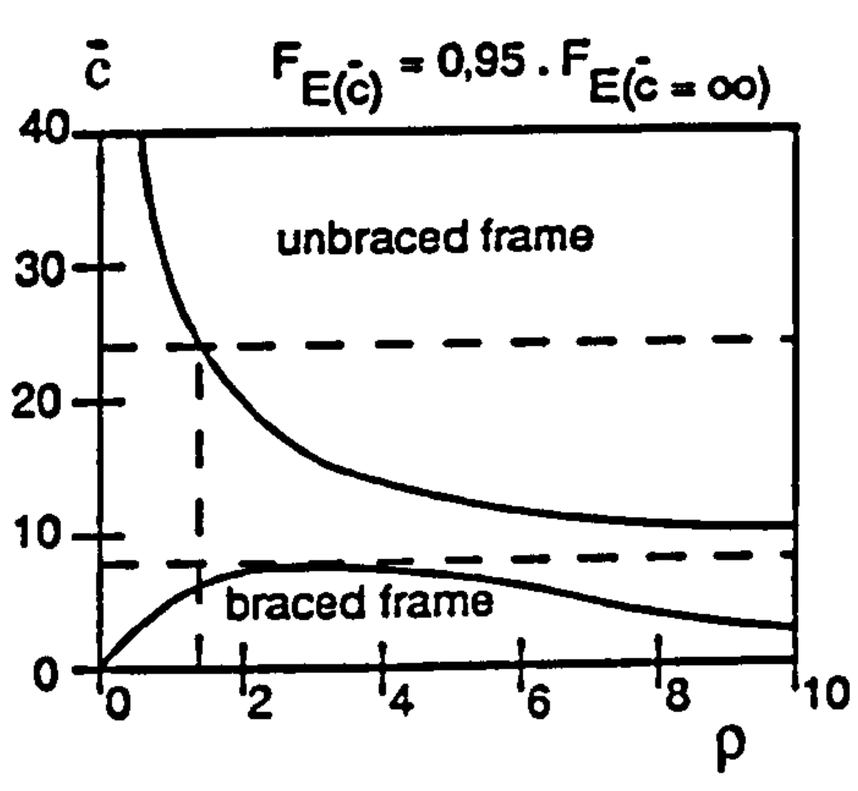

Figure 2.20: Relationship between $\bar{c}$ and ρ

Bijaard and Steenhuis (1991)

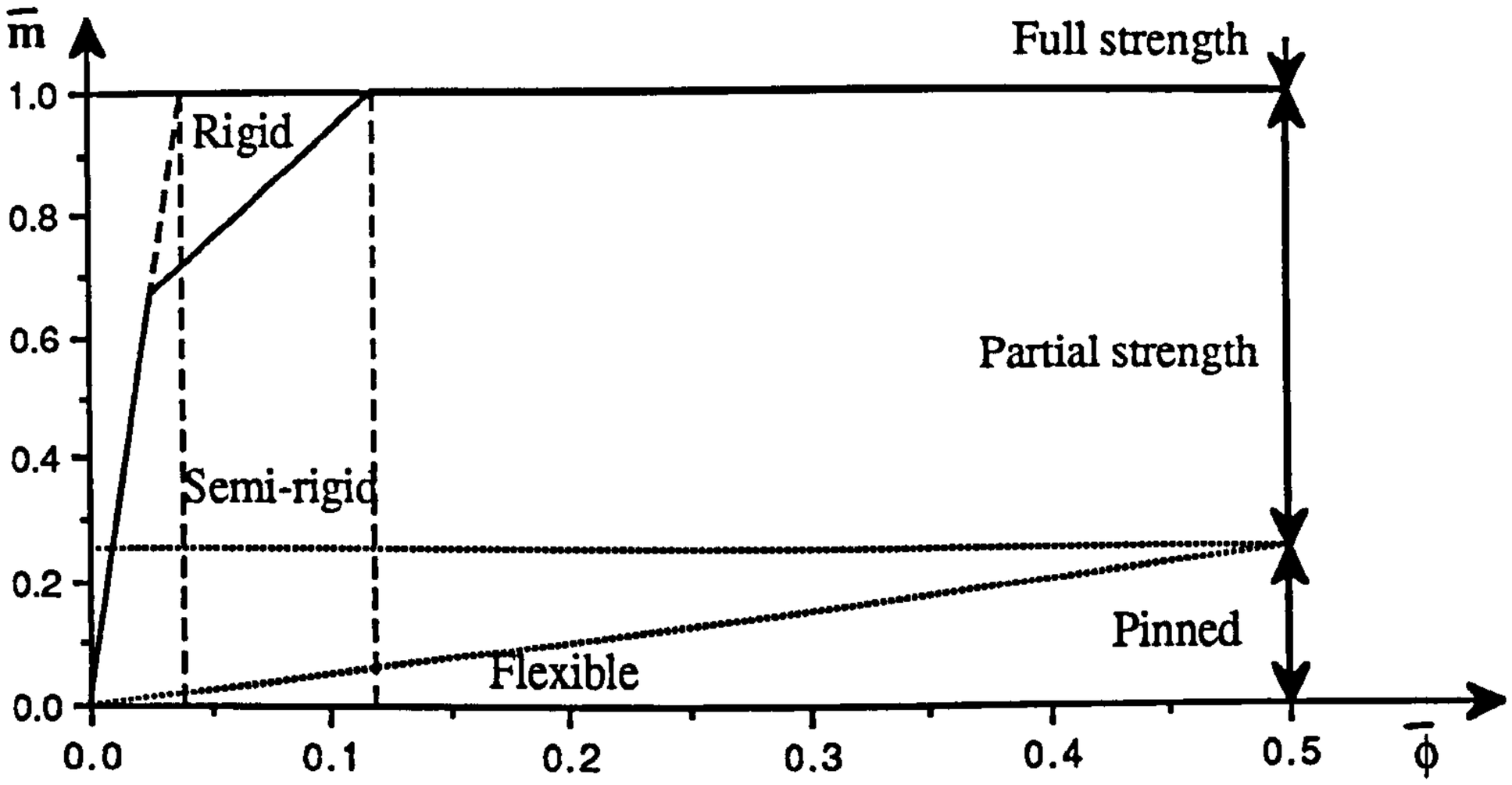

a)Unbraced frames

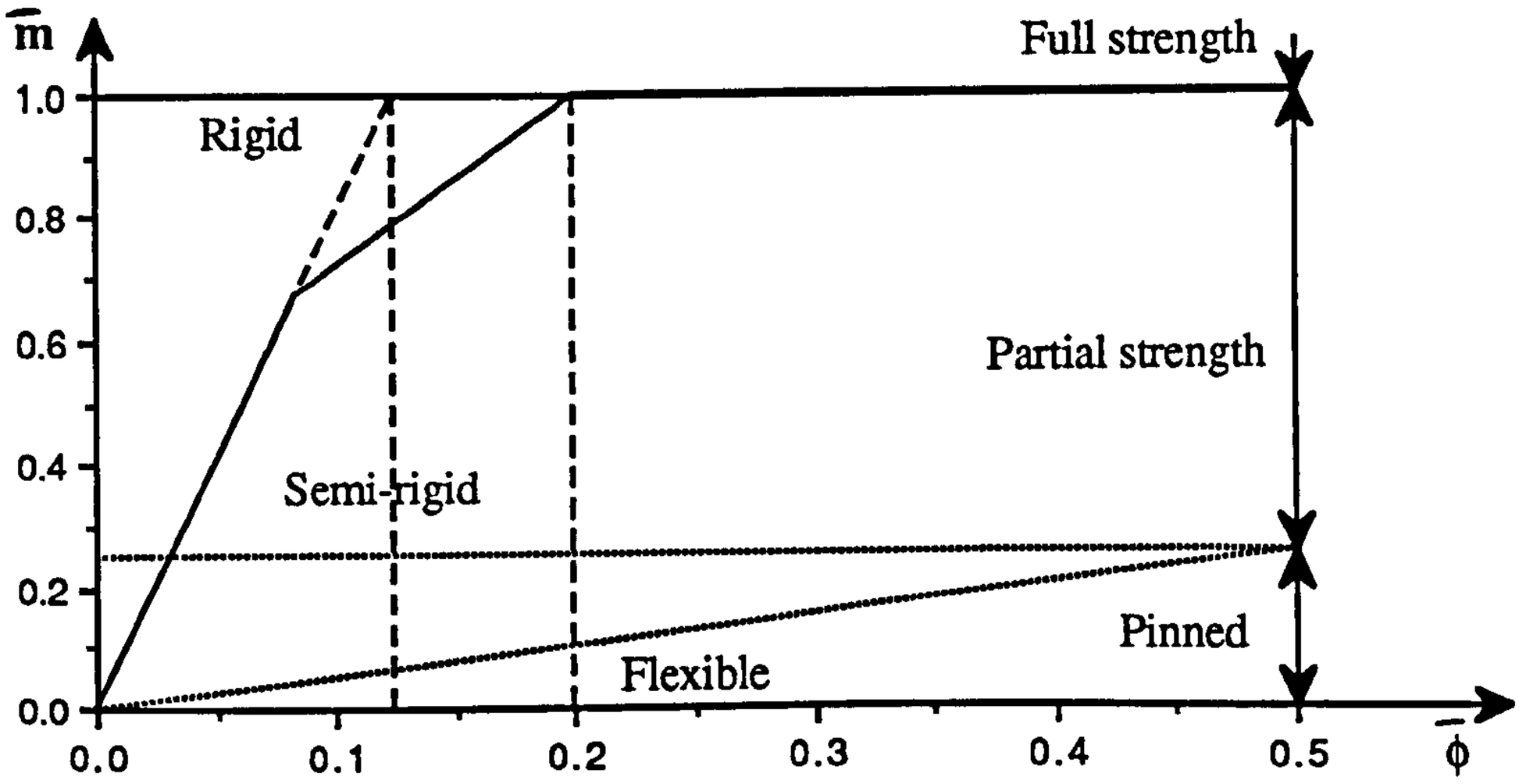

b)Braced frames

$$\bar{m} = \frac{M}{M_{pl.Rd}} \qquad \bar{\phi} = \frac{EI_b\phi}{L_bM_{pl.Rd}}$$

Figure 2.21: EC3 recommended classification boundaries for rigid beam-to-column connections

CHAPTER 3

ANALYTICAL STUDY

3.1 Stability analysis of precast structures

Under certain conditions the maximum load a structure can carry is determined by the stiffness of the structure not by the strength of the material. The condition is obtained at stresses below the elastic limit and is called elastic stability. An example of such conditions is Euler column buckling. The analysis required to determine these loads is called elastic stability analysis and resulting loads are called critical or buckling loads. The analysis is independent of materials, providing the moment curvature characteristics of the members are recognised.

Precast concrete skeletal structures are designed using pinned-jointed connections between beams, columns and floor slabs. The stability of unbraced structures may only be provided by cantilever action of the columns because transfer of bending moments is not permitted into the beams or slabs. This gives rise to large sway deflections and second - order $P-\Delta$ bending moments in columns of 3 or more storeys in, or about 10 m to 12 m, height for columns typically, 300 mm in size.

BS 8110 allows a precast concrete frame to be analysed as though it were a rigid framework but with $\alpha = 10$, where α = ratio of the stiffness of the columns to the beams at each connection. Clearly, with the wide range of different types of beam -

column connections used in precast frames, this arbitrary approach is neither rational nor representative of real behaviour.

Consider the standard beam as shown in Figure 3.1(a), and the beam modified by a semi-rigid connection of rotational stiffness J at the end of the beam in Figure 3.1(b). The rotational stiffness of the standard beam is :-

$$\frac{M}{\theta} = \frac{4E_bI_b}{L_b} \qquad Eq.\ 3.1$$

with the presence of the semi-rigid connection the same moment is applied to the LHS of the semi-rigid connection so that the total end rotation is given by :-

$$\theta = \theta_b + \phi = \frac{ML_b}{4E_bI_b} + \frac{M}{J}$$

This rotational stiffness

$$\frac{M}{\theta} = \frac{\frac{4E_bI_b}{L_b}}{\left(1+\frac{1}{K_s}\right)} \qquad Eq.\ 3.2$$

where $K_s = JL_b/4E_bI_b$

is reduced from that given in *Eq.* 3.1 because of the presence of the semi-rigid connection. This modified relation can be used to represent a beam with semi-rigid connection in a frame analysis (see Figure 3.1(c)).

$$\frac{\left(\frac{M}{\theta}\right)_{col}}{\left(\frac{M}{\theta}\right)_{Eq\,3.2}} = \frac{\frac{E_cI_c}{L_c}}{\frac{E_bI_b}{L_b}}\left(1+\frac{1}{K_s}\right) \qquad Eq.\ 3.3$$

By combining the stiffnesses of the beam AND the connection in one equation, the frame stiffness function α is modified to α' where

$$\alpha' = \alpha\left(1+\frac{1}{K_s}\right) \qquad \textit{Eq.}\ 3.4$$

For example if the column-to-beam stiffness ratio is $\alpha = 0.5$, and the connection stiffness is $K_s = 0.6$ (say), then the effect of the semi-rigid connection is to increase the apparent stiffness of the column to $\alpha' = 1.33$, thus increasing the column effective length factor β (see *Eq.* 3.6 later). Adopting a value of 10 for this function for every situation in precast construction is clearly unreasonable.

Extending this simple analysis to full 2-d, and even 3-d frames, computer programs (Görgün, 1992; SWANSA) are used to determine maximum column loads, bending moments and sway deflections. In these programs the beam and column components may be considered as either linear-elastic or non-linear (reflecting yielding of the steel bars), and the connections can be considered linear-elastic with infinite strength, or non-linear with finite strength. In all cases maximum column loads, and hence β factors are obtained for given values of α and K_s.

If linear-elastic components are specified then the resulting value of β may be used to compute M_{add} according to BS 8110, Part 1, clause 3.8.3.

If non-linear components with linear connections are specified, the computer program will give column bending moments which will replace the BS 8110 method.

This is because second order $P-\Delta$ effects are built into the program, and M_{add} is given implicitly.

If non-linear components AND connections are specified, the program not only determines $P-\Delta$ effects but also checks for the finite strength of the connection M_{con}. This is a very important design consideration because if M_{con} is greater than M_{add}, the $P-\Delta$ moments may be distributed into the beam, and need not be successively accumulated to the foundation as in the present practice when pinned connections are used.

Thus if the strength, stiffness and moment - curvature characteristics of the beam and column components are known, and the $M_{con}-\phi$ characteristics of the connection are either measured from tests or calculated from design equations, the frame may be designed to allow for the effects of non-linearity in the components and connections. These effects may be studied in the realistic range to determine the importance of each parameter on frame design.

In the context of the present work, stability implies general stability, i.e. if a buckling load is reached in a column, immediate collapse of the frame will take place. This also means that the columns will not buckle independently. It is therefore necessary to investigate the stability of the frame as a whole and to take into account the beam - column effect. This effect is incorporated into the analysis by using stability functions that enable the member stiffness matrix equations to be modified to include the influence of axial load on bending stiffness.

It is therefore possible to study the elastic stability of frames and obtain the elastic buckling loads, maximum loads at large lateral deflections, (and hence effective

lengths) of simple sub - frames in which the stiffness of the beams, columns and joints are varied in the realistic range of typical concrete structures.

3.2 The definition of effective length

The critical loads for columns with various end conditions can be related to the critical load of a pin-ended column through the concept of effective length factor which is commonly used in design. This can be expressed in terms of an effective length factor β:

$$L_e = \beta L \qquad \textit{Eq.}\ 3.5$$

Here L_e is the effective length, L is height of the column and β is calculated from the buckling load of the frame (Gregory, 1967) as :-

$$\beta = \frac{1}{\sqrt{\frac{P_{cr}}{P_E}}} \qquad \textit{Eq.}\ 3.6$$

Here P_{cr} is the buckling load and P_E is the Euler load ($\pi^2 EI/L^2$) of the column.

The effective length factor β is a major parameter in the design of columns. Codes of practice have adopted different criteria for determining this parameter. The structural steelwork code BS 5950 (1985) regards the β as a quantity dependent upon whether the column is effectively held in position and restrained in direction at its ends. The code also specifies β ratio for columns in multi-storey beam-column frames by

using the limited frame method applied only to rigid joints for the braced and unbraced situations.

The structural concrete code BS 8110 (1985) specifies equations and provides simplified recommendations for the calculation of β depending on the relative stiffness of the rigidly connected elements at the ends of the column. It specifies intermediate values of effective length factor between 1.2 and 2.2 for the case of unbraced columns and between 0.75 and 1.0 for the braced column, depending upon the efficiency of the directional restraints.

The American code AC1318 (1990) provides equations for calculating β using a similar approach to that of BS 8110.

3.3 Method of analysis

The sub-frames shown in Figure 3.2 were analysed using the computer program (Görgün, 1992) (mounted on a 486 series PC) with the rotational and axial stiffness of the beams and columns calculated for the uncracked section. The linear - elastic rotational stiffness of the beam-column connections was specified as follows:-

(a) $K_s = 1x10^{-9}$; to simulate a pinned-joint.

(b) $1x10^{-9} < K_s < 10$; to simulate the semi-rigid joint stiffness*

(c) $K_s = 1x10^{9}$; to simulate a fully rigid joint

* except $K_S = 0.1$ in frame F1.

The computer program analysis starts with zero axial forces in all members, giving the linear solution at the first step load increment. Then, at each new load step the axial forces and frame deflections found in the previous step are used in the stiffness matrix

and the final displacements and rotations, member end forces, and bending moment distributions are determined.

If the value of frame loads are known beforehand the output from the program gives member axial forces, shear forces, and bending moments, and joint deflections and rotations. These data may be used to design the components. Alternatively the maximum frame loads may be determined given the axial and moment capacities of the components. This is given when the sway deflections increase without bound. In this case a small lateral disturbance (force or displacement) is given to the frame to induce sway.

3.4 Assumptions of parametric study

i) - One of the fundamental assumptions of the present work is that there is only axial deformation of columns if the frame is perfectly symmetric. To allow a large deflection problem, a non vertical frame is considered. In this case a small lateral disturbance (δ_o = 1 mm displacement) is given to the frame to induce sway. See Fig. 3.3.

ii) - The present work focuses on the problem of in-plane buckling because the associated stiffness is the flexural stiffness of the members and connections.

iii) - The critical loads is designated P_{cr} at which the frame becomes unstable and the lateral deflections of the members increase without bound. See Fig. 3.3(b).

iv) - The present work assumes that at failure the stresses in the structure remain elastic and that the effect of changes in the geometry of the frame on the failure load (second order analysis) is taken into account.

3.5 Parametric study

In order to study both the effect of the ratio K_s of the stiffness of the connection to the flexural stiffness of the beam, and the ratio α of the stiffness of the columns to the beams at each connection on the buckling capacity of a multi-storey structure a linear-elastic analysis was carried out to determine β factors in the single-storey sub-frames which would represent the common situation shown in Figure 3.2. The sub-frames were as follows:

F1 represents an upper floor unbraced sub-frame.

F2 represents a ground floor unbraced subframe with rigid foundations.

F3 represents an upper floor unbraced sub-frame in which only one of the columns has a rigid foundation

These sub-frames F1 and F2 were chosen because they are compatible with the standard cases for determining β of columns as presented in BS 8110, Part 1, clause 3.8.1.6. Sub-frame F3 was selected as being intermediate between F1 and F2.

The values given in BS 8110 are due to Cranston (1972) in which the degree of restraint provided by the connecting beam was expressed in terms of the factor α but assuming rigid joints. Cranston considered a range of α values between 0.0 and 5.0, and for consistency the same range of values of α was adopted here. The computer program used (Görgün, 1992) requires a value for α greater than 0 for the above sub-frames. For this reason $\alpha = 0.001$ was used to simulate $\alpha = 0$. Using rigid joints the sub-frame F1 was compared with solutions given by Mahdi (1992) and

Cranston (1972). The sub-frame F2 was compared with a solution given by Mahdi (1992) and Timoshenko (1961).

The next task was to replace the rigid connections with rotational springs in the ends of the beams (not in the columns) in order to observe the effects of semi-rigidty of connections. The results could then be used to map both the influence of K_s and α as defined above, on β factors. A range of values for K_s was used as shown in Table 3.1. As it can be noted that the minimun values of K_s used 0.1 for F1, because this frame is unstable for $K_s = 0$.

The results are reported on and discussed in Chapter 4 and are given in Figures 4.1 to 4.9. Curves drawn for the column effective length equations given in BS 8110, Part 2, clause 2.5.5 are also shown in these figures for completeness.

F1		F2		F3	
K_s	α	K_s	α	K_s	α
0.1	0.001	0	0.001	0	0.001
0.2	0.005	0.1	0.2	0.1	0.2
0.5	0.2	0.5	0.5	1.0	0.5
1.0	0.5	1.0	1.0	2.0	1.0
1e9	1.0	4.0	2.0	10	2.0
	2.0	1e9	5.0	1e9	5.0
	5.0		10.0		10.0
	10.0				

Table 3.1: K_s and α values used for F1, F2 and F3.

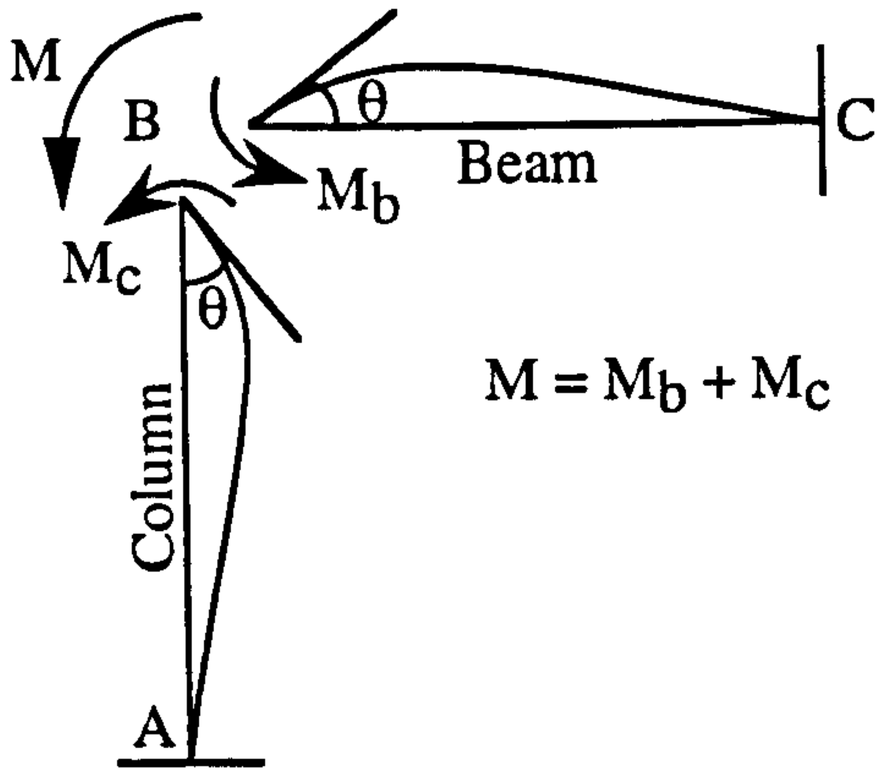

(a)

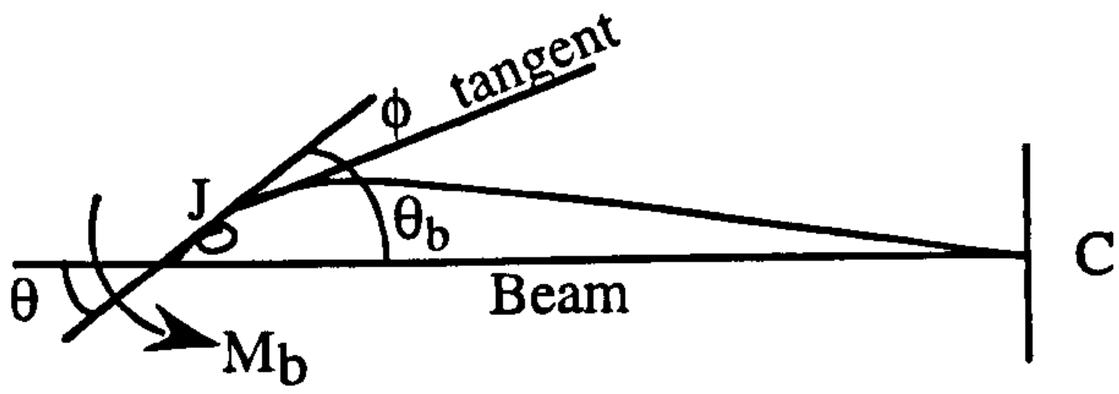

(b)

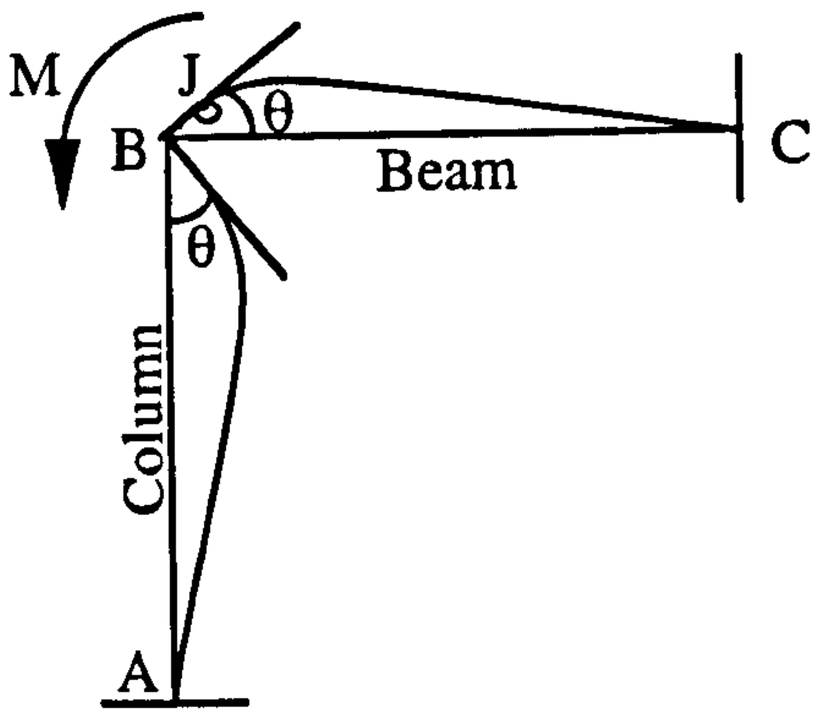

(c)

Figure 3.1: Implication of semi - rigid joints

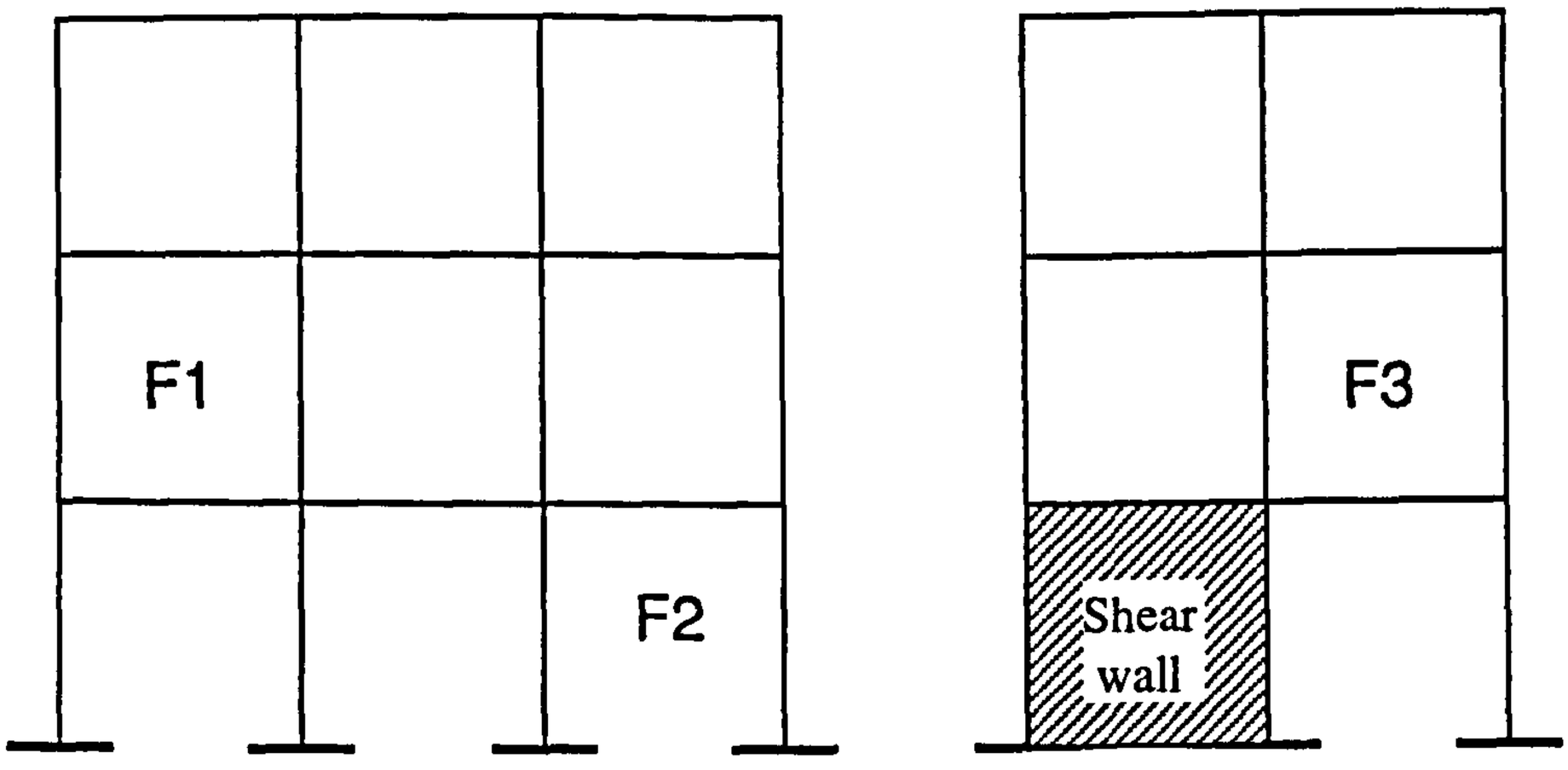

Figure 3.2: Types of precast frames (a) unbraced (left) and partially braced.

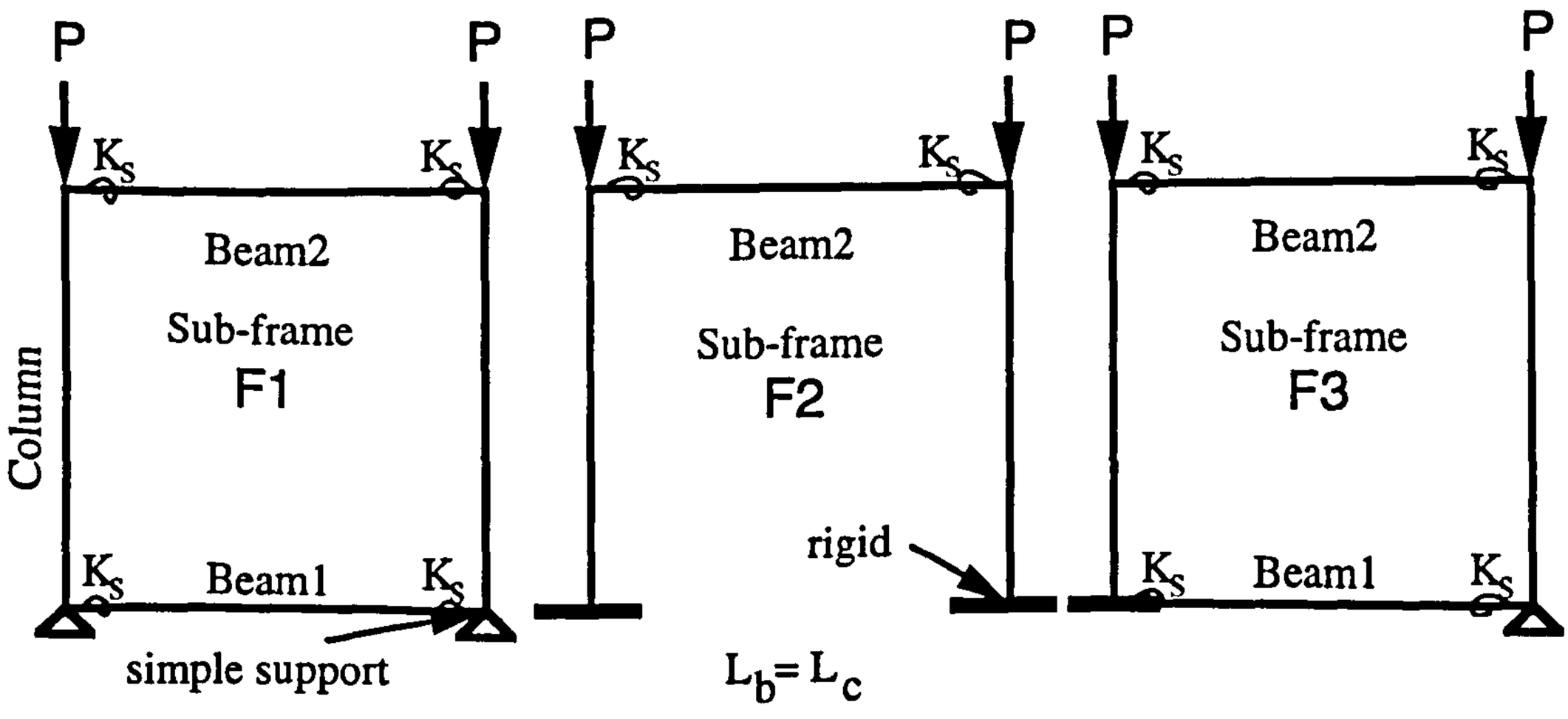

Figure 3.2(c): Definition of sub-frames used in the analysis.

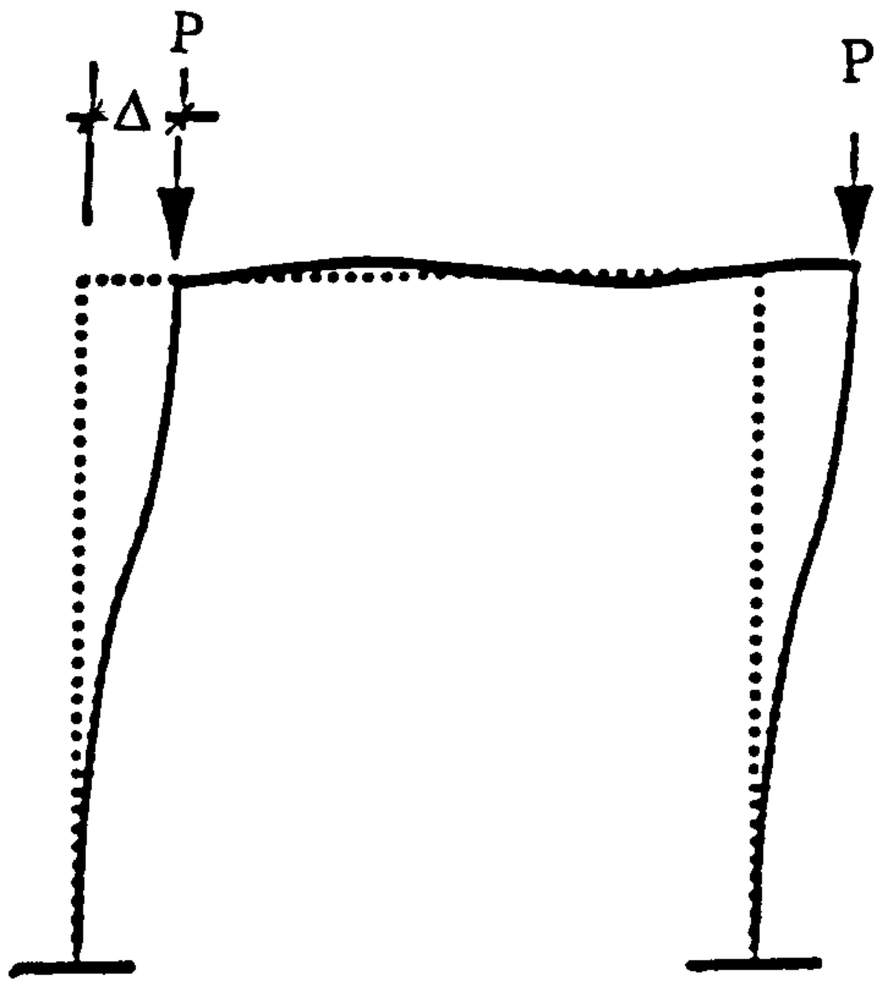

(a)

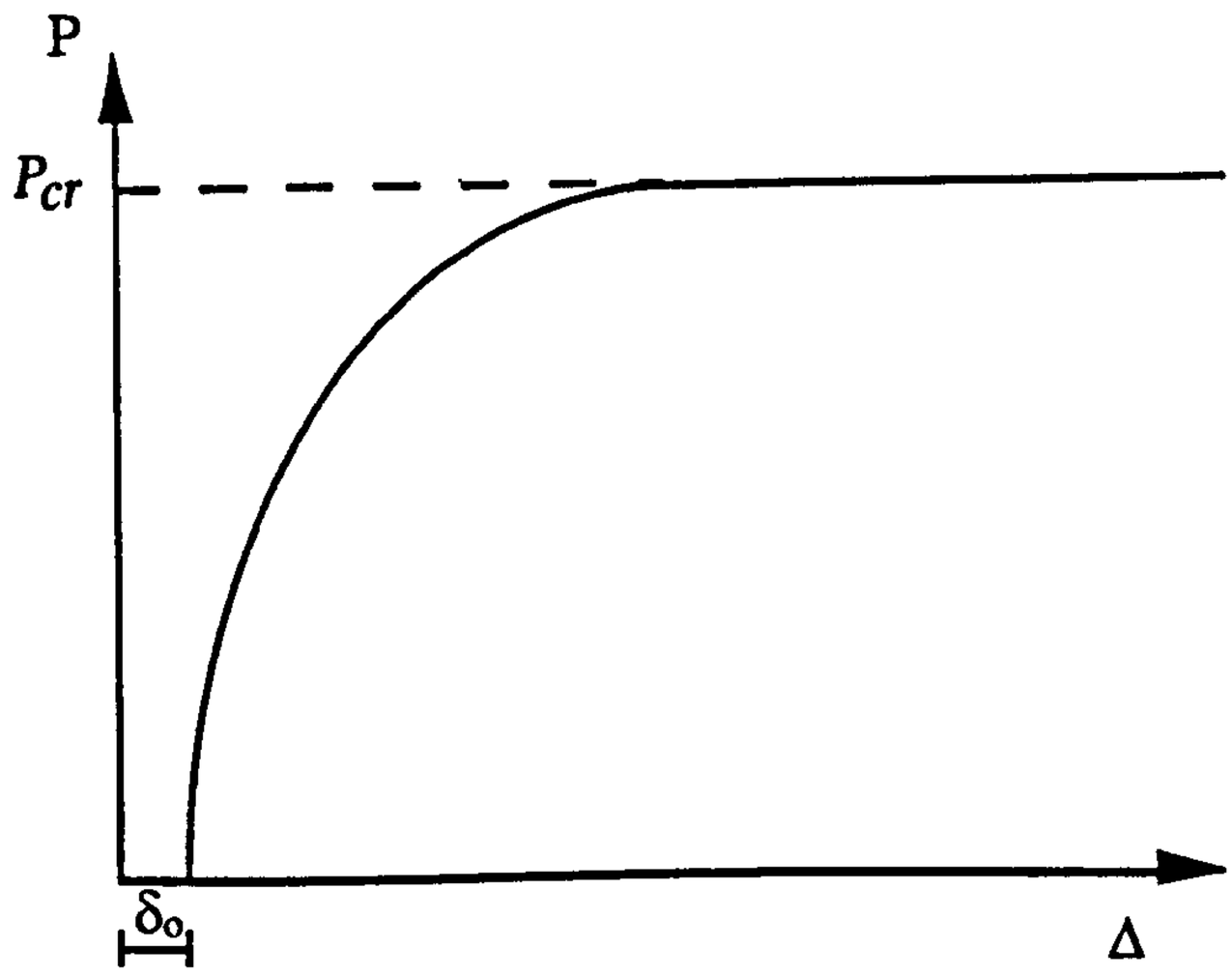

δ_o = initial disturbance

(b)

Figure 3.3: Deformation of sway frame

CHAPTER 4

RESULTS AND DISCUSSION OF PARAMETRIC STUDY FOR EFFECTIVE LENGTH FACTOR FOR SWAY FRAMES

4.1 Results

4.1.1 Variations in column effective length factors for rigid connections

Comparing the results obtained from this work and those calculated using BS 8110, Part 2 equations 5 and 6. Figures 4.1, 4.4 and 4.9 present the results for the variation in β with α assuming fully rigid connections. Note that in the case of sub-frame F1, $\alpha_1 = \alpha_2$, where α_1 and α_2 are the relative stiffnesses of the column to the lower and upper beams, respectively. In sub-frame F2, $\alpha_1 = 0$ because the foundation is rigid. There is no equation in BS 8110 to deal with sub-frame F3. The results in Figures 4.1 and 4.4 show that the code equations are in good agreement with analytical results for $0 < \alpha < 2$, and conservative thereafter. It is postulated that an equation for sub-frame F3 may be taken as the mean of the equations for F1 and F2. The results suggest that the code equations might be modified for values of $\alpha > 3$.

4.1.2 Variations in column effective length factors for semi-rigid connections

Figure 4.2 shows the results for the variations in β with α for selected values of K_s and Figure 4.3 with K_s for selected values of α in the upper storey sub-frame F1.

Although a mapping function is required to demonstrate the full parametric variations, the five selected values for K_s and α show the trends clearly. The results in Figure 4.3(a) show that for values of $K_s > 2$ or 3 the change in β is no more than about 5 per cent of its fully rigid value. For this reason Figure 4.3(b) is an enlargement of Figure 4.3(a) for values of $K_s \leq 2$.

Figures 4.5 and 4.6, and Figures 4.7 and 4.8 show similar sets of results for selected values of K_s and α for sub-frames F2 and F3, respectively. As expected the values of β in the ground floor sub-frame F2 converge at $\beta = 2.0$, and are independent of α. The corresponding value in sub-frame F3 is $\beta = 2.7$. A major difference between the upper floor (F3) the ground floor (F2) sub-frames is the more rapid decrease in β with K_s in the upper floor sub-frame. This is because F3 contains four semi-rigid connections, (although one of them is located adjacent to a rigid column foundation) whereas F2 contains only two. Also, F3 has eight degrees of freedom whereas F2 has only six. This result has obvious implications for frameworks containing a small number of bays in the plane of bending, say 2 or 3, where the number of semi-rigid connections is disproportionately large to the number of columns. The variation in α does not appear to have any major influence on the behaviour of the various sub-frames once the effects of changes in K_s have been removed.

4.2 Parametric equations

Subtracting the value of 1.0 from all the data and normalising the results with respect to α, the variation in $1/\beta$ with K_s is primarily linear and marginally quadratic. A

simple analysis of a right angled knee-joint (comprising one beam and one column connected by a semi-rigid rotational spring) will show that the effect of the semi-rigid connection is to modify the relative stiffness of the members from α to α' (see *Eq.*3.4).

For example if $\alpha = 0.5$ and $K_s = 0.6$ (say), then the effect of incorporating a semi-rigid connection is to increase the apparent stiffness of the column to $\alpha' = 1.33$, thus increasing β according to the results in Figure 4.1. Thus the influence of the connection stiffness K_s is paramount in the present parametric equations, whilst that of α is of lesser influence over the range studied. The influence of K_s on β is greater for values of $K_s < 2$ than when $K_s > 2$, and therefore separate equations are presented to cater for the differences in behaviour at these points.

Referring to Figures 4.2 and 4.3, the data for the upper storey sub-frame F1 may be approximated by using the following empirical relationship (derived in Görgün (1996) and subsequently modified) :

$$\beta = 1 + \frac{1}{0.2 + 10.0K_s} + \frac{\alpha}{0.3 + 1.8K_s - 0.45K_s^2} \quad \text{for } 0.1 \le K_s \le 2 \qquad Eq.\ 4.1(a)$$

$$\beta = 1.1 + \frac{1}{7.4 + 7.4K_s - 0.4K_s^2} + \frac{\alpha}{1.6 + 0.3K_s} \quad \text{for } 2 < K_s \le 10 \qquad Eq.\ 4.1(b)$$

Thus, $\alpha = 0.5$ and $K_s = 0.6$ for example, equation [*Eq.*4.1(*a*)] gives $\beta = 1.50$. If the value for the equivalent stiffness from *Eq.* 3.4 . ($\alpha' = 1.33$) is used in the BS 8110

equation, then $\beta = 1.40$. This shows that equating a semi-rigid connection to a rigid connection in an equivalent frame under estimates β for these particular parameters.

Referring to Figures 4.5 and 4.6, the data for the ground floor sub-frame F2 may be given as:

$$\beta = 1 + \frac{1}{2.0 + 2.0K_s + 4.0K_s^2} + \frac{\alpha}{4.0 + 0.5K_s} \quad \text{for } 0.1 \le K_s \le 2 \qquad Eq.\ 4.2(a)$$

$$\beta = 1 + \frac{1}{8.6 + 8.4K_s - 0.4K_s^2} + \frac{\alpha}{3.9 + 0.9K_s} \quad \text{for } 2 < K_s \le 10 \qquad Eq.\ 4.2(b)$$

Referring to Figures 4.7 and 4.8, the data for the upper storey sub-frame F3 may be given as:

$$\beta = 1 + \frac{1}{1.25 + 2.5K_s + 2.5K_s^2} + \frac{\alpha}{2.5 + 0.5K_s} \quad \text{for } 0.1 \le K_s \le 2 \qquad Eq.\ 4.3(a)$$

$$\beta = 1 + \frac{1}{6.5 + 5.6K_s - 0.3K_s^2} + \frac{\alpha}{2.7 + 0.3K_s} \quad \text{for } 2 < K_s \le 10 \qquad Eq.\ 4.3(b)$$

To demonstrate the full parametric variations, the three selected values for α show the trends clearly. The dashed lines in Figures 4.10 to 4.12 show the plots of the proposed parametric equations. Results are presented only for values of $K_s \le 2$ for the reasons outlined above in Section 4.1.2.

4.3 Discussion

The primary objective of the parametric analytical study has been to observe both the influence of the linear rotational stiffnesses of joints and flexural stiffnesses of the linear elastic members on buckling loads and hence on the effective length factors of the sub - frames presented in Figure 3.2. In the analysis α was calculated by keeping the cross sectional area and the second moment of area of the beams constant. The second moment of area of the beams and columns were based on the uncracked section.

It has been established that where column effective length factors β are determined within a structural framework, the nature of that framework and its boundary conditions will influence the results. All the results show an increase in β with:

i) an increasing number of degrees of freedom, and an increasing number of connections per sub-frame

ii) an increase in α

iii) a decrease in K_s.

In the context of precast concrete frame connections, where full scale experimental results indicate values of K_s between 0.1 and 3.35 [Chapter 11] it is significant that for values of $K_s < 2$ the influence of connection stiffness on β is much greater than that of the relative stiffness of the frame members, particularly in sub-frame F1 where all connections are semi-rigid (see Figure 4.3). In the sub-frames comprising at least one rigid foundation (i.e. F2 and F3) the variation in β with K_s and α is about equal for $K_s < 1$, and more dependent on α for $K_s > 1$. It is therefore concluded that

maximum benefit in obtaining reductions in β with greater connection stiffness will accrue in upper storey sub-frames where $K_s < 1$, and in the ground floor sub-frame where $K_s < 0.5$.

The results obtained for the upper storey in the partially braced sub-frame F3 are of particular interest to designers because the boundary conditions for the column which is not adjacent to a shear wall is unspecified in codes of practice. Treating the column alone would lead to very high β factors and an impossible design situation (which can be appreciated from the design rules given in BS 8110, Part 2 equations 5 and 6). A pinned jointed frame can be idealised as shown in Figure 4.13. In Figure 4.13(a) the deflected profile of a column held in position but not in direction at level N, and a free cantilever above this level will have a β factor of at least 3.0 (assuming equal storey heights). However the true manner of slenderness induced deflections would be as shown in Figure 4.13(b) where the effective length of *all* columns is 2.7. The restoring force in the beam is small but very significant in terms of frame stability. Bending moments resulting from sway in the unbraced part are carried over into the braced part of the frame, diminishing to zero with distance to the level of the floor below, such that β for the columns in the lower braced regions may be taken as 1.0.

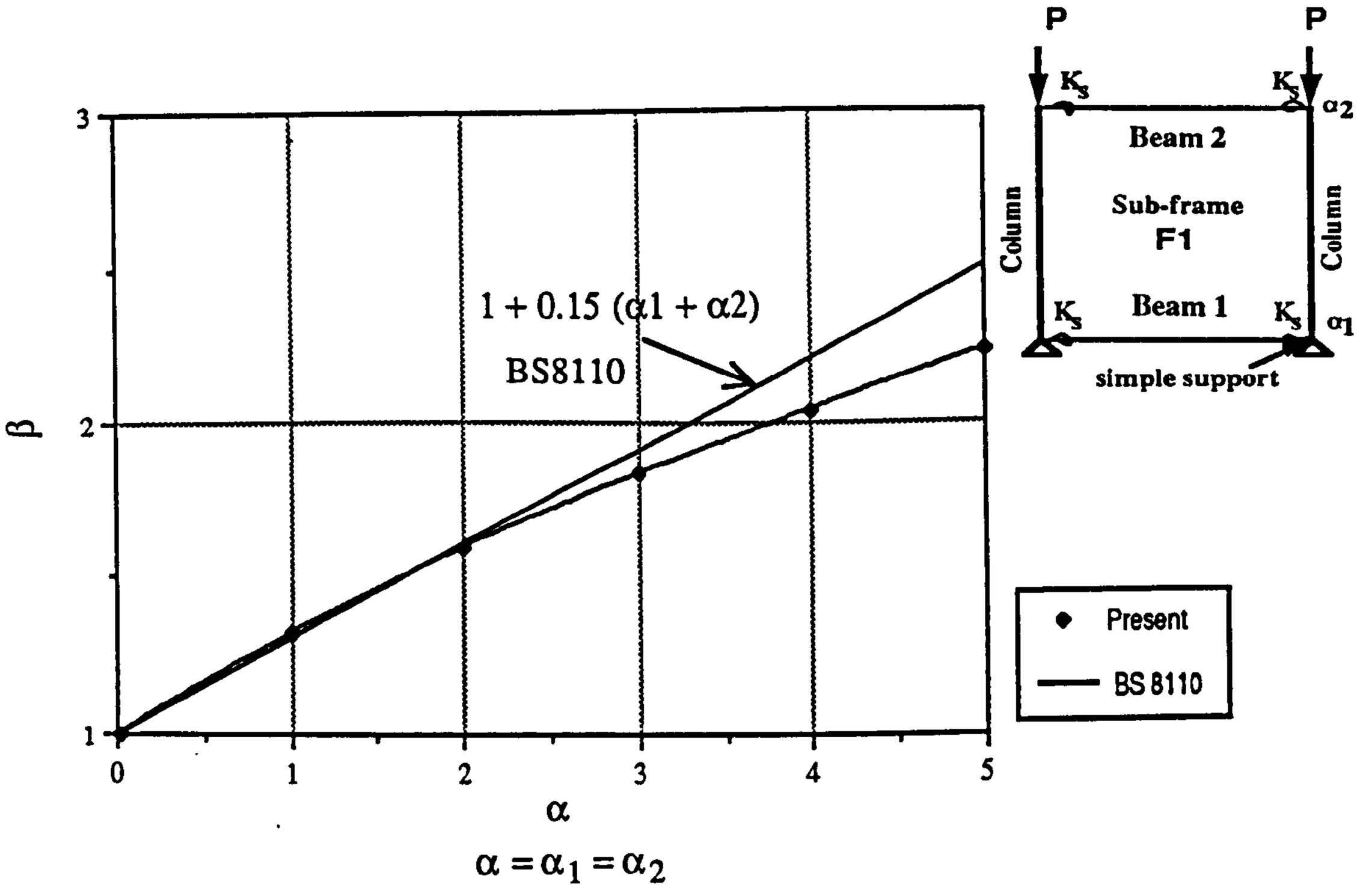

Figure 4.1: Comparison with BS8110 using F1 with fully rigid joints

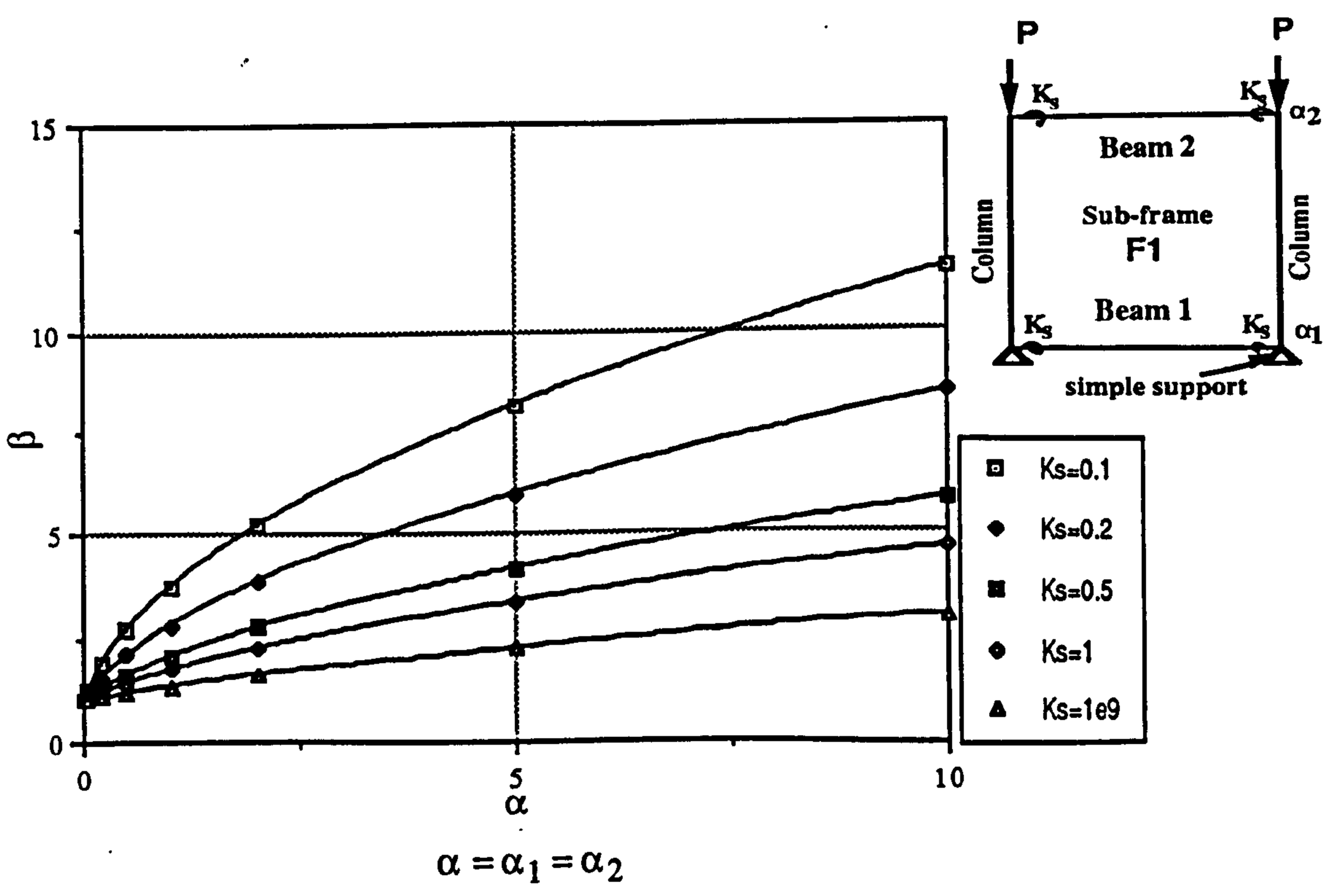

Figure 4.2 (a): Variation in β factor with $0.001 \leq \alpha \leq 10$ for upper floor sub-frame F1

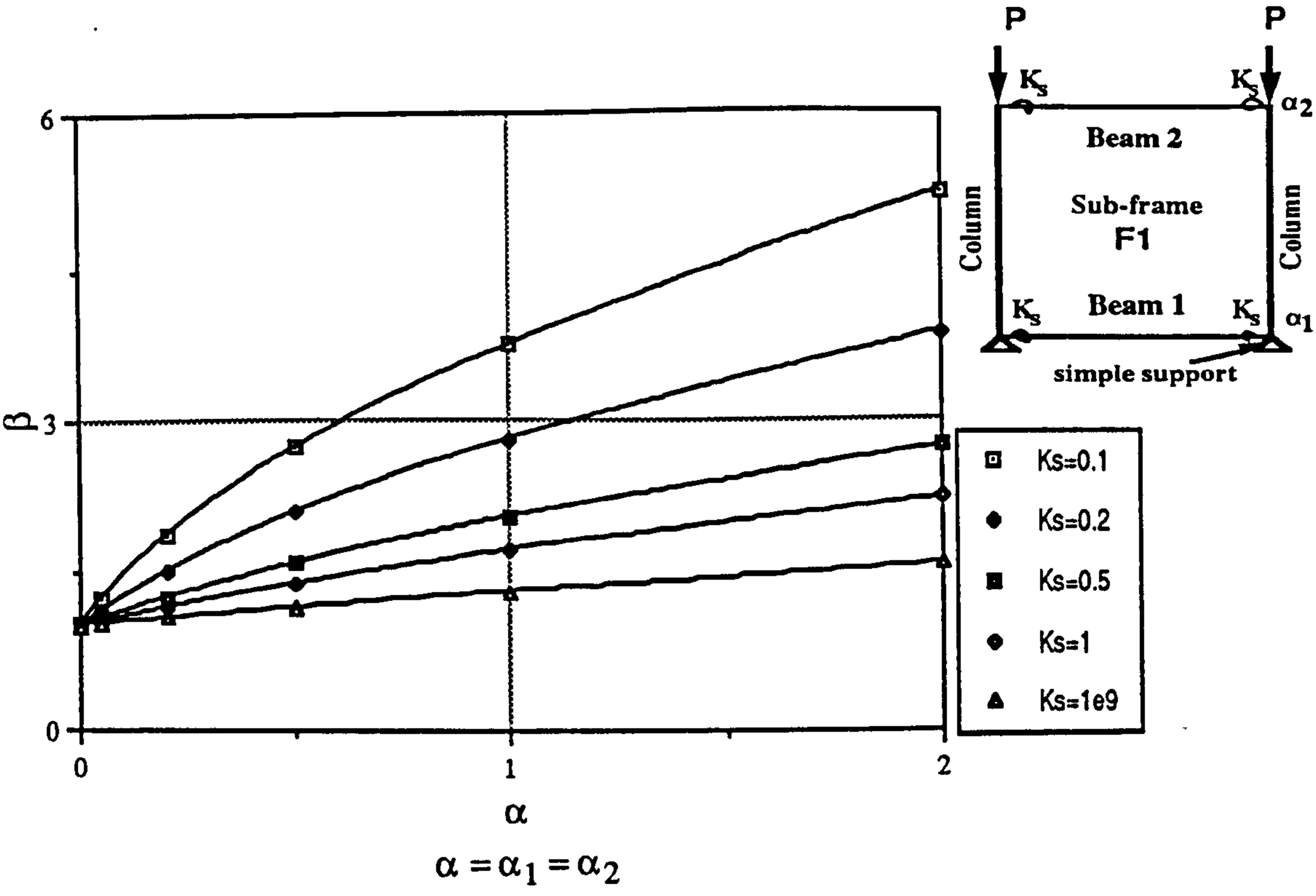

$$\alpha = \alpha_1 = \alpha_2$$

Figure 4.2 (b): Variation in β factor with $0.001 \leq \alpha \leq 2$ for upper floor sub-frame F1

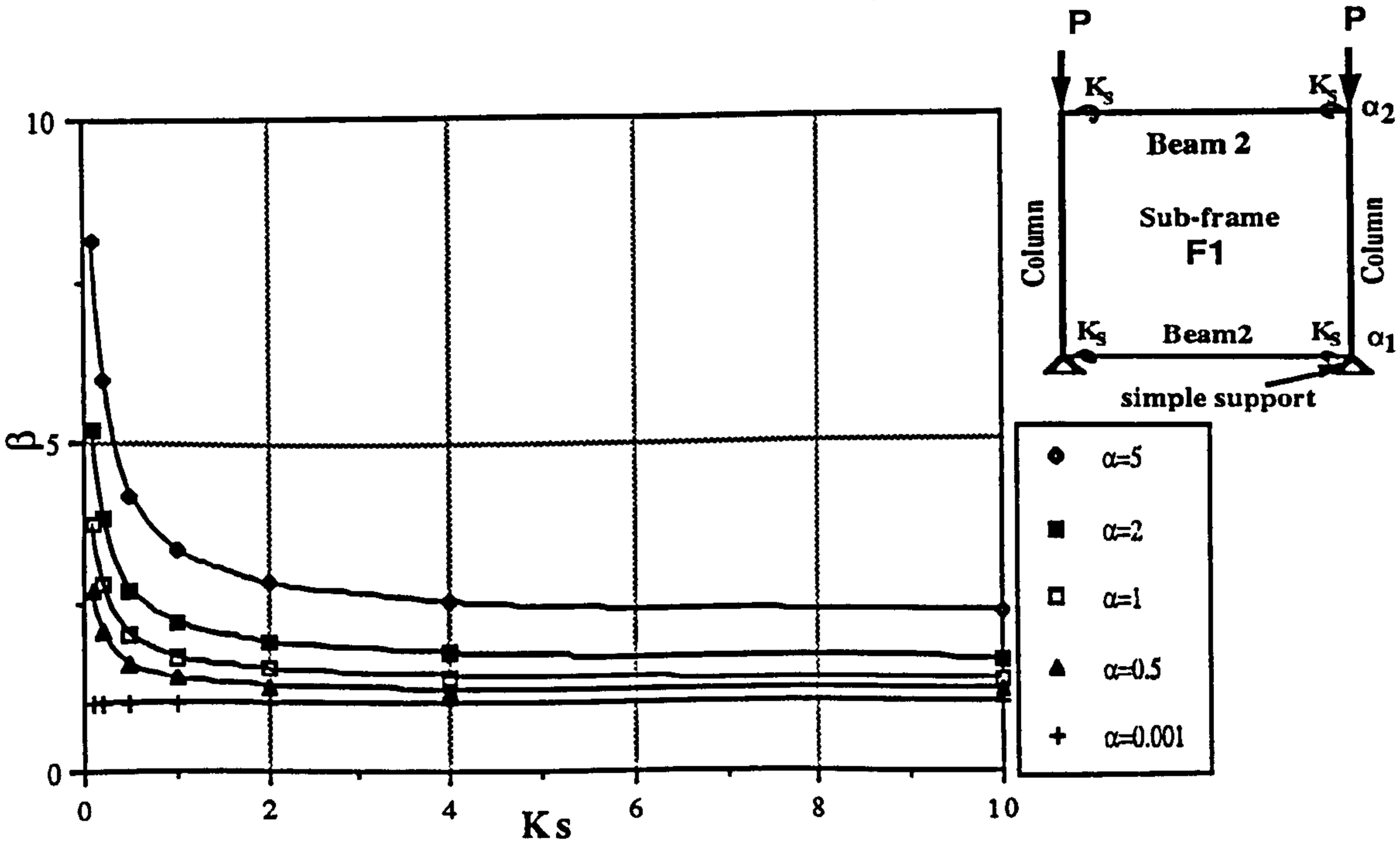

Figure 4.3 (a): Variation in β factor with $0.1 \leq K_S \leq 10$ for upper floor sub-frame F1

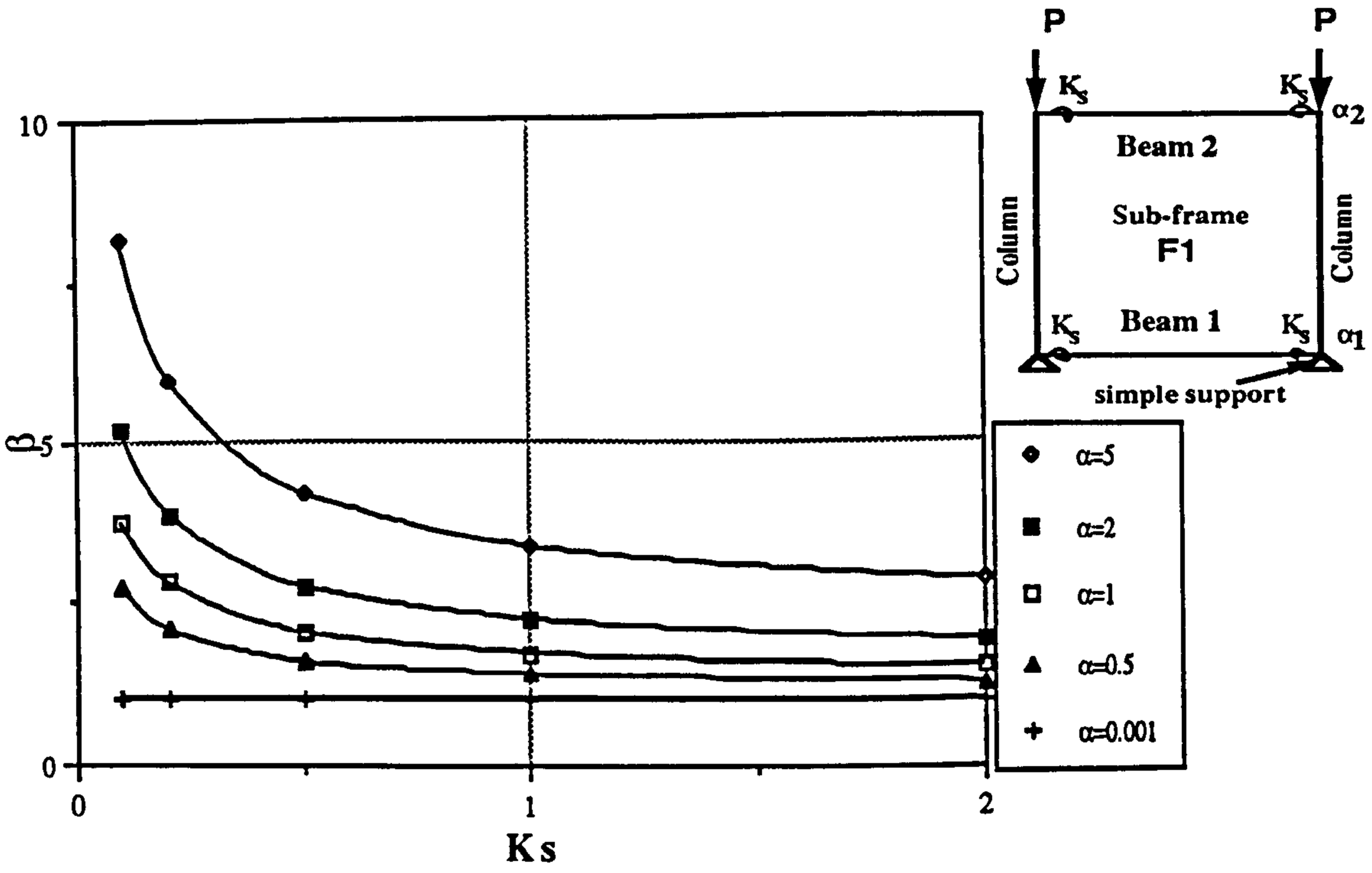

Figure 4.3 (b): Variation in β factor with $0.1 \leq K_S \leq 2$ for upper floor sub-frame F1

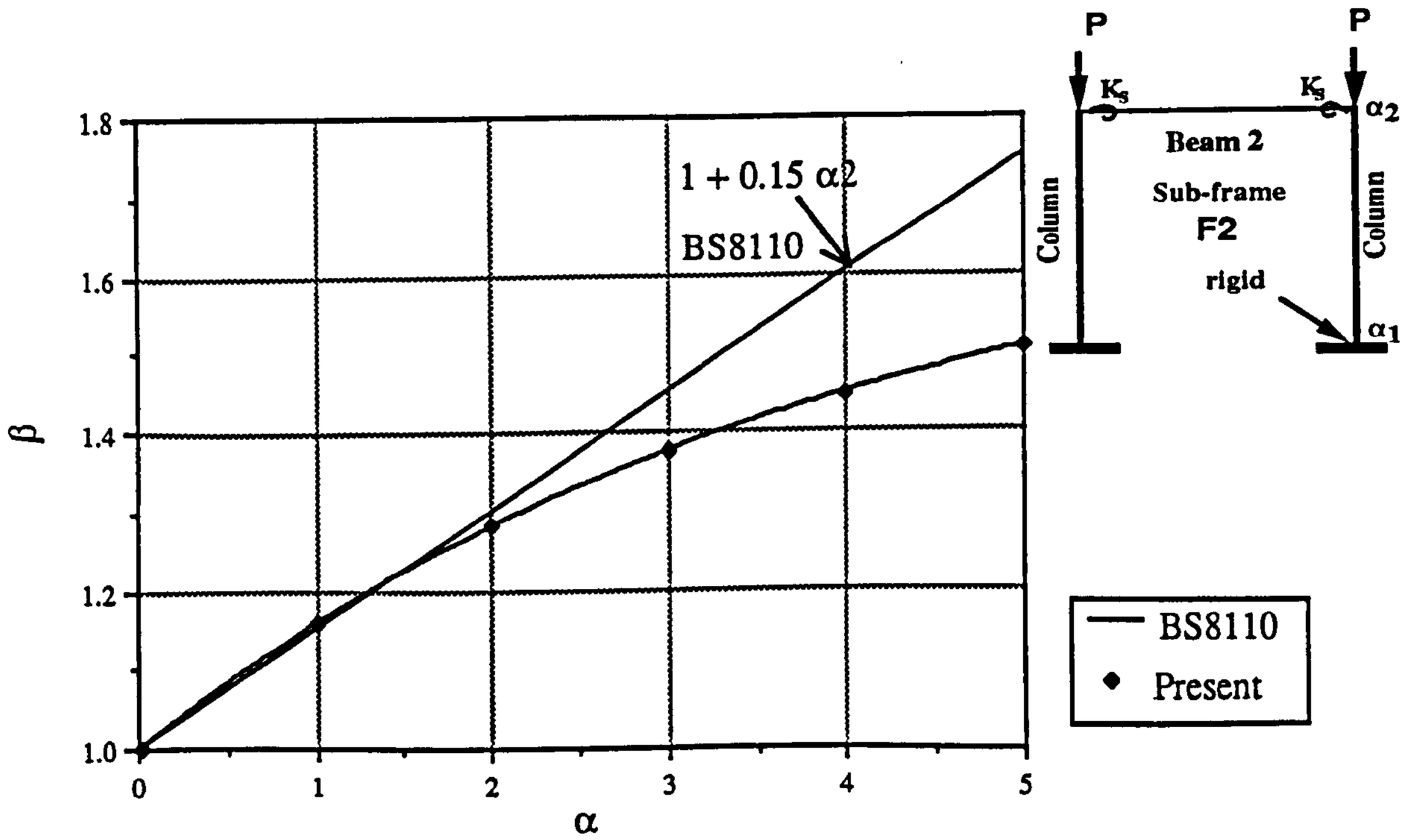

Figure 4.4: Comparison with BS8110 using F2 with fully rigid joints, where $\alpha_1 = 0$

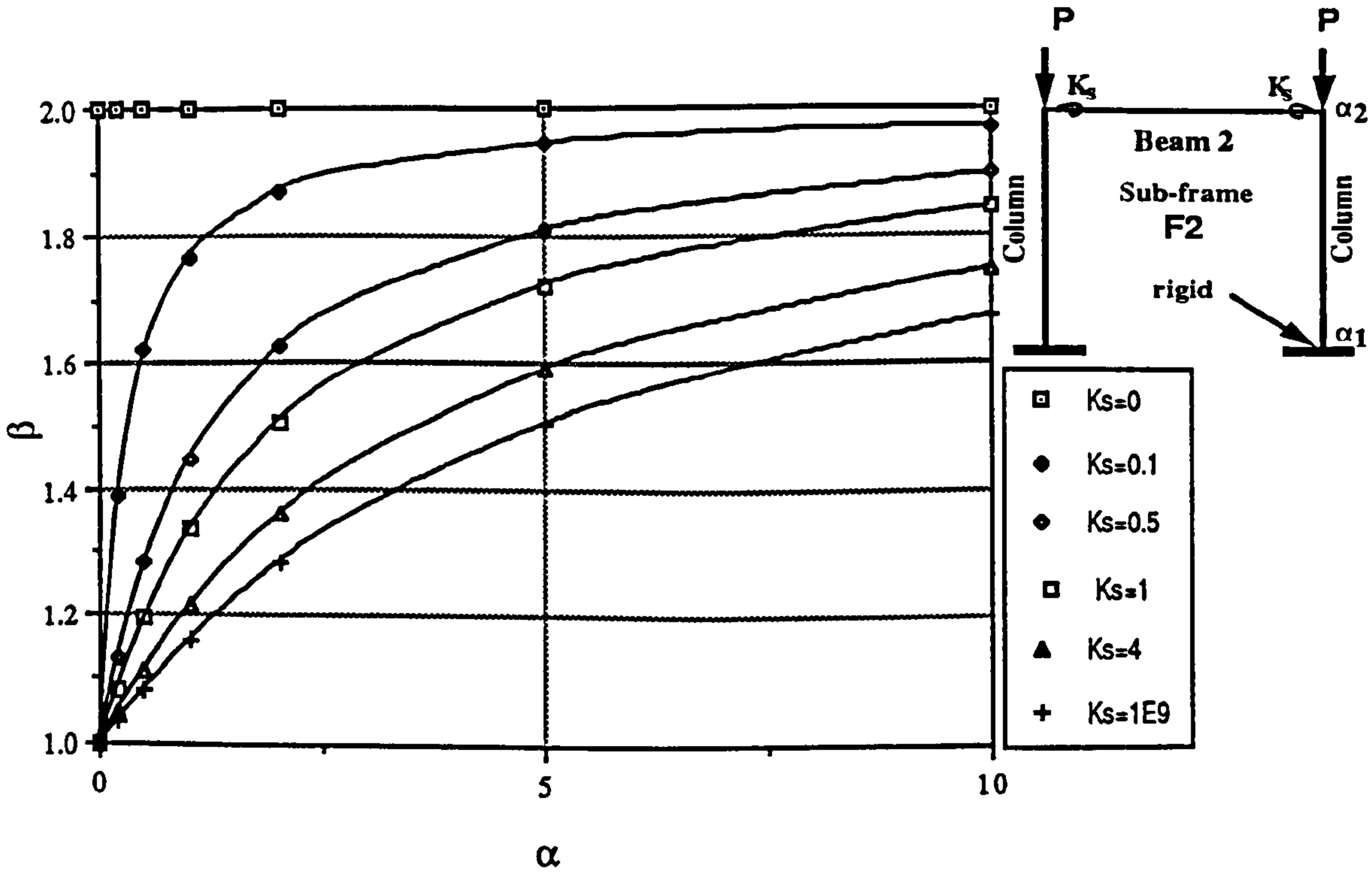

Figure 4.5 (a): Variation in β factor with $0.001 \leq \alpha \leq 10$ for sub-frame F2

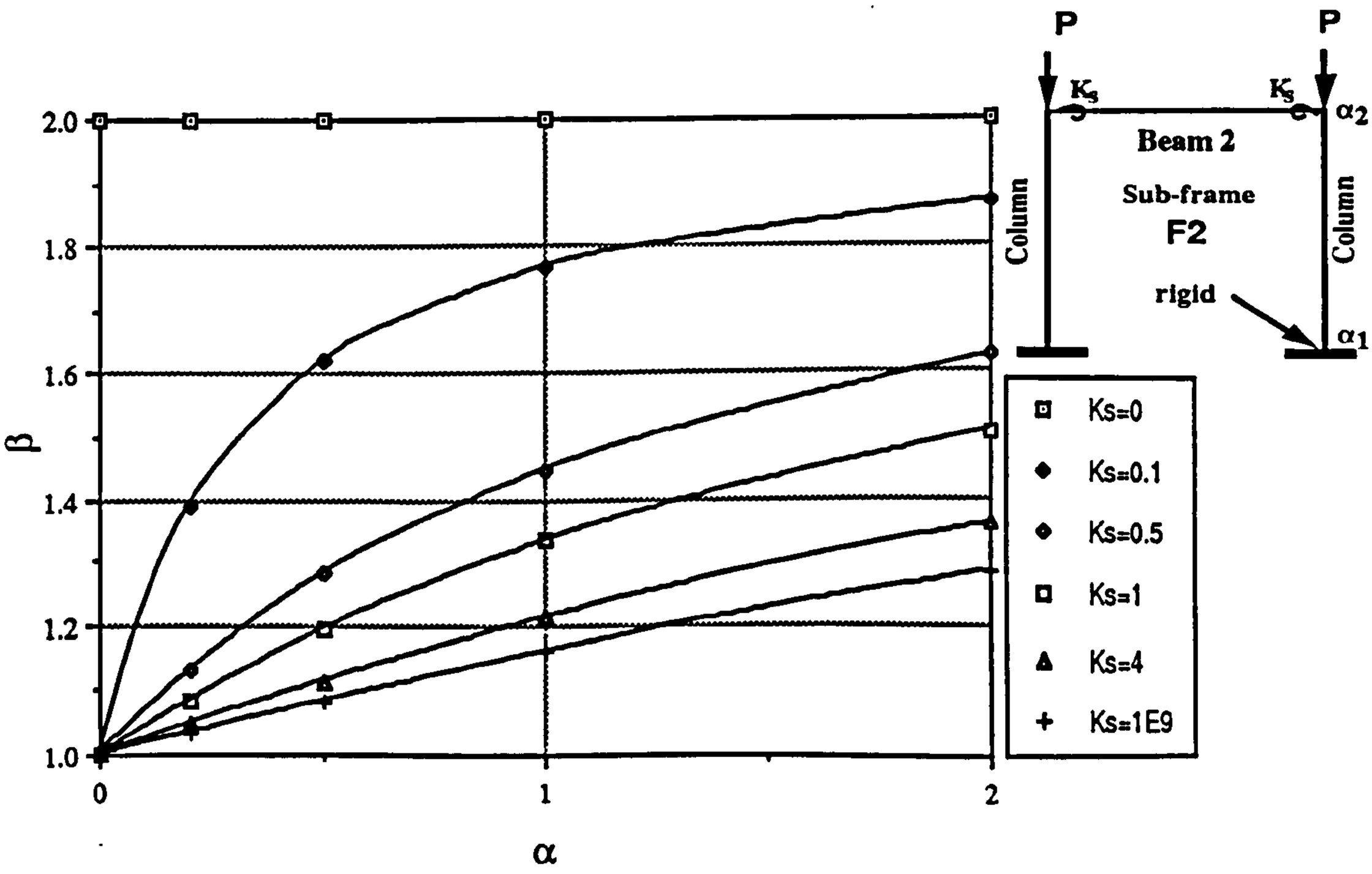

Figure 4.5 (b): Variation in β factor with $0.001 \leq \alpha \leq 2$ for sub-frame F2

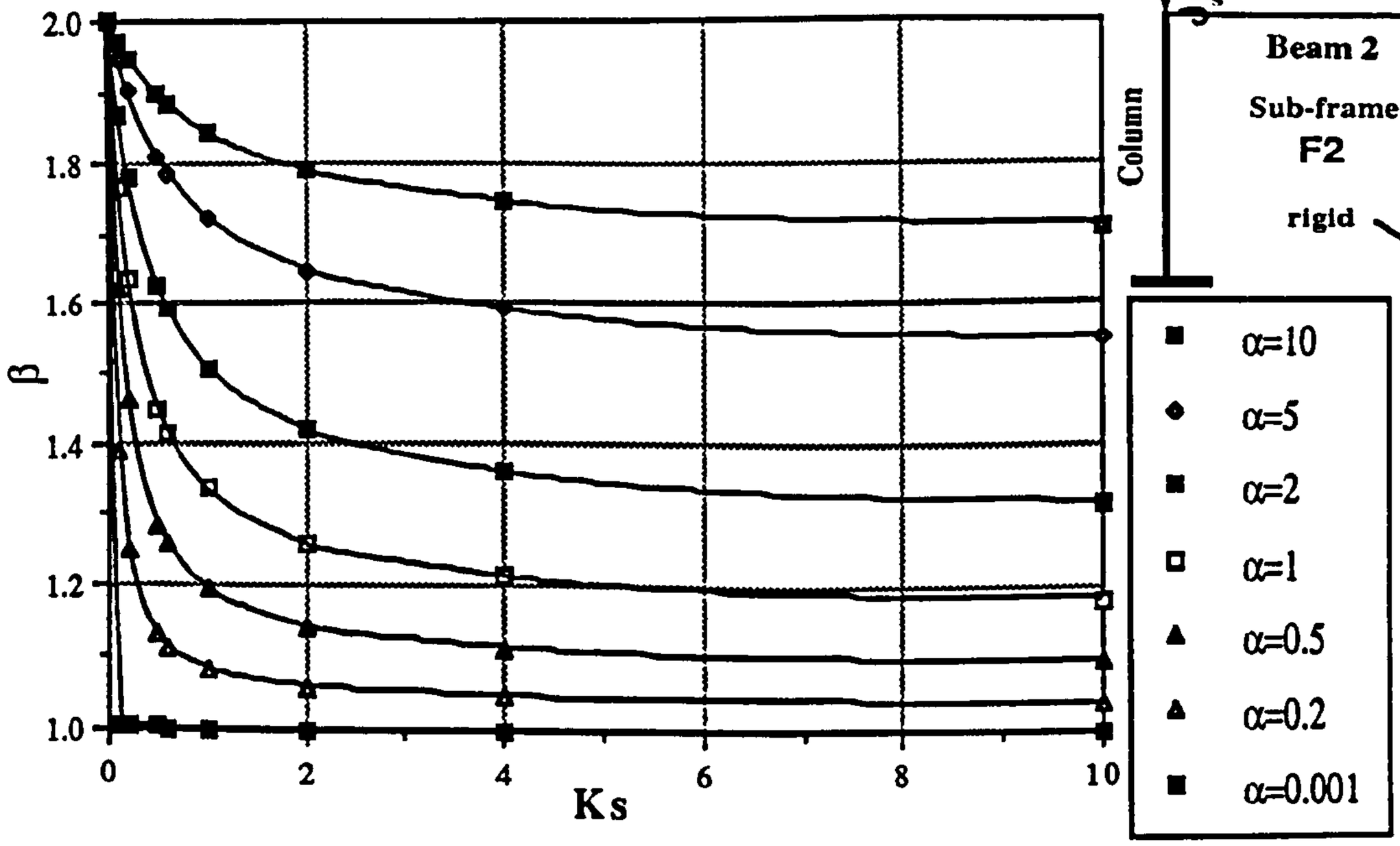

Figure 4.6 (a) : Variation in β factor with $0 \leq K_S \leq 10$ for sub-frame F2

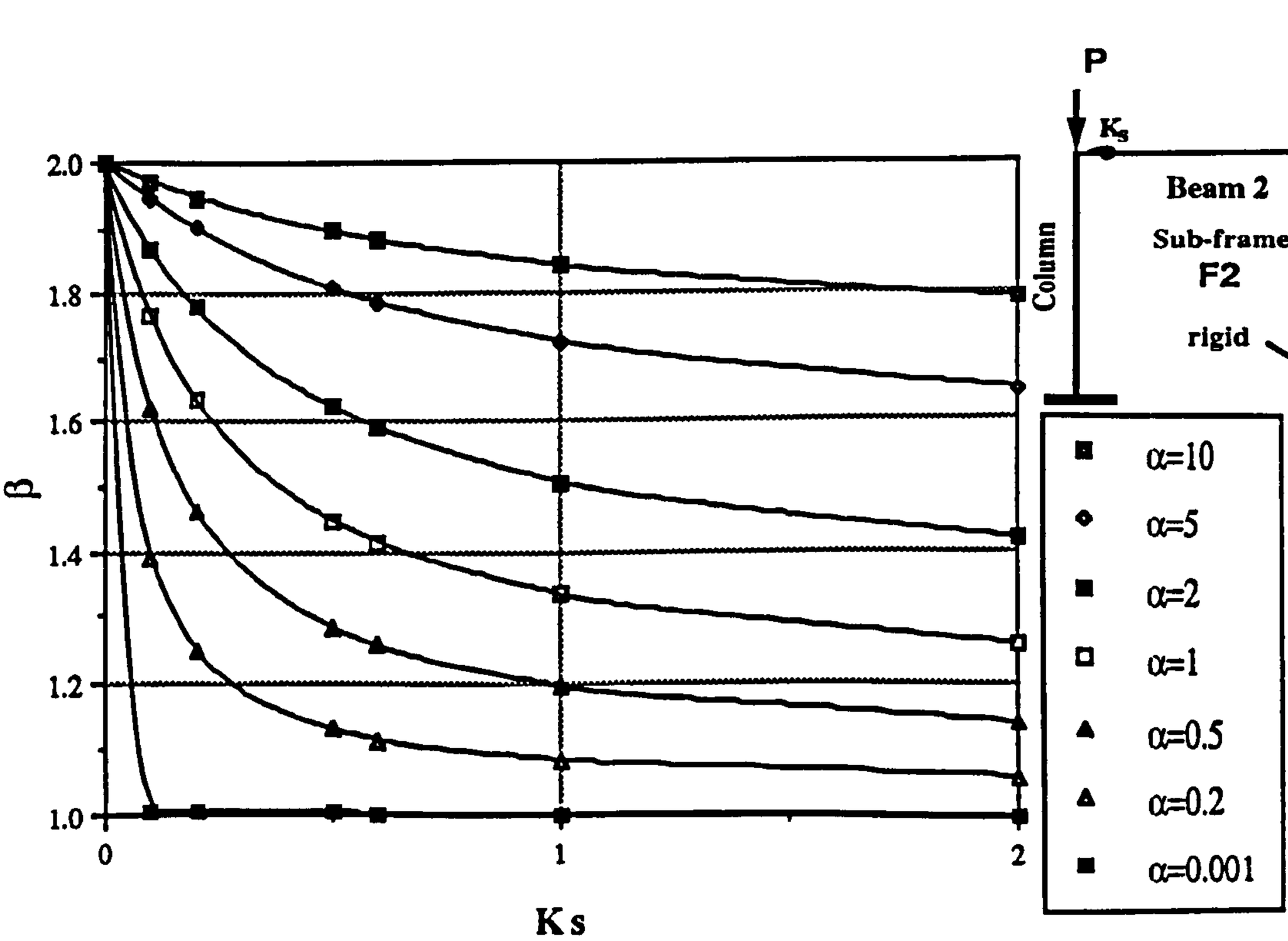

Figure 4.6 (b):Variation in β factor with $0 \leq K_S \leq 2$ for subframe F2

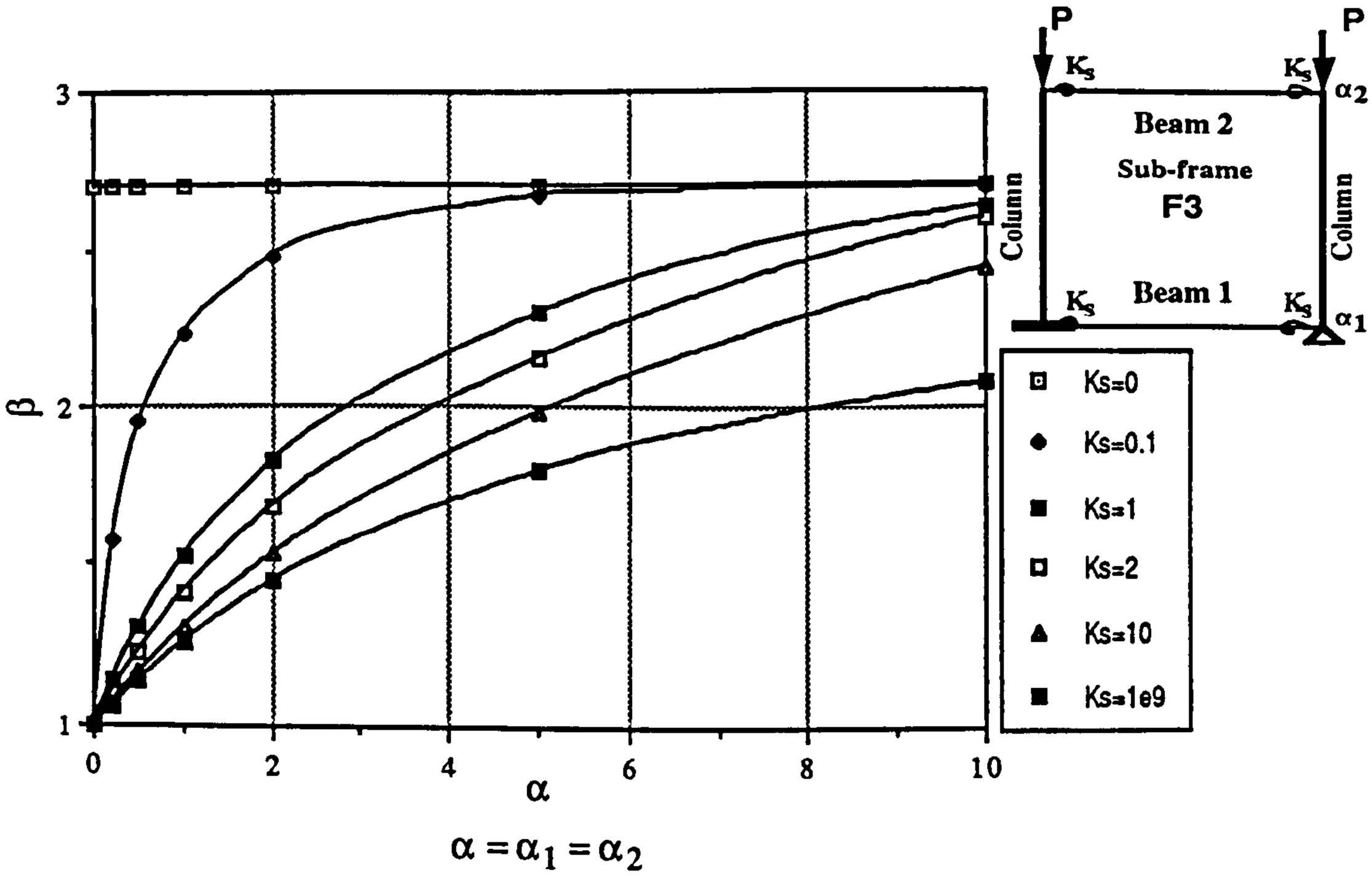

$$\alpha = \alpha_1 = \alpha_2$$

Figure 4.7 (a): Variation in β factor with $0.001 \leq \alpha \leq 10$ for sub-frame F3

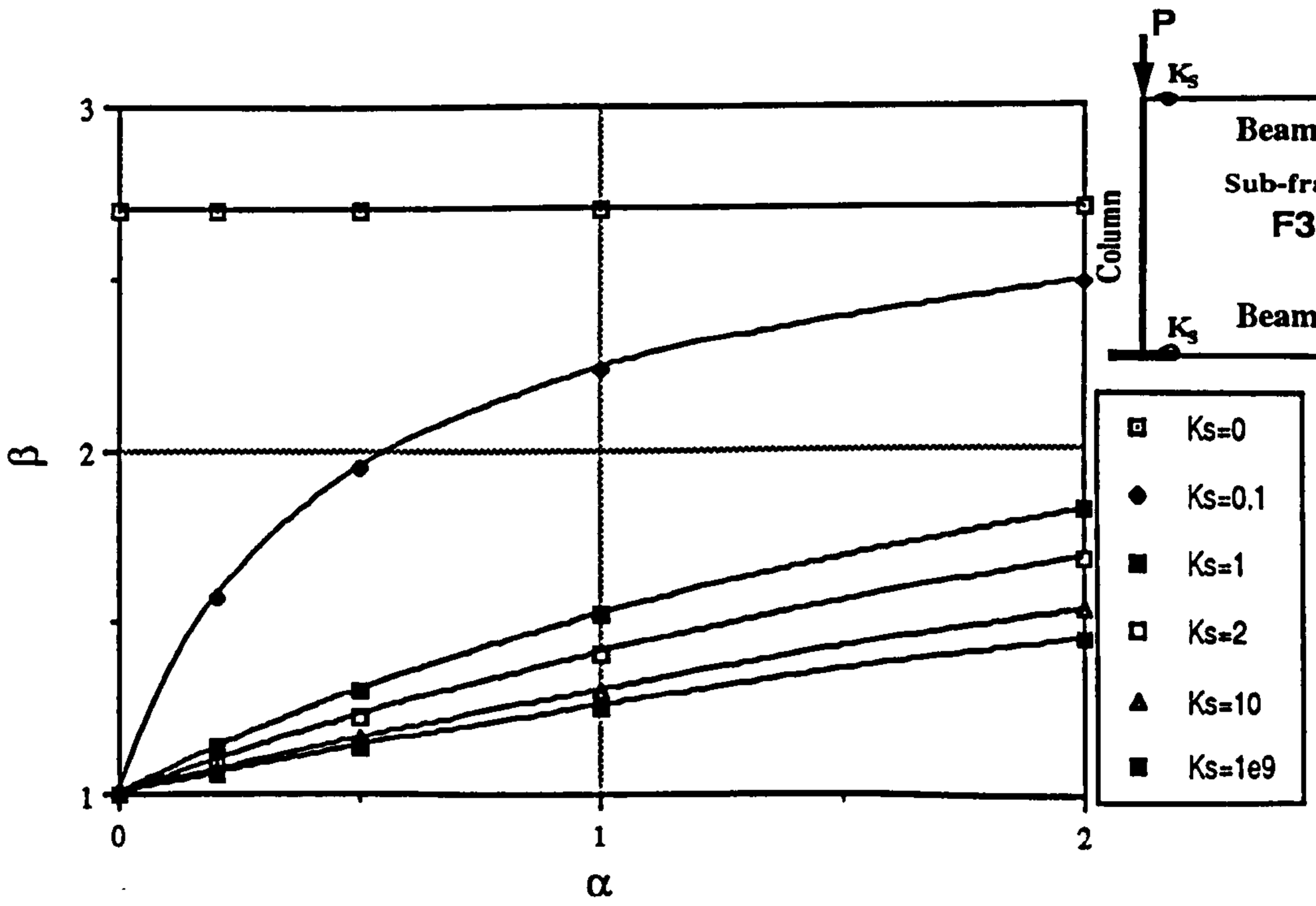

$$\alpha = \alpha_1 = \alpha_2$$

Figure 4.7 (b): Variation in β factor with $0.001 \leq \alpha \leq 2$ for sub-frame F3

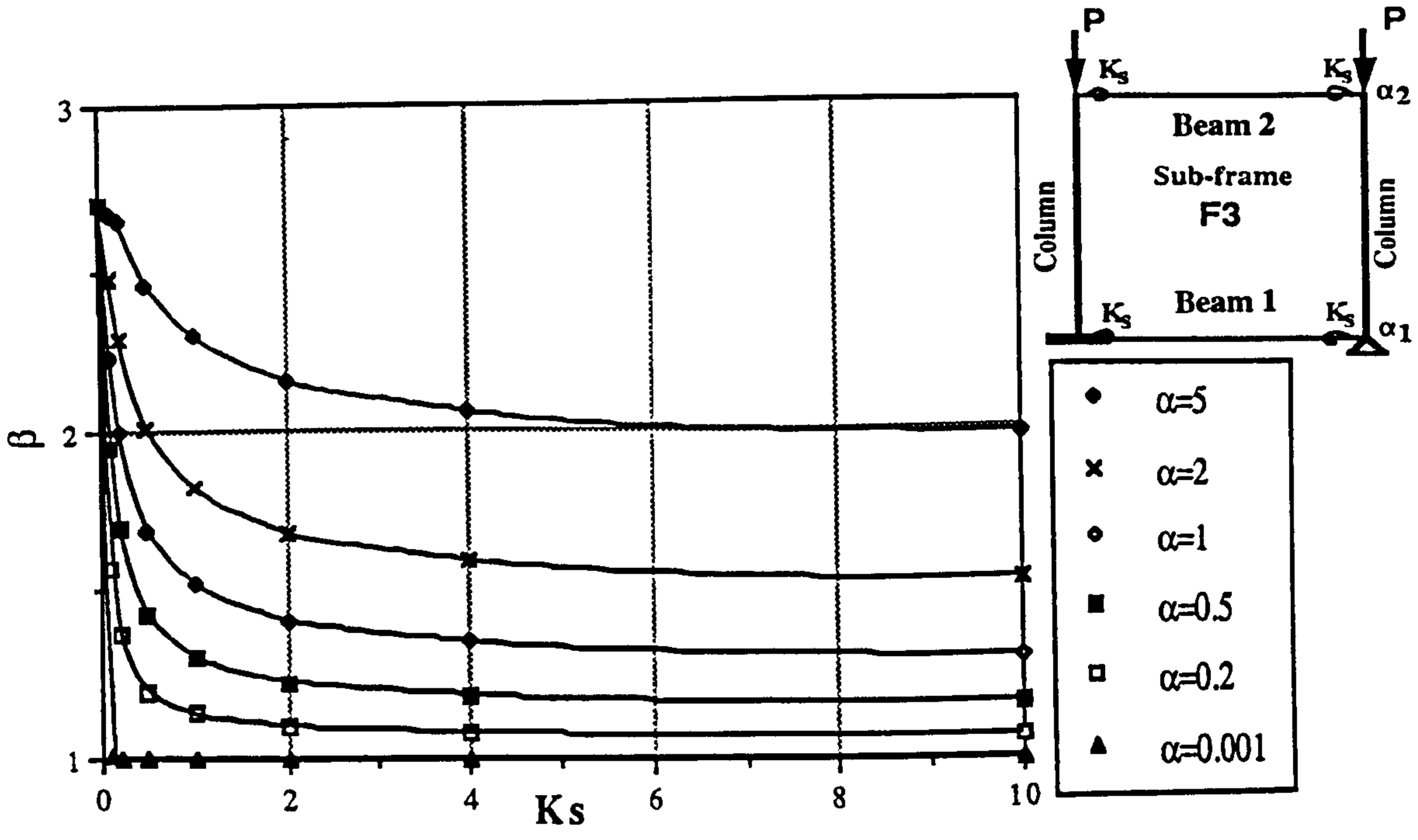

Figure 4.8 (a): Variation in β factor with $0 \leq K_S \leq 10$ for sub-frame F3

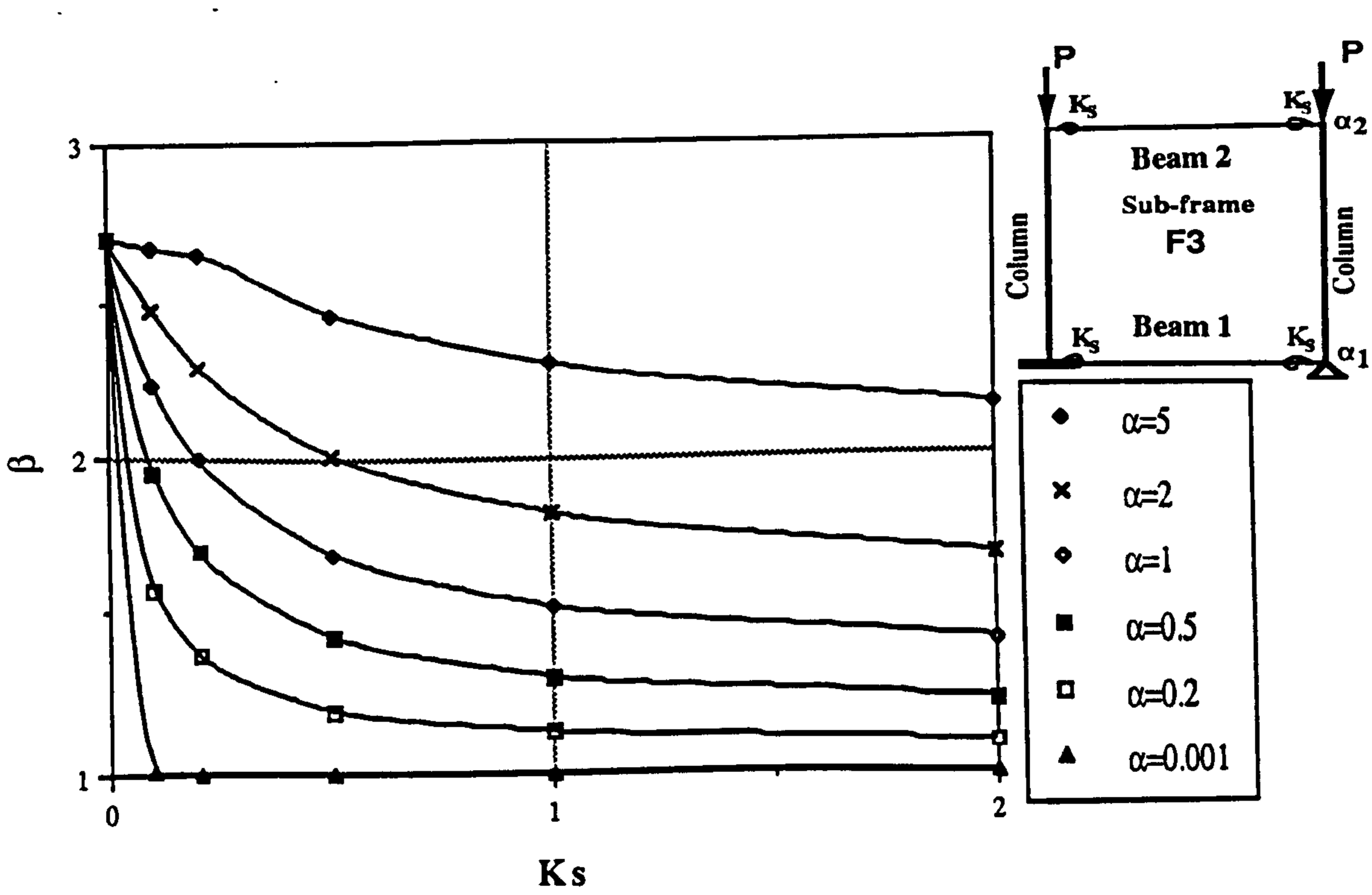

Figure 4.8 (b): Variation in β factor with $0 \leq K_S \leq 2$ for sub-frame F3

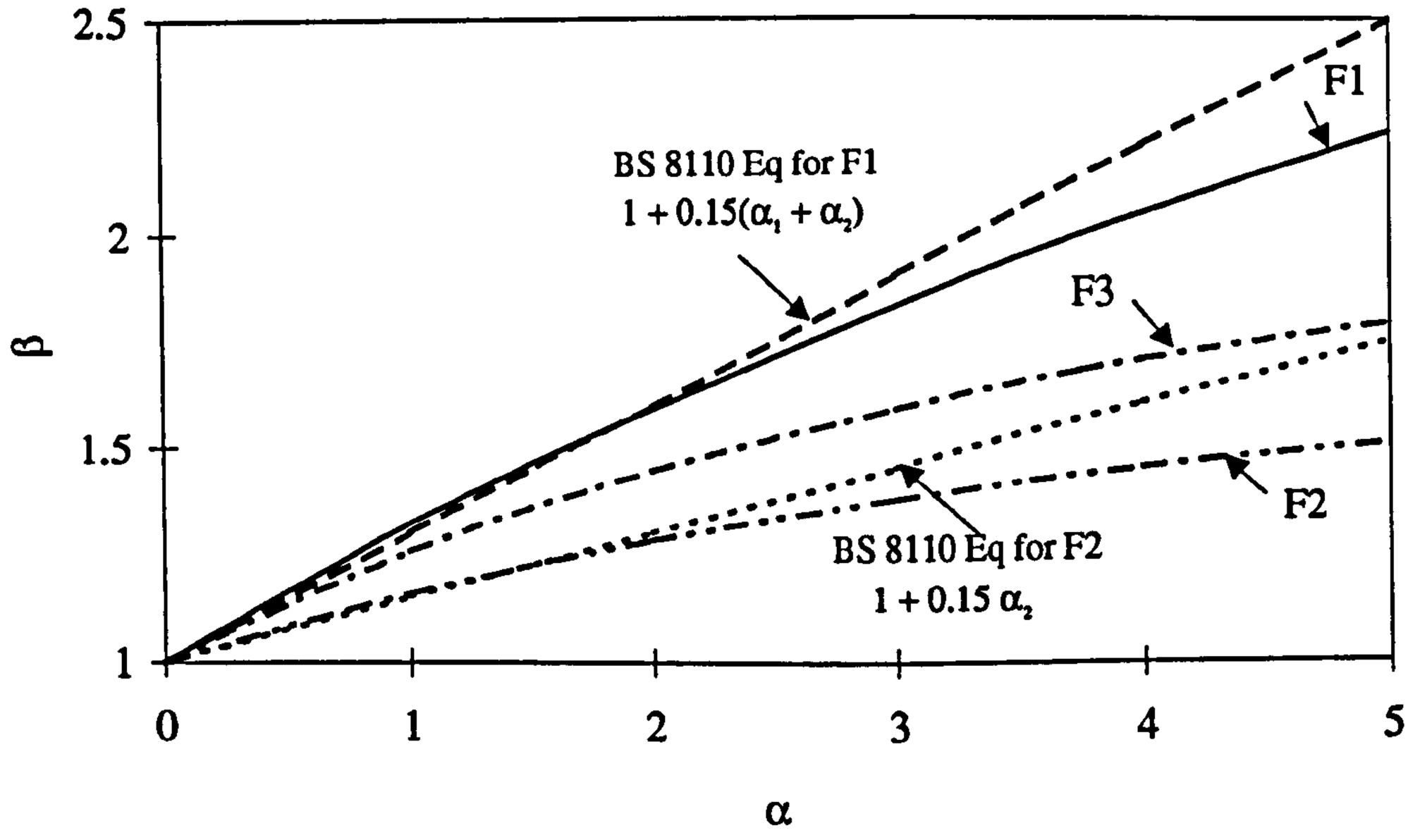

Figure 4.9: Variation in column effective length factor β with frame stiffness α for rigid joints

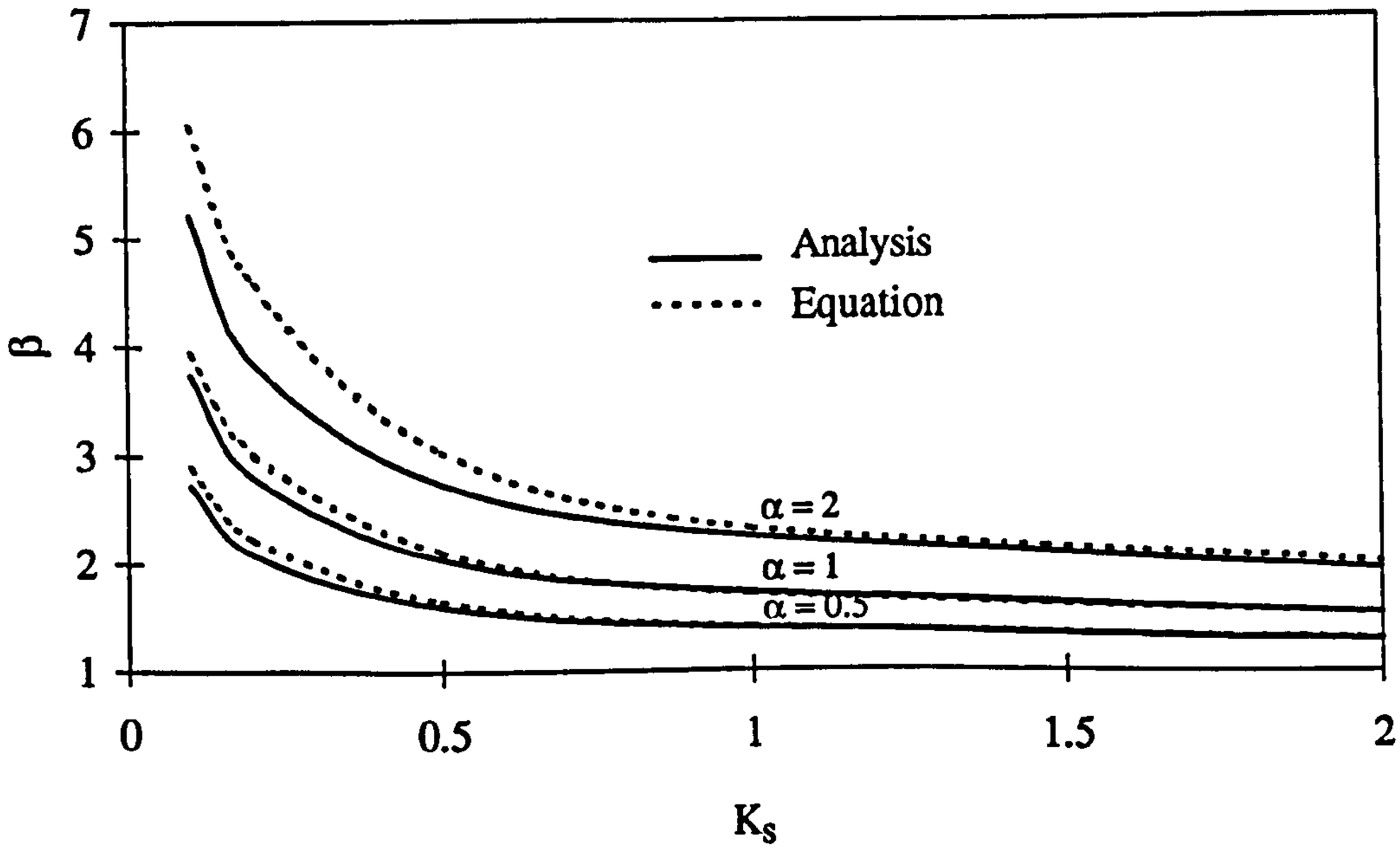

Figure 4.10: β factors vs $K_s \leq 2$ for selected values of α in sub-frame F1

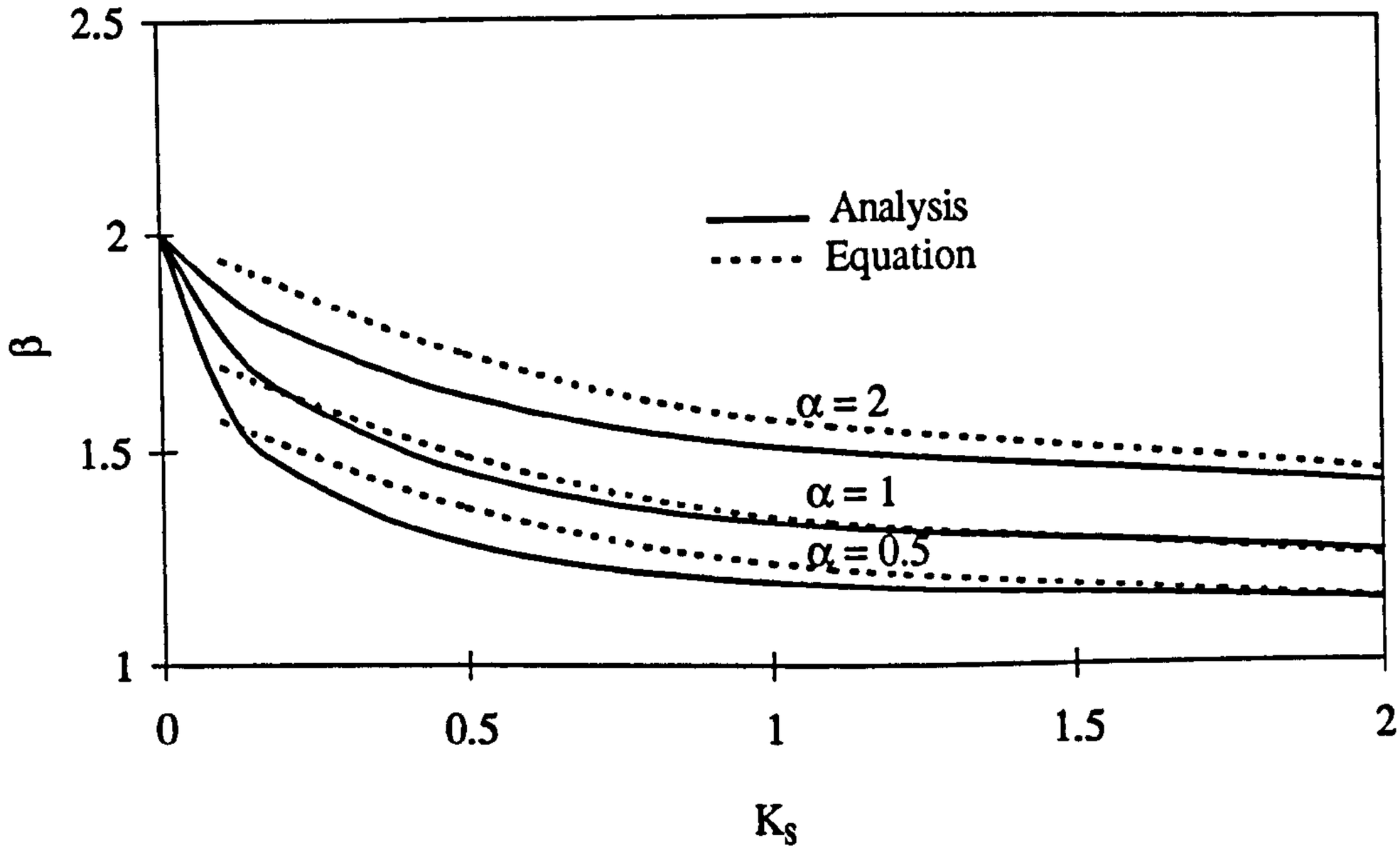

Figure 4.11: β factors vs $K_s \leq 2$ for selected values of α in sub-frame F2

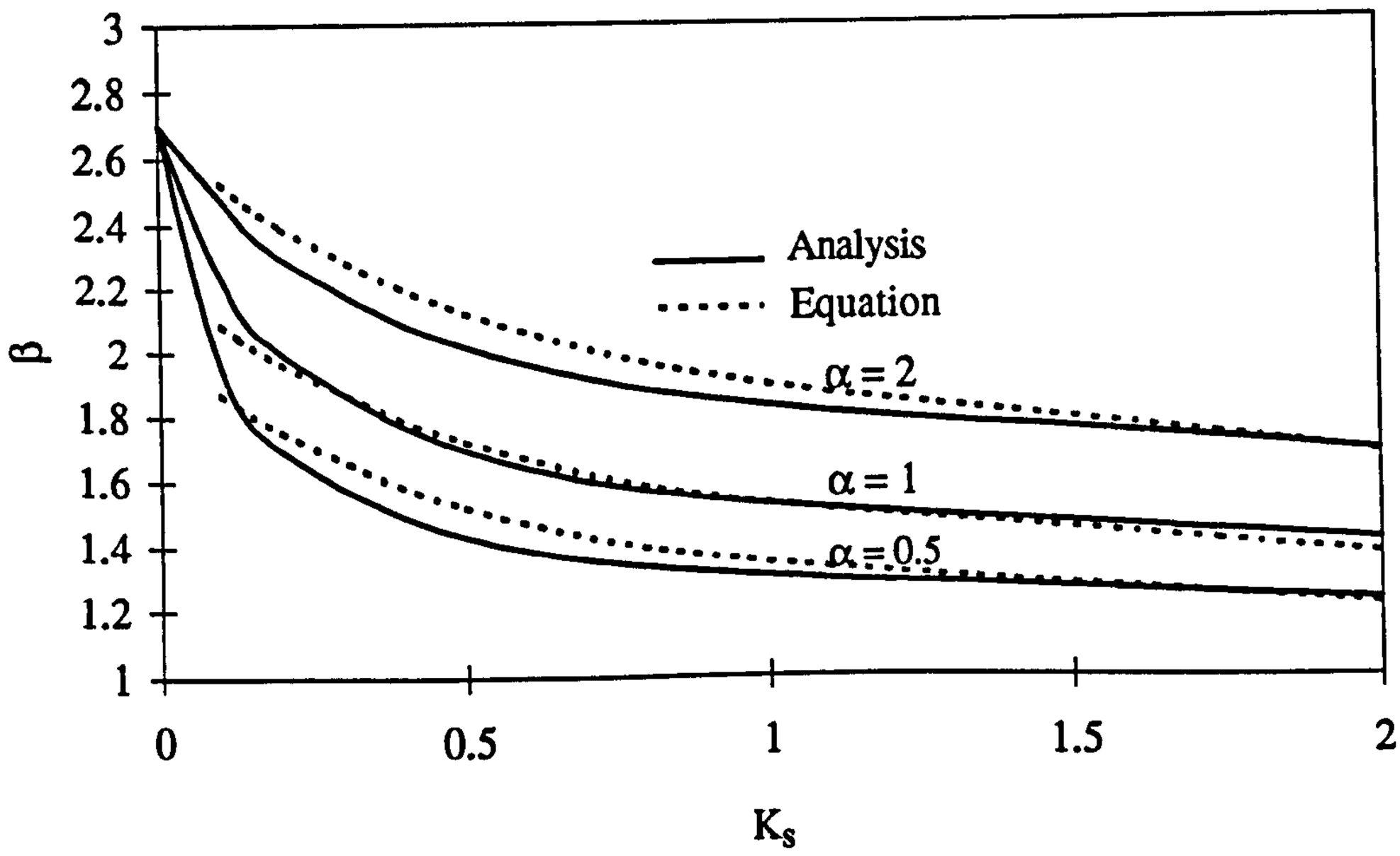

Figure 4.12: β factors vs $K_s \leq 2$ for selected values of α in sub-frame F3

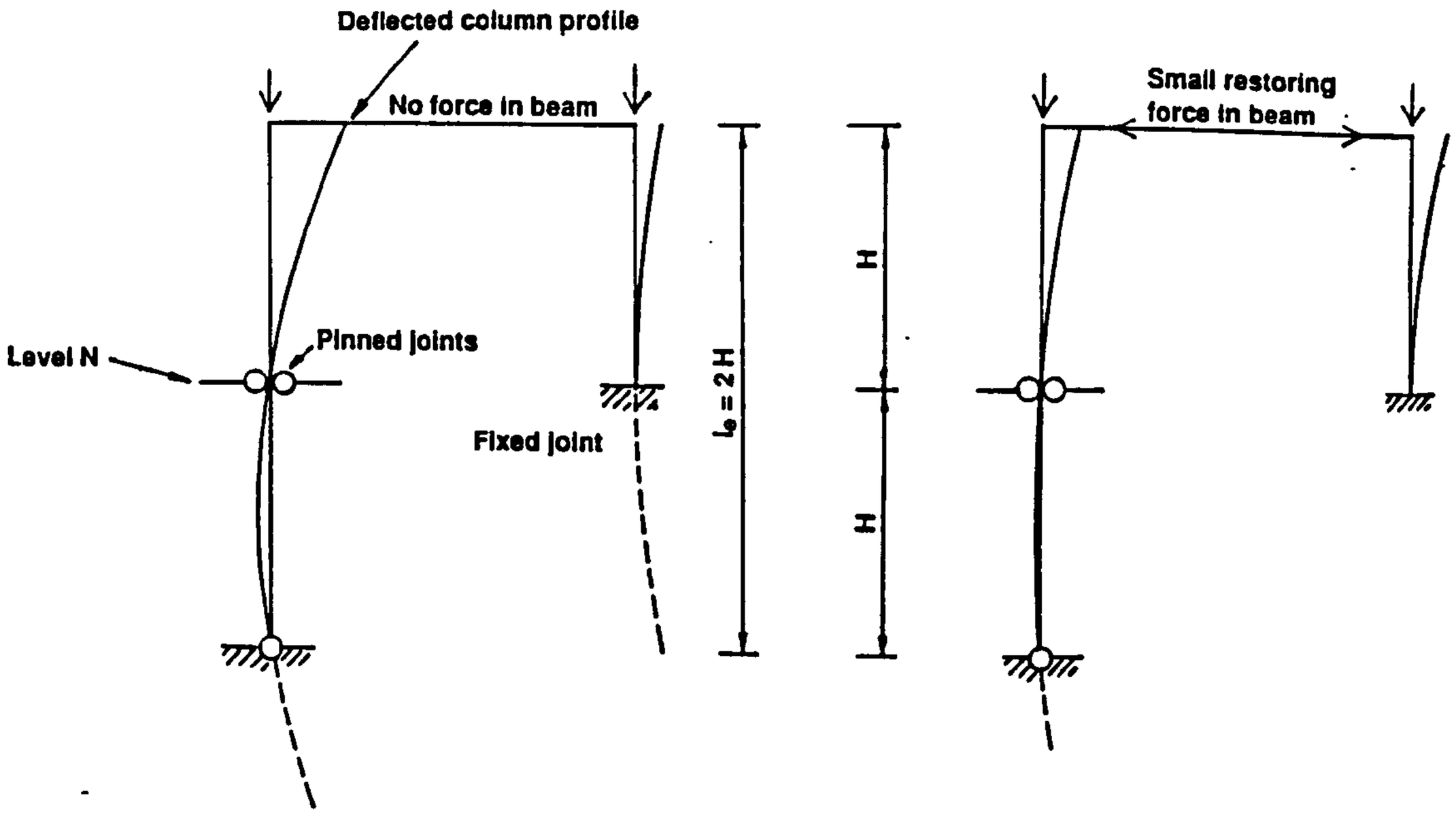

Figure 4.13: Behaviour of a partially braced frame, (a) discrete column deflection profiles (left), (b) column deflection profiles in a frame environment (right)

CHAPTER 5

EXPERIMENTAL PROGRAMME FOR FULL SCALE FRAME CONNECTION TESTS

5.1 Introduction

The main aim in the full scale precast concrete frame connection tests is the determination of the moment-rotation $M-\phi$ characteristics of the most common types of beam-to-column connections used in the precast concrete frames in the UK as shown in Figure 1.1. From these characteristics it will be possible to abstract the rotational stiffness, bending strength and ductility of the corresponding connections and hence their effects on the stability of these frames. Because currently, beam connections are rated and identified by their shear capacity only, a shear test TW1(B) was carried out after the bending test TW1(A) was completed to ensure that the shear resistance of the entire connection was satisfactory.

In this project study it is hoped that the connections can be identified not only by their shear capacity but also by their rotational stiffness, flexural strength as well as ductility.

The contribution of these main characteristics of the connections (also referred to as joints on completion) to frame behaviour under gravity cycling loading is well studied in braced (nonsway) precast concrete frames where the precast concrete

connections are subjected to hogging bending moments. For this reason braced frames were considered in the present study.

Consider the master braced nonsway skeletal frame shown in Figure 5.1. All beams are loaded equally. The joints in this frame may be classified according to their locations, as those required to connect beams to internal columns, subframe SF1, and those required to connect beams to external columns, subframe SF2. Therefore two separate investigations are required on internal and external subframes.

The subframes SF1 and SF2 can now be shown separately, as in Figures 5.2 to 5.5. The length of the beams, and hence the position of the bending load P was selected to represent the point of contraflexure in a uniformly distributed loaded beam. Assuming that the maximum bending moment is recorded at the face of the column, the shear span / beam effective depth ratio for the load is 2365 / 400 = 5.91. The effective depth to the reinforcement, 2T25 tie bars, is 500 - 100 = 400 mm. The lever arm distance at 2.365 m was kept constant, even though it will change when plasticity is reached in the connection. The subframe SF1 (essentially symmetrical) was simulated in test series 1 and 3, and SF2 in test series 2 and 4, with and without the precast concrete proprietary slip formed hollow core floor slabs (supplied by Bison Floors, UK). This was done in order to investigate the influence of incorporating the floor slabs on the main properties of the connections in a double sided and single sided precast concrete connections shown in Figure 1.1. As can be seen the overall dimensions of these subframes indicate that they are full scale tests. It is important to have full scale test data for each of the connections shown in Figure 1.1 to compare with those derived from the isolated joint tests, and to be able to predict the behaviour

of a number of full scale frame connections from the isolated joint tests reported in Chapter 8.

Eight tests were carried out according to Table 5.1 in four test series. The schedule was organised so that the relationship between the moments and shear forces acting at the beam connection were all identical, except for the case of tests TB1(B) and TB1(C) where smaller length beams were tested in an attempt to simplify even further the full scale tests.

Four series of experimental tests were carried out as follows :-

- Test series 1 included three tests (TW1(A), TW1(B) and TW1(C)) on double sided full scale (internal) subframe SF1 assemblages with (TW1(A) and TW1(B)) including floor slabs and (TW1(C)) without floor slabs as shown in Figures 5.2 to 5.4 and incorporating two way welded plate connection (Figure 1.1(a)).
- Test series 2 included one test (TW2) on single sided slab-beam-column full scale (external) subframe SF2 assemblage as shown in Figure 5.5 incorporating three way welded plate connection (Figure 1.1(b)).
- Test series 3 included three tests (TB1(A), TB1(B) and TB1(C)) on double sided slab-beam-column full scale (internal) subframe SF1 assemblage (TB1(A)) as shown in Figure 5.2, and double sided in-situ-beam-column subframes as shown in Figures 5.6 and 5.7 incorporating two way billet connection (Figure 1.1(c)). In the test TB1(C) the RHS billet in the column and beam end plate (Figure 5.9) were not incorporated.
- Test series 4 included one test (TB2) on single sided slab-beam-column full scale (external) subframe SF2 assemblage as shown in Figure 5.5 incorporating three way billet connection (Figure 1.1(d)).

Test series	Test reference	Connection type	Subframe type	Floor slab
1	Test 1 [TW1(A)]	Welded plate	Double sided	Hollow core
	Test 2 [TW1(B)]*	Welded plate	Double sided	Hollow core
	Test 3 [TW1(C)]	Welded plate	Double sided	None
2	Test 4 [TW2]	Welded plate	Single sided	Hollow core
3	Test 5 [TB1(A)]	Billet	Double sided	Hollow core
	Test 6 [TB1(B)]$^{+}$	Billet	Double sided	In-situ infill only
	Test 7 [TB1(C)]$^{+}$	Billet	Double sided	In-situ infill only
4	Test 8 [TB2]	Billet	Single sided	Hollow core

TW = Welded plate. TB = billet.

* shear test. $^{+}$ flexural test with short length components

Table 5.1: Schedule of full-scale frame connection tests

In the tests, the subframes were subjected to vertically applied bending loads at the free end of the precast concrete cantilever beams in an attempt to simulate the pattern of gravity loading shown in Figure 5.1. A shear test TW1(B) was also carried out as shown in Figure 5.3. The frames consisted of continuous 300 x 300 mm columns, 300 x 300 mm beams spanning in x-direction, and 200 mm deep hollow core floor slabs spanning at right angles to the beams. The in-situ concrete infill placed over the top of the beams gives a composite floor beam section 500 mm deep. The compressive cube strength for the precast beam, column and beam-to-column joint concrete and grout is specified as 40 N/mm^2, for the slab as 60 N/mm^2, and for in-situ concrete infill over the top of the beams as 30 N/mm^2.

5.2 Details of beam-to-column connections

The beam-to-column connections that use steel inserts at the beam end and at the column to transfer load are considered in three parts (I Struct E, 1978):-

- as a column insert alone, transferring load to the concrete of the column
- as a beam-end detail, transferring load from the concrete of the beam, and
- as a totality, with inserts from the beam and column joined together, and the joint completed

The way in which the connection is assembled and completed affects the choice of inserts. Methods of calculation for some of the more commonly used inserts are given in the I Struct E Manual (1978). In most cases beam shear force is transferred through direct bearing between the inserts

The welded plate and billet beam-to-column connection (to be referred to as welded plate connection) used in this project study (see Figures 1.1(a) and (b)) uses a 25 mm thick, cast in mild steel, narrow beam connection plate (see Figure 5.8 and Plate 5.2) (the ISE, 1978: Narrow beam plates Type III) projecting from the end of the beam and a projecting wide section solid steel billet insert embedded in the column (see Figure 5.10, Figures 5.11(a), (b) and (c) and Plate 5.1).

The design method is used where the projecting plate cannot be fully contained in the depth of the beam (see Figure 5.12(a)). Typical applications are in the ends of the precast parts of composite beams. It is located on the vertical centre-line of the beam (see Figure 12(b)). Shear reinforcement in the beam is carried through to the end of the beam so that the insert is well contained by links. The links project above the precast section, and the precast beam is propped until its in-situ topping has reached an adequate strength. The main tension bars in the beam are taken through to the end

of the beam and adequately connected to the plate anchor bars by special links (see Figure 5.12(b)). The beam end plate bears on the projecting wide section solid billet in the column and is welded using 20 mm fillet weld (see Figure 1.1(a) and Plate 5.5).

Welding the steel inserts requires skilled labour and is a special operation to ensure that weld cooling does not cause permanent twist in the precast members.

The connection (the 100 mm gap between beam and column) is subsequently filled up to the top level of the beam with nominal $f_{cu} = 40$ N/mm^2 strength in-situ concrete using 10 mm aggregate without additives and is now called a joint (Plates 5.6 and 5.7).

The bolted billet beam-to-column connection (to be referred to as billet connection) (see Figures 1.1(c) and (d)) comprises a simply supported connection in which a cast-in bearing plate (Figure 5.9) in the beam end (Figure 5.13(a) and (b)) bears on a projecting structural hollow section in the column (Plates 5.15 and 5.17). A tie rod passes through bolt plate and billet and is connected at the top of the beam to an angle cleat bolted to the column face (Plate 5.18). The whole connection, including the inside of the RHS, is subsequently grout filled. The expanding agent "Tricosal" (1% of cement weight) is used to reduce shrinkage.

The design of the column RHS billet is based on the method outlined in I Struct E (1978) and is based on the assumption that the load is transmitted by bearing from the beam to the column. The I Struct E recommendations ignore the influence of the reinforcement in the column near the column billet. Clarke (1978) studied the influence of reinforcement on the bearing capacity of the billet. In the same study a series of tests to examine the shear capacity of steel billets of various sections cast into the columns with different reinforcement details was studied. It was

concluded that the design method based solely on the bearing strength allowed by the code was satisfactory. It was also concluded that in order to control splitting of the column below the billet sufficient links should be provided within a distance equal to the column breadth to prevent a premature failure. The billet width should not exceed one third of the column width.

5.3 Design and manufacture of precast concrete test components

Geometric and reinforcement details of the column, around the billets are presented in Figures 5.10 and 5.11 (see also Plate 5.1 for reinforcement around the solid billet for double sided test and Plate 5.15 the RHS billet for single sided test). The column size 300 x 300 mm was used throughout the experimental work. This is the minimum size required to accommodate the types of wide section column inserts under investigation. Only the height of the column was reduced from 2000 mm to 800 mm in the tests TB1(B) and TB1(C) in test series 3. Other provisions in the column were sleeves to allow the passage of continuing longitudinal reinforcement in test series 1 and 3, and two M16 dia, cast-in sockets to facilitate fixing the instrumentation. The column reinforcement contained 4T25 main bars and T12 links @ 185 mm c/c. The design ultimate axial capacity of a short column with zero moment was 2085 kN for $f_{cu} = 40$ N/mm^2 and $f_y = 460$ N/mm^2.

Geometrical and reinforcement details of the beams for welded plate and billet connections are presented in Figures 5.12 and 5.13, respectively. The ends of the beams connected to both sides of the column vary in accordance with the requirement of casting in a standard beam connection plate of 278 kN (Bison literature reference

K/278/ Figure 5.8 and Plates 5.2 and 5.3) and 260 kN (Crendon literature reference, beam end plate BA Figure 5.9 and Plate 5.16) design ultimate shear capacity, respectively for welded plate and billet connections. The beams are considered as acting compositely with the floor slabs and contained 4T20 bars, top and bottom, and T10 shear links @ 100 mm c/c. Design ultimate moment of resistance of the composite beams were 241.10 kNm ($f_y = 460$ N/mm^2, $f_{cu} = 40$ N/mm^2, partial safety factors for strength γ_m: ultimate limit state taken as 1.15 and 1.50 for reinforcement and concrete respectively, using BS 8110 simplified stress block). The design ultimate ($\gamma_m = 1.25$) and calculated ultimate ($\gamma_m = 1.0$) shear resistance were 250 and 312.5 kN, respectively

The cross section of the slabs, reinforcement details, and continuity reinforcement are presented in Figure 5.14(a), (b) and Figure 5.15, respectively. The slab units were 1200 mm nominal width by 200 mm depth and 1000 mm long precast prestressed hollow core units (Roth type), each of which contained cut outs (see Plate 5.9) to permit the placement of reinforced (T12 transverse bars) in-situ concrete infill. The thickness 200 mm of the slabs represents the most widely used thickness in precast concrete structures. The slab units contained 33 no. 5 mm diameter crimped prestressed wires. The ultimate design sagging moment and shear resistance of the slabs were 125.6 kNm and 162.10 kN, respectively (Bison literature reference).

5.4 Horizontal ties for building integrity

The specific requirements relating to ties in precast concrete structures are given in BS 8110, Part 1, clause 5.1.8. Tie passing through precast columns (double sided tests,

see Plate 5.8) are fed through oversized sleeves (usually two to three times the diameter of the tie bars) (Elliott, 1996a) and later concreted in. In the single sided tests the tie steel passes outside the face of the column, rather than through it due to practical difficulty of forming these sleeves. This means that the width of the beam, over which the tie bars are placed, must be greater than the width of the column around which they will pass. Otherwise, part of the floor slab has to be broken out to allow the ties to be bent and cranked around the corners of the column. In the tests carried out, the width of the beam is equal to the width of the column. The only remaining option was to break out the top corner of the floor slabs to place the cranked 45° tie bars (see Plate 5.13). The tie steel is implicitly provided for precast frame stability, and not for the sole purpose of these tests.

The tie steel was designed according to BS 8110, Part 1, clause 3.12.3.4.2 assuming that the structure was 5 storeys in height, and the floor dead (g_k) and live (q_k) loads were each 5.0 kN/m^2, respectively. The spans for the beam and slabs were both taken as 6 m.

Thus, the basic tie force F_t is :-

$$F_t = (20 + 4n_o) = (20 + 4 \times 5) = 40 \text{ kN / m} \qquad Eq.\ 5.1$$

where n_o is the number of storeys in the structure, and the modified tie force F_t' (to allow for larger spans and greater floor loads) is given by :-

$$F_t' = \frac{(g_k + q_k)}{7.5}\frac{l_r}{5}F_t = \frac{(5+5)}{7.5}\frac{6}{5}40 = 64 \text{ kN/m run} \qquad Eq.\ 5.2$$

Slab tie steel A_s required by the larger requirement F_t' is :-

$$A_s = \frac{64 \times 10^3}{460} = 139 \text{ mm}^2/\text{m}$$

$\therefore$ Use T12 @ 600 c/c (188 mm^2) shown in Figure 5.15.

If the beam is supporting 6 m long slabs on each side, then the collective tie force at the beam is :-

$$F_t' \text{ per beam} = 64\left(\frac{6}{2} + \frac{6}{2}\right) = 384 \text{ kN}$$

$$A_s = \frac{384 \times 10^3}{460} = 834.8 \text{ mm}^2$$

$\therefore$ Use 2 no T25 bars (982 mm^2) shown in Figure 5.15.

Note: $\gamma_f = 1.0$ for this situation

5.5 Concrete mixes

10 mm single-sized Trent River Valley coarse (gravel) uncrushed aggregate specified in Table 3 of BS 882: 1992 were used in all the test carried out. The fine aggregate consisted of uncrushed sand complying to medium grading zone of BS 882: 1992 Table 4. The grading of the coarse and fine used in all tests carried out are presented in Tables A5.1.1 and A5.1.2, respectively in Appendix 5.1. Ordinary Portland cement complied with the standard requirements specified in BS 12: 1983 was used in all the tests.

The correct quantities of cement, aggregates and water were batched and mixed using a 0.1 m^3 capacity laboratory mixer. It was not big enough to cast a beam or column at once. Totally 13 mixes were cast for the full scale subframe shown in Figure 5.2. All mix proportions used in the tests are presented in Tables A5.2.1 to A5.2.4 in Appendix 5.2, together with corresponding slump values.

5.6 Test rig

A test rig (Figure 5.16 and Plate 5.11) was designed according to BS 5950: 1985 to accommodate the test subframes. The rig consists of two parallel tie back steel frames aligned perpendicular to the test subframes. Both of the tie back frames are capable of carrying 600 kN working load at the centre of the horizontal 250x150x16 RHS cross beam between two 152x76x10 channel-stanchions. This was calculated on the basis of the available number of the holding down bolts. Vertical bending loads at the free ends of the concrete cantilever beams of the test subframes were applied incrementally through hand operated hydraulic jacks and measured using 200 kN capacity electrical resistance load cells. The jacks were clamped to the cross beams as shown in Plate 5.12. The beams were loaded so as to provide in-plane bending only and to keep the continuous column in a vertical plane. This induced the correct bending moments and shear forces in the connections by keeping the lever arm constant.

Two semi-roller load spreaders were used underneath the load cells to make sure that the positions of the applied loads were kept constant.

Two 100 kN capacity load cells were also positioned beneath the end of the beams as shown in Figure 5.16(c) and used to measure the self weight of the test

components in order to find out the initial bending moment of the connections due to self weight.

For single sided tests the test rig was modified by using two 120 x 120 x 10 angles for diagonal bracing as shown in Plate 5.14 for the horizontal column reaction (see Figure 5.5) in test series 2 and 4.

5.7 Test procedure

The column was lifted vertically using a crane and a pin passing through the top sleeve of the column. It was placed on to the strong laboratory floor on smooth casting face. It was decided to cast the bottom face of the column as smooth as possible before casting. The length of the mould available in the laboratory was longer than the required overall height of the column by 400 mm. A 25 mm thick timber plate was used between the free end of the mould and the top of the column. This end could be move during casting and vibrating the fresh concrete. Thus, one of the ends of the mould was chosen as reference for the bottom face of the column to make sure that this face is smooth enough to keep the column in its vertical position after erecting.

The column was permanently braced against in and out of plane movements to ensure stability during the replacement of the beams and slab units as shown in Plate 5.4. The bracing used two 630 mm long 120x120x16 angles, four 690 mm long "Acrow SGB" props (two for each plane). Four 100x100x5x900 mm long RHS were used to support the props to transfer their loads acting on to the laboratory floor.

The beams were placed at one end on the column connection and at the other were seated on to a timber plate support were placed on to the load cell. The load cell was supported by a large travel hydraulic jack to lift the free end of the beam into the

correct horizontal position (see Plate 5.12) before welding the ends of the beam unclamped to prevent twisting during the welding of welded plate connections. The beam connections were welded to the column connections using the fillet weld (NOVOF IL 70 SG2, 1.2 mm wire) made using covered electrodes complying with BS 639 and steel complying with BS 4360 obtained from Table 36 for mild steel. (It was carried out by a professional welder from the Engineering Faculty Workshop.) The welding was done slowly to prevent twisting because of high temperature during the welding. After each layer of weld it was left to cool before for the next run. Plate 5.5 shows the welding region of the connections in test series 1. Beam 2 had a 5 mm initial twisting (out of plane) before welding. The imperfections were re-measured after welding, and the maximum imperfections (twisting) were about 7 and 8 mm for the beams 1 and 2, respectively in test series 1. The throat thicknesses and the leg lengths welds were measured using weld measuring apparatus and a small steel ruler in the narrow connection regions (see Appendix 5.4).

During joint concreting or grouting, the ends of the beams seated on to the billets projecting from the column face were held providing timber formwork for both sides of the column (for double sided connections) and were clamped using large G clamps, as shown in Plates 5.6 and 5.18, respectively for welded plate and billet connections.

The beam-to-column joints were concreted using mix proportions presented in Table A5.2.1. Plate 5.7 shows the joints after completion. They were concreted without vibrating, but tamped carefully.

Two plastic tube sleeves passing through the column were removed and 2T25 (grade 460) longitudinal tie bars with steel strain gauges on were passed through the

open sleeves and were placed over the beams. The bars were tied to the shear links projecting from the beams. New measurements were taken after positioning the bars, i.e. centre distance of the bars from the top of the beams. It was not possible to measure from the top of the beams. Owing to some casting problems the top edges of the beam had a 25 mm wide rebate, which reduced the bearing distance between the slab units and the beams from 75 mm to 50 mm. The bottom edges of the beams were used as reference points to measure the distances required. Plate 5.8 shows the location of the 2T25 tie bars and steel strain gauges.

Trestles, timber shims and a RHS cross beam were provided to support the slab units temporarily. These units were then seated at one end on to the beams with a bearing distance of 50 mm and the remote end on to the timber shims that were placed on the top of the RHS cross beam seated on to the trestles (see Plate 5.9). The horizontal position of the slab units was adjusted using small timber packs. The ends of the slab-to-slab joints and sides of the column at the bottom level of the slabs were moulded to cast slab-beam-column in-situ concrete.

The transverse reinforcement as placed into the opened cores of the slabs as shown in Figure 5.15 (see Plate 5.10).

The construction was completed filling the gaps between the slabs, over the top of the beams and around the column using the slab-beam-column in-situ concrete, to the mix proportions presented in Table A5.2.1. The entire subframe was then coated with a brittle white wash coat to detect the formatting cracks (Plate 5.11). Testing dates were determined by the cube strength of the in-situ concrete.

The same general procedure was followed for the remainder of the tests.

5.8 Instrumentation and measurement

Figure 5.17(a) presents the layout of the different measuring instruments that were used in tests

The functions and locations of the instruments used are presented in details in Tables A5.3.1 to A5.3.5 of Appendix 5.3.

The important measurements were:-

(a) Vertical deflections of the beams

(b) crack width δ_T at boundaries of the slab, beam and column

(c) compressive deformation δ_B in the compression zone

(d) strain in the tie bars in the tension zone

(e) strain in the concrete in the compression zone

For one of the main tests e.g. test TW1(A) twenty deflection transducers (potentiometric type), called "POTs", were used to measure the vertical deflections, crack width and compressive deformation. All of the offsets were measured at the beginning of each test after the attachments of the POTs were completed

Six 30 mm concrete strain gauges (type: PL - 30-11, gauge resist: 120 ± 3 Ω, gauge factor: 2.12) and ten 10 mm steel strain gauges (type: FLA - 10-11, gauge resist: 120 ± 3 Ω, gauge factor: 2.13) as shown in Figures 5.17(b) and (c) were used to record the strains.

All signals from the sensors were automatically recorded using a model 3535D Scorpio data logger. The signals were then linearized by inputting the respective calibration factors (the load cells were calibrated before carrying out the tests) for the various sensors into the data logger and the results were displayed directly in the units

of millimetre for POTs and kN for the load cells. The data logger was linked to an PC and operated using the proprietary software, Scorpio through Windows. This package allowed the live plotting of the data during each test. Subsequently, the logged data in the hard disk was transferred into a floppy disk and the data was processed using the software package Excel (version 5.0) through Windows.

5.9 Material testing

5.9.1 Reinforcement

For the stability tie bars for each test, two T25 x 1000 mm long hot-rolled deformed high tensile bars were cut at random from the lengths used in the tests. They were tested in accordance with the requirements of BS EN 10 002-1: 1990 for the yield stress and elastic modulus in the 2000 kN INSTRON 8500 testing machine. Results for four test series are presented in Table A5.4.1 in Appendix 5.4.

5.9.2 Tie rods

Tensile tests were carried out on M16 diameter grade 8.8 tie rods used in the bolted billet connections. Two M16 x 400 mm long tie rods were cut at the random from the lengths used in the tests and were tested in accordance with the requirements of BS 18: 1987 to estimate the shear capacity P_s from the tensile load. Testing was carried out using a ZWICK 1484 testing machine. Results are presented in Appendix 5.4.

5.9.3 Concrete

Slump testing (to BS 1881, Part 102) was carried out to ensure uniformity of workability of the mix. The desired slump measurement for precast units is between 50 and 100 mm. Actual results are given in Tables A5.2.1 to A5.2.4 in Appendix 5.2.

Compressive strength tests (to BS 1881, Part 116) were carried out on 100 mm size cubes which were cast simultaneously with the beam and column specimens, and with the infill concrete. The strength of the latter were used to dictate the testing date. All results are shown in Tables 5.2 to 5.5.

5.10 Prediction of collapse load

The predicted collapse load was calculated according to the simplified stress block of BS 8110 :1985 with safety factor γ_m taken as 1.0 using the internal forces induced in the connections at the column face. The maximum hogging bending moment of the connections was predicted at the column faces from the internal forces presented in Figures A5.4.1 and A5.4.2 in Appendix 5.4 as:-

For welded plate connection with slabs:

$$x = \frac{(F_t' + F_{wt})}{0.67 f_{cu} b} \times 10^3$$

x is the depth of the stress block (mm), from the condition of internal forces to be in equilibrium (see Appendix 5.4).

where

F_t' is the total tensile yield load (kN) in the 2T25 longitudinal tie bars tested

F_{wt} is the total fillet weld tensile yield load (kN). The weld length and throat thickness was measured on completion of the welding.

f_{cu} is the actual compressive cube strength of beam-to-column joint concrete at test day (N/mm^2)

b is breadth of the section = 300 mm

The predicted moment was found as:-

$$M_{pred} = F_t'\left(400 - \frac{1}{2}x\right)10^{-3} + F_{wt}\left(200 - \frac{1}{2}x\right)10^{-3} \text{ in (kNm)} \qquad Eq.5.2$$

For welded plate connection without slab:

$$x = \frac{F_{wt}}{0.67 f_{cu} b} \times 10^3$$

$$M_{pred} = F_{wt}\left(200 - \frac{1}{2}x\right)10^{-3} \qquad Eq.5.3$$

For billet connection with slabs:

$$x = \frac{(F_t' + P_s)}{0.67 f_{cu} b} \times 10^3$$

$$M_{pred} = F_t'\left(400 - \frac{1}{2}x\right)10^{-3} + P_s\left(300 - \frac{1}{2}x\right)10^{-3} \qquad Eq.5.4$$

where

P_s is the shear force in the tie rod tested

f_{cu} is the actual compressive cube strength of beam-to-column joint grout at test day (N/mm^2)

The predicted moments were calculated in this way by substituting corresponding F_t', F_{wt} and P_s values in the relevant equation above for each test reducing to a function of f_{cu}. The calculated predicted moments are presented in Tables 5.6 to 5.9. with F_t', F_{wt}, P_s and f_{cu} values.

The predicted collapse load was found as:-

$$P = \frac{M_{pred}}{2.365} \text{ (ignoring self weight of test specimens)} \qquad Eq.5.5$$

where 2.365 (0.765 in tests TB1(B) and TB1(C)) is the lever arm distance from the face of the column to the centre of the applied load.

The internal forces have been simplified by ignoring criteria such as shear friction and tension stiffening. The strain in the tie bars and that in the adjacent concrete (assuming perfect bond) was assumed that they were equal up to failure.

5.11 Test monitoring and loading history

Each test was monitored by the live plotting of the applied bending load versus crack opening, beam-to-column joint compressive deformation, and concrete and steel

strains. The performance of the connection was viewed on a PC monitor using the live results during the loading.

The loading scheme was aimed at simulating the cyclic action of the gravity force on a precast concrete skeletal frame. This action causes hogging bending moment to the beam-to-column connections.

At the beginning of the tests, the first recording scan was taken soon after the slab units' temporary supports were removed. The aim of this scan was mainly to record the initial bending load at the free end of the beams due to the self weight of the test specimens. The second scan was taken as soon as the load cells used at the underneath of the free ends were removed to record the initial deflections.

The bending load was applied in four reversible cycles prior to loading monotonically to failure. The cyclic tests were performed to measure reductions in stiffness with increasing damage. The first three cycles (three cycles were chosen as being the least number) were applied in increments of 5 kN up to 30% (Mahdi, 1992 showed major changes in behaviour at about 30% of ultimate load or moment) of the predicted failure load (see later Figure 6.1). The fourth cycle was applied to 50% (Behaviour when normalised with respect to ultimate values there is a marked change at about 0.47 x ultimate load or moment (Minutes of 4th Concrete Structures Working Group WG1 Meeting, Graz, Austria, 15 December 1995) of the load with 10 kN load increment (see later Figure 6.1). At the end of the each cycle, at load zero level (load off), a scan was taken to calculate permanent deflections. When the monitored deflections indicated the onset of non-linearity, the load increments were reduced from 20 to 10 then 5 kN in the last cycle. Between any two successive increments a visible check was carried out on cracks in the critical zones of the subframe, and the stroke of

the POTs and jacks. Where these were exceeded a scan was taken and the appropriate POT was reset followed by a further scan and the resumption of the loading.

It was decided to measure the flexural stiffness of the connections at the bending moment in the connections at the face of the column M_{con} ranging from 30 and 50 per cent of the M_{pred}. These limits have also been used at Tampere University of Technology (Finland). Because the stiffness decreases with an increase in moment, the moment at which the stiffness has been determined should always be stated. Repeated loading and unloading reduces the effect of the tensile stiffness of the floor slabs where cracks occur at low loads and give an artificially low stiffness so that the moment-rotation curve on second, third, fourth and final loading exhibits only small curvature.

The test procedure was to apply load increments until the joints were not capable of supporting any further bending load.

5.12 Calibration of load measuring equipment

Load cells were calibrated in the Dennison M/C testing machine which was in turn calibrated for accuracy and certificated to National Physical Laboratory Standards annually by an independent Testing Organisation.

	Specified cube (28 day) strength (N/mm^2)	Actual cube strength (N/mm^2) (at testing)		
		TW1(A)	TW1(B)	TW1(C)
Column	40	56.3	56.3	56.3
Beam 1	40	54.9	54.9	54.9
Beam 2	40	50.4	50.4	50.4
Beam/column joint	40	45.4	45.4	45.0
Slab/beam/column in situ	30	33.8	33.8	N/A

Table 5.2: Specified and average compressive cube strengths in test series 1

	Specified cube (28 day) strength (N/mm^2)	Actual cube strength (N/mm^2) (at testing)
		TW2
Column	40	57.3
Beam 1 (Ready mix)	40	44.5
L beams	40	56.1
Upstand	40	53.3
Beam/column joint	40	45.0
Slab/beam/column in situ	30	39.3

Table 5.3: Specified and average compressive cube strengths in test series 2

	Specified cube (28 day) strength (N/mm^2)	Actual cube strength (N/mm^2) (at testing)		
		TB1(A)	TB1(B)	TB1(C)
Column	40	38.3	38.7	38.7
Beam 1	40	50.3	52.0	48.4
Beam 2	40	48.4	52.0	48.4
Beam/column joint grout	40	46.4	51.9	51.9
Slab/beam/column in situ	30	27.8	32.4	32.4

Table 5.4: Specified and average compressive cube strengths in test series 3

	Specified cube (28 day) strength (N/mm^2)	Actual cube strength (N/mm^2) (at testing)
		TB2
Column	40	45.4
Beam 1 (Ready mix)	40	34.2
L beams	40	34.2
Upstand	40	34.2
Beam/column joint grout	40	41.8
Slab/beam/column in situ	30	38.7

Table 5.5: Specified and average compressive cube strengths in test series 4

	M_{pred} (kNm)	F_t' (kN)	F_{wt} (kN)	f_{cu} (N/mm^2)
TW1(A)	$\left(309.84 - 2599.59\frac{1}{f_{cu}}\right)$	526.91	495.36	45.4
TW1(B)	N/A	526.91	495.36	45.4
TW1(C)	$\left(99.07 - 610.40\frac{1}{f_{cu}}\right)$	N/A	495.36	45.0

F_t' tensile force in stability ties (tested)

F_{wt} tensile force in fillet weld (measured)

f_{cu} cube strength of joint concrete (on test day)

Table 5.6: Predicted moments of the connections in test series 1 using simplified stress block in BS 8110 and forces, F_t' and F_{wt}, given in the table

	M_{pred} (kNm)	F_t' (kN)	F_{wt} (kN)	f_{cu} (N/mm^2)
TW2	$\left(294.00 - 2402.09\frac{1}{f_{cu}}\right)$	487.31	495.36	45.0

Table 5.7: Predicted moment of the connection in test series 2 using simplified stress block in BS 8110 and forces, F_t' and F_{wt}, given in the table

	M_{pred} (kNm)	F_t' (kN)	P_s (kN)	f_{cu} (N/mm^2)
TB1(A)	$\left(219.34 - 809.98\frac{1}{f_{cu}}\right)$	481.56	89.07	46.4
TB1(B)	$\left(236.34 - 935.12\frac{1}{f_{cu}}\right)$	524.06	89.07	51.9
TB1(C)	$\left(221.22 - 823.34\frac{1}{f_{cu}}\right)$	486.25	89.07	51.9

F_t' tensile force in stability ties (tested)

P_s shear force in the tie rod (tested)

f_{cu} cube strength of joint grout (on test day)

Table 5.8: Predicted moments of the connections in test series 3 using simplified stress block in BS 8110 and forces, F_t' and P_s, given in the table

	M_{pred} (kNm)	F_t' (kN)	P_s (kN)	f_{cu} (N/mm^2)
TB2	$\left(220.45 - 817.86\frac{1}{f_{cu}}\right)$	484.33	89.07	41.8

Table 5.9: Predicted moment of the connection in test series 4 using simplified stress block in BS 8110 and forces, F_t' and P_s, given in the table

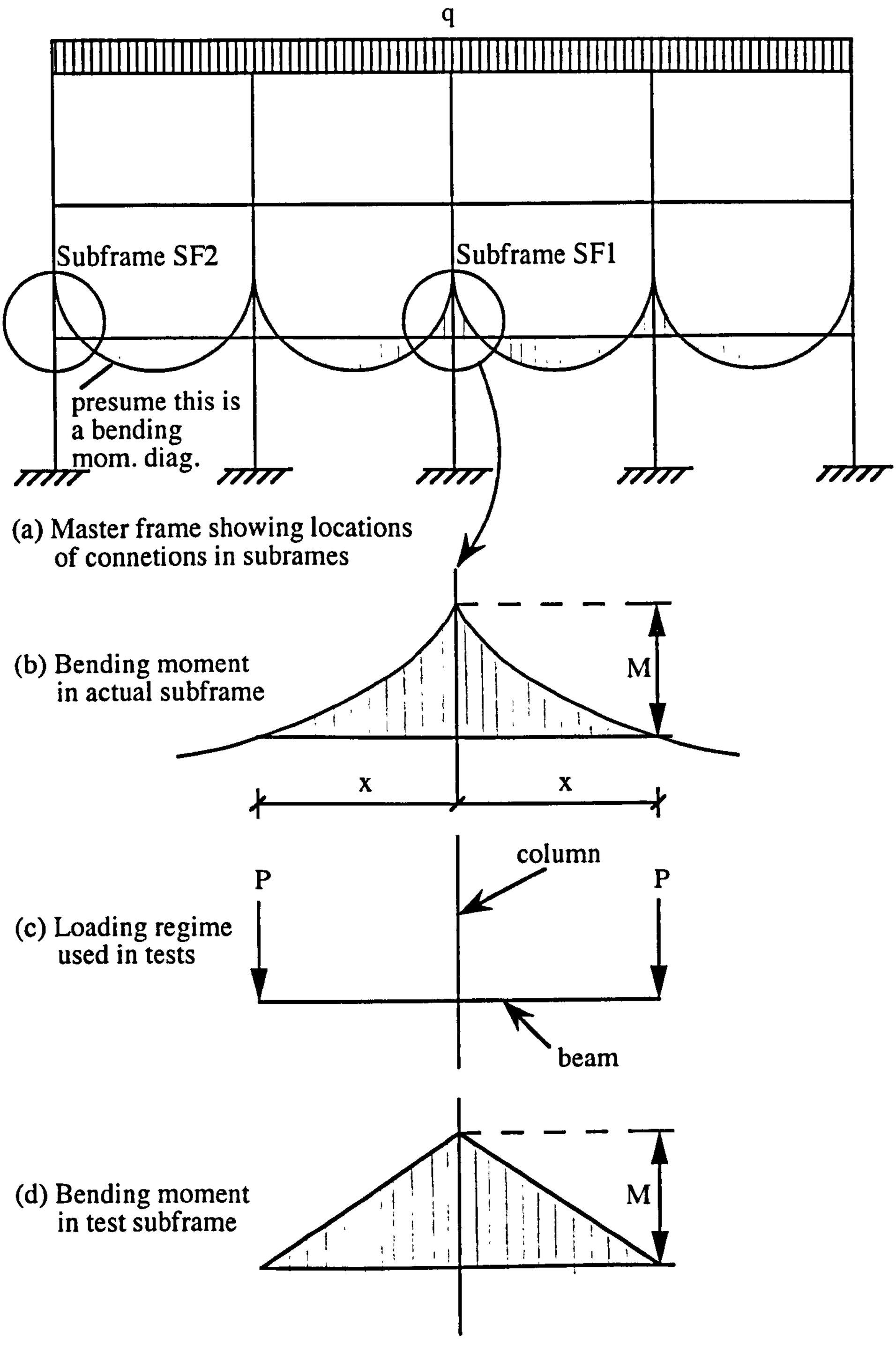

Lever arm used in these tests was x = 2.515 m. The difference between the parabolic BM diag. above and the triangular one used in the test is slight.

Figure 5.1: Location of connections in the moment resisting frame

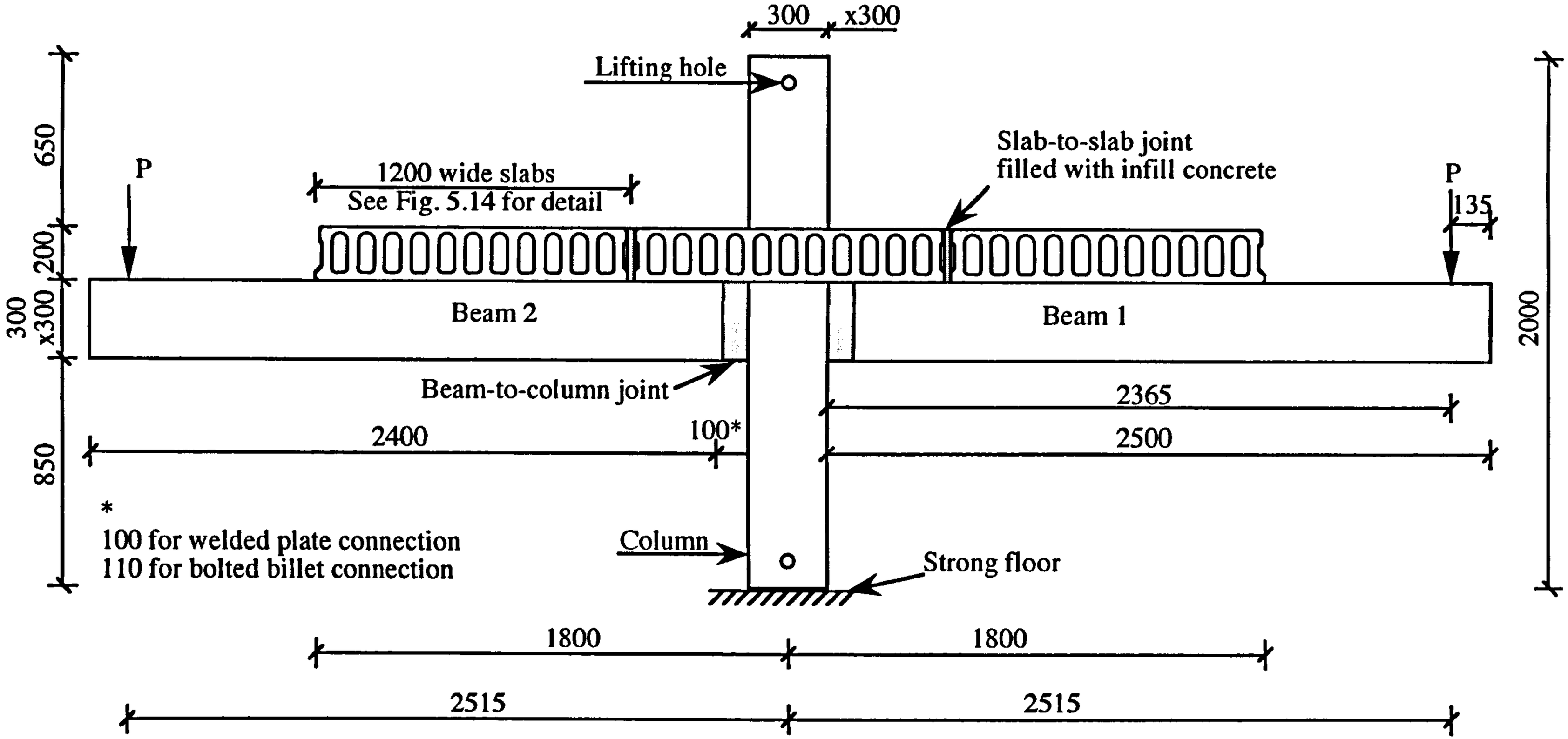

Figure 5.2(a): Front elevation of subframe SF1 with floor slabs for test series 1-TW1(A) and test series 3-TB1(A)

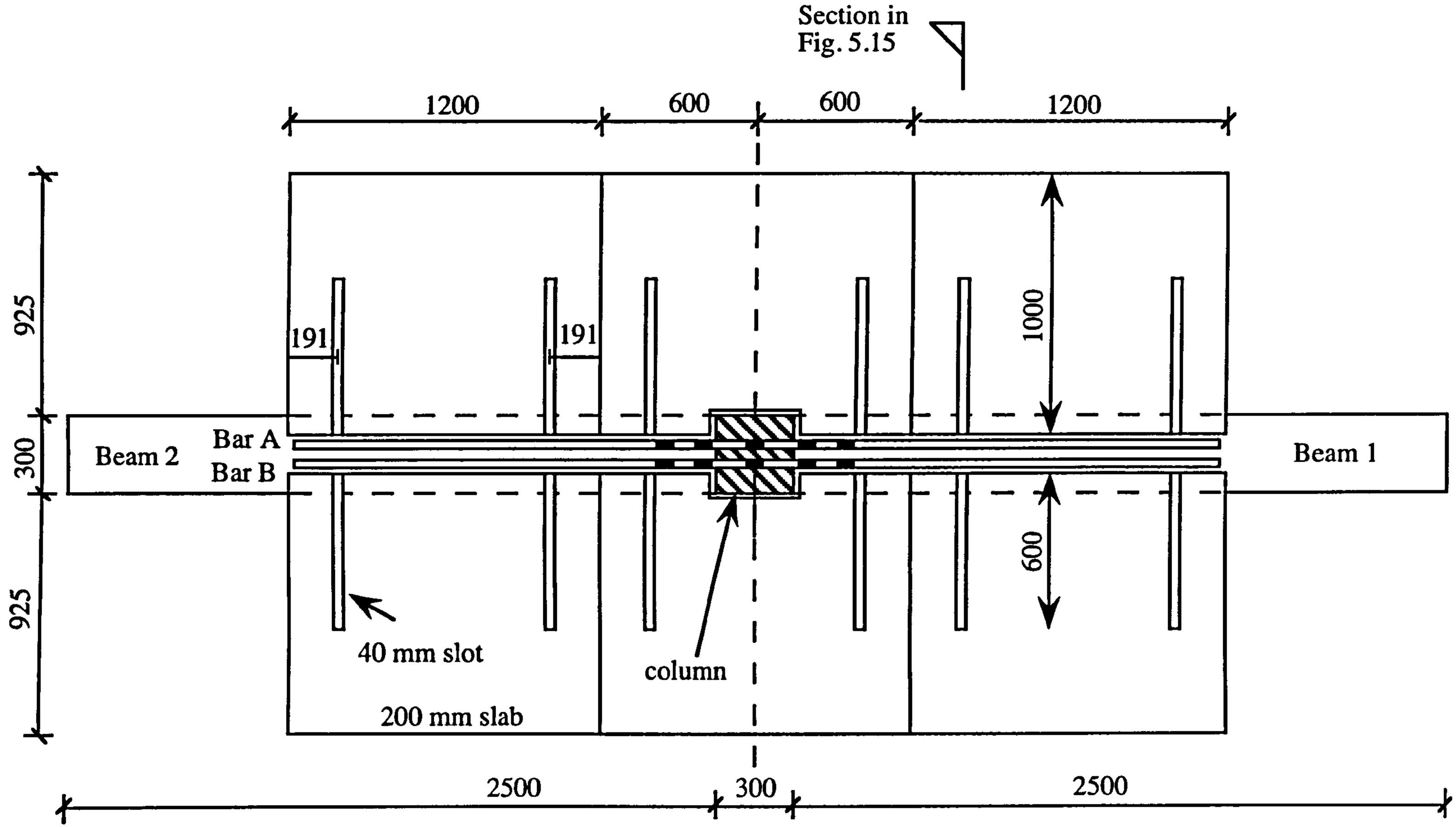

Figure 5.2(b): Plan view of subframe SF1 with floor slabs

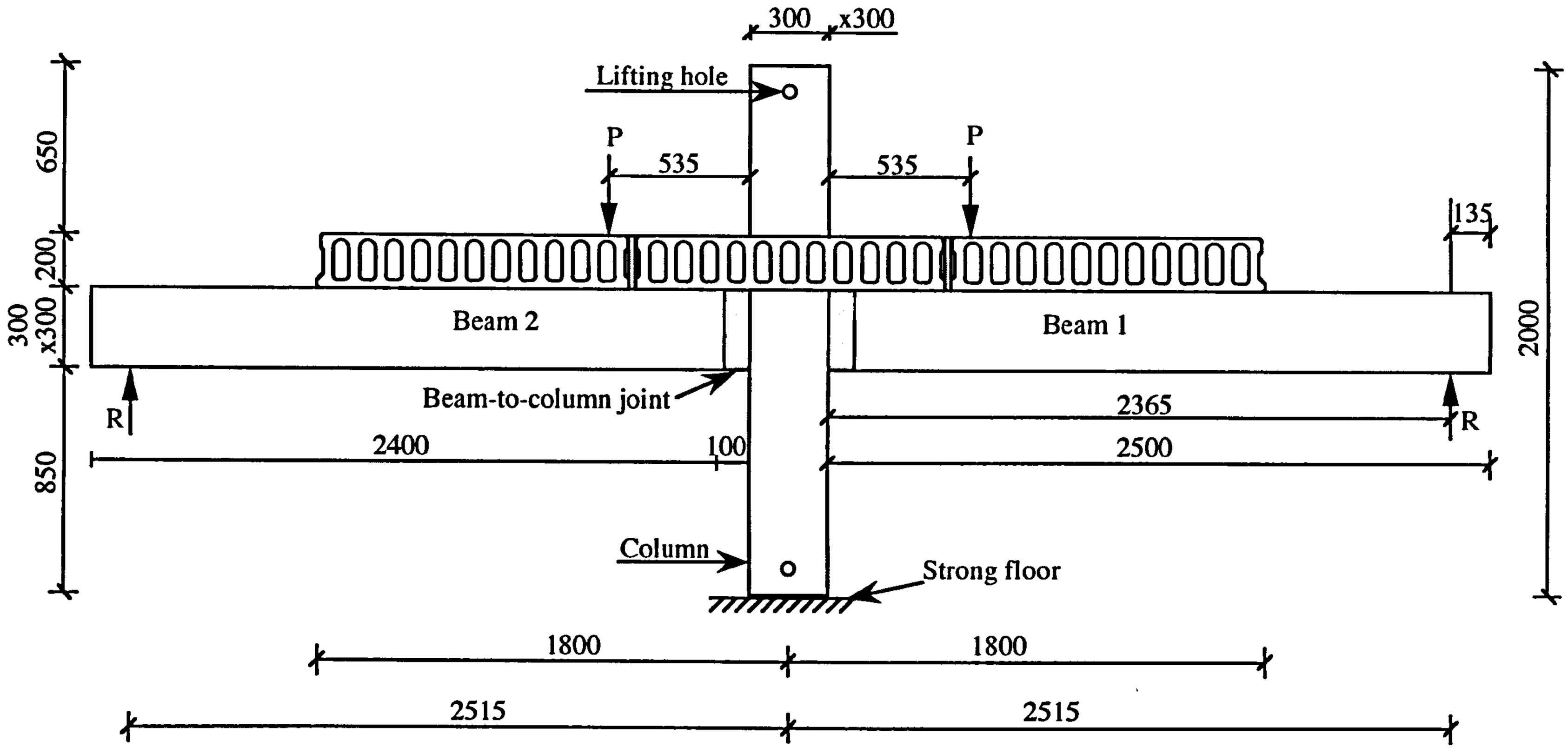

Figure 5.3: Front elevation of subframe SF1 with floor slabs for test series 1-TW1(B)

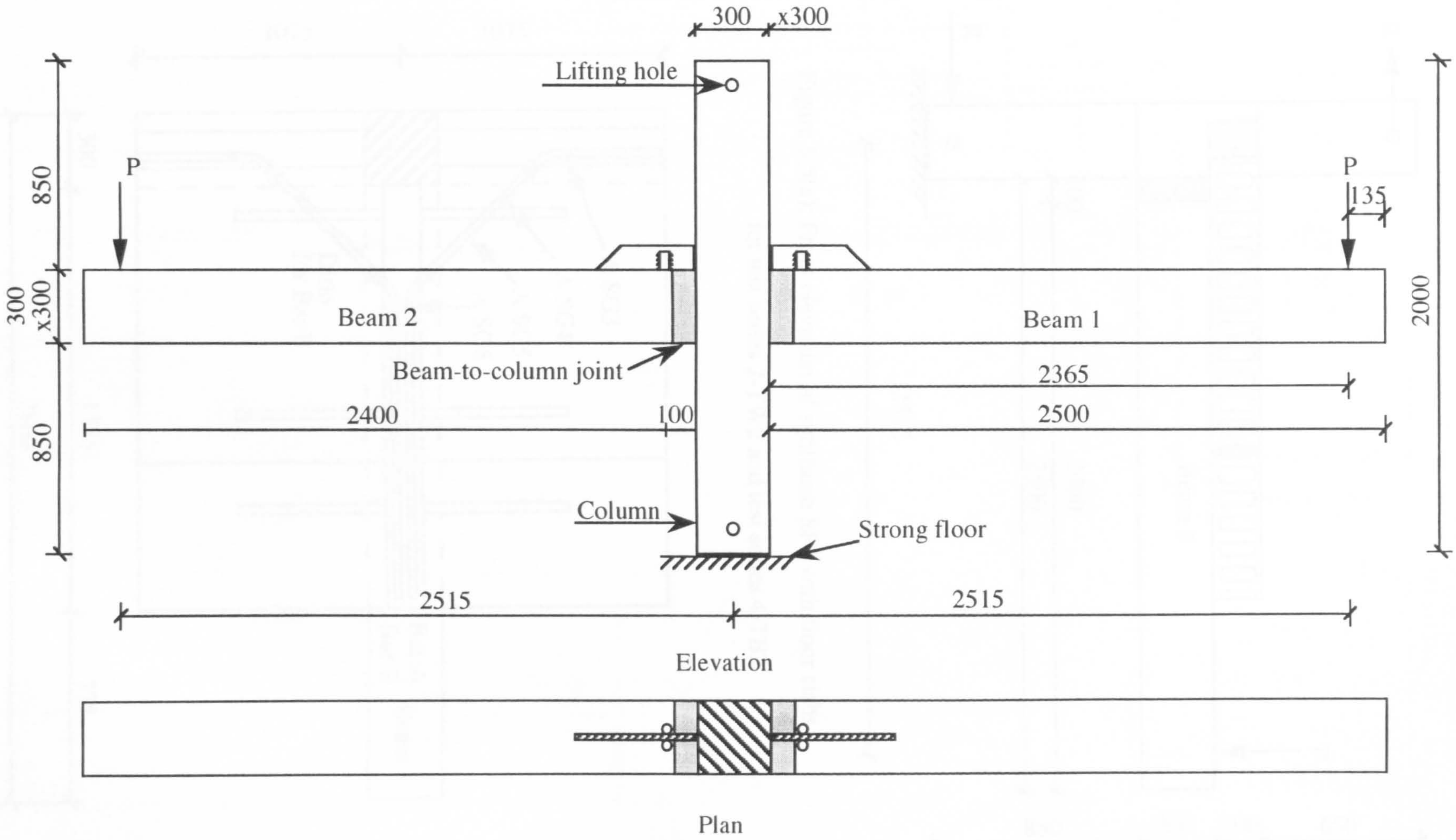

Figure 5.4: Subframe SF1 without floor slabs for test series 1-TW1(C)

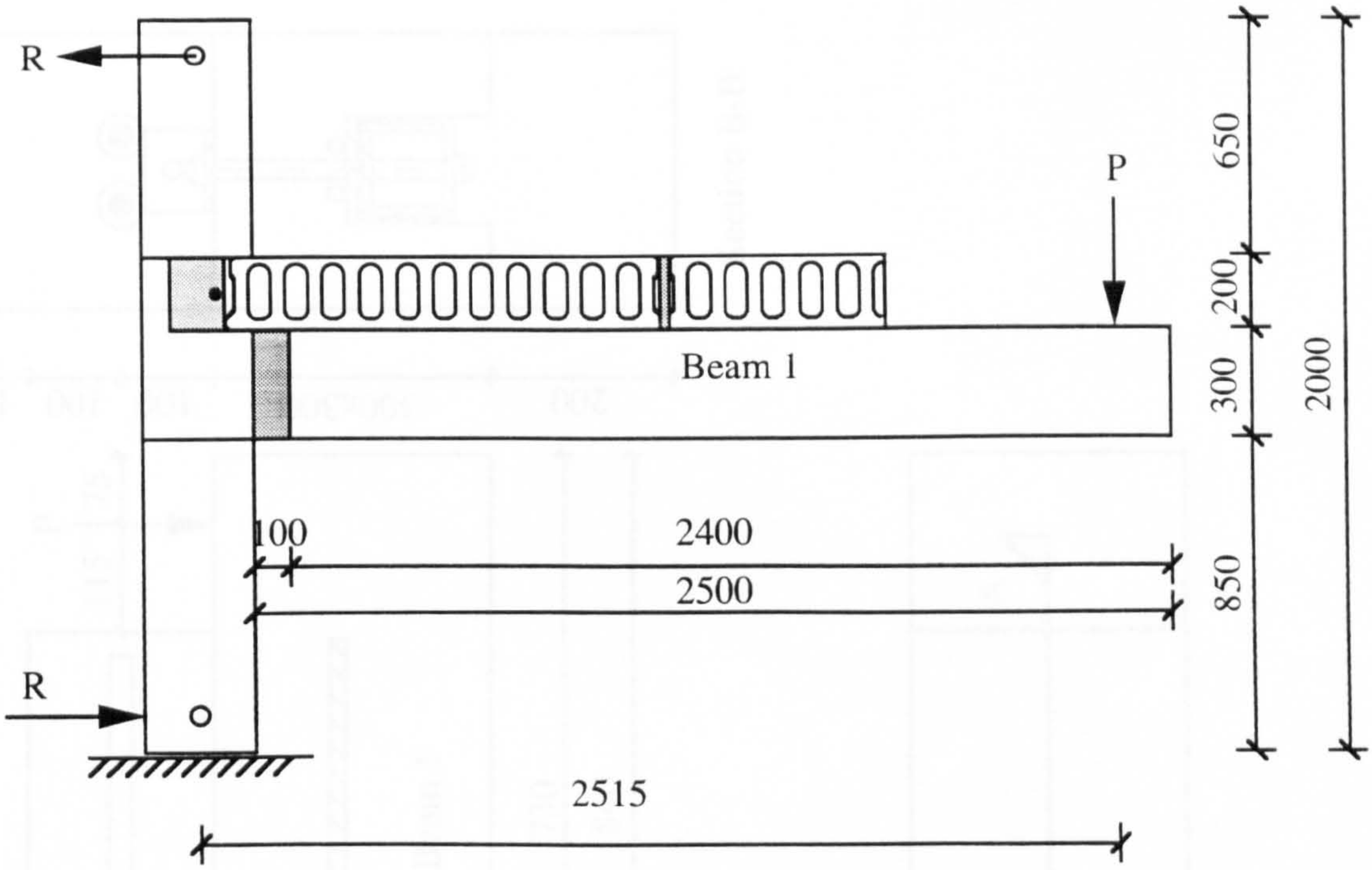

Figure 5.5(a): Front elevation of subframe SF2 with floor slabs

for test series 2-TW2 and test series 4-TB2

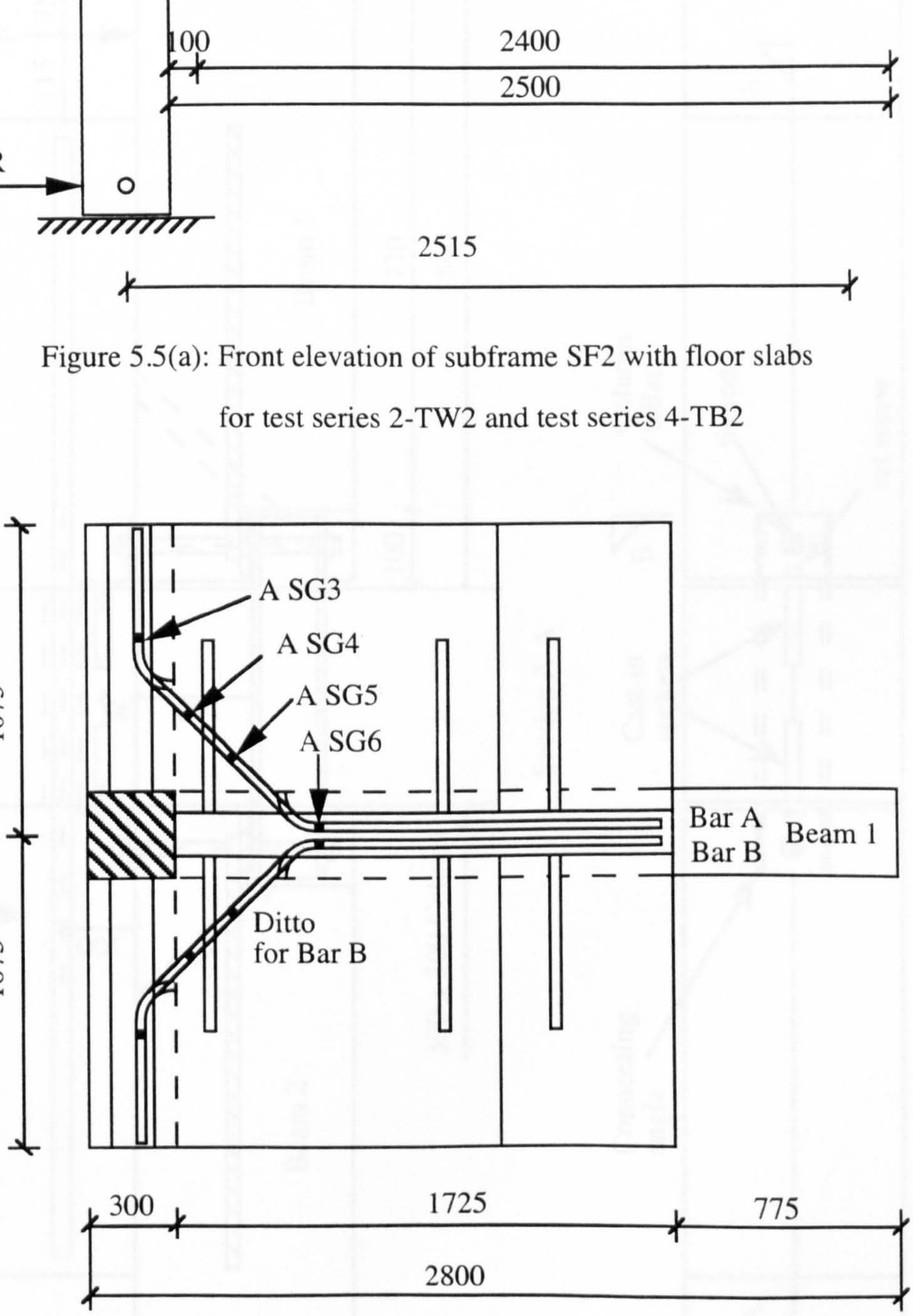

Figure 5.5(b): Plan view of subframe SF2 with floor slabs

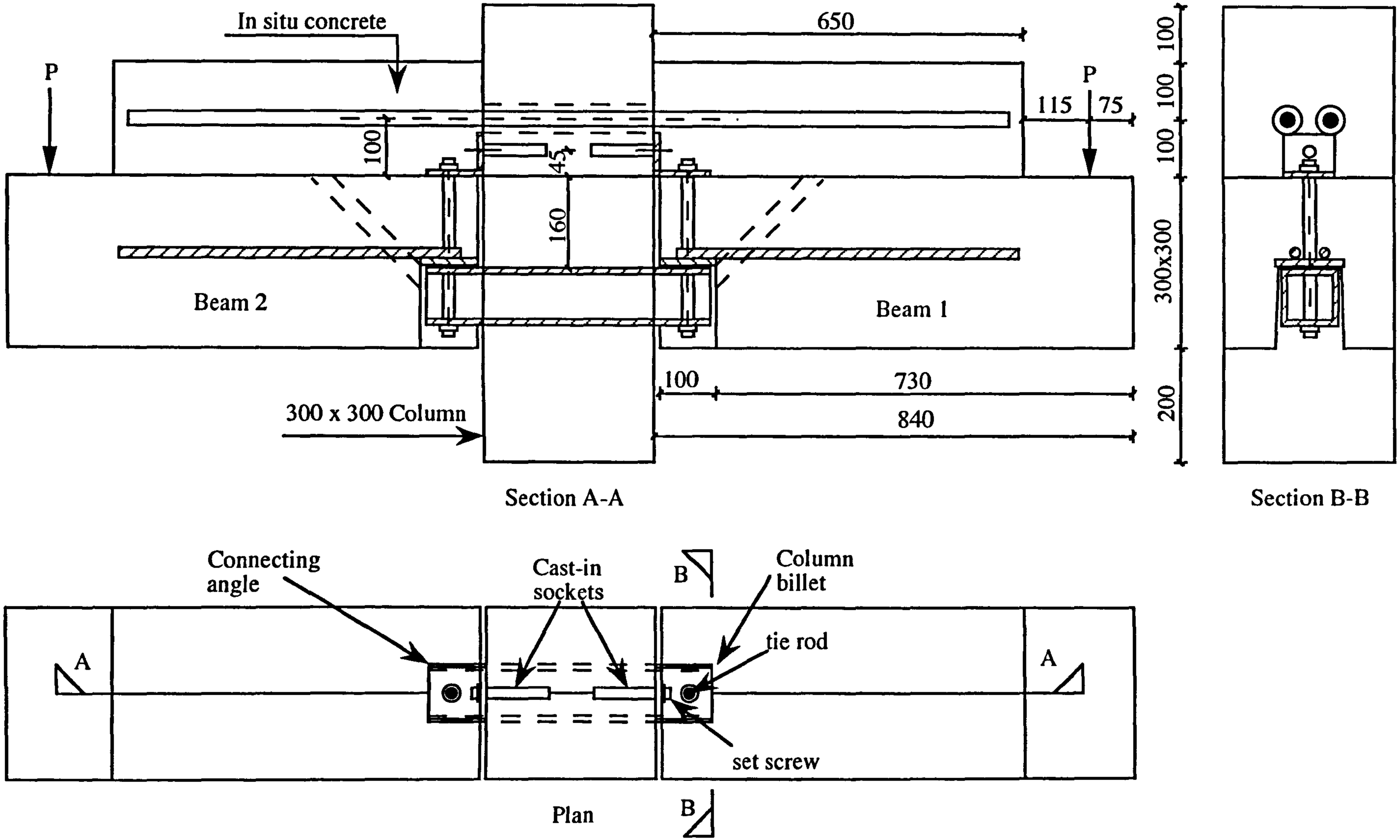

Figure 5.6: Test series 3-TB1(B)

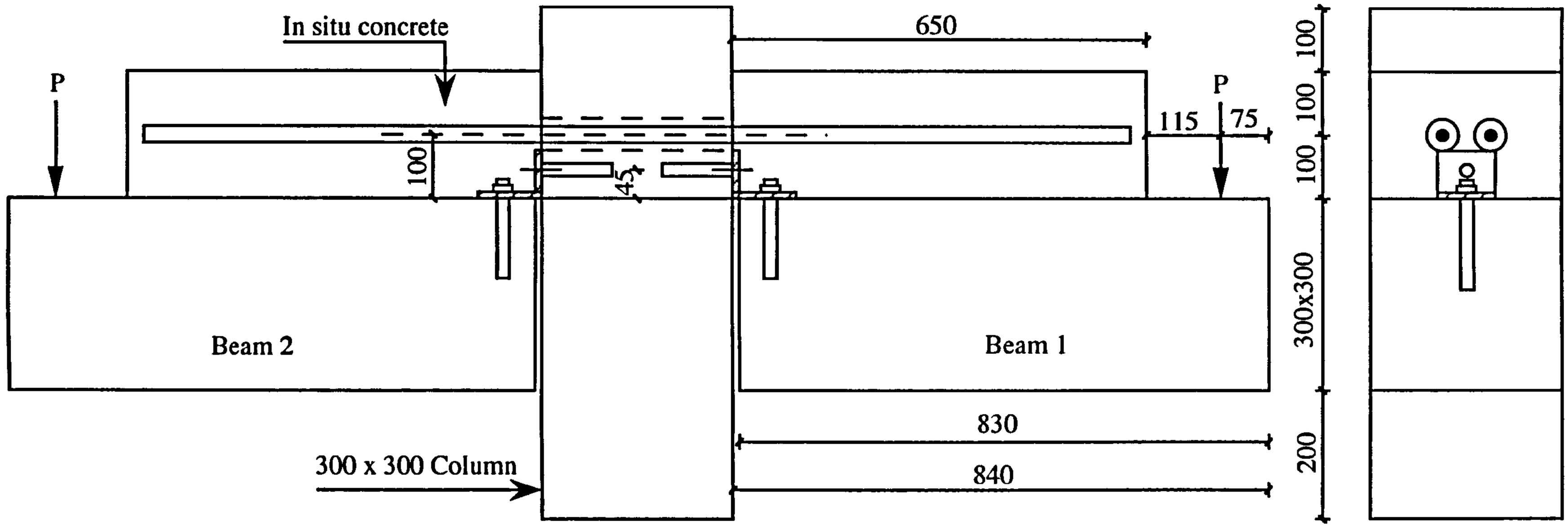

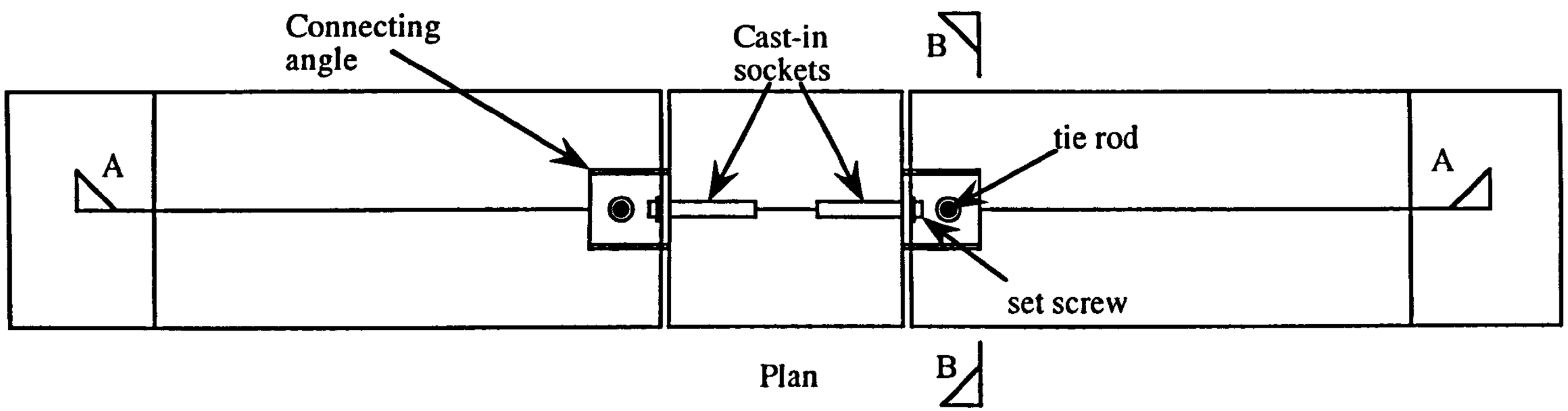

Figure 5.7: Test series 3-TB1(C)

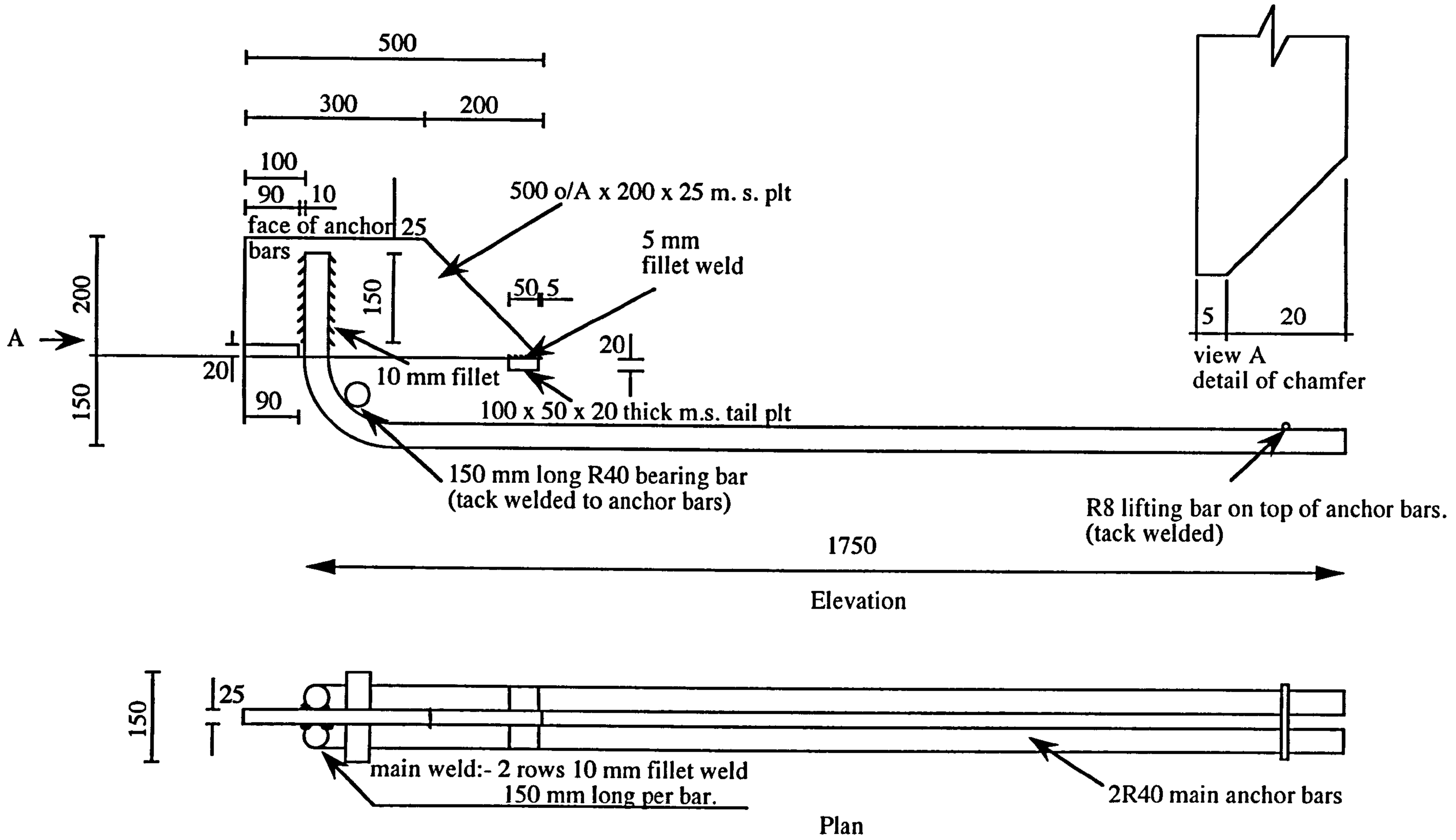

Figure 5.8: Details of standard beam connection plate

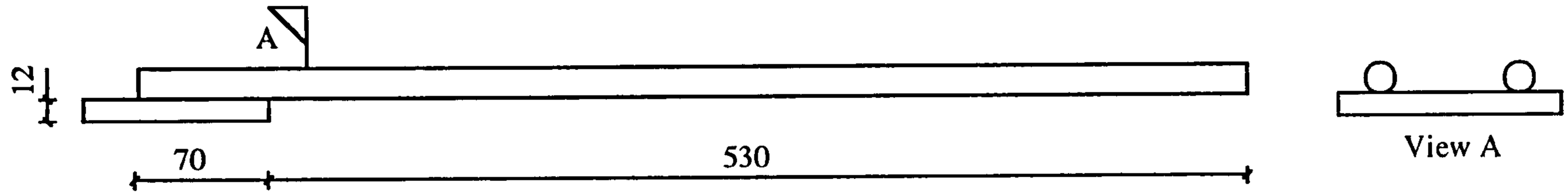

Elevation

View A

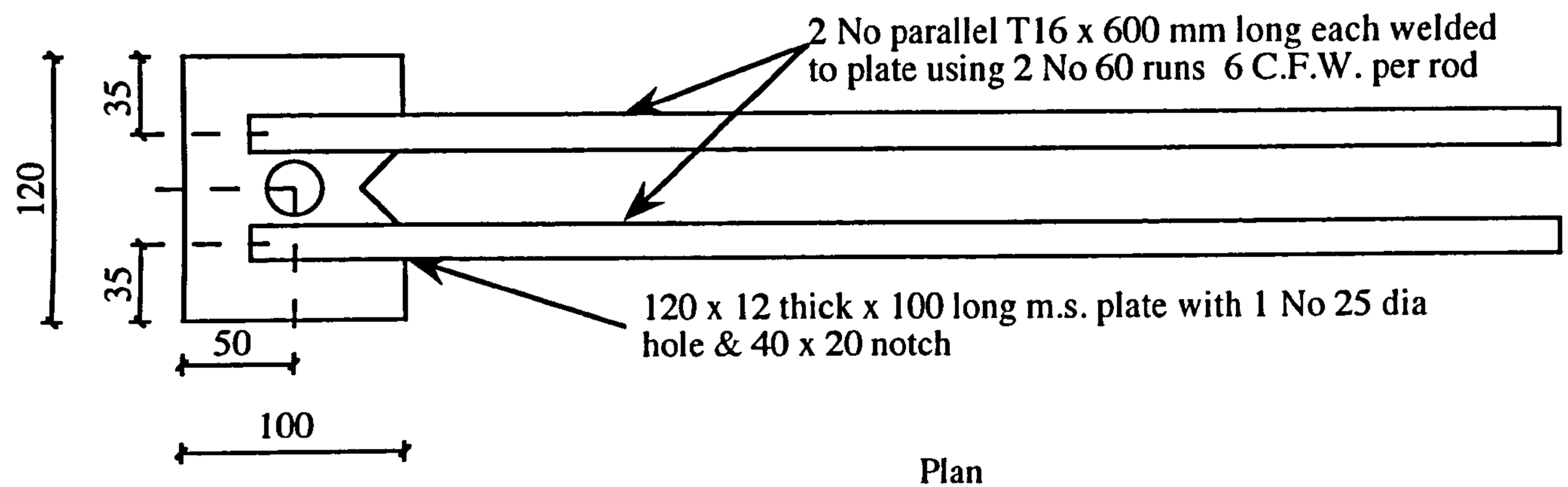

Plan

Figure 5.9: Details of beam end plate for bolted billet connection (see Fig. 5.13(a))

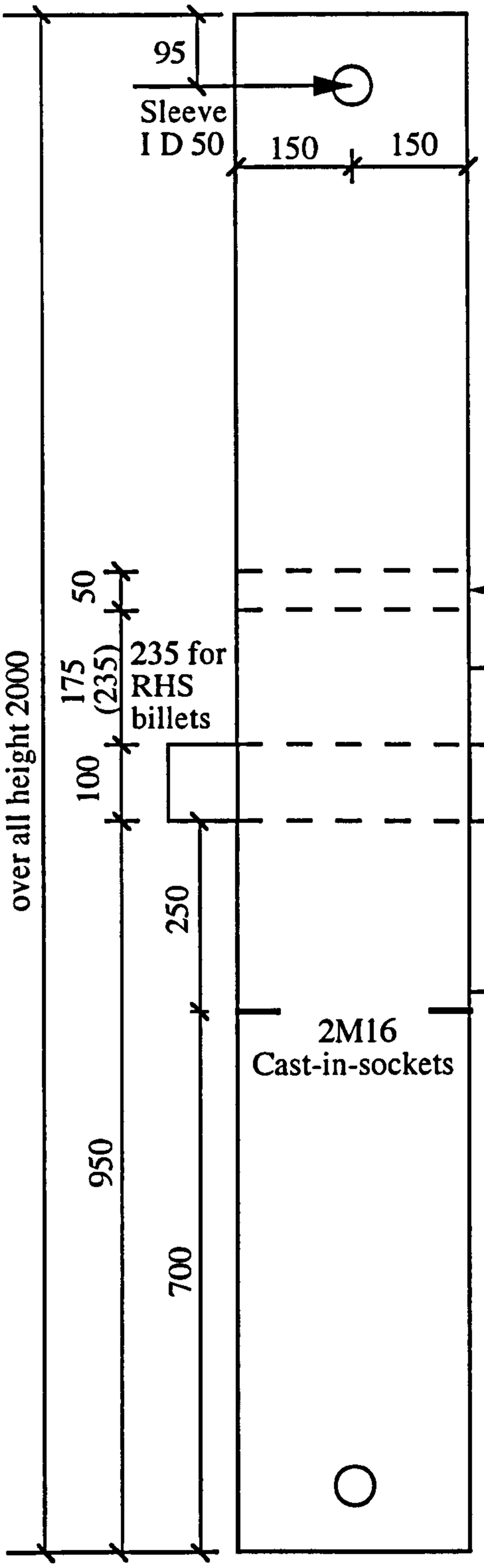

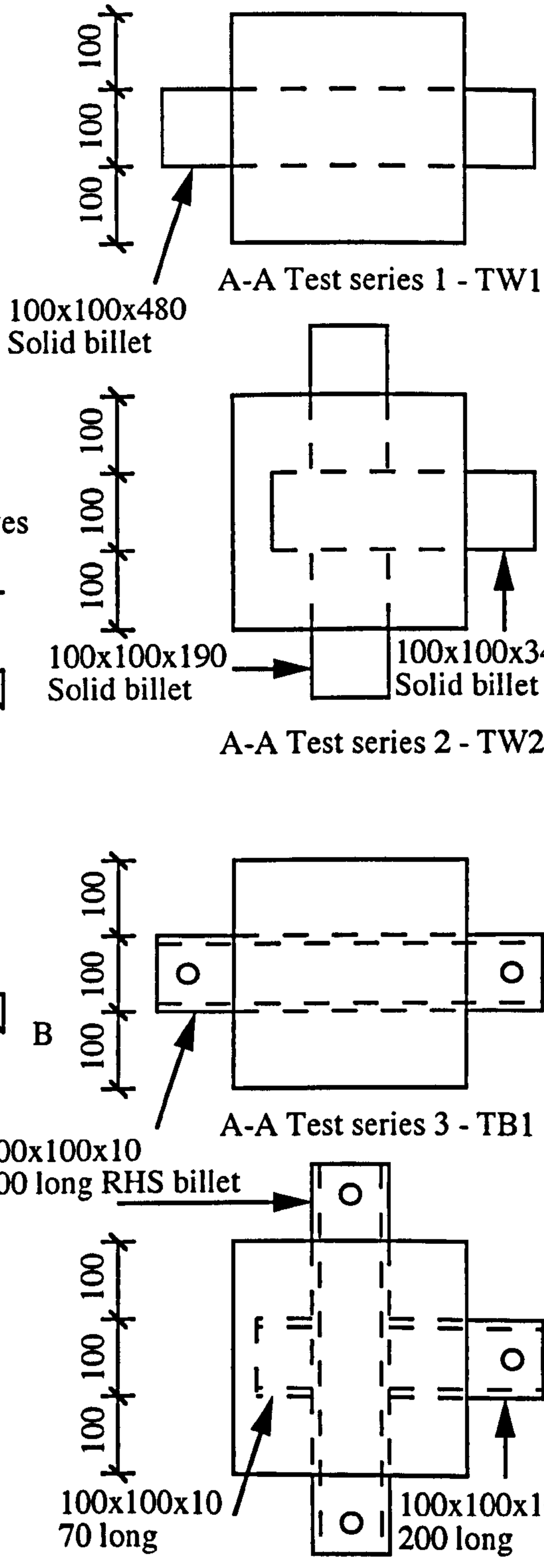

Figure 5.10: Geometrical details of column

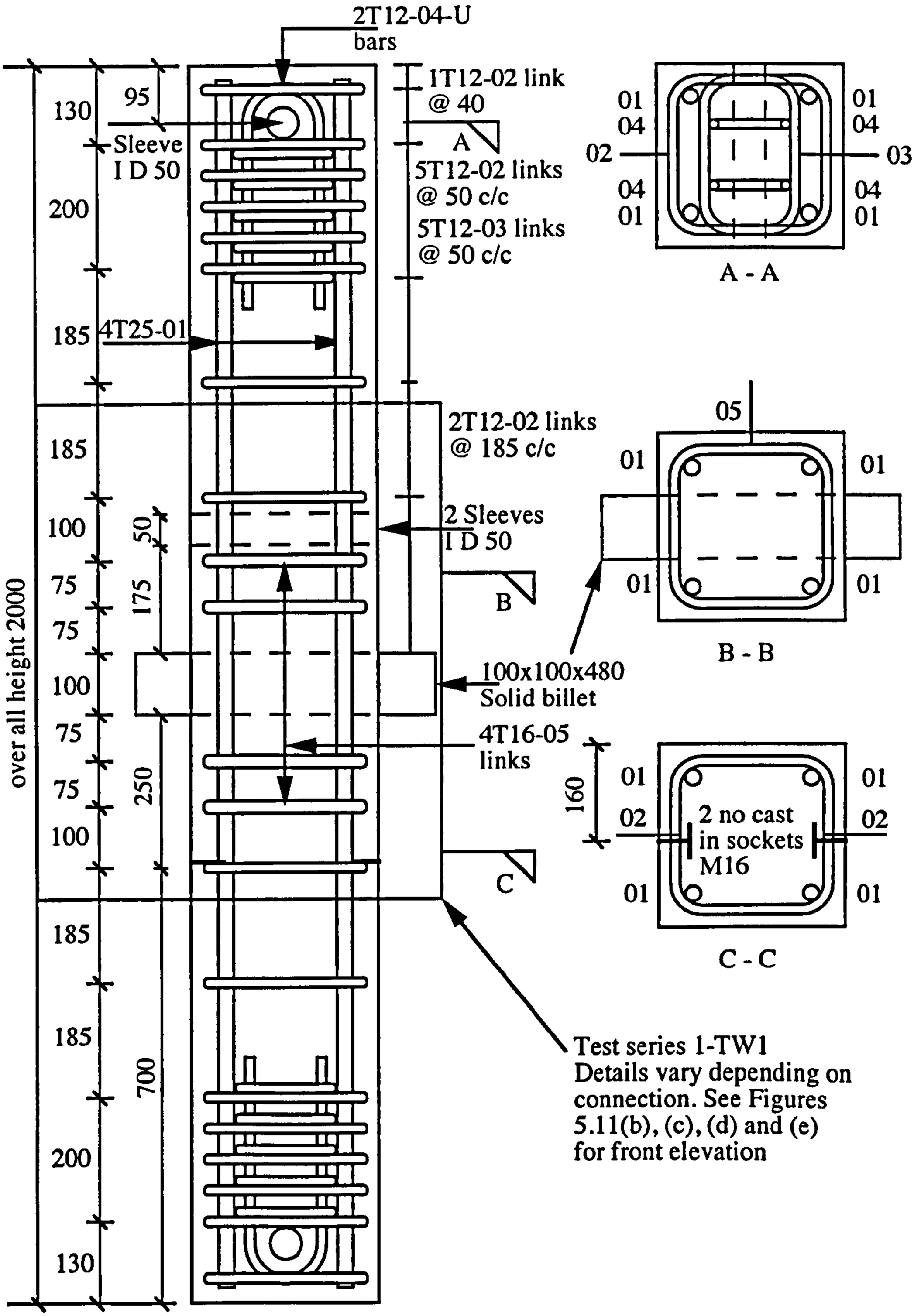

Figure 5.11(a): Reinforcement details of column

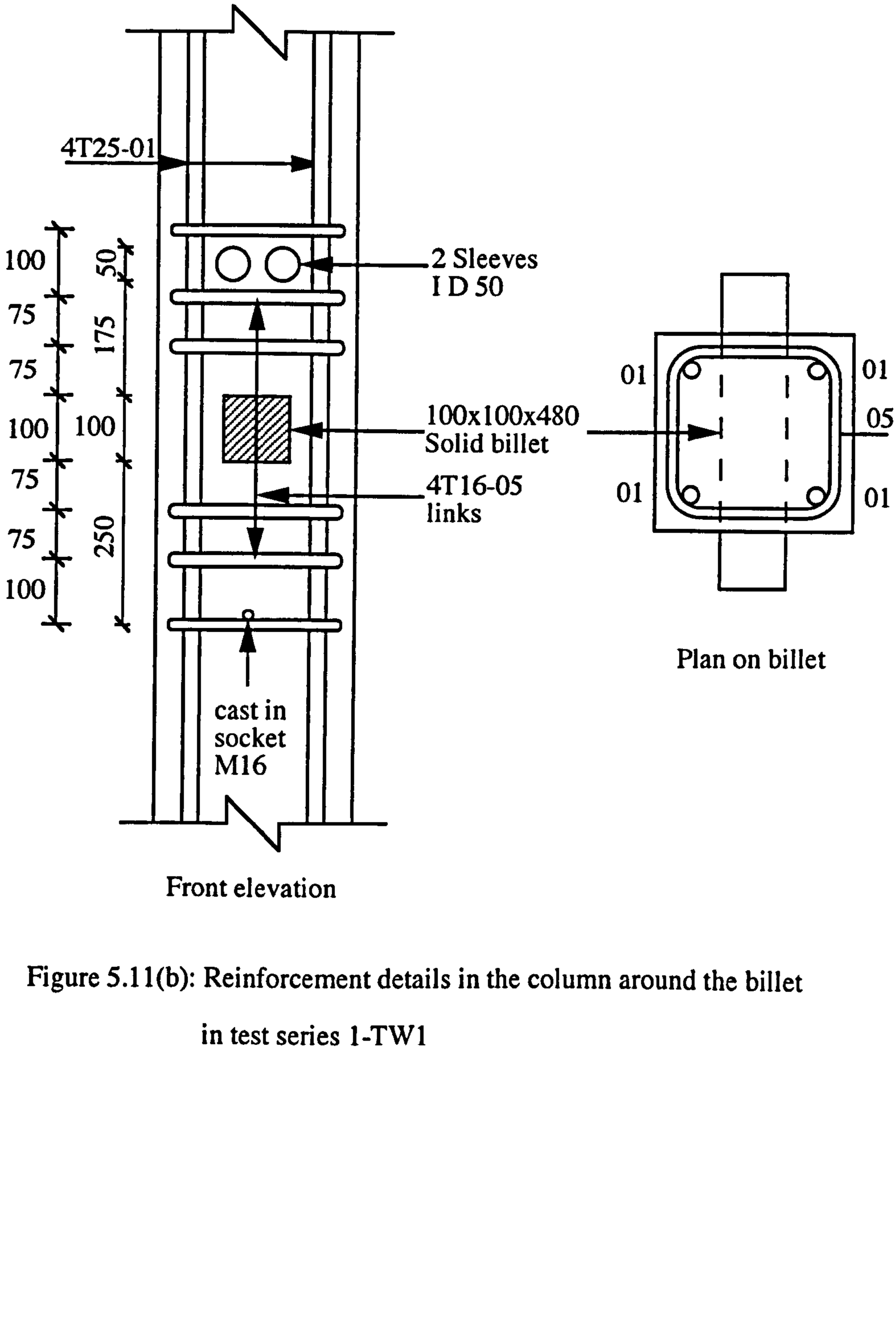

Figure 5.11(b): Reinforcement details in the column around the billet in test series 1-TW1

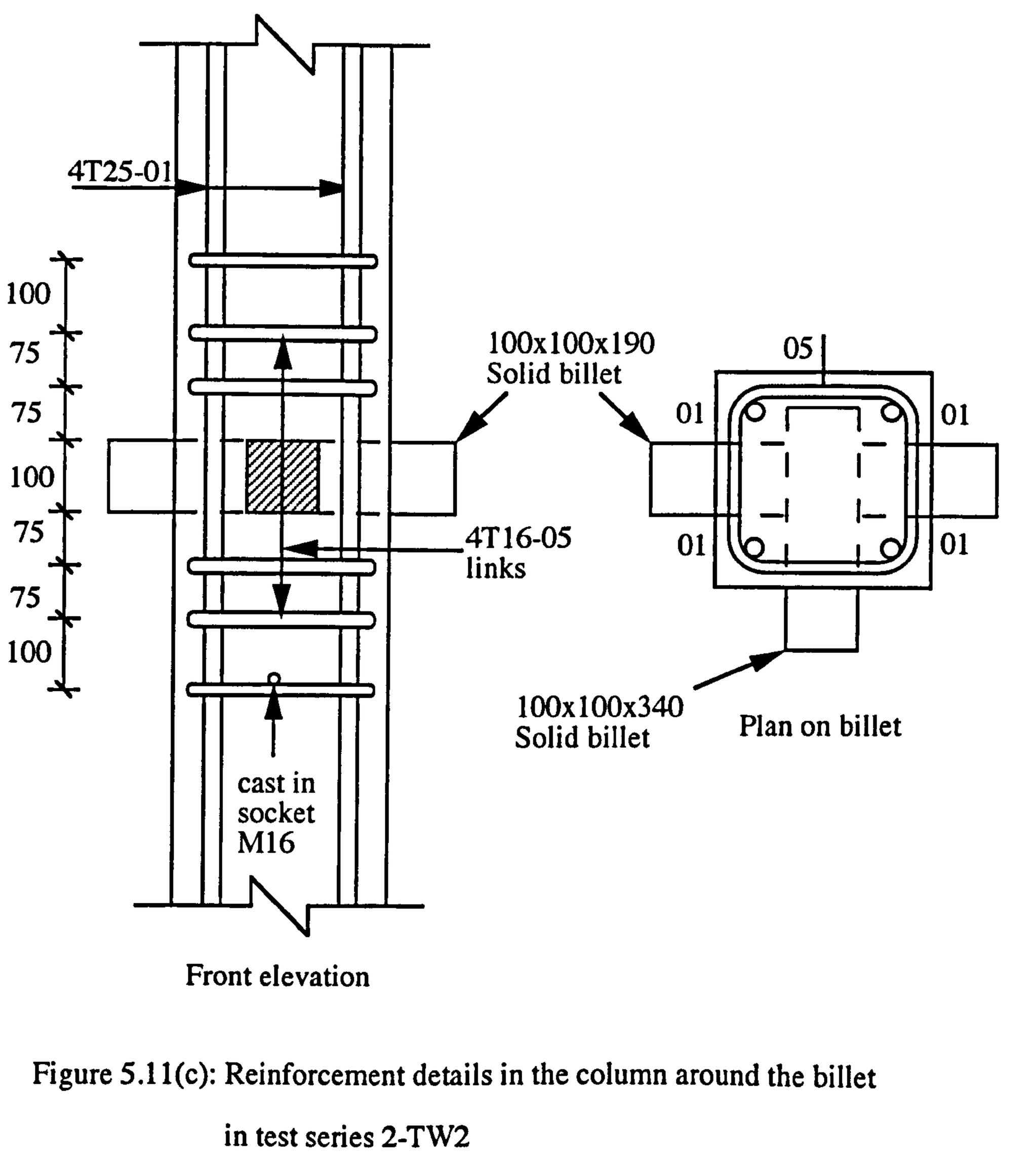

Front elevation

Figure 5.11(c): Reinforcement details in the column around the billet in test series 2-TW2

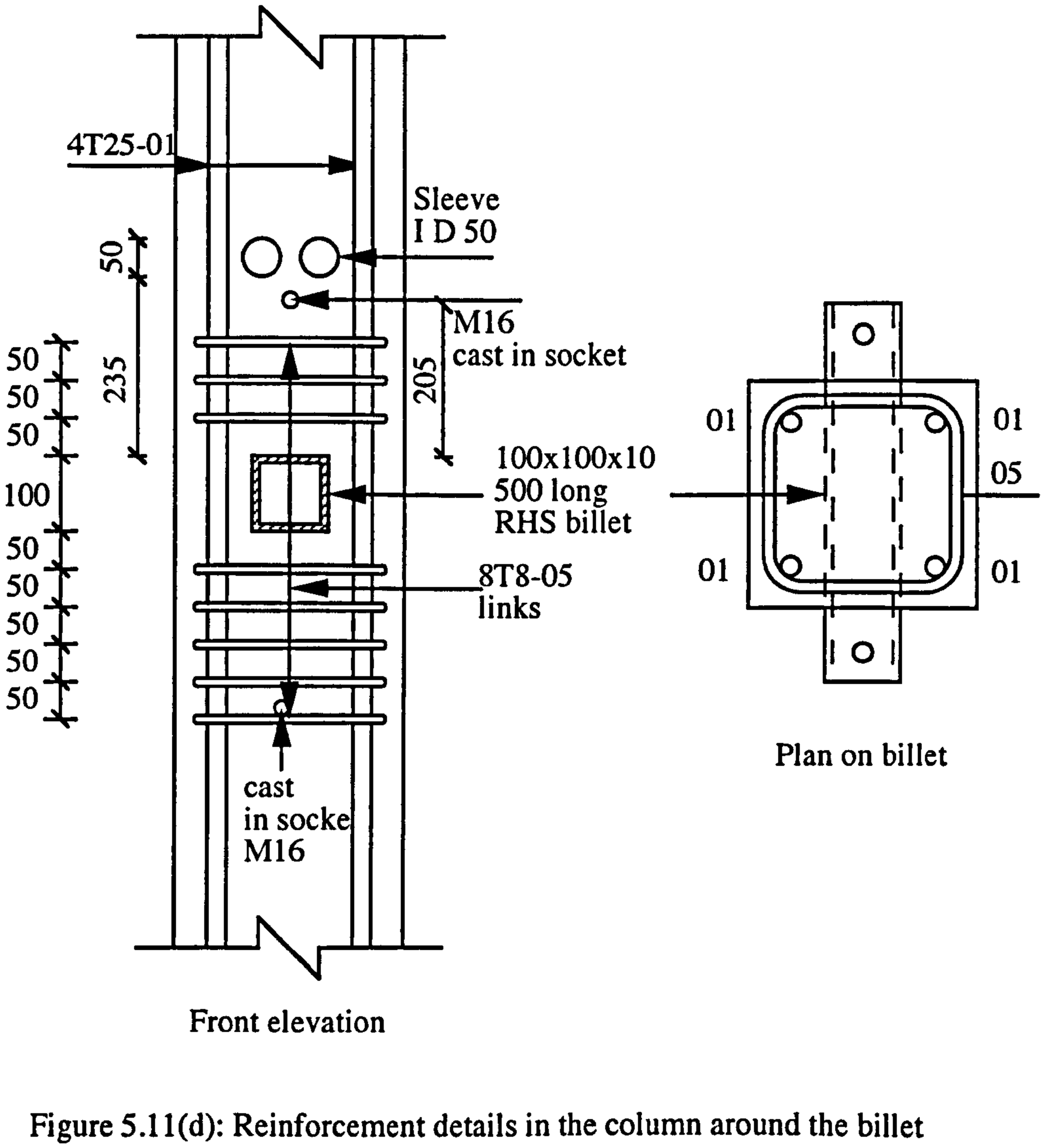

Figure 5.11(d): Reinforcement details in the column around the billet in test series 3-TB1

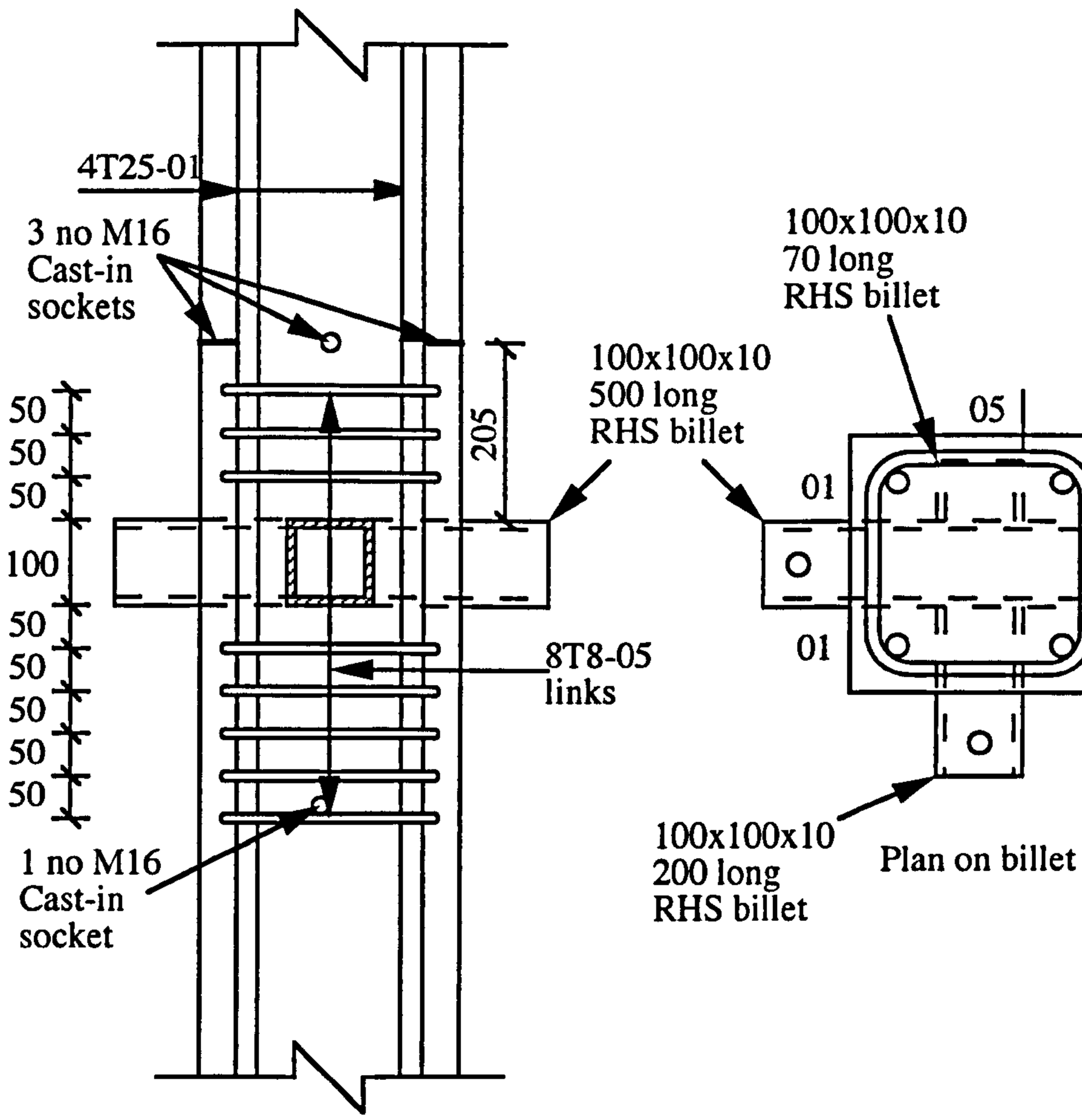

Figure 5.11(e): Reinforcement details in the column around the billet in test series 4-TB2

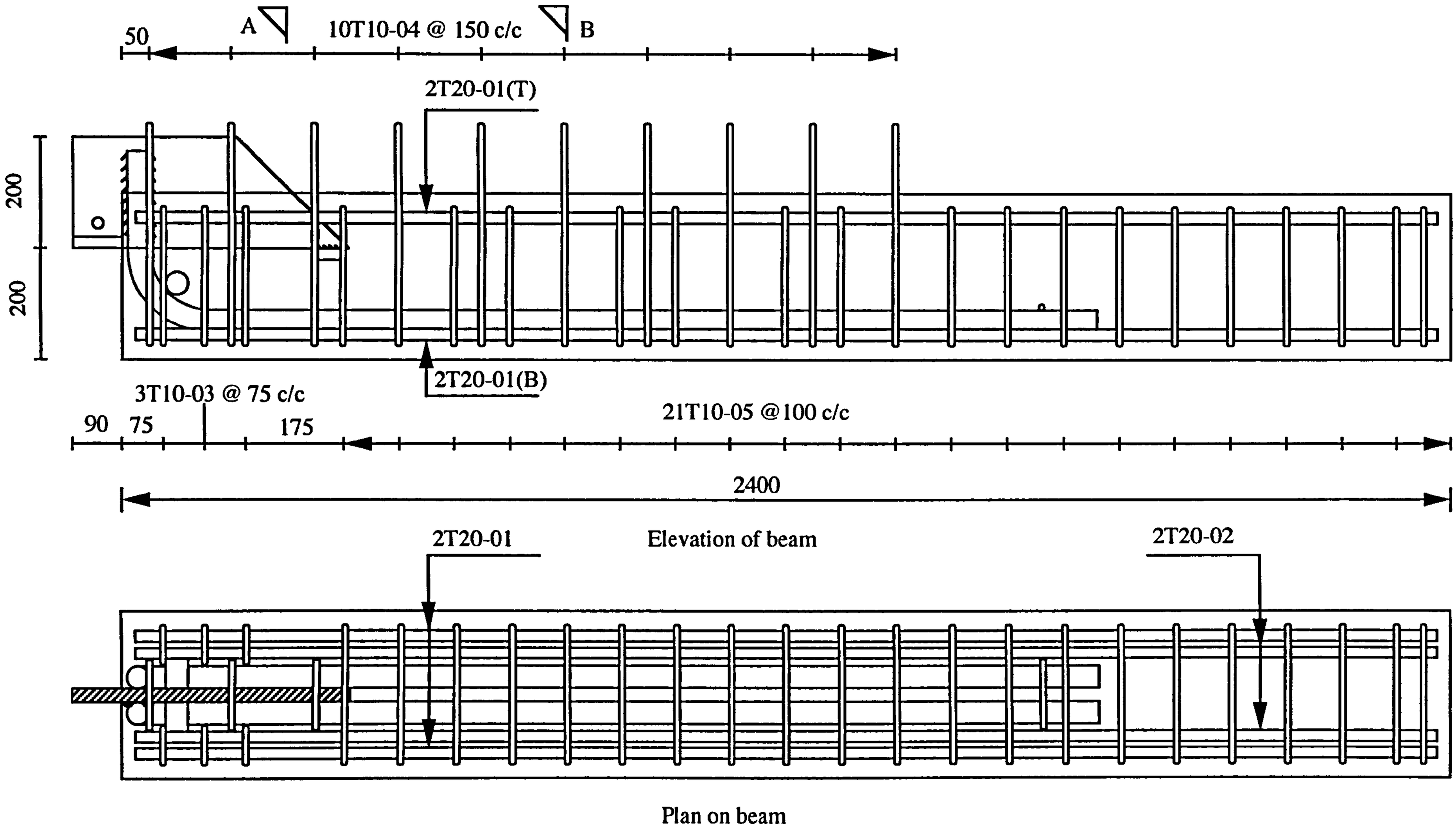

Figure 5.12(a): Reinforcement details of beam in test series 1 and 2

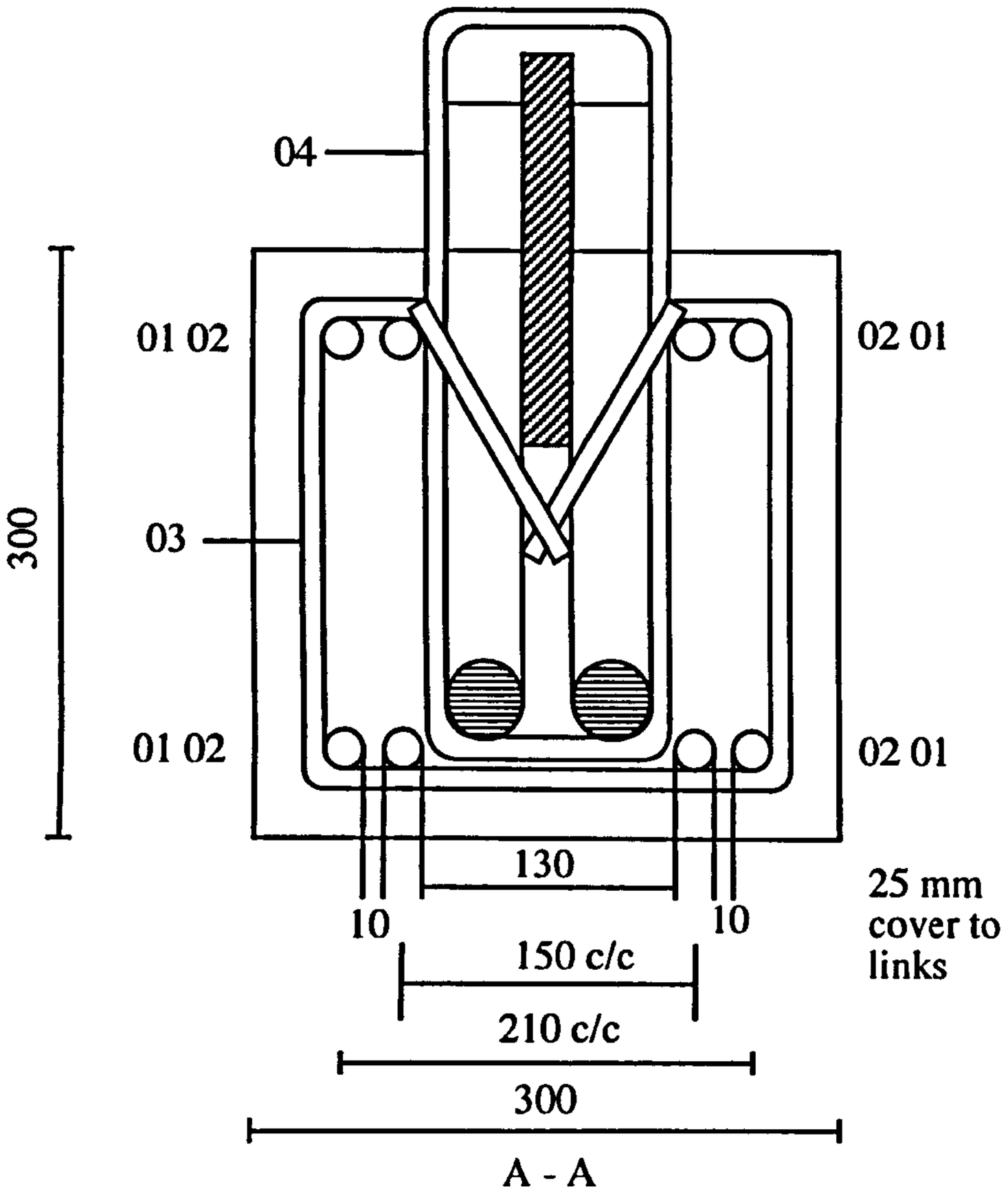

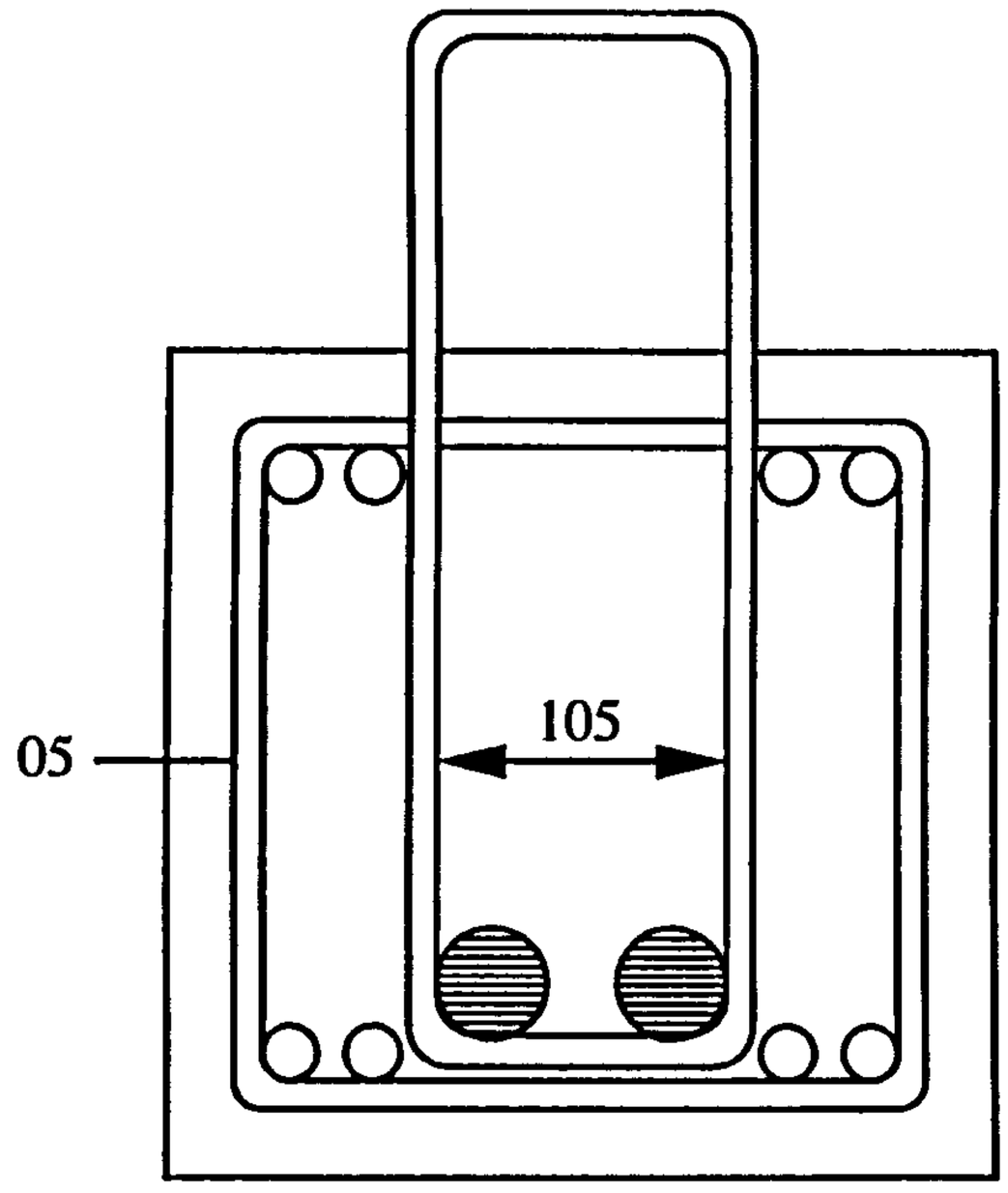

Figure 5.12(b): Cross sections of beam

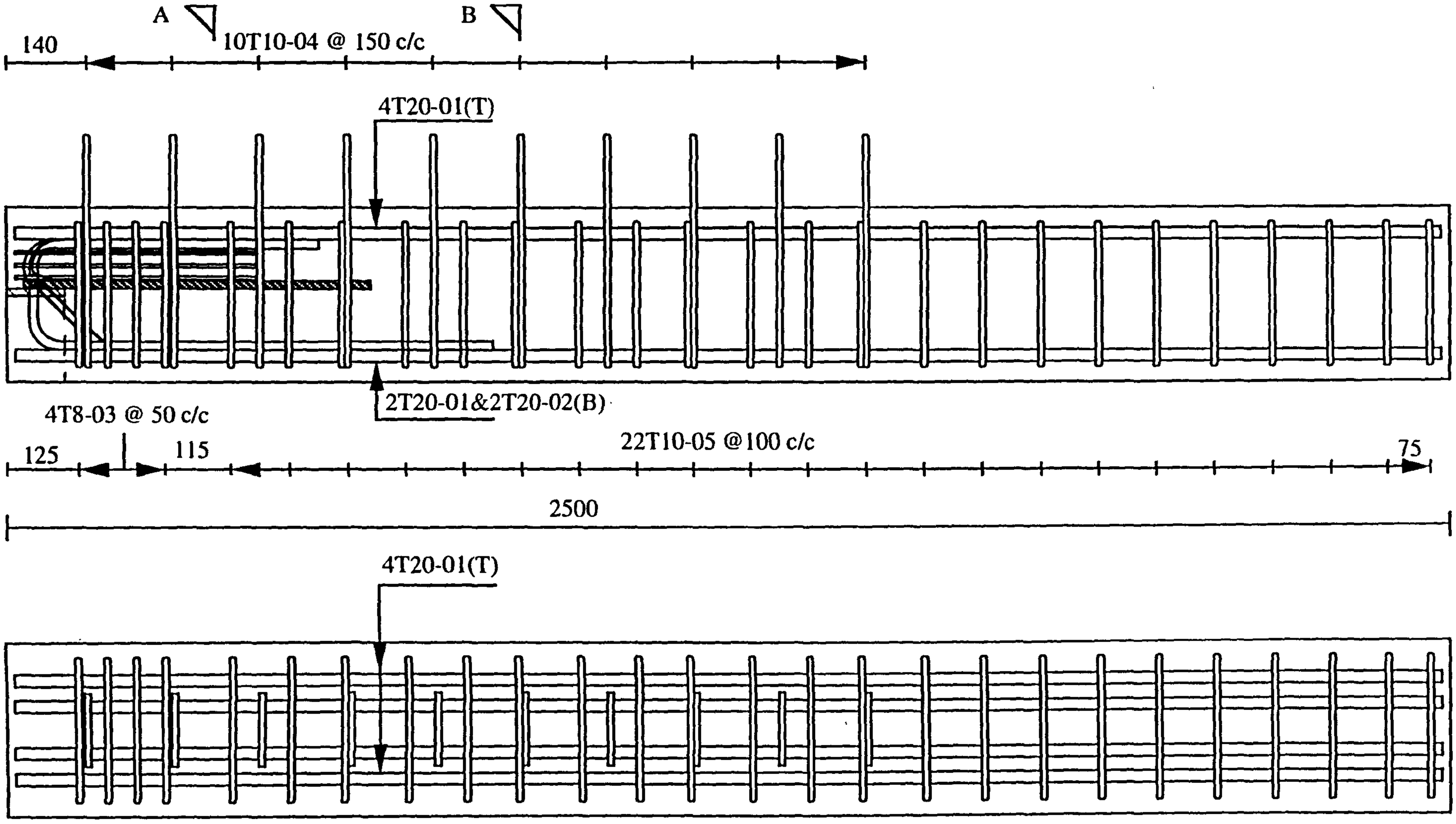

Figure 5.13(a): Reinforcement details of beam in test series 3 and 4

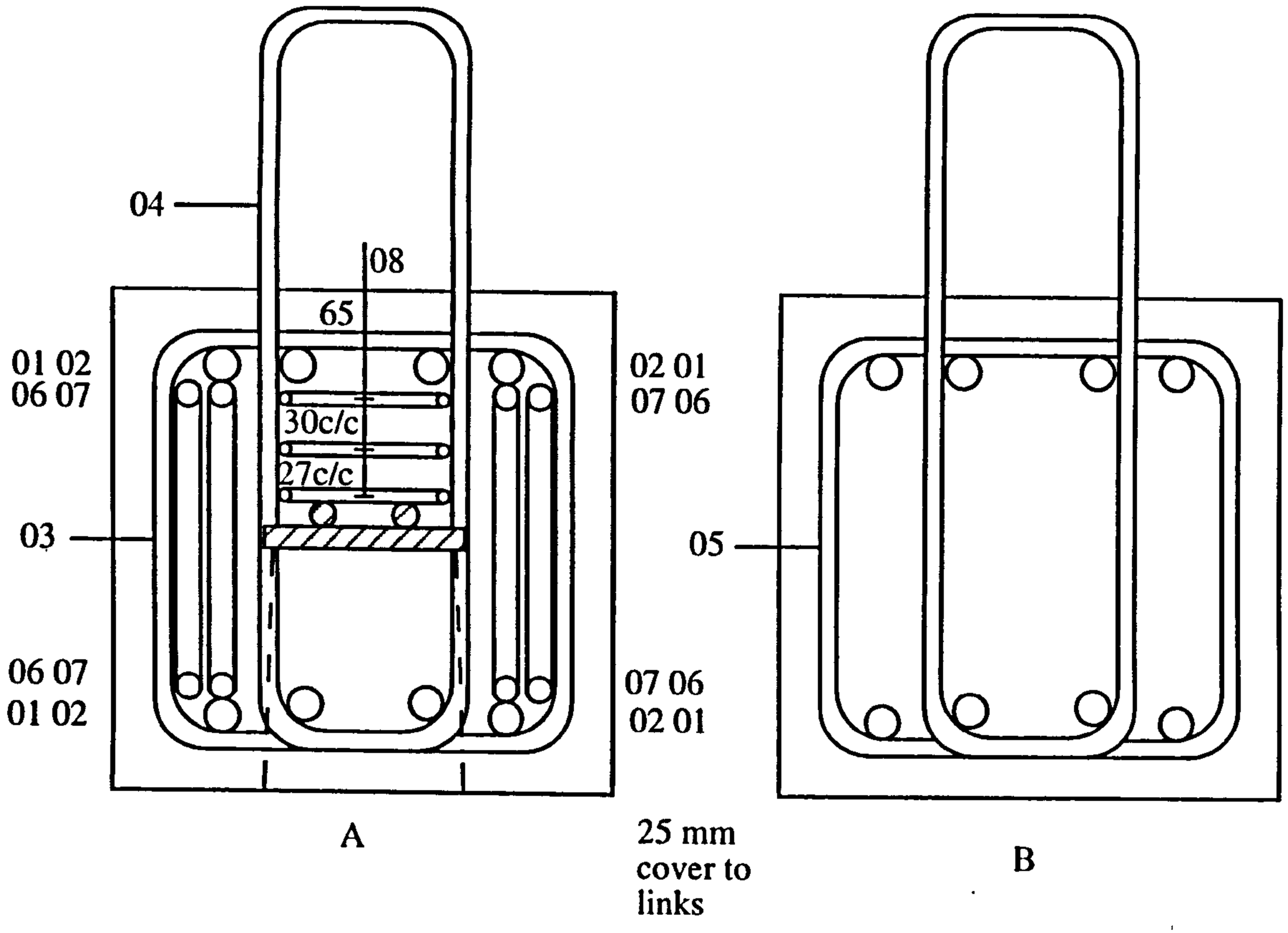

Figure 5.13(b): Cross sections of beam

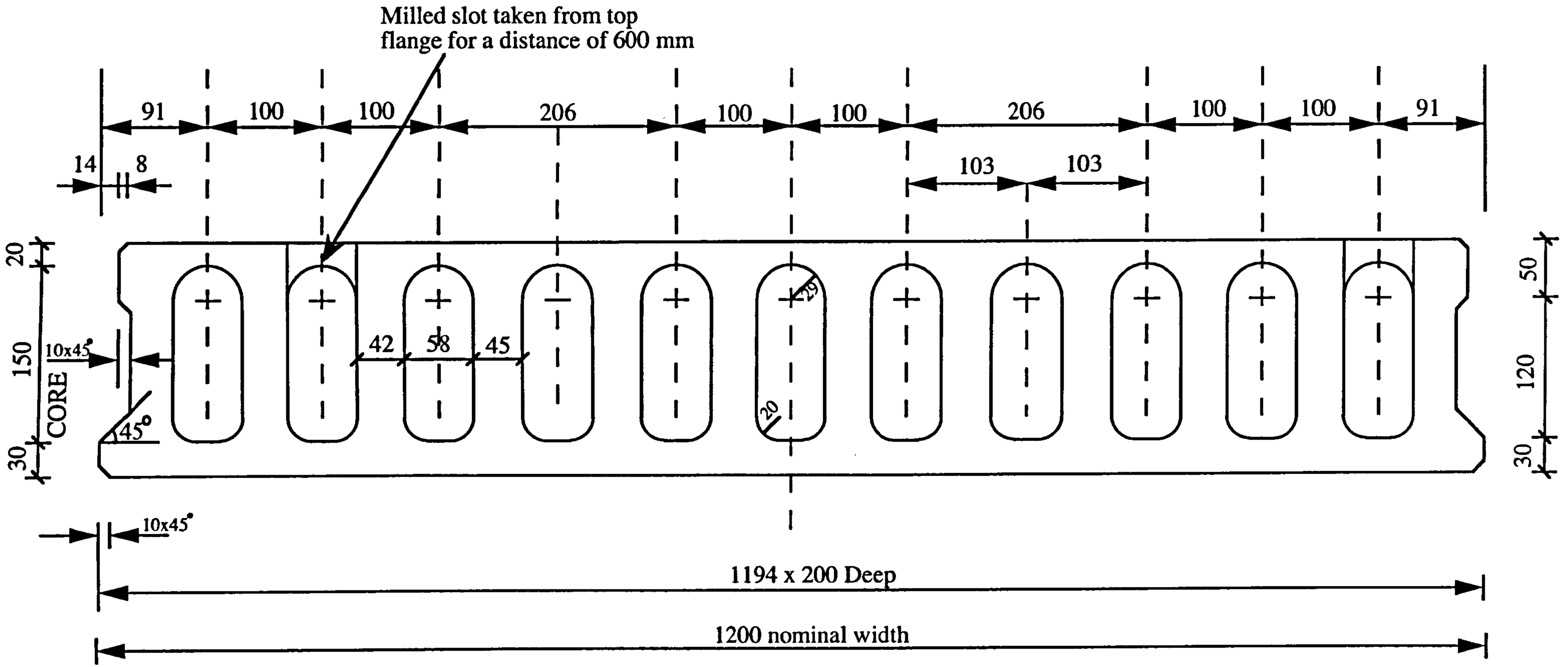

Figure 5.14(a): Cross section details of slab

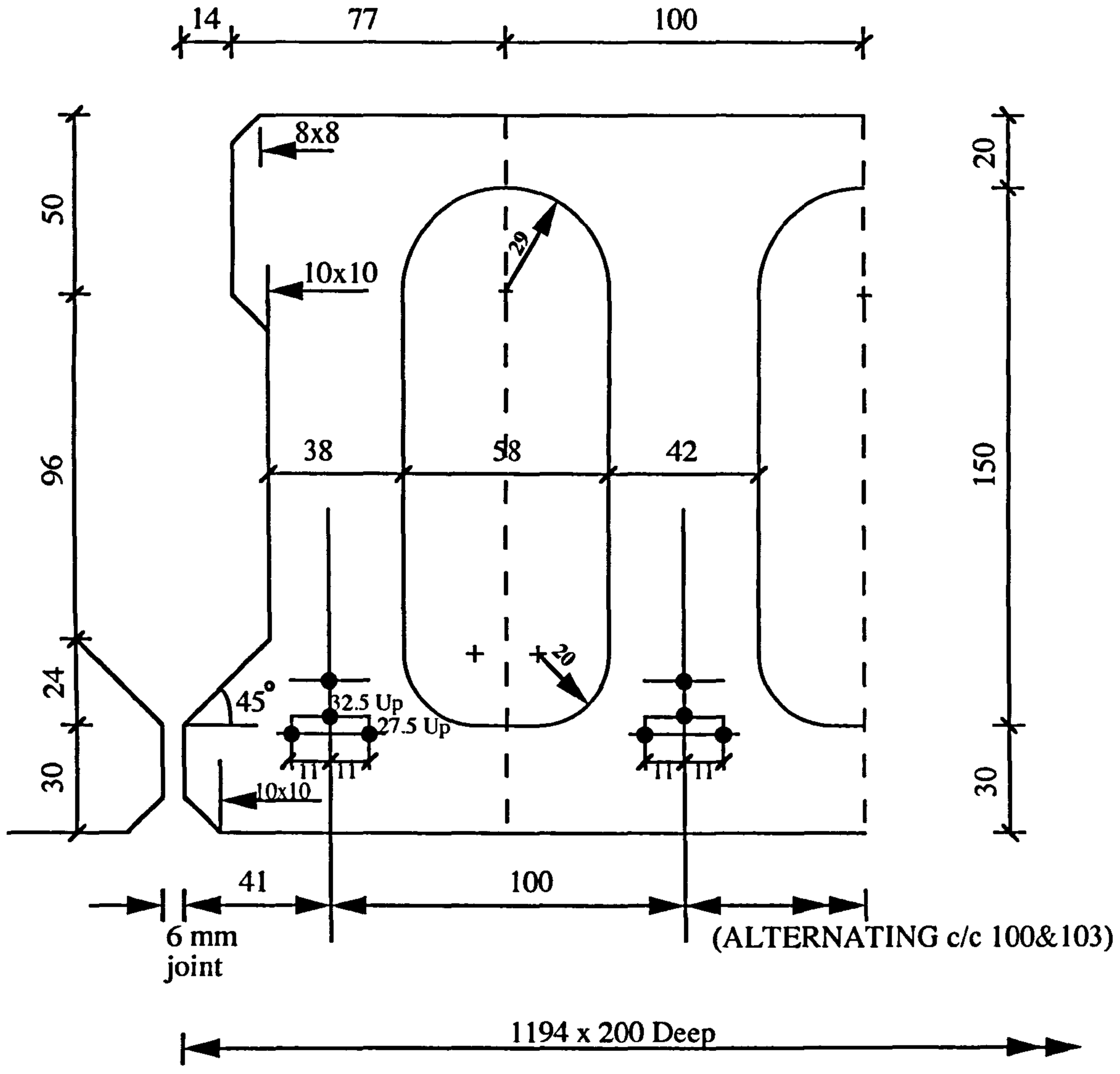

Figure 5.14(b): Reinforcement details of slabs

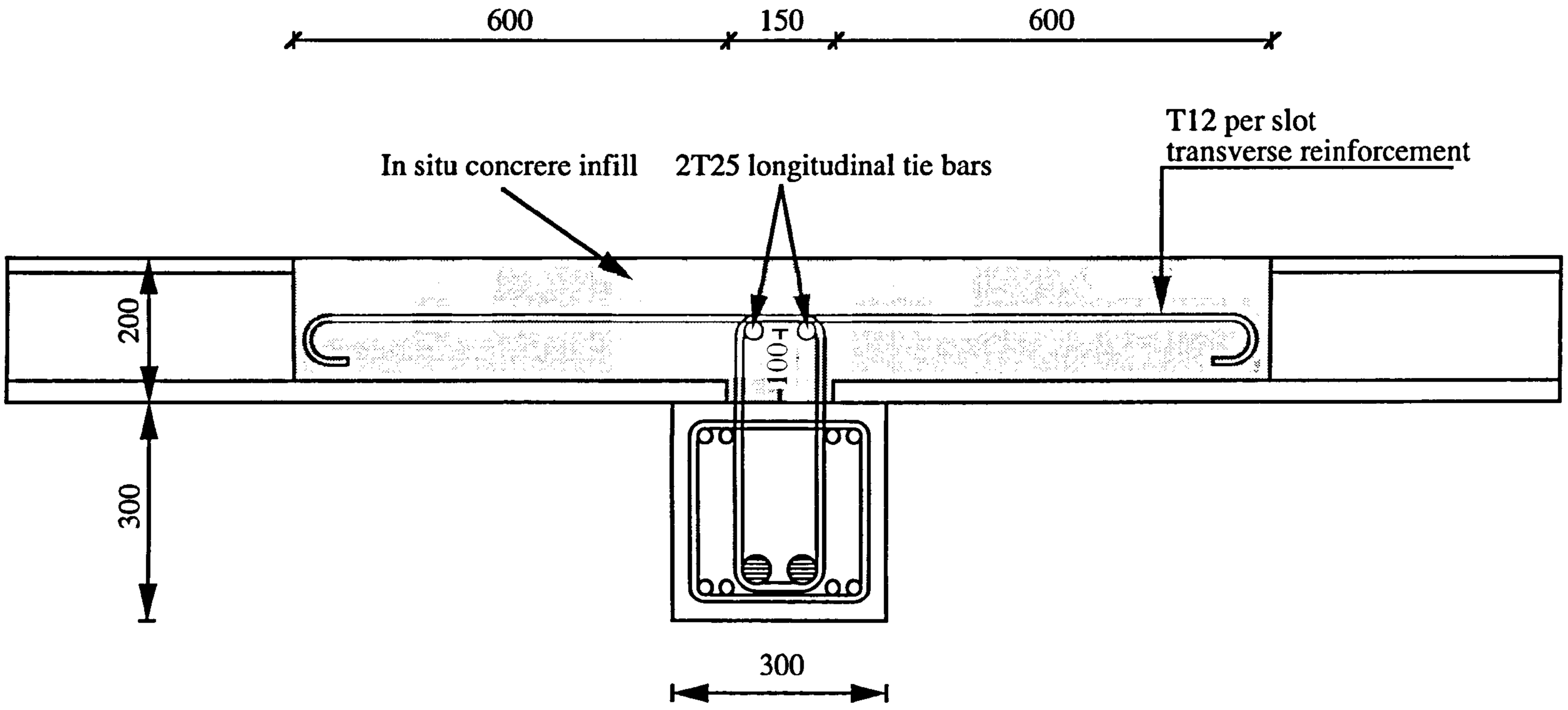

Figure 5.15: Continuity reinforcement at slot section

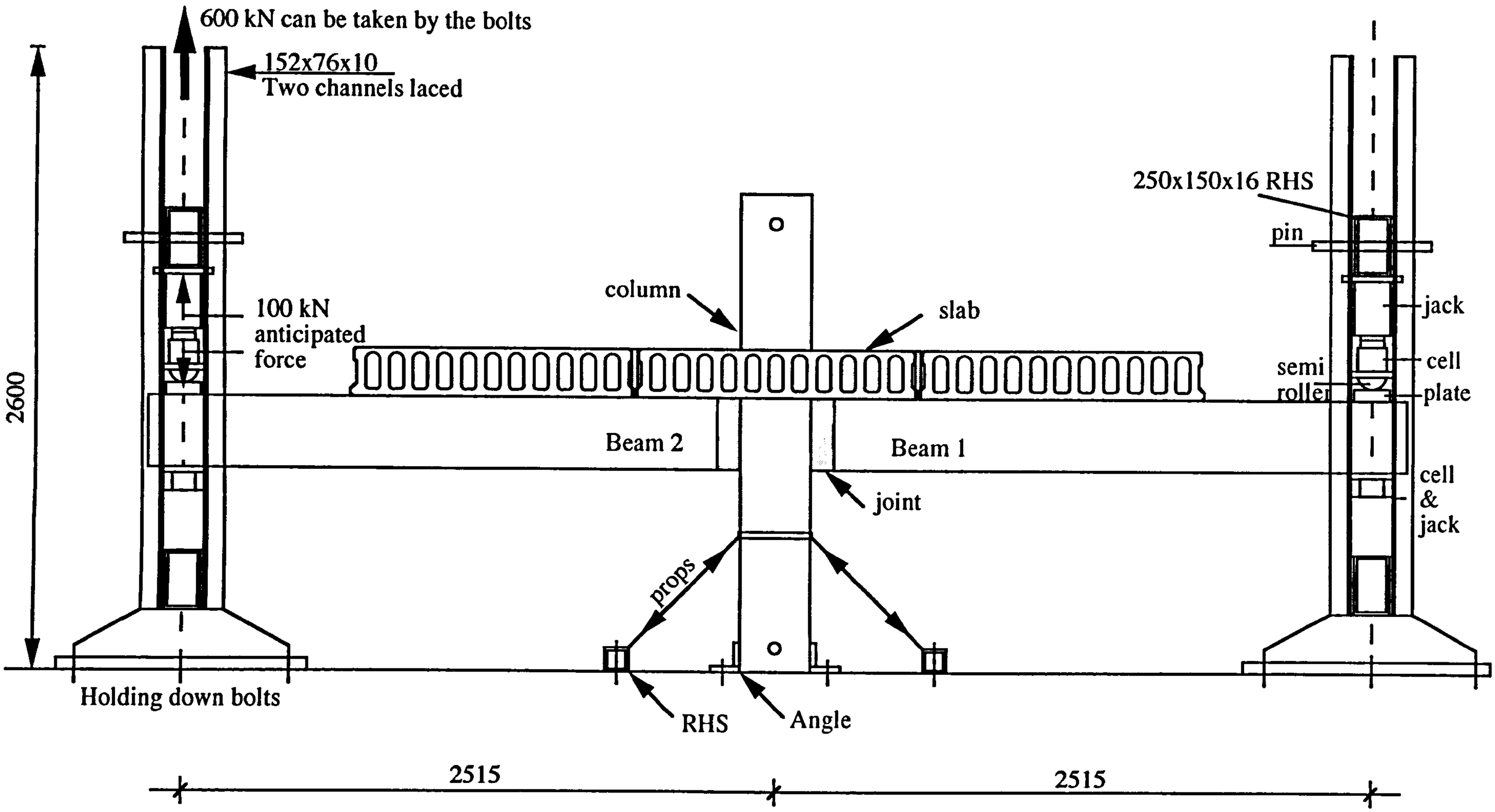

Figure 5.16(a): Front elevation of the test rig with subframe SF1

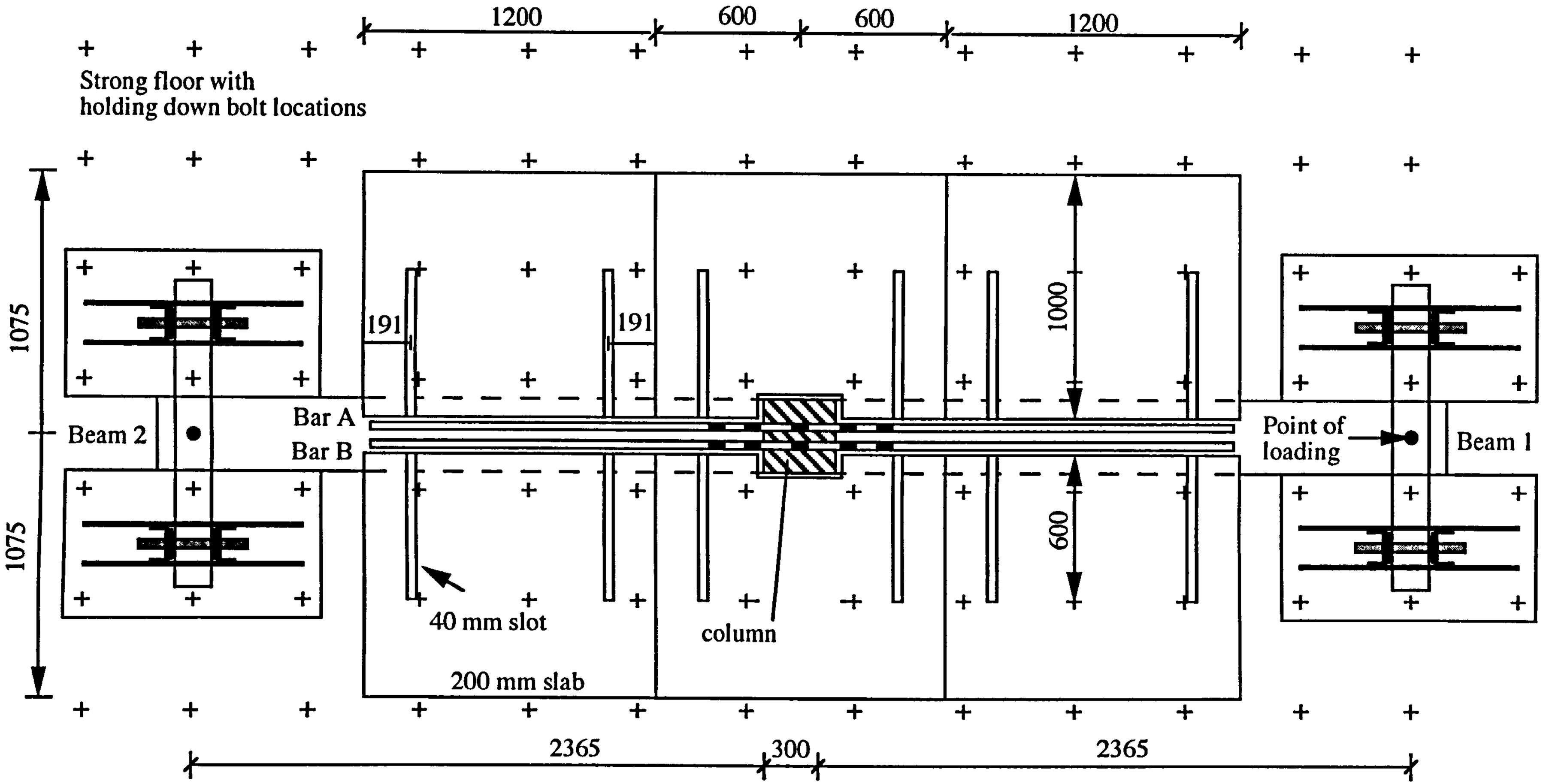

Figure 5.16(b): Plan view of test rig with subframe SF1

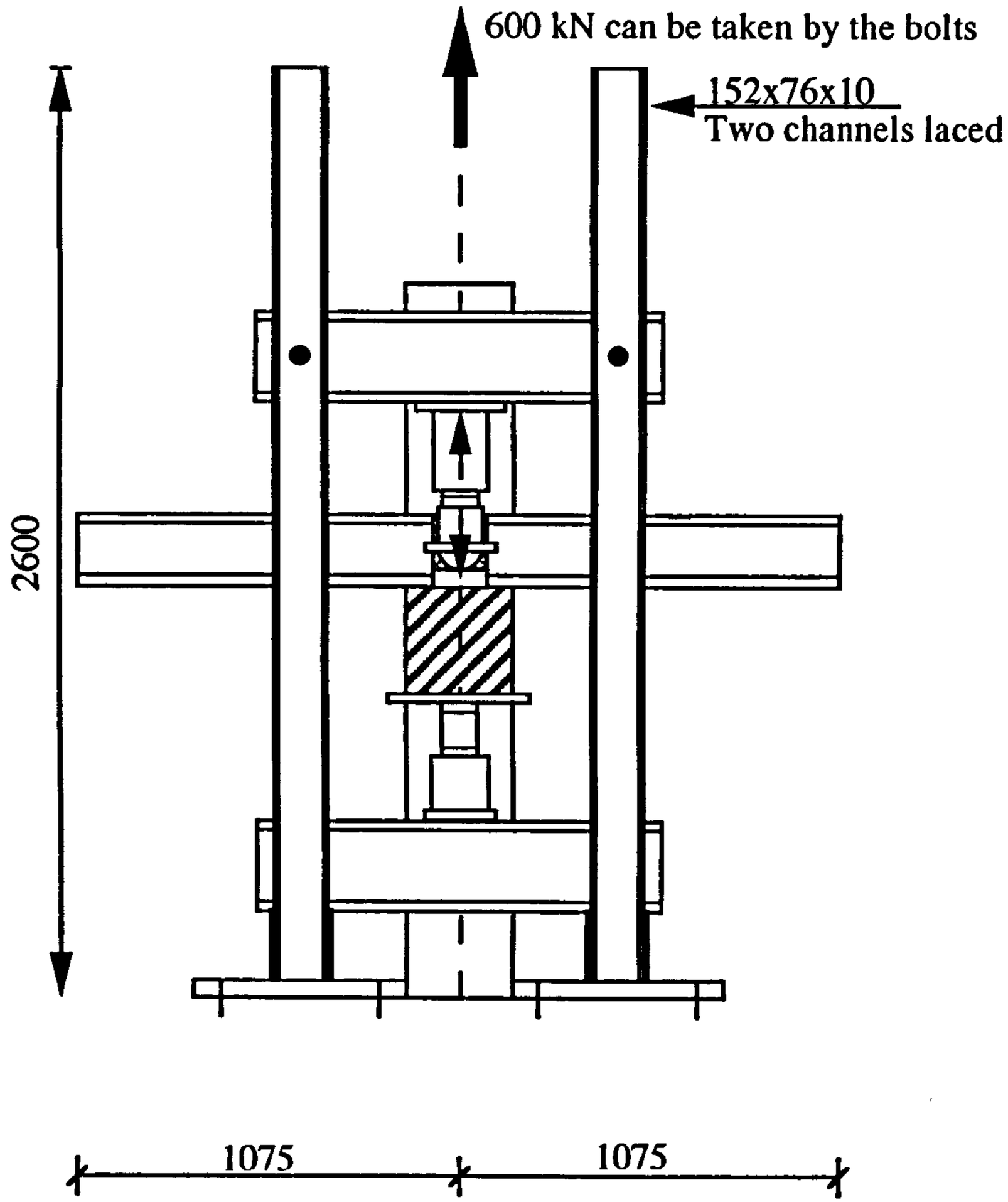

Figure 5.16(c): End elevation of test rig with subframe SF1

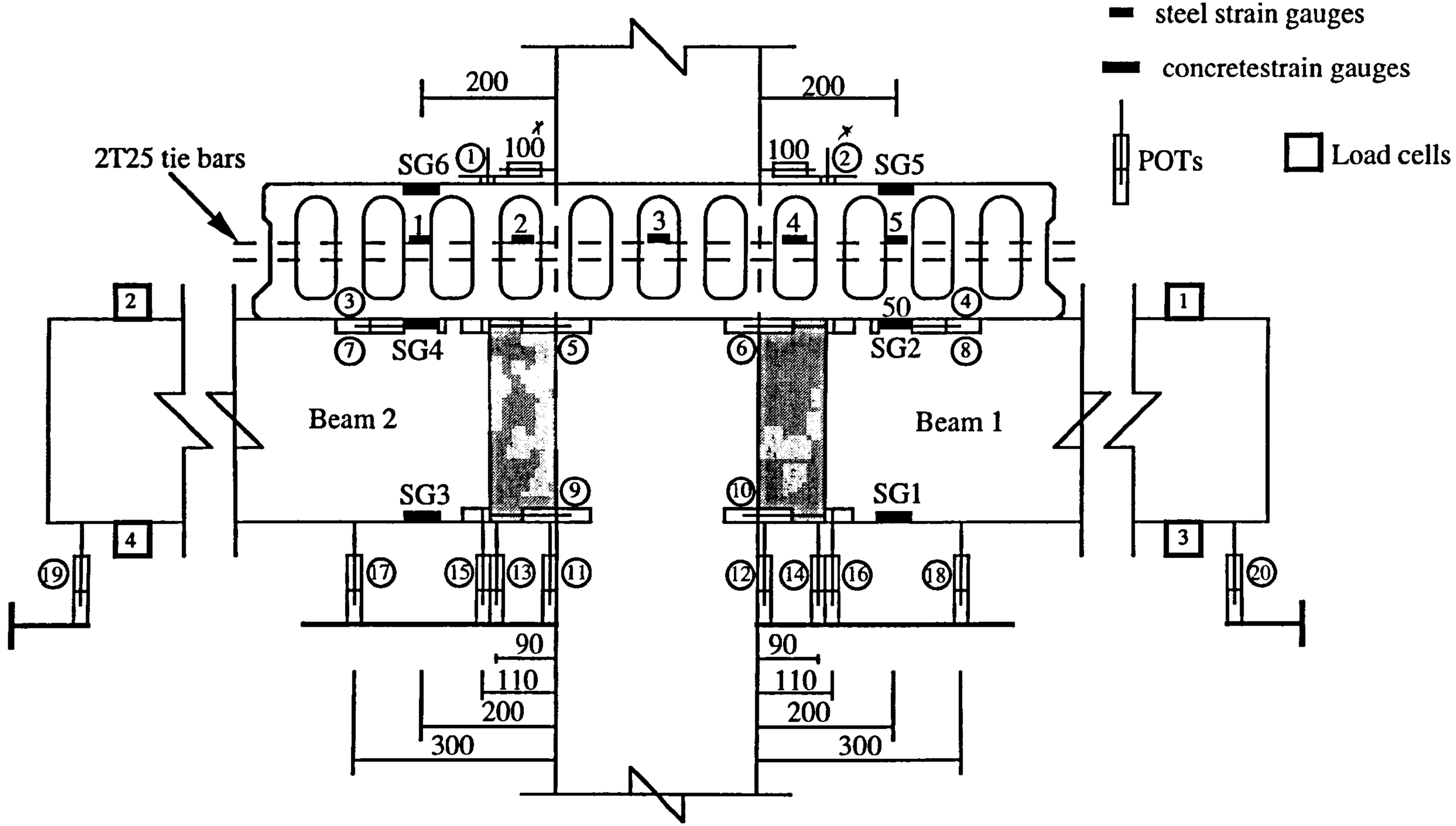

Figure 5.17(a): Instrumentation (see (b) and (c) for detail)

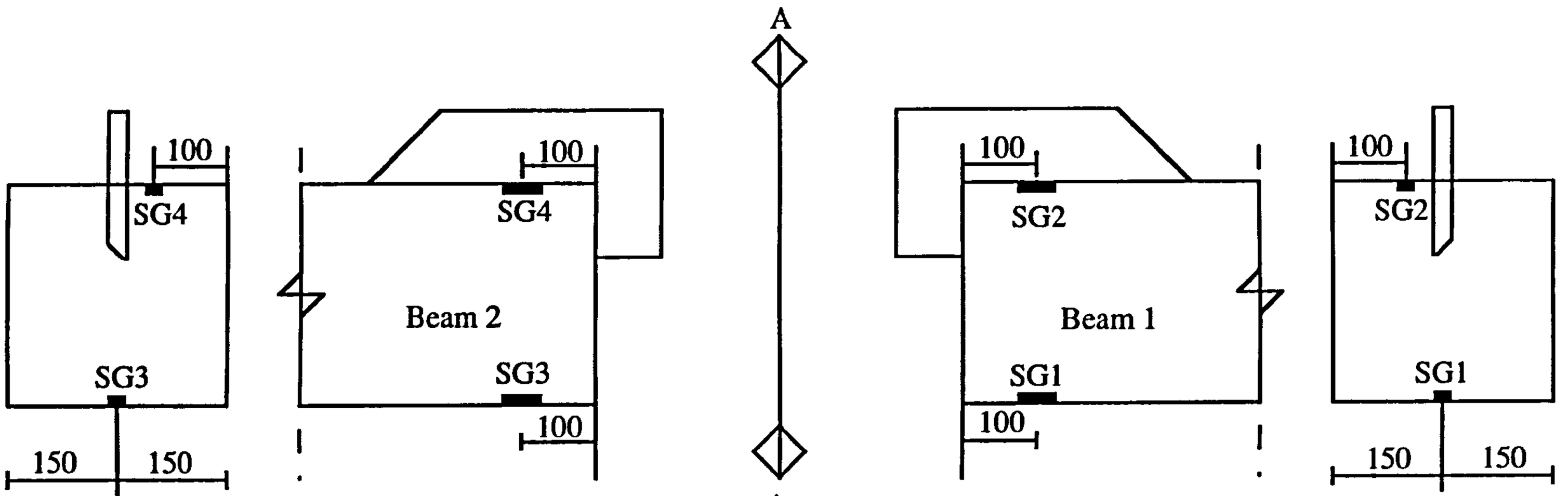

End cross section of beam 2 next to the column face

SG = Strain Gauge

End cross section of beam 1 next to the column face

Figure 5.17(b): Location of concrete strain gauges on the beams

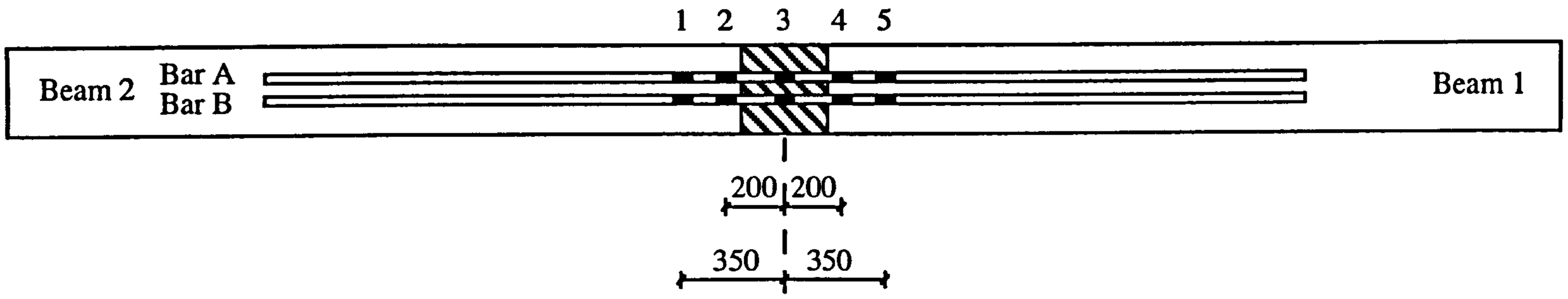

Figure 5.17(c): Location of steel strain gauges on 2T25 tie bars (see Fig. 5.5(b) for single sided tests)

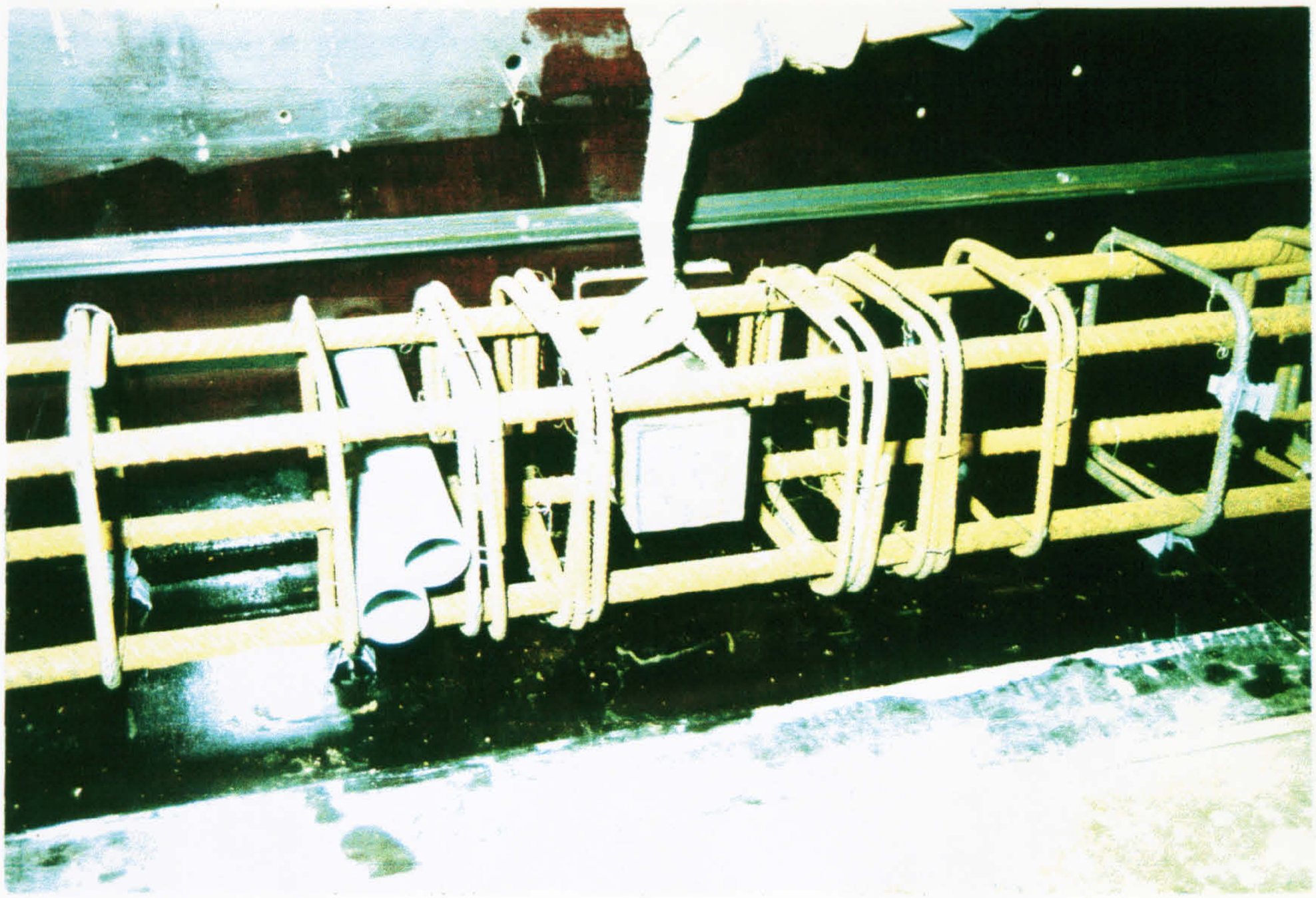

Plate 5.1: Column reinforcement with solid billet and sleeves

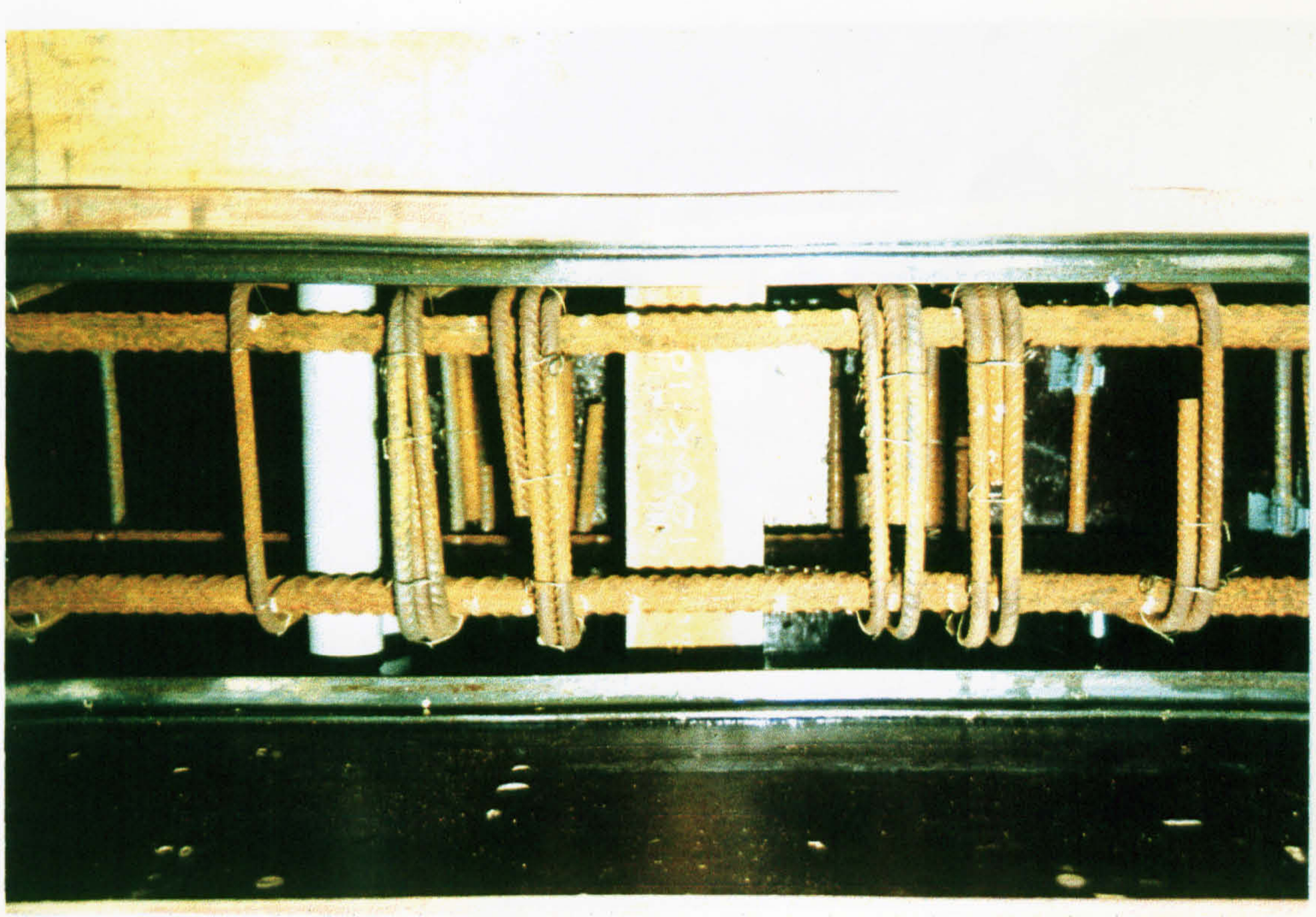

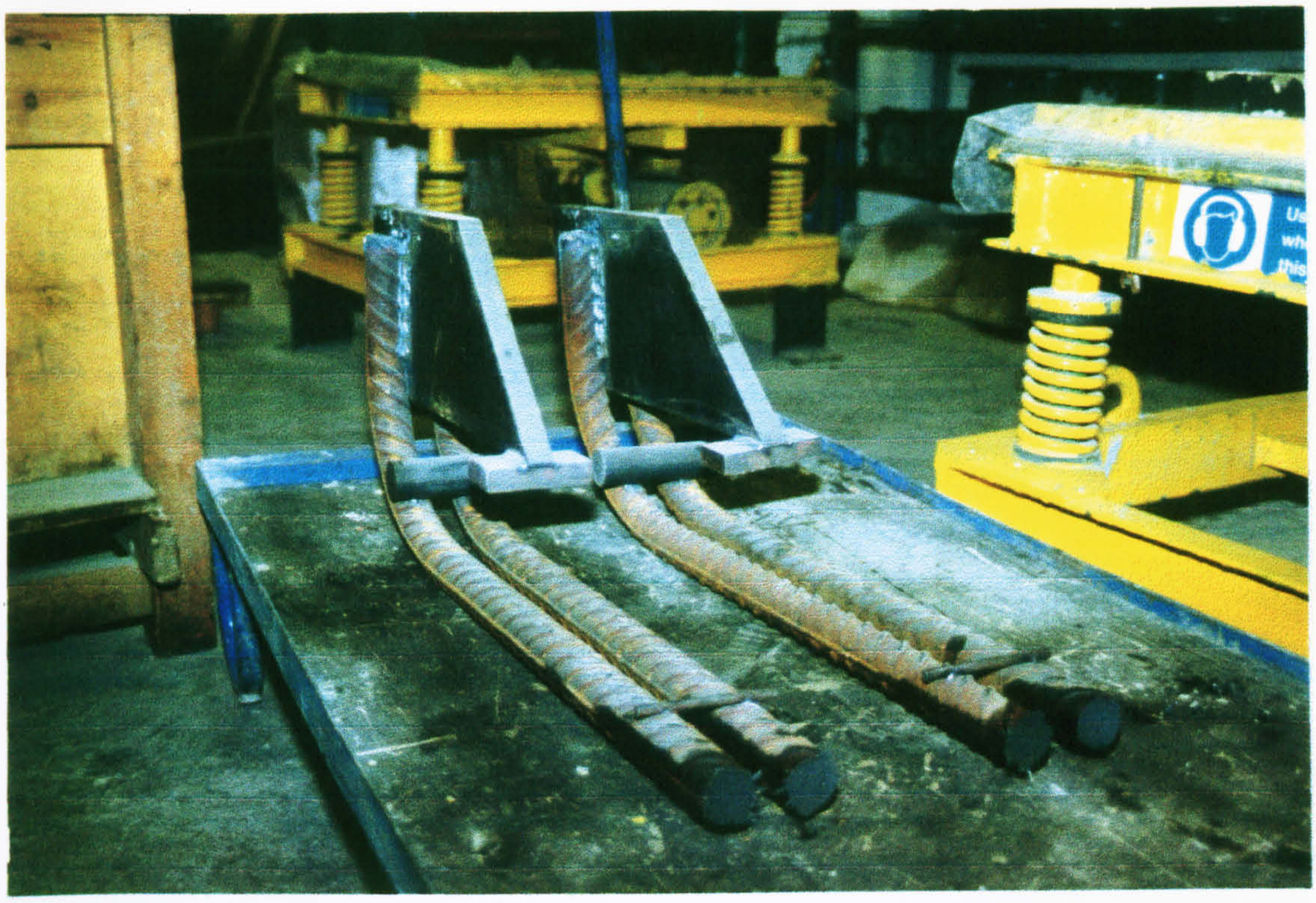

Plate 5.2: Standard beam connection plate

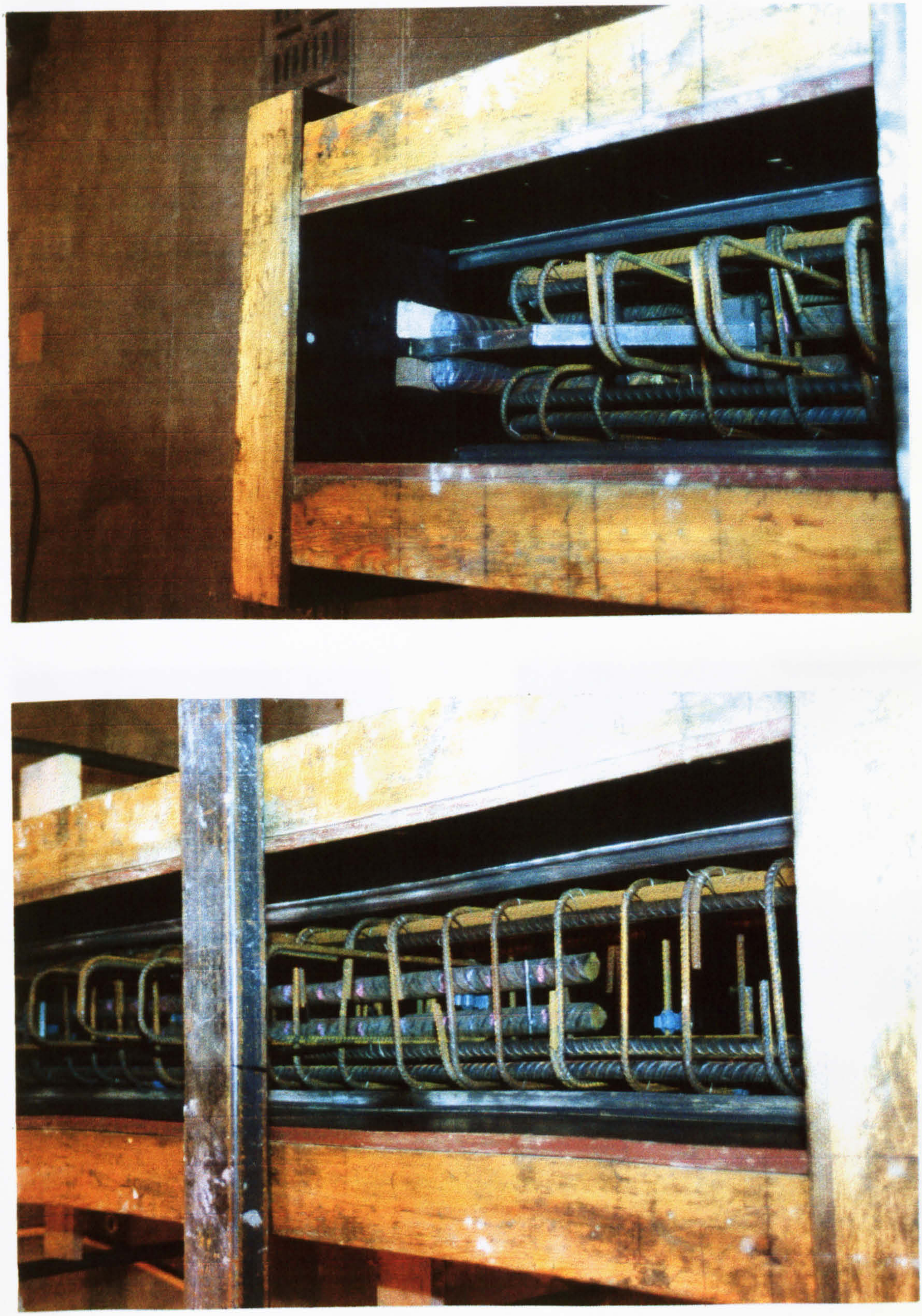

Plate 5.3: Beam reinforcement with standard beam connection plate and special links

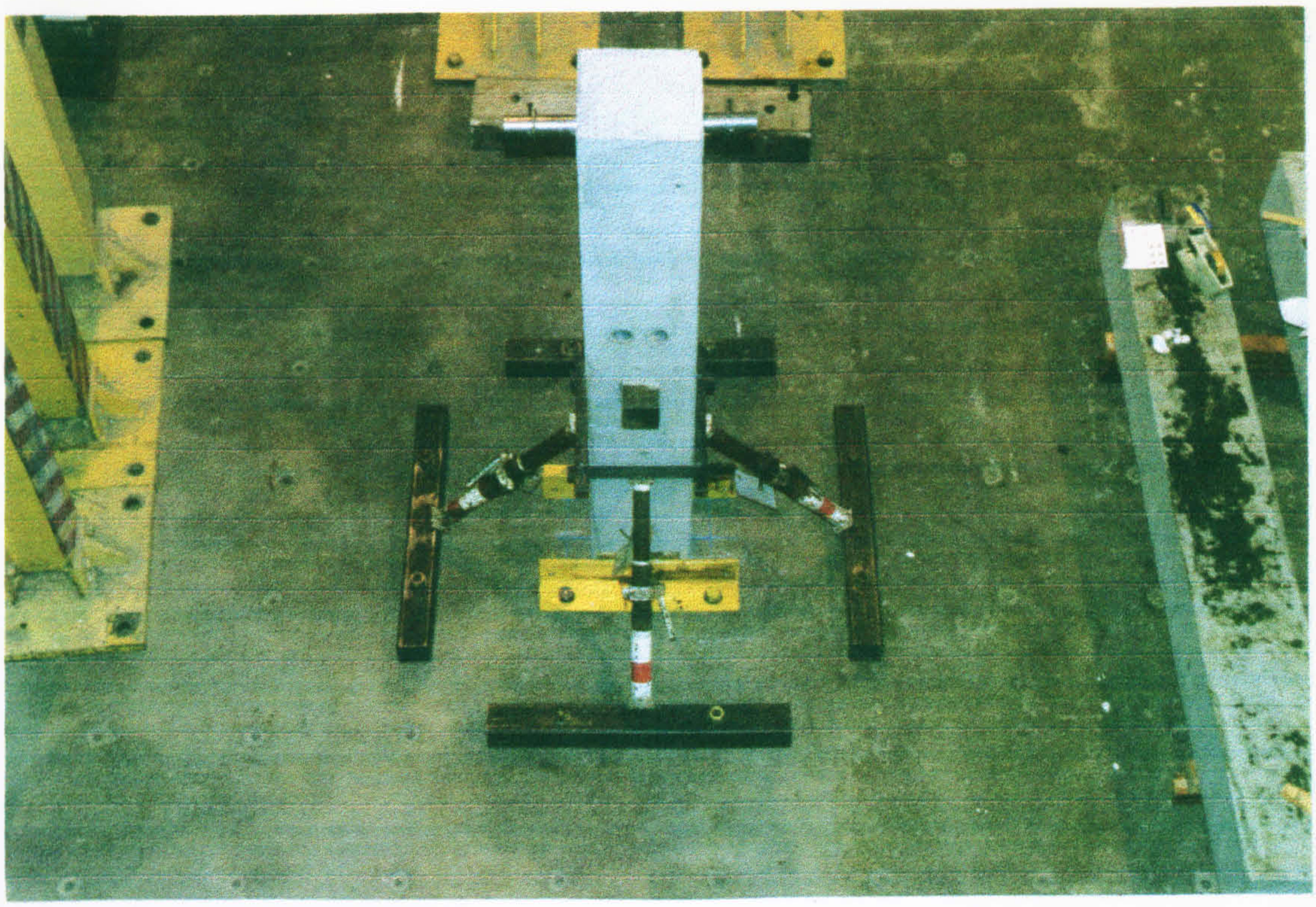

Plate 5.4: Column with bracings against sidesway movements

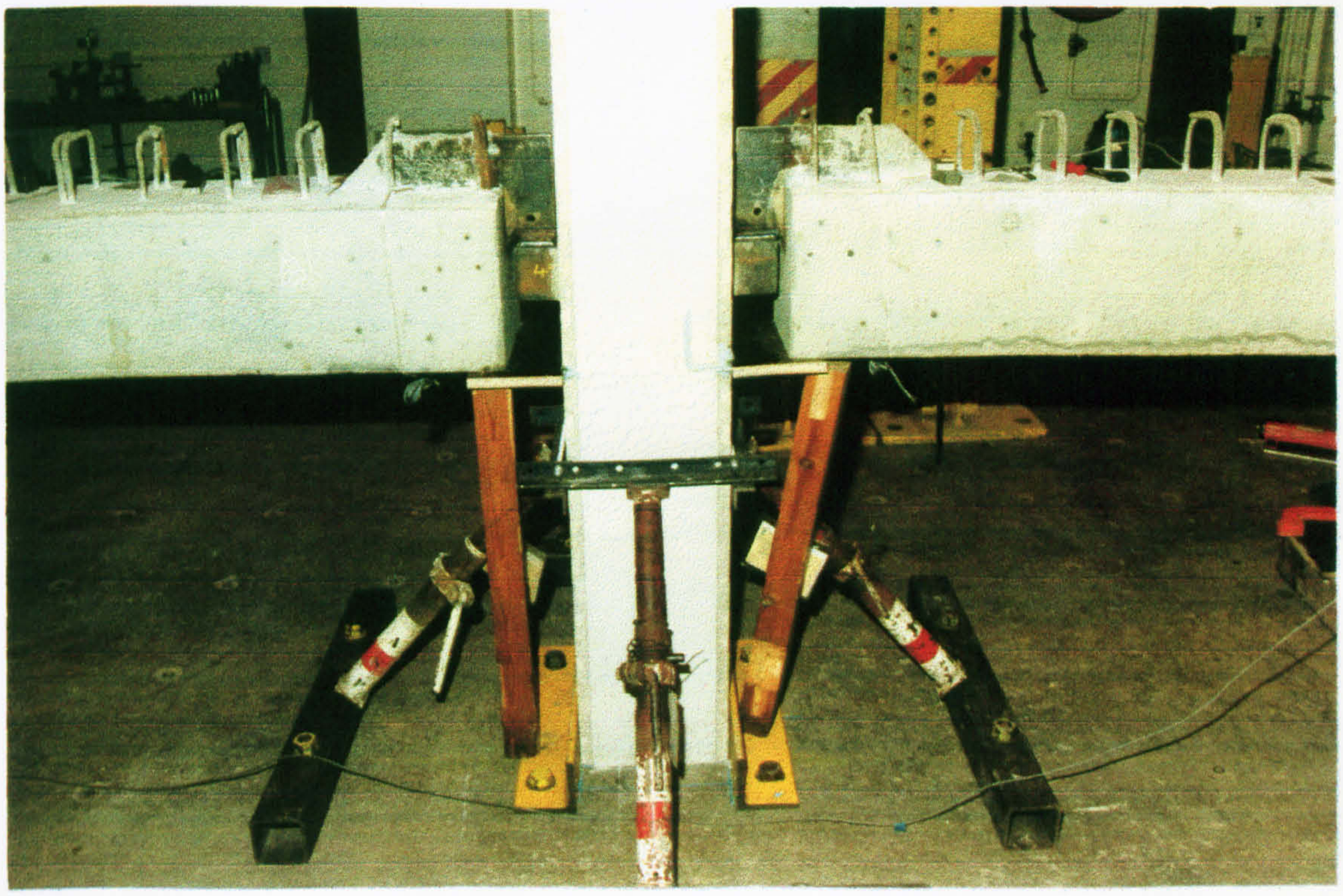

Plate 5.5: Welded plate connections after welding

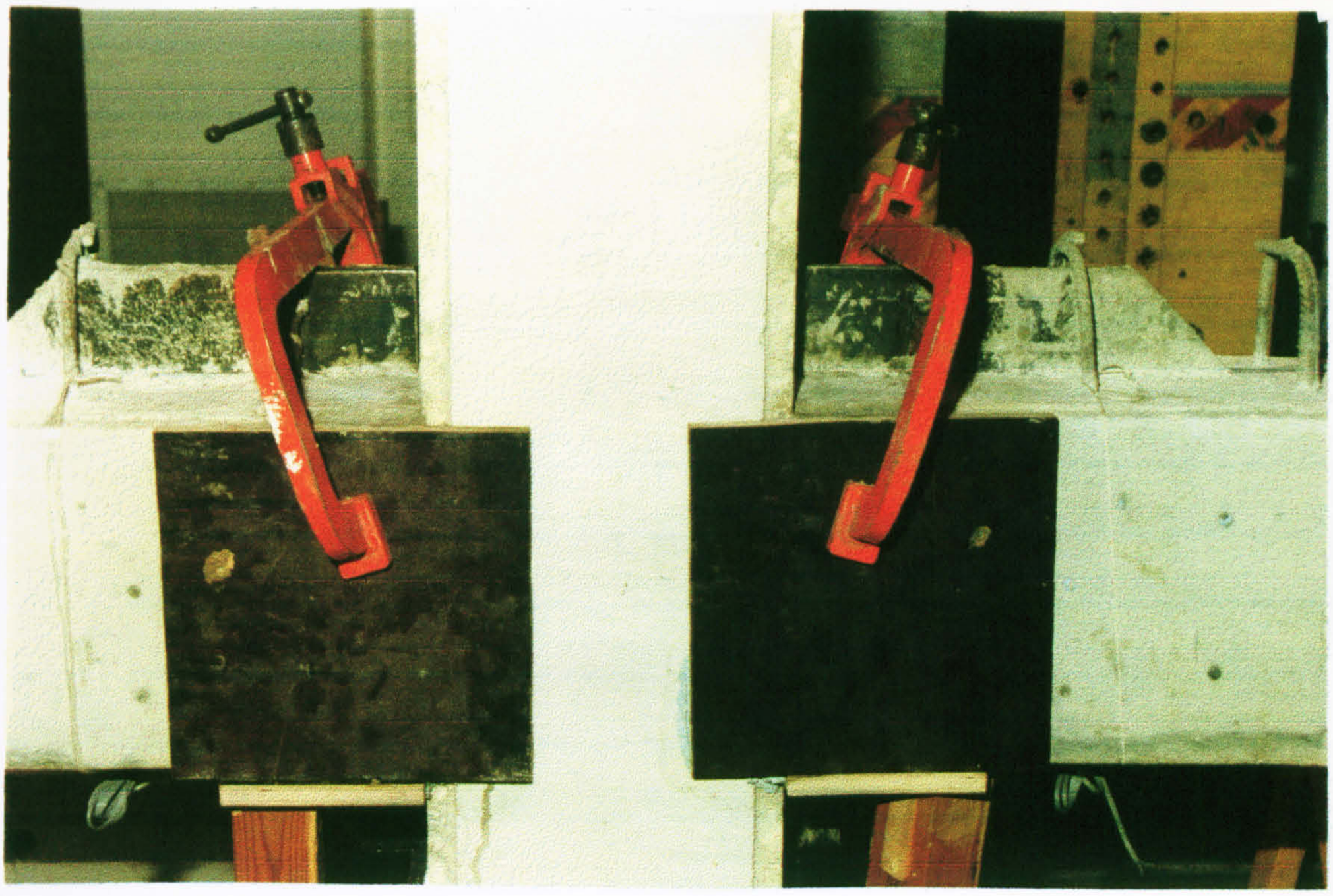

Plate 5.6: Casting joints concrete

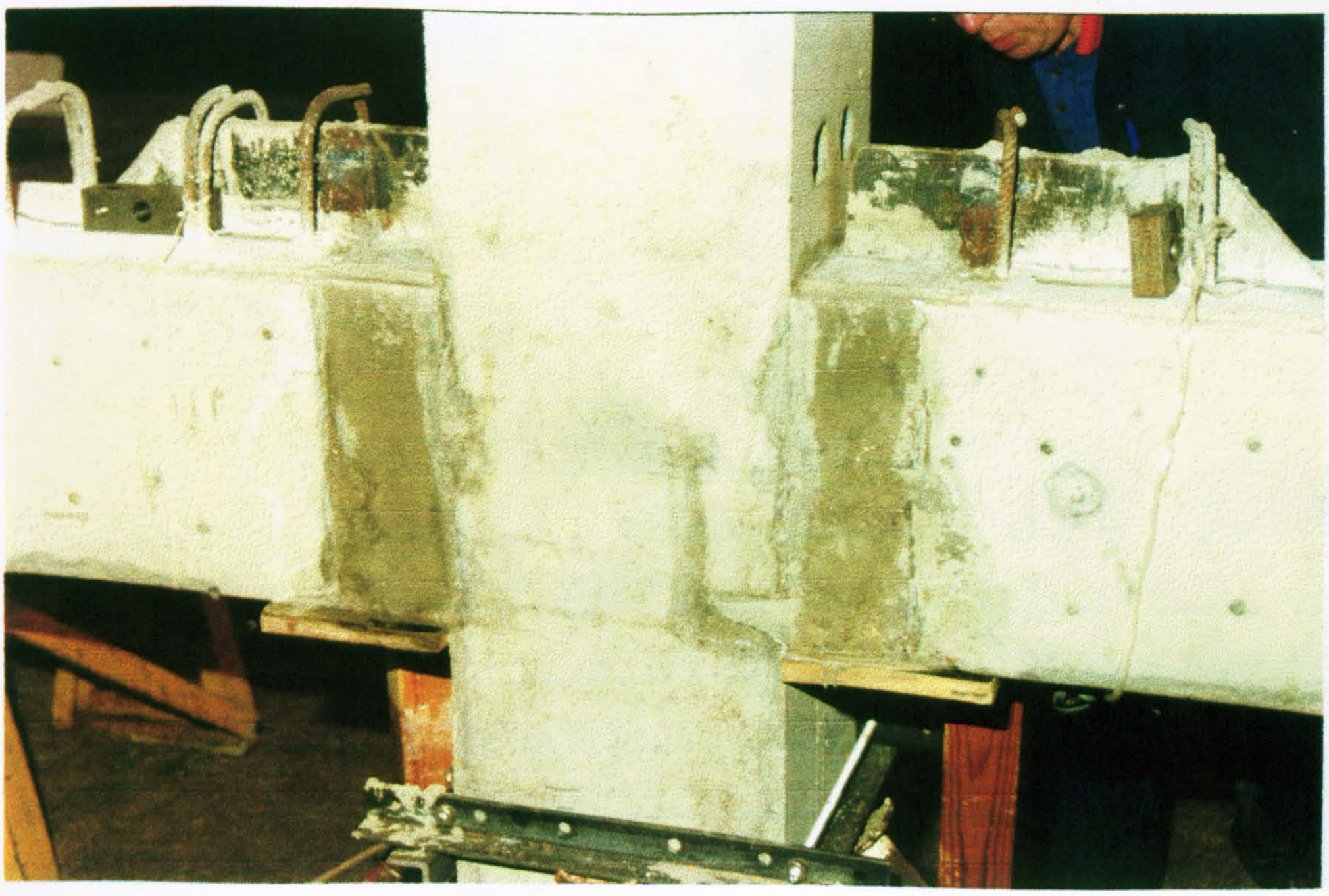

Plate 5.7: Joints concrete after casting

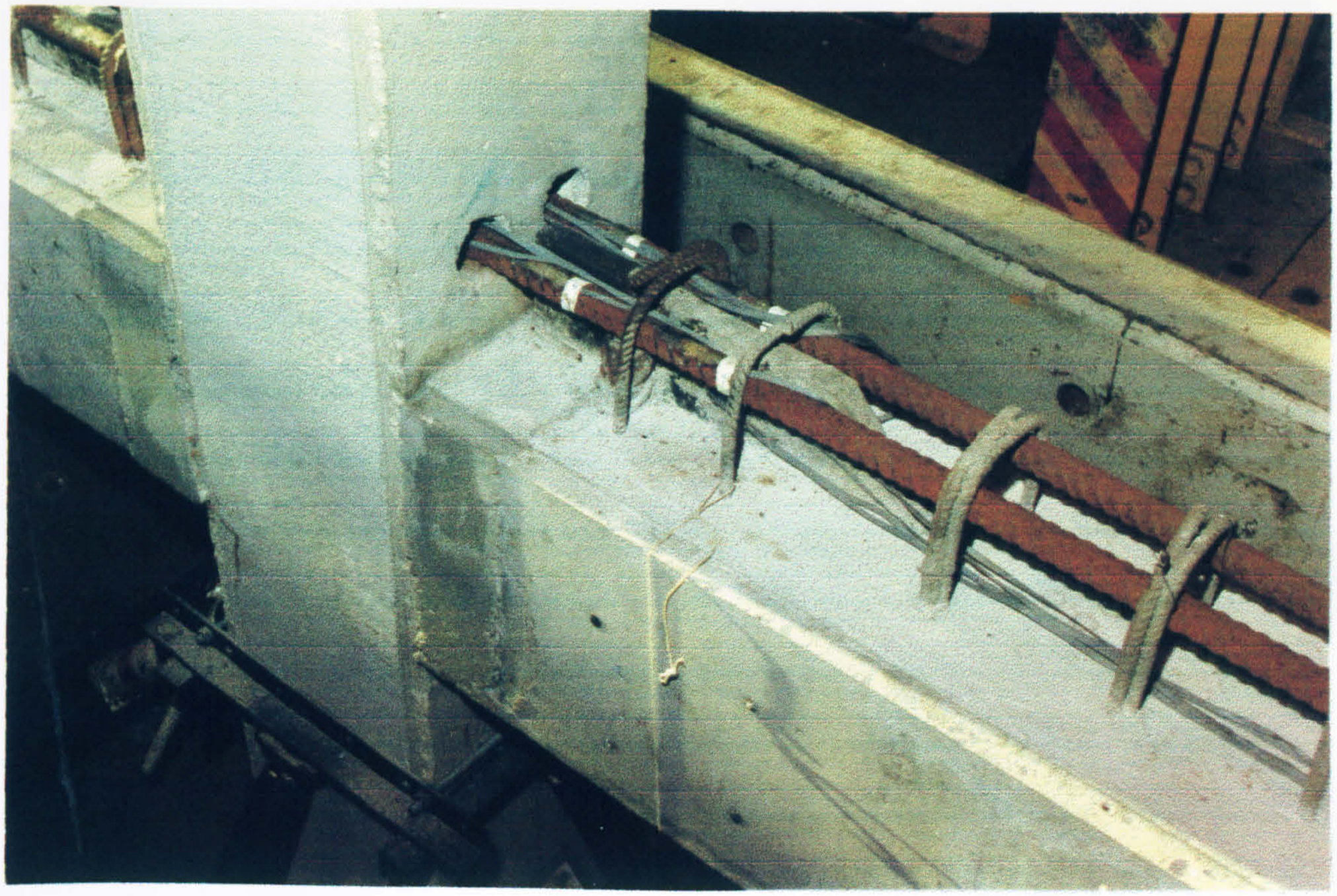

Plate 5.8: Location of stability tie bars with steel strain gauges for subframe SF1

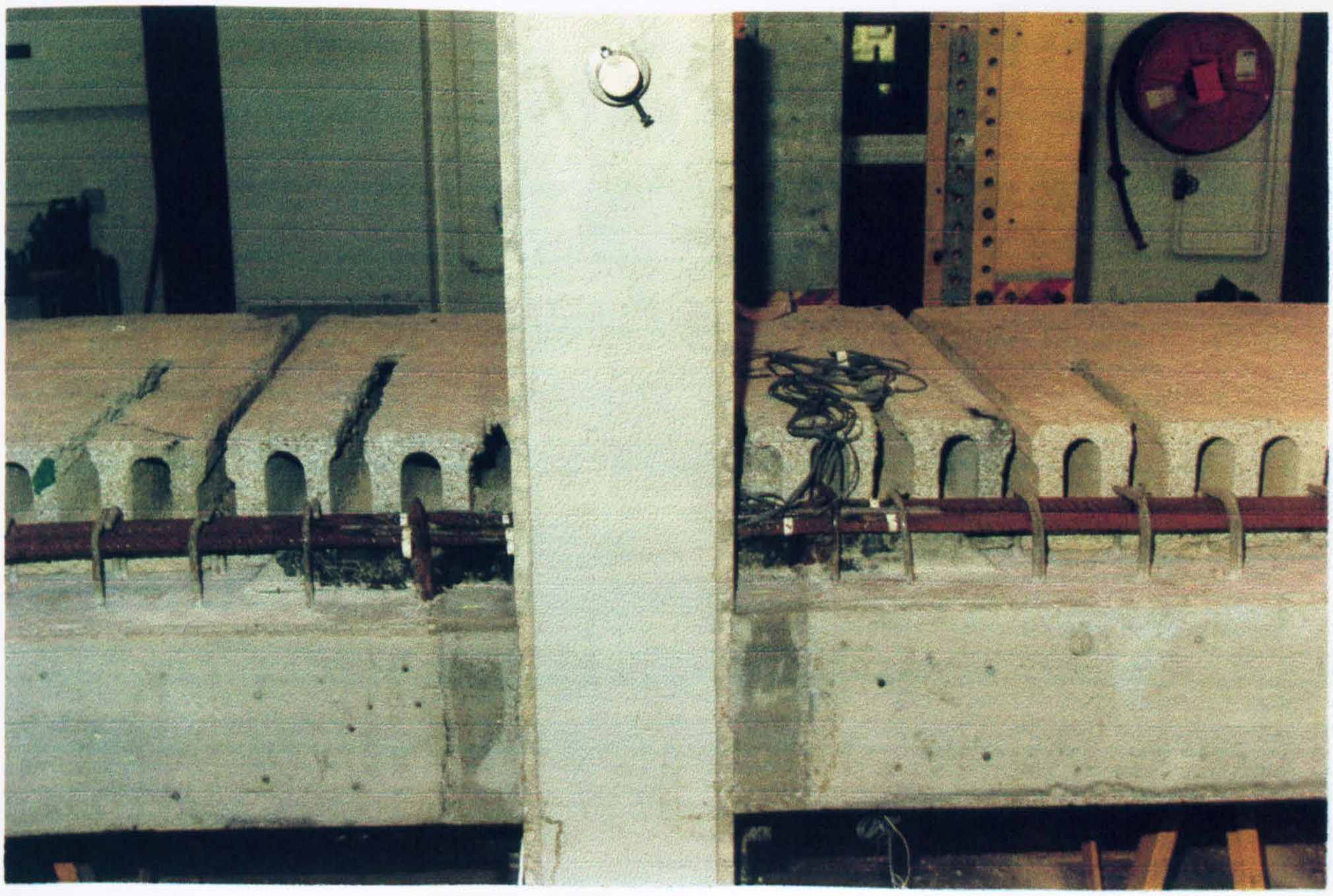

Plate 5.9: Subframe under construction

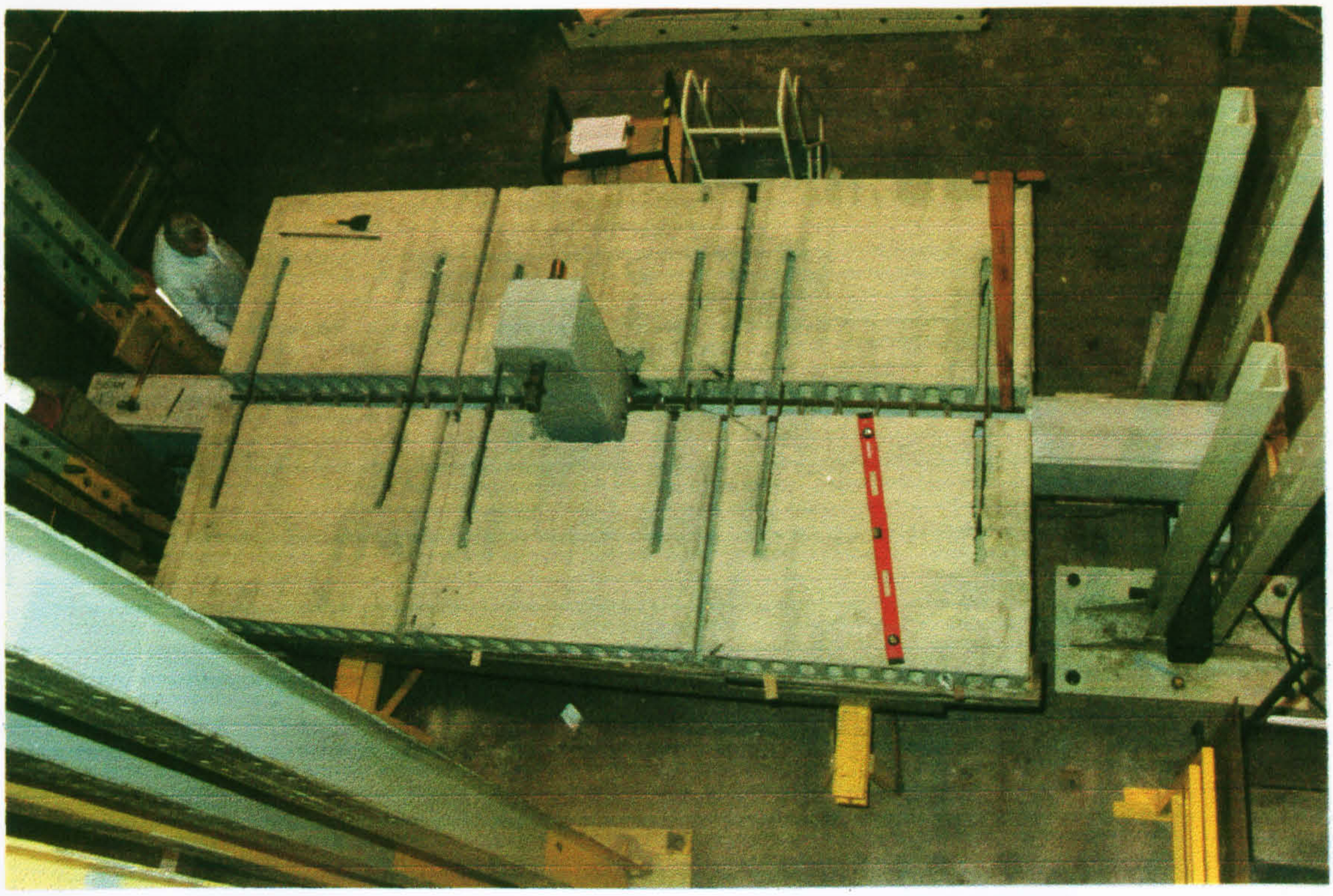

Plate 5.10: Subframe ready to cast slab-beam-column in situ concrete

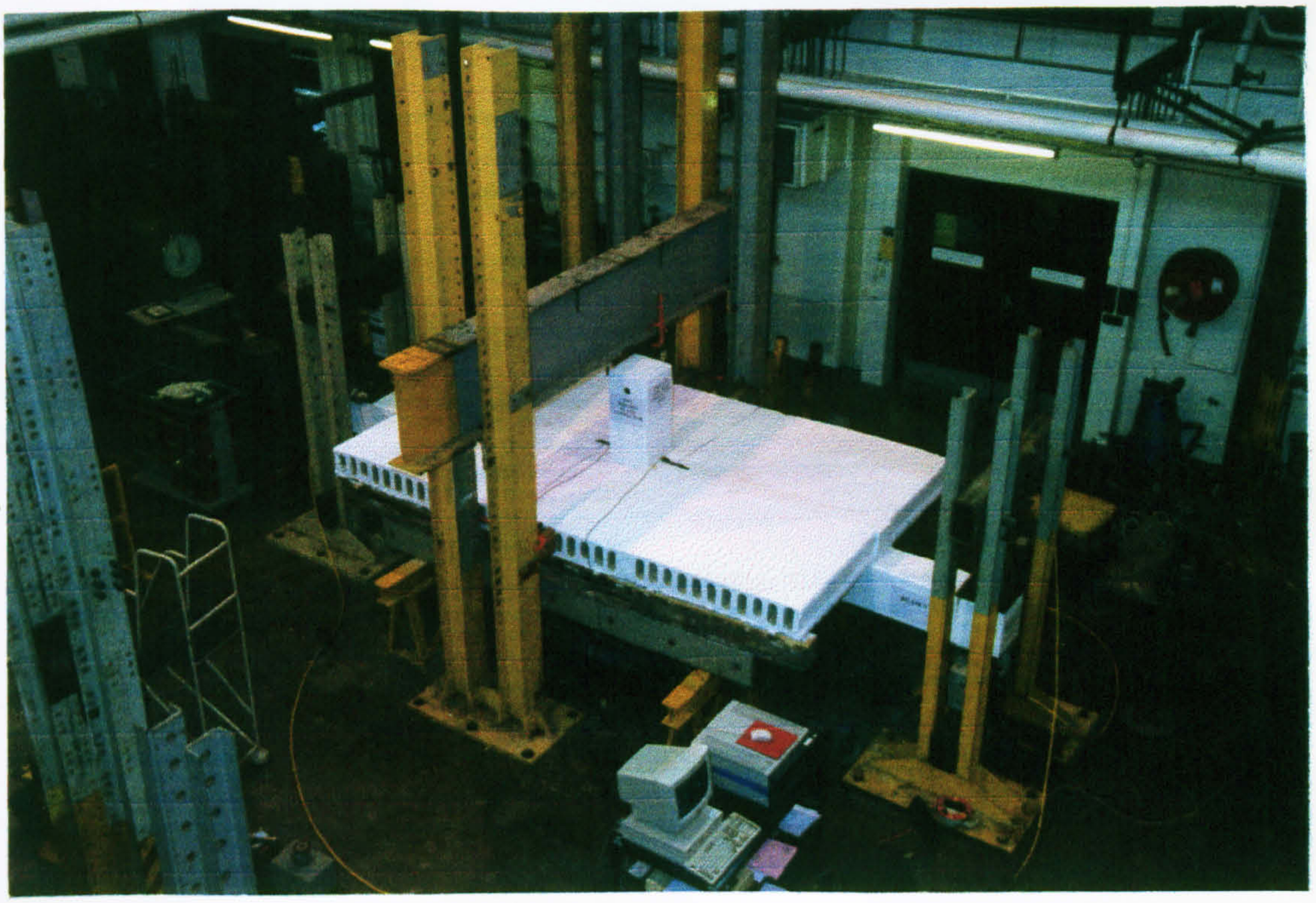

Plate 5.11: General assembly in Structures Laboratory for test series 1

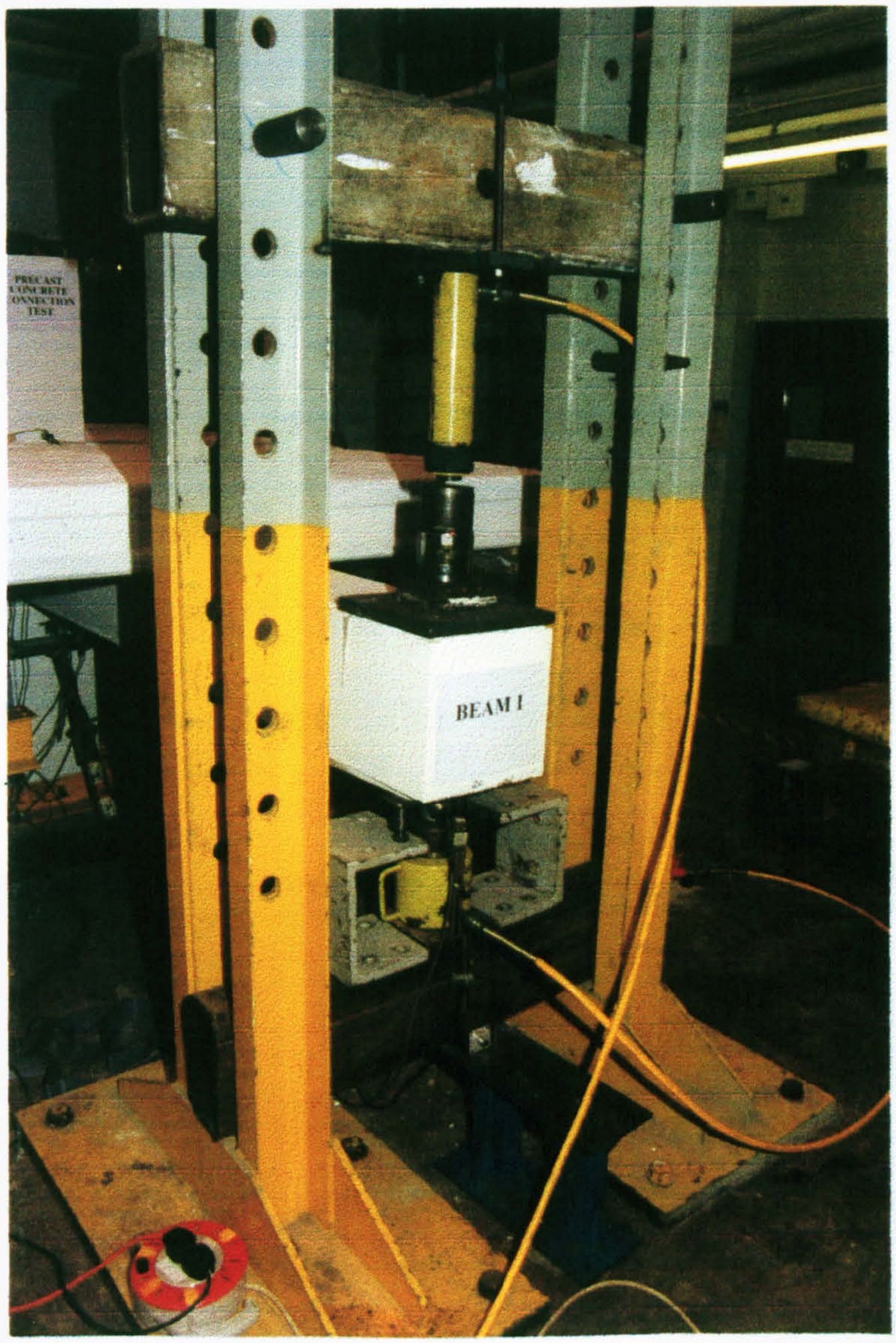

Plate 5.12: Mechanisims at the free ends of the beams

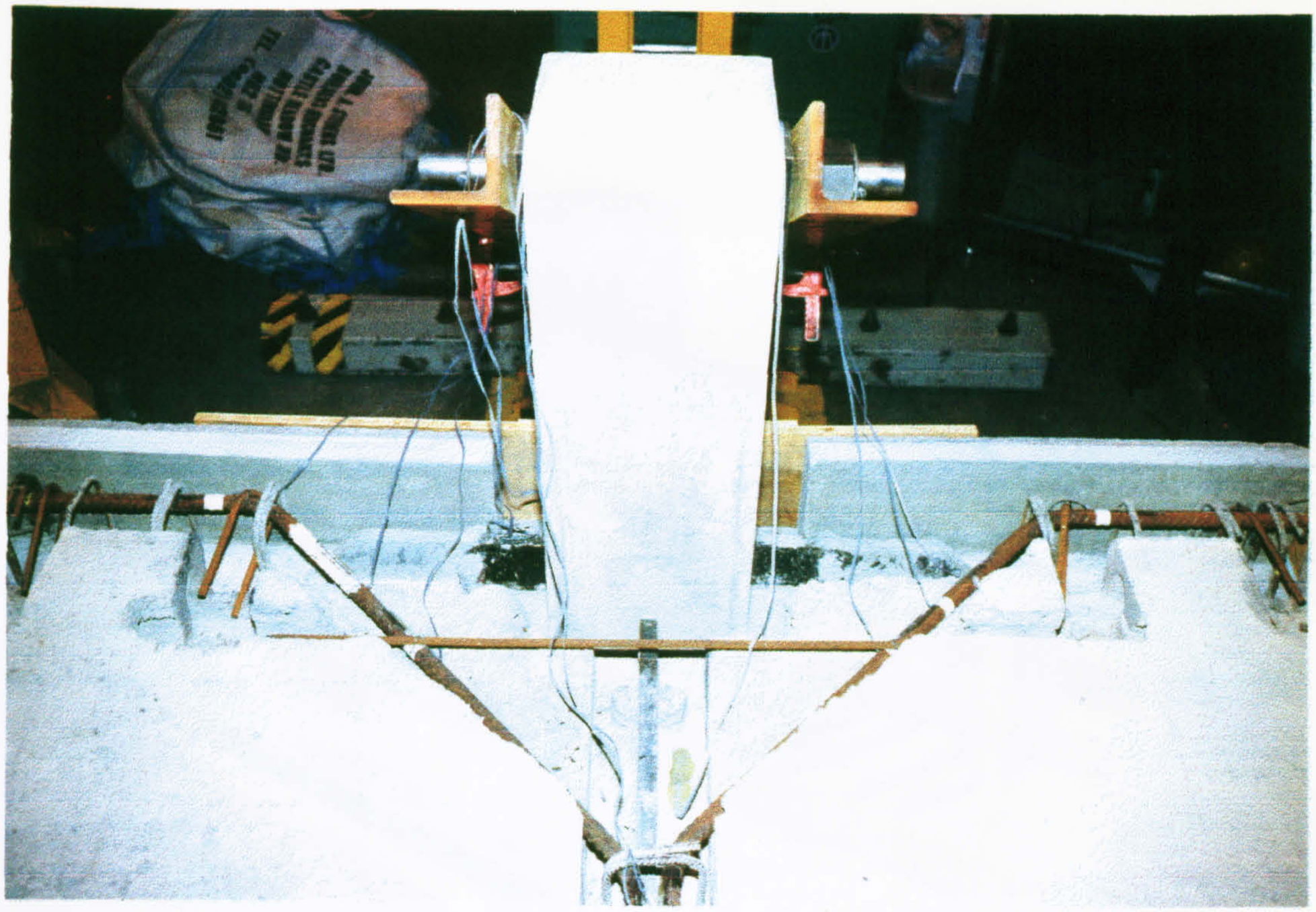

Plate 5.13: Location of stability tie bars with steel strain gauges for subframe SF2

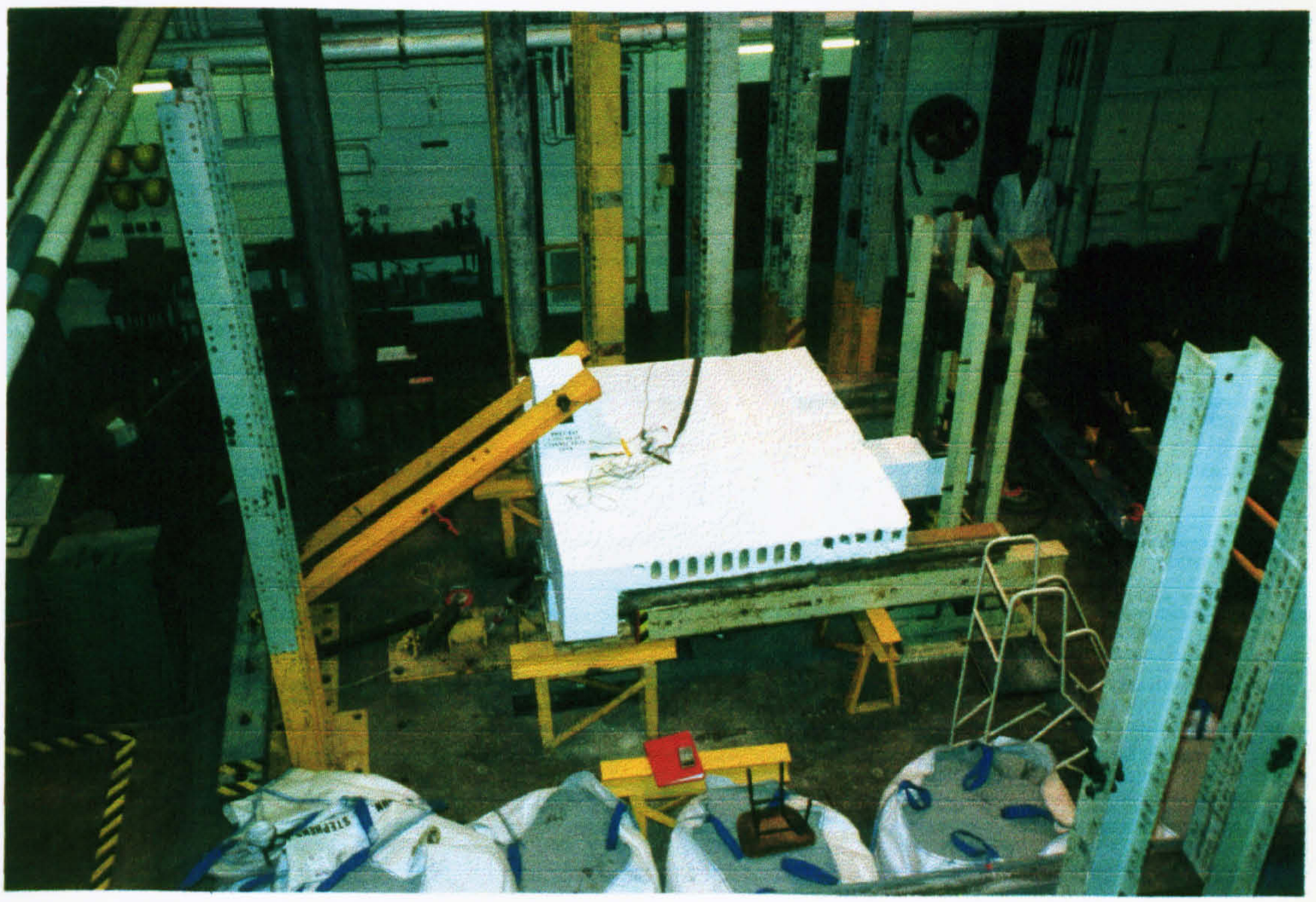

Plate 5.14: General assembly in Structures Laboratory for test series 2

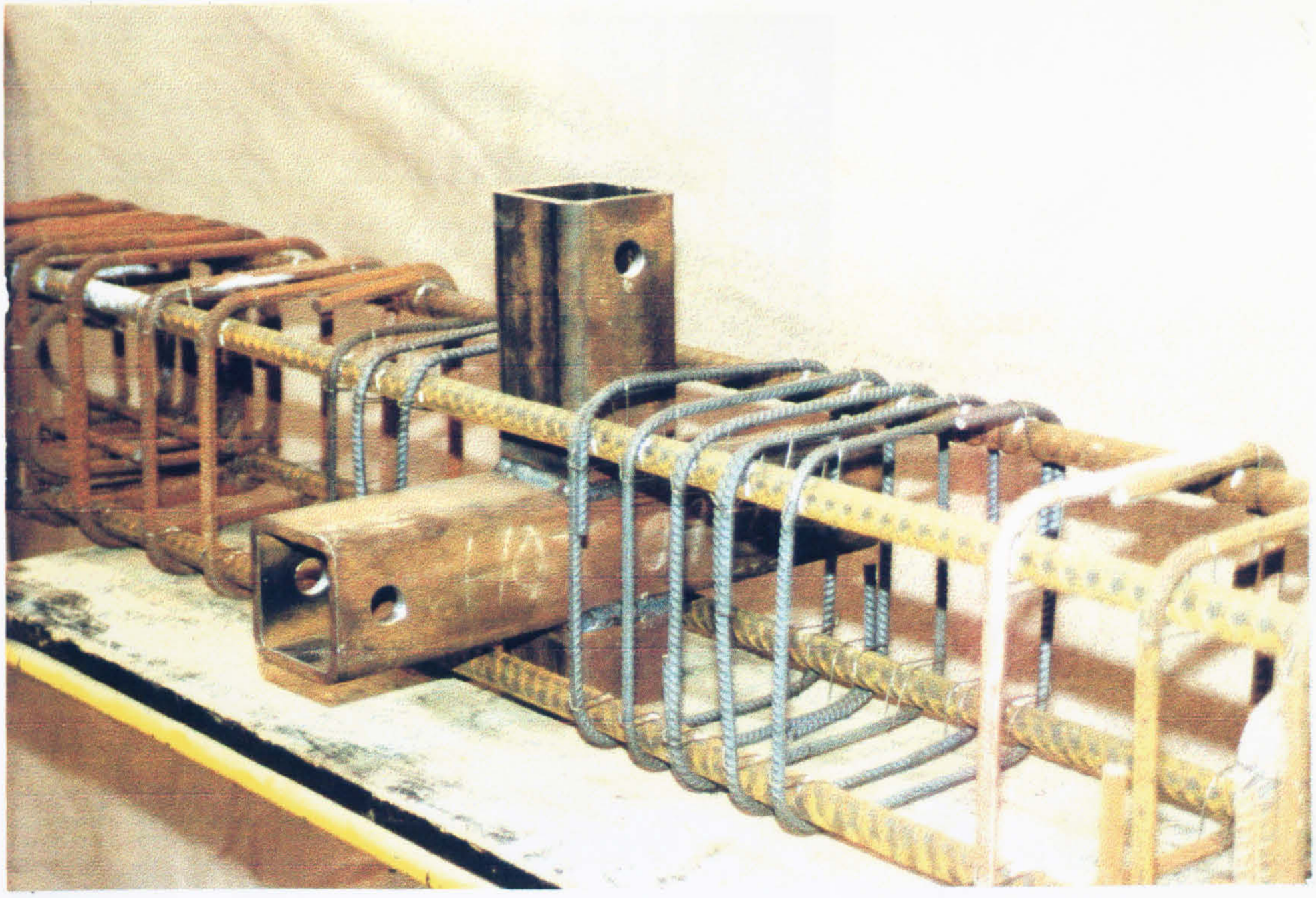

Plate 5.15: Column reinforcement with RHS billet

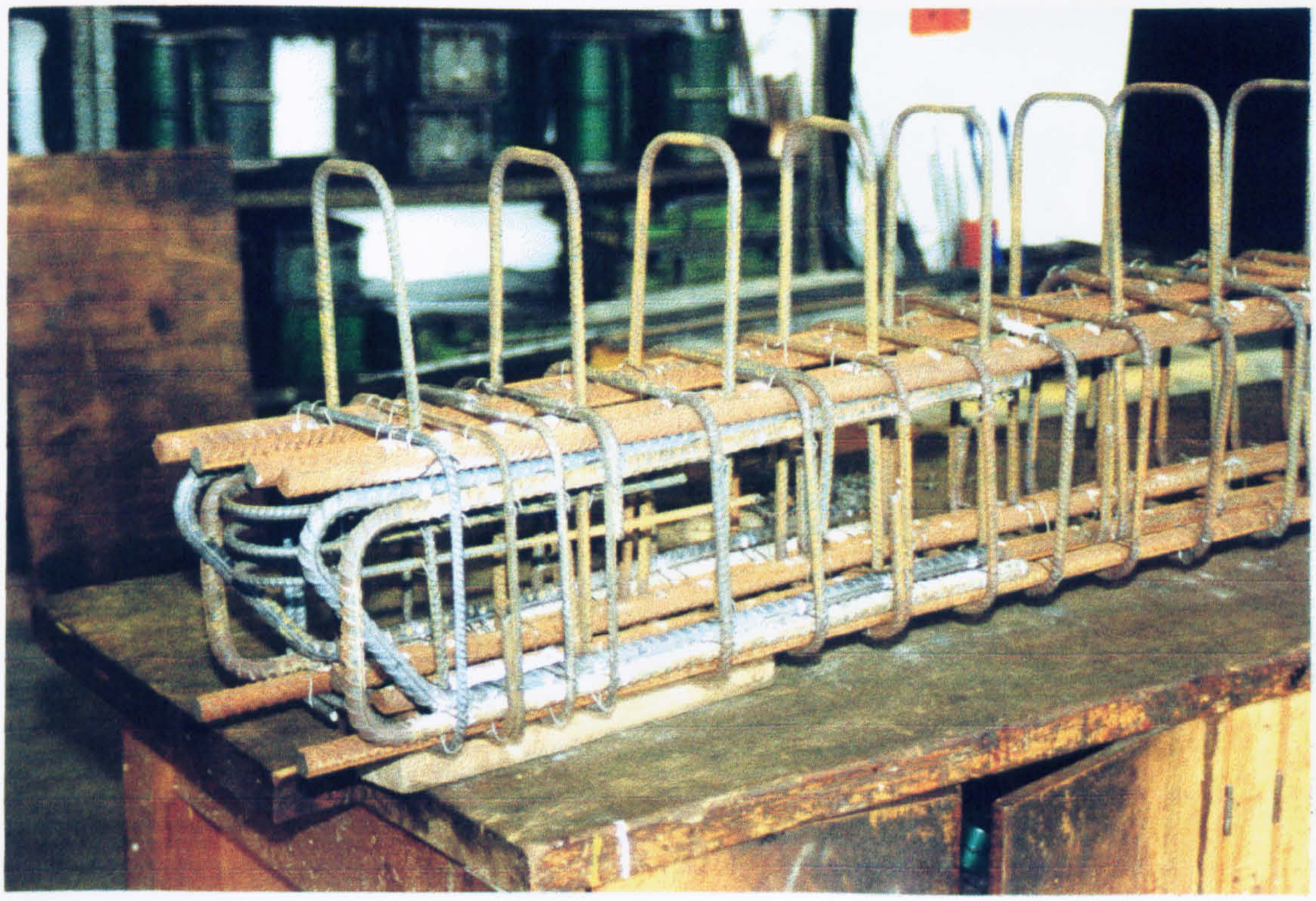

Plate 5.16: Beam reinforcement for bolted billet connection

Plate 5.17: Construction of bolted billet connnection in test series 3

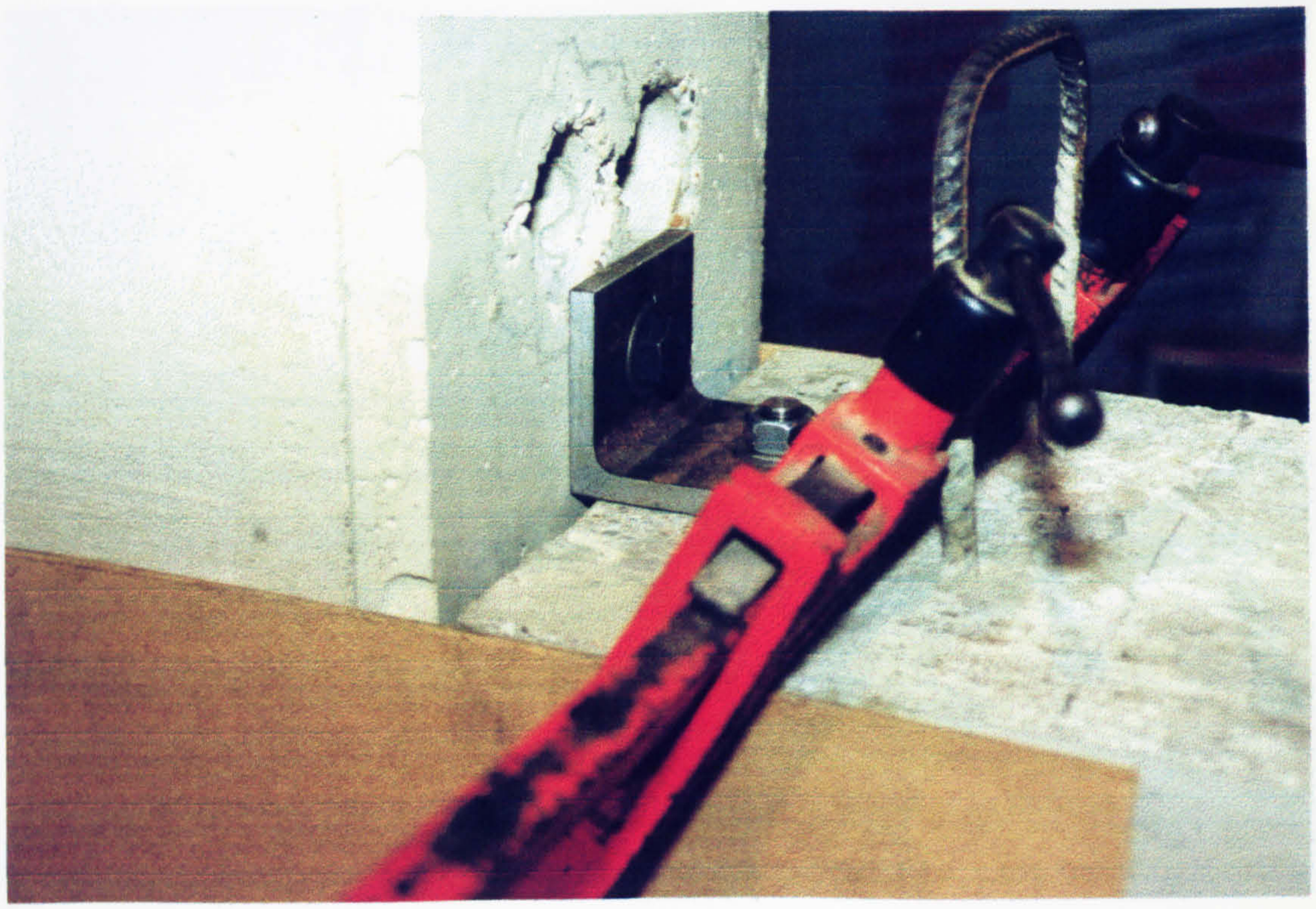

Plate 5.18: Column connecting angle (connections ready for grouting)

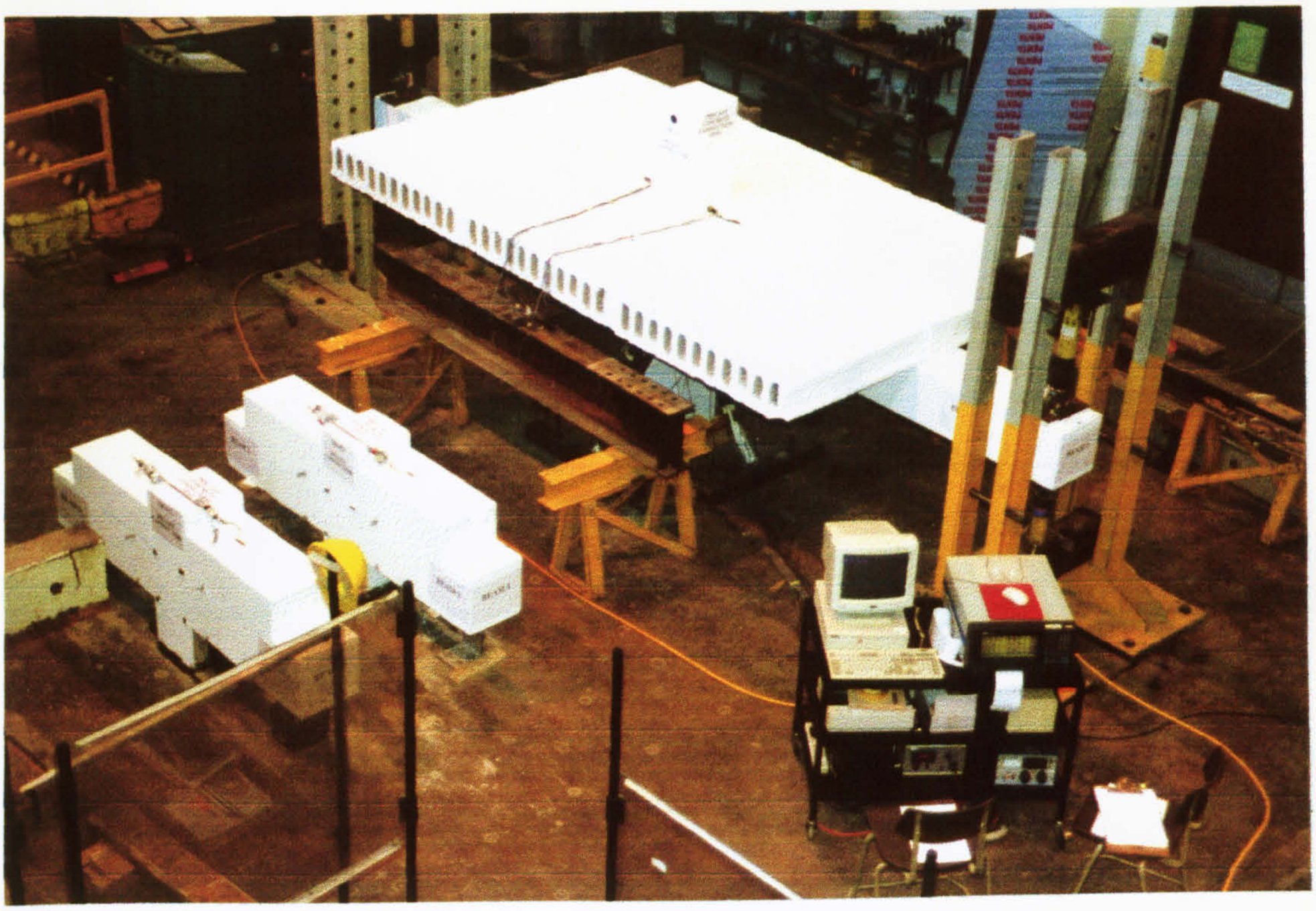

Plate 5.19: General assembly in Structures Laboratory for test series 3

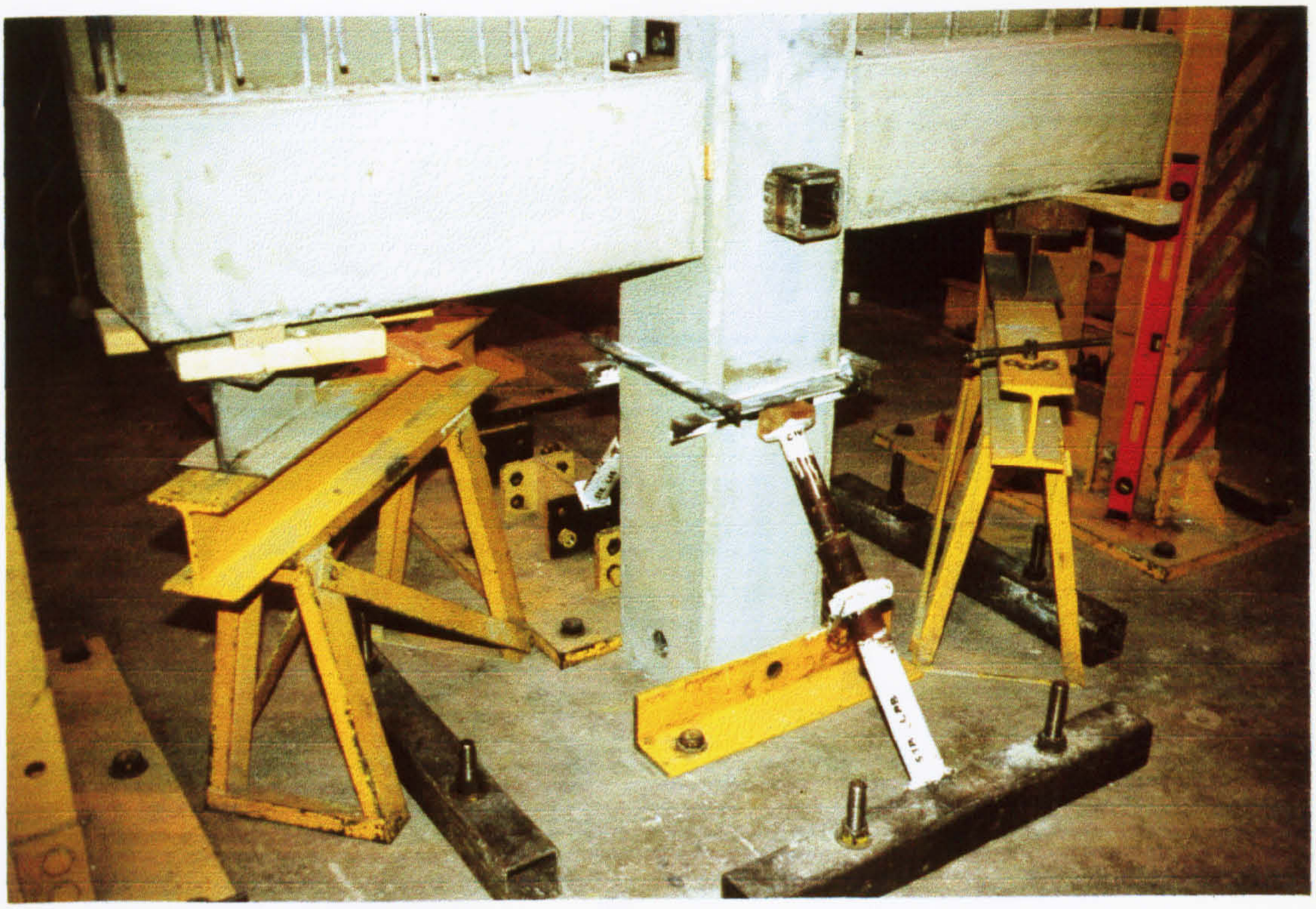

Plate 5.20: Construction of subframe in test series 4

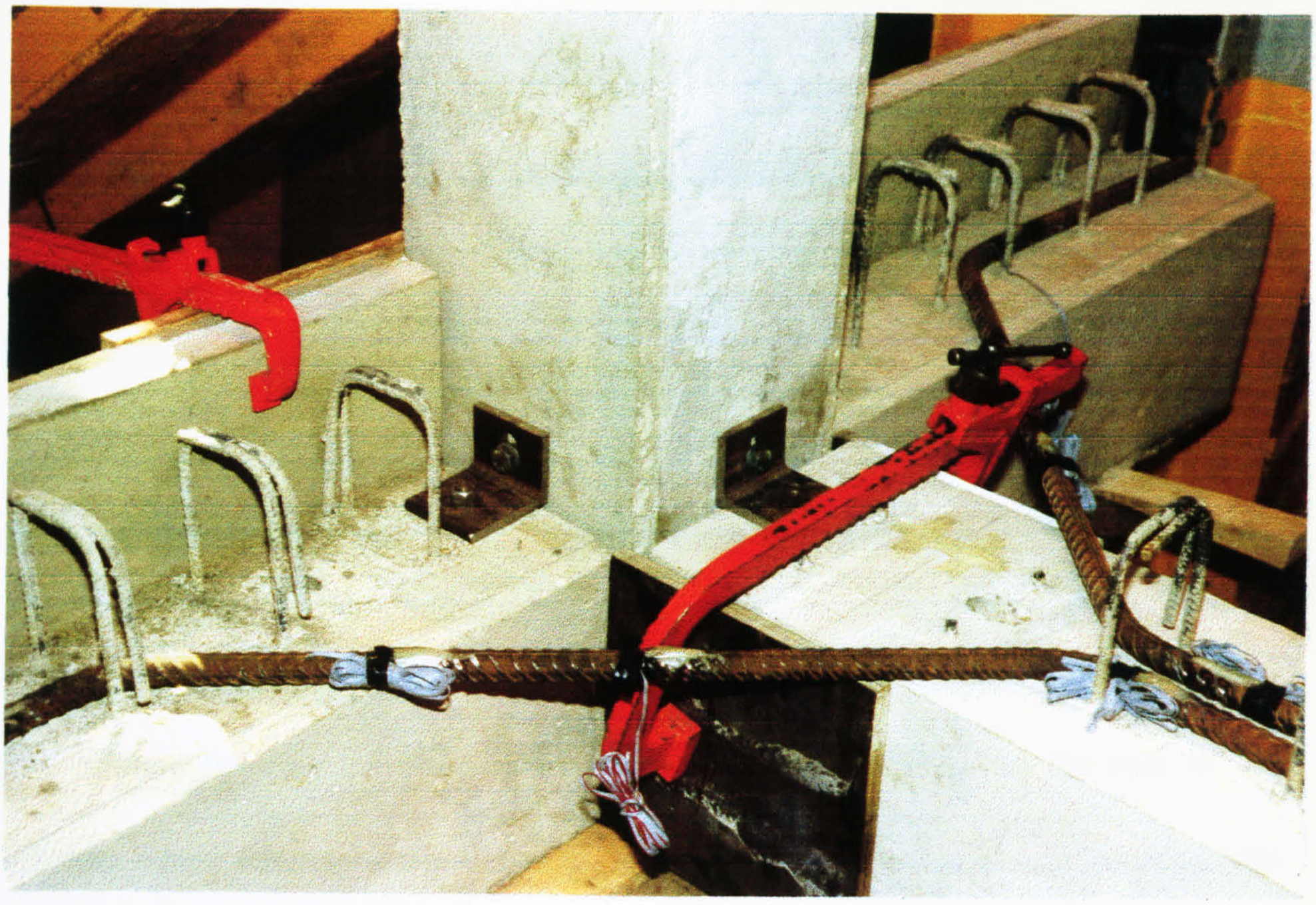

Plate 5.21: Connections ready for grouting in tests series 4

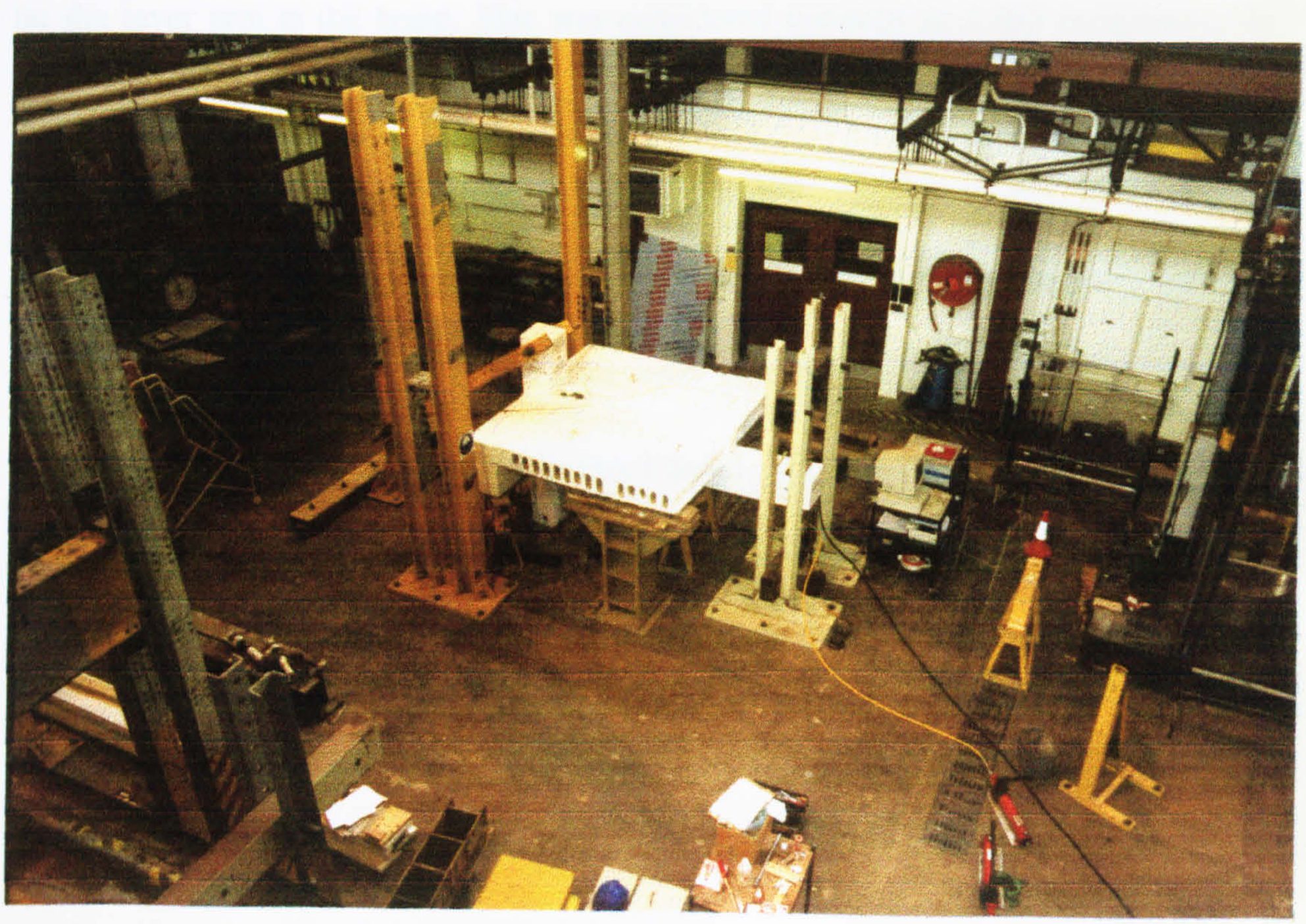

Plate 5.22: General assembly in Structures Laboratory for test series 4

CHAPTER 6

RESULTS OF FULL SCALE FRAME CONNECTION TESTS

6.1 Calculation of moment-relative rotation and stiffness

6.1.1 Calculation of moments

The applied hogging bending moment in the connection M_{con} at the face of the column, where the most critical zone of the connection is located due to the maximum bending stresses, was calculated by multiplying the magnitude of applied bending load P, recorded by the load cells 1 and 2 for the beams 1 and 2 respectively (Figure 5.1), by the lever arm in the beam. This was considered constant at 2.365 m between the line of action of the applied loads at the ends of the beams and the faces of the column.

The initial bending moment of the connection M_i due to self weight of the components was calculated using the same lever arm and the magnitude recorded by load cells 3 and 4 (Figure 5.17(a)) after removing the wedges of the slab units. M_i values were 6.80 and 6.45 kNm for beams 1 and 2, respectively in test TW1(A). These were ignored to be on conservative side and not involved in calculating actual (test) values of the joint M_{con} or M_u and not measured in the rest of the tests.

6.1.2 Calculation of relative rotations

The relative rotations ϕ between beam and column were calculated using two methods as follows:-

Method 1 (M1): Using vertical POTs mounted on two steel rods bolted to the column as shown in Figure 5.17(a). They measured the vertical deflections (e.g. "POT14" means the deflection measured by POT no 14) of the beams and joints relative to the column including shear effects. Shear deflections are thus eliminated. The deflection divided by their respective distances (actual distances) from the column faces produced the required relative rotations as follows:-

For the beam 1 (B1) side:-

$$\text{M1 B1 V1: } \phi = \left(\frac{\text{POT14}}{90}\right) \qquad \textit{Eq}.6.1(a)$$

$$\text{M1 B1 V2: } \phi = \left(\frac{\text{POT16}}{110}\right) \qquad \textit{Eq}.6.1(b)$$

$$\text{M1 B1 V3: } \phi = \left(\frac{\text{POT18}}{300}\right) \qquad \textit{Eq}.6.1(c)$$

$$\text{M1 B1 V4: } \phi = \left(\frac{\text{POT18} - \text{POT16}}{300 - 110}\right) \qquad \textit{Eq}.6.1(d)$$

Ditto for the beam 2 (B2) side.

Method 2 (M2): Using the horizontal POTs clamped to the top of the slab in-situ concrete and near to the top and bottom of the beams. They were clamped by drilling the slab in-situ, beams and column. They measured the crack openings δ_T and

compressive deformations δ_B in the joints relative to the column (see Figure 5.17(a)). This method assumes full shear interaction between the floor slab and the beam. The required relative rotations were produced as follows:-

For the slab 1 (S1) and beam 1 (B1) side:-

$$\text{M2 S1: } \phi = \left(\frac{\text{POT2} + \text{POT10}}{500}\right) = \left(\frac{\delta_T + \delta_B}{500}\right) \qquad Eq.6.2(a)$$

where δ_T (mm) is the crack opening at the top of the slab 1 recorded by POT2

δ_B (mm) is the compressive deformation in the joint recorded by POT10

500 (mm) is the actual vertical distance between strokes of POT2 and POT10

$$\text{M2 B1: } \phi = \left(\frac{\text{POT6} + \text{POT10}}{260}\right) = \left(\frac{\delta_T + \delta_B}{260}\right) \qquad Eq.6.2(b)$$

where δ_T (mm) is the crack opening at the top of the beam 1 recorded by POT6

260 (mm) is the actual vertical distance between strokes of POT6 and POT10

Ditto for the slab 2 (S2) and beam 2 (B2) side.

The rotations ϕ were then used in the presentation of the moment-relative rotation ($M_{con} - \phi$) graphs. The sidesway of the column in and out of the plane of bending were ignored due to the symmetrical loading of the beams, equal span slabs and the way of measuring deflection, because the POTs measured the deflections relative to the column itself.

6.1.3 Calculation of stiffnesses

The rotational stiffnesses, J (general), were calculated from the slope of the $M_{con} - \phi$ curve on the basis of both tangent stiffness and the secant stiffness of the chord of the curve. Each loading and unloading curve was analysed using regression analysis. Cycle 1 has five different estimates of rotational stiffness J as follows (see Figure 6.1(a)):-

a) Before cracking

(1) The initial tangent flexural stiffness J_u, which is the slope of the $M_{con} - \phi$ curve from the beginning of the test to the first crack moment of the connection M_{cr}

(2) The initial secant flexural stiffness J_{is}, which is the slope of the chord of the same curve in (1)

b) After cracking

(3) The tangent flexural stiffness J_c, which is the slope of the $M_{con} - \phi$ curve from the M_{cr} to the peak moment of the cycle M_{peak}

(4) The flexural stiffness of unloading curve J_{unl}

(5) The secant flexural stiffness J_s, which is the slope of the chord of the $M_{con} - \phi$ curve from the beginning of the cycle to the M_{peak}

For the second, third and fourth cycles J_c and J_s were calculated from the beginning of reloading $M_{con} - \phi$ curves to the peak moment of the corresponding cycle M_{peak}. For the last cycle, C5, J_c was calculated up to a moment value at which the slope of the graph decreased rapidly (see Figure 6.1(b)).

6.2 Presentation of results

The results are presented from derived calculations. These include hogging bending moment in the connection M_{con} at the faces of the column versus crack opening δ_T at boundaries between the slabs and column and between the beams and column in the case of the test incorporating floor slabs and in-situ concrete, and between the beams and column only in the case of the test TW1(C). Moment versus compressive deformations δ_B in the joints, concrete and steel strains $\mu\varepsilon$, and relative rotations ϕ of the joints are also presented graphically. Where necessary the behaviour during the loading cycles 1-3 is enlarged and presented separately (as Figure(a)) before each of the corresponding results to failure (as Figure (b)). The latter do not show the unloading cycles and are derived by the sequential superposition of peak values. This enables a full picture of the behaviour to be realised.

6.3 Test series 1

6.3.1 Test TW1(A)

Figures 6.2 to 6.3 represent the moment M_{con} versus crack opening δ_T, at boundaries of slabs and column, and beams and column, and M_{con} versus compressive deformations δ_B in the beam-to-column joints for the double sided welded plate connection. These results show the relative displacements which induces the relative rotations between the slabs and column, and the beams and the column. The displacements are a measure of the elastic and plastic deformation of the connection as a whole and represent a release in concrete strain in tension, which

increases steel strains at the cracked section, the compressive strain generally, and strain in the joint concrete particularly

Calculated moment versus concrete strains in compression in the precast beams, and steel strains in bars A and B are presented in Figures 6.4 to 6.6, respectively. They define limits of the strains in the joint zone.

Figure 6.7 shows vertical displacement profiles along each of the beams for selected values of moment in cycle 5 only. The gradients of these plots enable beam-to-column rotation to be derived using the Method 1. POTs 12 and 14 were used to record the vertical deflection of the joint that would give relative rotation of the joint to the column face, the POTs 16 and 18 recorded the vertical deflections of the beam 1. The rotation obtained from the gradient of these two POTs (not effected by the shear deformation) would give the relative rotation of the beam-to-column by dividing the relative deflections of the sensors by their relative offsets (see Section 6.1.2 for M1 B1 V4). This is the relative rotation commonly used in many computer programs, i.e. SWANSA, by ignoring the length of the joint element and assuming the rotation of the joint takes place at its centre which varies according to the type of the connection, i.e. 50 mm from the face of the column for welded and 60 mm for the billet connection. The total relative rotation does not include the curvature of the beam, the location of POTs 17 and 18 were 200 mm from the end of the beams which is less than the overall depth of the beam ($h = 300$ mm).

The derived moment versus relative rotation graphs obtained from the two methods described in Section 6.1.2 are presented in Figures 6.8 to 6.10. Figure 6.11(a) presents the tangent loading and unloading stiffnesses J calculated using Method 1 for V4 only for both beams. Figure 6.11(b) presents the stiffnesses calculated using

Method 2 for both slabs and beams. The solid lines and dashed lines are used for the loading and unloading stiffnesses, respectively. The solid symbols present beam 1 side and open symbols beam 2, respectively.

Typical damaged zones for this test are presented in Plates 6.1 to 6.4. (The notation refers to applied target increment load P in kN. It was convenient to mark cracks at the applied target increment load P they observed during the tests. It is important to note that (a) the recorded P values are slightly different from the marked P values, i.e. the above marked P = 15 kN has been recorded as 15.5 kN for beam 1 and 15 kN for beam 2, (b) the actual P values at which the cracks appeared are in between two recorded increments. This means that the marked values are the upper limits for the cracks). The first crack appeared at the column face and spread to the outer edge of the hollow core slab. Plates 6.3 and 6.4 show the damaged area of the joints. A circle has been drawn around the bottom right hand corner of the joint (Plate 6.4) to indicate the extent of the concrete compression zone and the final position of the neutral axis, i.e. about 100 mm from the bottom of the beam. Horizontal bursting cracks are a clear indication of unconfined concrete compressive failure in the in-situ concrete infill. A second horizontal crack occurs at the level of the top surface of the solid steel billet, and is possibly indicative of local stress concentrations there. A summary of the test results is presented in Table 6.1. The actual (test) cracked moment M_{cr}, the peak moments of each cycle M_{peak} and ultimate moment capacity of the connection M_u, the actual (predicted) ultimate moment capacity of the connection M_{pred} and beam M_{beam}, the ratio of the actual cracked moment to the actual ultimate moment of the connection and ratio of the actual moment of the connection to those predicted are also presented. The tangent and unloading flexural stiffnesses of

the connections for each cycle in TW1(A) from the Methods 1&2 are presented in Tables A6.1.1 to A6.1.2 and the secant flexural stiffnesses are presented in Tables A6.1.3 to A6.1.4 in Appendix 6.1 with corresponding relative rotations and calculated K_s (see *Eq*.1.1) values from the secant stiffnesses in cycle 5. Details for calculating K_s values are given in Chapter 7.

6.3.2 Test TW1(B)

This test was carried out after the bending test, TW1(A), to ensure that the shear resistance of the entire connection was satisfactory. The ultimate experimental design resistance previously obtained was 278 kN. With known distances of the applied shear load P and end reaction V from the centre of the column (see Figure 5.3 and Plate 6.5), ratios of P/V were found analytically as 1.113 and 1.374, assuming rigid and pinned joints, at the centre of the column respectively.

The test was stopped after a satisfactory shear resistance V = 300 kN of the connection was achieved. The reason for stopping the test was to prevent damage to the precast beams and column for re-use in the flexural beam test TW1(C).

Test results are presented in Figure 6.12 together with analytical values. The test set up, and the damaged region around the column after test was completed are presented in Plates 6.5 to 6.10.

6.3.3 Test TW1(C)

This test is a continuation of test TW1(A) in which 200 mm deep hollow core slabs and tie bars were removed in order to evaluate the reductions in the main characteristics of the connection due to the absence of these items.

Figure 6.13 presents moment versus crack opening at boundaries of the beams/column. The moment versus compressive deformations in the joints are presented in Figure 6.14. Vertical deflections profiles are presented in Figure 6.15. The reasons for the apparent reversals in deflections within the joint zone are explained in Chapter 7 (Section 7.4.3). The moment-rotation characteristics of the two beams are plotted in Figures 6.16 to 6.18 and the stiffnesses in Figure 6.19 for both beams.

Typical damaged zones for this test are presented in Plates 6.11 and 6.12. A summary of the test results is presented in Table 6.1. The rotational stiffnesses values are presented in Tables A6.1.6 to A6.1.8 as in TW1(A).

6.4 Test series 2

6.4.1 Test TW2

Referring to Figures 6.20 to 6.21, these graphs represent the moment M_{con} versus crack opening δ_T, at boundary of the slabs and column only (at the boundary of the beam and column is not available due to a fault in POT6) and M_{con} versus compressive deformations δ_B in the beam-to-column joint for the single sided welded plate connection.

The moment versus concrete strains in compression, and steel strains in bars A and B are presented in Figures 6.22 to 6.24, respectively. In addition to the concrete compressive strain gauge SG1 in test TW1(A) two more concrete strain gauges SG1b and SG1c were used in the compression zone at interface between the end of the beam and adjacent face of the joint and at the centre of the joint, respectively.

Figure 6.25 shows vertical displacement profiles along the beam for selected values of moment in cycle 5 only.

The derived moment versus relative rotation graphs obtained from the two methods are presented in Figures 6.26 to 6.27. Figure 6.28 presents the tangent stiffnesses for loading and unloading.

Typical damaged zones for this test are presented in Plates 6.13 to 6.17. Plates 6.14 and 6.17 show the damaged area of the joints and precast concrete members. A tape measurement has been used at the top of the edge beam and around the bottom right hand corner of the joint (Plate 6.15) to indicate the extent of the concrete tension and compression zones. The zone of influence in the beam in compression was measured at 300 mm from the face of the column. A summary of the test results is presented in Tables 6.1. The tangent and unloading flexural stiffnesses of connections for each cycle in TW2 from the Methods 1&2 are presented in Table A6.1.9 and the secant flexural stiffnesses are presented in Table A6.1.10 in Appendix 6.1 with corresponding relative rotations and calculated K_s values.

6.5 Test series 3

6.5.1 Test TB1(A)

Figures 6.29 to 6.30 represent the moment M_{con} versus crack opening δ_T, at boundaries of slabs and column, and beams and column, and M_{con} versus compressive deformations δ_B in the beam-to-column joints for the double sided billet connection. There is no compressive deformation value after cycle 1 in beam 2 side due to a fault in POT9.

Calculated moment versus concrete strains in compression in the precast beams and joint, and steel strains in bars A and B are presented in Figures 6.31 to 6.33, respectively. An addition to the strain gauge SG1 in test TW1(A), two extra strain gauges SG1d and SG1e, 60 mm from the column face (ditto for beam 2 side), were used at the bottom of the beam and at the joint centre, respectively. The number of the steel strain gauges were reduced from 5 to 3 for each bar in this test series (TB1(A), TB1(B) and TB1(C)). There was no need to use steel strain gauges SG1 and SG5, 200 mm far from the column face.

Figure 6.34 shows vertical displacement profiles along each of the beam for selected values of moment in cycle 5 only. POT18 failed to record deflections.

The derived moment versus relative rotation graphs obtained from the two methods are presented in Figures 6.35 and 6.36. Figure 6.37(a) presents the tangent stiffnesses for loading and unloading calculated from the Method 1 for V4 for beam 2 (not available for beam 1 due to a fault in POT18). Figure 6.37(b) presents the stiffnesses calculated from the Method 2 for both slab 1 and beam 1 (not available for sab 2 and beam 2 due to a fault in POT9).

Typical damaged zones for this test are presented in Plates 6.18 to 6.20. Plates 6.19 and 6.20 show the damaged area of the beams and joints. Flexural cracks have been marked on the top of the beams and in the joints to indicate the extent of the concrete compression zone and the final position of the neutral axis, i.e. about 160 mm from the bottom of the beam in the beam and 100 mm from the bottom of the beam in the joint. Horizontal bursting cracks (see Plate 6.20) are a clear indication of unconfined grout compressive failure in the joint and concrete in the part of the beam that covers the joint which is also unconfined about 125 mm from the end of the beam (see Figure 5.13(a)). A summary of the test results is presented in Tables 6.1. The flexural stiffnesses for tangent and unloading of connections for each cycle from the Methods 1&2 are presented in Tables A6.1.11 to A6.1.12 and the secant flexural stiffnesses are presented in Tables A6.1.13 to A6.1.14 in Appendix 6.1 with corresponding relative rotations and calculated K_s values from the secant stiffnesses in cycle 5.

6.5.2 Test TB1(B)

Figures 6.38 to 6.39 represent the moment M_{con} versus crack opening δ_T, at boundaries of slabs (in-situ) and column, and beams and column, and M_{con} versus compressive deformations δ_B in the beam-to-column joints for the double sided billet connection.

Calculated moment versus concrete strains in compression in the precast beams, and steel strains in bars A and B are presented in Figures 6.40 to 6.42, respectively. The strain gauge SG1e was not used in this test (ditto for beam 2 side).

The derived moment versus relative rotation curves obtained from the Method 2 (the Method 1 was not used in this test) are presented in Figure 6.43. The stiffnesses calculated from the Method 2 are presented in Figure 6.44 for both slabs and beams.

Plates 6.21 and 6.22 show the damaged area of the beams, in-situ infill topping and joints. Flexural cracks have been marked on the top of the beams and in the joints to indicate the extent of the concrete compression zone and the final position of the neutral axis in the beams. A summary of the test results is presented in Tables 6.1. The tangent and unloading flexural stiffnesses of connections for each cycle from the Method 2 are presented in Table A6.1.15 and the secant flexural stiffnesses are presented in Tables A6.1.16 in Appendix 6.1 with corresponding relative rotations and calculated K_s values from the secant stiffnesses in cycle 5

6.5.3 Test TB1(C)

Figures 6.45 to 6.46 represent the moment M_{con} versus crack opening δ_T, at boundaries of slabs (in-situ) and column, and beams and column, and M_{con} versus compressive deformations δ_B in the beam-to-column joints.

The moment versus concrete strains in compression in the precast beams, and steel strains in bars A and B are presented in Figures 6.47 to 6.49, respectively.

The moment versus relative rotation curves obtained from the Method 2 (the Method 1 was not used in this test) are presented in Figure 6.50. The stiffnesses calculated from the Method 2 are presented in Figure 6.51 for both slabs and beams.

Typical damaged zones for this test are presented in Plates 6.23 to 6.24. The damaged areas, cracked pattern, are similar to that of the test TB1(B). Most of the flexural cracks initiated at 80 kN in cycle 4 at the horizontal interface between the in-

situ infill concrete and the beams. These cracks were extended horizontally then down to beams as the load was increased. A summary of the test results is presented in Tables 6.1. The tangent and unloading flexural stiffnesses of connections for each cycle from the Method 2 are presented in Table A6.1.17 and the secant flexural stiffnesses are presented in Tables A6.1.18 in Appendix 6.1 with corresponding relative rotations and calculated K_s values from the secant stiffnesses in cycle 5

6.6 Test series 4

6.6.1 Test TB2

Figures 6.52 to 6.53 represent the moment M_{con} versus crack opening δ_T, at boundaries of slab and column, and beam and column, and M_{con} versus compressive deformations δ_B in the beam-to-column joint for the single sided billet connection.

Calculated moment versus concrete strains in compression in the precast beams and joint, and steel strains in bars A and B are presented in Figures 6.54 to 6.56, respectively.

Figure 6.57 shows vertical displacement profiles along each of the beam for selected values of moment in cycle 5 only.

The derived moment versus relative rotation graphs obtained from the two methods are presented in Figures 6.58 to 6.59. Figure 6.60(a) presents the tangent loading and unloading stiffnesses calculated from the Method 1 for V4 for beam 1 side. Figure 6.60(b) presents the stiffnesses calculated from the Method 2 for both slab 1 and beam 1.

Typical damaged zones for this test are presented in Plates 6.25 to 6.32. The zone of influence in the beam in compression was measured at 120 mm from the face of the column being the end of the joint hidden in the beam. A horizontal bursting crack is a clear indication of unconfined concrete compressive failure in the part of the beam covering the joint grout (see Plate 6.30 right). A summary of the test results is presented in Table 6.1. The tangent and unloading flexural stiffnesses of connections for each cycle from the Methods 1&2 are presented in Table A6.1.19 and the secant flexural stiffnesses are presented in Table A6.1.20 in Appendix 6.1 with corresponding relative rotations and calculated K_s values from the secant stiffnesses in cycle 5.

Test Ref.	C1		C2	C3	C4	C5					
	M_{cr} (kNm)	M_{peak} (kNm)	M_{peak} (kNm)	M_{peak} (kNm)	M_{peak} (kNm)	M_u (kNm)	M_{pred} (kNm)	M_{beam} (kNm)	$\frac{M_{cr}}{M_u}$	$\frac{M_u}{M_{pred}}$	$\frac{M_u}{M_{beam}}$
TW1(A)	24.59	71.13	72.36	75.00	118.72	238.78	252.58	340.28	0.10	0.95	0.70
	23.05	72.78	71.24	72.65	118.38	237.01	252.58	338.01	0.10	0.94	0.70
TW1(B)	N/A	N/A	N/A	N/A	N/A	N/A	N/A	N/A	N/A	N/A	N/A
TW1(C)	9.29	26.20	25.90	25.50	41.90	74.78	85.51	161.59	0.12	0.87	0.46
	9.07	25.60	25.50	25.50	41.60	76.34	85.51	160.30	0.12	0.89	0.48
TW2	34.84	70.19	70.55	70.78	115.15	156.43	240.62	321.89	0.22	0.65	0.49
TB1(A)	23.32	72.01	72.53	71.97	117.19	191.34	201.89	323.09	0.12	0.95	0.59
	23.90	70.96	71.07	70.81	115.38	188.21	201.89	322.15	0.13	0.93	0.58
TB1(B)	24.23	58.04	58.00	58.61	96.50	183.60	218.31	337.91	0.13	0.84	0.54
	23.02	56.48	56.77	57.43	95.10	183.60	218.31	337.91	0.13	0.84	0.54
TB1(C)	15.42	57.00	58.08	57.92	96.50	177.48	205.34	323.68	0.09	0.86	0.55
	15.57	56.40	57.61	57.01	94.41	177.48	205.34	323.68	0.09	0.86	0.55
TB2	28.48	55.58	56.46	56.49	58.02*	54.92	200.89	314.48	0.49	0.29	0.18

* M_u=58.02 kNm in test TB2 in cycle 4 (C4)

Table 6.1: Summary of test results

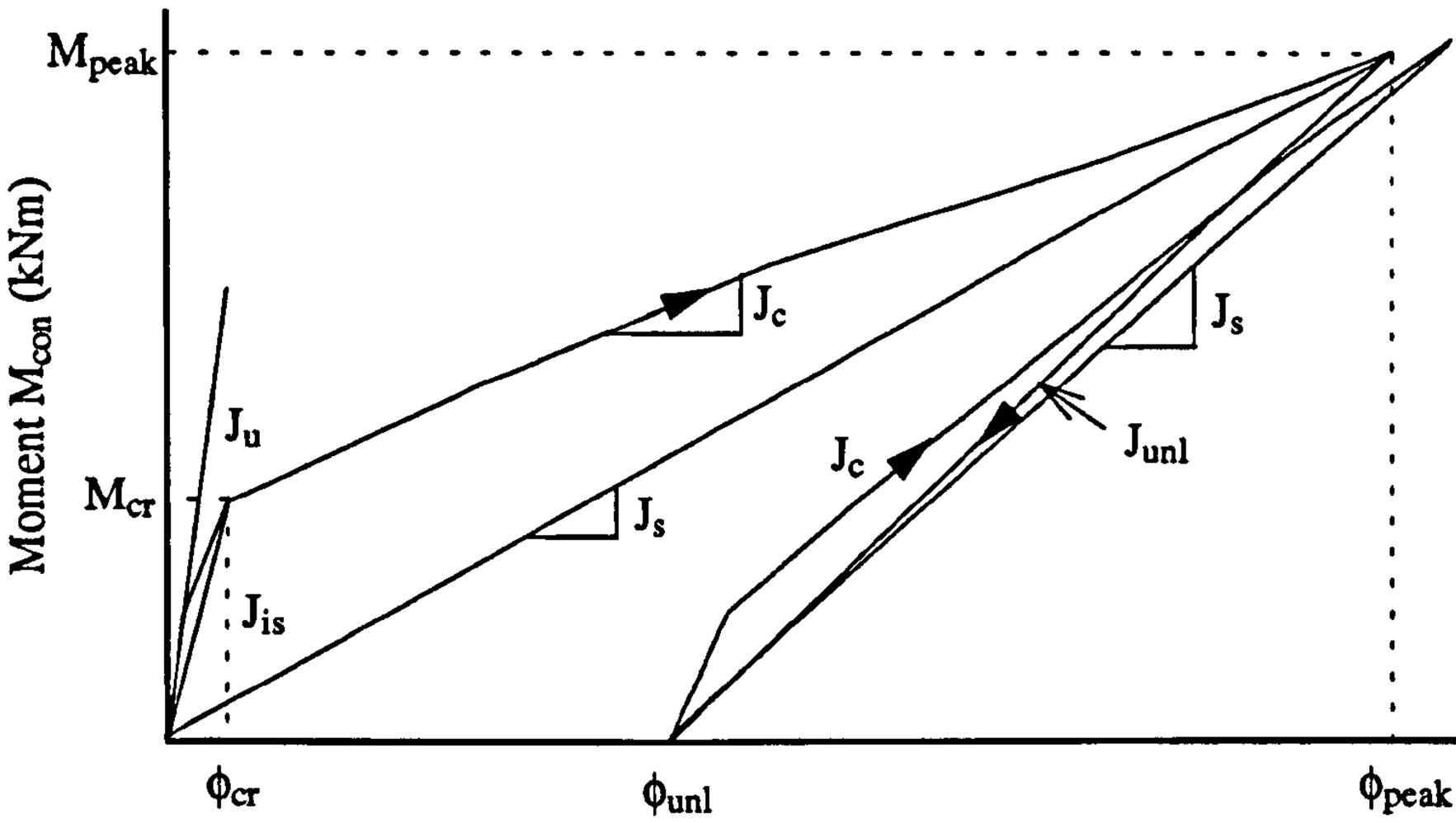

Figure 6.1(a): Actual moment versus relative rotation curve at which flexural stiffnesses were defined for cycles 1-2

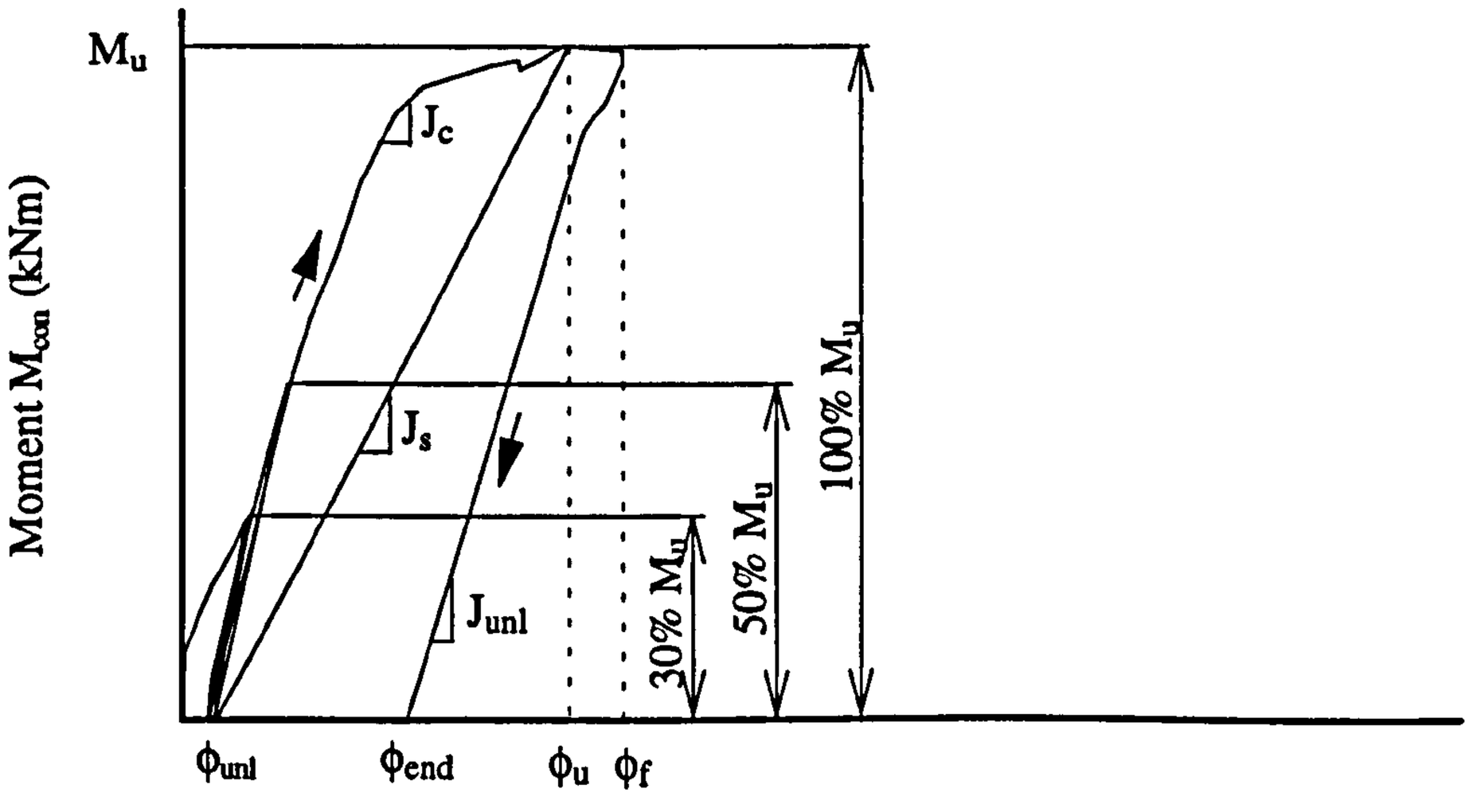

Figure 6.1(b): Actual moment versus relative rotation curve at which flexural stiffnesses were defined for cycle 5

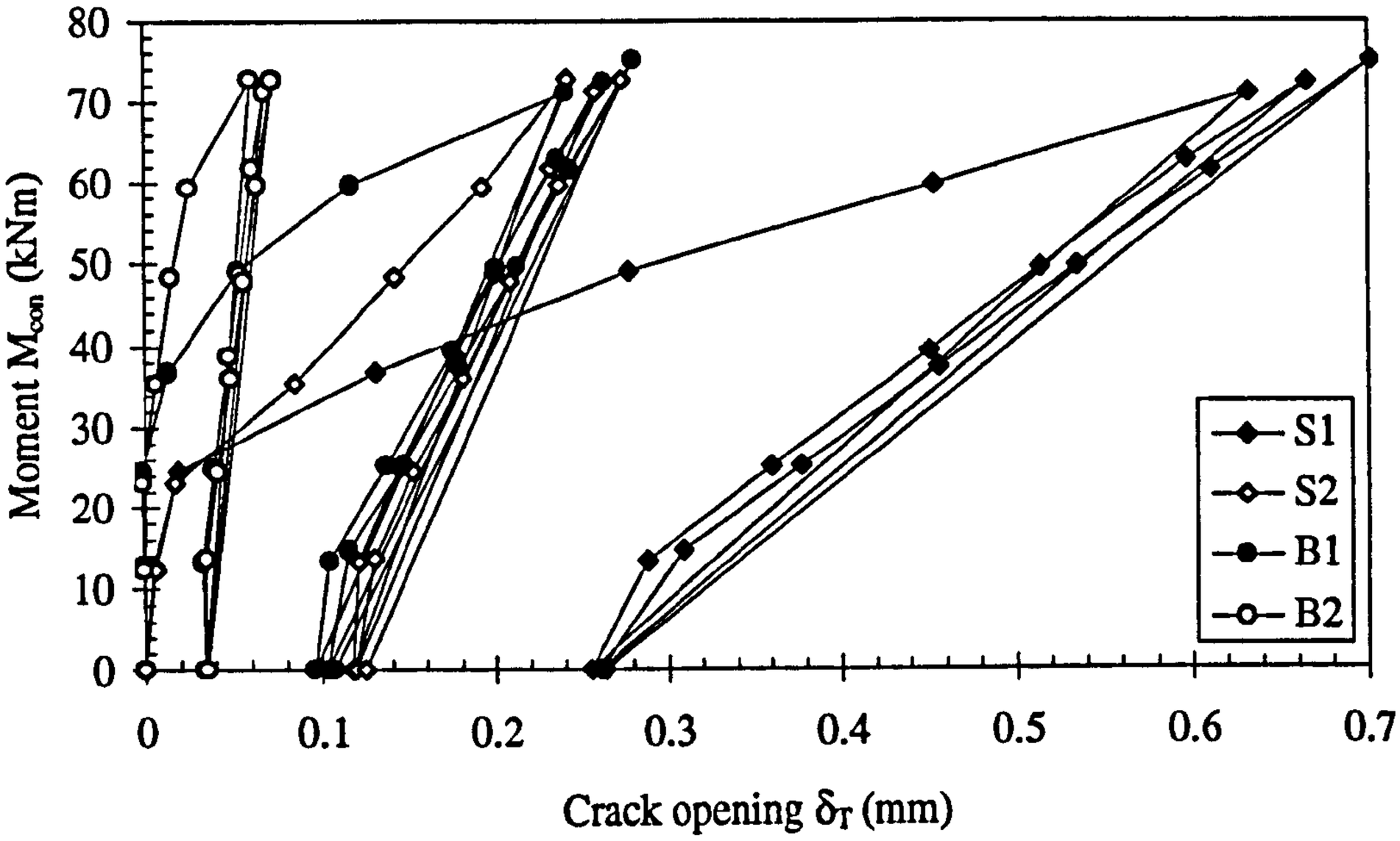

Figure 6.2(a): Moment versus crack opening at slab/column and beam/column boundaries in TW1(A) for cycles 1-3

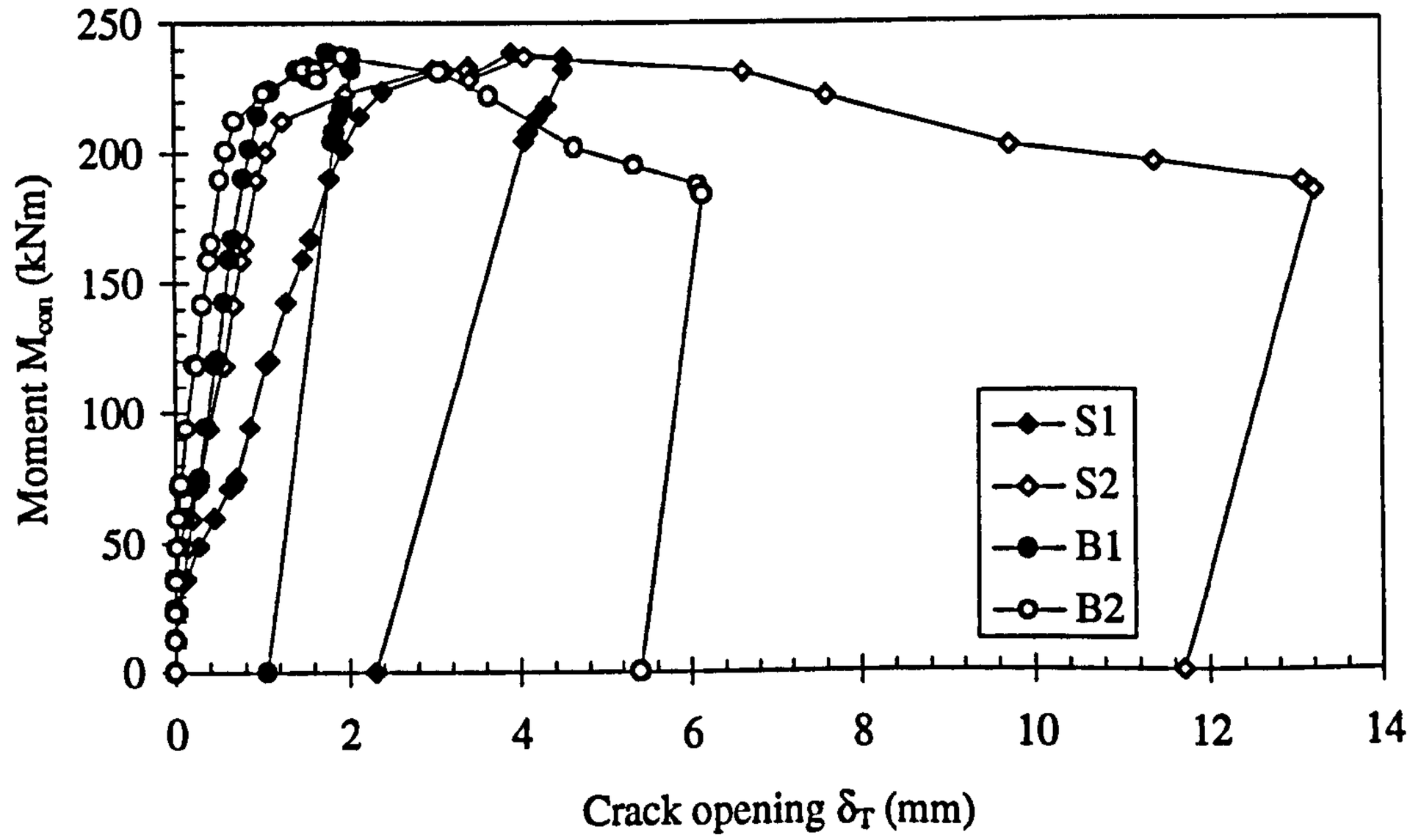

Figure 6.2(b): Moment versus crack opening at slab/column and beam/column boundaries in TW1(A)

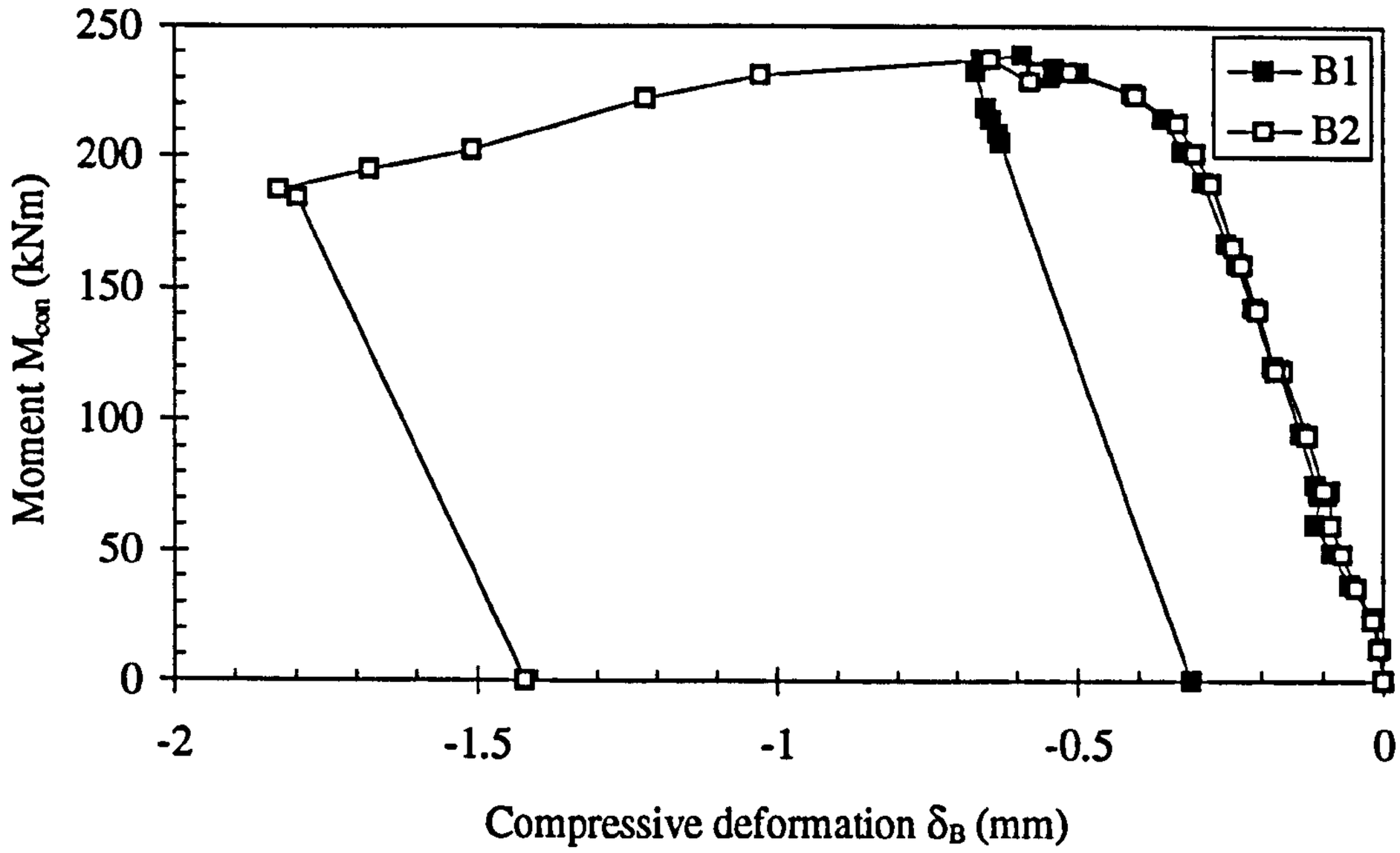

Figure 6.3: Moment versus compressive deformation in joints in TW1(A)

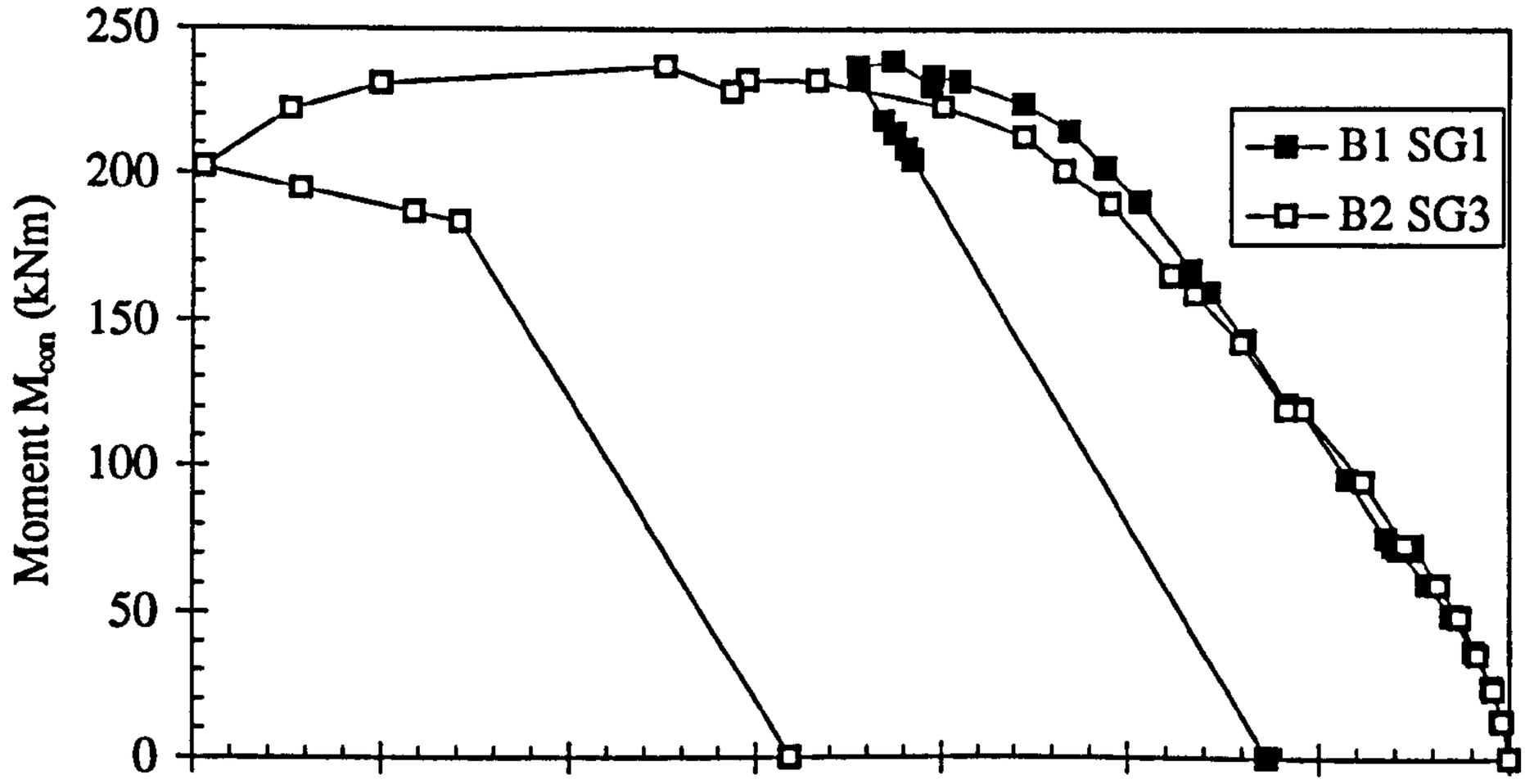

Figure 6.4: Moment versus concrete strains in beams in TW1(A)

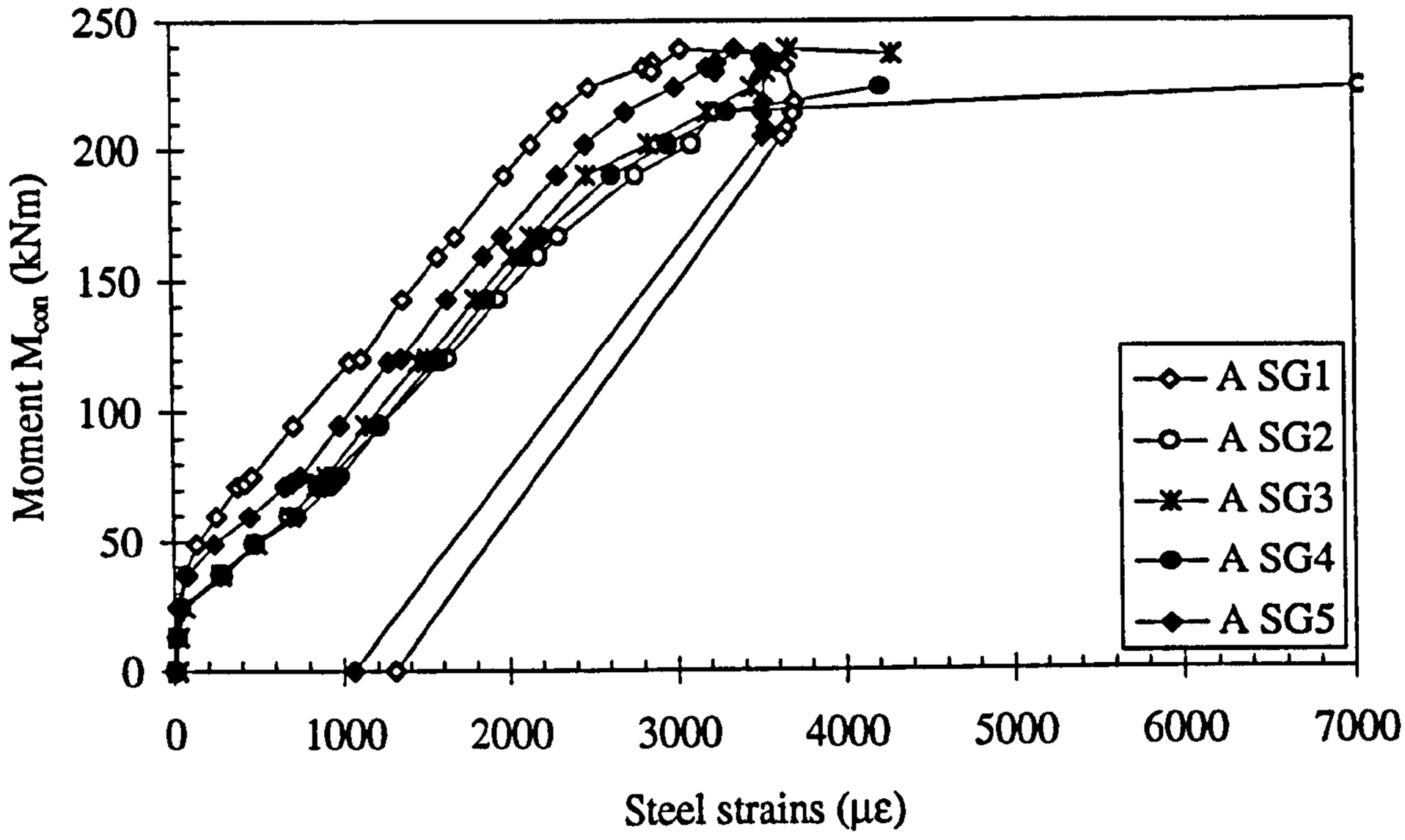

Figure 6.5: Moment versus steel strains in bar A in TW1(A)

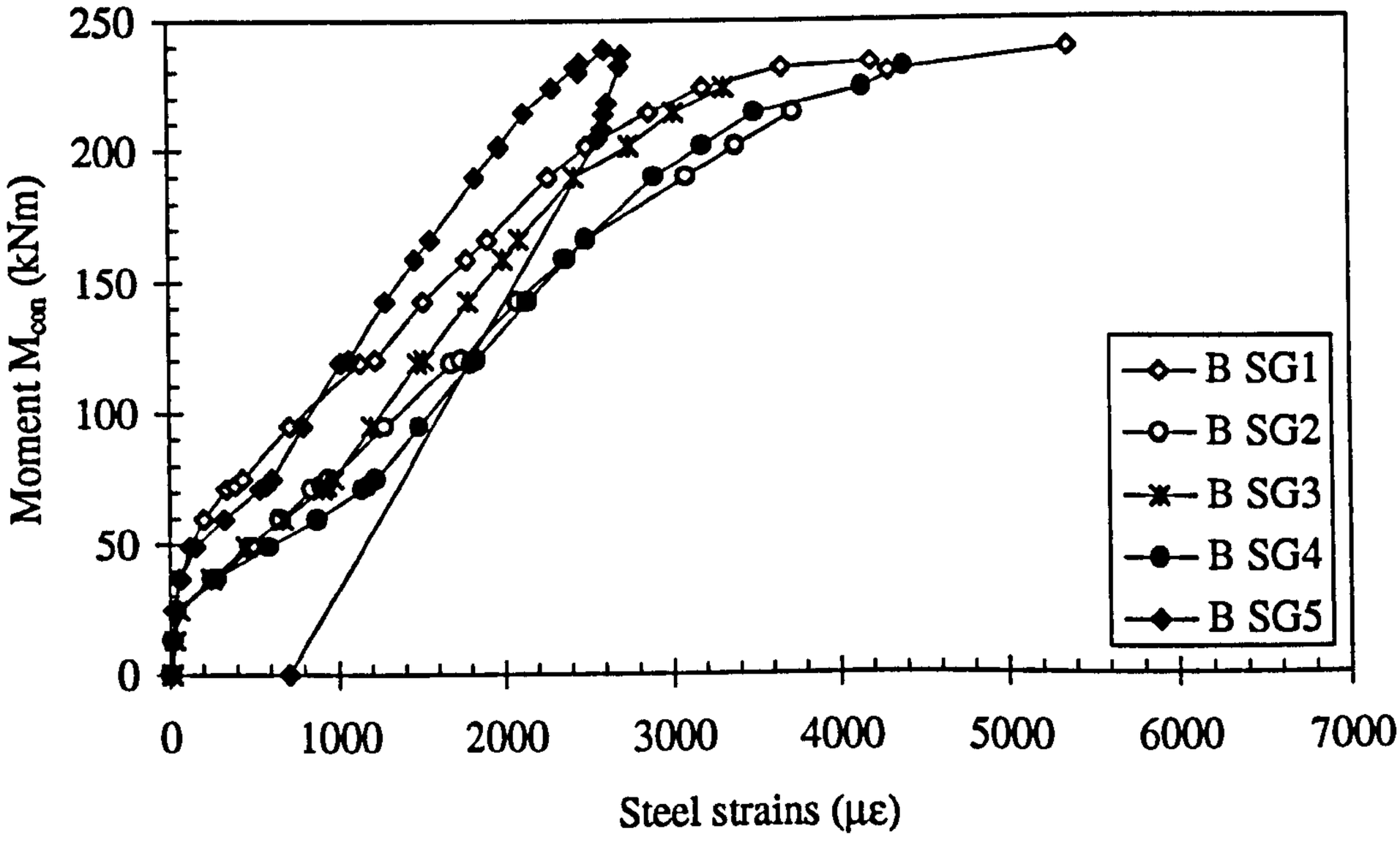

Figure 6.6: Moment versus steel strains in bar B in TW1(A)

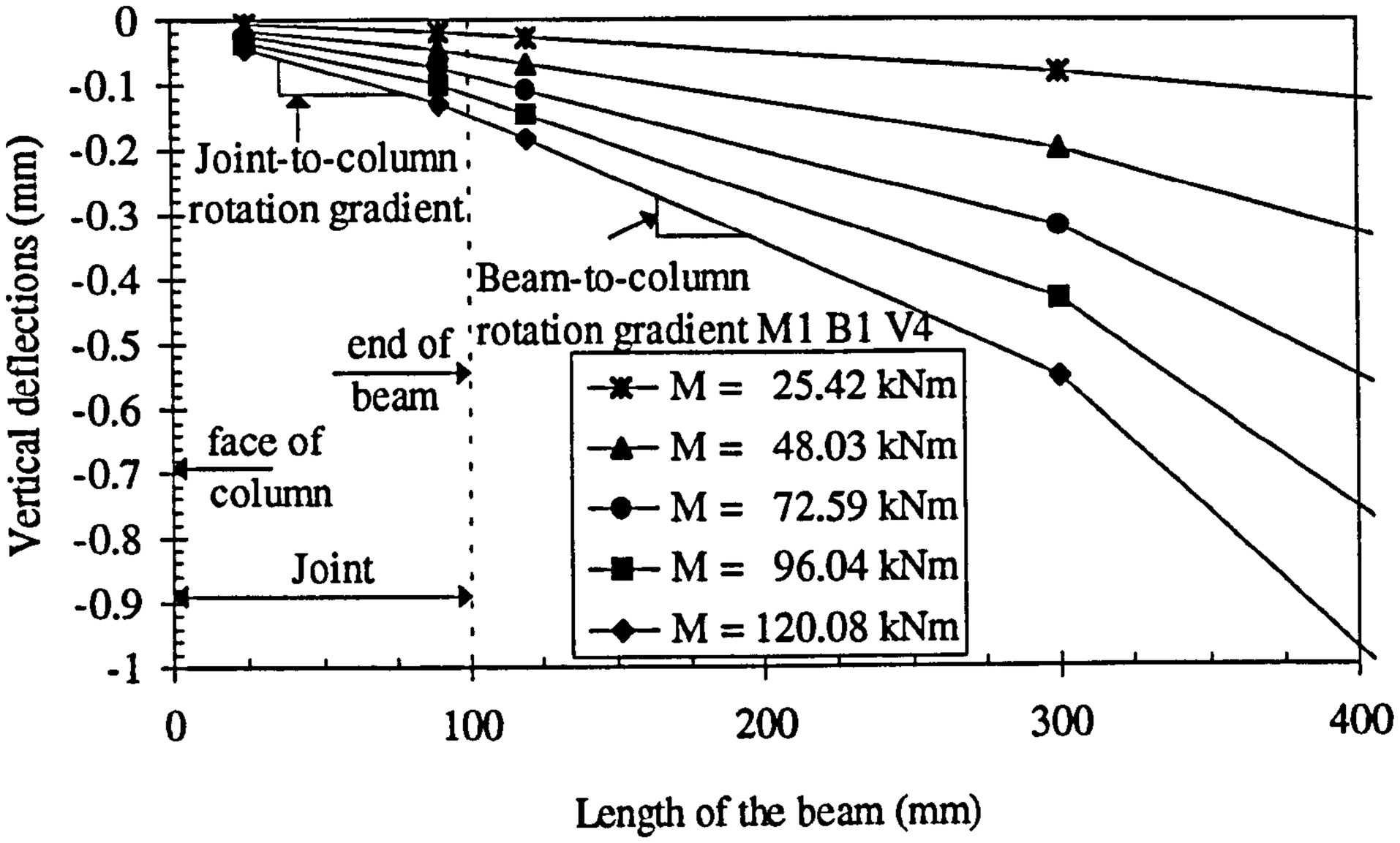

Figure 6.7(a): Moment versus vertical deflections in beam 1 in TW1(A) with various moment level

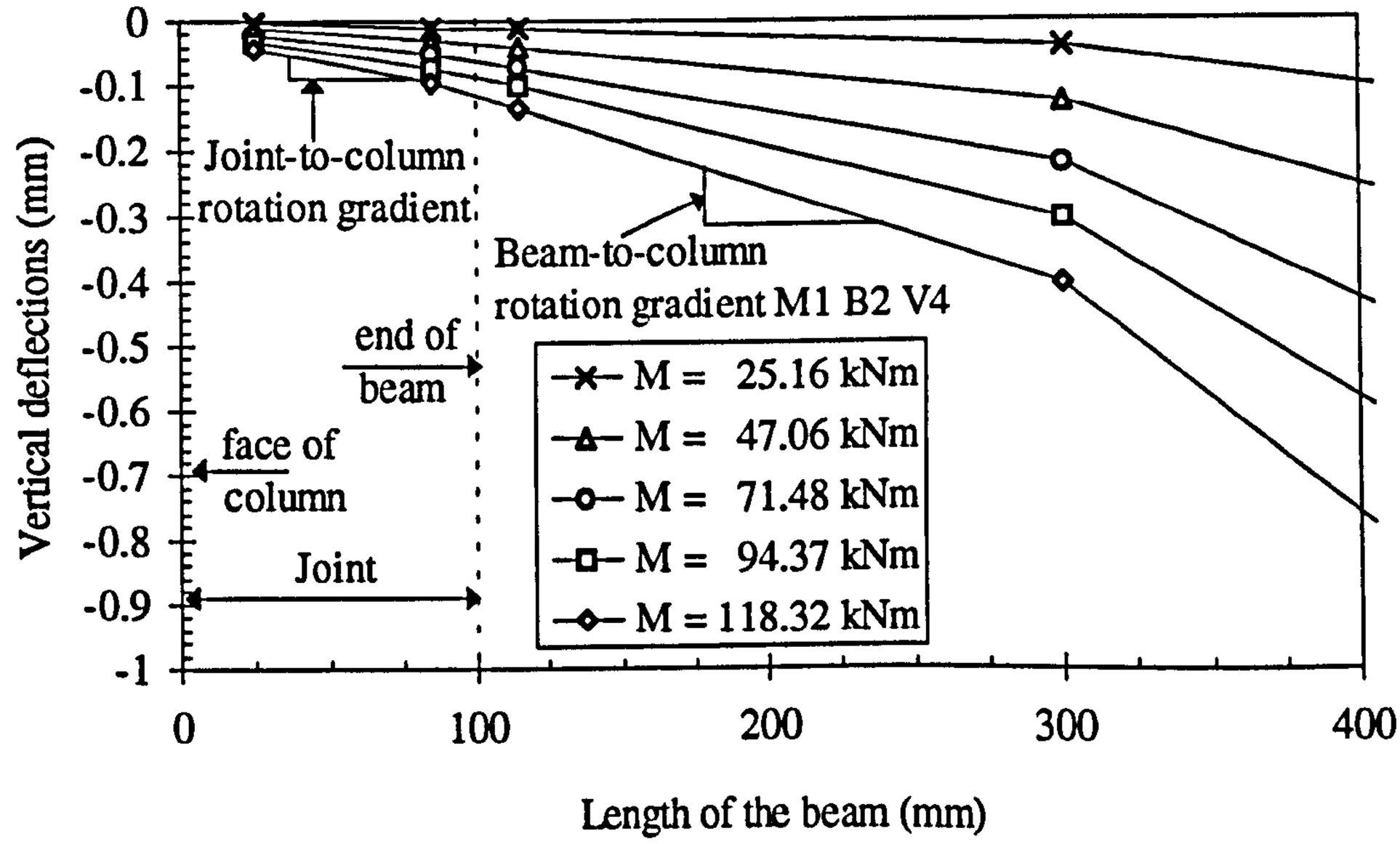

Figure 6.7(b): Moment versus vertical deflections in beam 2 in TW1(A) with various moment level

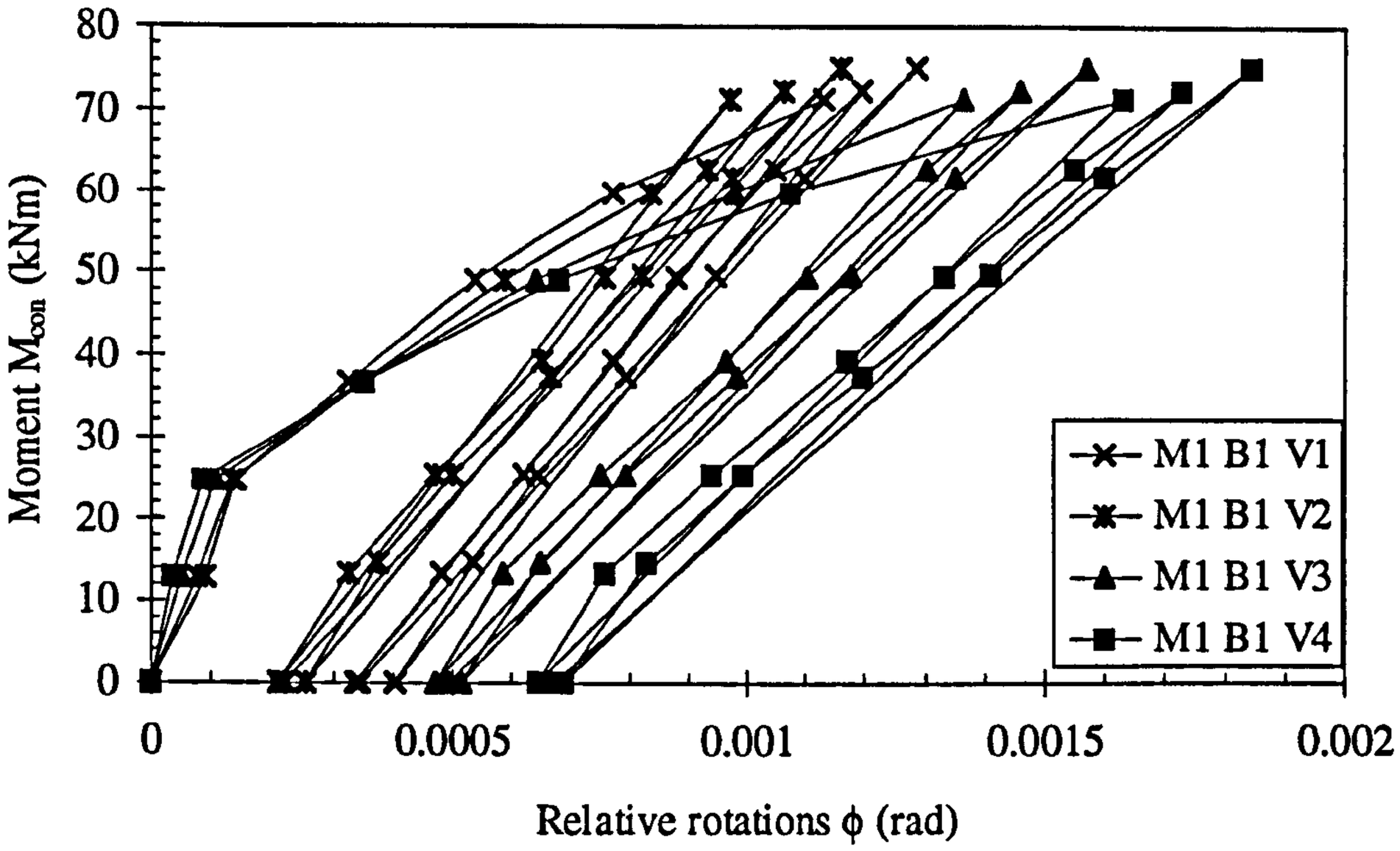

Figure 6.8(a): Moment versus relative rotations in beam 1 in TW1(A) using method 1 for cycles 1-3

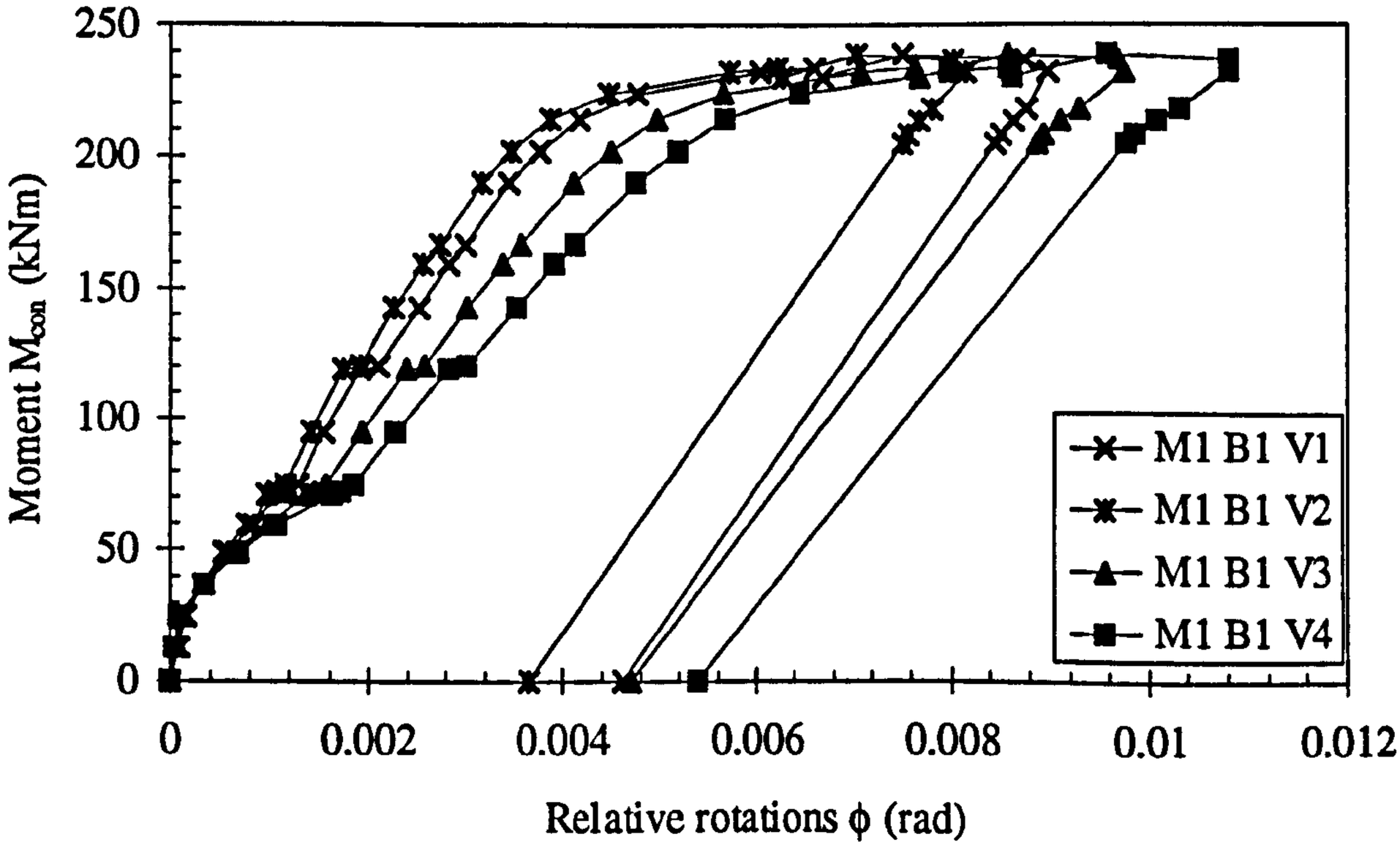

Figure 6.8(b): Moment versus relative rotations in beam 1 in TW1(A) using method 1

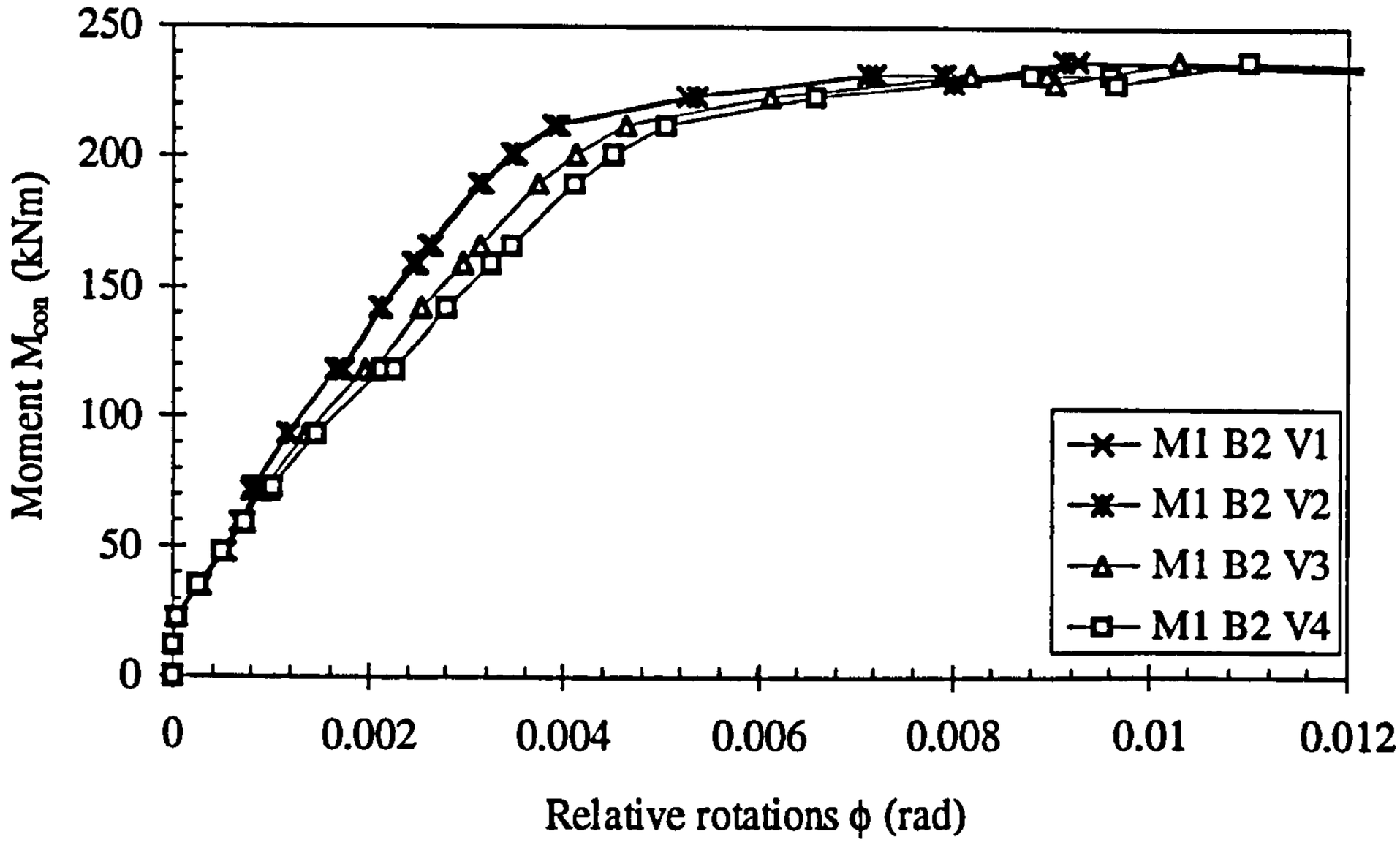

Figure 6.9: Moment versus relative rotations in beam 2 in TW1(A) using method 1

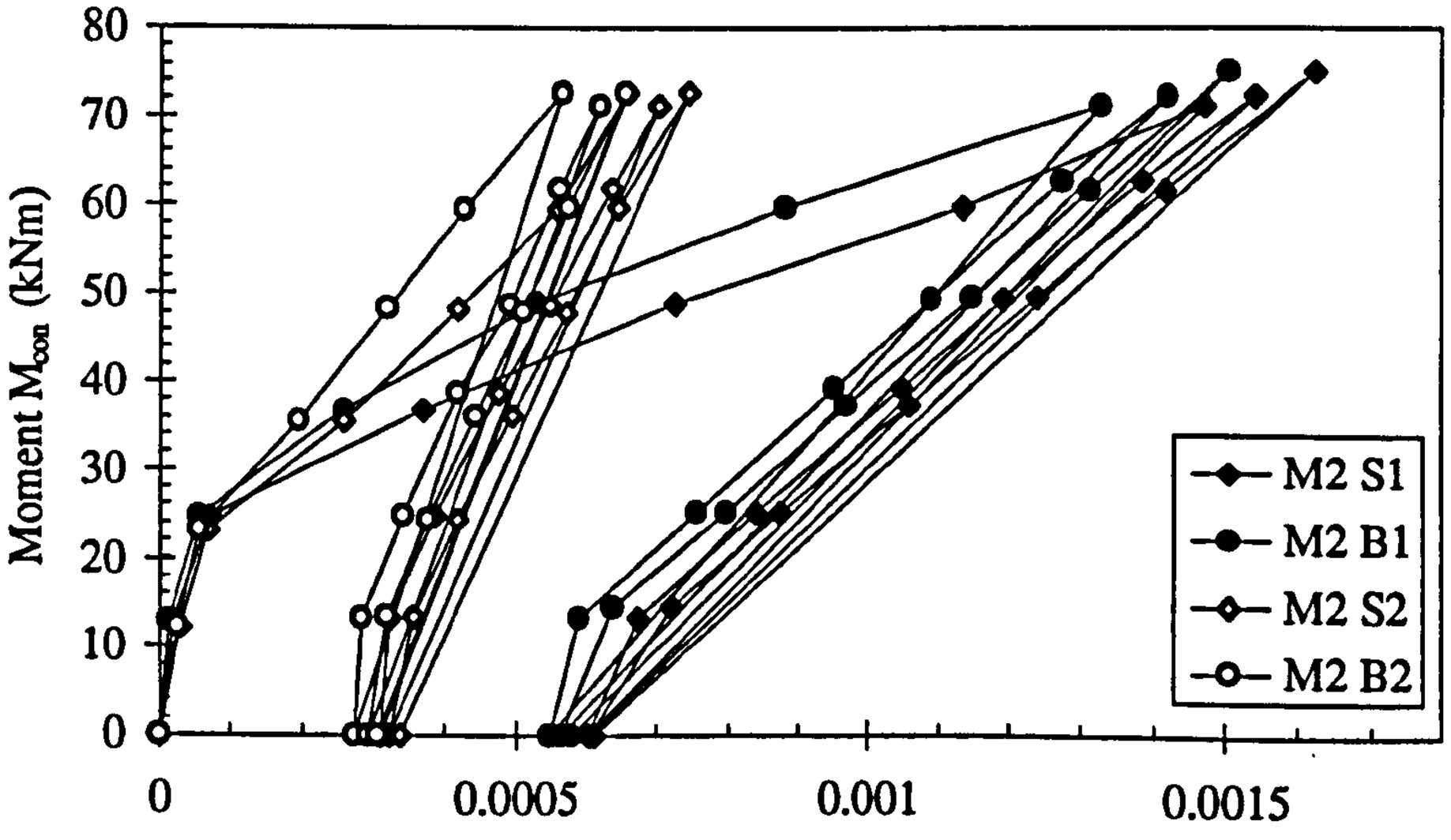

Figure 6.10(a): Moment versus relative rotations in TW1(A) using method 2 for cycles 1-3

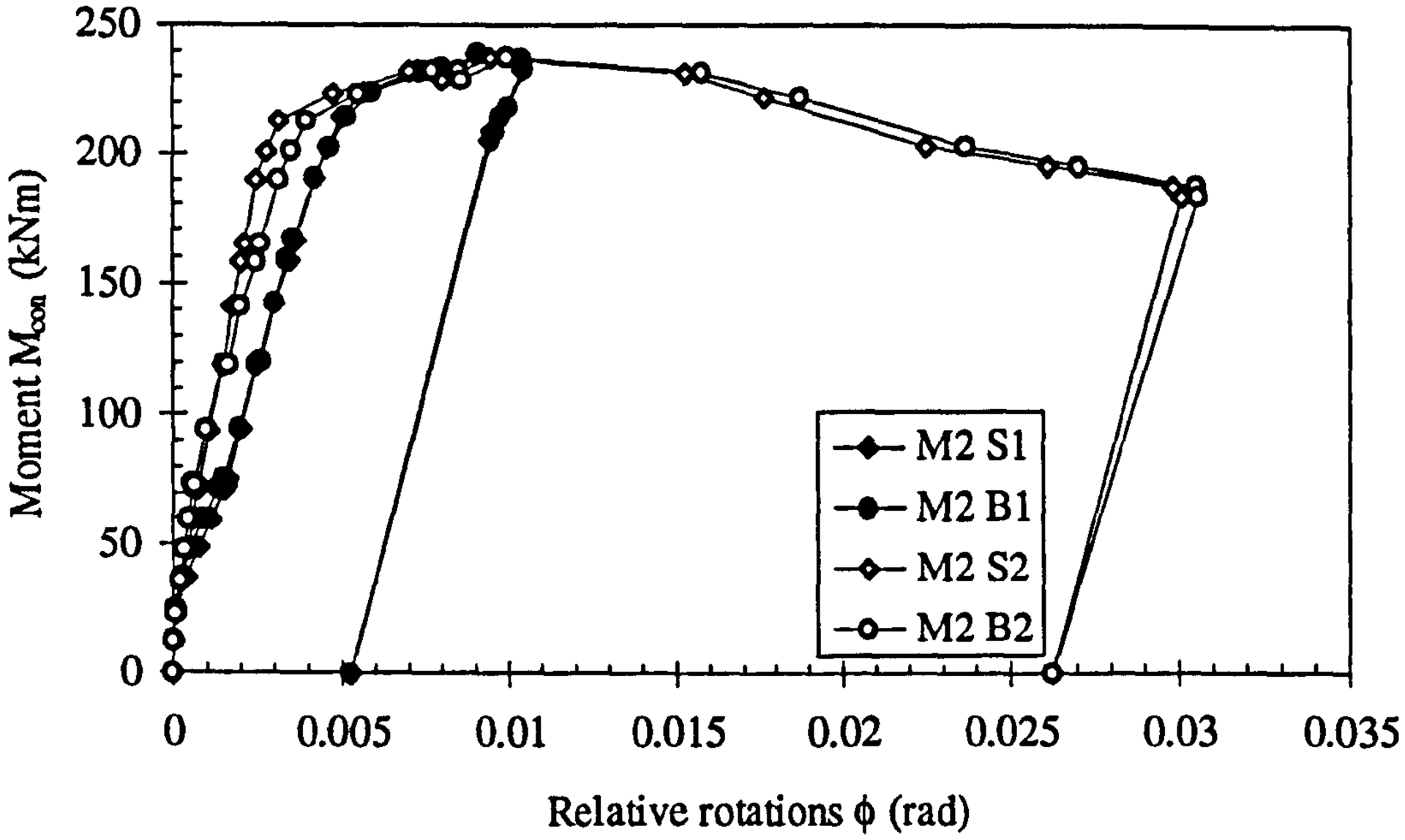

Figure 6.10(b): Moment versus relative rotations in TW1(A) using method 2

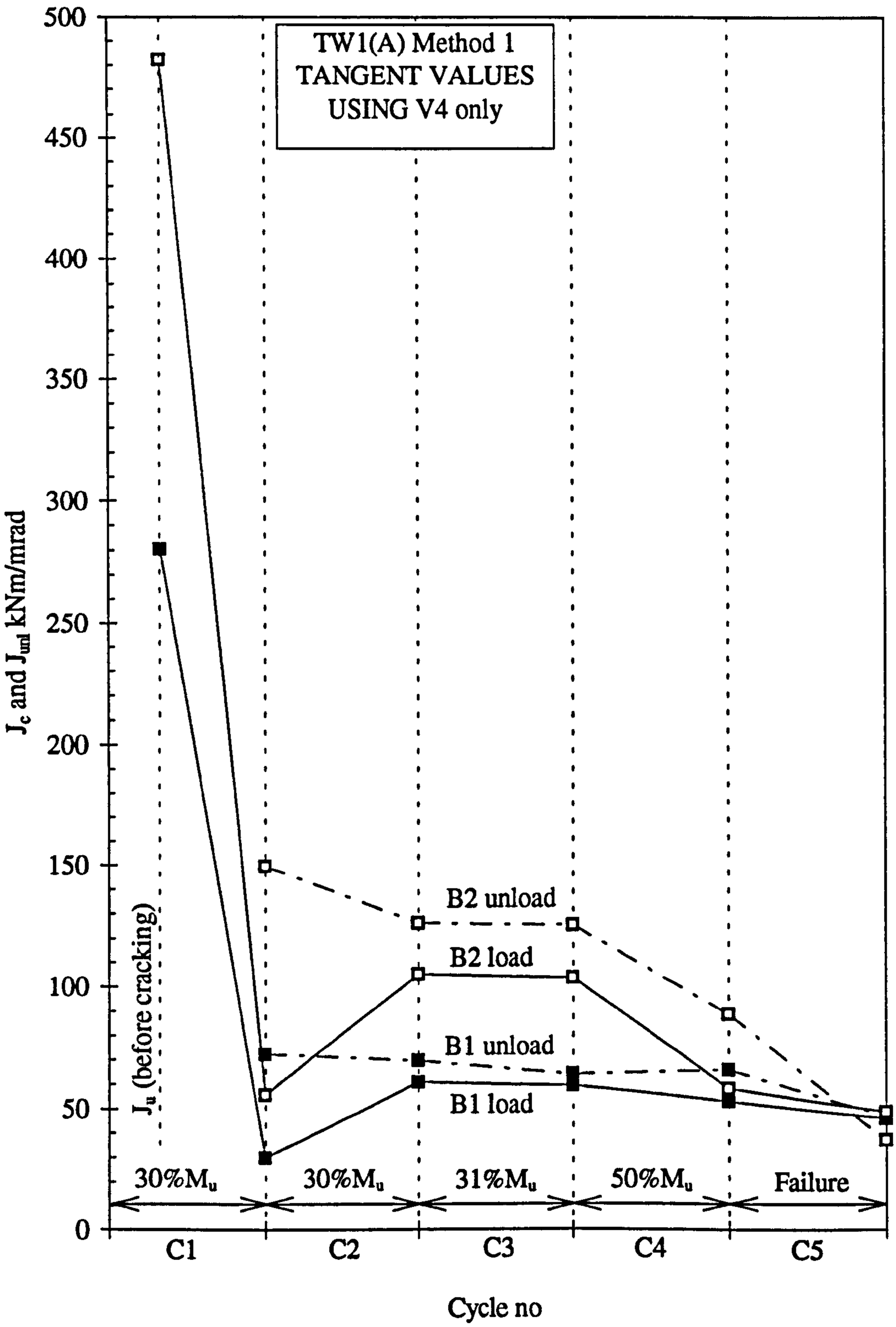

Figure 6.11(a): Tangent and unloading flexural stiffness versus cycles 1-5 in beams in TW1(A) using method 1

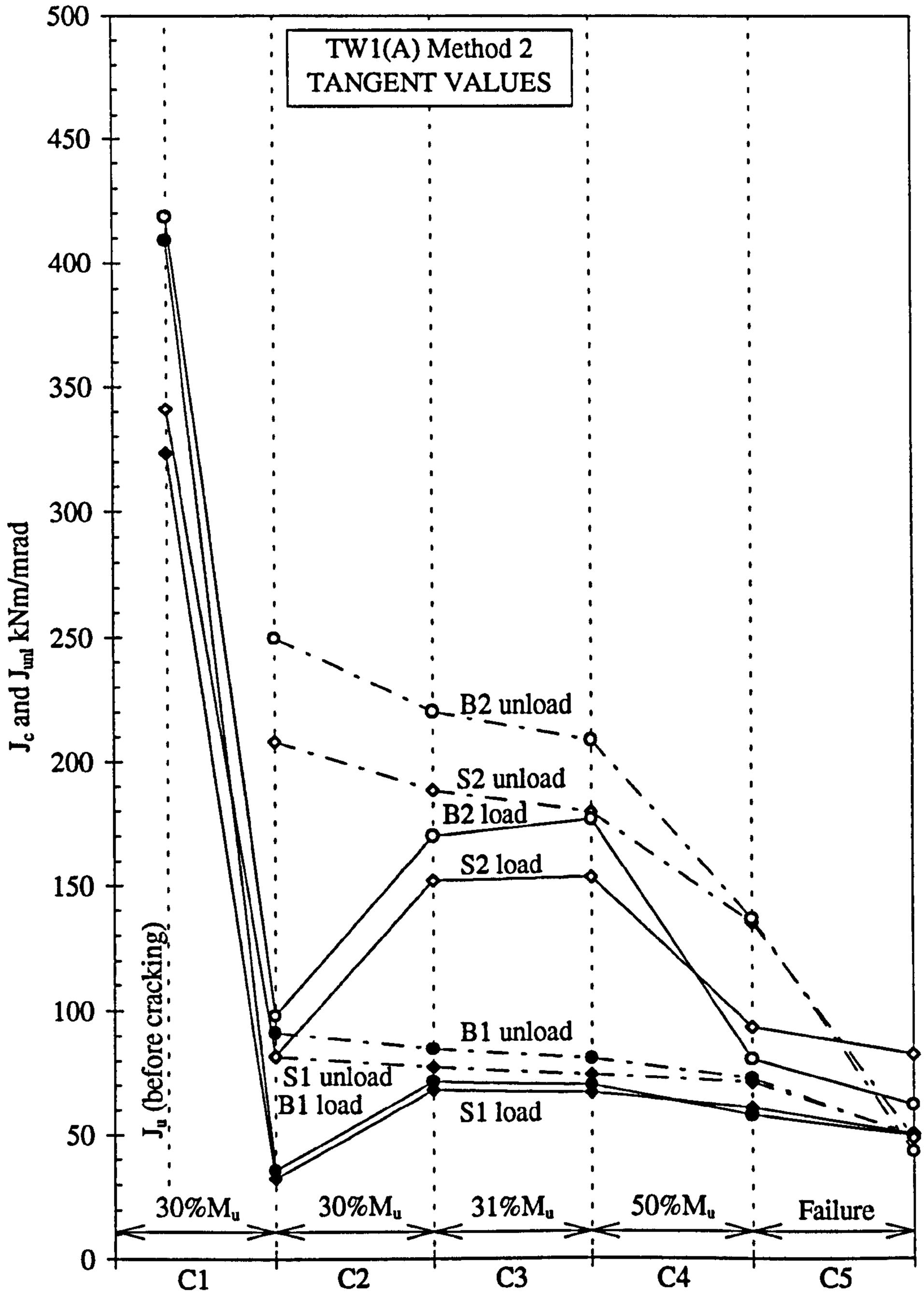

Figure 6.11(b): Tangent and unloading flexural stiffness versus cycles 1-5 in slabs and beams in TW1(A) using method 2

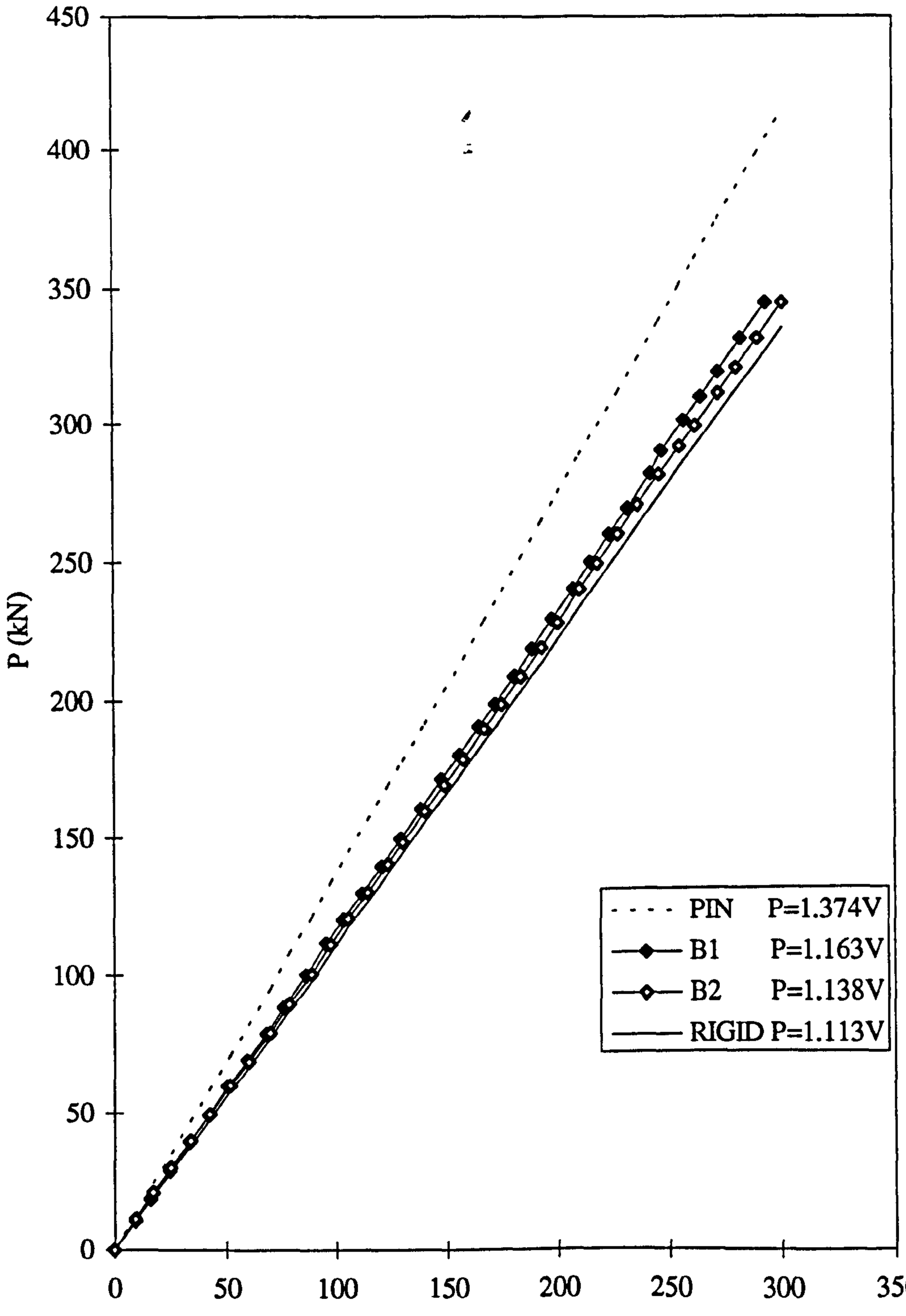

Figure 6.12: Applied shear load versus reaction of the connection in TW1(B)

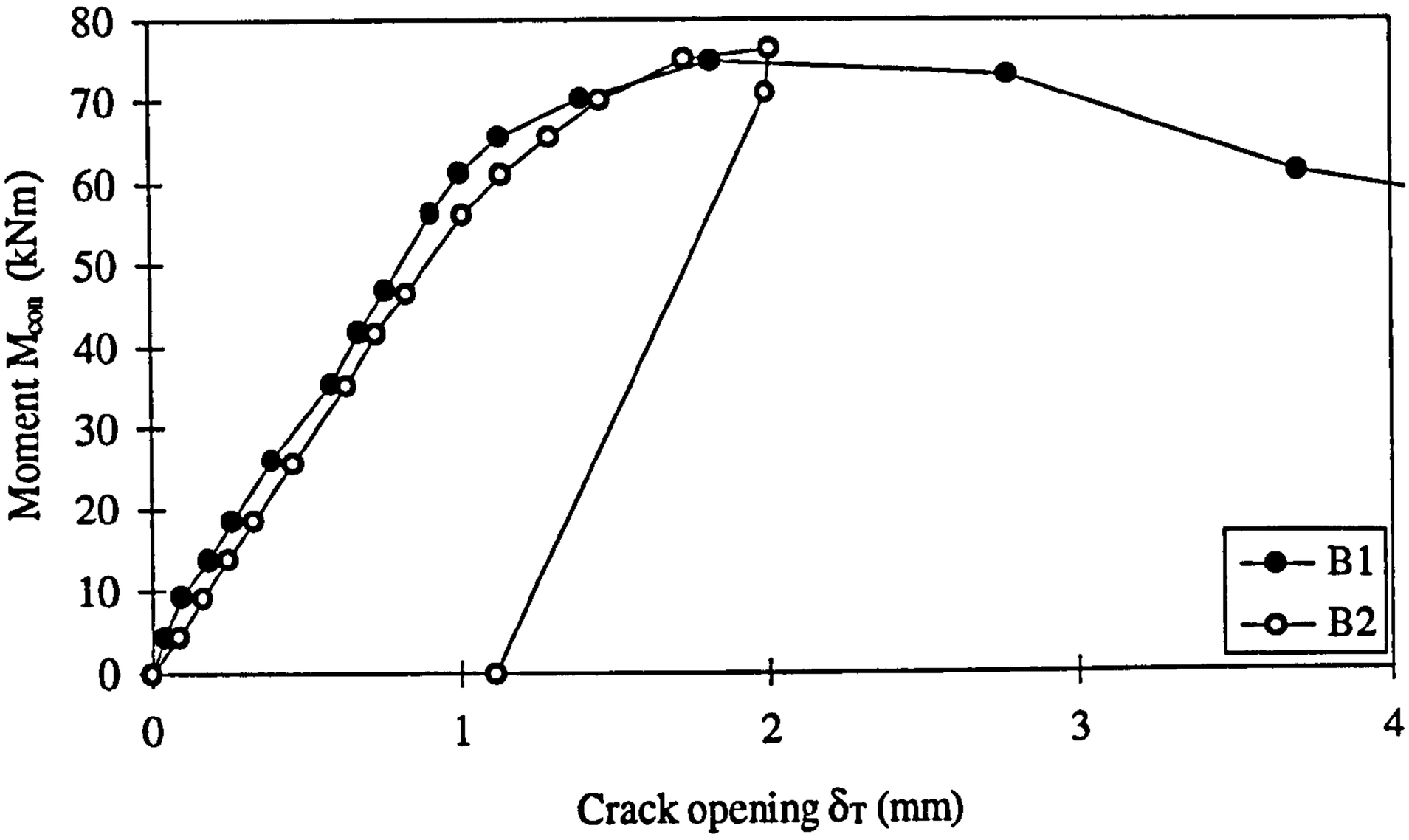

Figure 6.13: Moment versus crack opening at beam/column boundaries in TW1(C)

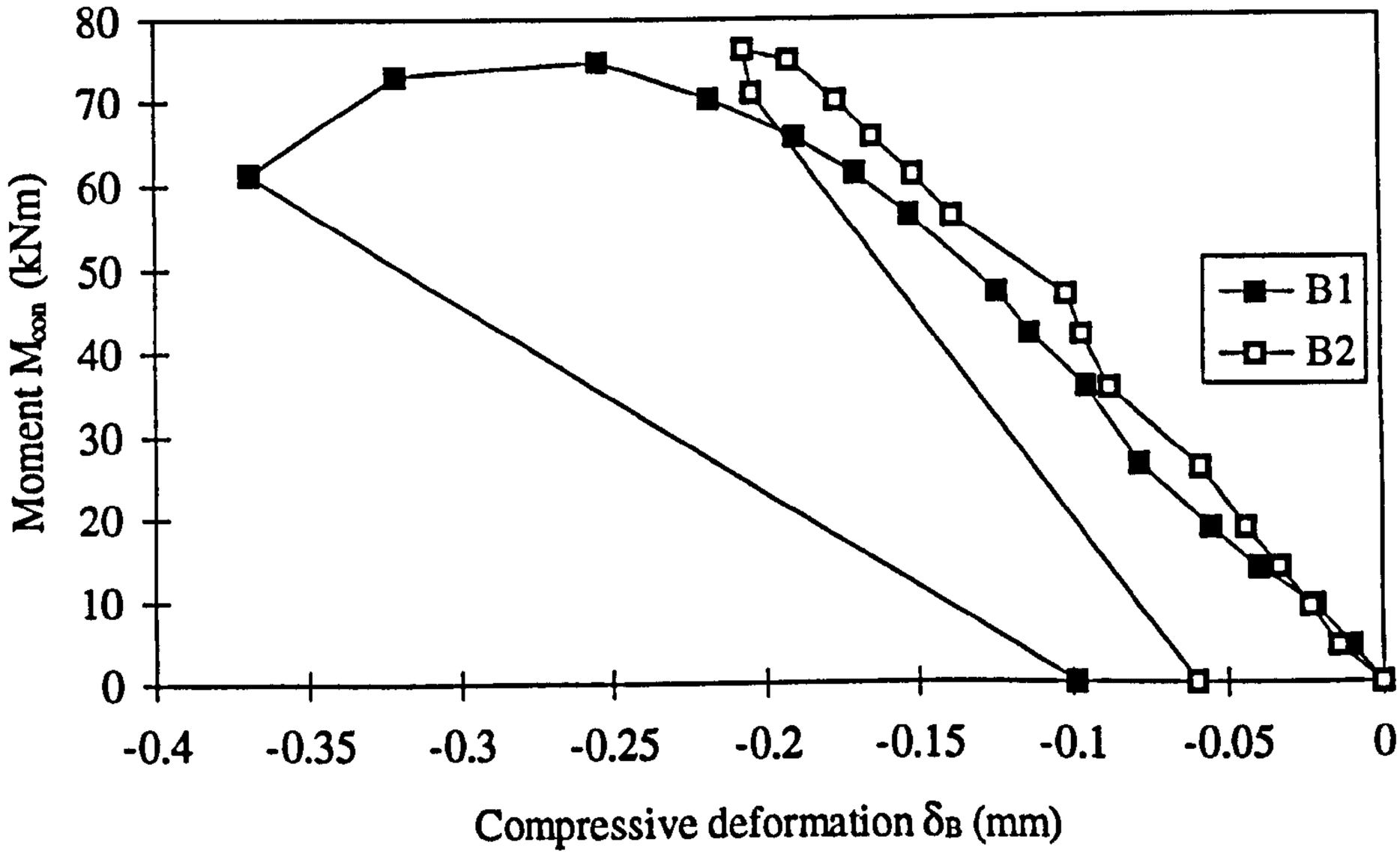

Figure 6.14: Moment versus compressive deformation in joints in TW1(C)

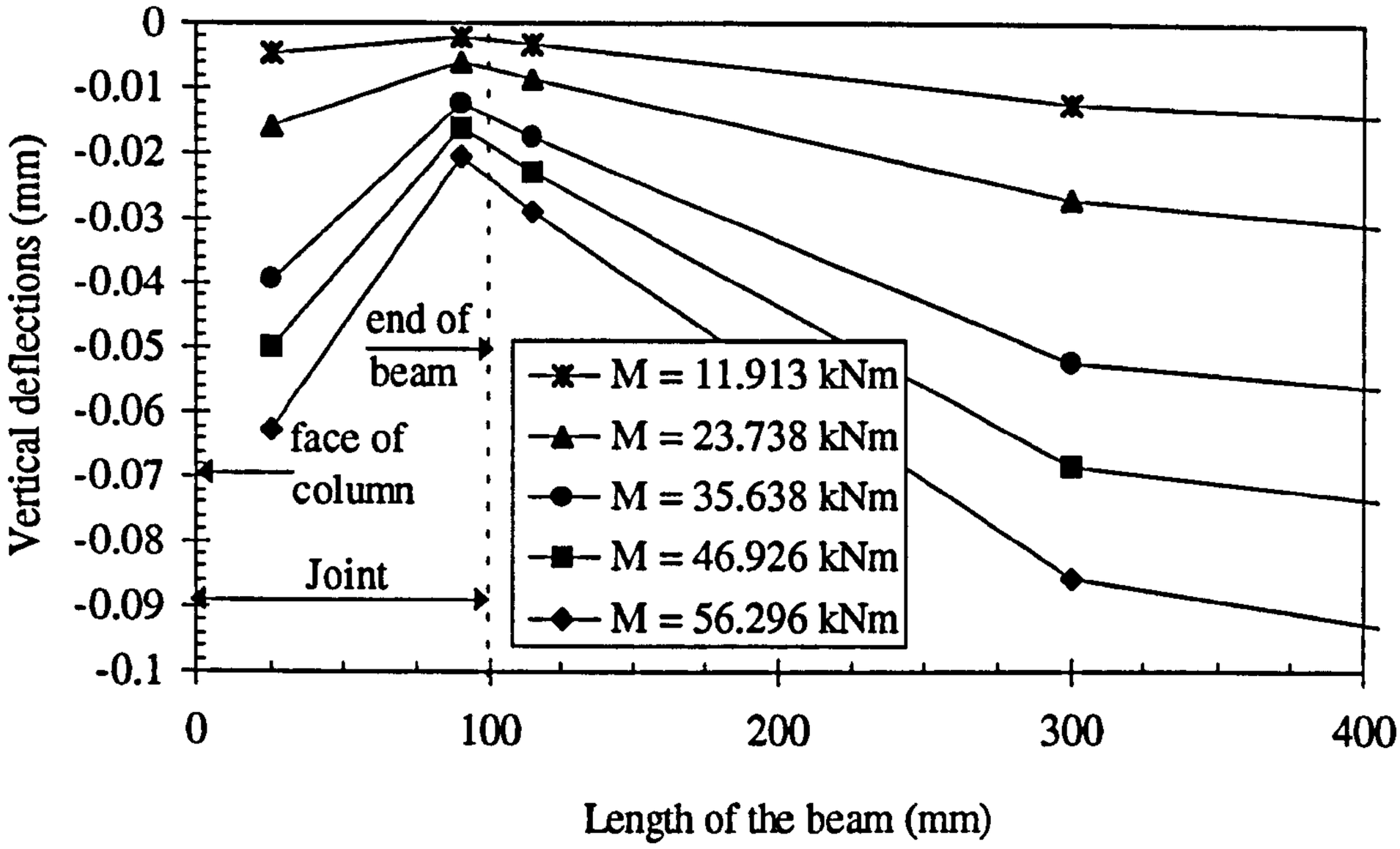

Figure 6.15(a): Moment versus vertical deflections in beam 1 in TW1(C) with various moment level

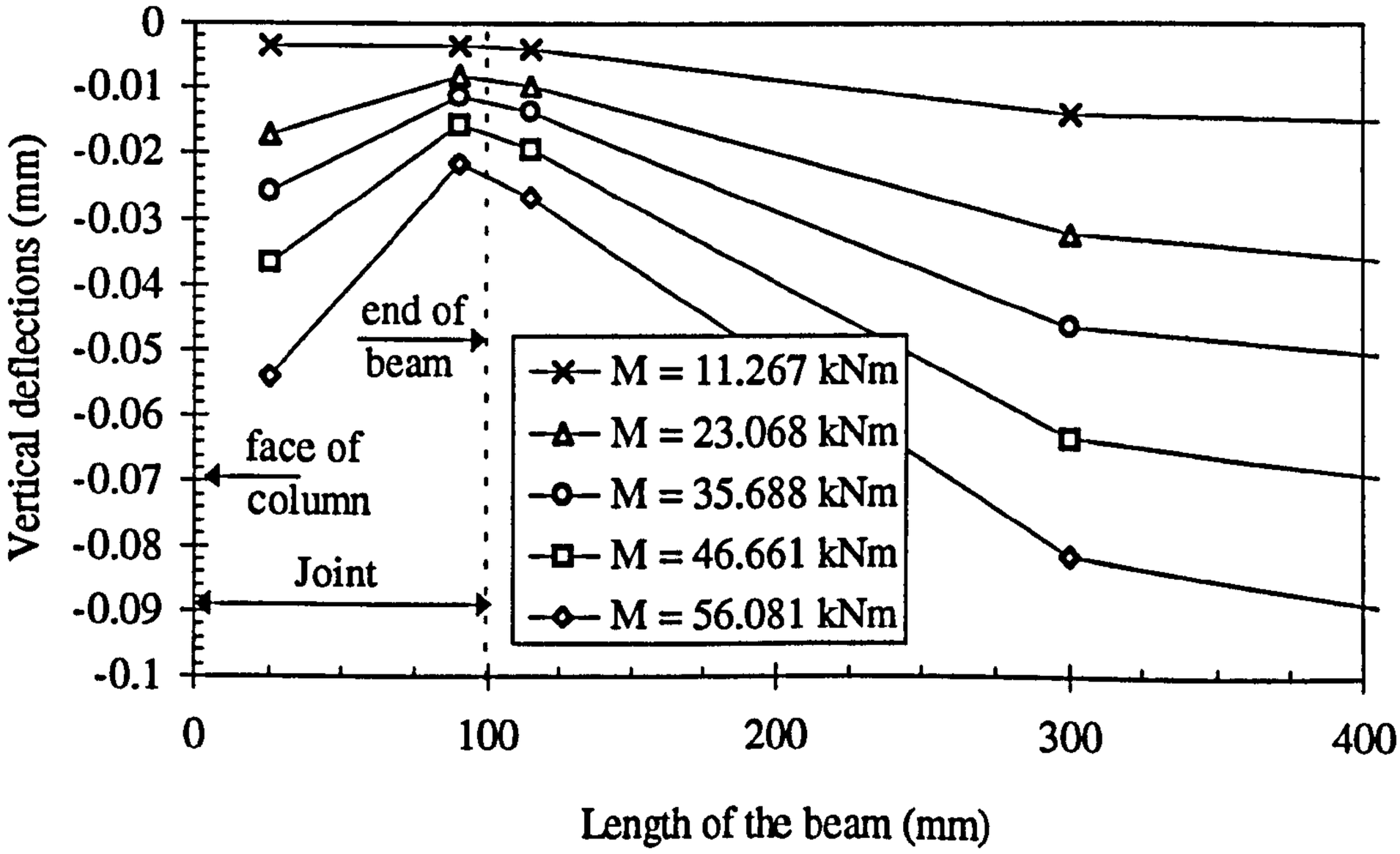

Figure 6.15(b): Moment versus vertical deflections in beam 2 in TW1(C) with various moment level

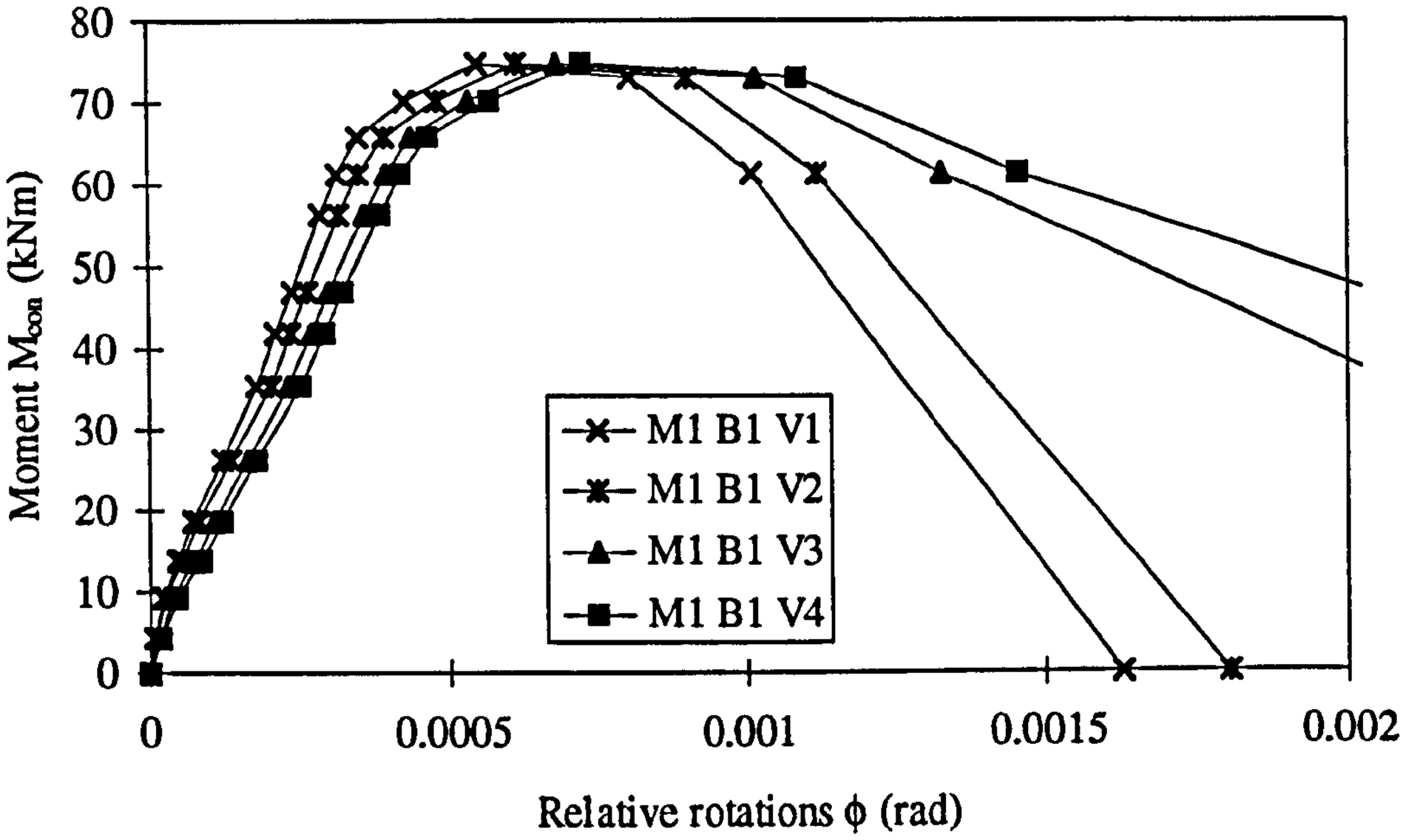

Figure 6.16: Moment versus relative rotations in beam 1 in TW1(C) using method 1

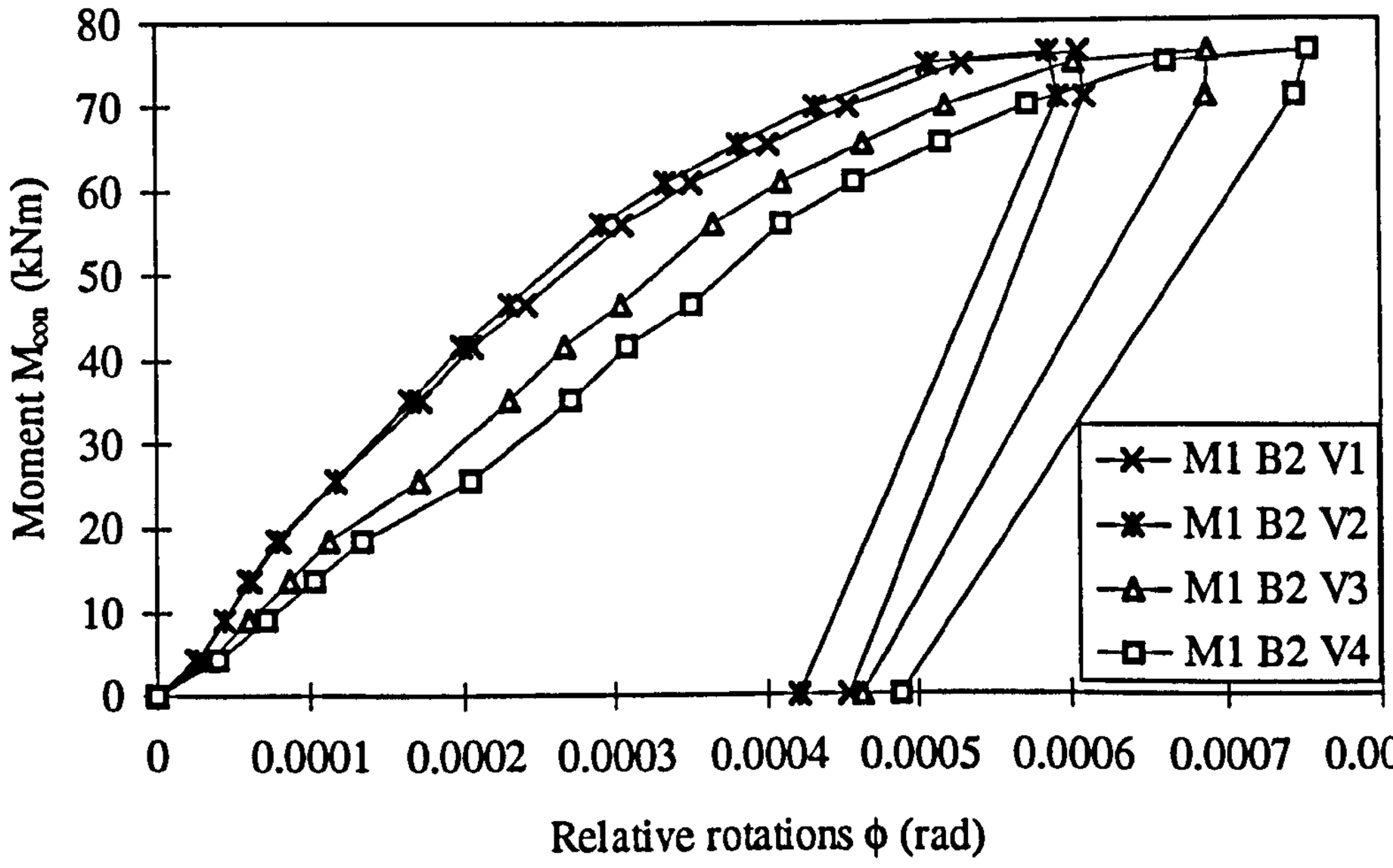

Figure 6.17: Moment versus relative rotations in beam 2 in TW1(C) using method 1

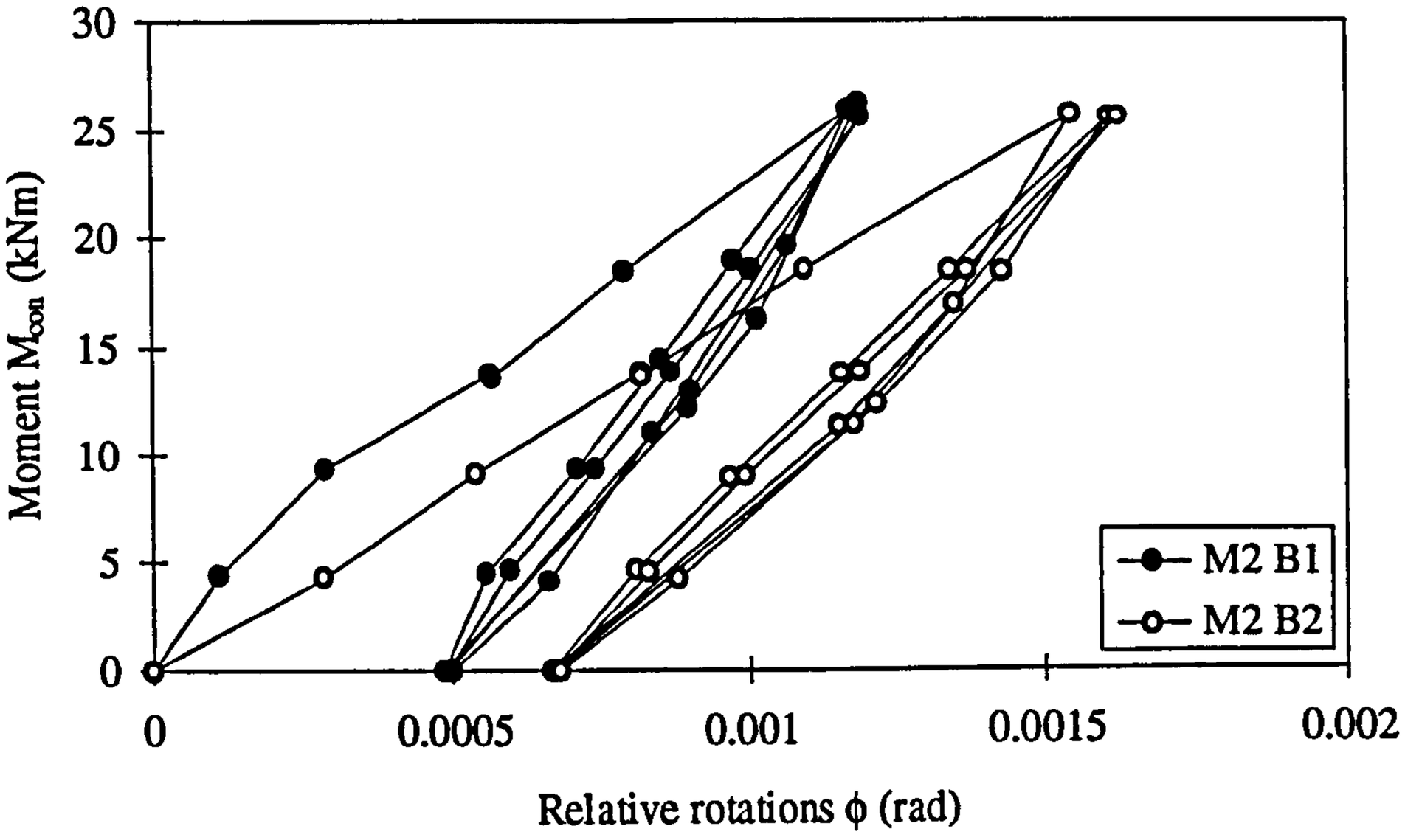

Figure 6.18(a): Moment versus relative rotations in TW1(C) using method 2 for cycles 1-3 for both beams

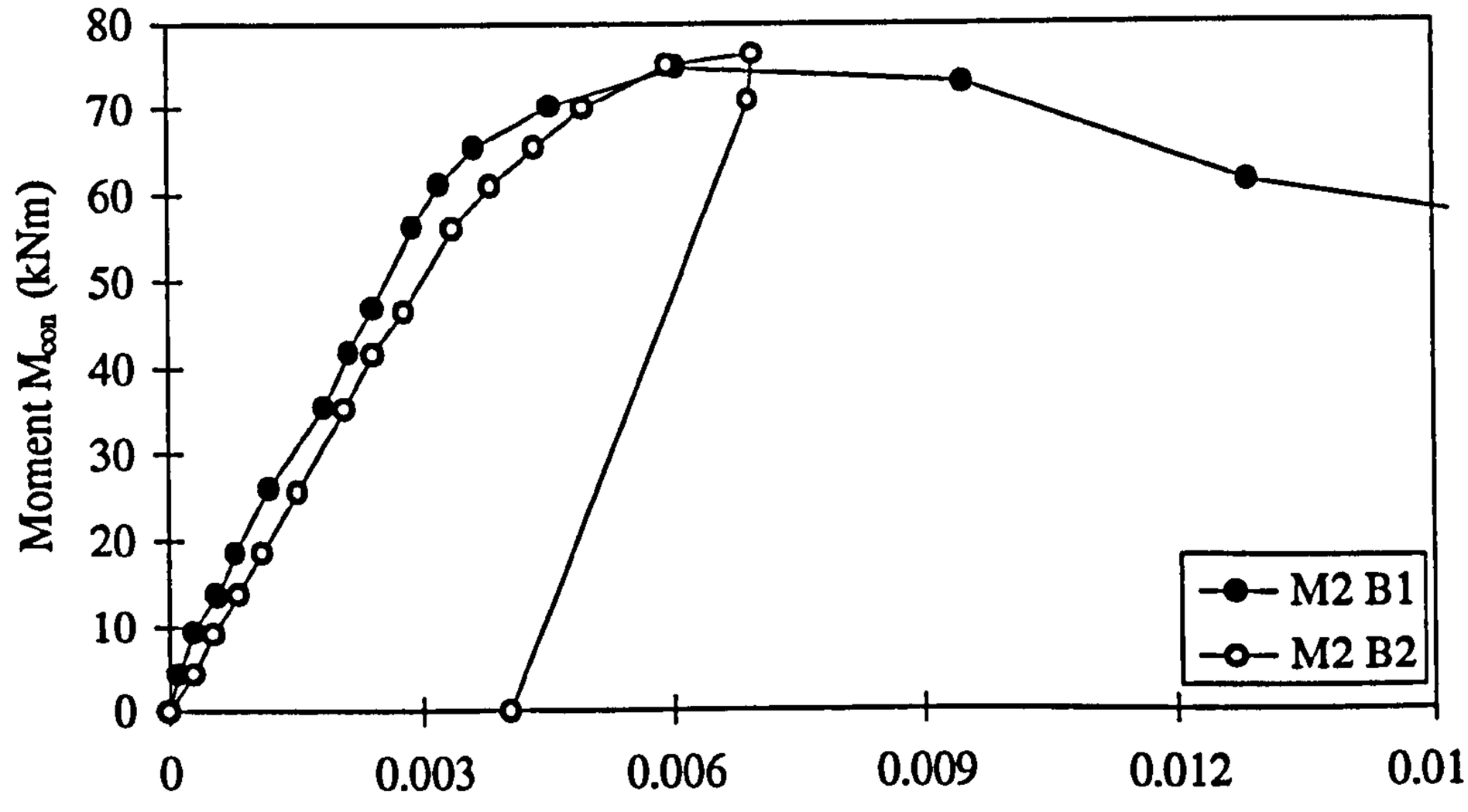

Figure 6.18(b): Moment versus relative rotations in TW1(C) using method 2 for both beams

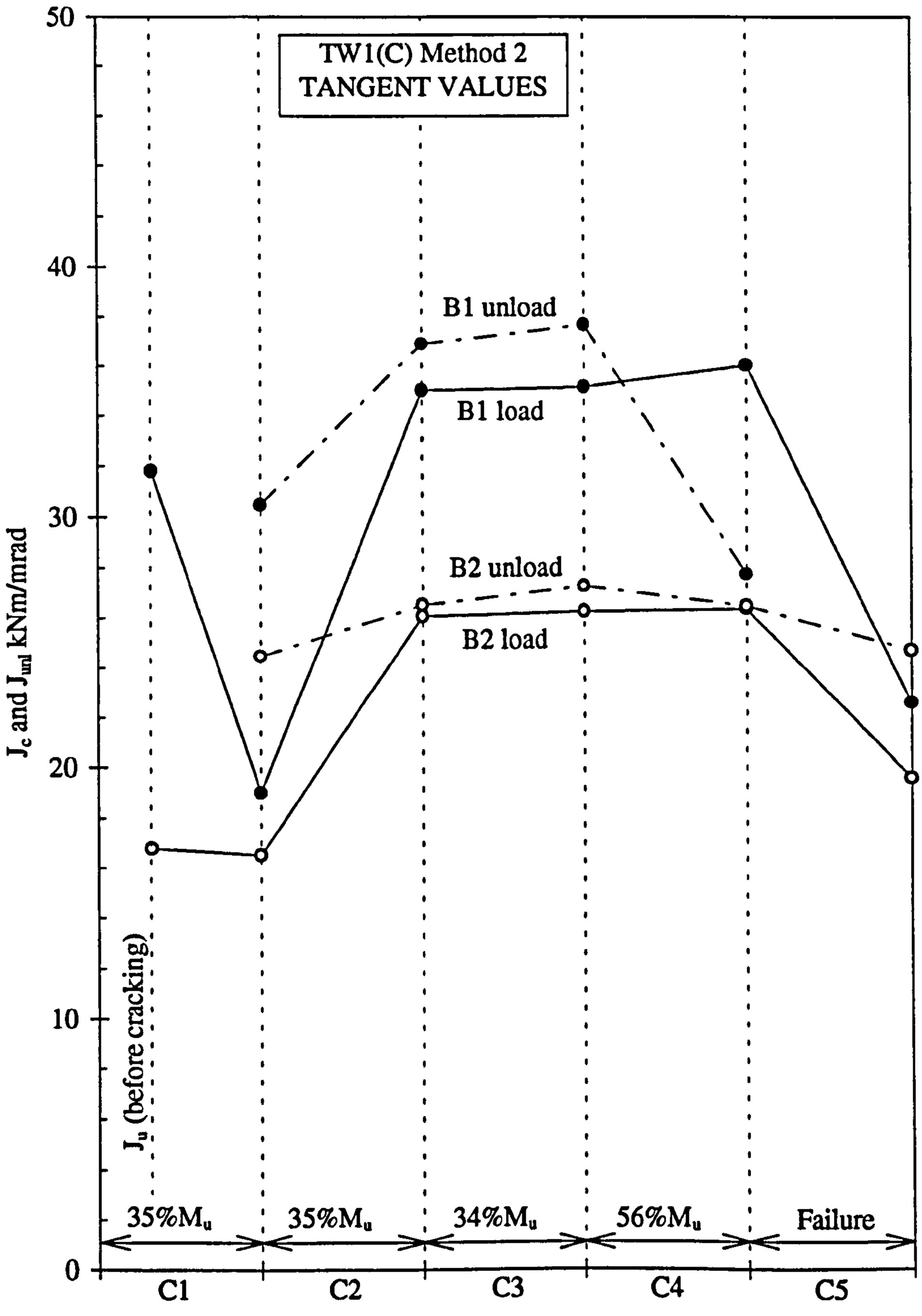

Figure 6.19: Tangent and unloading flexural stiffness versus cycles 1-5 in beams in TW1(C) using method 2

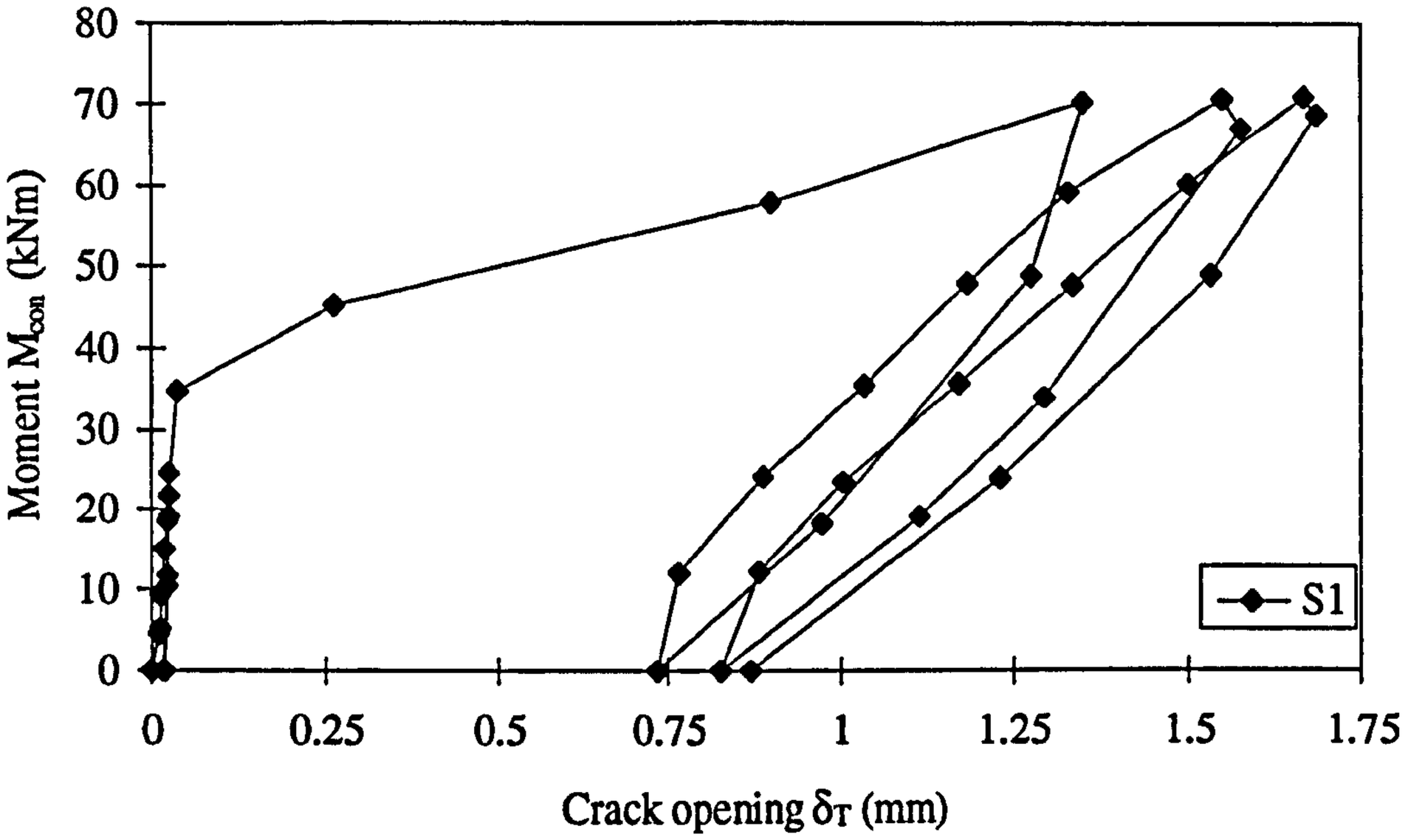

Figure 6.20(a): Moment versus crack opening at slab/column boundary in TW2 for cycles 1-3

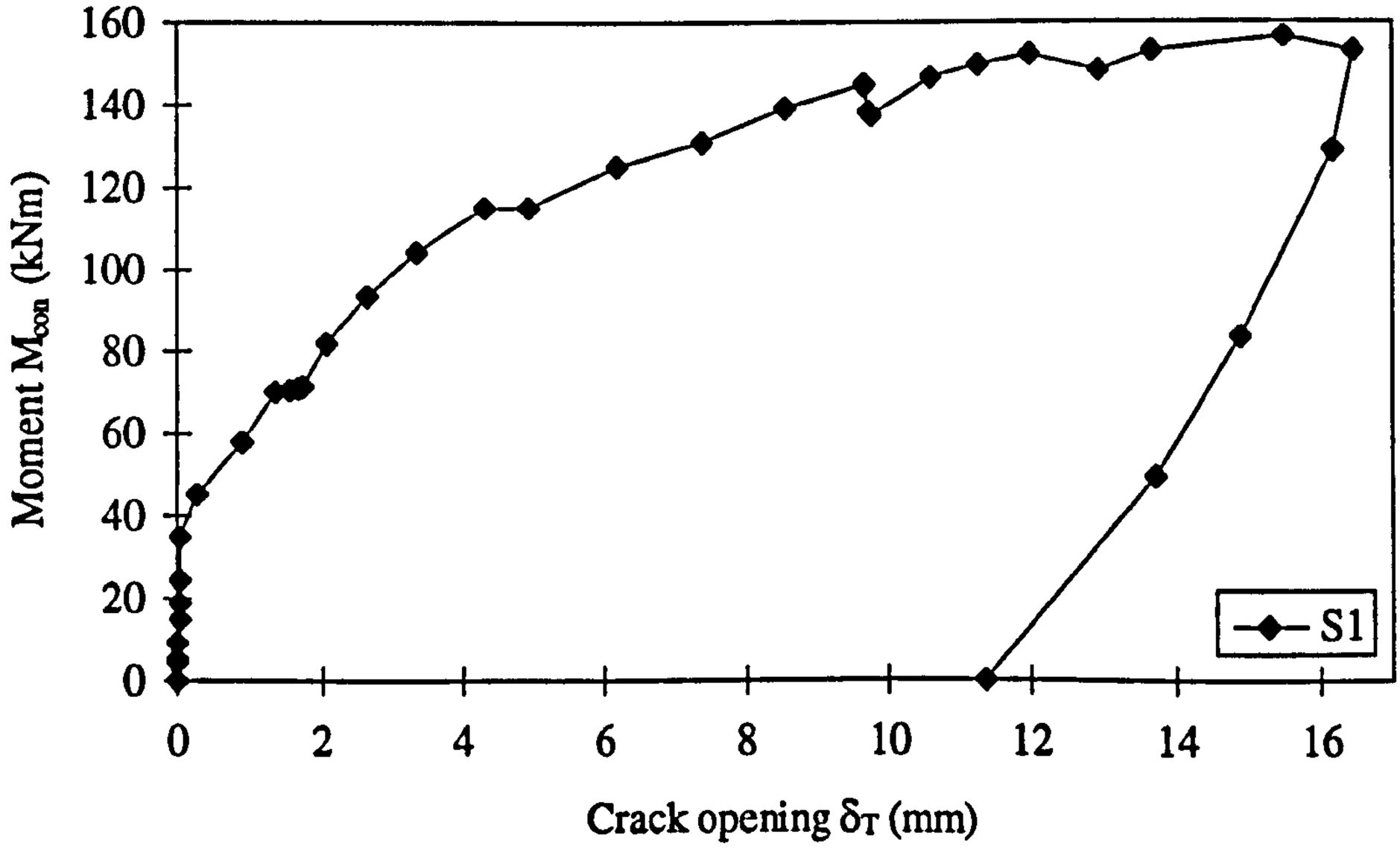

Figure 6.20(b): Moment versus crack opening at slab/column boundary in TW2

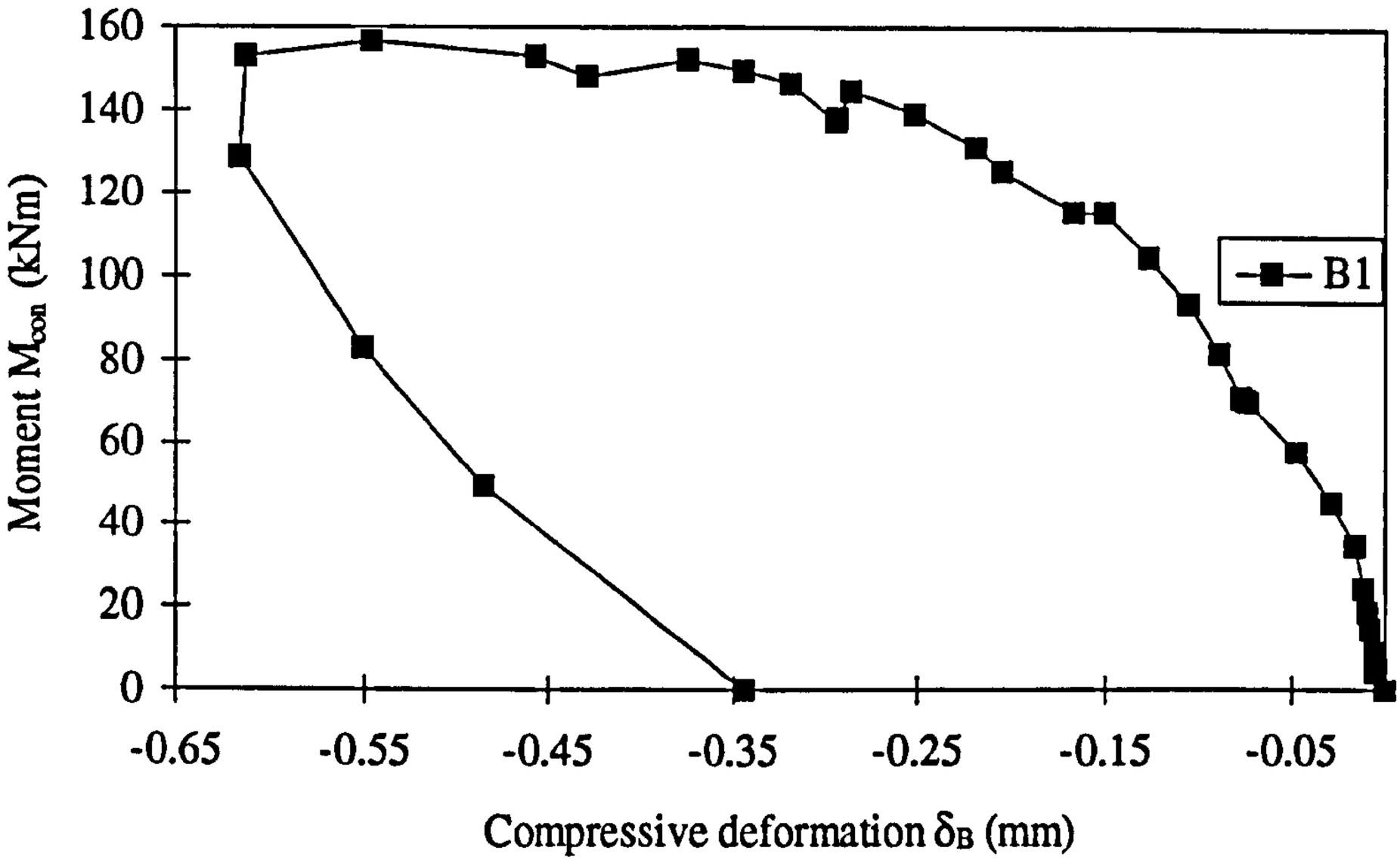

Figure 6.21: Moment versus compressive deformation in joint in TW2

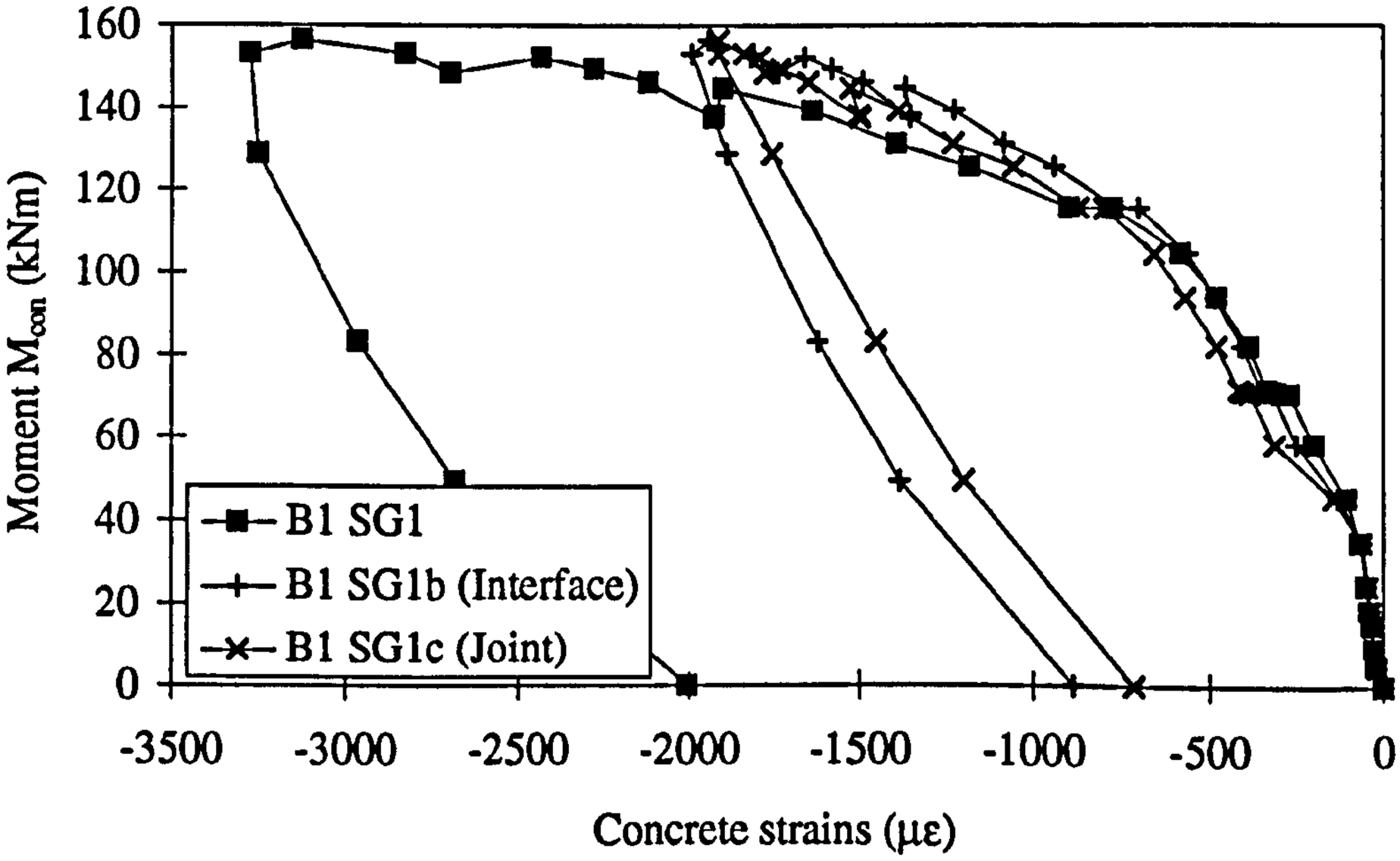

Figure 6.22: Moment versus concrete strains in beam 1 in TW2

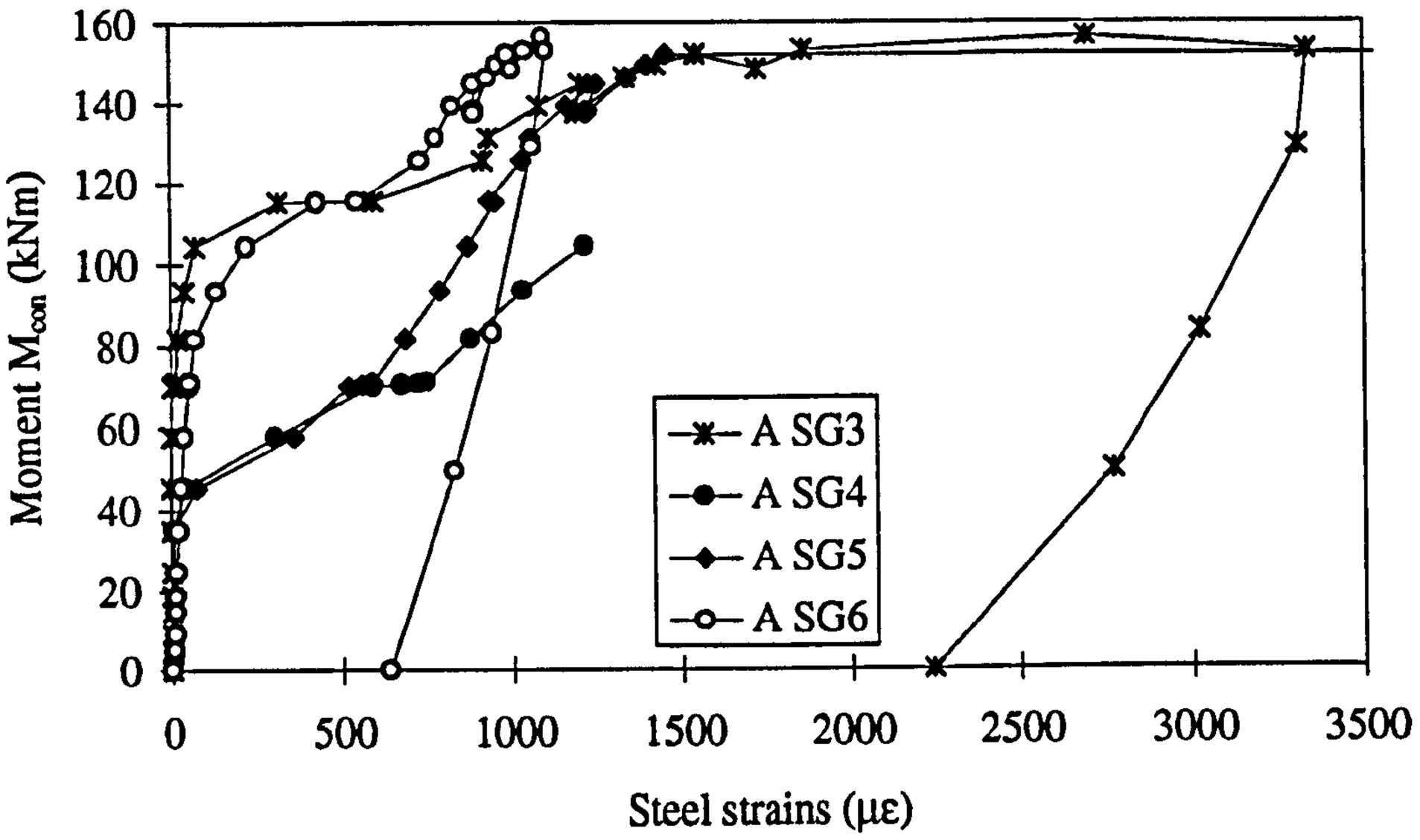

Figure 6.23: Moment versus steel strains in bar A in TW2

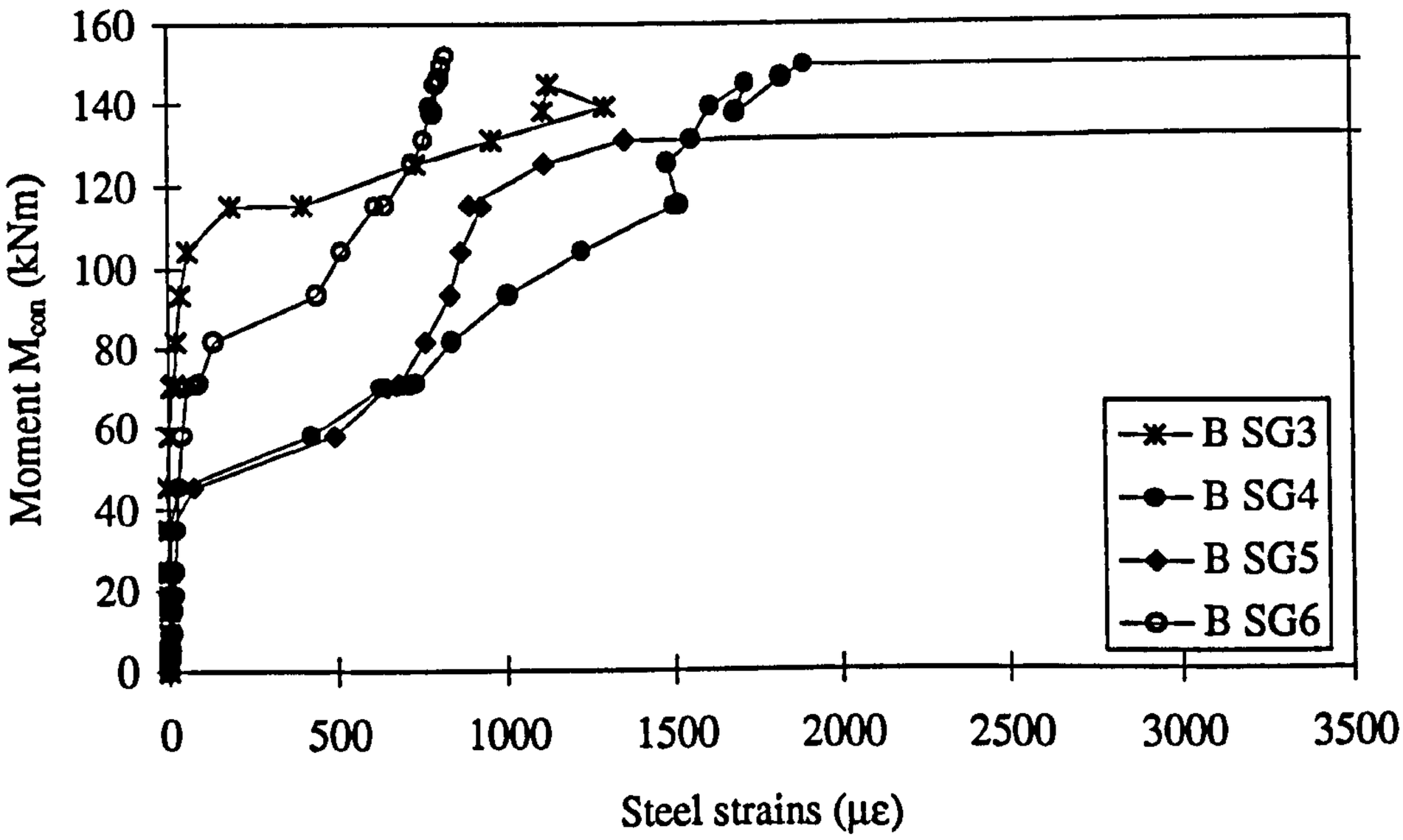

Figure 6.24: Moment versus steel strains in bar B in TW2

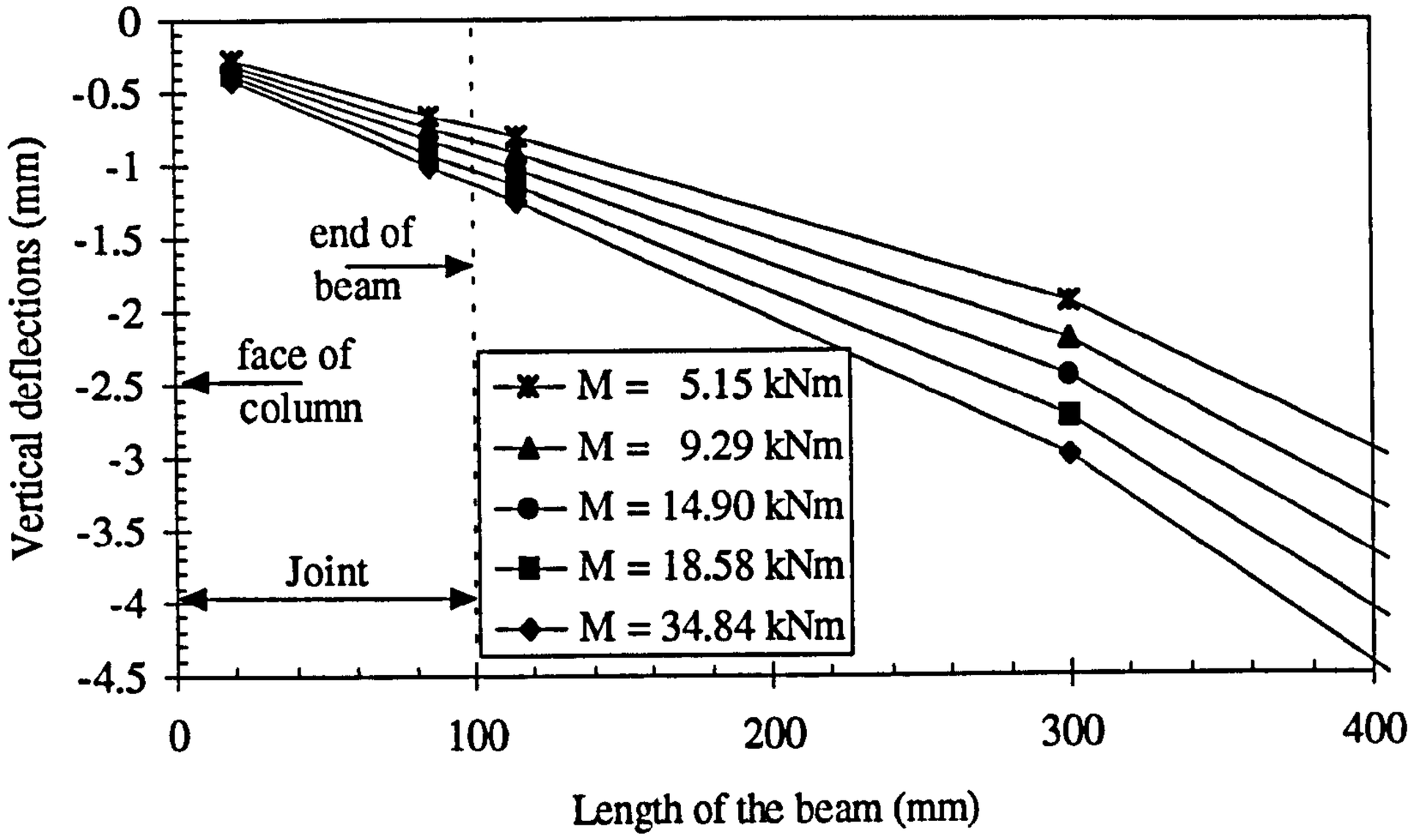

Figure 6.25: Moment versus vertical deflections in beam 1 in TW2 with various moment level

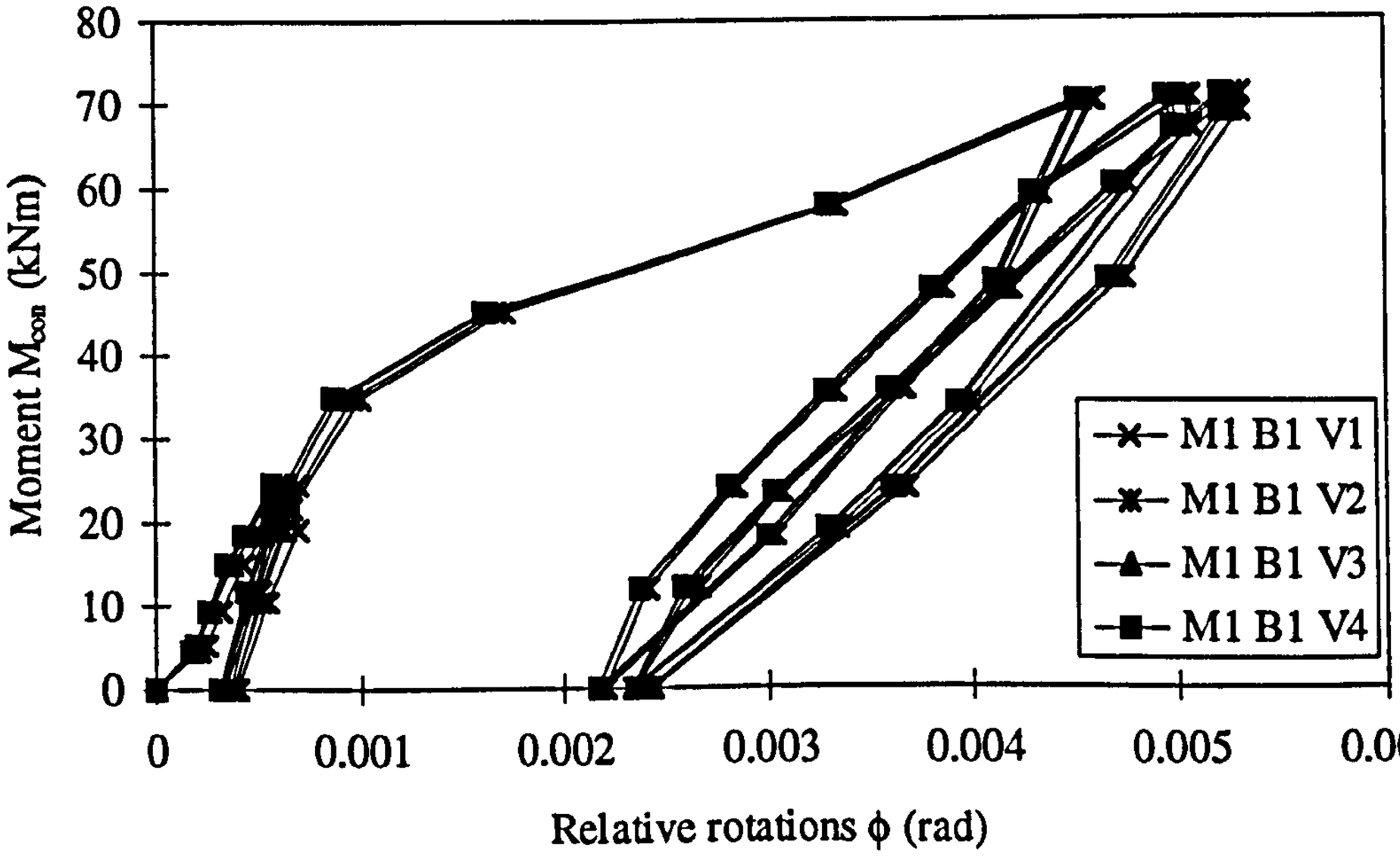

Figure 6.26(a): Moment versus relative rotations in beam 1 in TW2 using method 1 for cycles 1-3

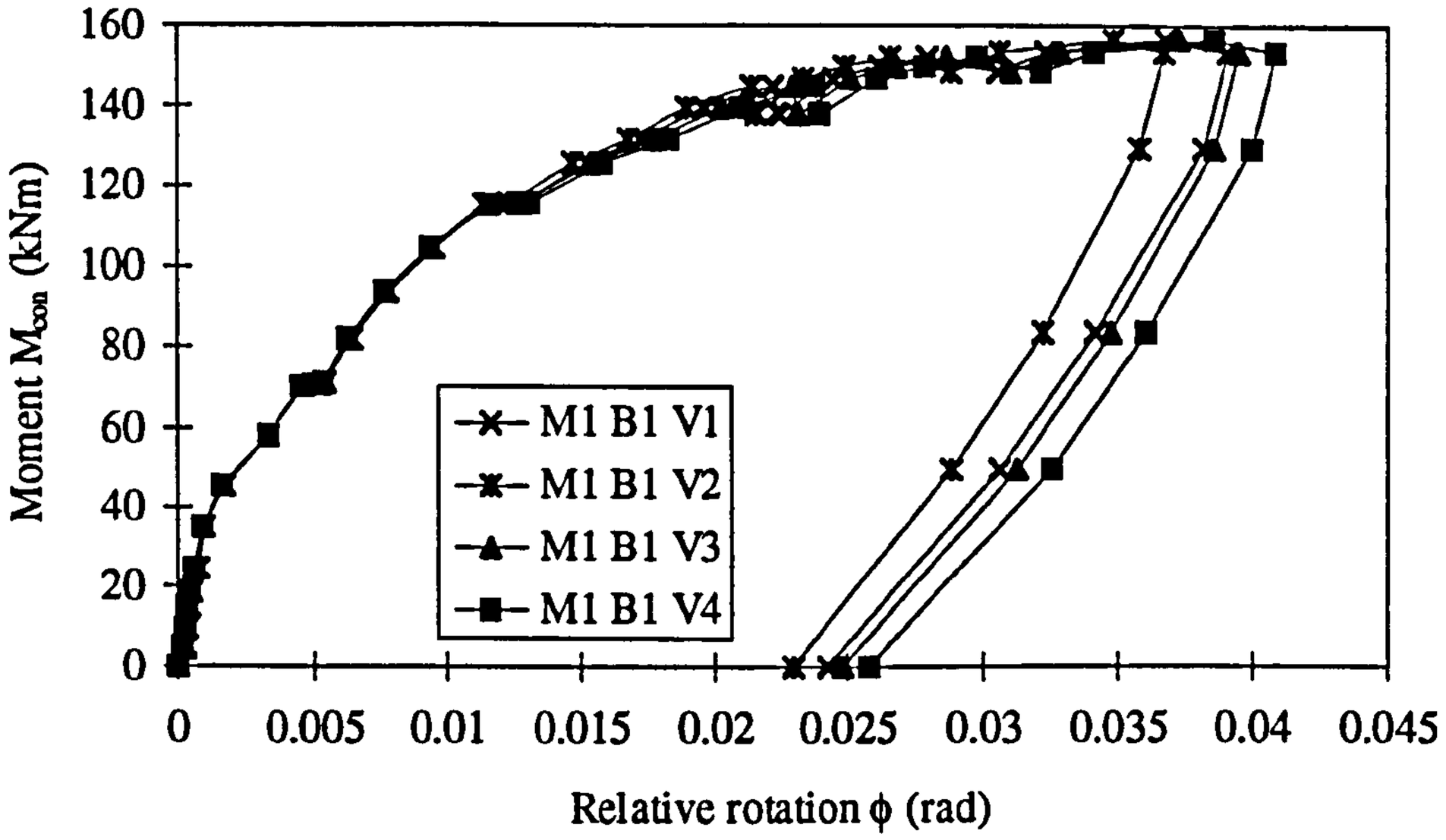

Figure 6.26(b): Moment versus relative rotations in beam 1 in TW2 using method 1

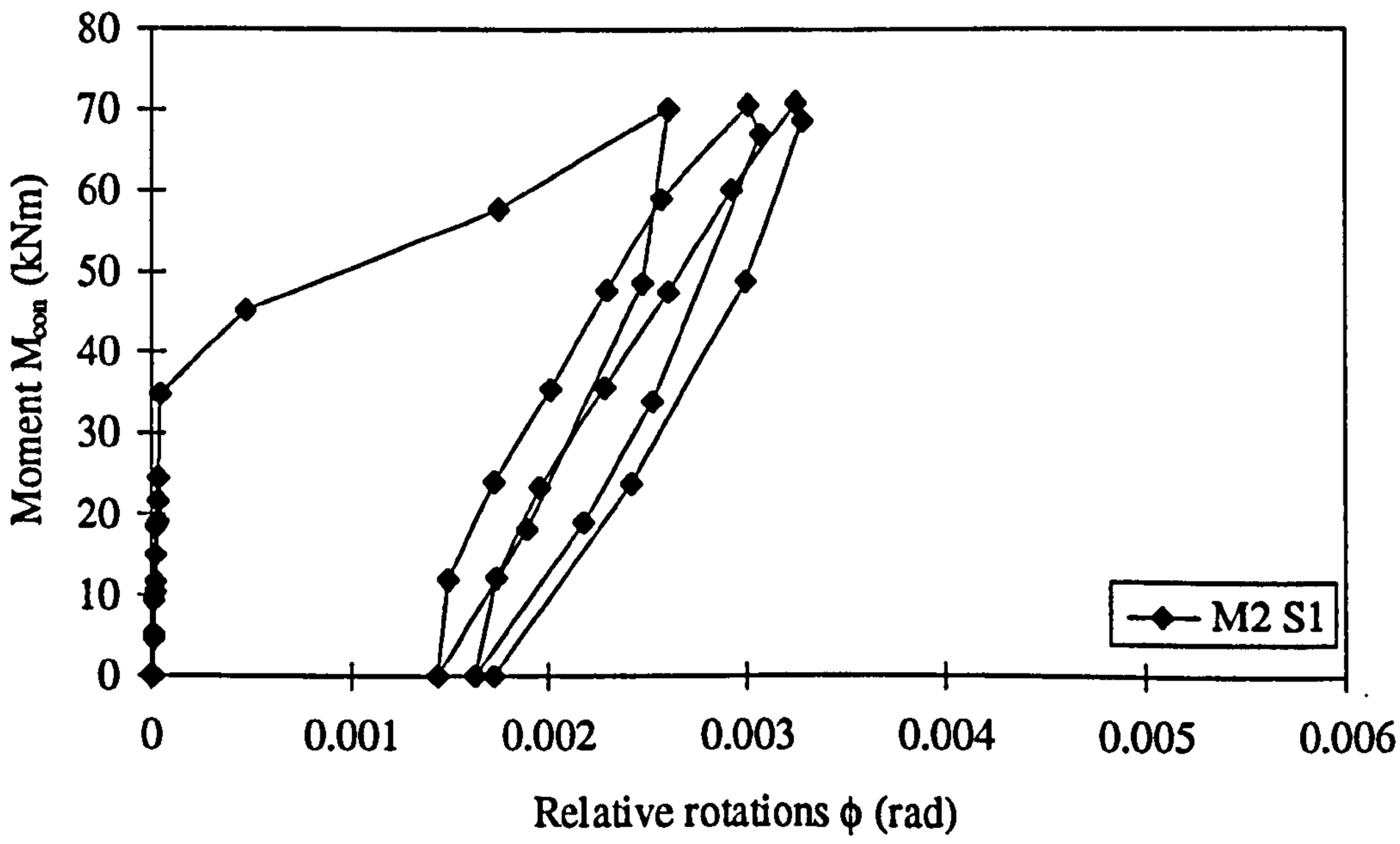

Figure 6.27(a): Moment versus relative rotations in TW2 using method 2 for cycles 1-3

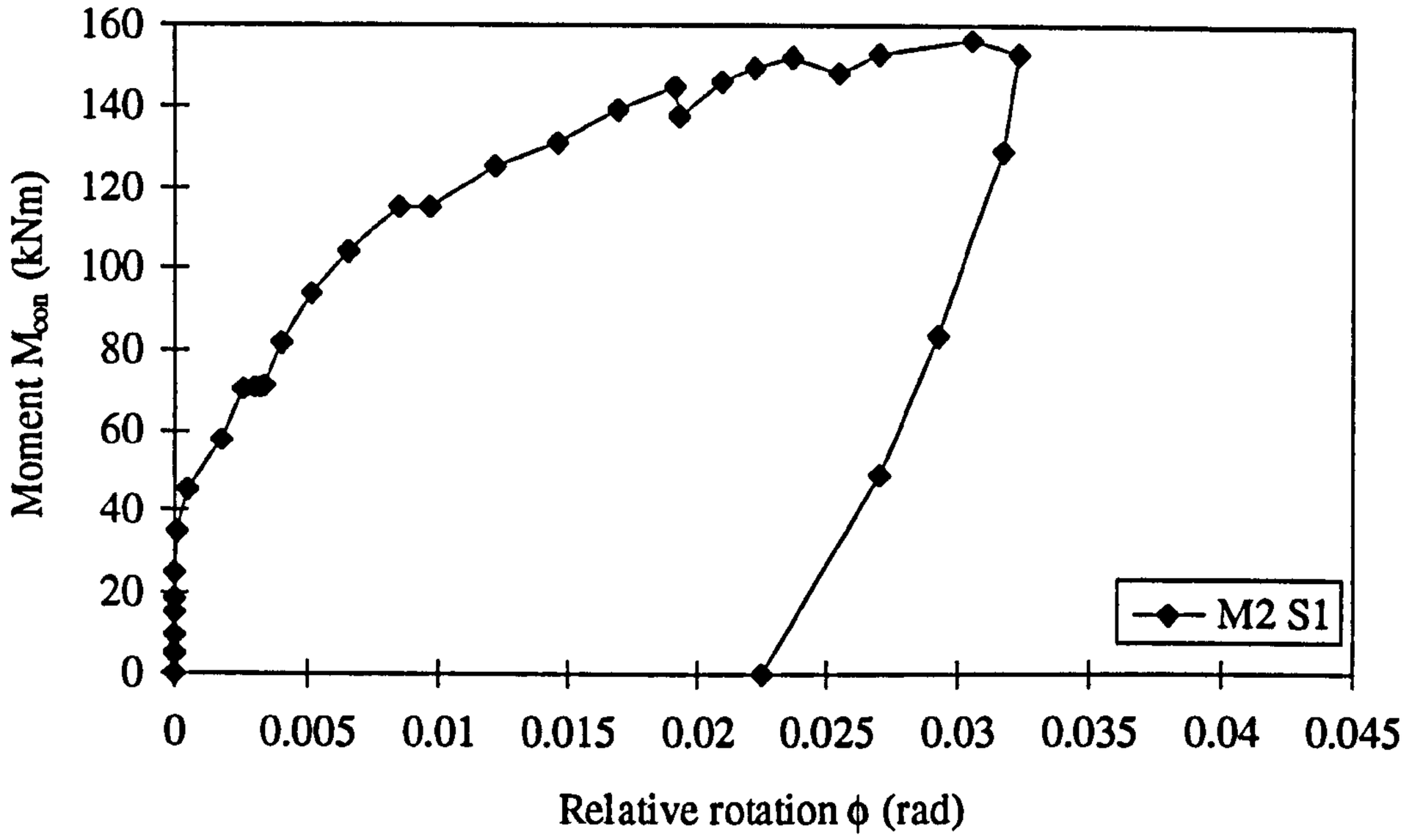

Figure 6.27(b): Moment versus relative rotations in TW2 using method 2

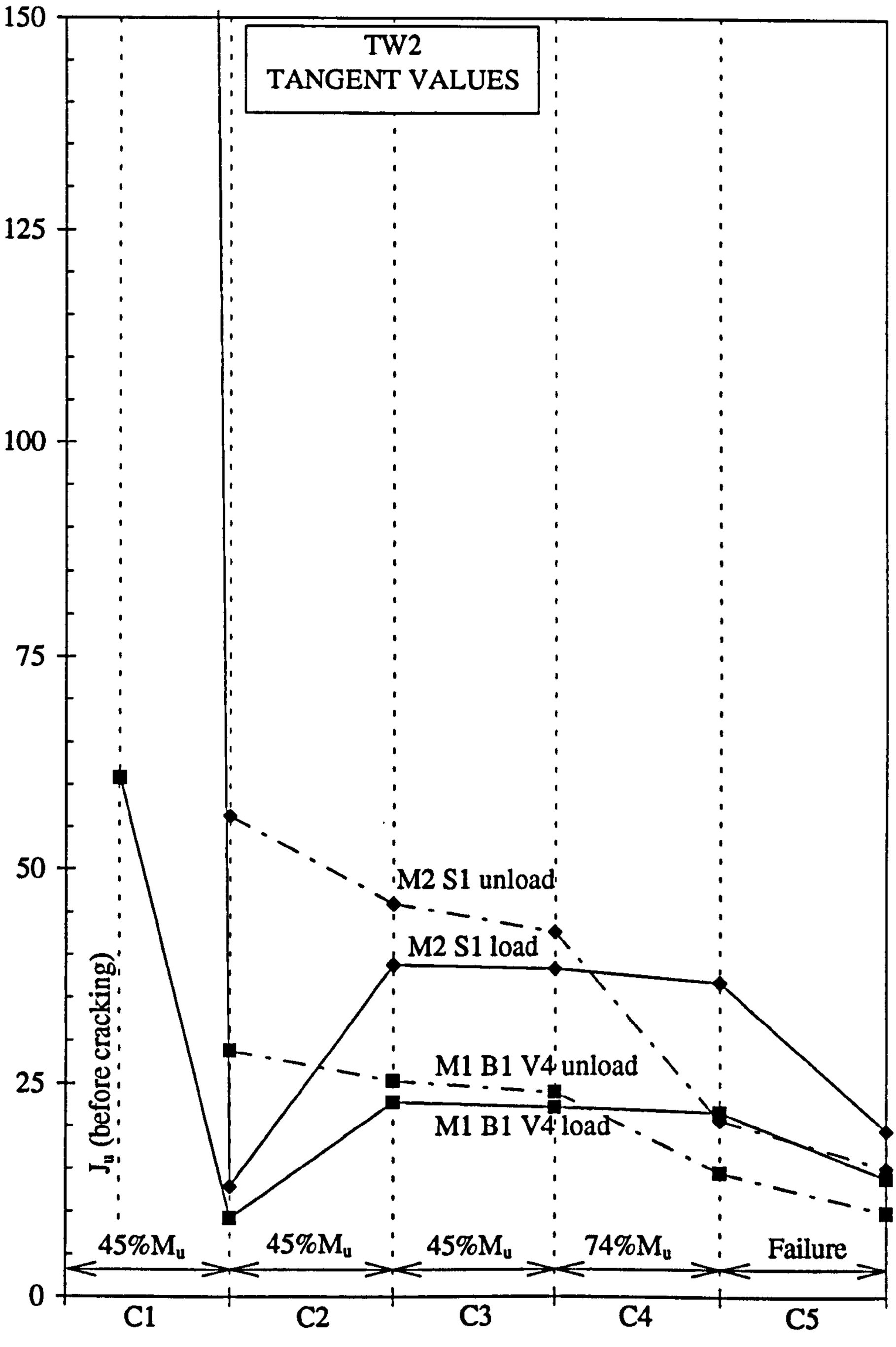

Figure 6.28: Tangent and unloading flexural stiffness versus cycles 1-5 in TW2 using methods 1 and 2

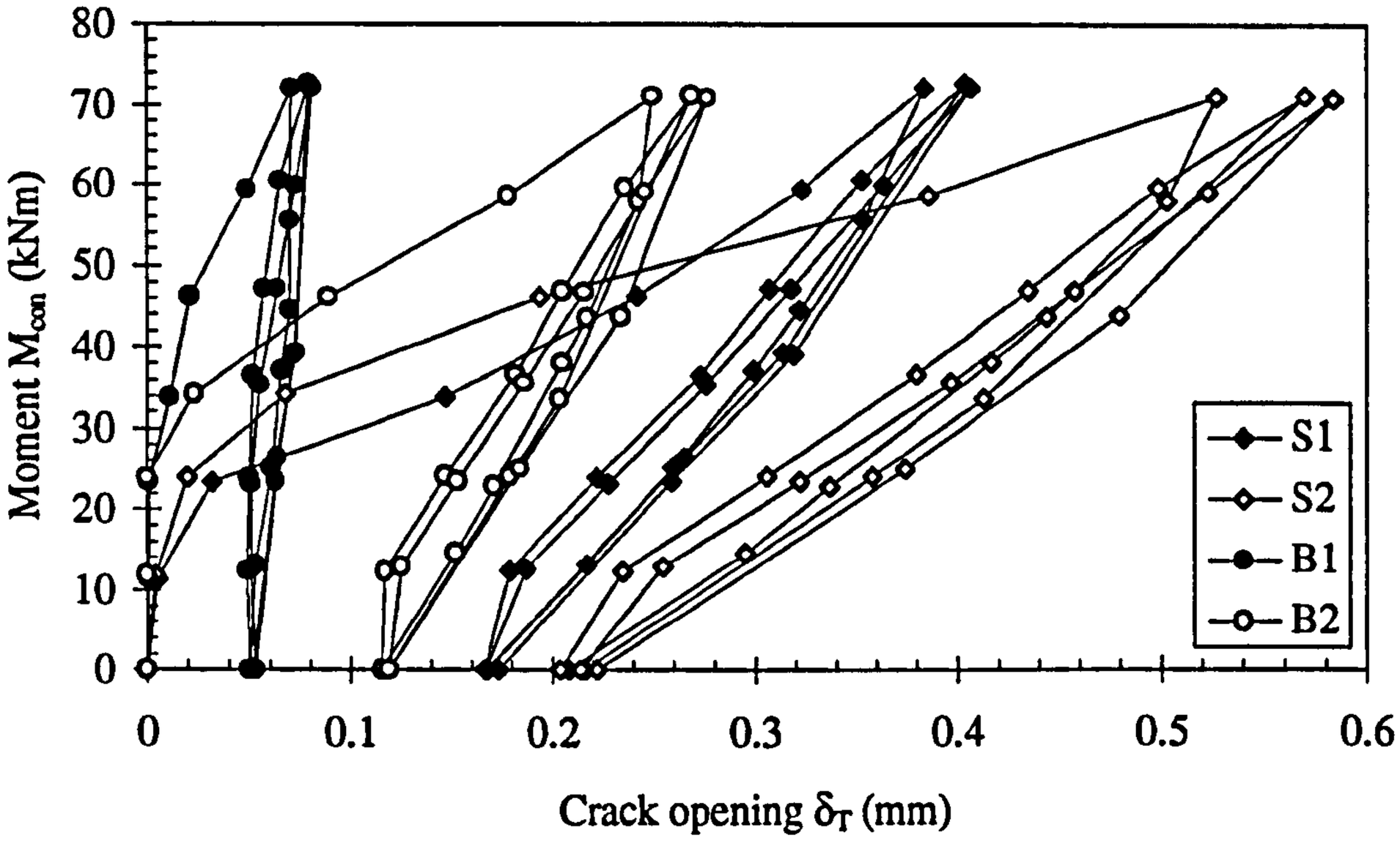

Figure 6.29(a): Moment versus crack opening at slabs/column and beams/column boundaries in TB1(A) for cycles 1-3

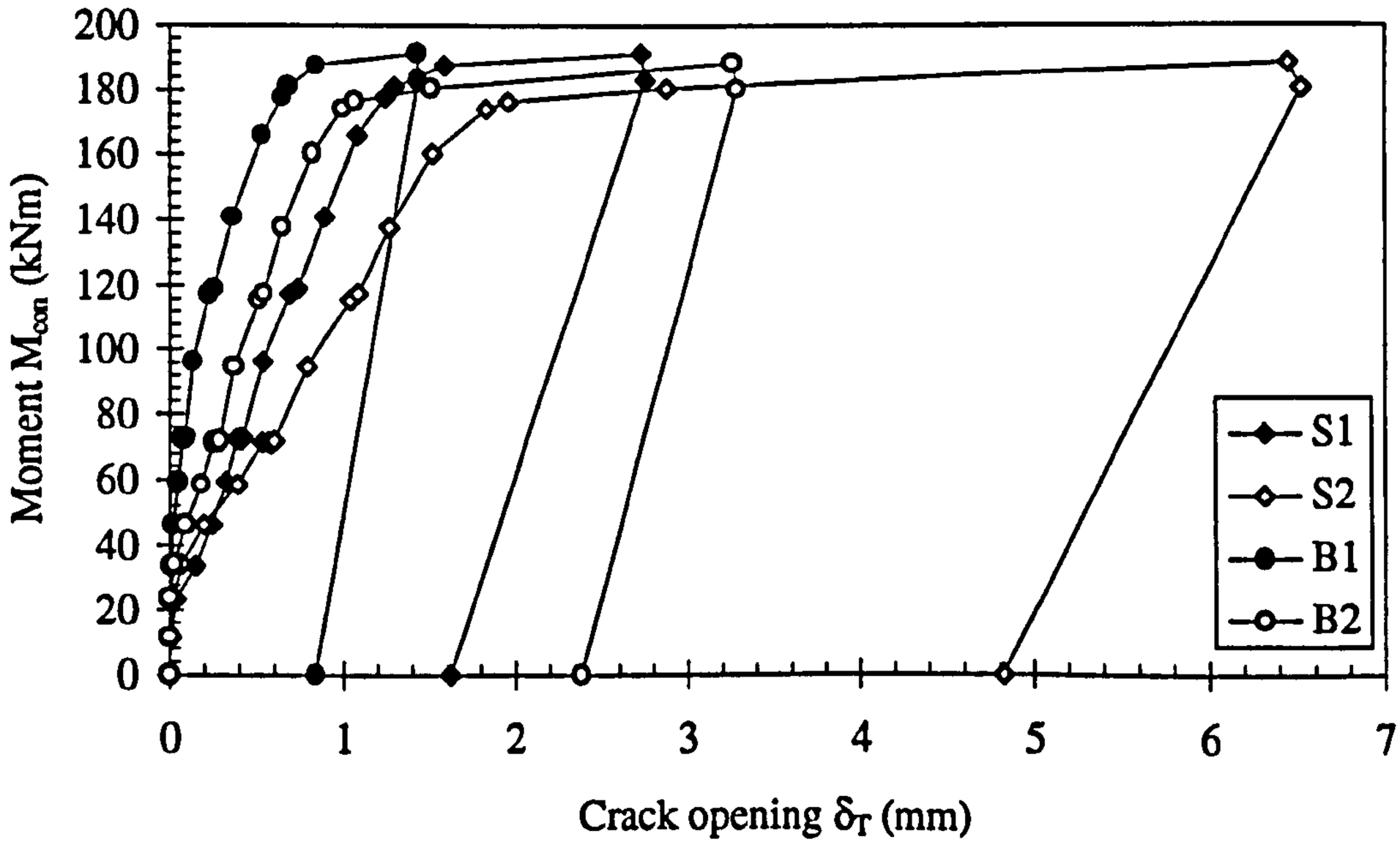

Figure 6.29(b): Moment versus crack opening at slabs/column and beams/column boundaries in TB1(A)

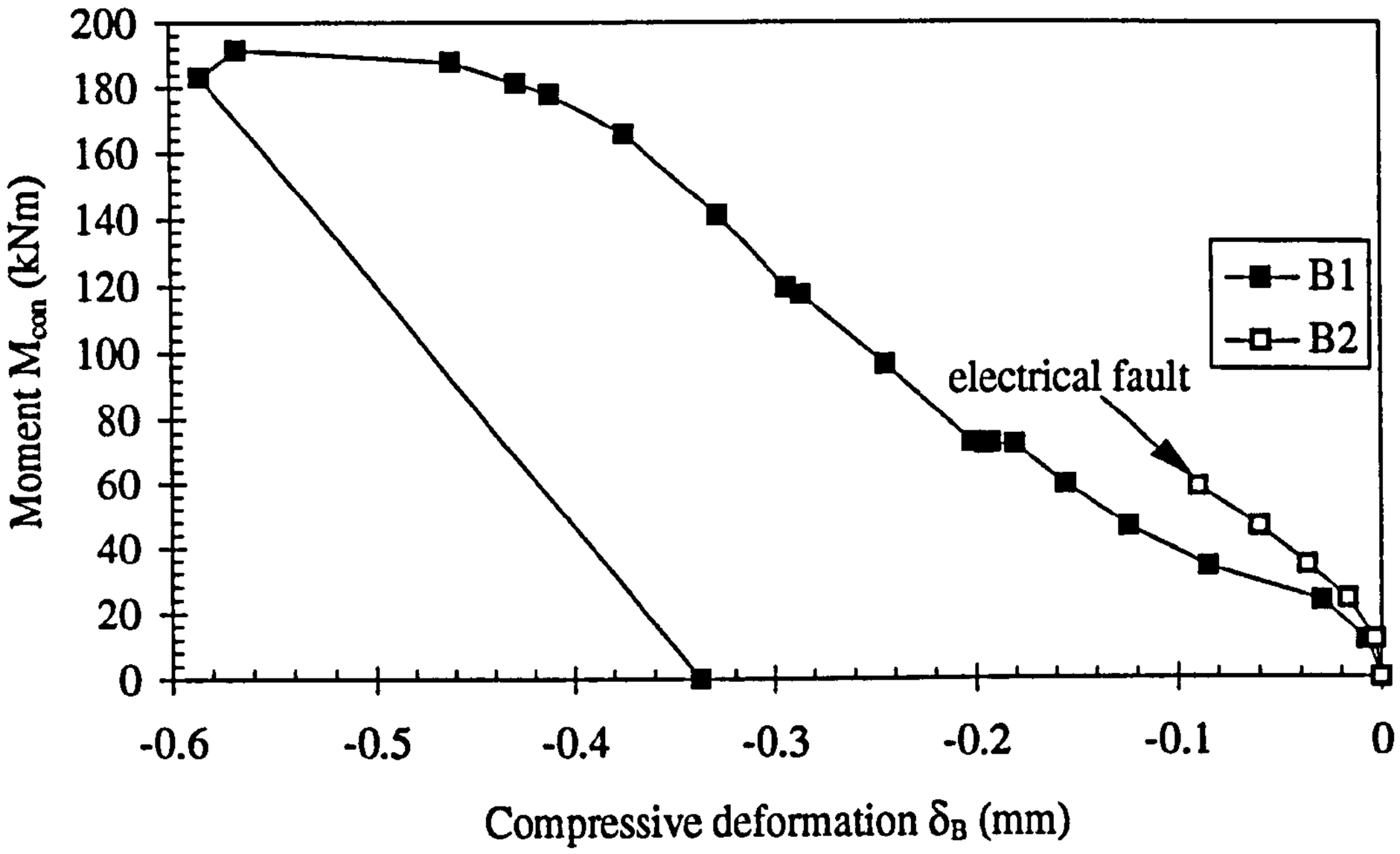

Figure 6.30: Moment versus compressive deformation in joints in TB1(A)

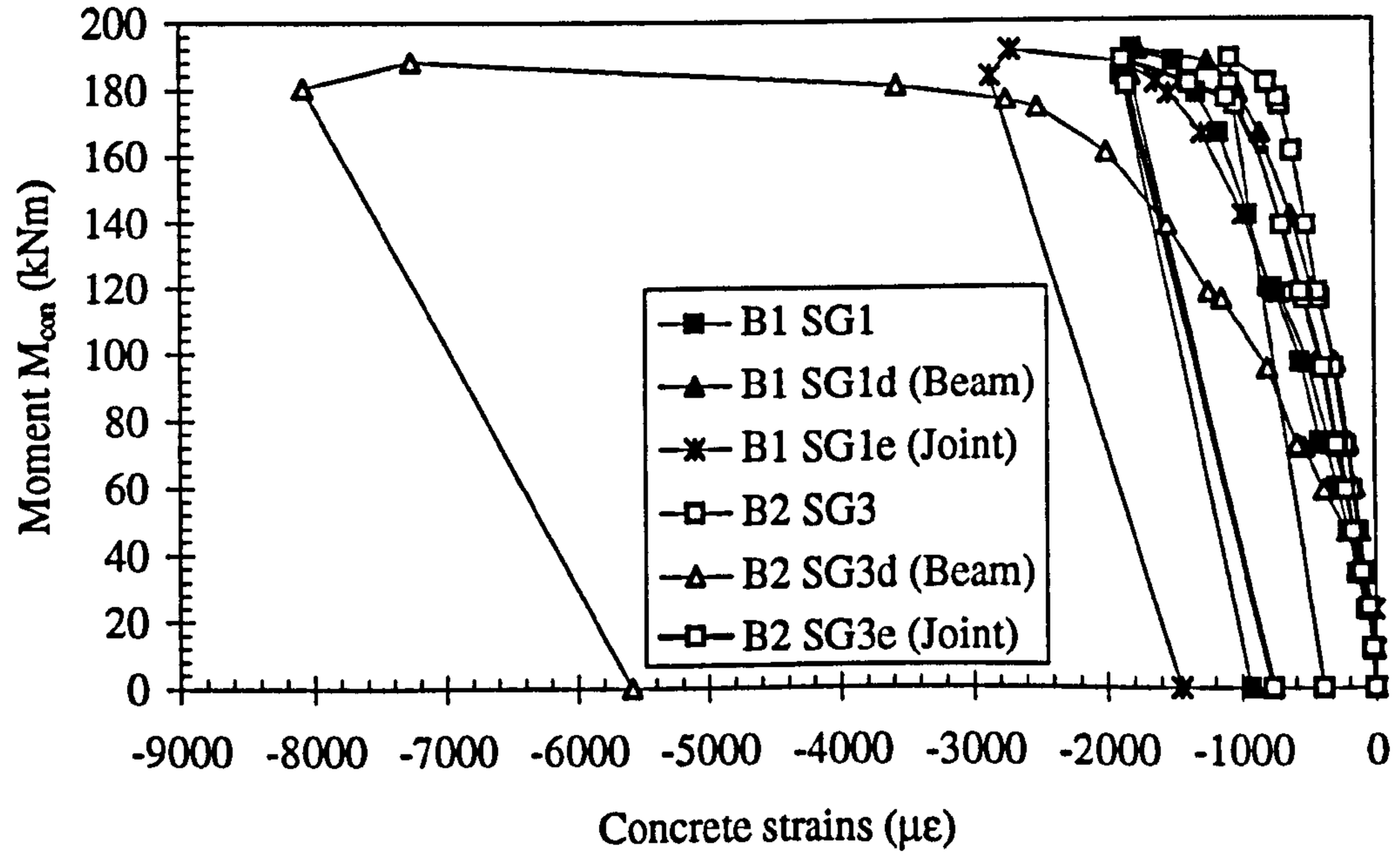

Figure 6.31: Moment versus concrete strains in beams in TB1(A)

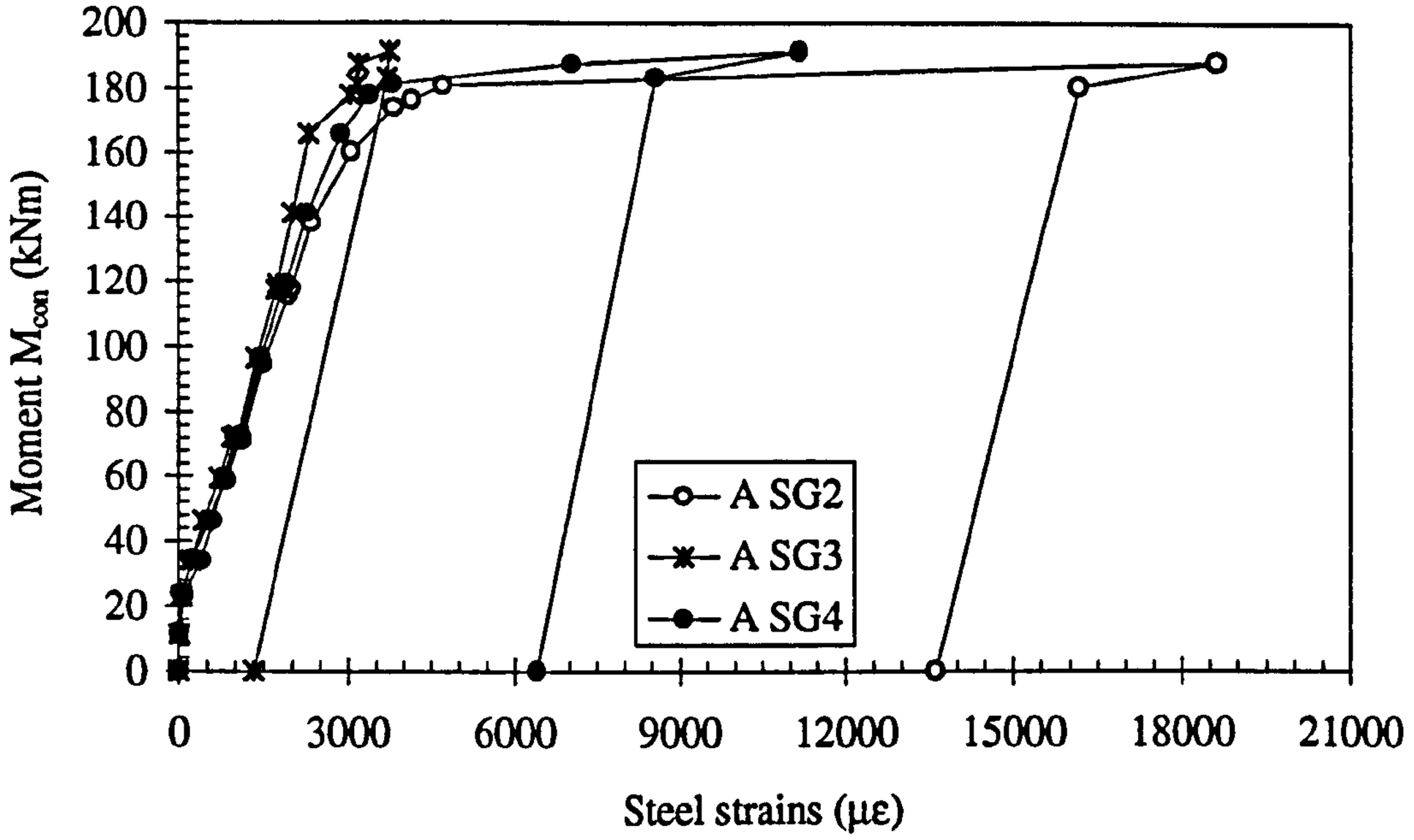

Figure 6.32: Moment versus steel strains in bar A in TB1(A)

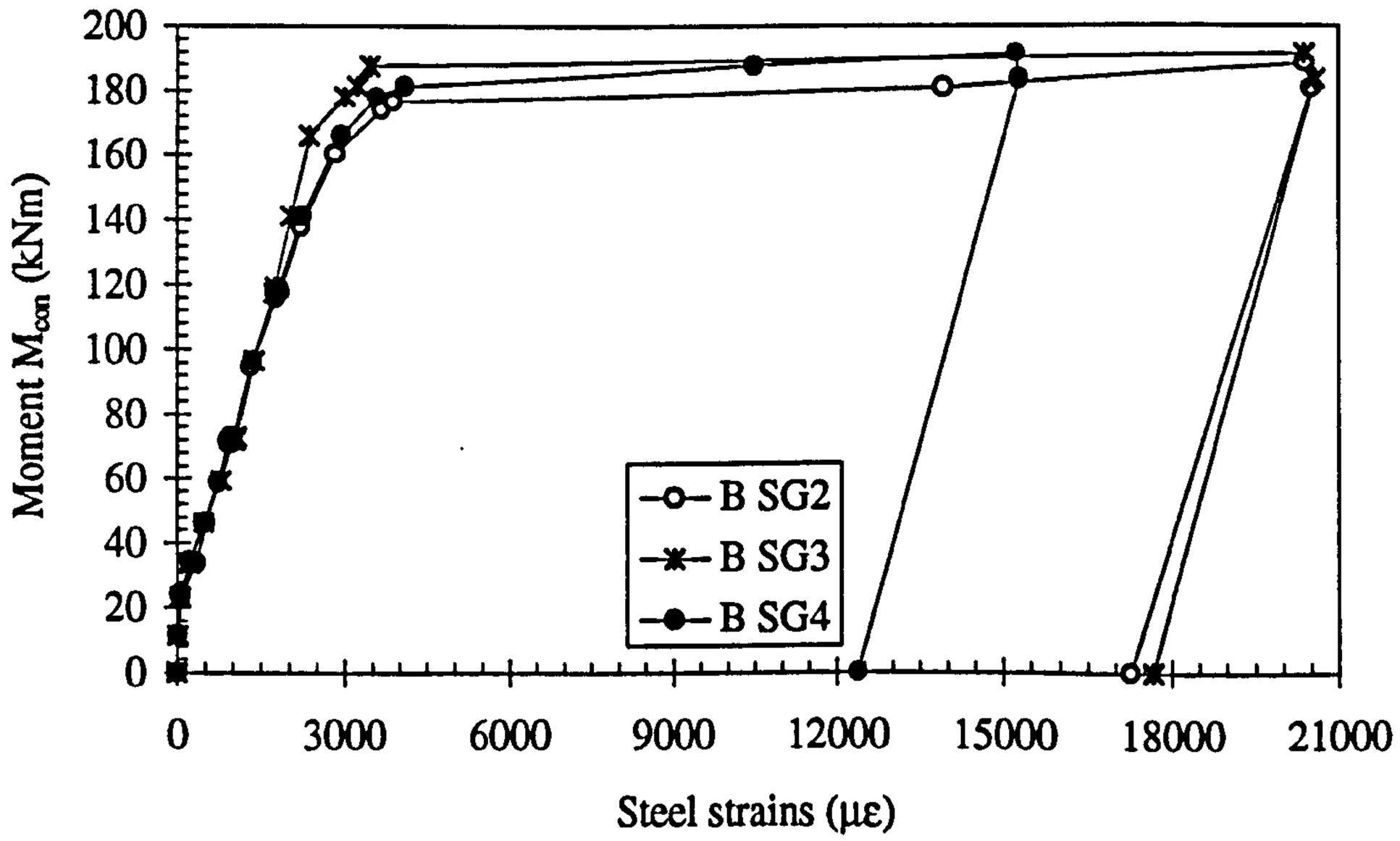

Figure 6.33: Moment versus steel strains in bar B in TB1(A)

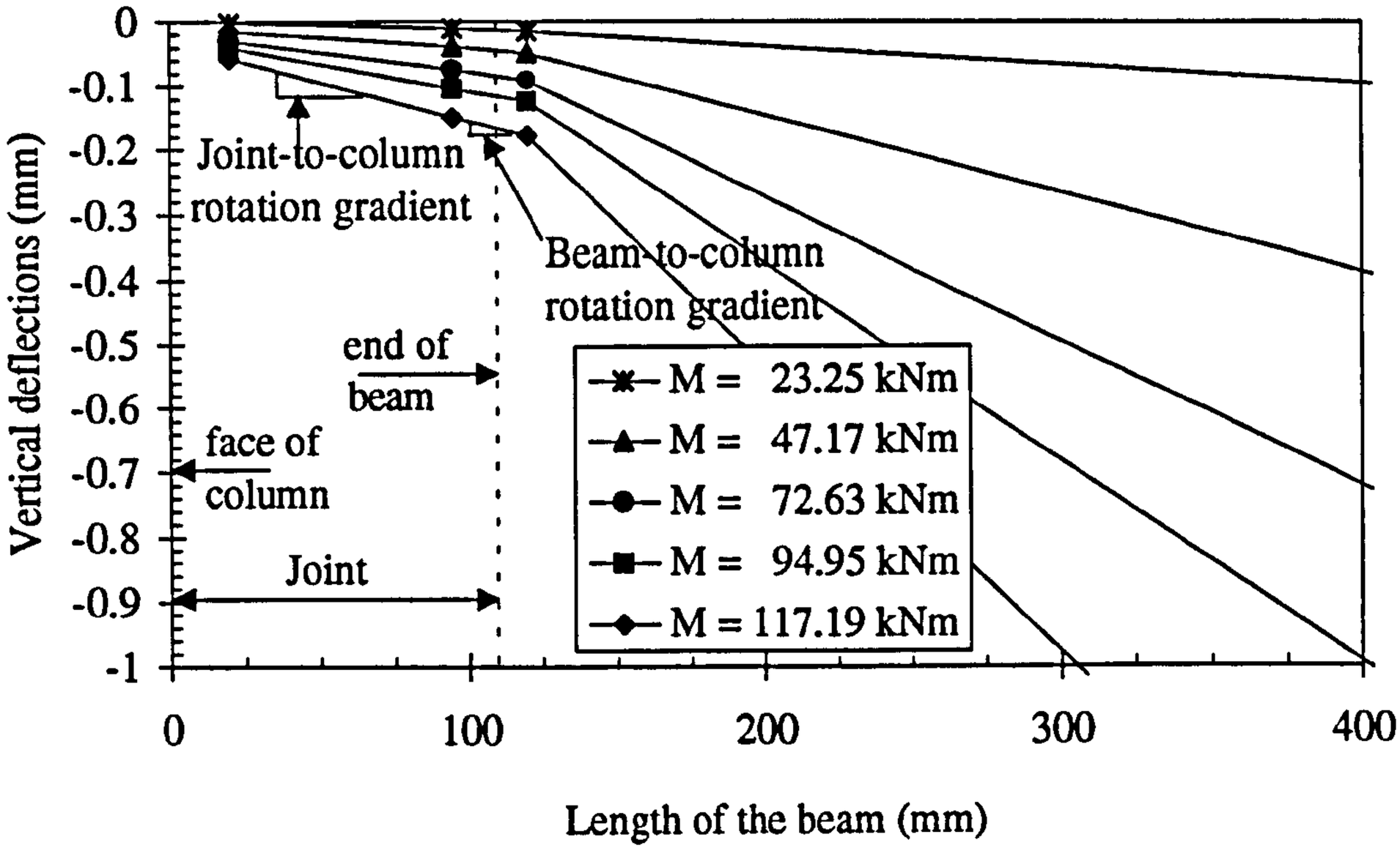

Figure 6.34(a): Moment versus vertical deflections in beam 1 in TB1(A) with various moment level

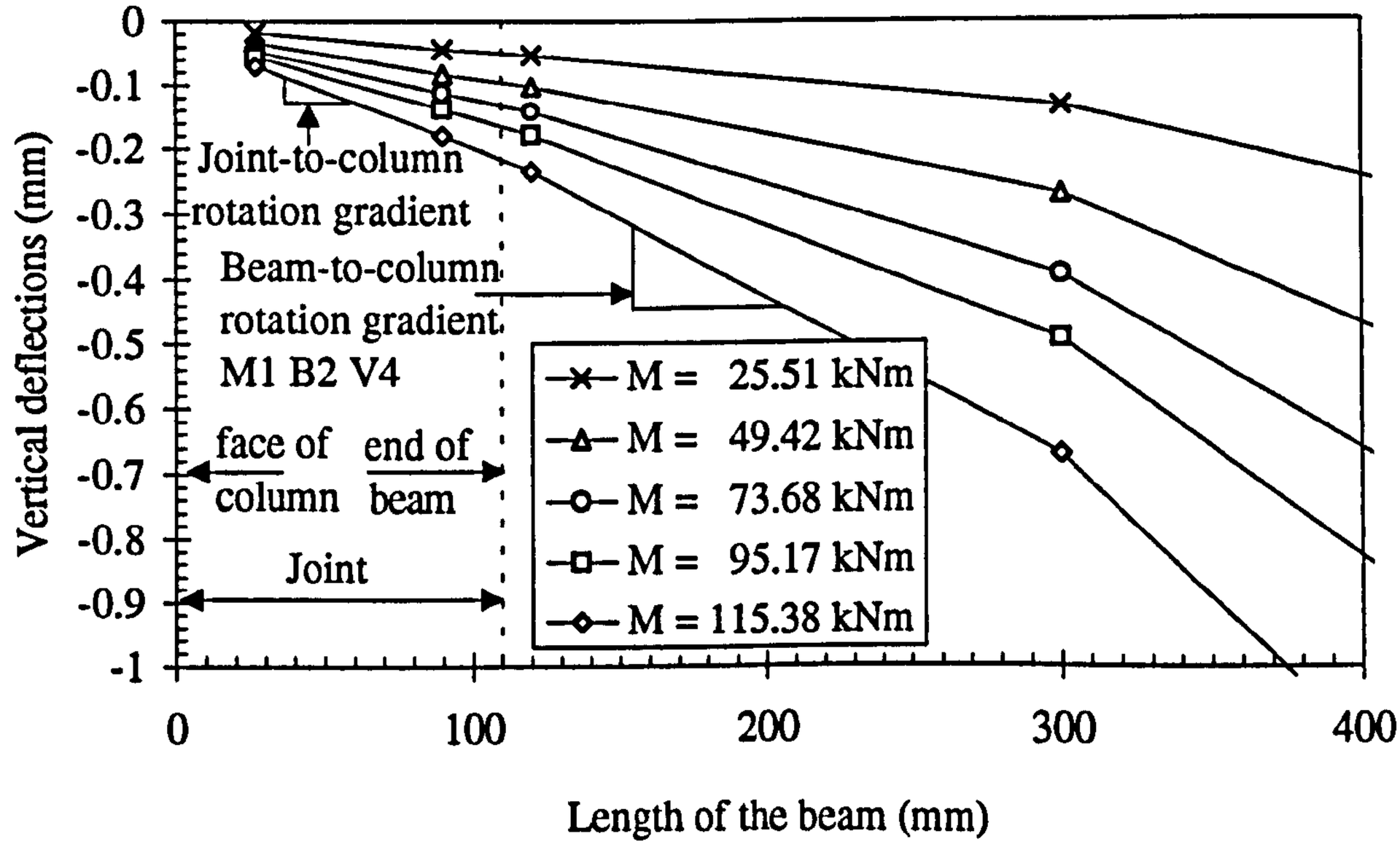

Figure 6.34(b): Moment versus vertical deflections in beam 2 in TB1(A) with various moment level

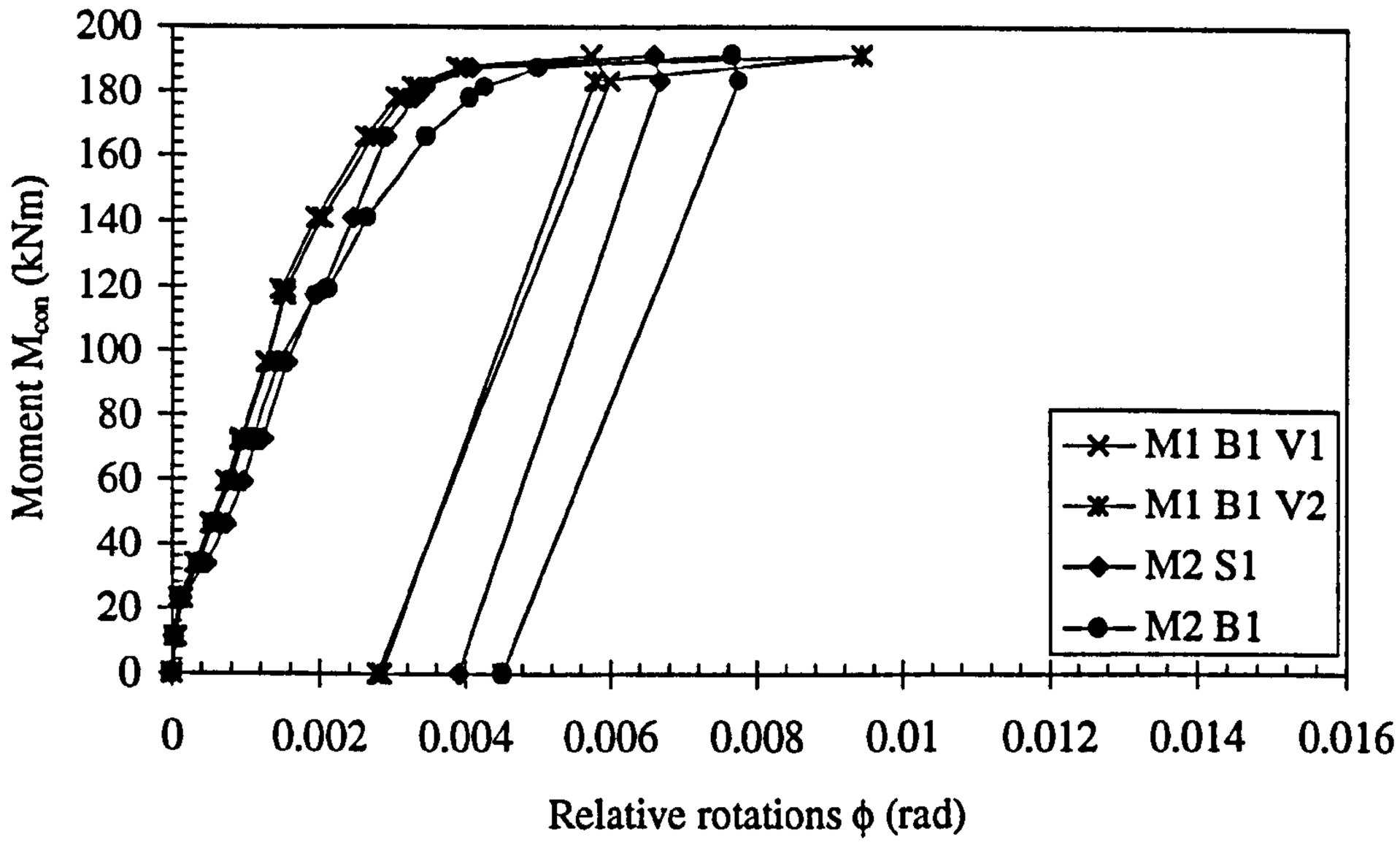

Figure 6.35: Moment versus relative rotations in beam 1 in TB1(A) using methods 1 and 2

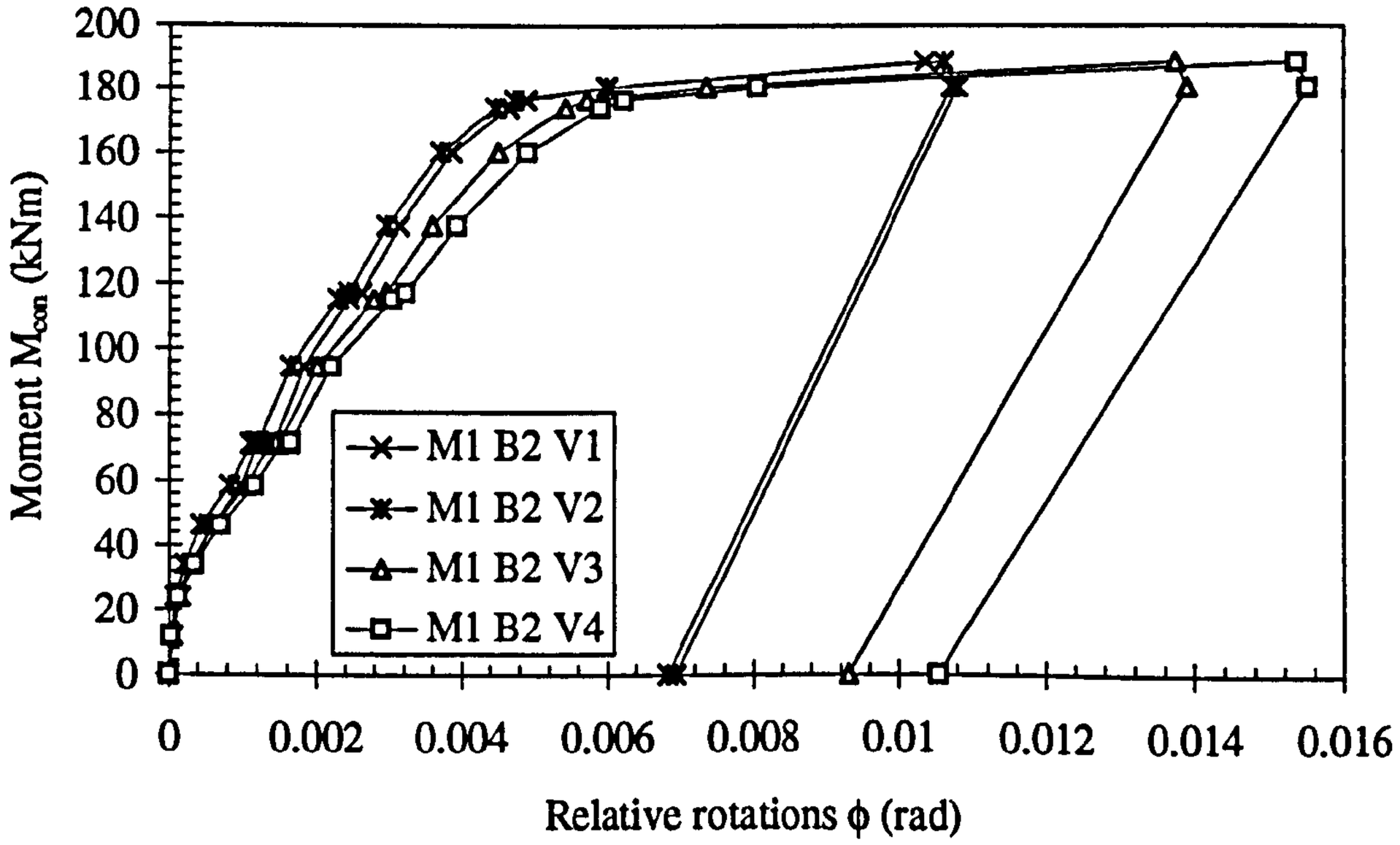

Figure 6.36: Moment versus relative rotations in beam 2 in TB1(A) using method 1

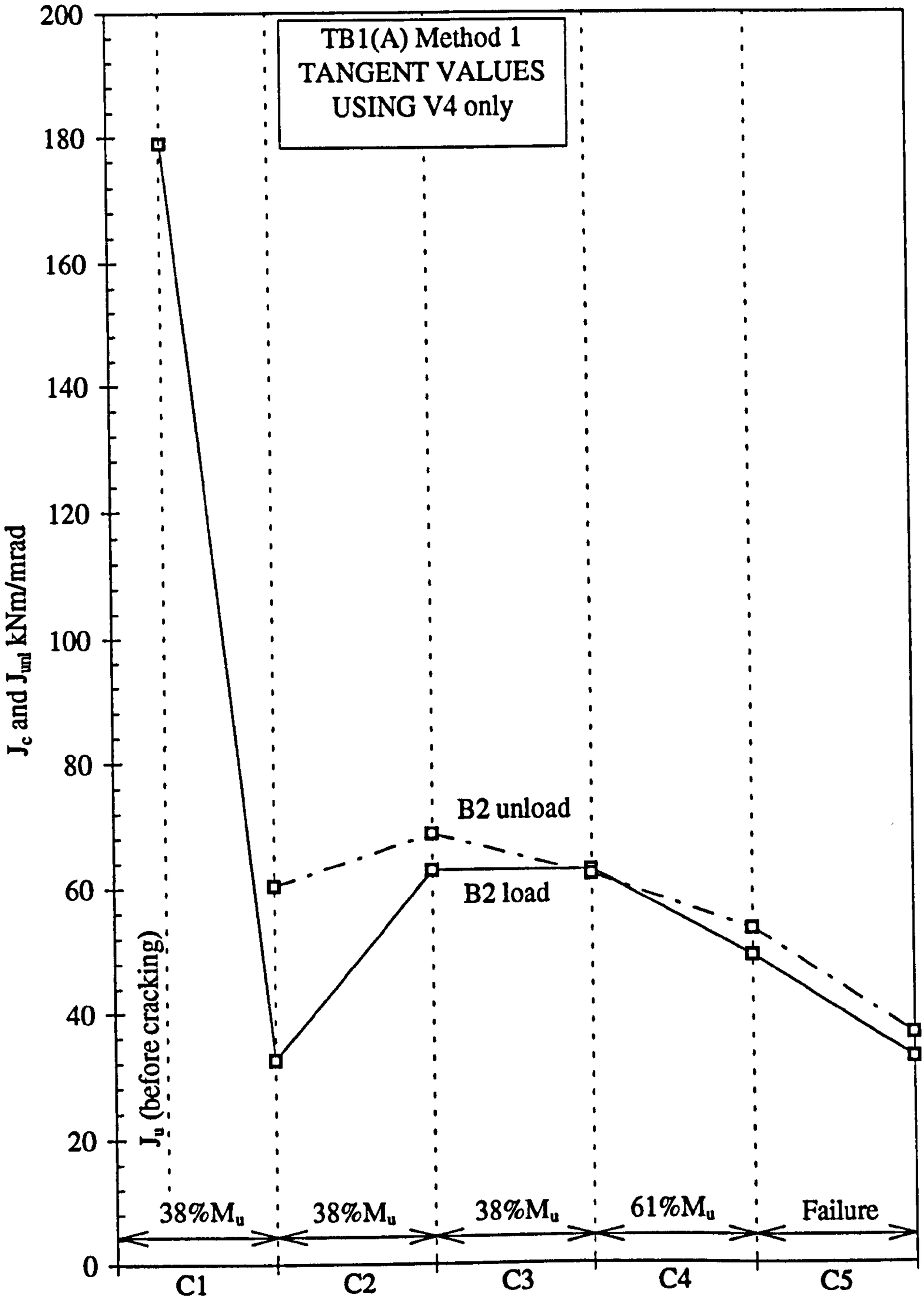

Figure 6.37(a): Tangent and unloading flexural stiffness versus cycles 1-5 in beam 2 in TB1(A) using method 1

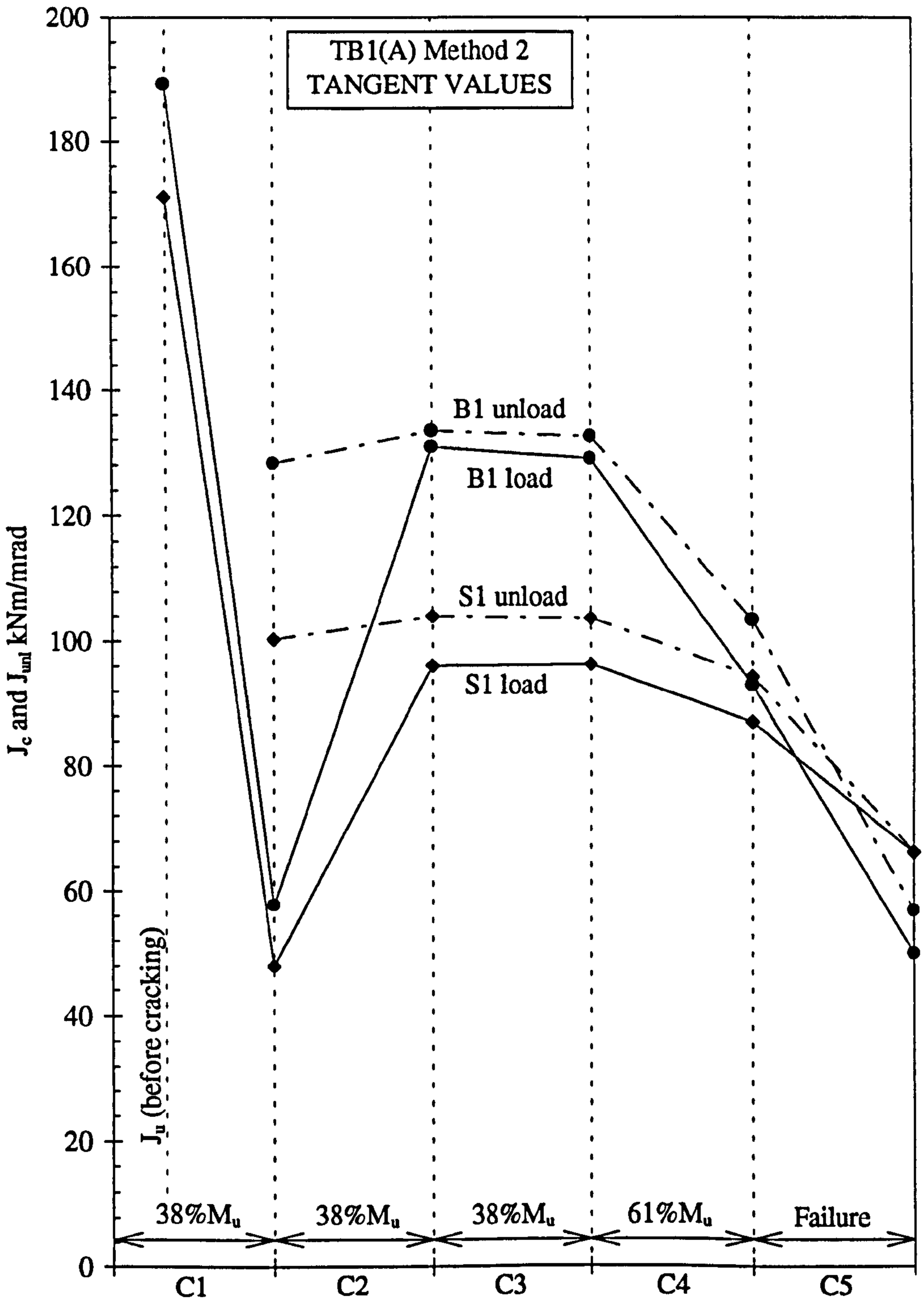

Figure 6.37(b): Tangent and unloading flexural stiffness versus cycles 1-5 in slabs and beams in TB1(A) using method 2

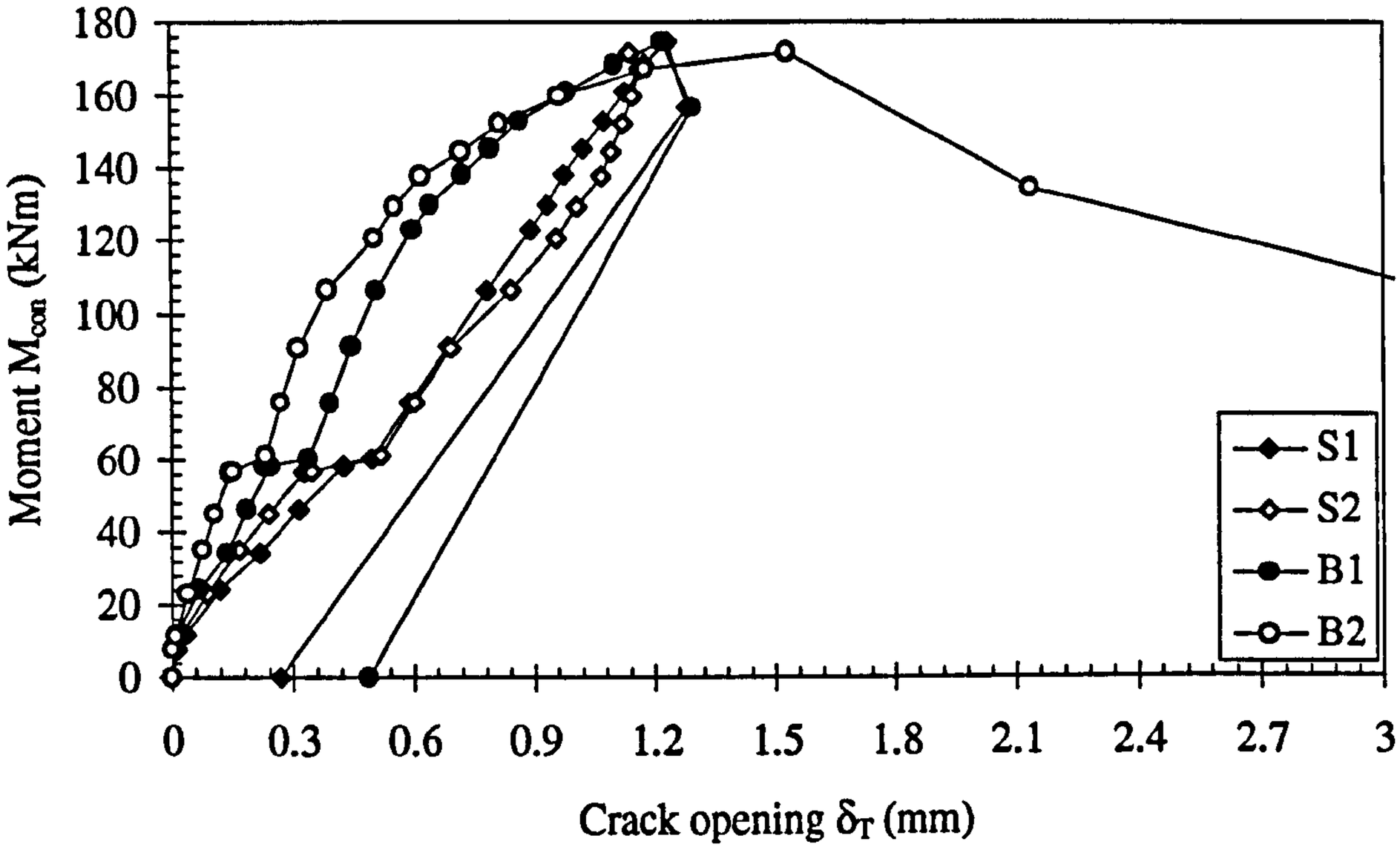

Figure 6.38: Moment versus crack opening at slab/column boundaries in TB1(B)

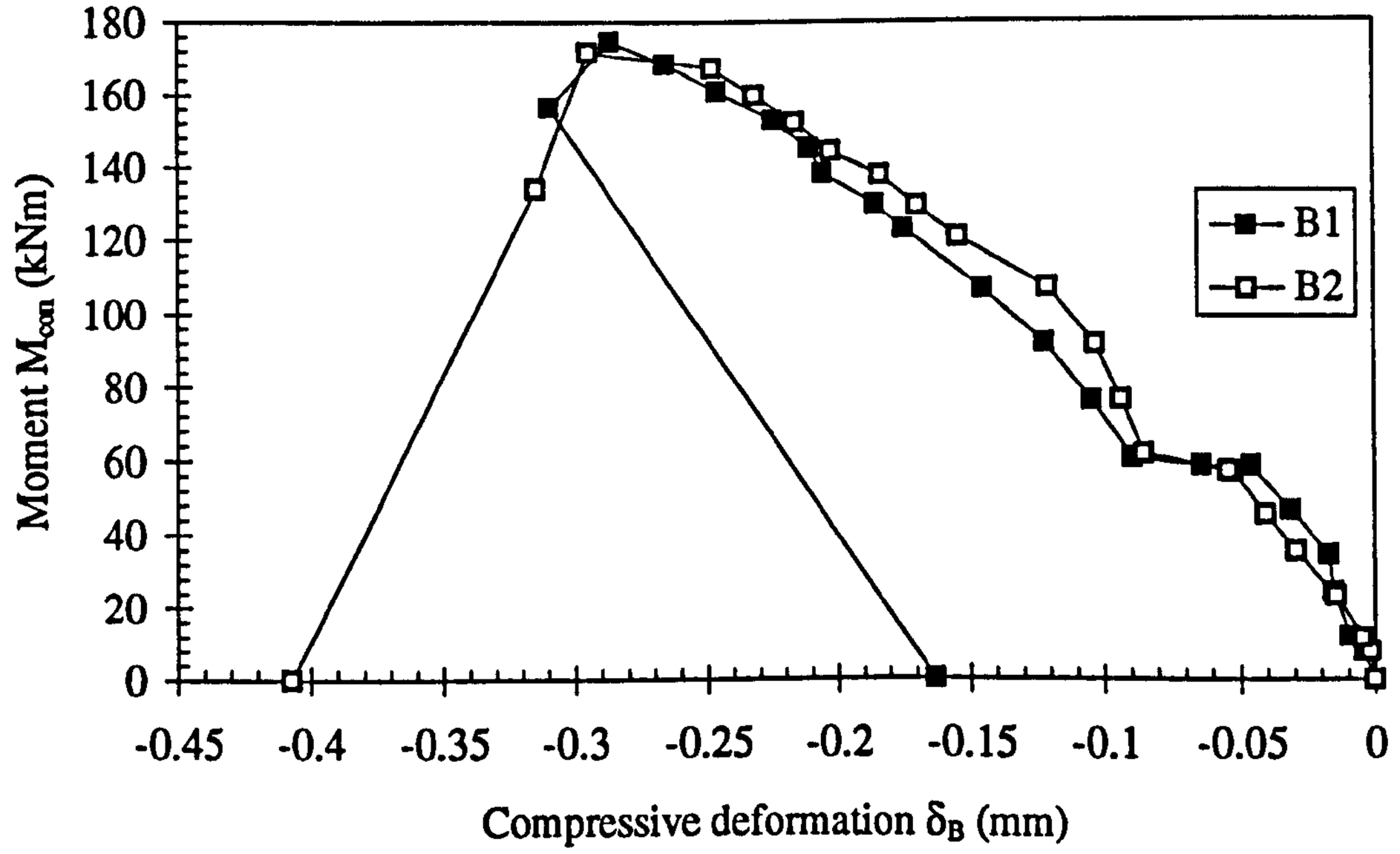

Figure 6.39: Moment versus compressive deformation in joints in TB1(B)

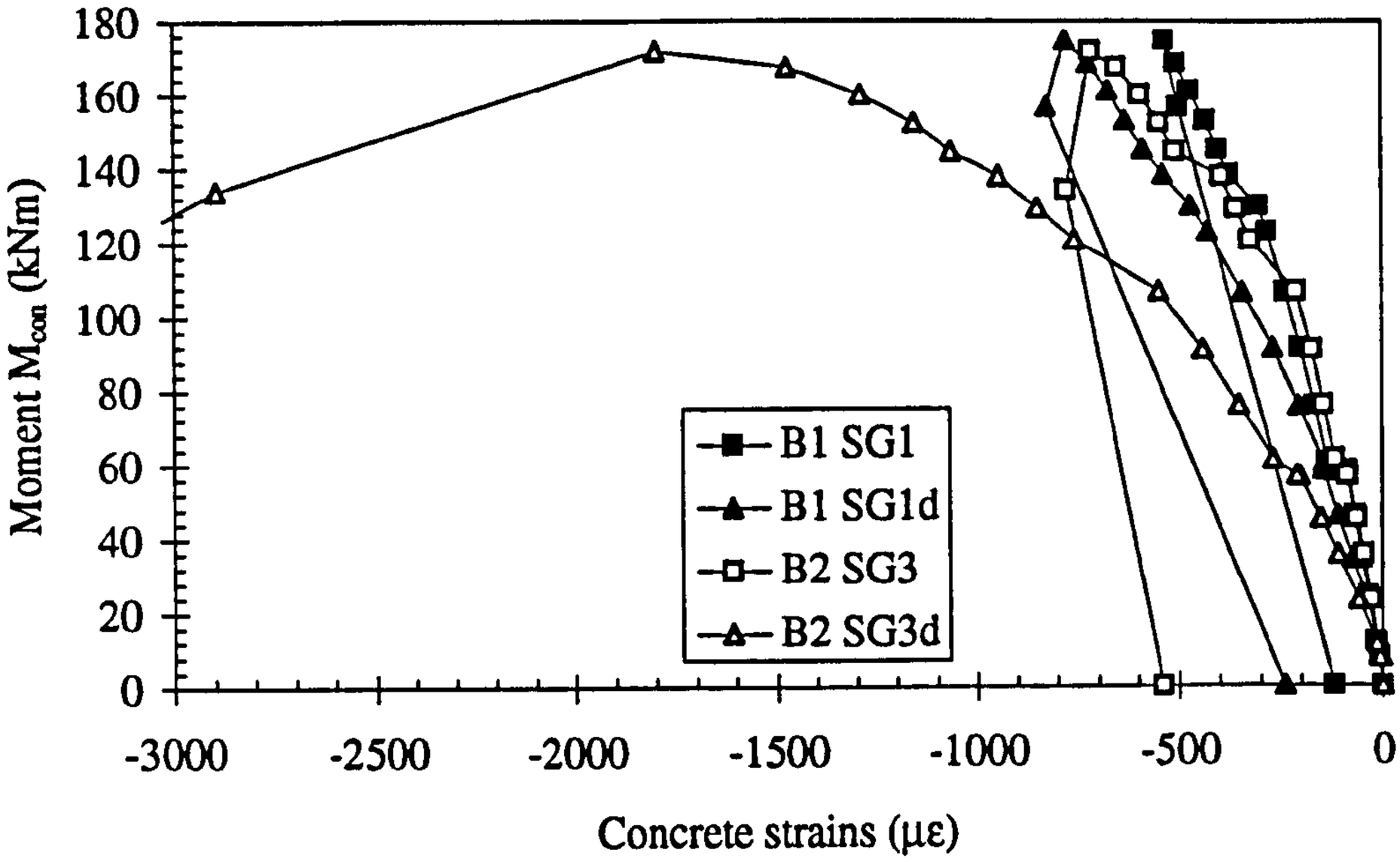

Figure 6.40: Moment versus concrete strains in beams in TB1(B)

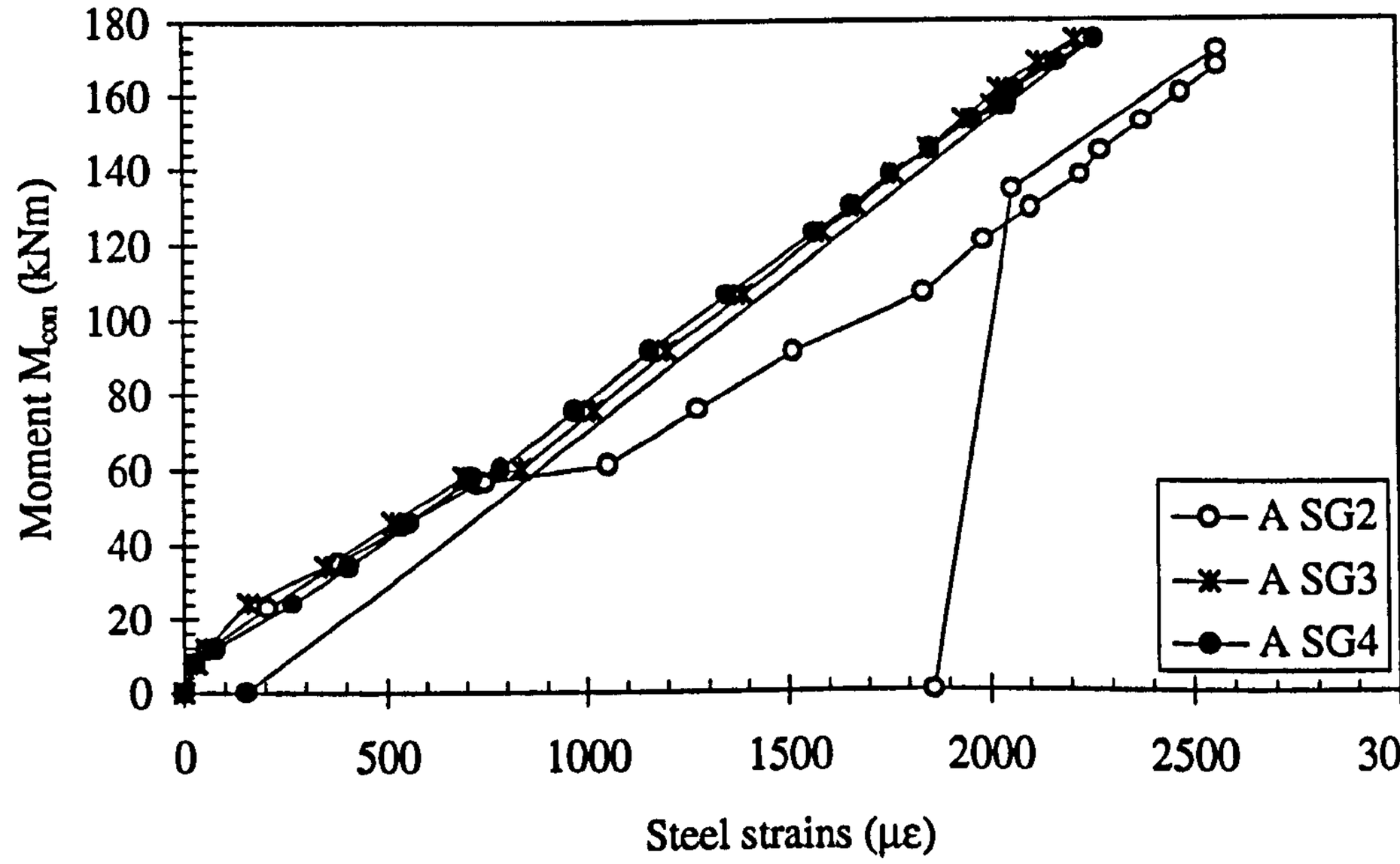

Figure 6.41: Moment versus steel strains in bar A in TB1(B)

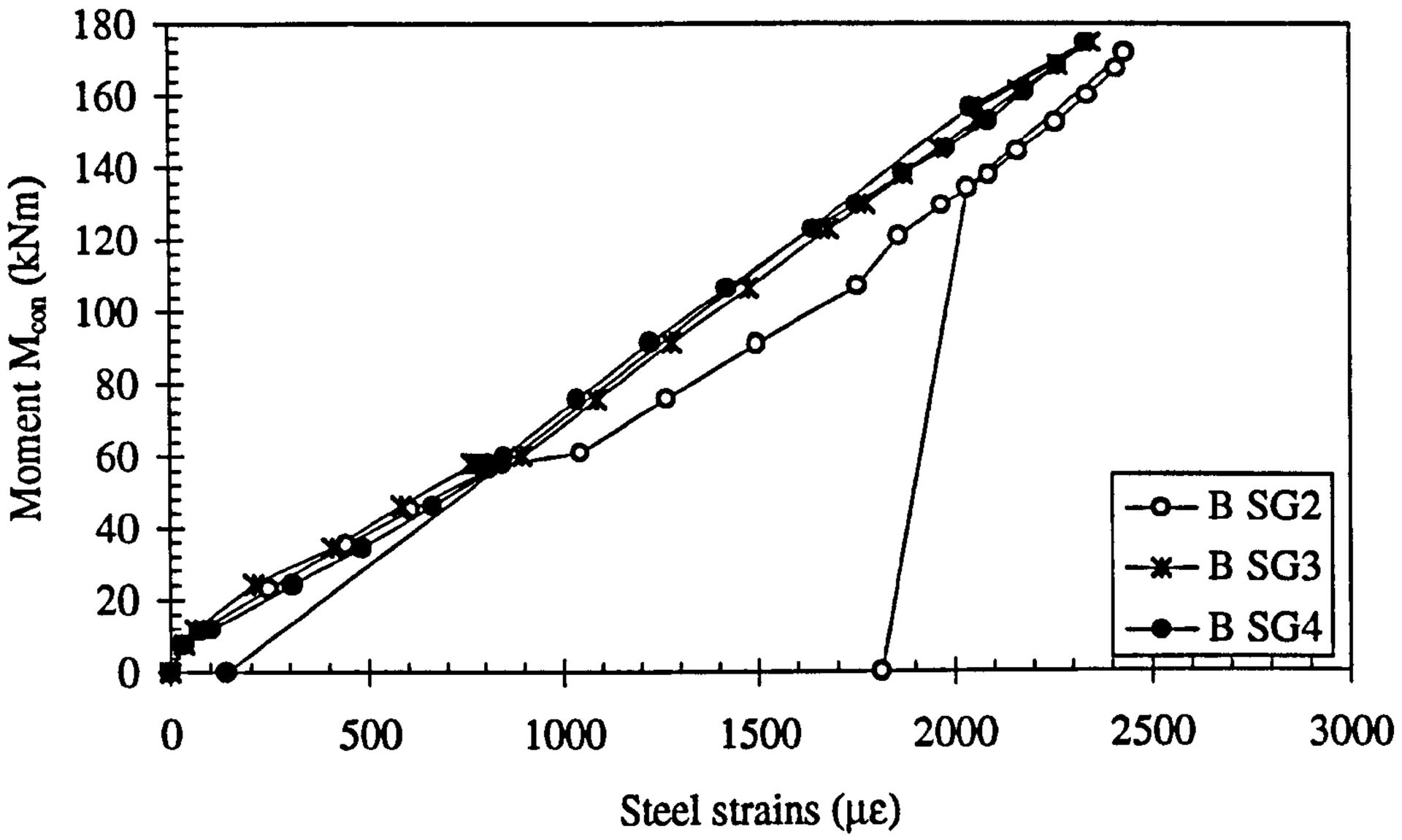

Figure 6.42: Moment versus steel strains in bar B in TB1(B)

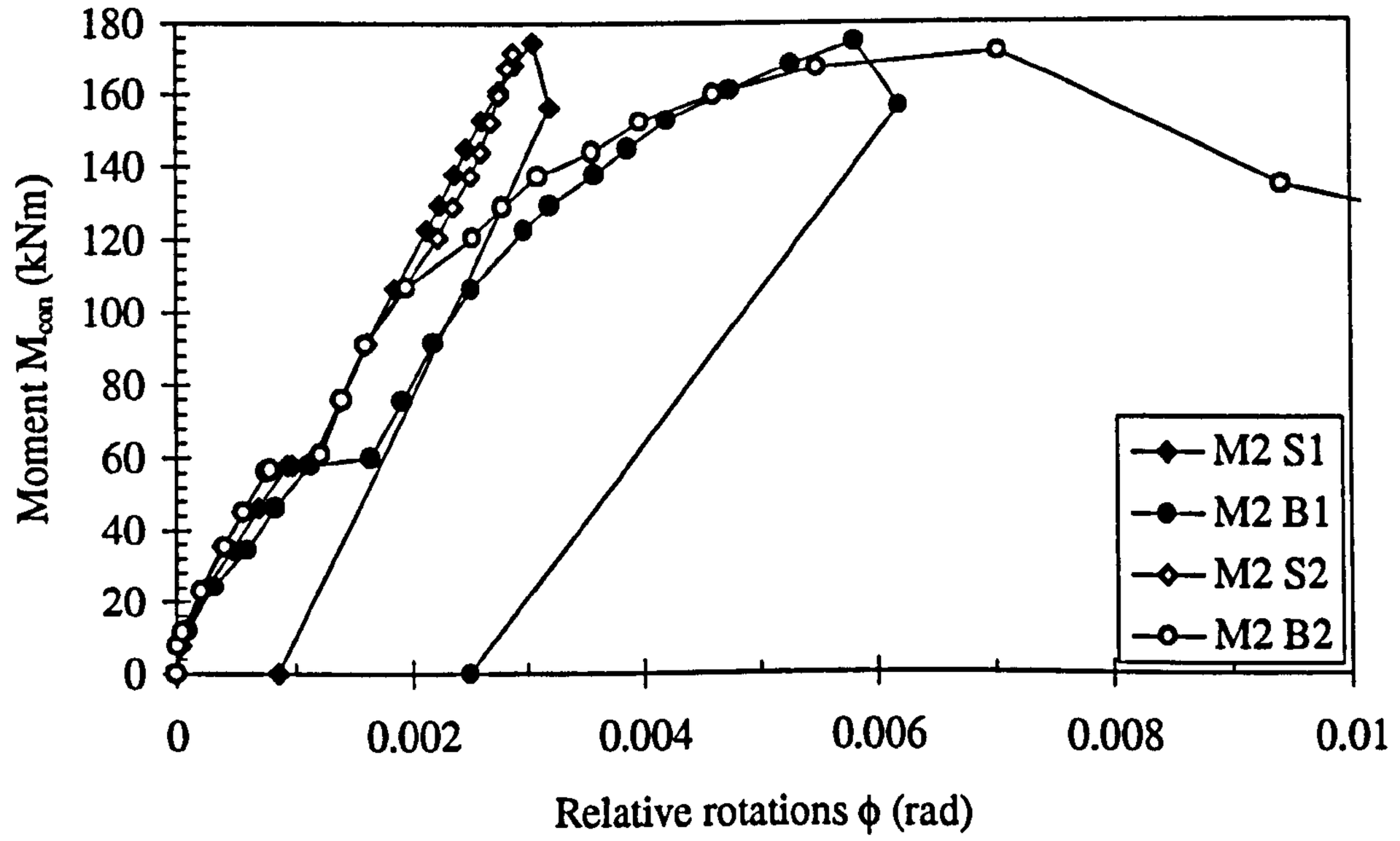

Figure 6.43: Moment versus relative rotations in beam 1 in TB1(B) using method 2

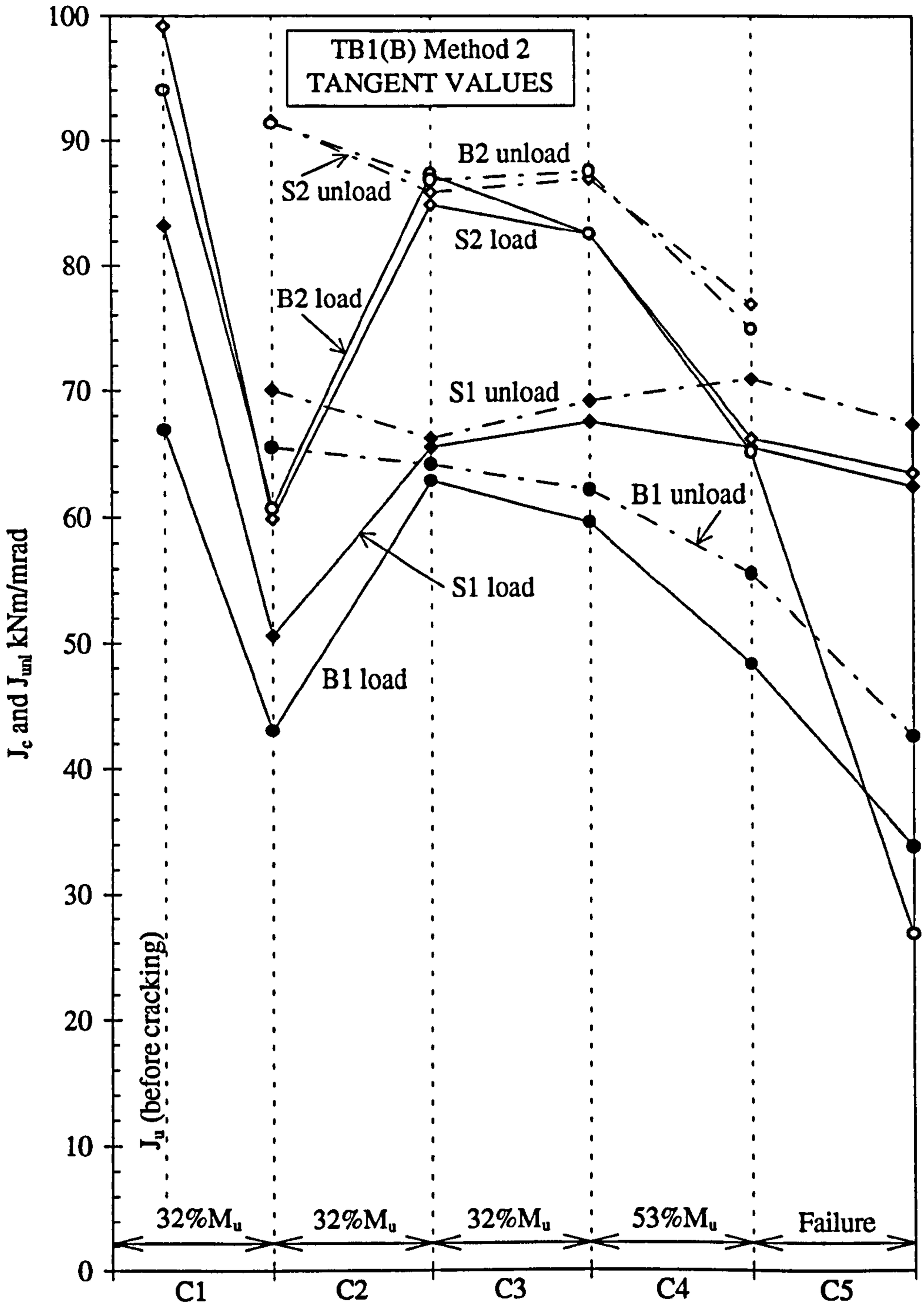

Figure 6.44: Tangent and unloading flexural stiffness versus cycles 1-5 in slabs and beams in TB1(B) using method 2

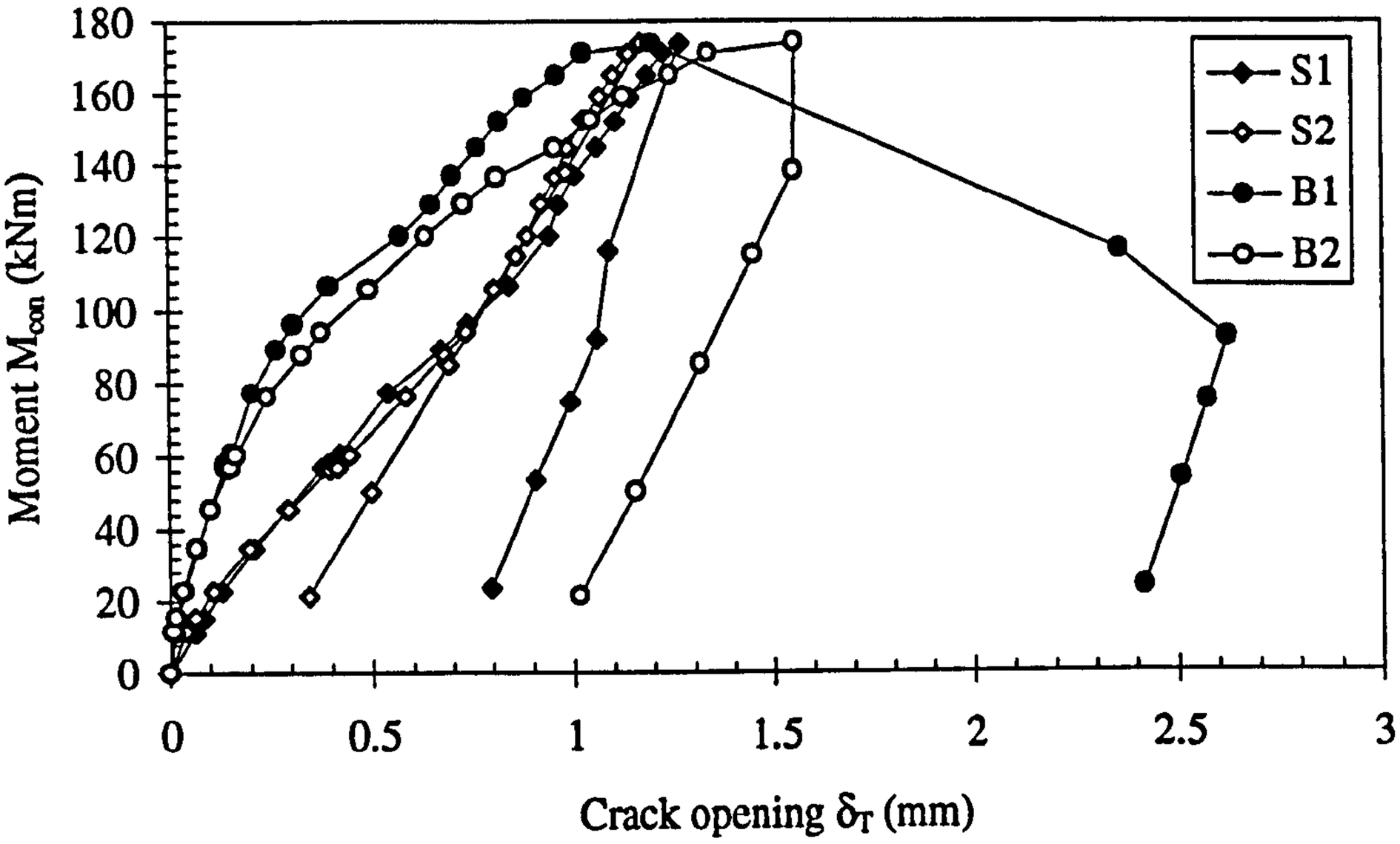

Figure 6.45: Moment versus crack opening at slab/column boundaries in TB1(C)

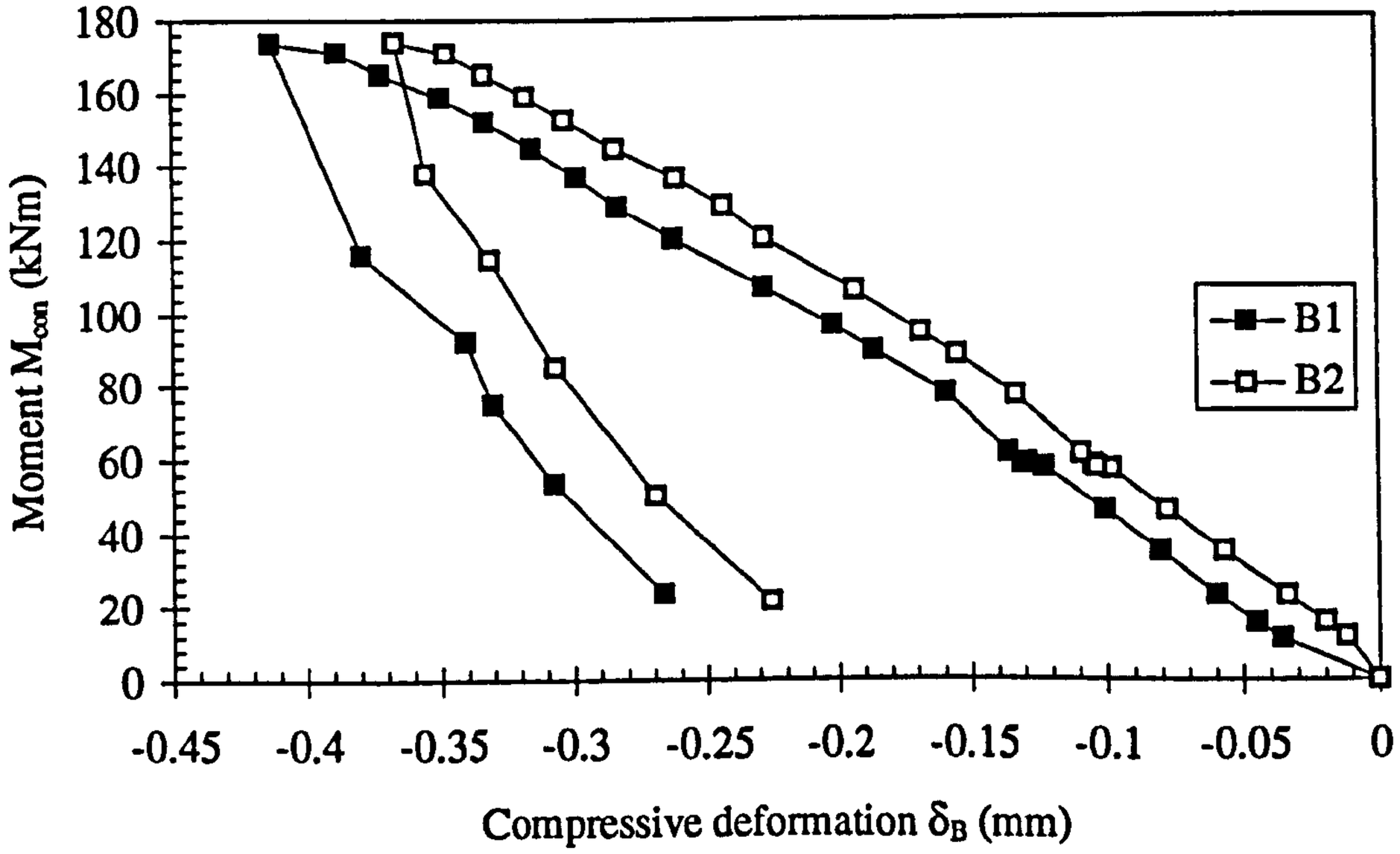

Figure 6.46: Moment versus compressive deformation in joints in TB1(C)

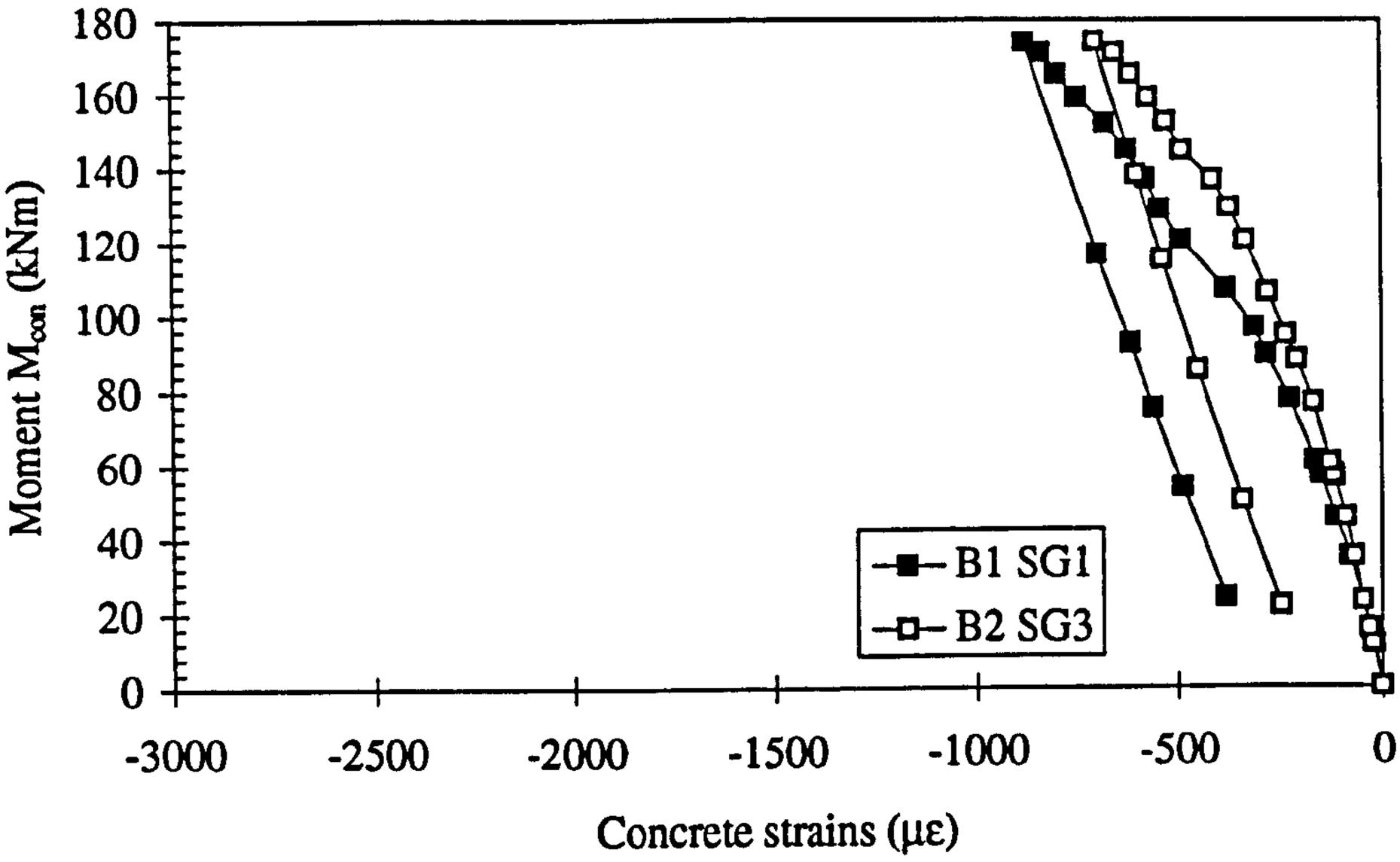

Figure 6.47: Moment versus concrete strains in beams in TB1(C)

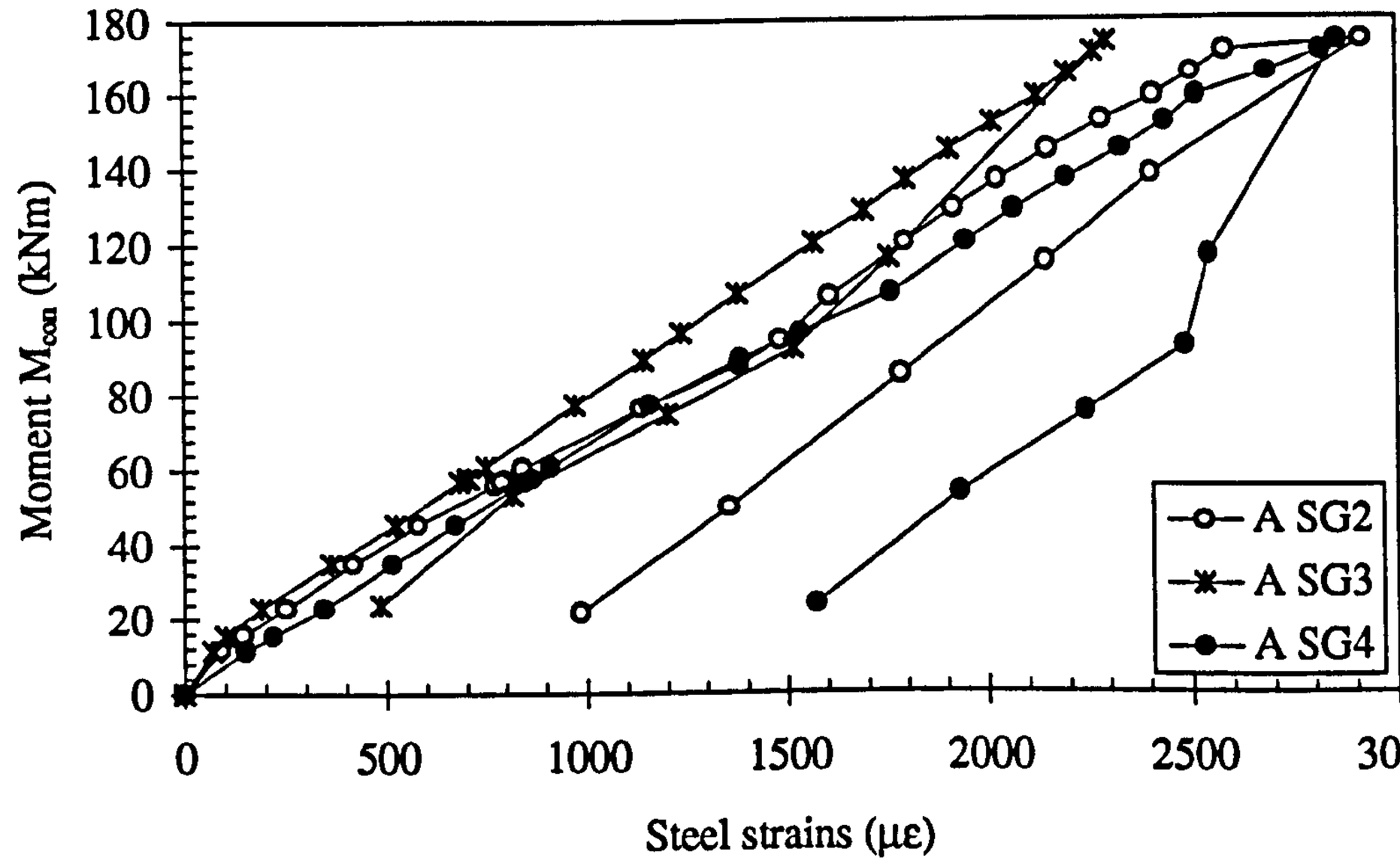

Figure 6.48: Moment versus steel strains in bar A in TB1(C)

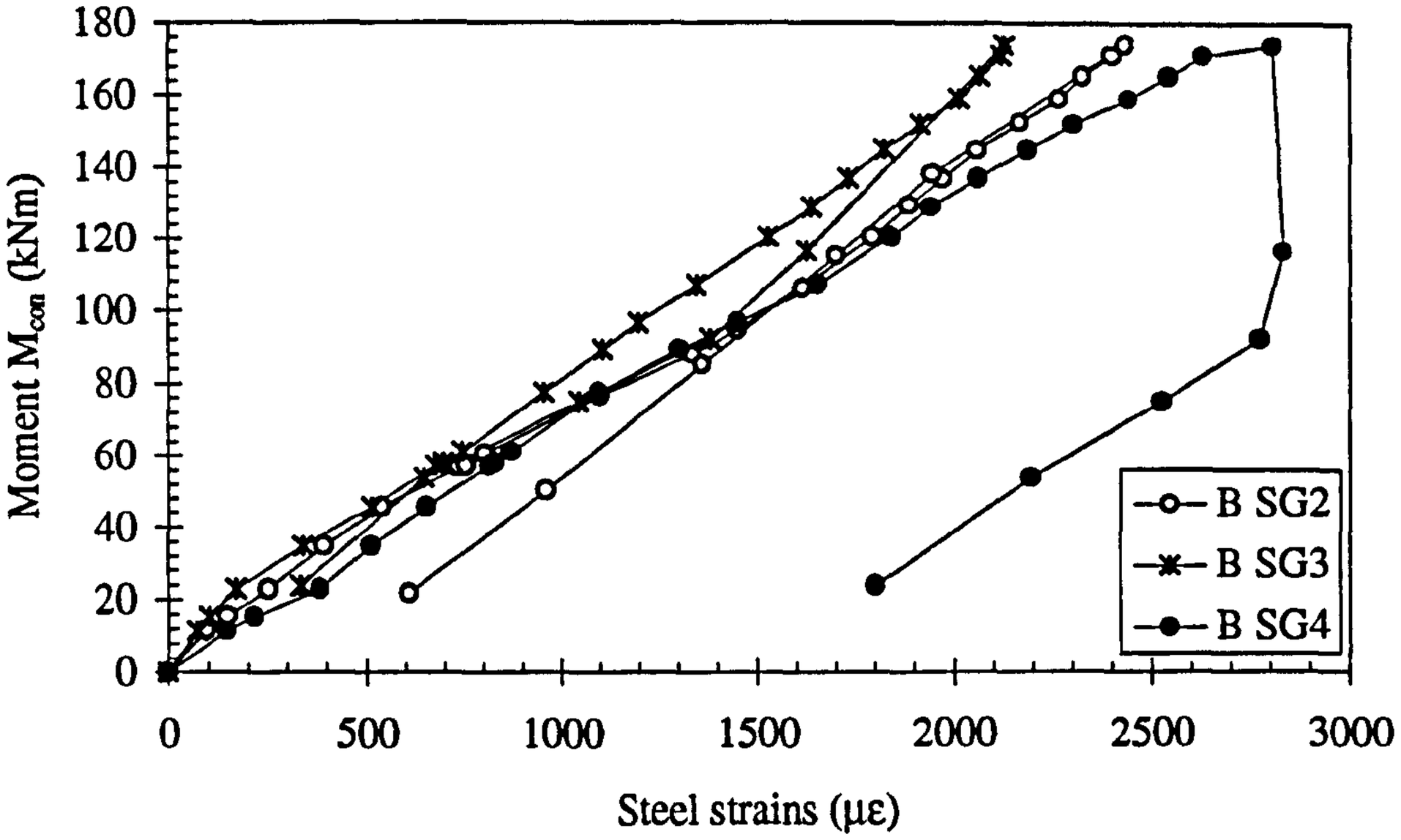

Figure 6.49: Moment versus steel strains in bar B in TB1(C)

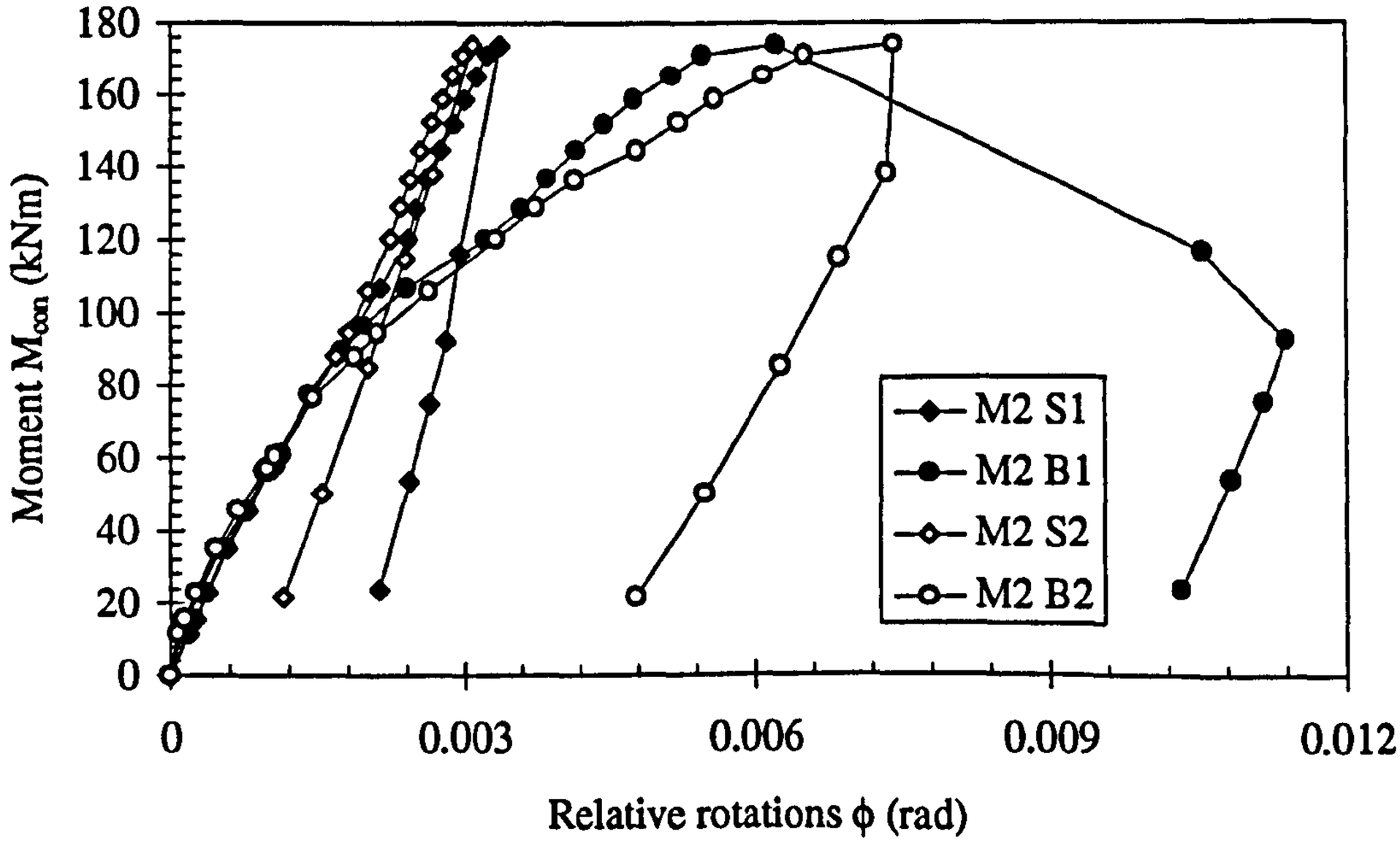

Figure 6.50: Moment versus relative rotations in beam 1 in TB1(C) using method 2

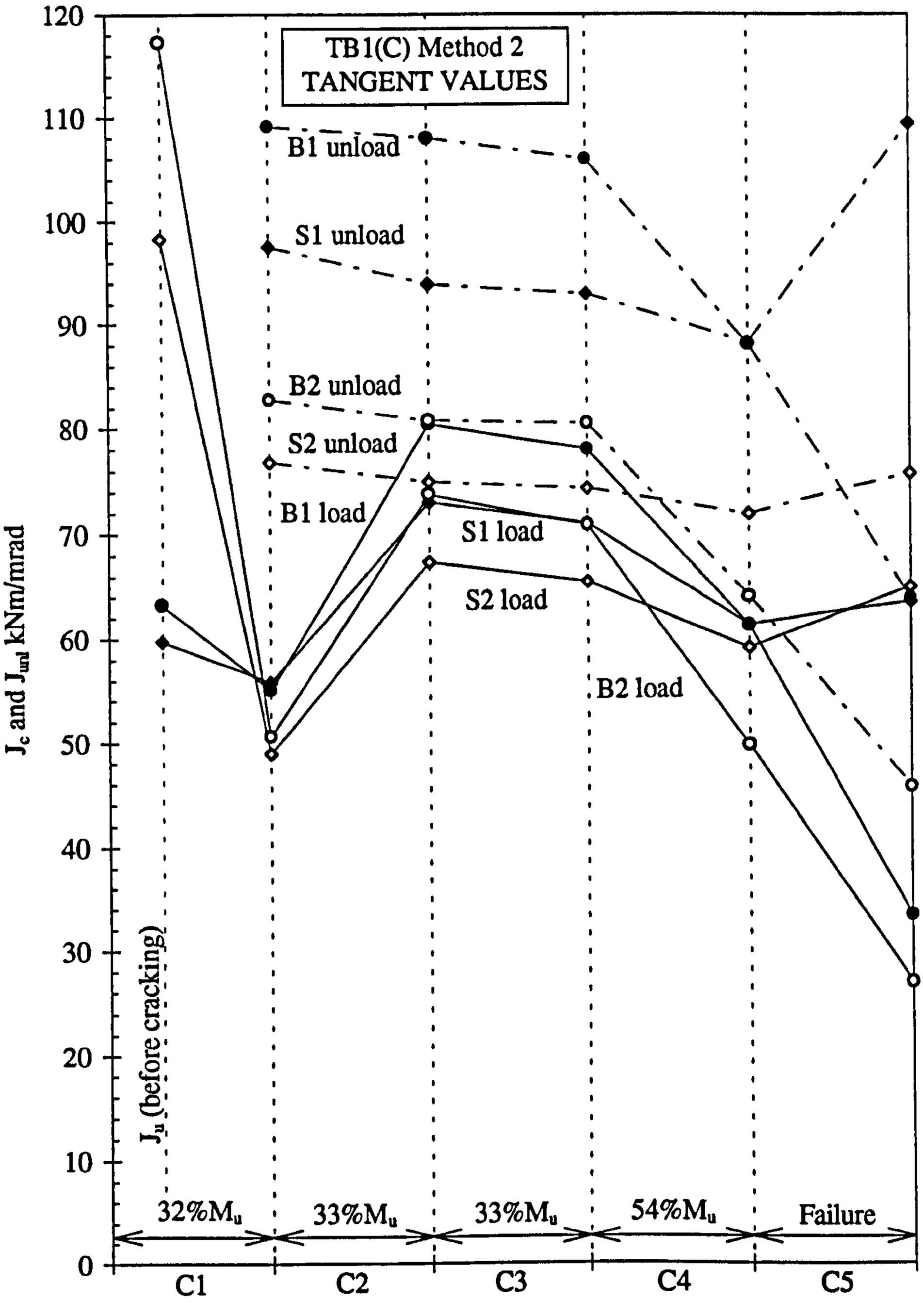

Figure 6.51: Tangent and unloading flexural stiffness versus cycles 1-5 in slabs and beams in TB1(C) using method 2

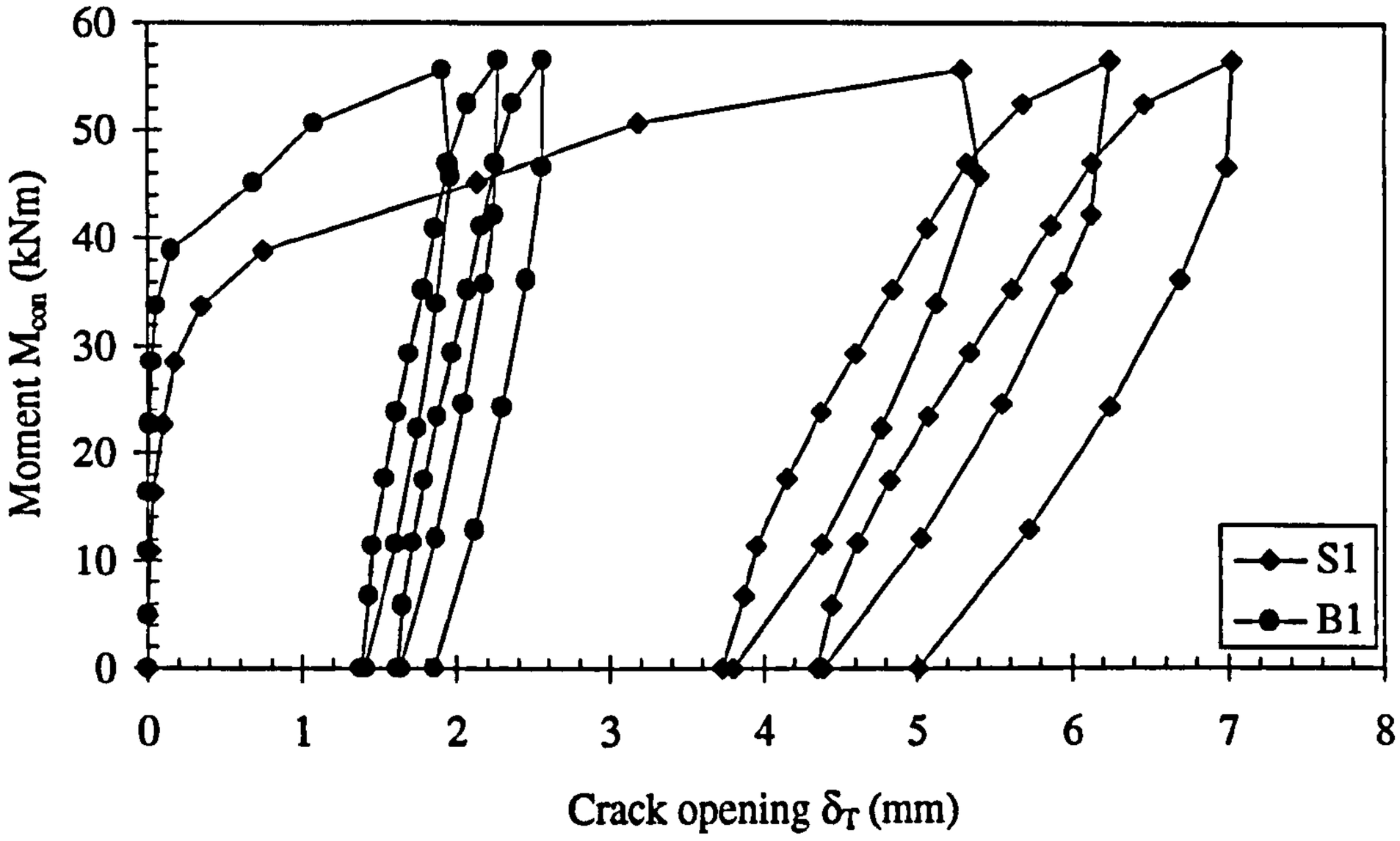

Figure 6.52(a): Moment versus crack opening at slab/column boundary in TB2 for cycles 1-3

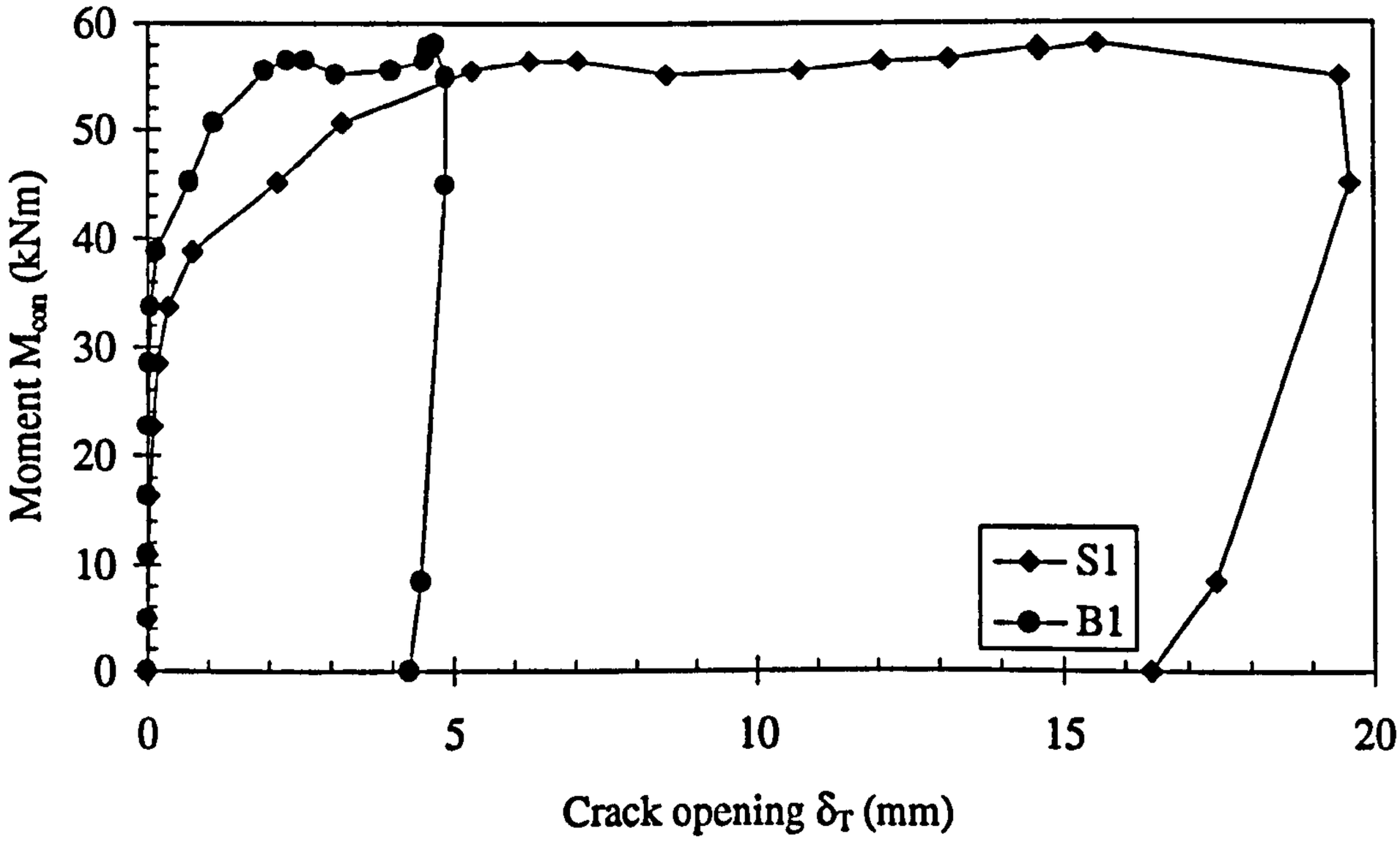

Figure 6.52(b): Moment versus crack opening at slab/column boundary in TB2

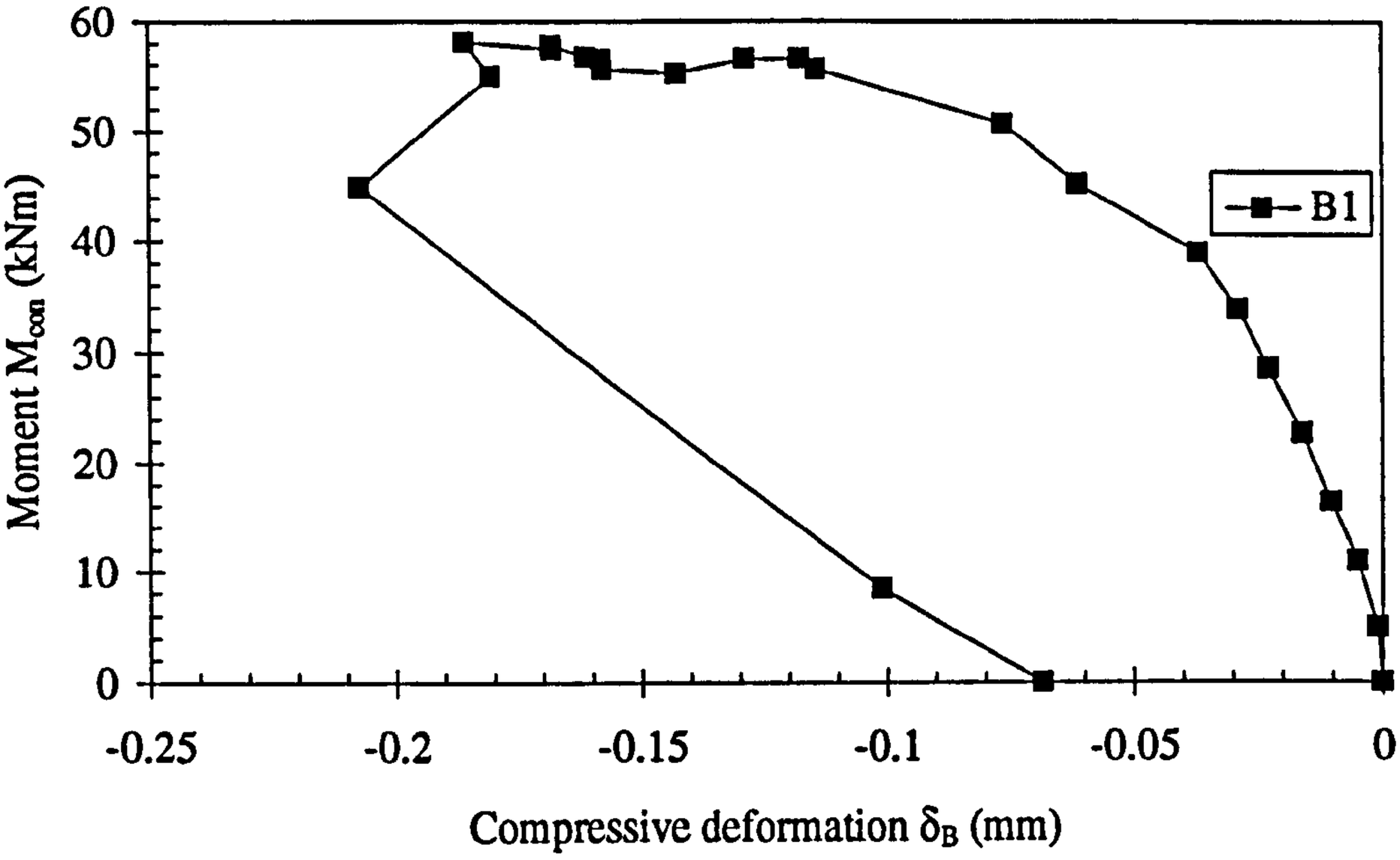

Figure 6.53: Moment versus compressive deformation in joint in TB2

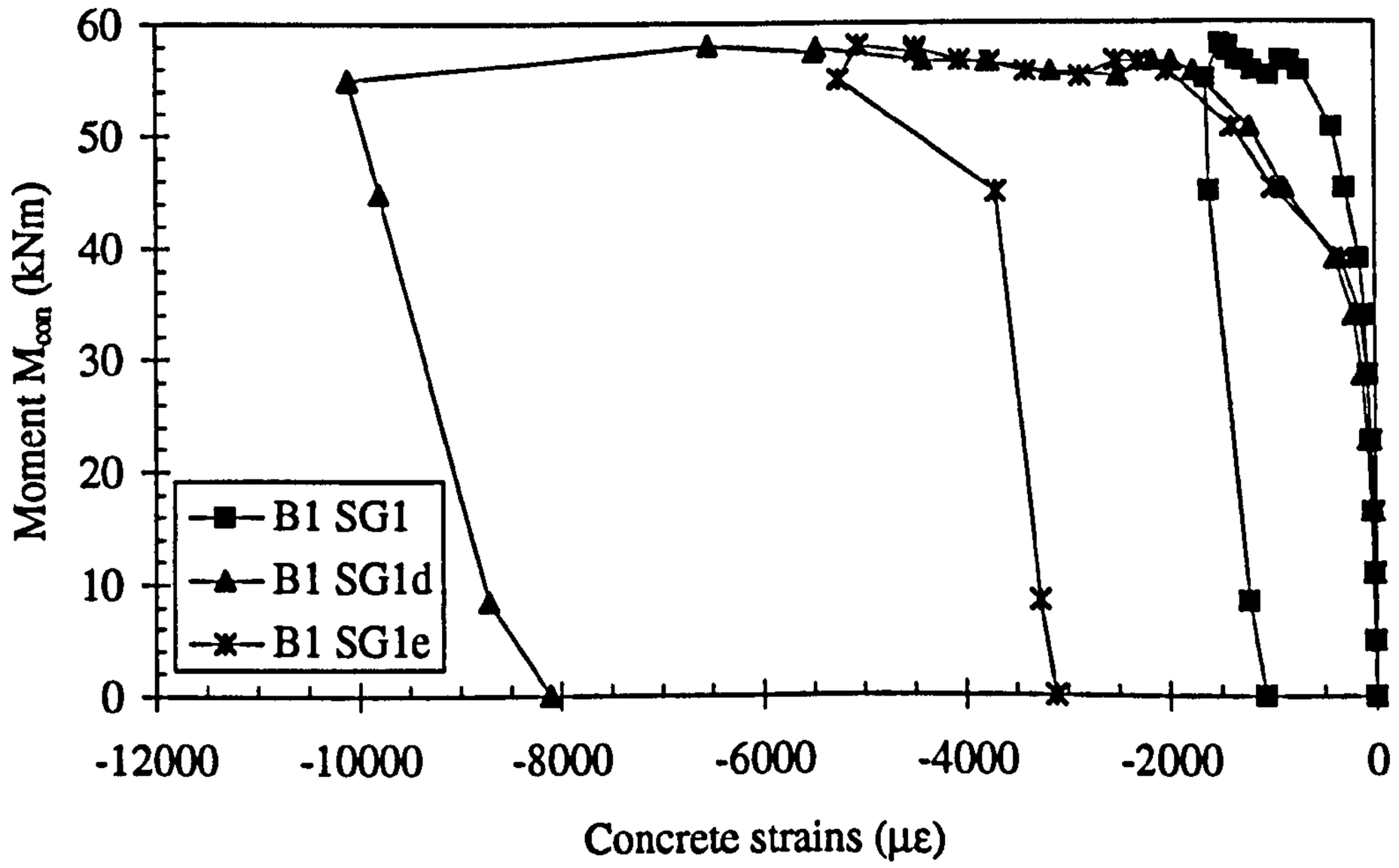

Figure 6.54: Moment versus concrete strains in beam 1 in TB2

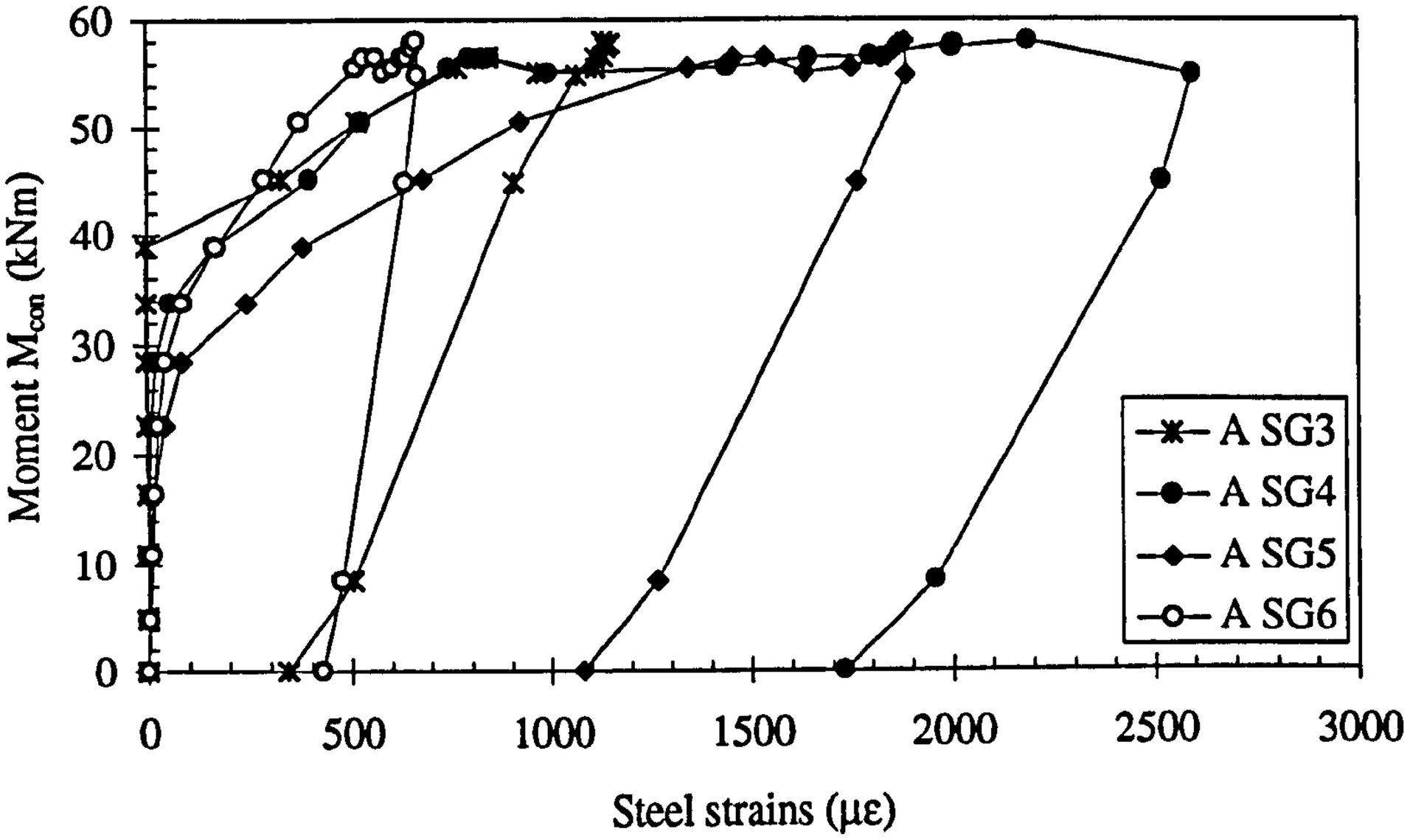

Figure 6.55: Moment versus steel strains in bar A in TB2

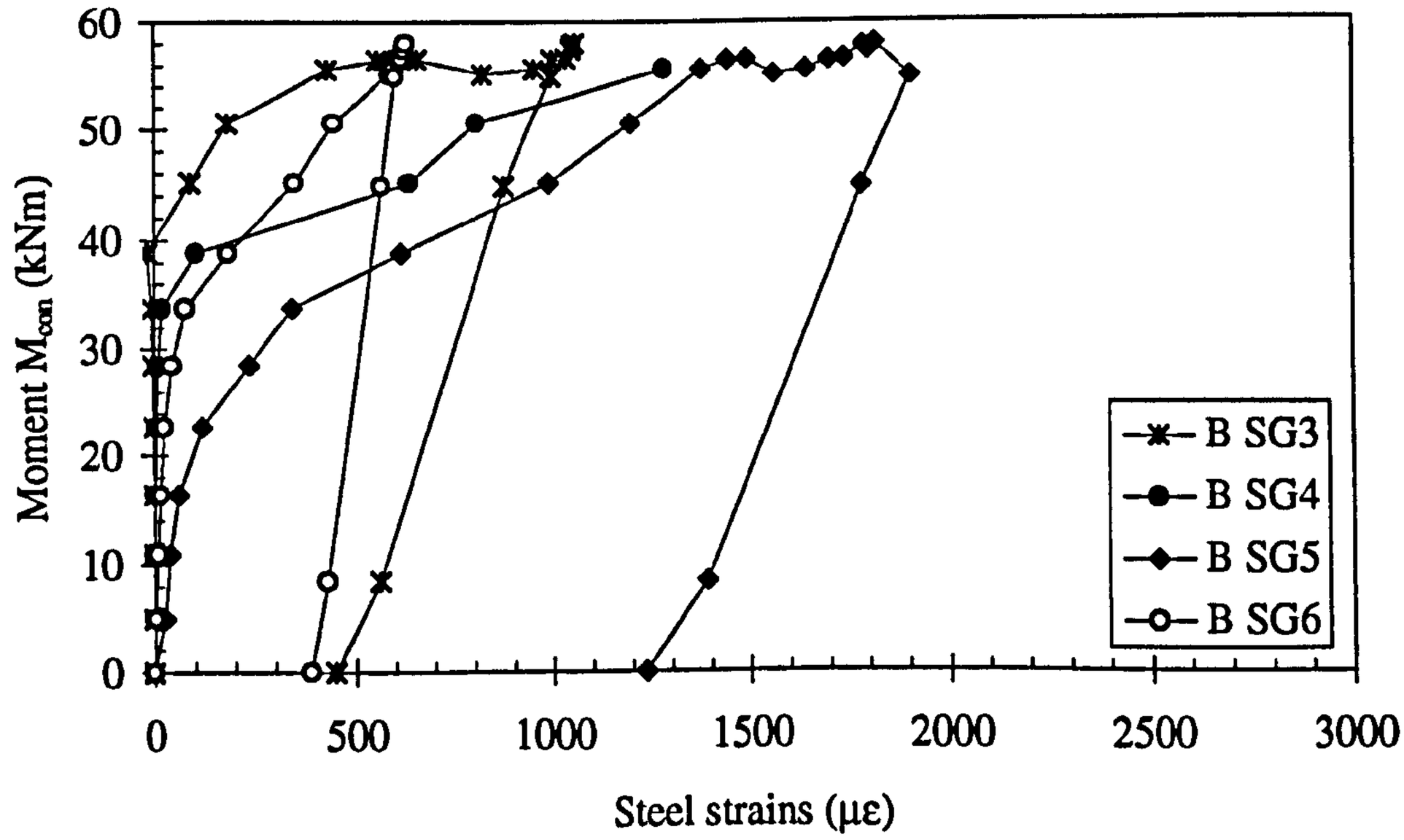

Figure 6.56: Moment versus steel strains in bar B in TB2

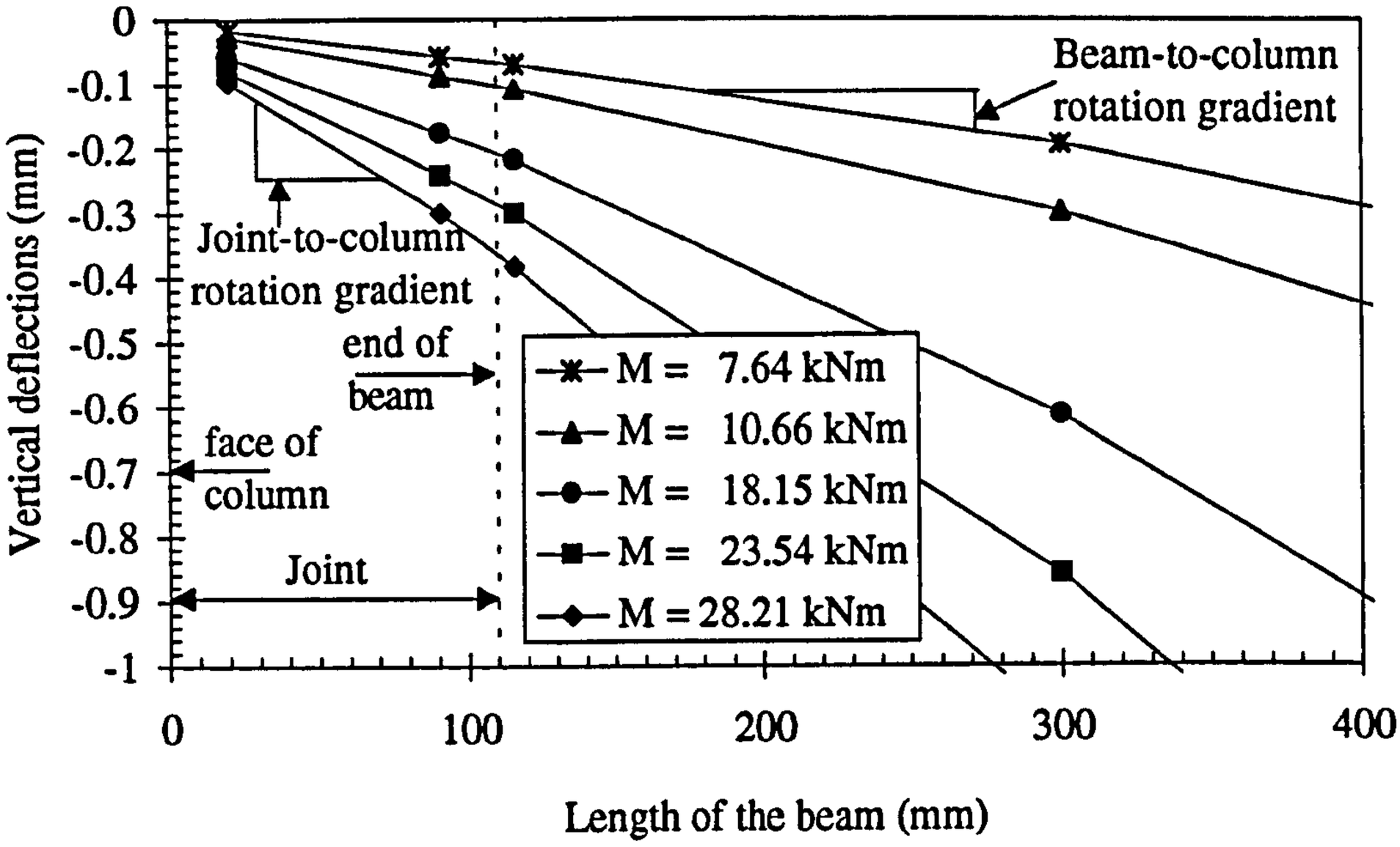

Figure 6.57: Moment versus vertical deflections in beam 1 in TB2 with various moment level

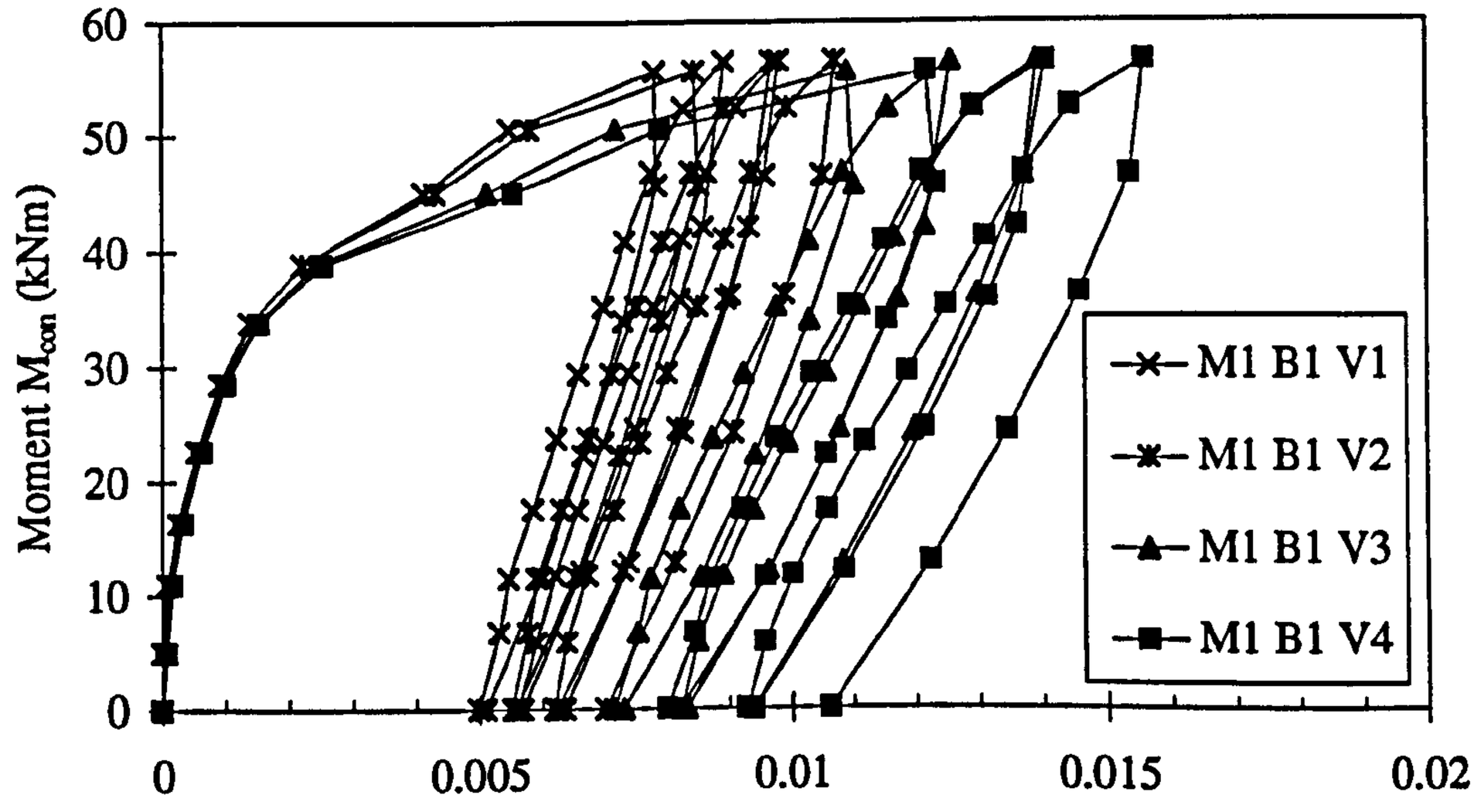

Figure 6.58(a): Moment versus relative rotations in beam 1 in TB2 using method 1 for cycles 1-3

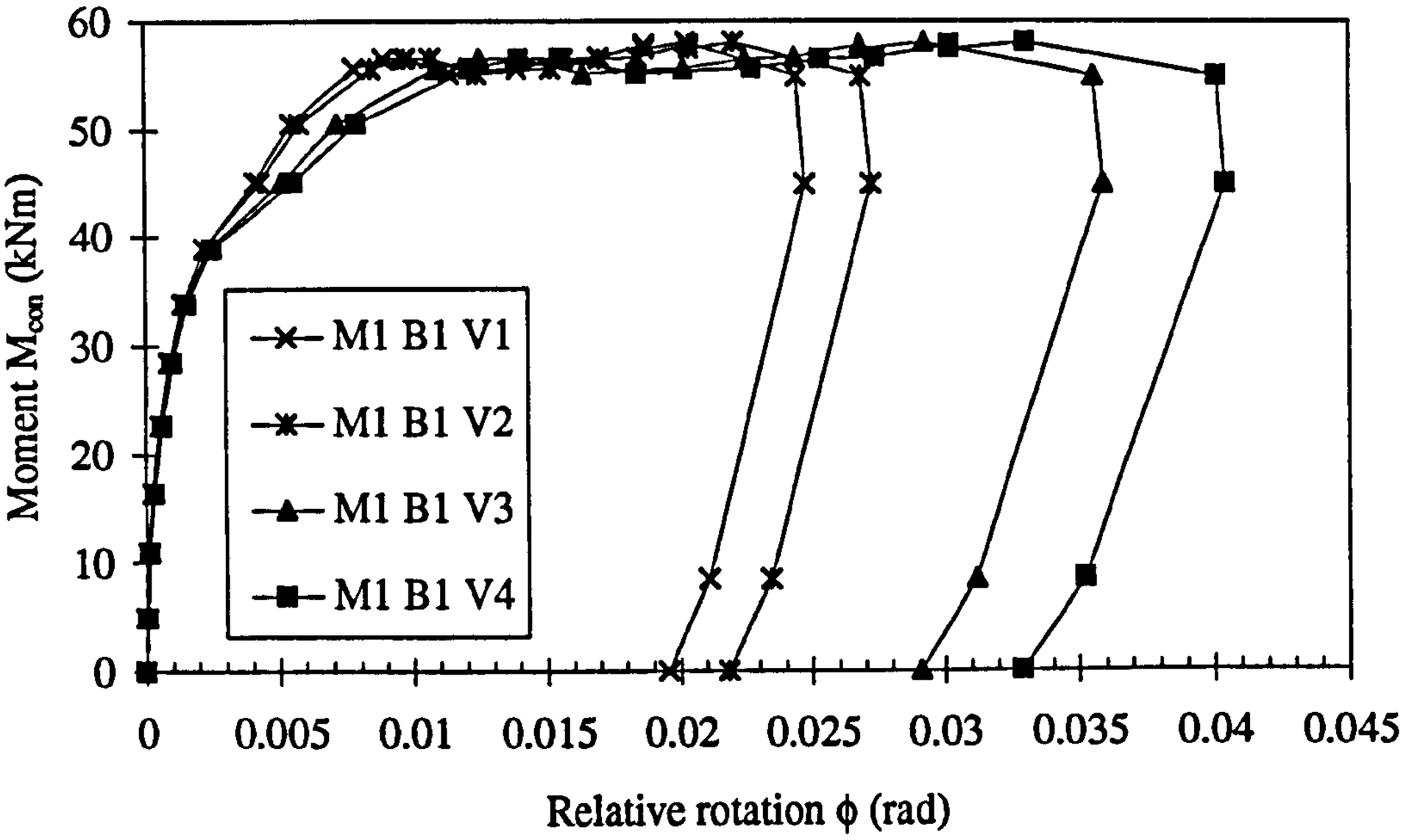

Figure 6.58(b): Moment versus relative rotations in beam 1 in TB2 using method 1

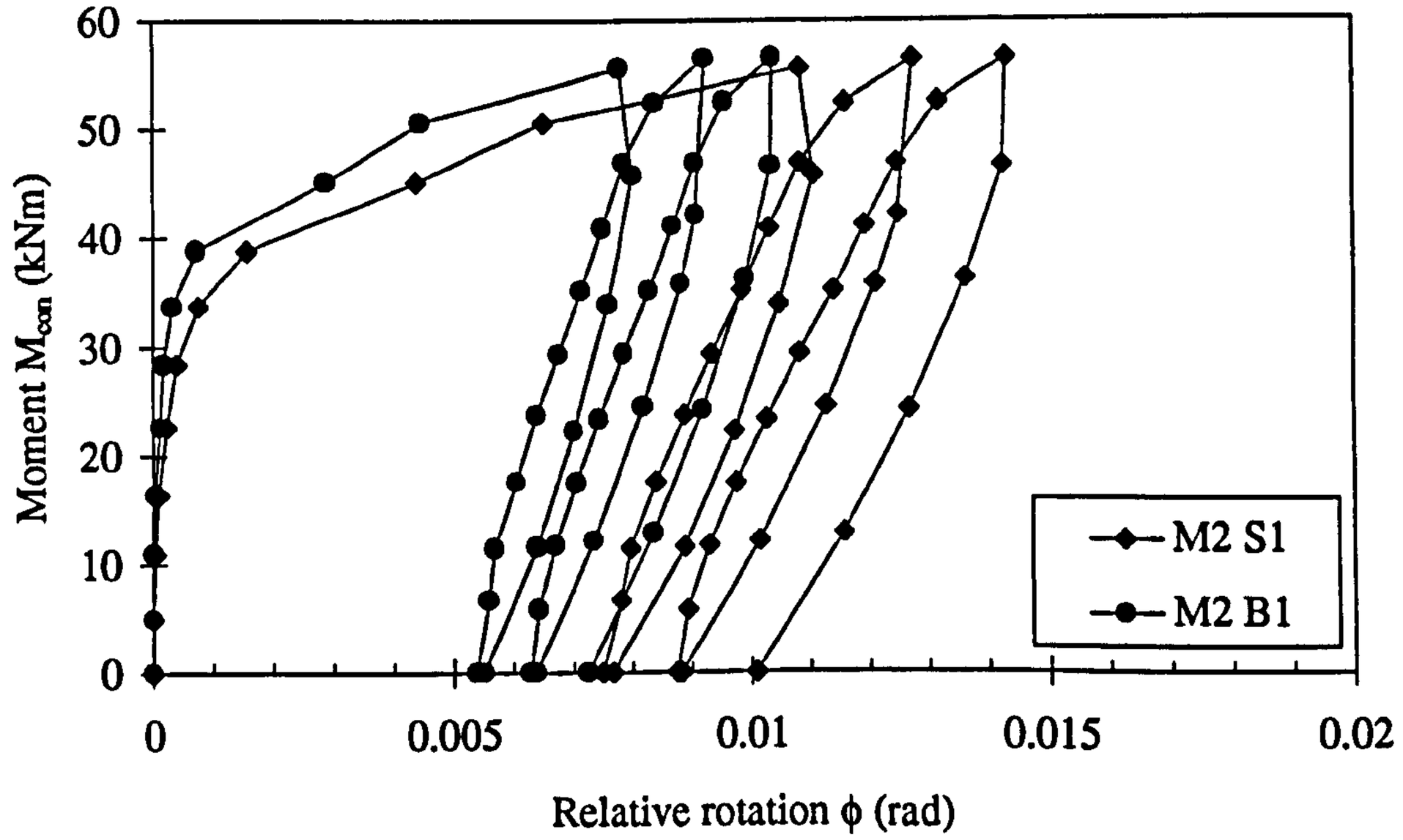

Figure 6.59(a): Moment versus relative rotations in TB2 using method 2 for cycles 1-3

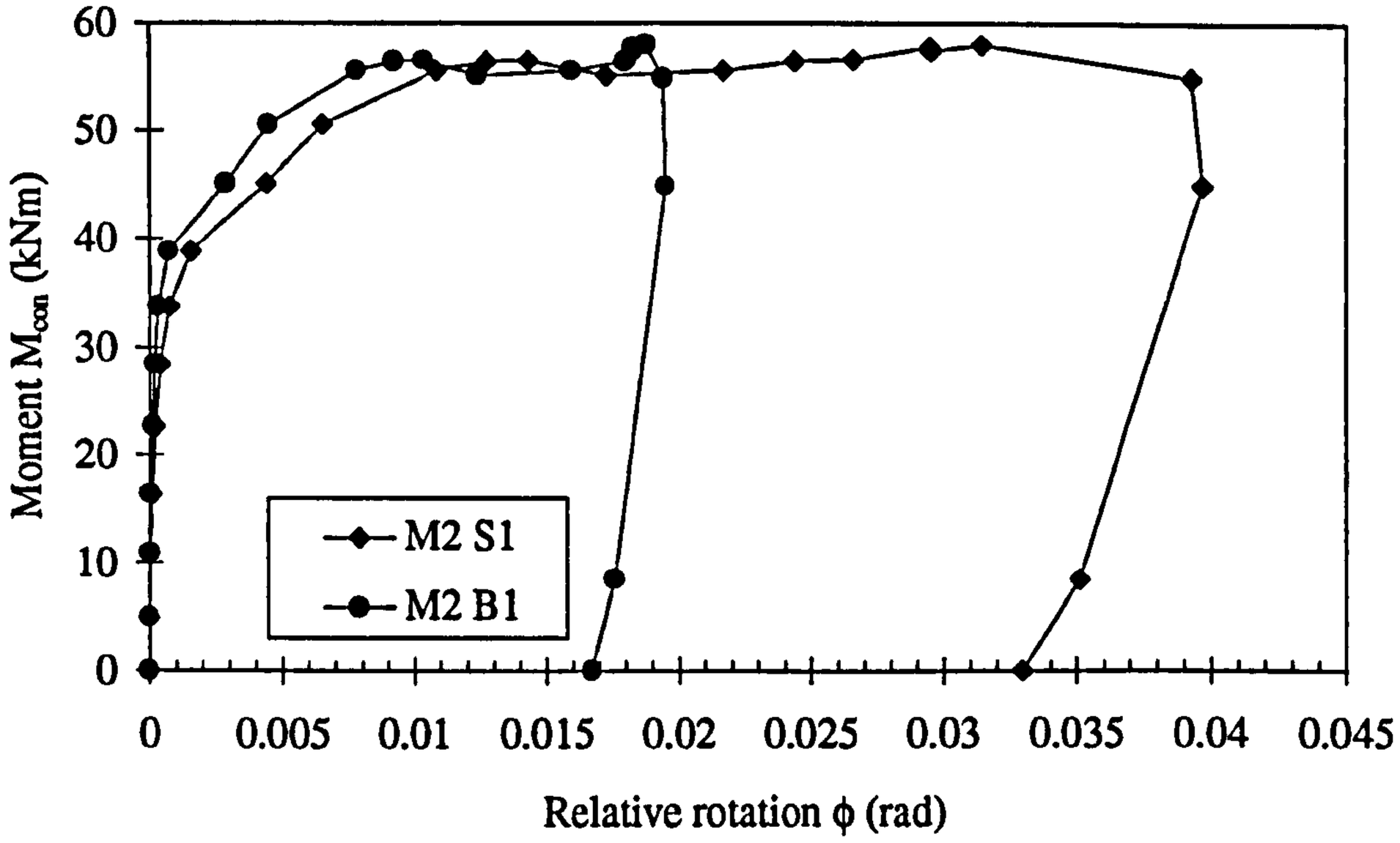

Figure 6.59(b): Moment versus relative rotations in TB2 using method 2

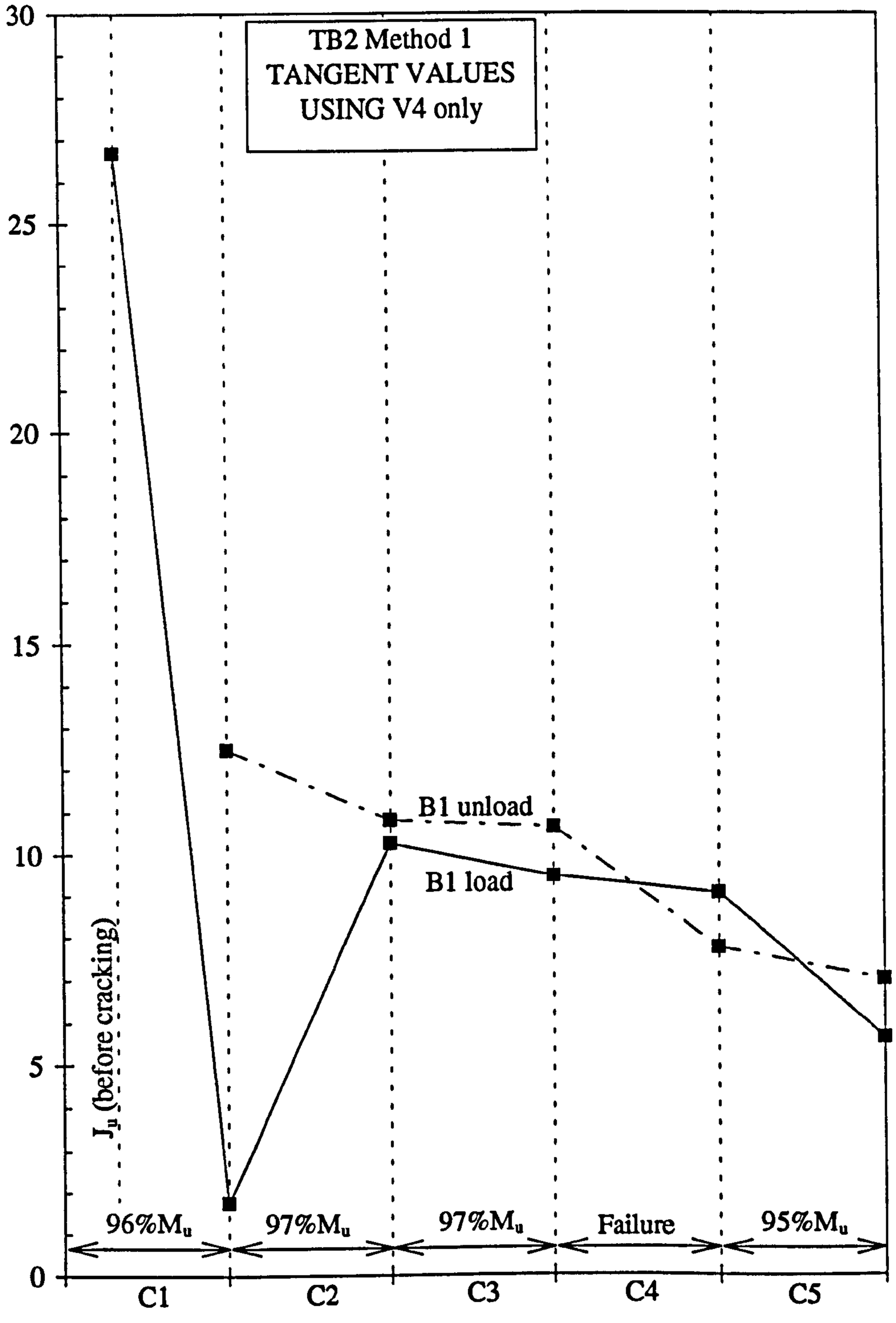

Figure 6.60(a): Tangent and unloading flexural stiffness versus cycles 1-5 in TB2 using method 1

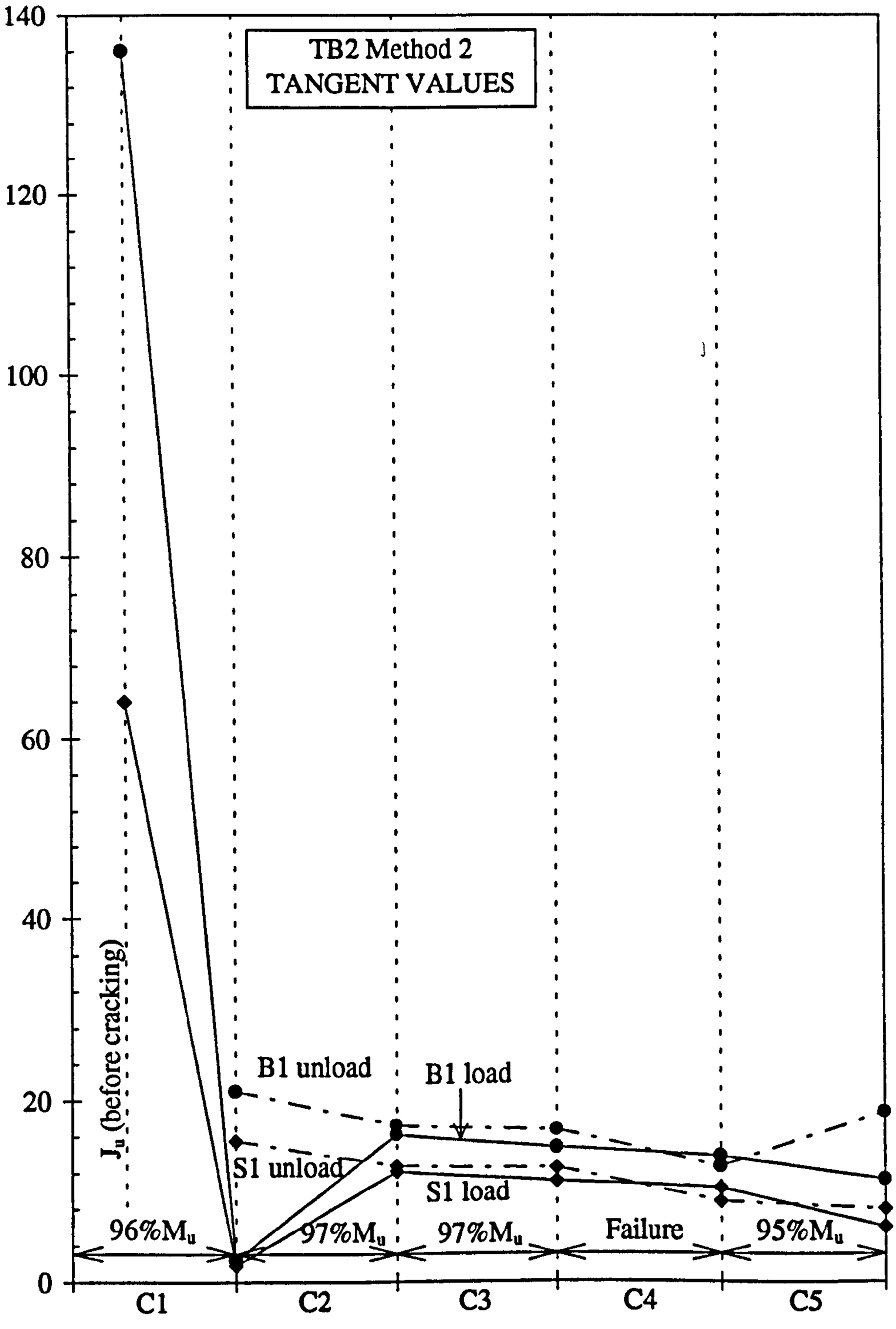

Figure 6.60(b): Tangent and unloading flexural stiffness versus cycles 1-5 in TB2 using method 2

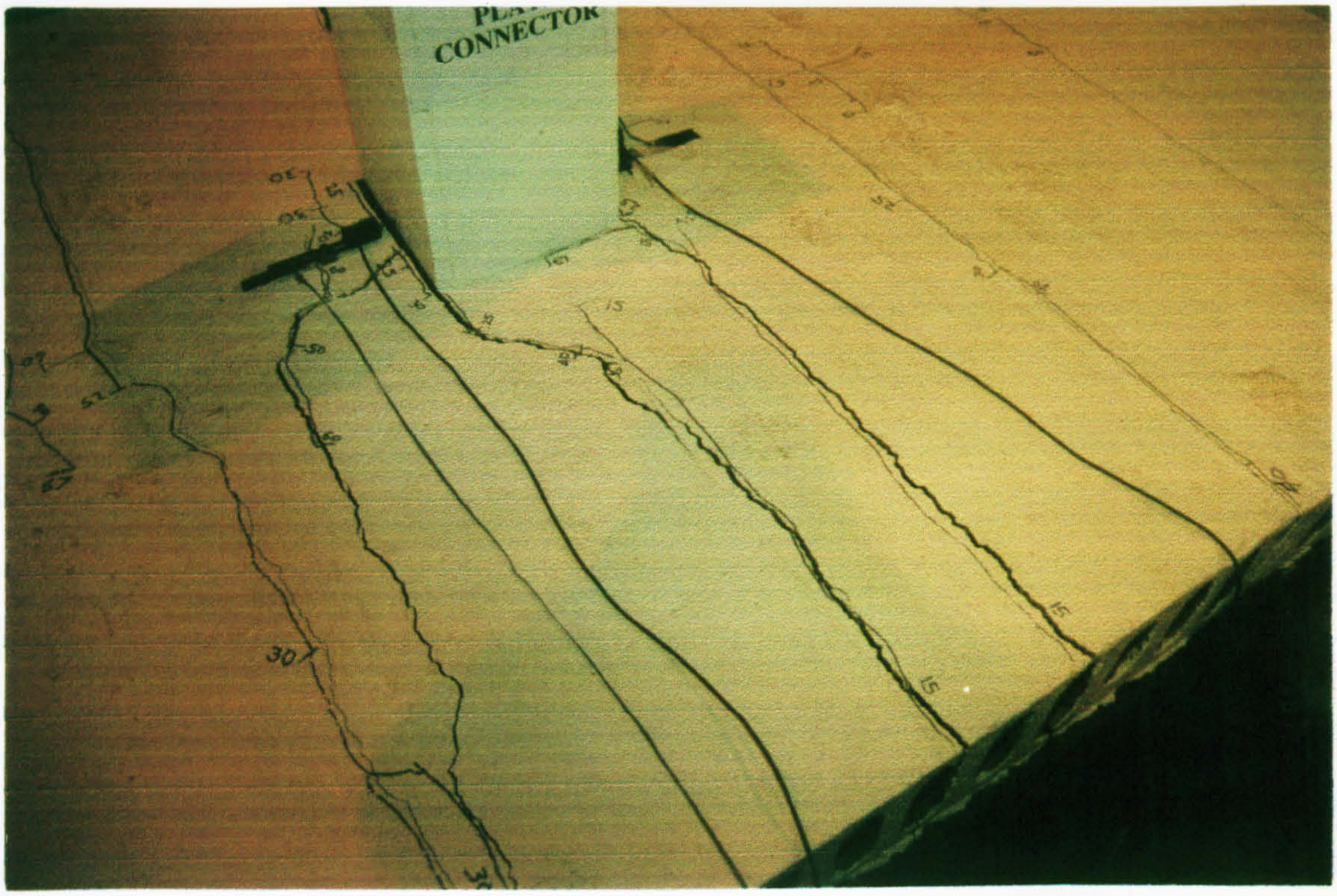

Plate 6.1: Failure region at top of slab from West in TW1(A)

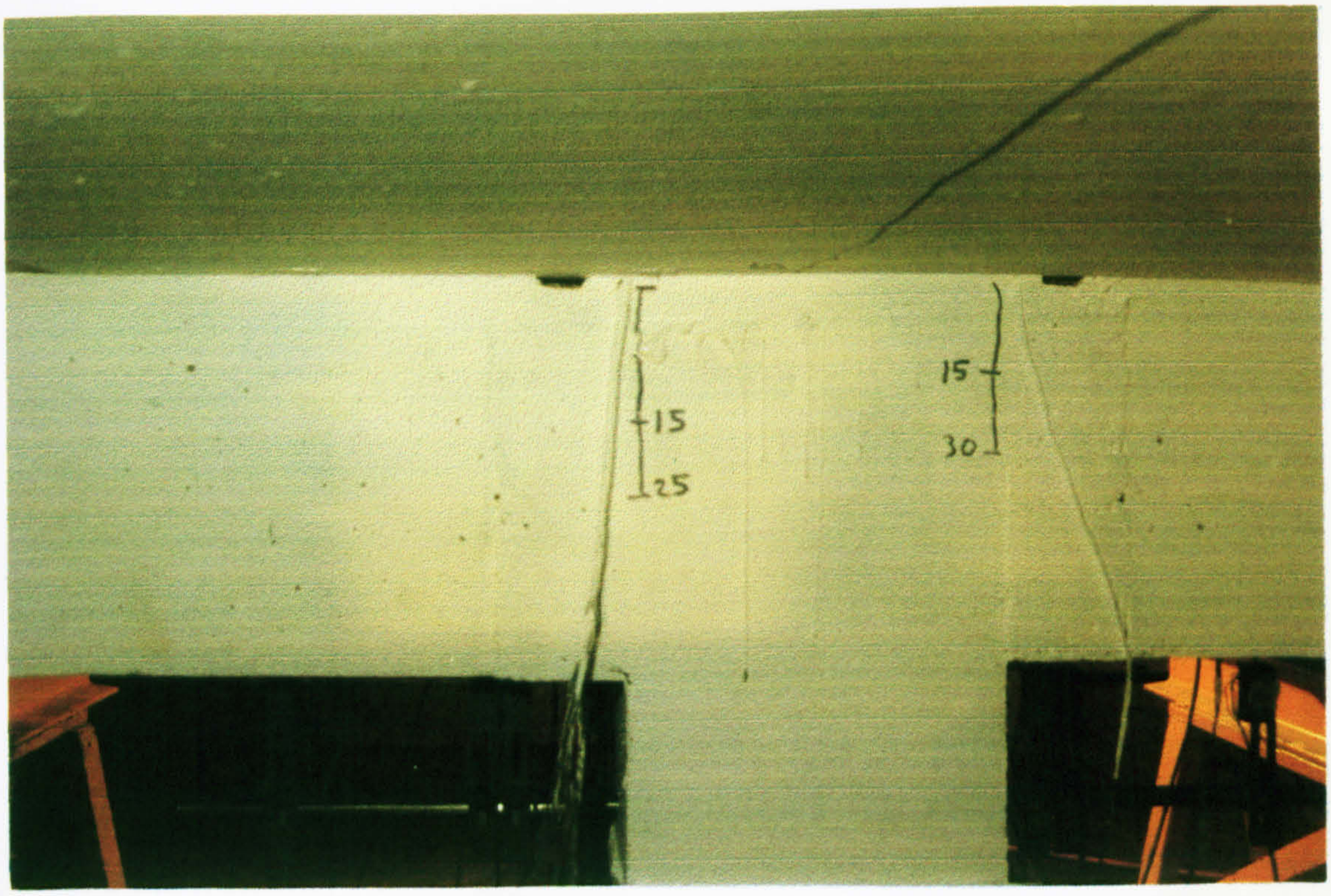

Plate 6.2: First cracks opening at joints-column boundaries from West in TW1(A)

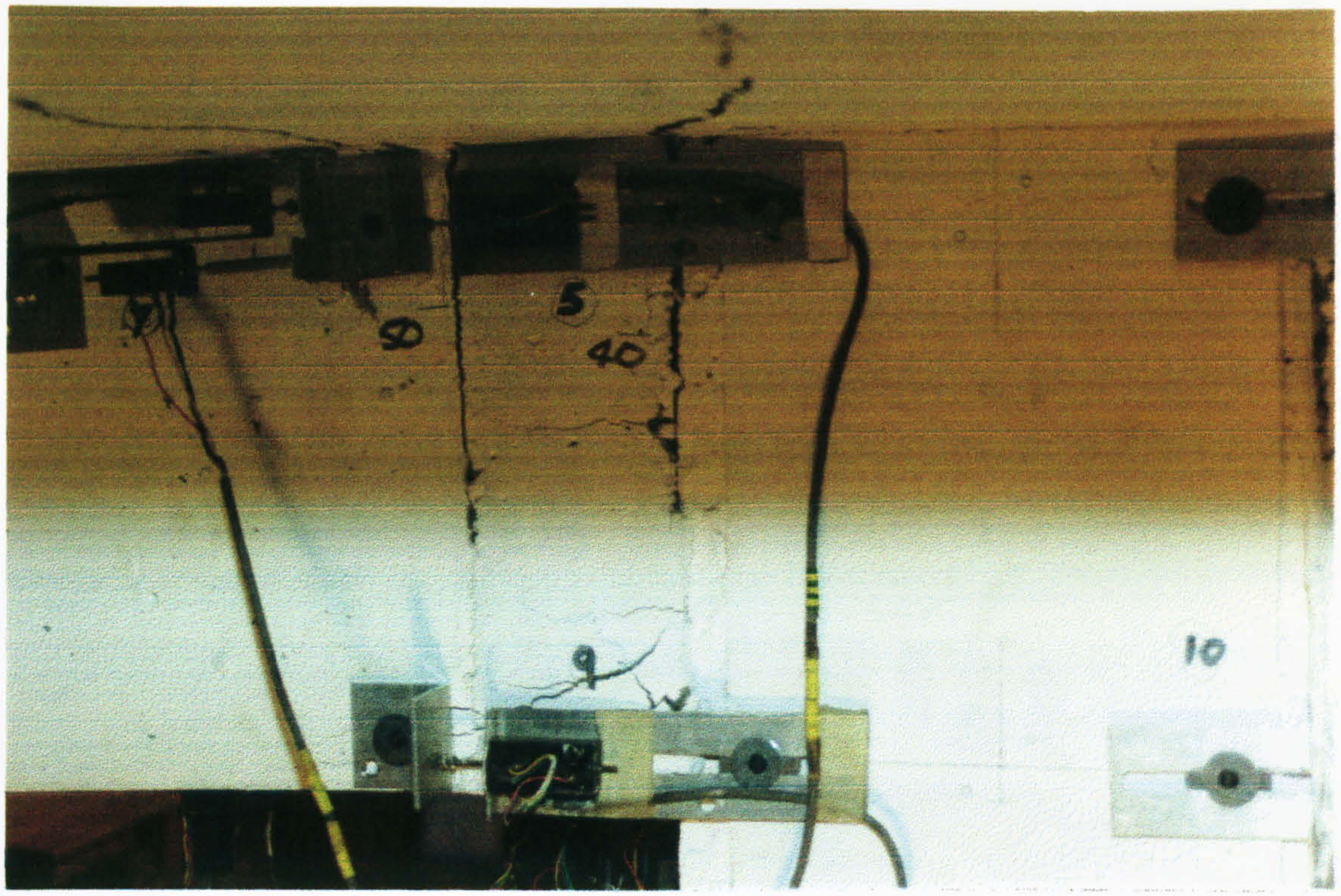

Plate 6.3: Failure region of beam 2-column joint from East in TW1(A)

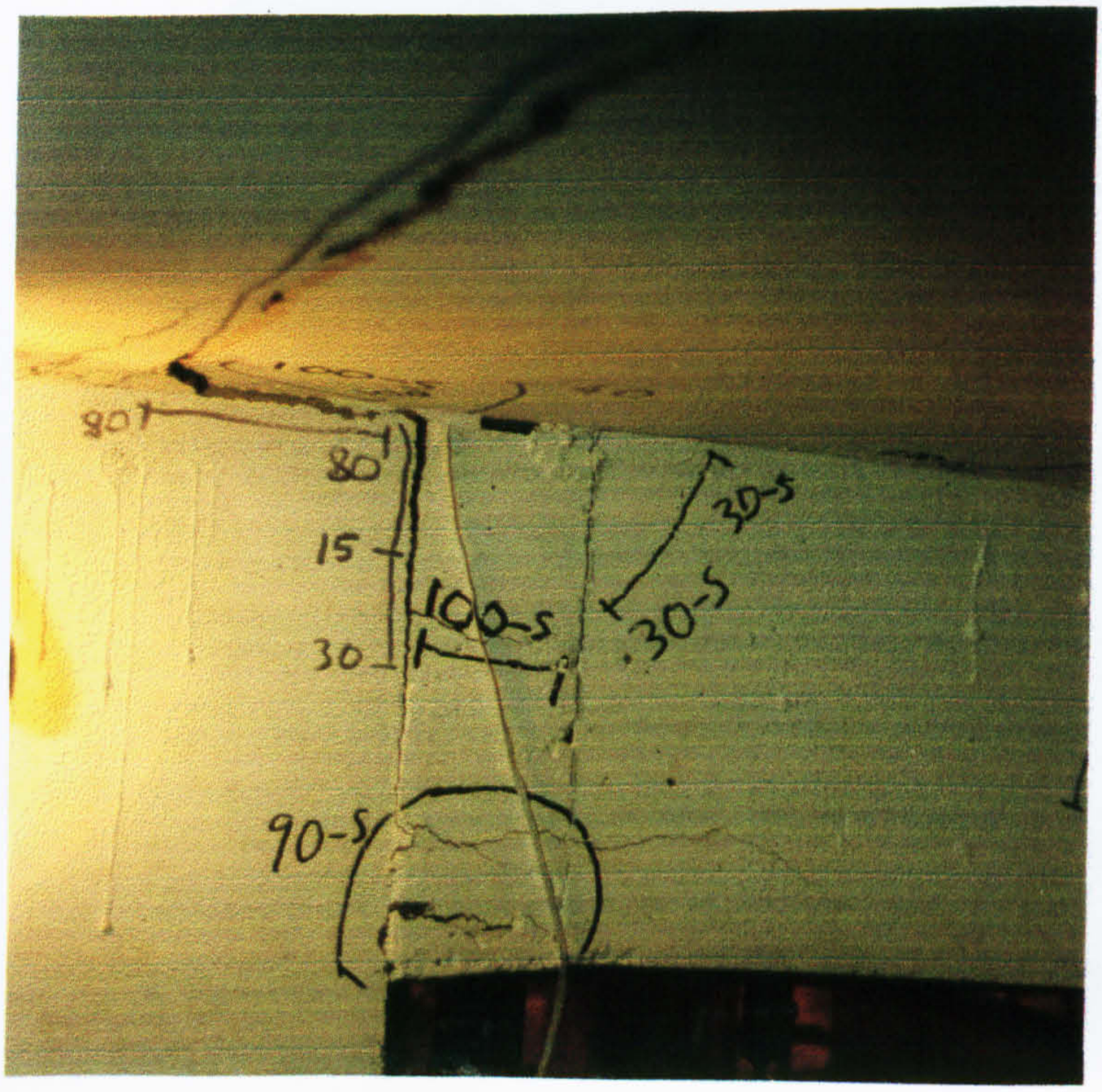

Plate 6.4: Failure region of beam 2-column joint from West in TW1(A)

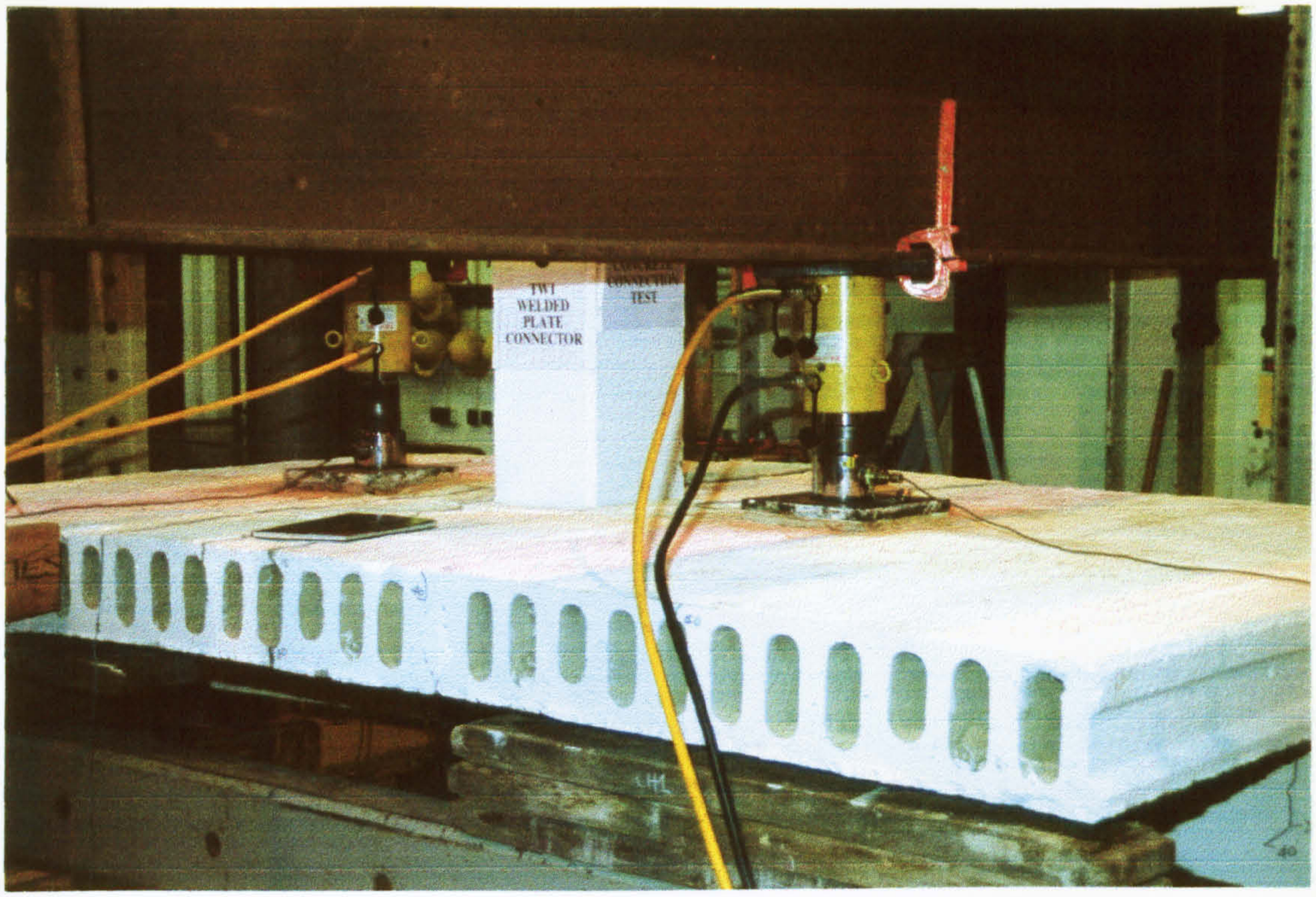

Plate 6.5: Shear subframe before testing from East in TW1(B)

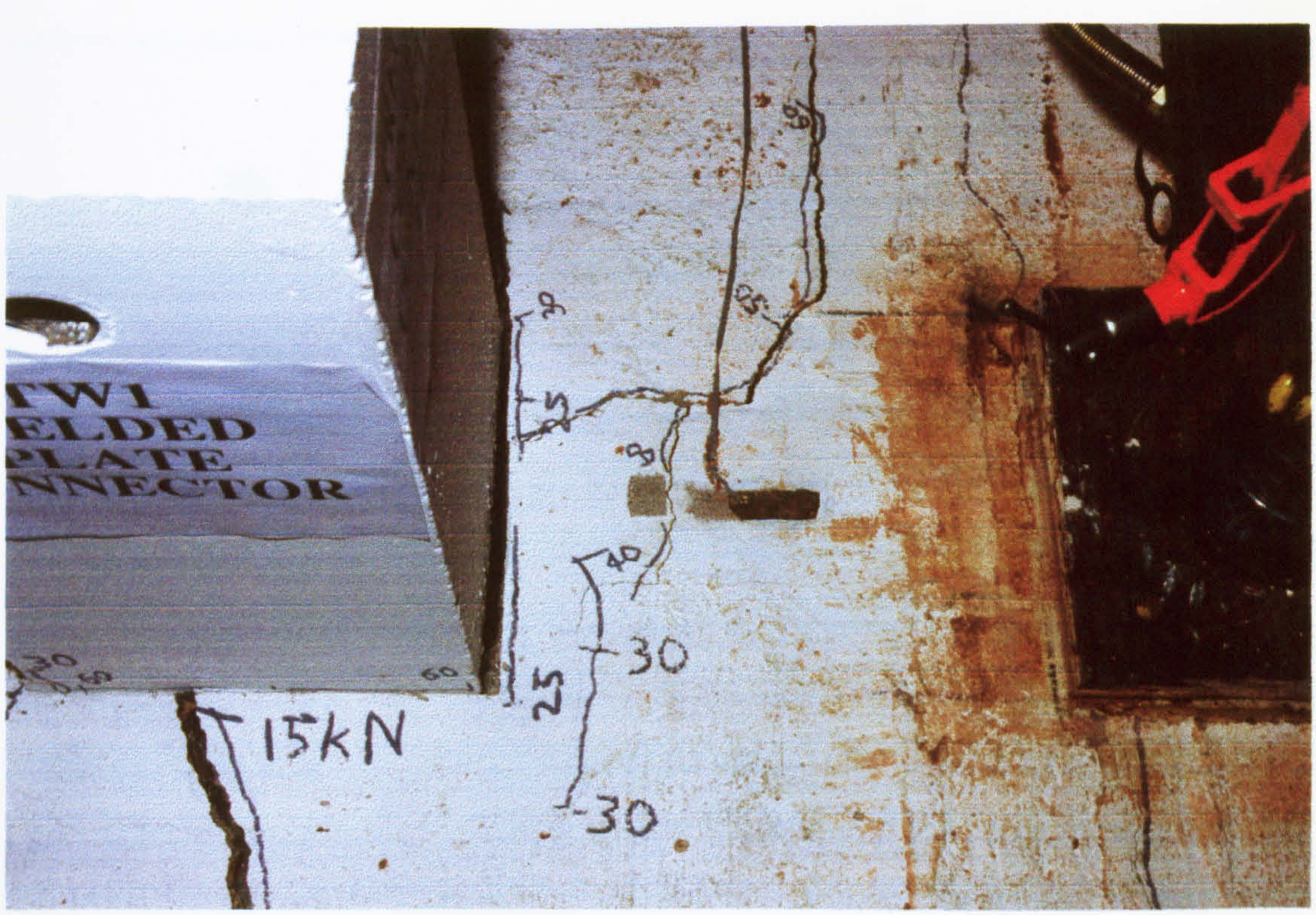

Plate 6.6: Damaged region around the column after shear test from West in TW1(B)

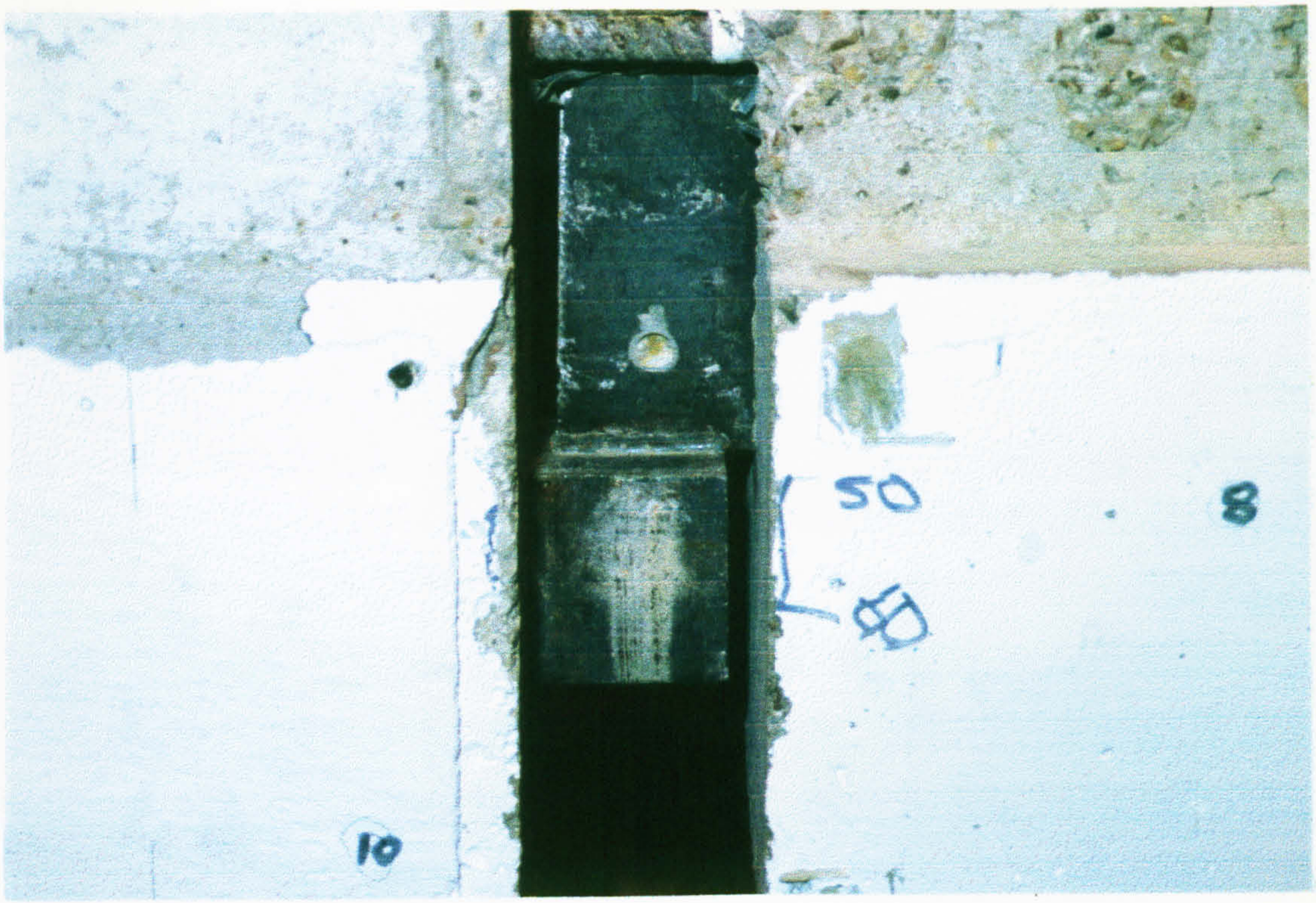

Plate 6.7: Weld region of beam 1 from East after testing TW1(B)

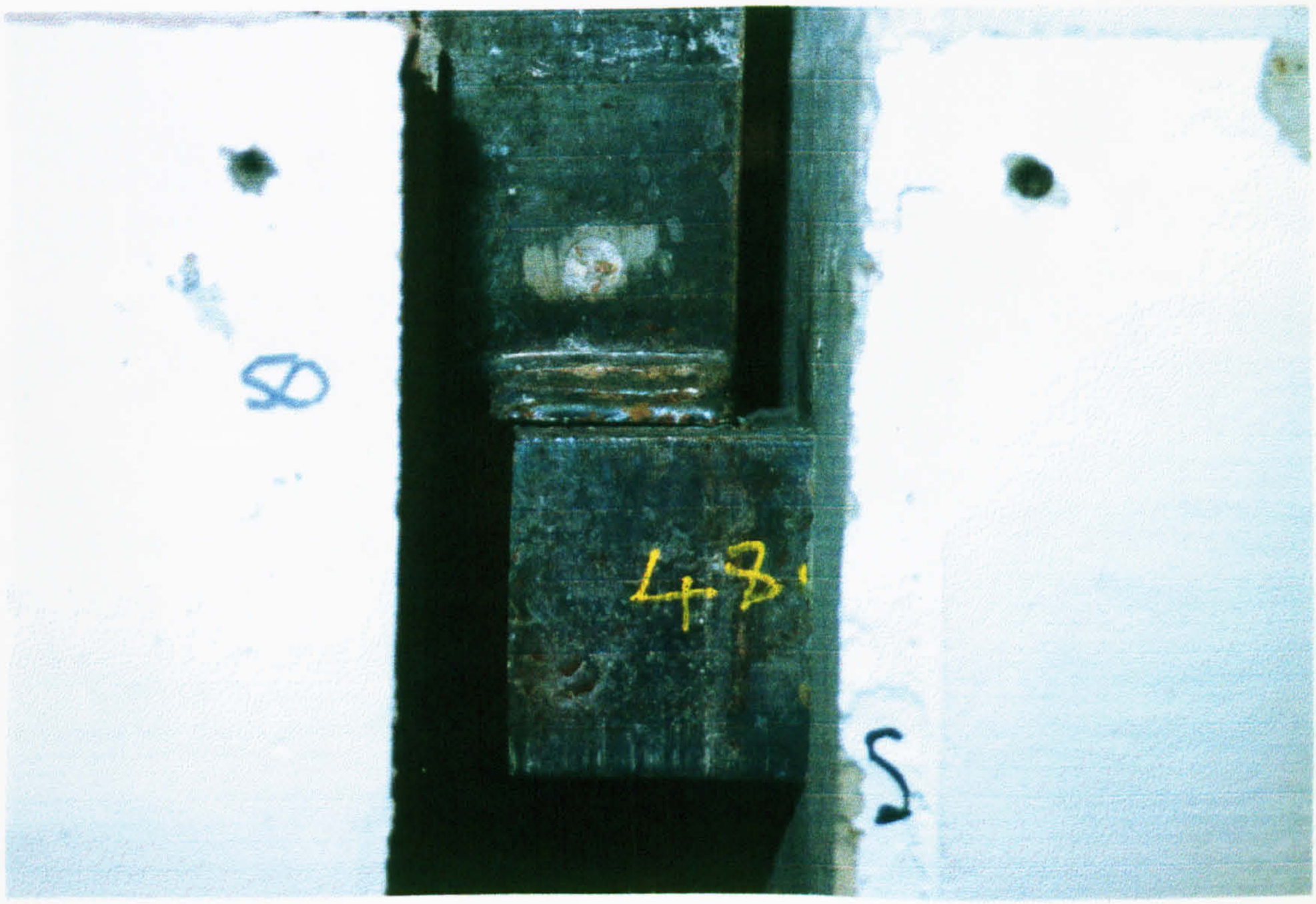

Plate 6.8: Completely broken weld in beam 2 from East after testing TW1(B)

Plate 6.9: Inspecting the weld after re-welding for TW1(C)

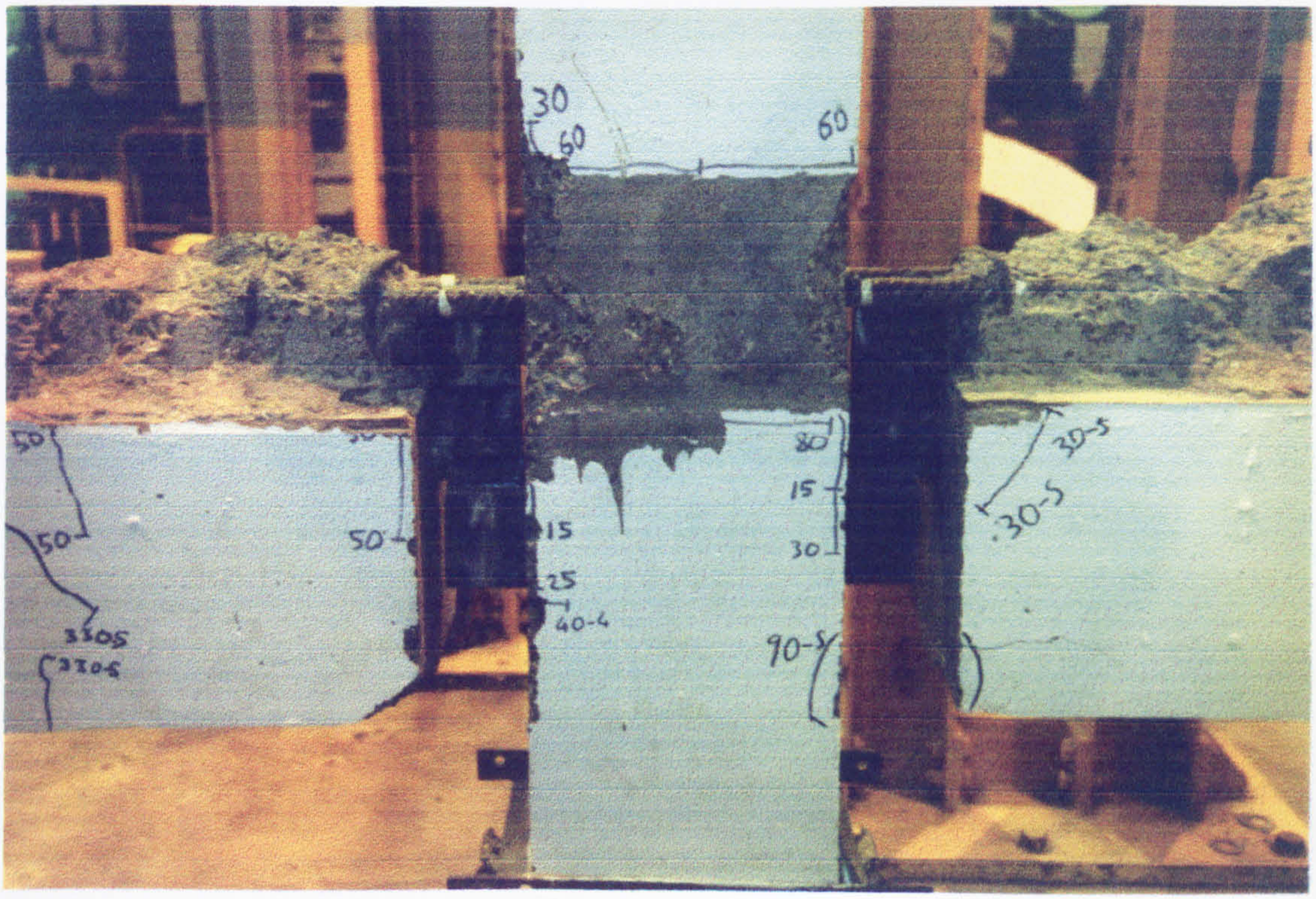

Plate 6.10: Damaged regions in the precast members from West after testing TW1(B)

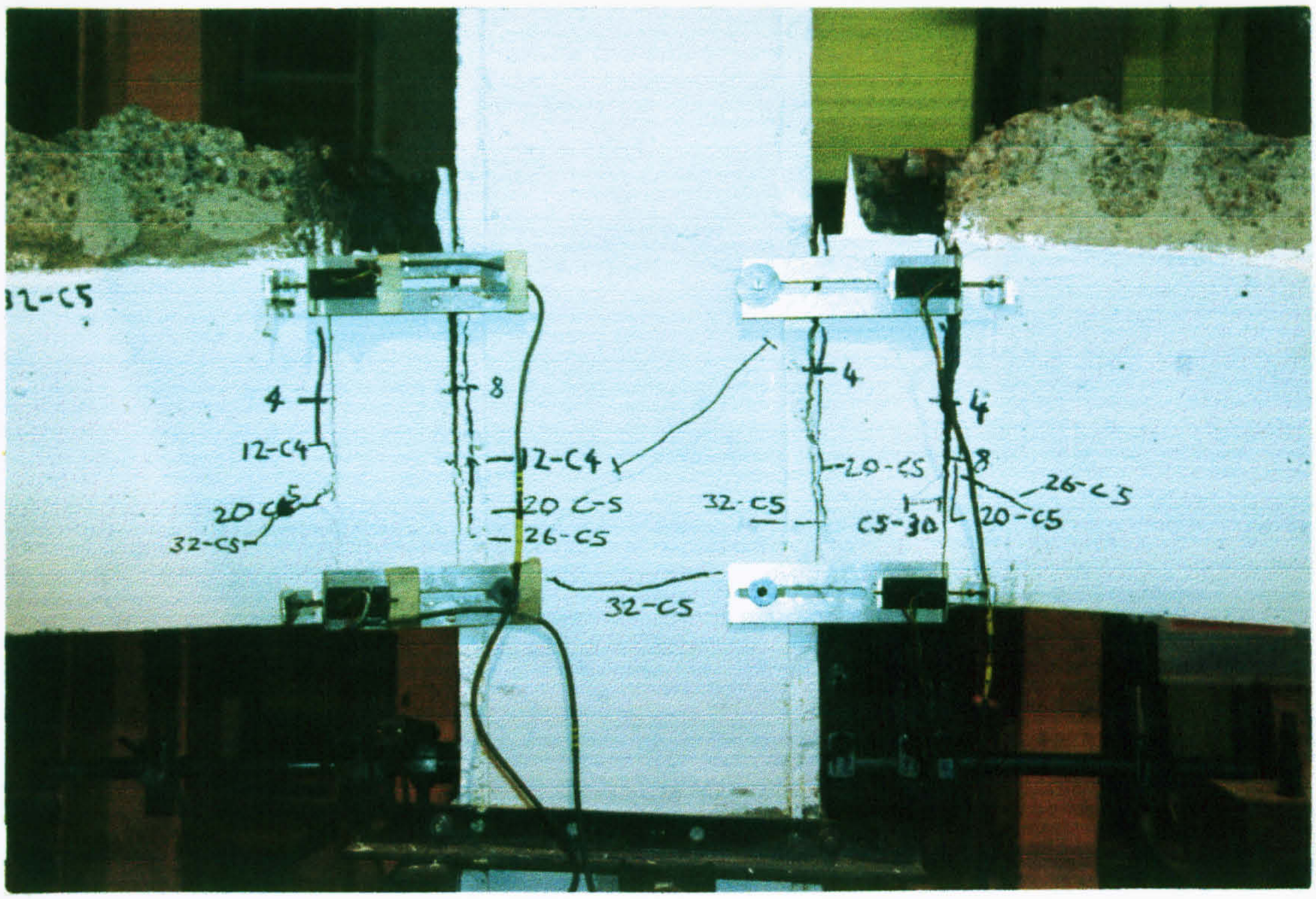

Plate 6.11: Damaged regions around joints from East in TW1(C)

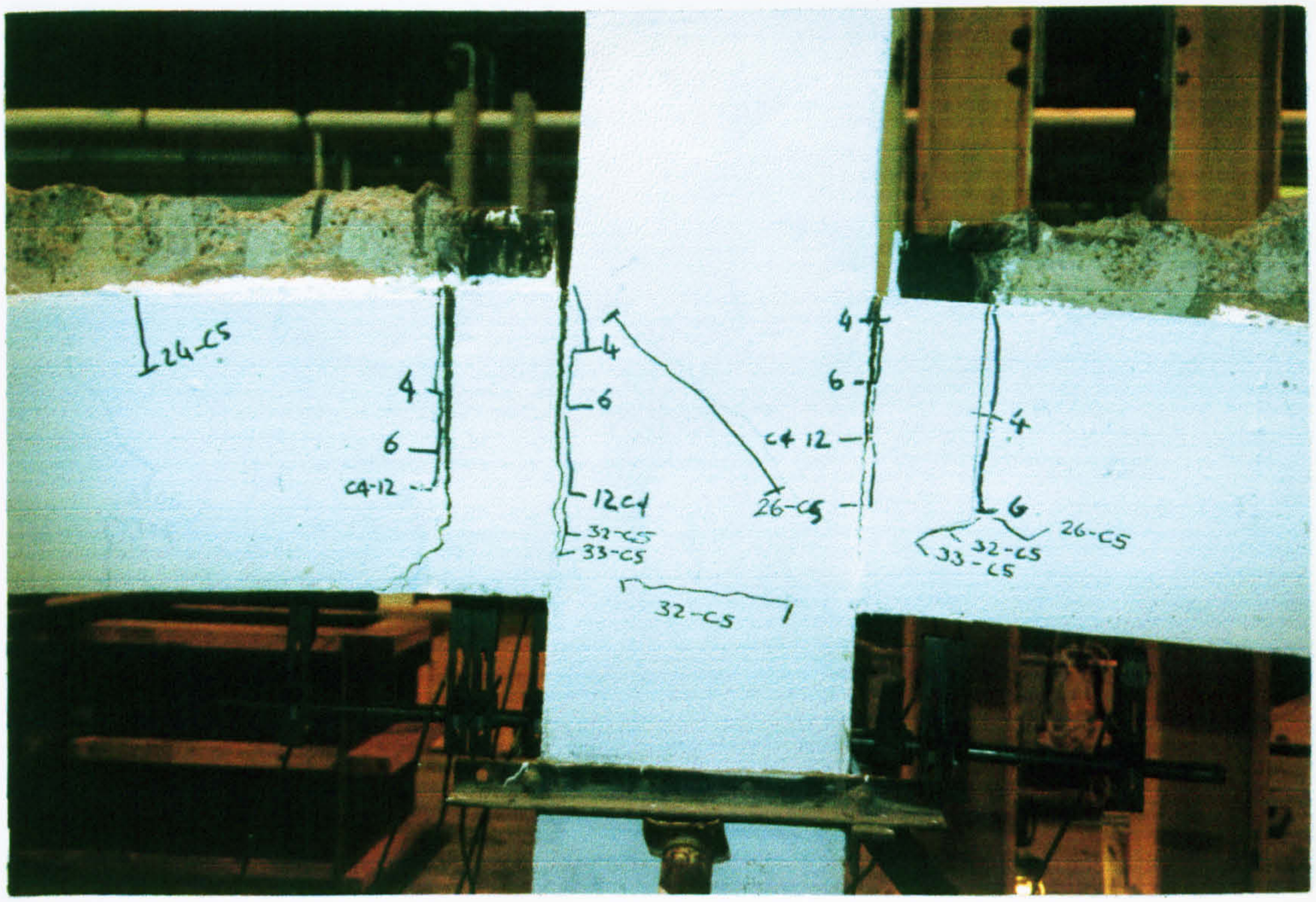

Plate 6.12: Damaged regions around joints from West in TW1(C)

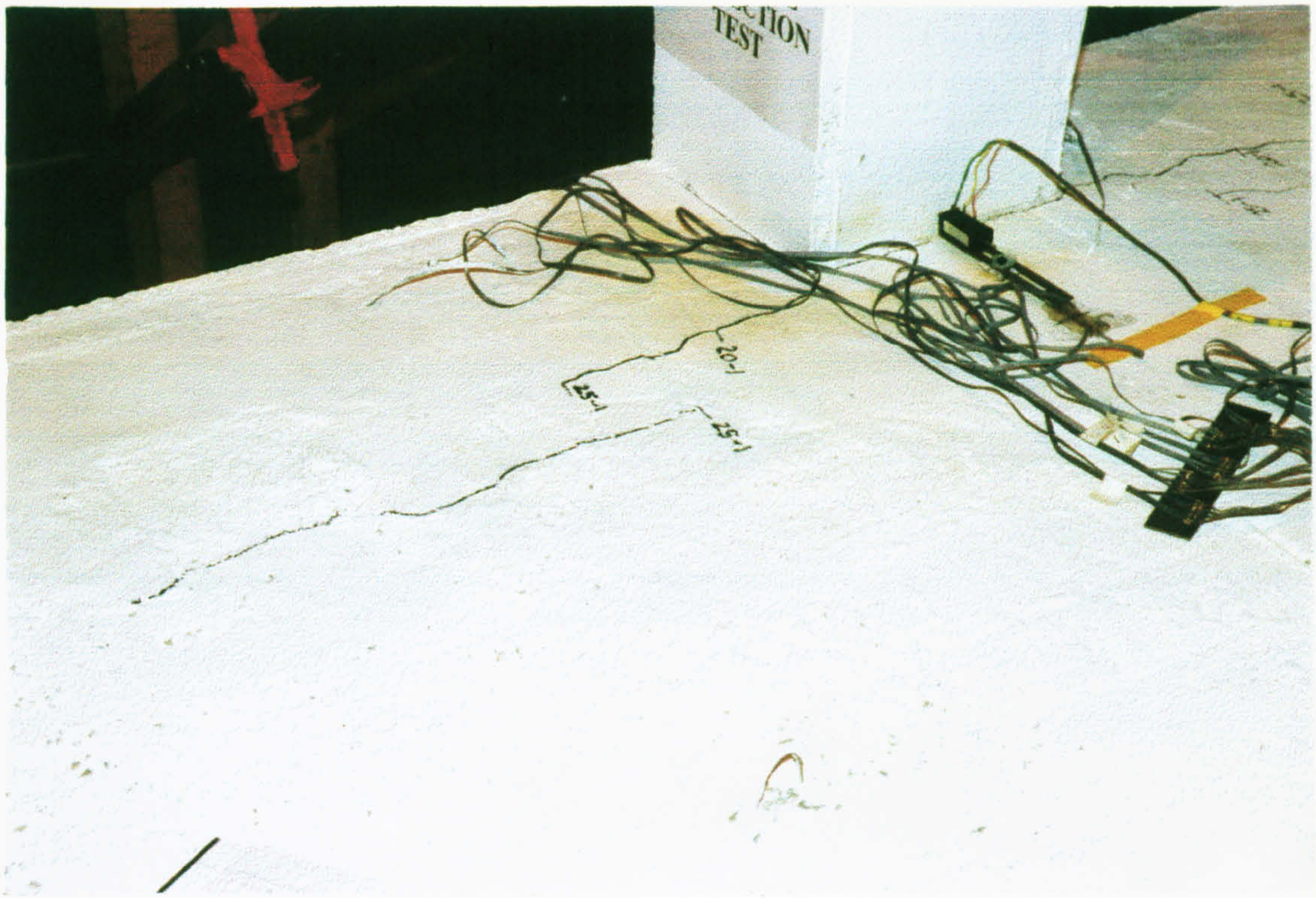

Plate 6.13: First cracks at top of slab from East in TW2

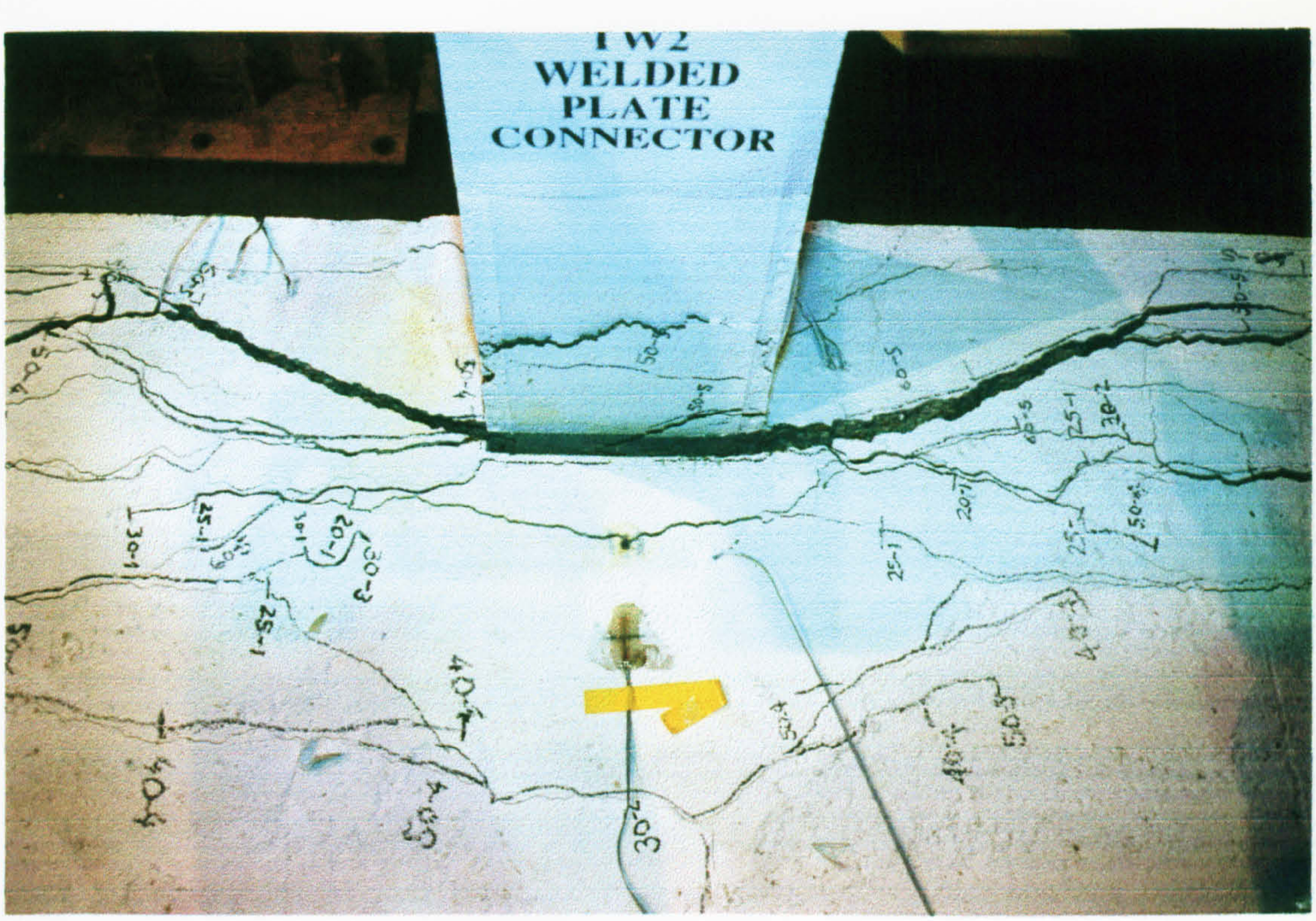

Plate 6.14: Failure regions at top of slab and around column from North in TW2

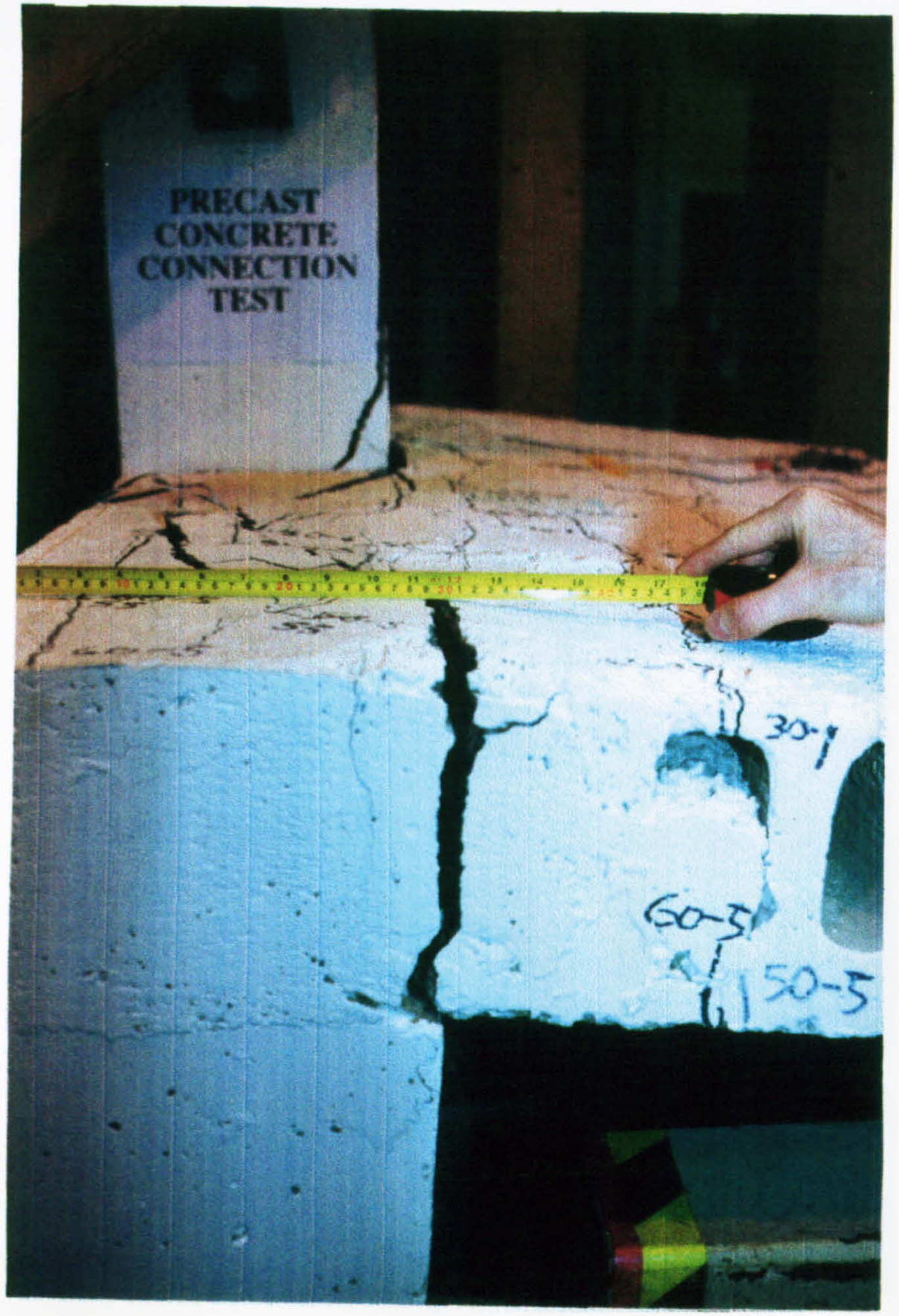

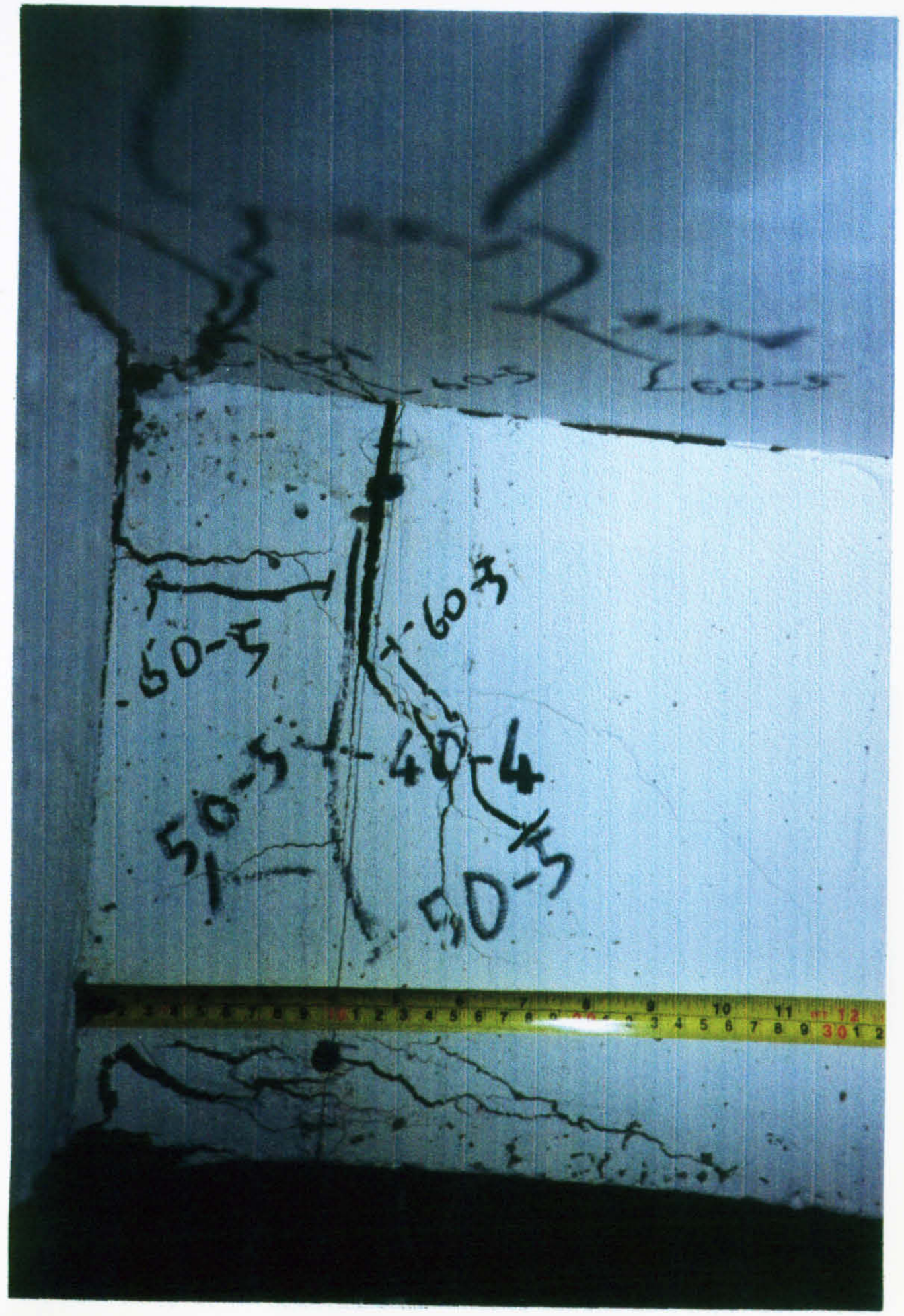

Plate 6.15: Failure regions at top of slab and around joint from East in TW2

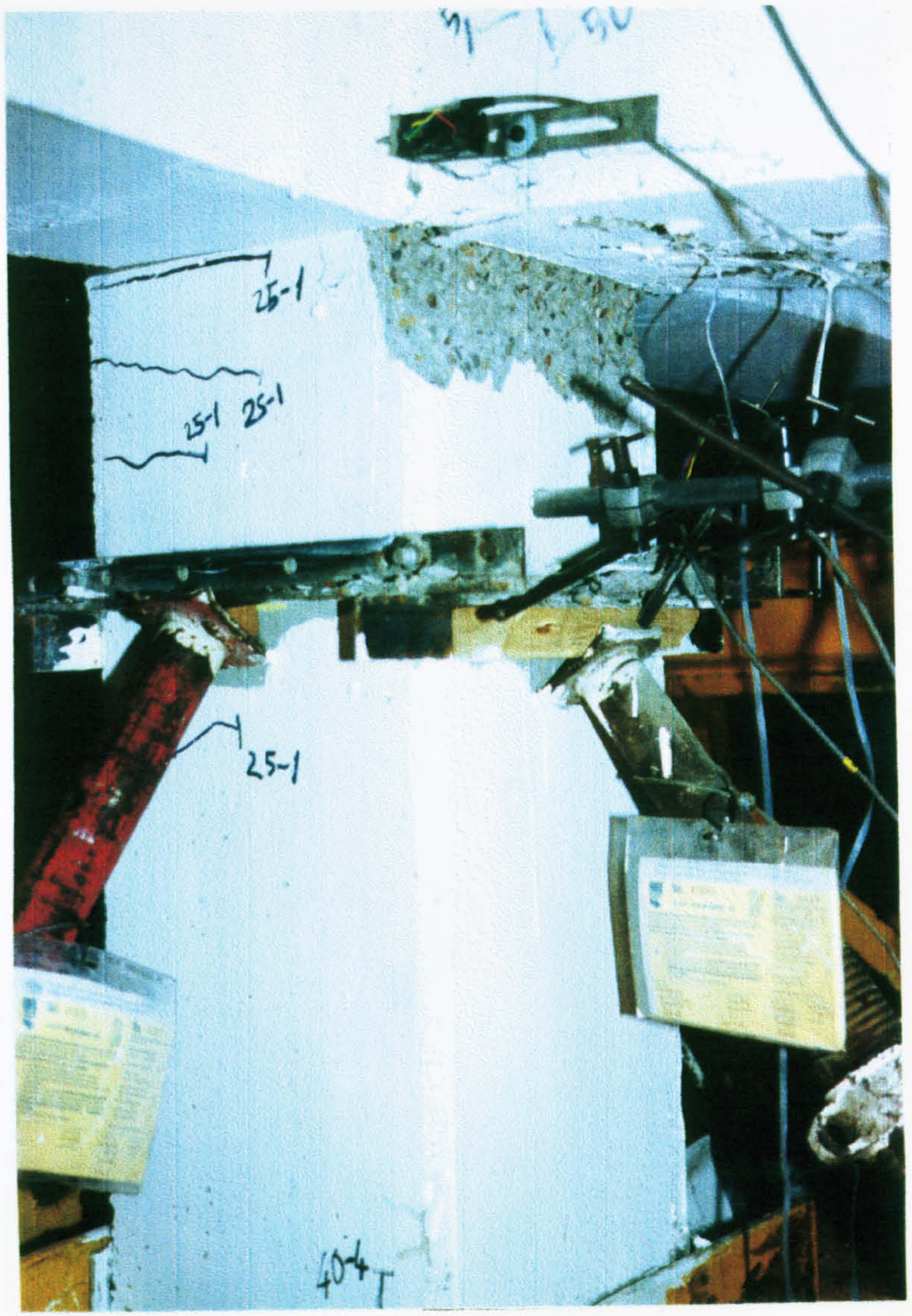

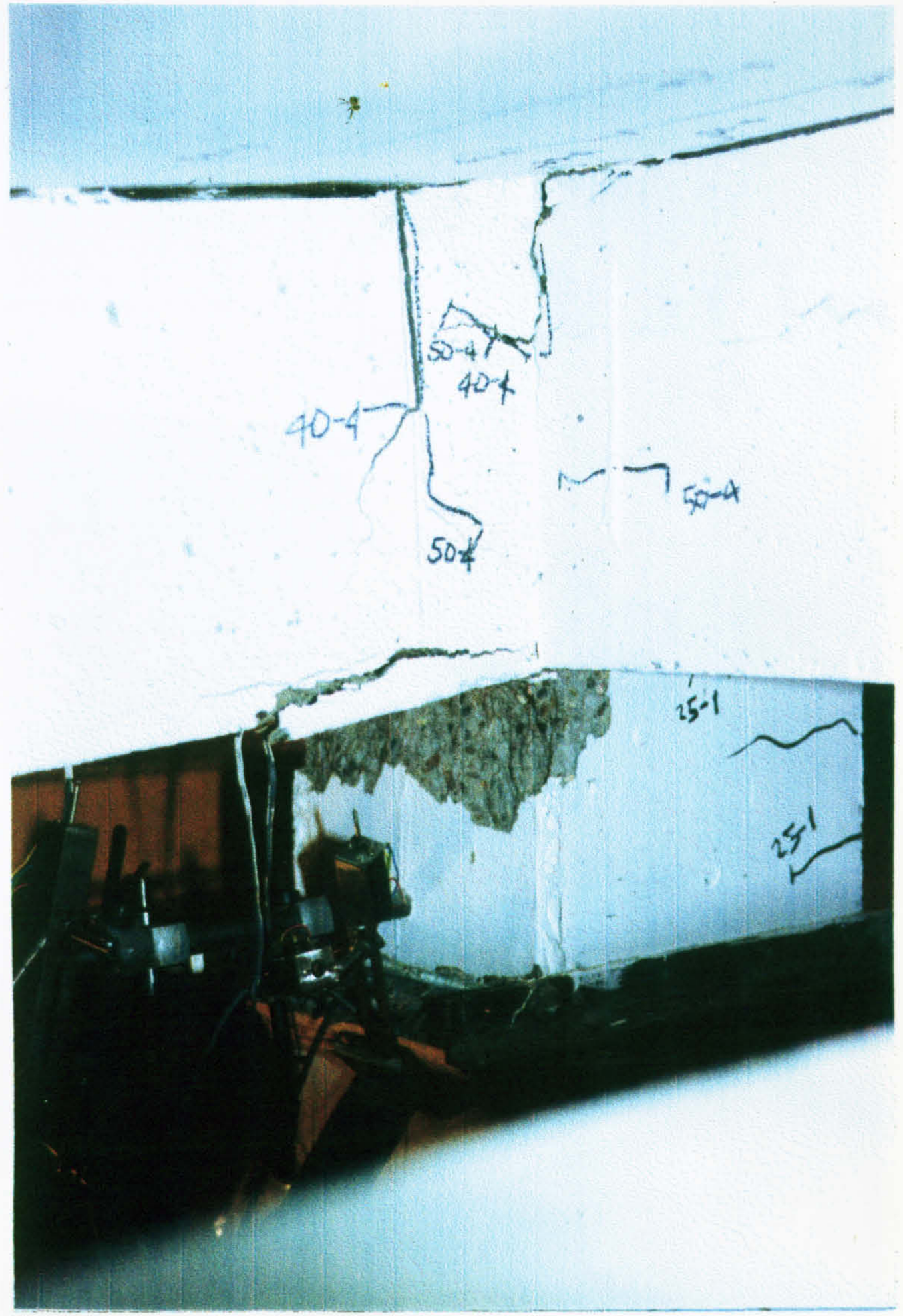

Plate 6.16: Damaged regions in the column in compression zone in TW2

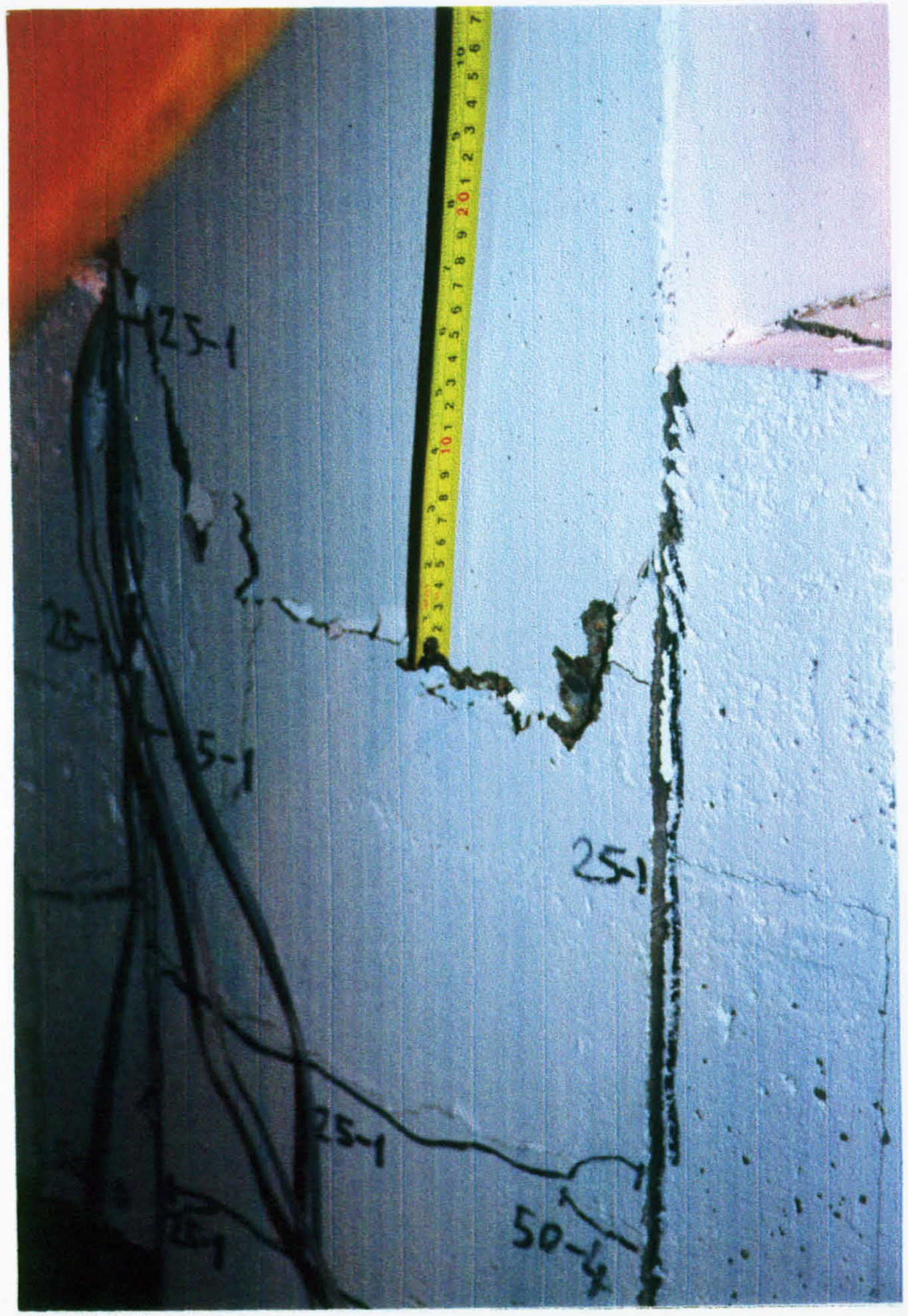

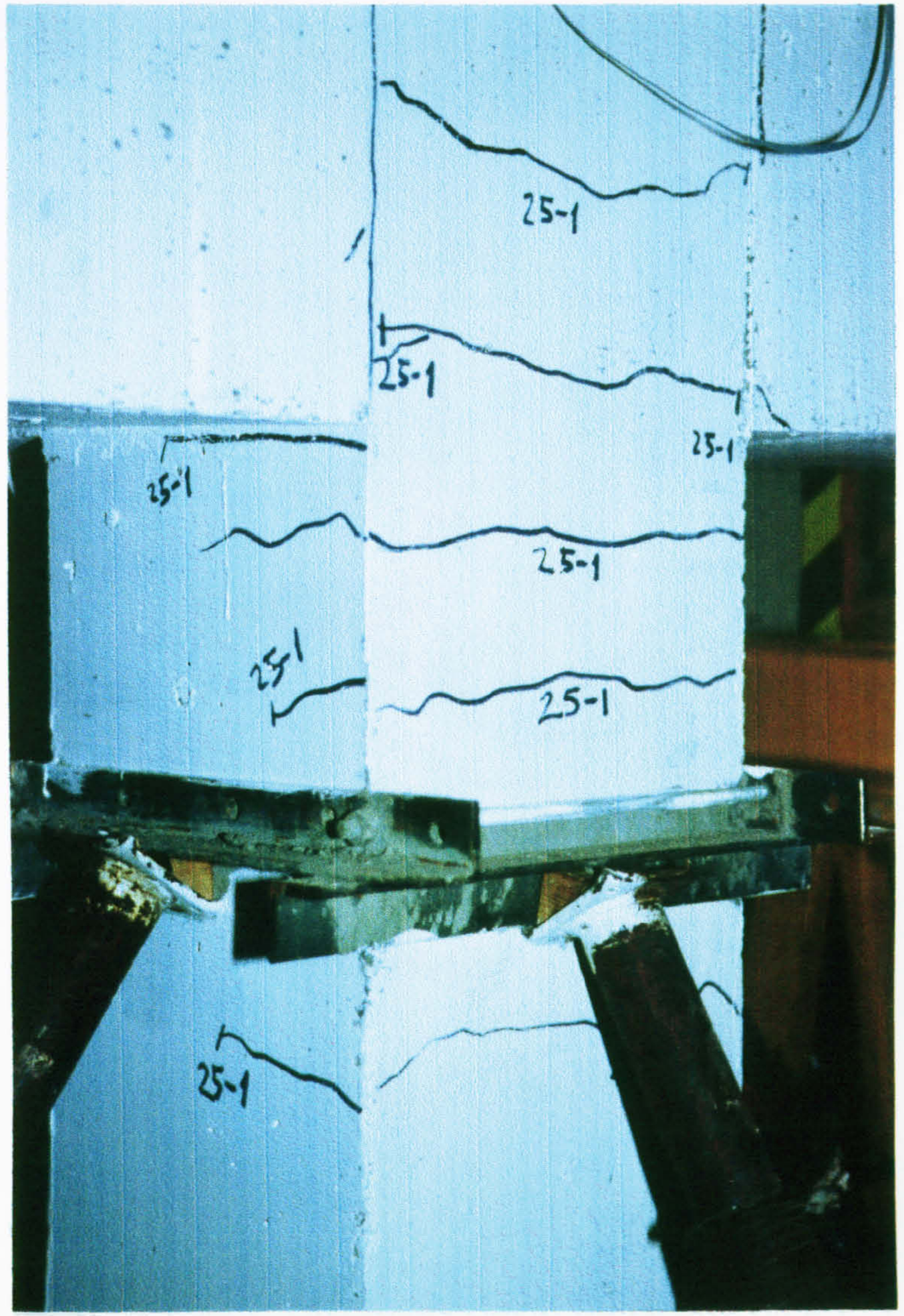

Plate 6.17: Damaged regions in the column from South in TW2

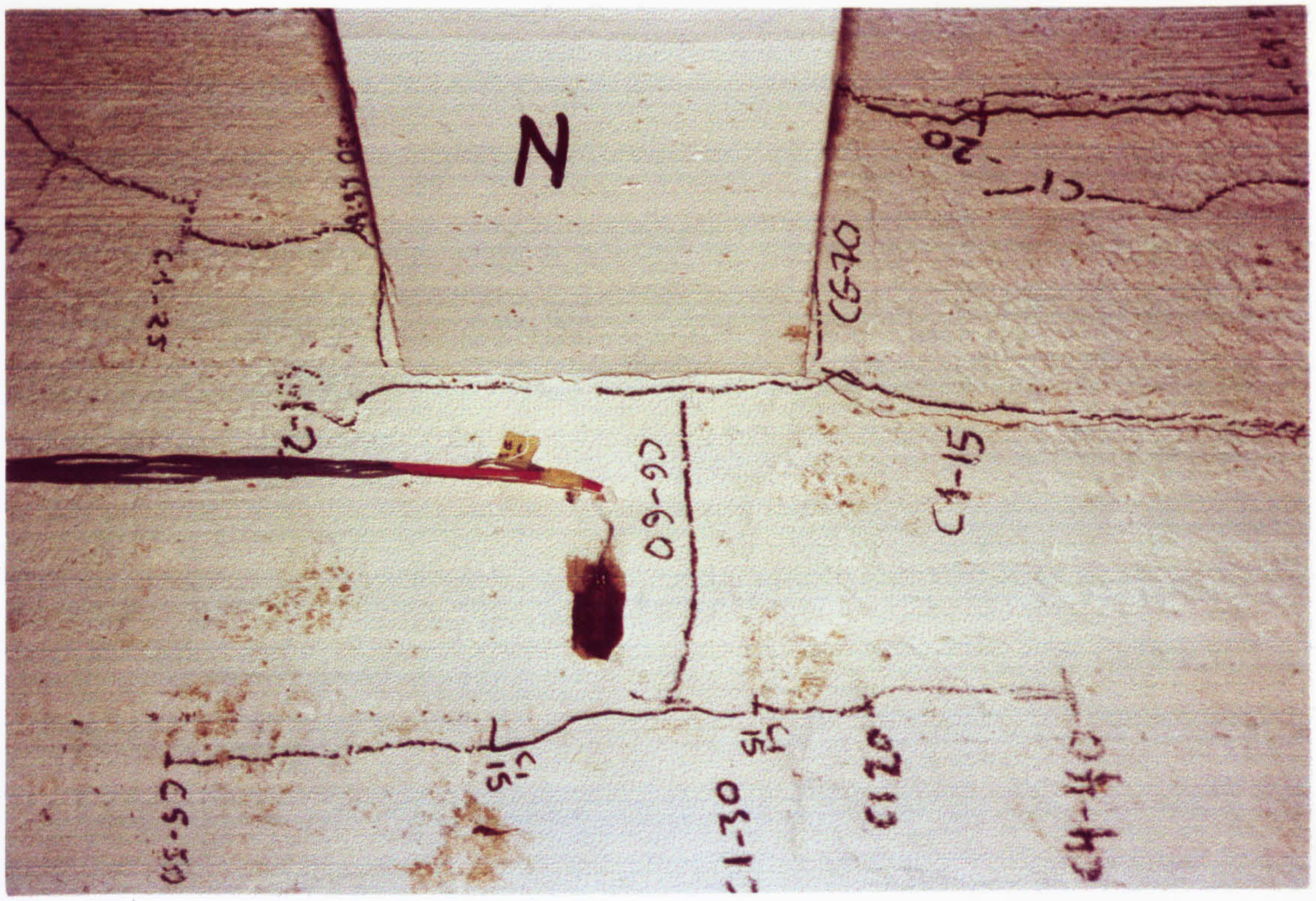

Plate 6.18: Failure region at top of slab from North and South in TB1(A)

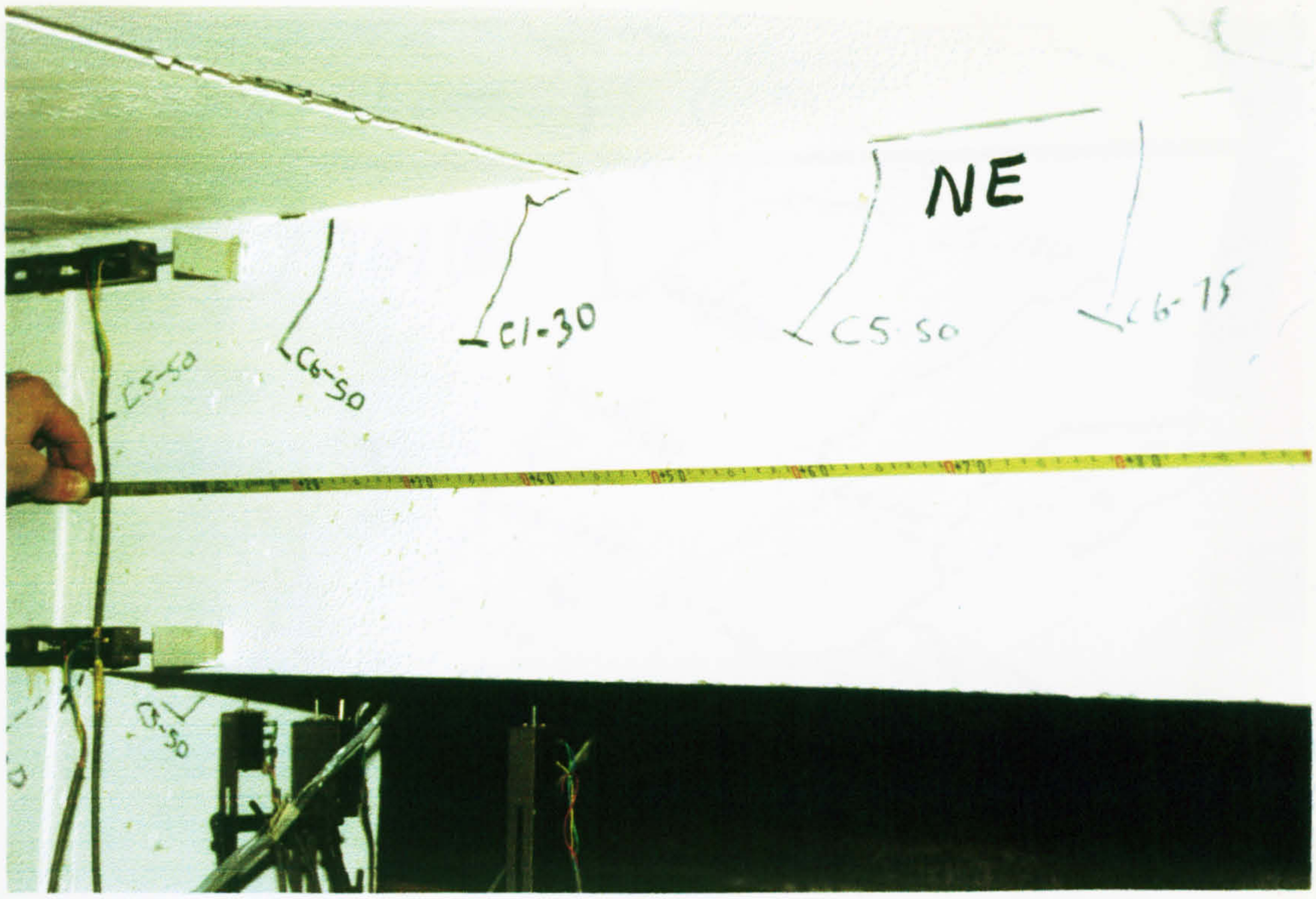

Plate 6.19: Flexural cracks in beam 1 from East in TB1(A)

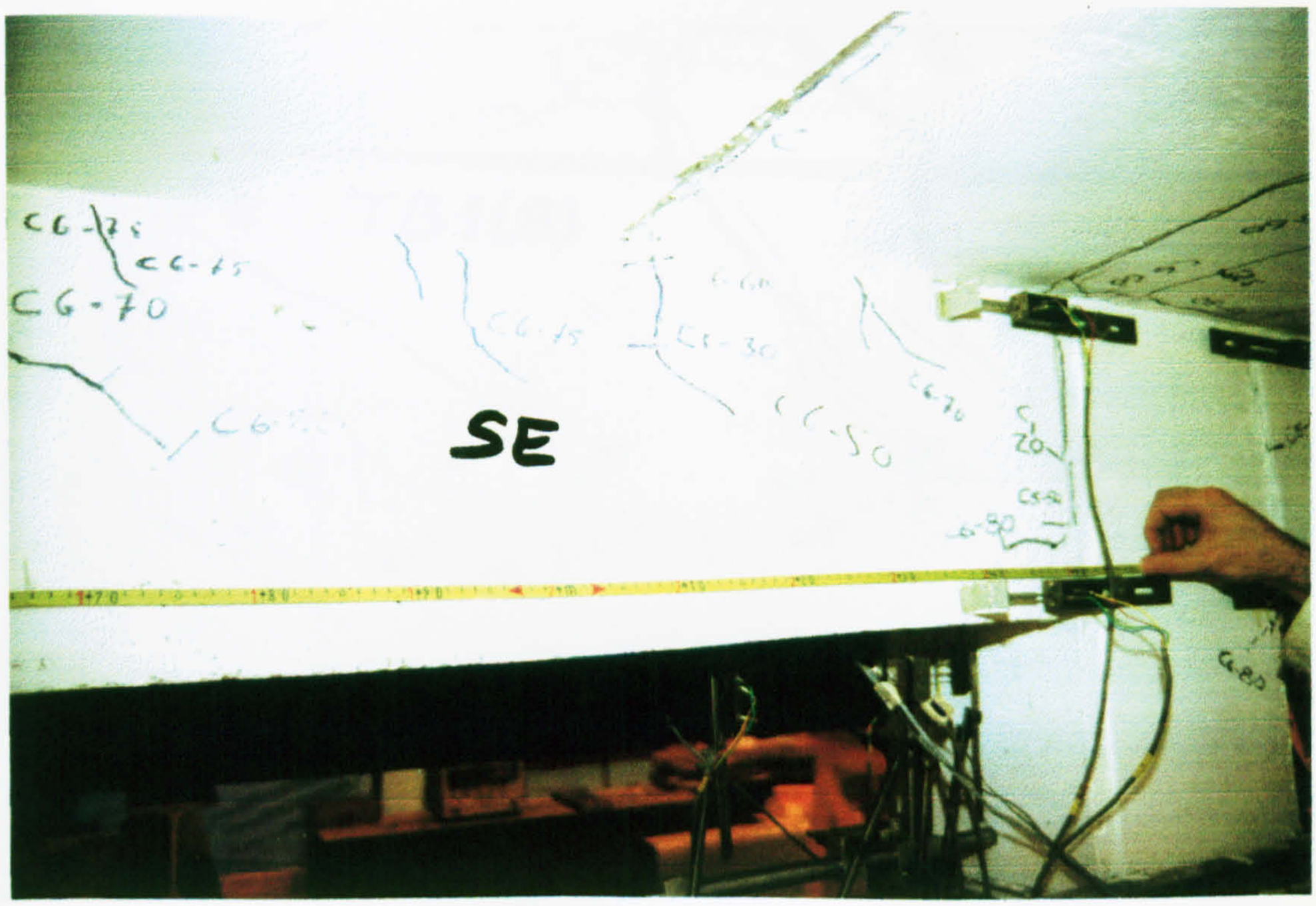

Plate 6.20: Flexural cracks in beam 2 from East in TB1(A)

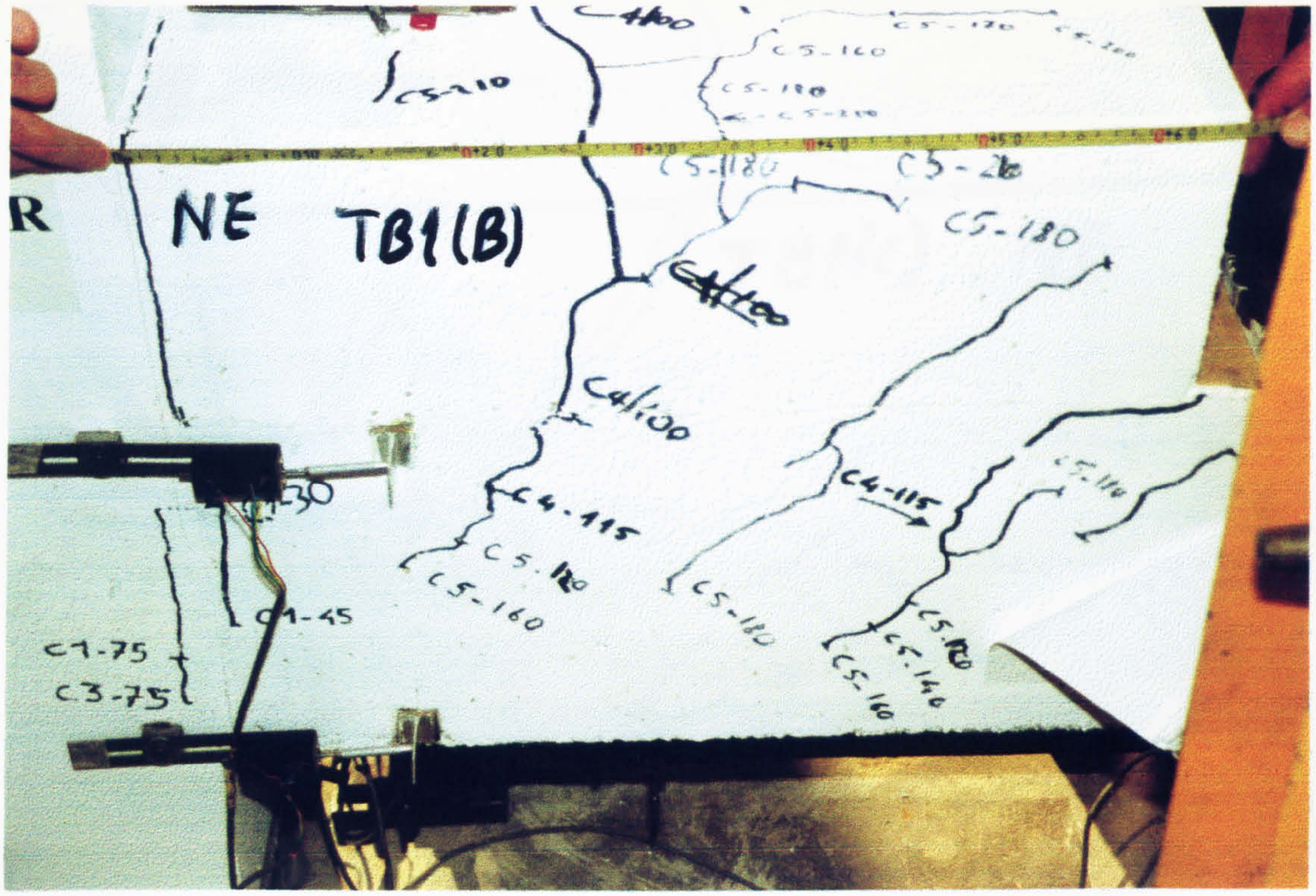

Plate 6.21: Failure regions in beam 1 from East in TB1(B)

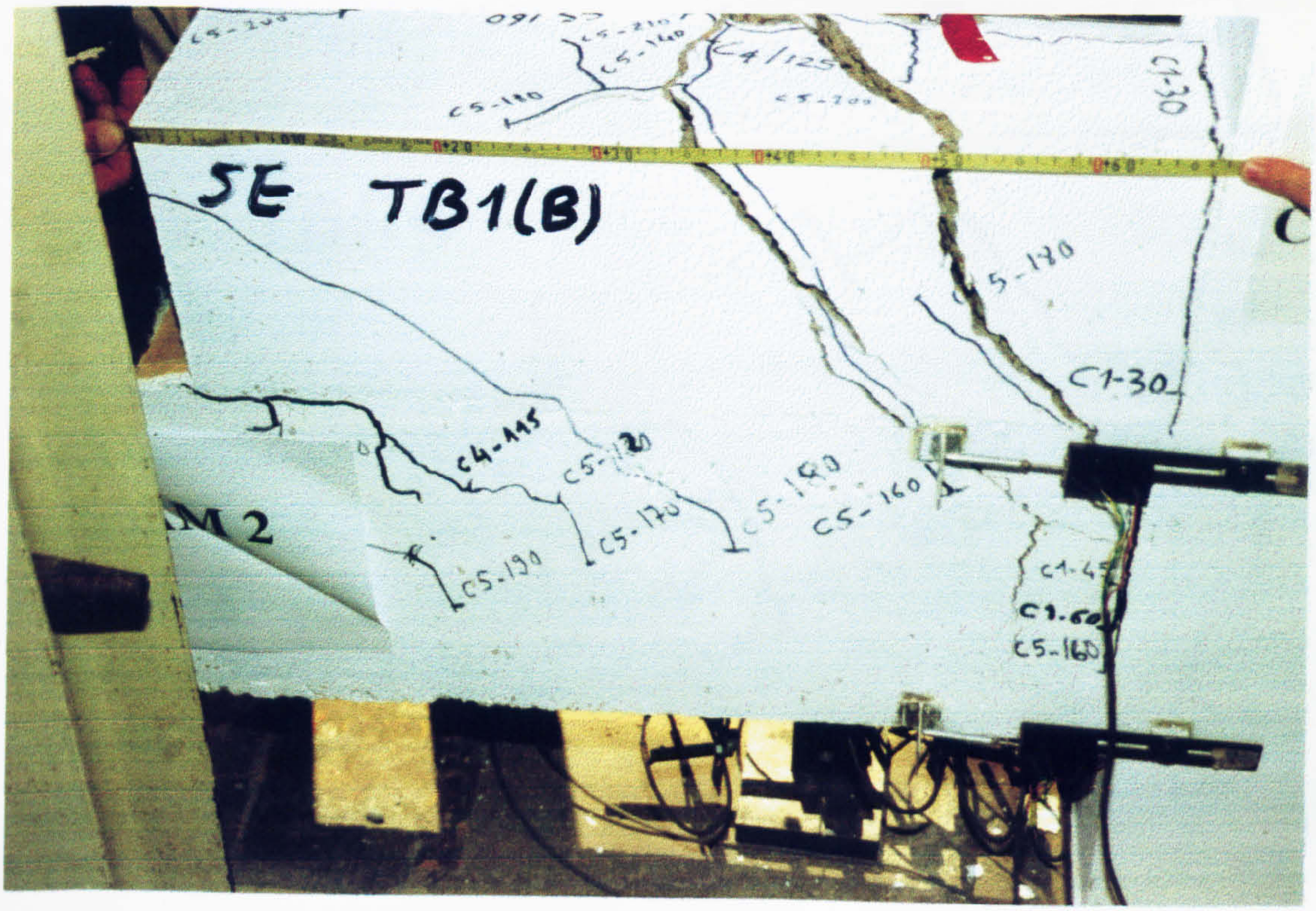

Plate 6.22: Failure regions in beam 2 from East in TB1(B)

Plate 6.23: Failure regions in beam 1 from East in TB1(C)

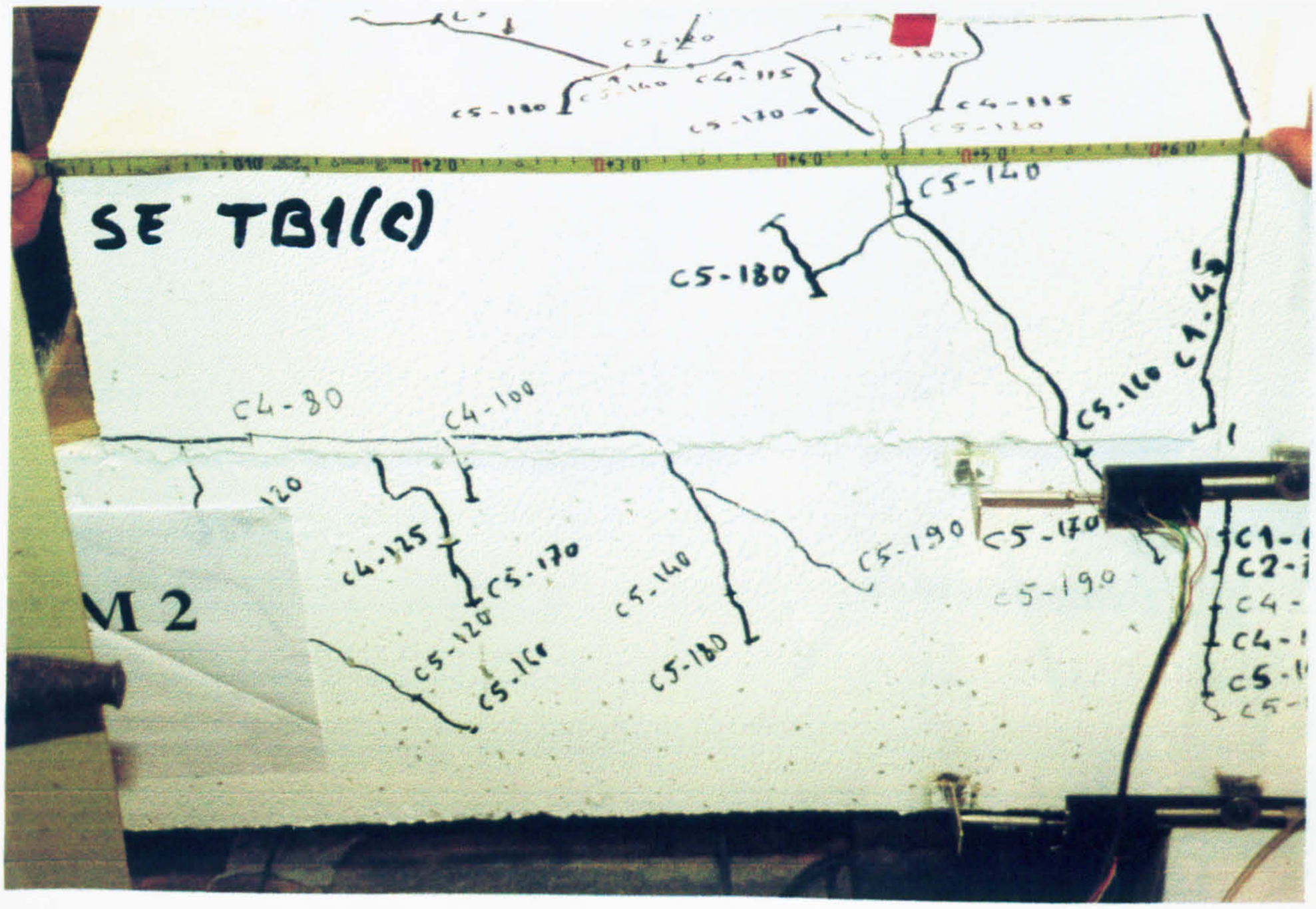

Plate 6.24: Failure regions in beam 2 from East in TB1(C)

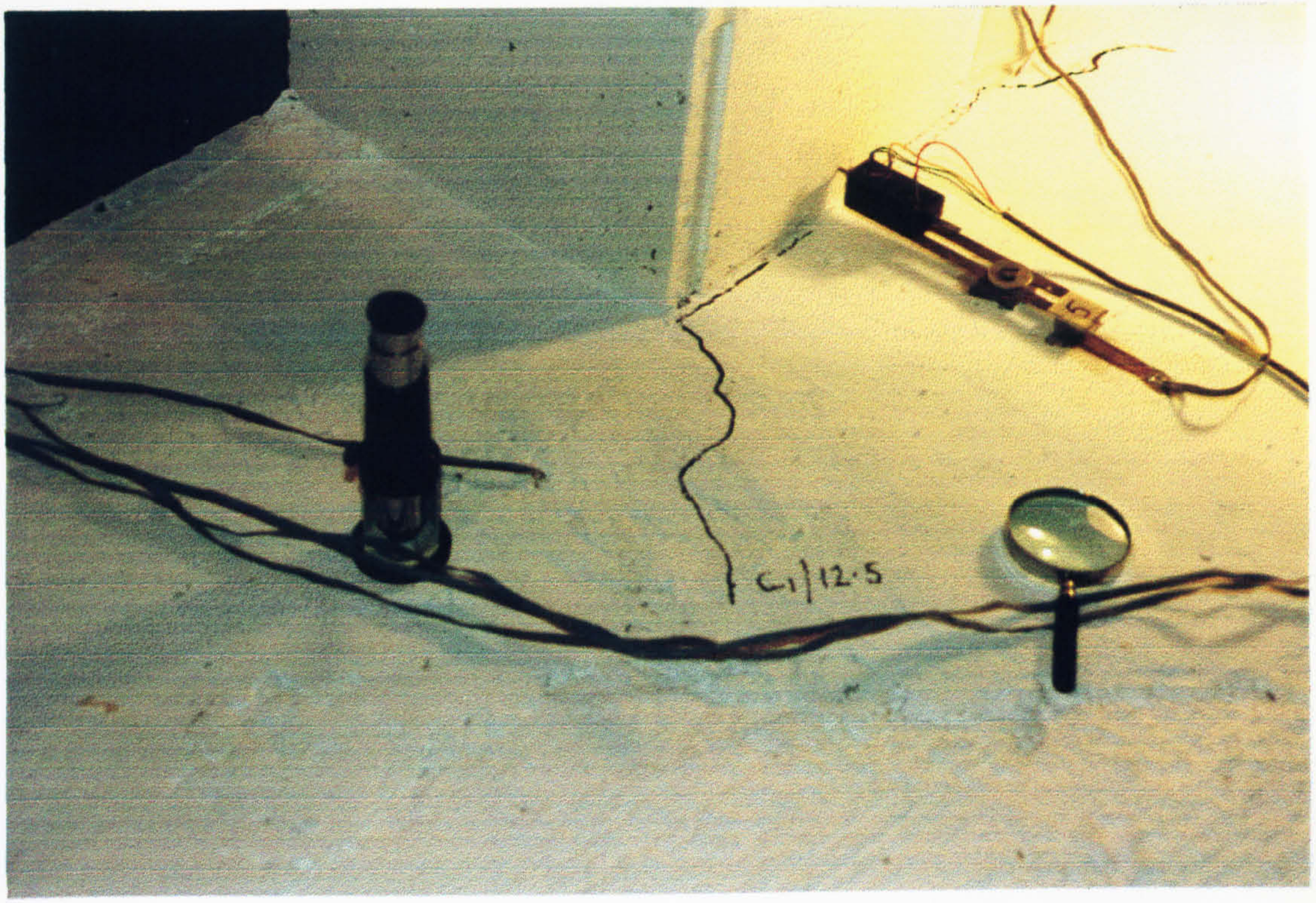

Plate 6.25: First cracks at top of slab from East in TB2

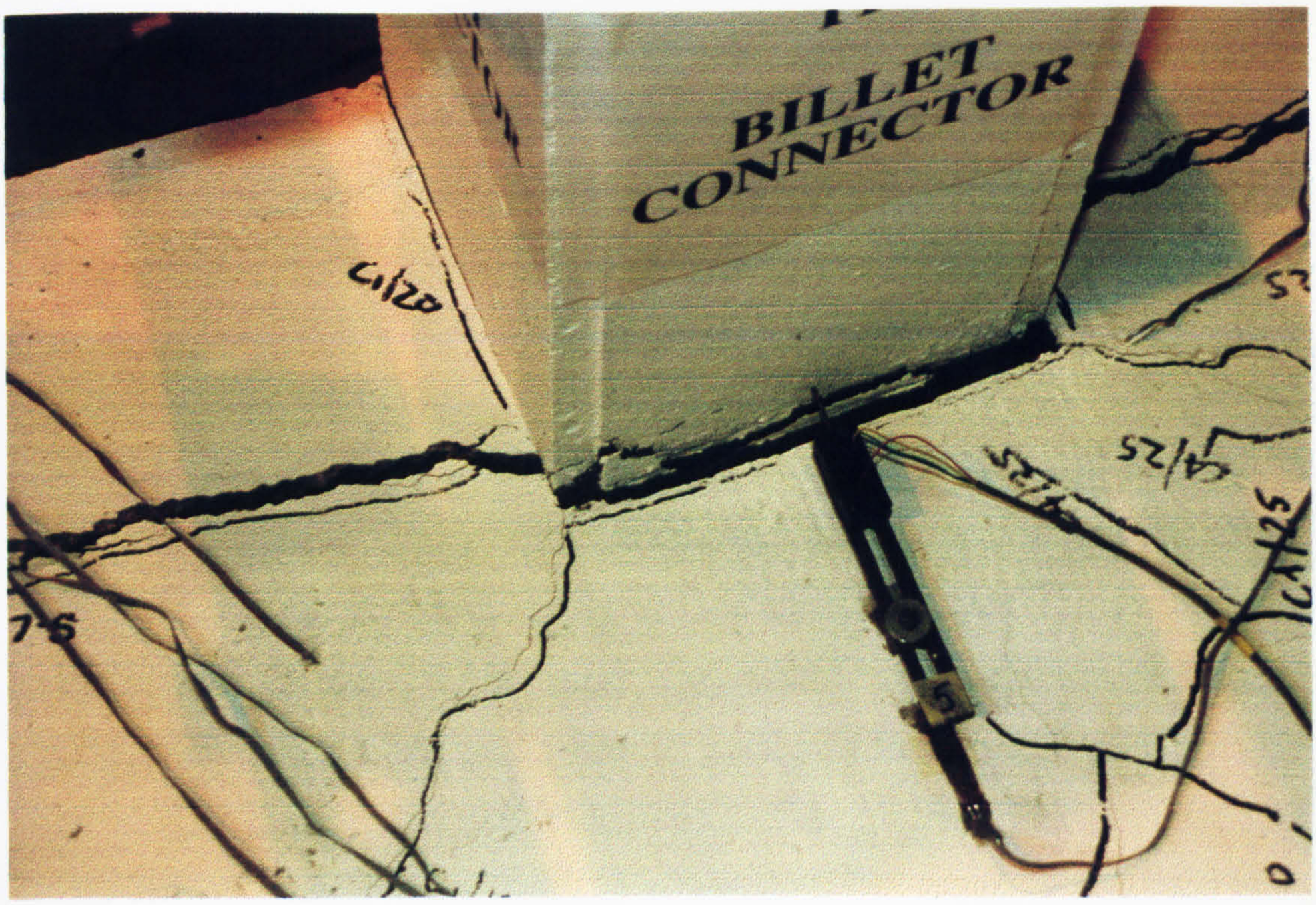

Plate 6.26: Failure regions at top of slab from East in TB2

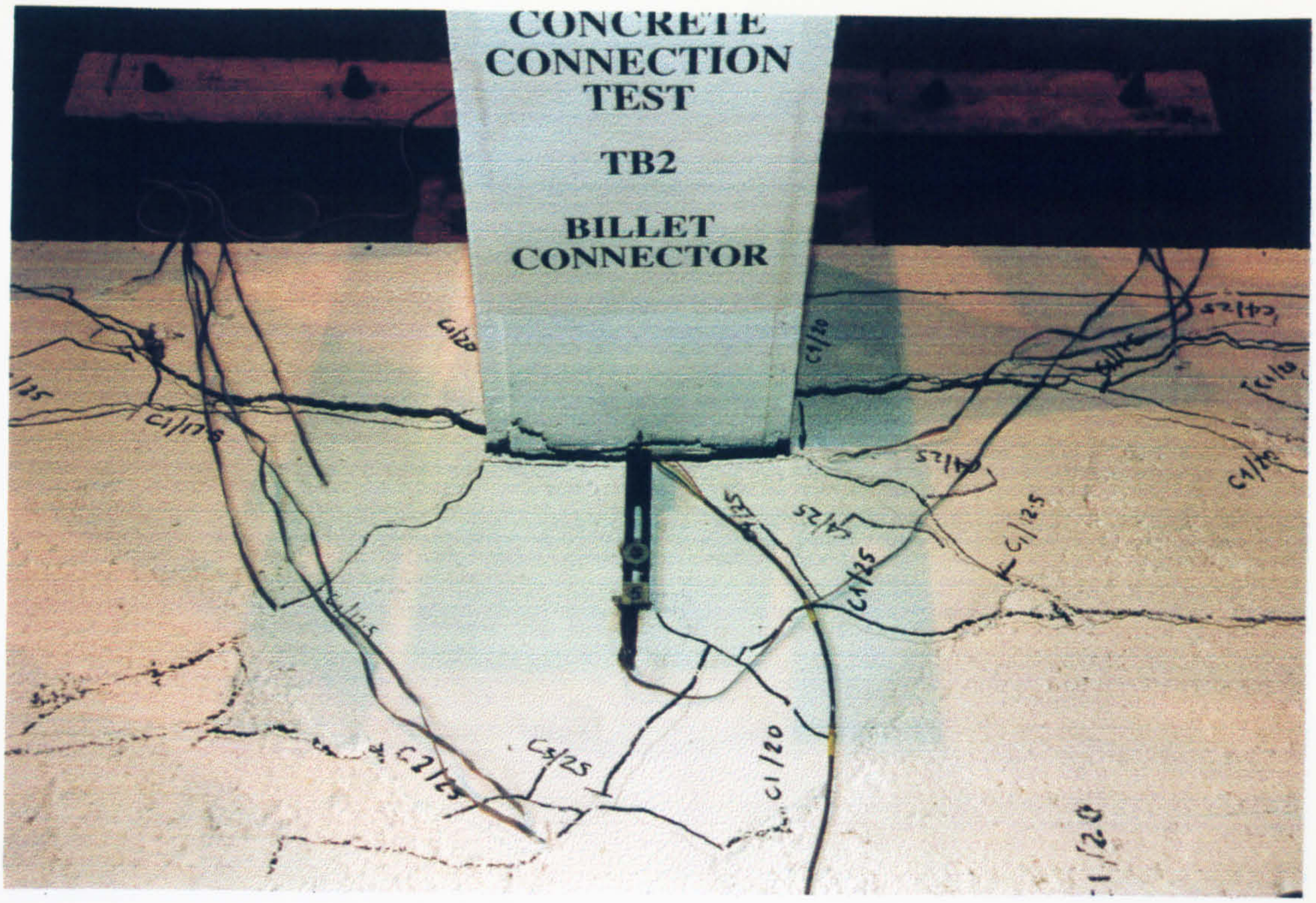

Plate 6.27: Hair cracks at top of slab from North in TB2

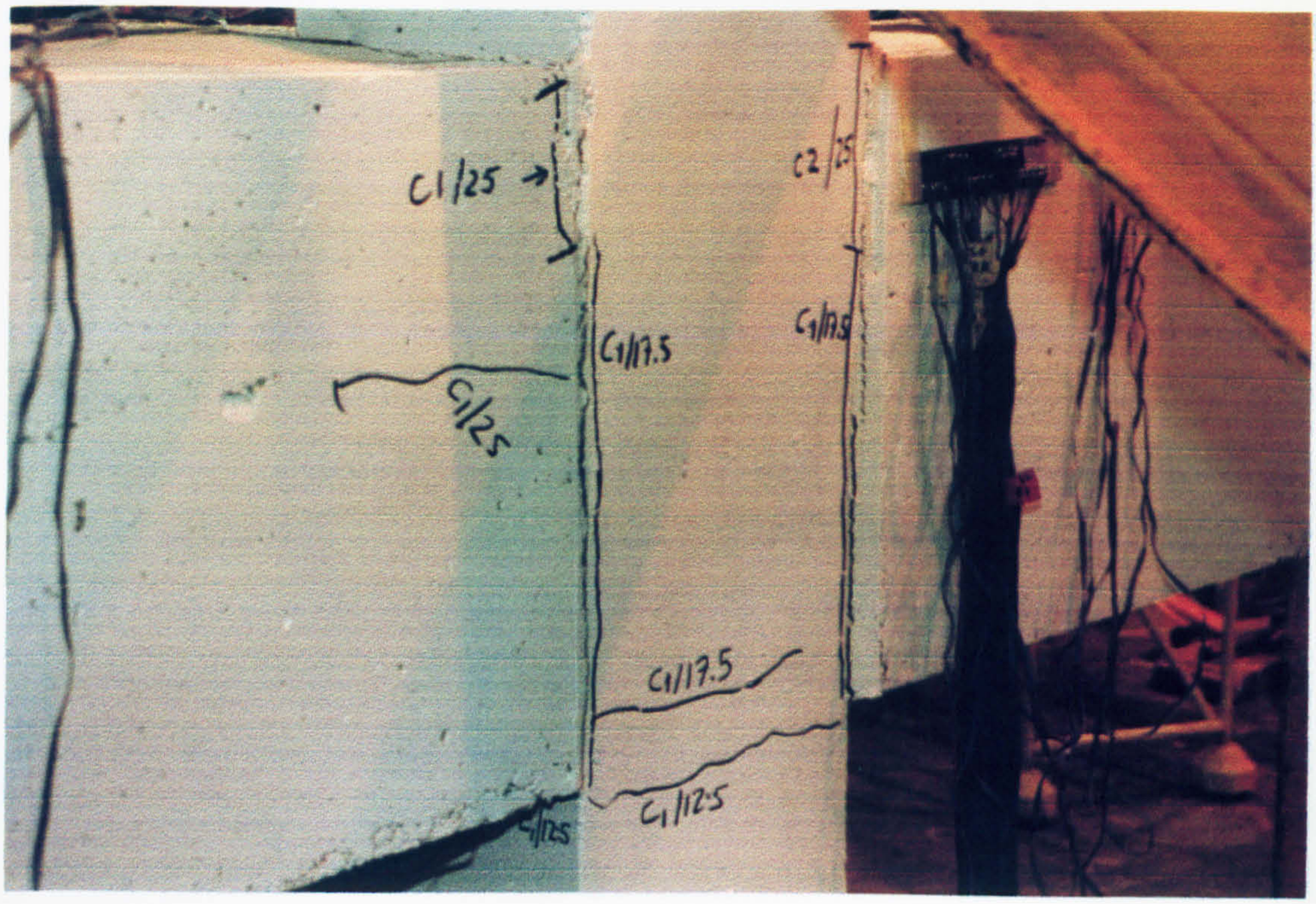

Plate 6.28: Damaged regions in the column from South in TB2

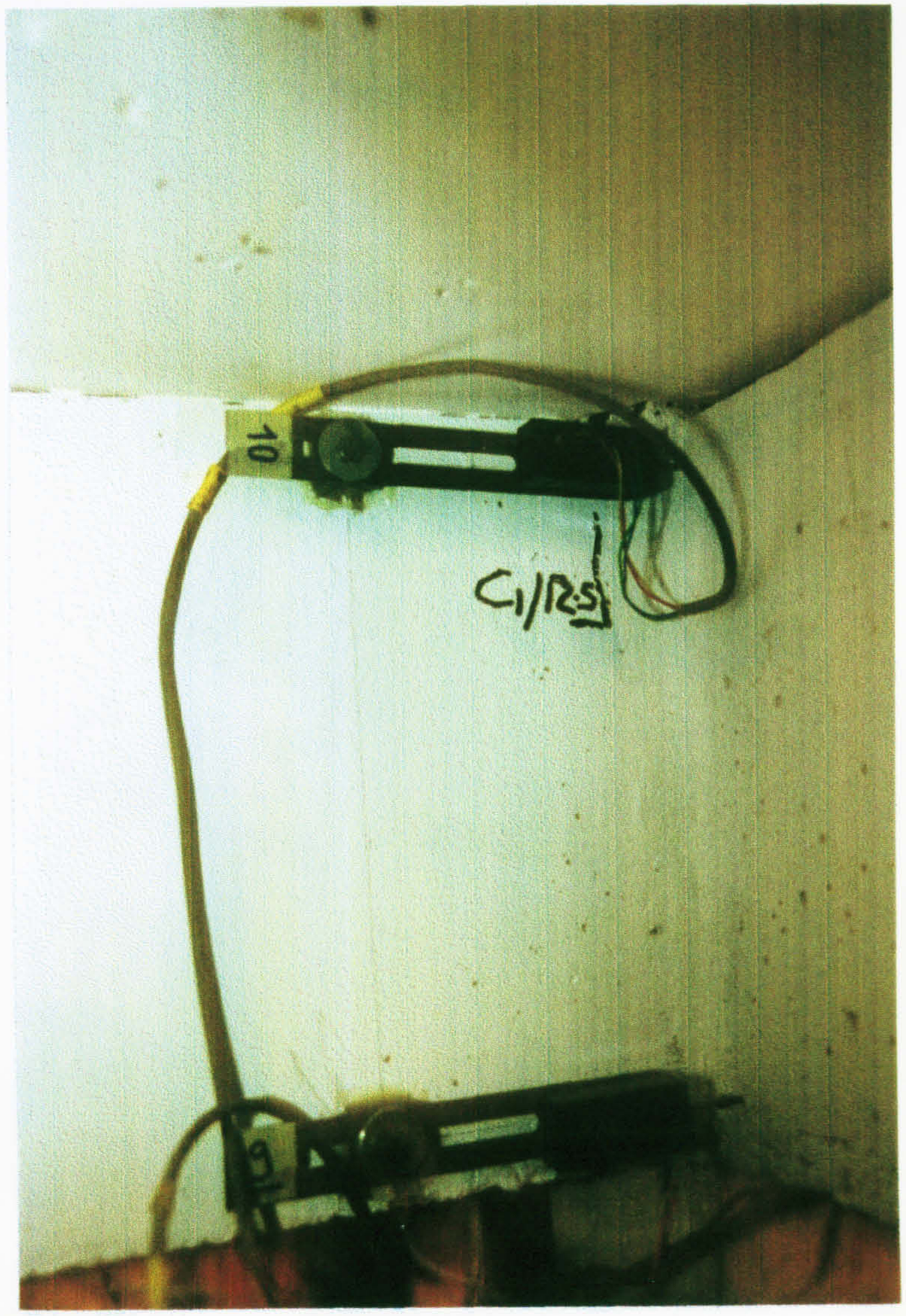

Plate 6.29: First cracks opening at joint-column boundary from East and West in TB2

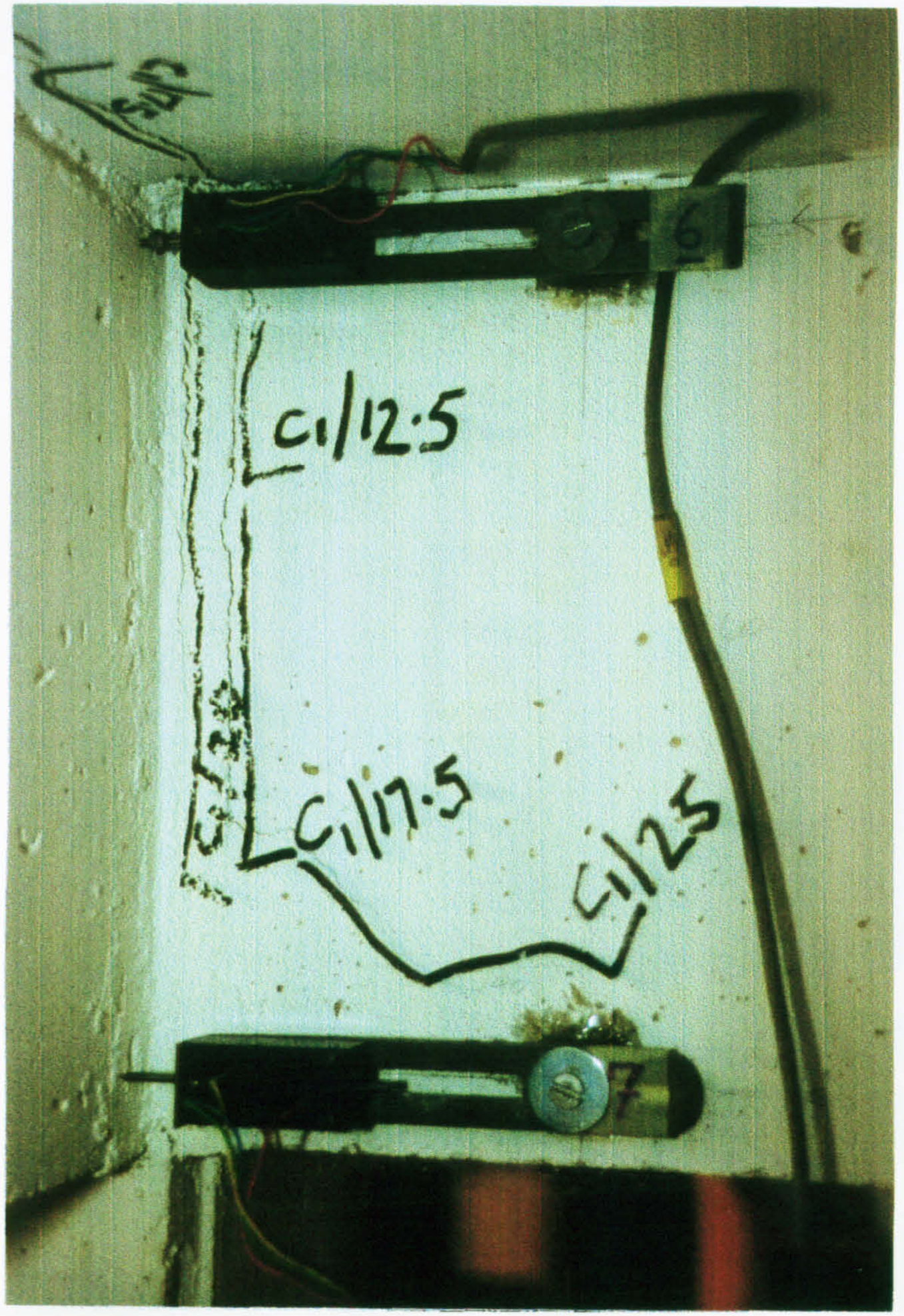

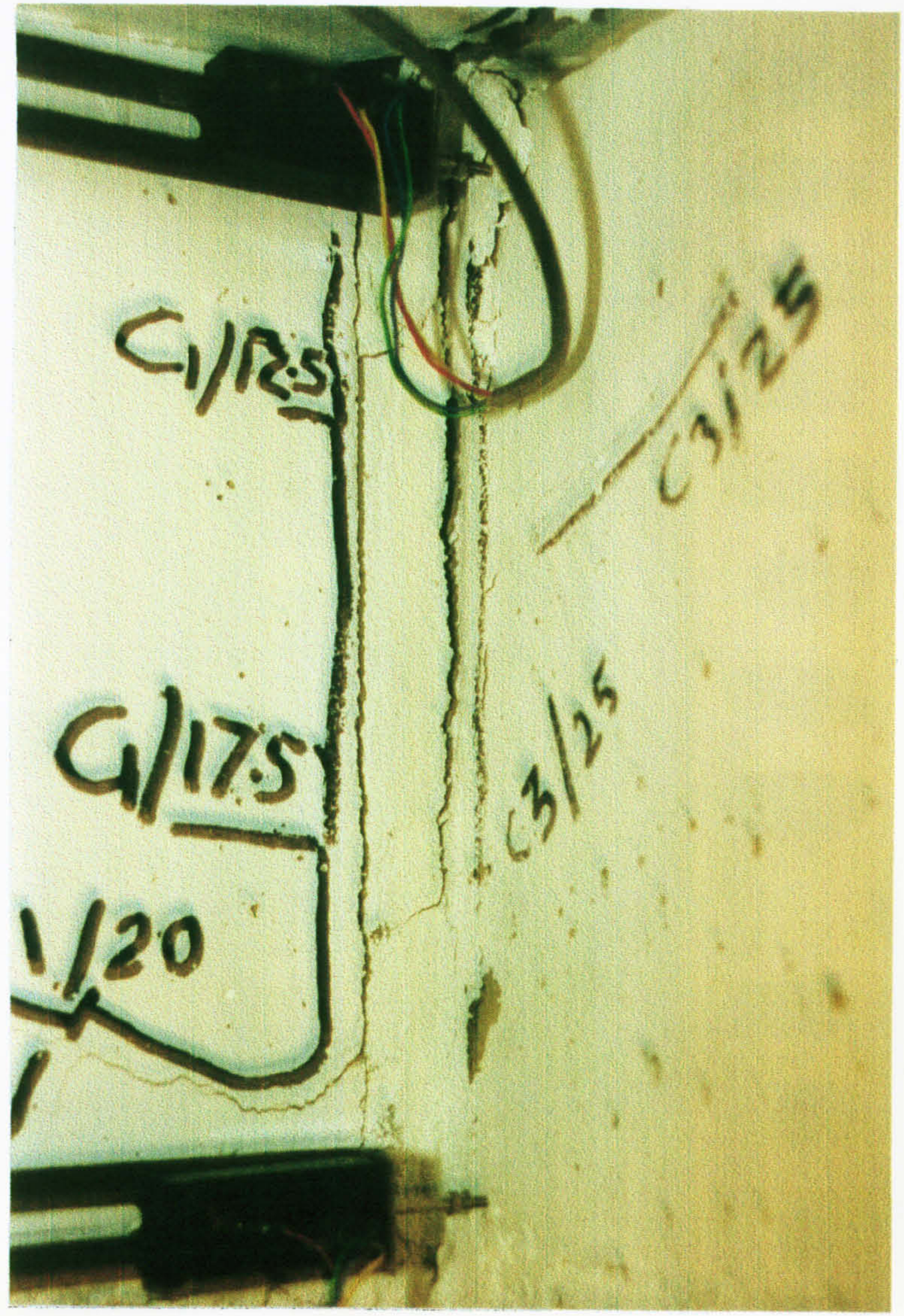

Plate 6.30: Damaged regions at joint-column boundary from East and West in TB2

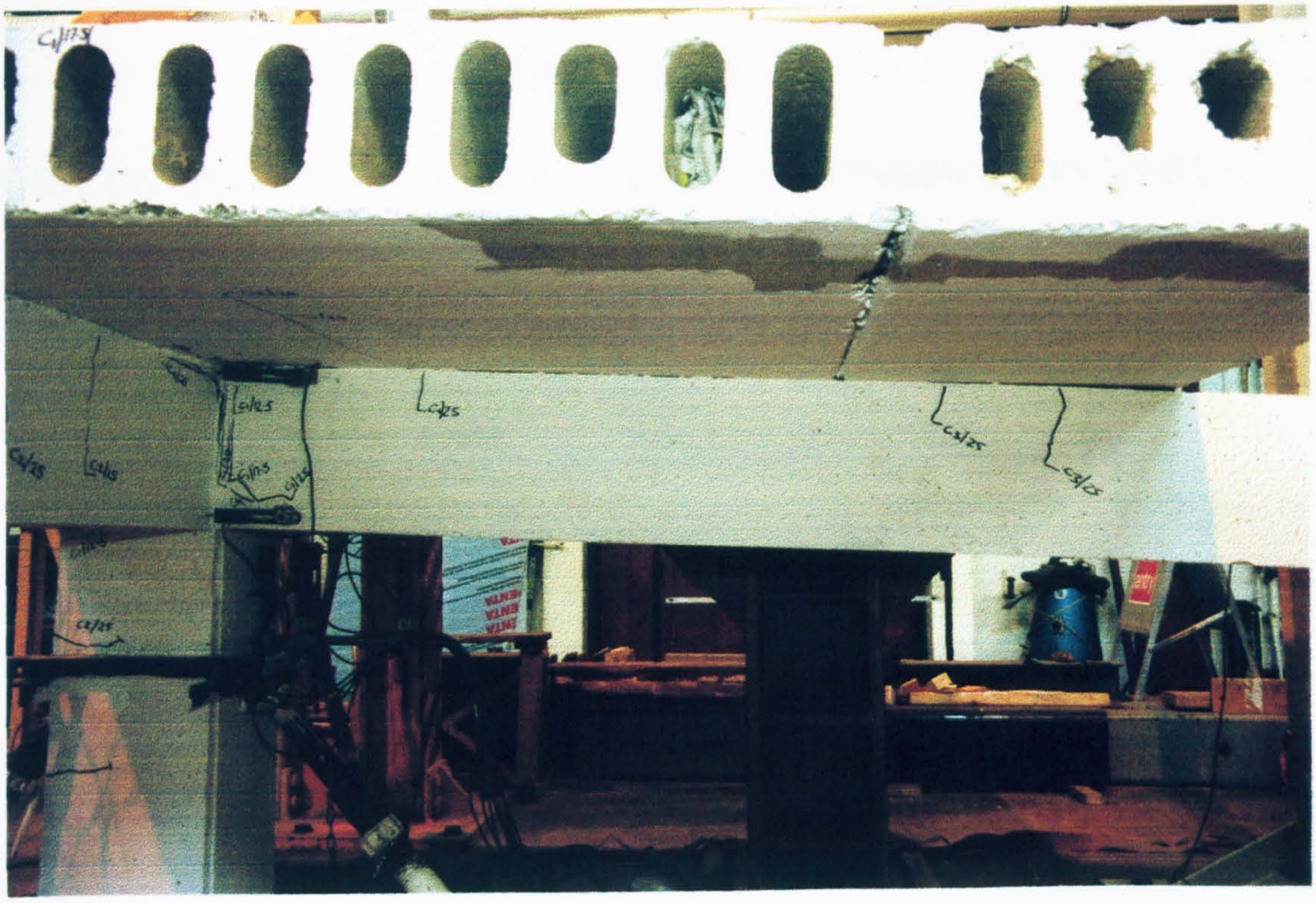

Plate 6.31: Damaged profile of the precast members from East in TB2

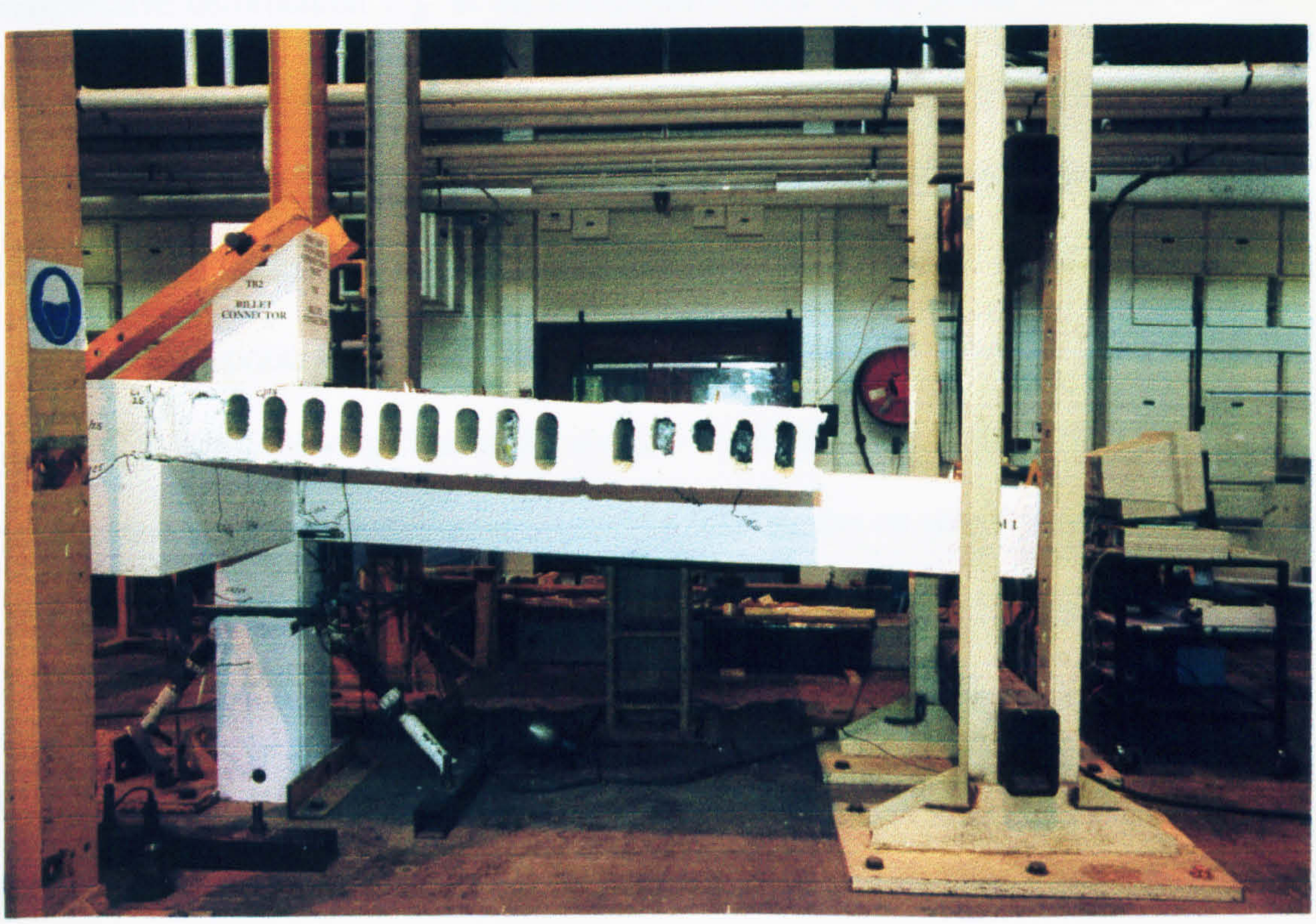

Plate 6.32: Deformed profile of the subframe from East in TB2

CHAPTER 7

DISCUSSION OF FULL SCALE FRAME CONNECTION TESTS

7.1 Introduction

The main aim of the experimental work on full scale frame connection tests has been to identify the moment-relative rotation $M_{con} - \phi$ characteristics and to recognise the inherent flexural stiffness J of the most widely used beam-to-column connections in precast concrete structures in the UK. Secondary behavioural information included crack opening δ_T at the boundaries of the slab (in-situ)/column and beam/column, compressive deformation δ_B in the compression zone in the joints, strain in the tie bars in the tension zone and strain in the concretes in the compression zone. The results, presented in Chapter 6, are discussed in this chapter and additional interpretative information, such as the comparison of all the tests in terms of the above mentioned behavioural is given. Figures 7.1 to 7.6 present moment versus crack opening. In the following figures the moment is plotted with respect to: Figure 7.7 compressive deformation in beams; Figure 7.8 steel strains on stability tie bars; Figure 7.9 compressive strains in beams and Figures 7.10 to 7.13 relative rotations.

The results indicate major differences in the response of the single sided test to the symmetrical double sided versions. The moment capacities of the connections are given in Table 6.1. The double sided connections achieved full capacity because the tie steel in the floor slab is fully effective, whilst single sided connections are limited by

the strength of the connection itself and less contribution from the slab as the tie steel is not fully effective. An important feature in the single sided tests results from the geometry of the tie steel which is a consequence of having to achieve continuity around a 90° bend. Forces in the tie bars are activated in two stages; firstly in the cranked part of the bars, and secondly in the part of the bars nearest to the main and edge beams. That the strains did not, in general, reach their uniaxial yield value indicates that the full plastic moment for the connections was not attained. This may be explained by the fact that the tie bars are cranked 45° to the direction of the tensile force. When the first cracks appeared in the in-situ concrete infill the bars are subjected to an eccentric tie force, thereby reducing their axial stiffness. Maximum strains were about 0.35 (TW2) to 0.50 (TB2) x yield strain, defined as 0.43% strain (BS 4461), when failure of the connection occurred due to bond slip in the tie bars and extensive cracking in the tops of the floor slab.

The results also show that at M_u the relative rotation ϕ_u = 10 to 15 mrad. for double sided and ϕ_u = 33 to 38 mrad. for single sided connections, respectively.

The zone of influence is defined as that region where the effects of the connection influence the $M_{con} - \phi$ behaviour both in the beam and column. It was found that the column contributes only to the flexibility of the single sided connections. The zone of influence in the beam depends on the type of connection. For the welded plate type, changes in rotation were measured at 450 mm from the centre line of the column, whereas in the billet type this distance was 300 mm.

7.2 Overview on the experimental work

The successful structural performance of precast concrete systems depends on the connection behaviour. The configuration of the connection affects the constructibility, stability, strength and flexibility of the structure. Furthermore, connections play an important role in the redistribution of forces as the structure is loaded.

Beam-to-column connections are essential to develop frame action in precast concrete buildings. The connections must develop sufficient strength to resist the applied loads and must have sufficient stiffness to limit the sidesway movement of the structure.

In this thesis, connections were examined for structural performance, as measured by forces and deflections from which the moment-rotation of the connections were calculated at the face of the column. Emphasis was placed on the behaviour of the connection subjected to gravity loading. Although seismic analyses were not performed, the connections were subjected to cyclic loading in order to observe their behaviour under reversed loading.

The action of the gravity and wind load on a building affects joint behaviour. The flexural strength and stiffness of the joint both affect sway of the columns and the moments transferred to connecting members such as beams and slabs.

In the case of the subframes tested, the simulated maximum gravity load applied at end of beam(s) induced moment in joints at the face(s) of column which are a measure of the moment transfer capacity of the joints. Consequently the load path which has been employed in the experimental work may be traced in three parts as follows :-

- load to beam by shear and bending

- beam to joint by shear and bending
- joint to column by shear and bending

The free ends of all beams and slabs in the experimental work were temporarily simply supported. Therefore, the shear forces at these locations in the beams, which were recorded by the load cells, are the actual applied bending forces from which the moments in the connections were calculated.

This load path has been defined as the global load path (Mahdi, 1992). It indicates that the joint constitutes an integral member (with zero length in analytical studies (Görgün, 1992)) of the structure particularly in transmitting forces to other connecting members. The magnitude of these forces depending on the type of subframe (double or single sided) and particularly the type of the connection (welded plate or billet) affects the size of the damaged zones in the joint and precast concrete members.

In addition to the global load path, there is a local load path associated with the joint being tested. This depends on how the connection was detailed. Figures A5.4.1 and A5.4.2 show the internal forces induced in the connections at the sections in the vicinity of the column faces, respectively for the welded plate and billet beam-to-column connections.

Using the local force path concept it was possible to formulate expressions for predicting moment capacity of the joints as presented in Tables 5.6 to 5.9. Due to the simplified nature of these expressions, it is therefore to be expected that the predicted moment capacities (Table 6.1) will be different from the experimental values. In the majority of the test carried out these expressions served as an approximate indicator of the maximum force applied to the end of the beam(s).

The member sizes and reinforcement of the precast concrete column and beam and their strength were chosen such as to simulate an actual building frame environment. The only exception was the length of the column and beams in tests TB1(B) and TB1(C), which were shortened due to mould restriction (casting two identical beams in the same mould) and location of holding down bolt holes in the strong floor in the laboratory.

7.3 Overview on the presentation of the test results

The graphical outputs of moment versus crack opening, compressive deformation, concrete and steel strains, vertical deflections and, most importantly moment versus relative rotations are assembled for tests carried out involving the welded plate and billet connections in order to facilitate comparison of the response of the joints to the applied bending moment.

In the presentation of the joint moment-rotation characteristics, the initial moment-rotation of the joints due to the self weight of the components was considered to be small.

7.4 Test series 1

7.4.1 Test TW1(A)

Figures 7.1 and 7.2 present a comparison of the moment versus crack opening at top of beams in the double sided, and at top of slabs in the double and single sided tests respectively, using welded plate connection.

In all the tests carried out flexural cracks were, as expected, first initiated at the column to joint interface at the top of the slab and the beam. This plane is therefore a plane of weakness due to the relative strength and stiffness of the two different materials in the joint and the beam.

A lower cover to the stability tie bars, longer span slabs and higher bond stiffness between the plate and the surrounding concrete could have reduced the value of the initial crack opening. The latter, without floor slabs, may be based on a pull out force calculated from the applied moment divided by a lever arm in the connection. This force may represent the integral of bond stresses operating along the welded plate. It is the deterioration in the bond strength which caused the crack opening in the tests (see later test TW1(C)). The variation in the magnitude of crack opening can be attributed to the quality of the concrete and the method of placing the concrete as these affect the bond strength.

It can be seen (see Figures 7.1 and 7.2) that the crack opening varies substantially in the region where the first flexural crack was induced in the connection. In the case of the double sided test TW1(A) the crack openings are much smaller than the corresponding ones in tests double sided beams only TW1(C) and single sided with floor slab and bar anchorageTW2 due to the effect of:-

a) for TW1(C) missing longitudinal bars at slab level as outlined in section 7.4.3

b) the slab in contact with the column was to lock the system due to bearing forces against the column, i.e. restrain the rotation

c) the symmetrical value of loaded connections, i.e. no moment in the column

Despite these effects, a transverse flexural crack (Plate 6.1) was first observed at an applied bending moment of M_{con} = 35.5 kNm corresponding a load of 15 kN being less than the 47.3 kNm observed in the single sided test TW2. The increase in the cracked moment in the test TW2 is due to the contribution of the bending flexibility of the column. The recorded crack widths at this point were 0.131 and 0.085 mm on either side of the column (Figure 6.2(a)). The largest cracks are, as expected, at the column to joint interface (Plate 6.2). These initiated at a moment of 35.5 kNm which coincides with the large reduction in stiffness seen in Figures 6.8(a) to 6.11(b) and may be interpreted as the point at which the section is cracked flexurally. With increasing rotation, the cracking became more widespread near the joints. The compressive and tensile stresses which the joint was not able to withstand led the crack to spread to larger areas around the joint, including the precast concrete beams. These cracks intensified in the zone, in the beam, at the soffit of the joint where they propagated horizontally indicating flexural overstressing resulting from the increased moment capacity of the joint. The column showed no sign of cracking. Apart from one or two minor deviations in the results the behaviour was generally anticipated with non-linear behaviour commencing at about 80 per cent of the ultimate moment, i.e. 190 kNm. Signs of compressive concrete failure in the bottom of the beam were evident.

Compressive deformations δ_B (Figure 7.7) were measured over a distance of 180 mm, i.e. 100 mm joint plus 40 mm precast beam and column. The maximum concrete strain calculated from these values is 0.0037, and being greater than 0.0035 ultimate strain at which concrete is normally assumed to crush explains the onset of failure at M_u. The 0.0037 strain including two interfaces between joint/column and joint/beam is greater than the compressive concrete strain 0.00347 recorded by the

surface strain gauges in the beams near to the joint zone at failure (Figure 6.4). One might say that 0.00347 ≅ 0.0037 when measuring concrete strains. It is true, but it indicates, however small, the effects of the presence of the interfaces which will be expanded on in Chapter 8. After the concrete in the tension zone failed to take any more tensile force, these were then taken by the tie bars which increased steel strains to more than 7000 με (A SG2 in Figure 6.5) and 5400 με (B SG1 in Figure 6.6), indicating significant yielding of the bars. Ultimate failure was due to significant yielding of the bars and concrete crushing failure in the joints

The moment-relative rotation $M_{con} - \phi$ results in Figures 7.10 to 7.13 and 6.8 to 6.10 show small variations in the different methods of measurement up to about M_{con} = 50 kNm, i.e. approximately 1/5 ultimate. The figures show the gradual deterioration in the stiffness soon after the cracks became widespread near the joints. This is because as the moment increased, this led to high compressive and tensile strain in the joint which resulted in cracking and spalling in the concrete and therefore a reduction in both the effective cross section area and the lever arm. The increase in the size of the cracked zone is an indication of the area of the plastification. A stage is reached where the joints are not able to withstand any more applied moment. At this stage the joint may be considered at its plastic moment of resistance M_u. Figure 7.10 shows that the moment-rotation behaviour is generally non-linear and the extent of the deviation from linearity is dependent on both the details of the connection and subframe. To this end, the scale of the moment-rotation curves reveal a great deal about the initial response of the joints, since the rotation is very small and therefore undetectable in the early stage of the loading history. Where necessary the behaviour during the loading cycles 1-3 is enlarged and presented separately (as Figure(a)) before

each of the corresponding results to failure (as Figure (b)) to evaluate the initial behaviour. Therefore the initial response of the moment-rotation results must be carefully interpreted. This is because in the majority of the moment-rotation graphs the joint might appear to have maintained full continuity of moment up to approximately 50% of the cracked moment M_{cr}. This could be attributed to the in-situ infill concrete which provided the initial tensile stiffness.

The increase in the moment capacity in the case of test TW1(A) compared with test TW1(C) is mainly due to the presence of the slab continuity longitudinal bars. These not only satisfied the stability requirements of the BS 8110 but also increased the main characteristics, moment (by 215%), rotation (by 46%) and stiffness (by 105%) of the connection. Currently, in practice this remarkable contribution of the floor strength and stiffness to the flexural capacity of the joint is neglected in the design process of the precast concrete frames.

The incorporation of the slabs satisfied other structural requirements such as composite action with the beam, and slab continuity in tension across the beam/column zone. These structural improvements significantly influenced the global strength and stiffness of the subframe tested. As mentioned this test was terminated because of the significant yielding of the bars and concrete crushing failure in the joints. This indicates that the flexural continuity of the connection was being maintained to the extent that it weakened the bars and joint concrete. Thus flexural behaviour of test TW1(A) suggests that the slab could be idealised as a 200 mm deep beam acting compositely with the main 300 mm deep beam. It has been found by Mahdi (1992) that the out of plane dimensions of slab carry no structural significance other than imposing gravity forces on the beam.

At no point do the rotations obtained using *Eq*.6.1(*d*) and *Eq*.6.2(*b*) differ by more than 8% and 13% of one another for beams 1 and 2, respectively. This will give greater confidence when using the "component method" based on the horizontal deflections from the isolated joint tests in Chapter 8.

The horizontal deformations at the top of the beam (Figure 7.11) were in linear relationship with δ_T and δ_B, showing that the beam and slab were rotating as a rigid block. These data also showed that the neutral axis for the flexurally cracked section was near to the level of the welded plate connection. An exact agreement was obtained between the rotations derived using M2 S1 and M2 B1 (see Figure 6.10(b)). This shows that, within the normal scatter experimental work of this type, either method may be used to generate $M_{con} - \phi$ data, and is the first step towards the validation of the "component method" (see later in Chapter 8)

The lowest tangent flexural stiffness, J_c = 45,800 kNm/rad. (M1 B1 V4), is obtained using Method 1, compared with values of about J_c = 50,000 kNm/rad. (M2 S1) and J_c = 49,500 kNm/rad. (M2 B1) using Method 2. It is for this reason that all subsequent results and design values will be based on Method 1 V4 (see *Eq*.6.1(*d*)).

In Figure 6.11(a) (Method 1) the tangent and unloading stiffnesses of the connection for Beam 2 is always greater than the Beam 1 because of more cracks on Beam 1 side (see Plate 6.1). The tangent stiffnesses decrease very rapidly due to the first flexural tensile (transverse) cracks occurring at low loads and gave low stiffness in cycle 1. These cracks reduced the contribution of the tensile stiffnesses of the slabs to the stiffnesses of the connections. Repeated loading and unloading in cycle 2 reduced this effect, hence increased the stiffnesses of the connections. There is no significant

change in stiffnesses in cycle 3. The stiffness decreased in beam 2 side in cycle 4, because the stiffness decreases with an increase in moment and damage in the previous cycles and came close to the stiffness in beam 1 side. This is an indication of the failure to take place at Beam 2 side.

In Figure 6.11(b) (Method 2) in addition to the observations in Figure 6.11(a), the stiffnesses obtained from the slab rotations are less than those obtained from the beam rotations in the cycles 1-3, unlike in the cycles 4-5 as a result of more cracks far from the column faces giving less crack opening at column/slab (in-situ) boundaries. By comparing the results of the two Methods it is found that the Method 1 gives a lower tangent stiffnesses than the Method 2 in each cycle for both beams and joints.

The mean ultimate moment M_u value 237.90 kNm, ultimate rotation ϕ_u = 10.3 and 9.5 mrad and secant stiffness J_s = 25450 and 27100 kNm/rad were achieved in this test using Methods 1 and 2, respectively. The value 0.70 x the actual ultimate moment capacity of the composite beam M_{beam} was attained. Currently, in practice this remarkable contribution of the strength and stiffness to the flexural capacity of the precast concrete members is neglected in the design process of the precast concrete frames.

7.4.2 Test TW1(B)

The shear resistance of the entire connection was found to be satisfactory after the bending moment capacity of the connection was obtained. The beam-to-column connection tested was of 278 kN design shear capacity, which was obtained in the test without significant change in the behaviour of the connection. It gave confidence that

the connections may be identified not only by their shear capacity but also by their rotational stiffness, flexural strength as well as ductility.

Although it was not intended to study the semi rigidity of the connection in this test, it was possible to gain some understanding of the degree of connection stiffness because the experimental ratios of applied load vs connection reaction P/V were 1.163 and 1.138 for the beams 1 and 2, respectively. These were closer to the rigidly connected analytical value of P/V = 1.113 than for the pinned connection value of P/V = 1.374, as shown in Figure 6.12.

7.4.3 Test TW1(C)

This test was a continuation of test TW1(A) in which 200 mm deep hollow core slabs and tie bars were removed in order to evaluate the reductions in the main characteristics of the connection due to the absence of these items. The crack openings and compressive deformations were obtained using the same POTs and drilled holes used in test TW1(A) for the beams to compare the results with those obtained in test TW1(A).

The joints in test TW1(C) showed different patterns of cracking from those of the test TW1(A) as the cracks are greater and more in linear registration with moment than in the test TW1(A) due to the absence of the slabs (see Figure 7.1). The variation in the magnitude of the crack opening can be attributed only to the quality of the weld. Because the first flexural tensile vertical cracks were initiated at an applied bending moment of 9 kNm at the boundaries between the joint and column, and beam and joint interfaces where the maximum flexural stress takes place. The change in the slope of the moment vs crack opening curve is too small to be considered after the first cracks.

The cracks spread rapidly and vertically down to the compression zone (see Plates 6.11 and 6.12). The total crack widths (Figure 6.13) reached to 0.39 and 0.46 mm at the peak value of the cycle 1 loaded up to 30% of the anticipated moment. At the end of unloading in cycle 1, the total crack widths were partly recovered elastically and the deformations 0.15 and 0.19 mm remained as permanent deformations in the joints. The crack widths increased to 1.83 and 2.02 mm for the beams 1 and 2, respectively, at the ultimate moment capacity of the connection. Both crack widths nearly attained the same value of 1.83 mm at the same moment as shown in Figure 6.13. This moment was the failure moment for the beam 1.

The stiffness of the joint slightly reduced after cracking. Two more cycles were repeated in a similar manner to cycle 1. There were no significant changes in stiffness although the linearly elastic regions increased. The fourth cycle was applied to 50 % of the anticipated ultimate moment. The initial stiffness of the fourth cycle was similar to the previous two cycles, but it reduced after the peak values of the first three cycles was exceeded. Finally the fifth cycle was applied to failure to obtain the ultimate strength of the joint regardless of the slabs and the bars.

The compressive deformation of the joints δ_B (Figure 6.14) increased rapidly after the first flexural cracks. Greater crack widths of the beam resulted in greater compressive deformation of that beam to column joint concrete, due to the rigid body movement of the end of the beam as in test TW1(A). The maximum compressive deformations δ_B at failure were 0.25 and 0.21 mm for beams 1 and 2, respectively, measured over the same distance of 180 mm in the test TW1(A). The maximum concrete strain calculated from these values are 0.0014 and 0.0012, and being smaller than 0.0035 ultimate strain at which concrete is normally assumed to fail explains the

onset of unfailure at M_u (see Plates 6.11 and 6.12). After the concrete in the tension zone failed to take any more tensile forces, all forces induced in this zone were taken by the weld. The failure was due to weld breaking failure in the joint in beam 1. This indicates that the flexural continuity of the connection was being maintained to the extent that it weakened the weld. This provided important information on the pure plastic moment capacity of the welded plate connection itself to give a reference datum being independent of the slabs, the stability tie bars to evaluate performance of the connection with these two items used in test TW1(A). This has been done as presented in Section 7.4.1.

Unlike in test TW1(A) a disagreement between the joint and beam deflections and their distance from the face of the column was observed (Figure 6.15). The beam-to-column joints give more deflections in POTs 11 and 12 due to the splitting of the joints concrete. The gradients of the beam deflections in Figures 6.15(a) and (b), and Plates 6.11 and 6.12 clearly indicate that joint has two rotations at its ends, namely (a) at the infill-to-column interface, and (b) beam-to-infill interface. The latter is greater in this test due to the absence of the removed items giving a freedom to the beam end plate to rotate at the face of the solid billet projecting from the column face as if it was the centre of the joint. This does not enable the use of Method 1 to derive the rotations as it gives very small rotations (as shown in Figures 6.16 and 6.17) and hence very high stiffnesses. It was decided to use Method 2 to evaluate moment-rotation behaviour of the connections in this test.

The moment-rotation curves in Figure 6.18 obtained using Method 2 showed similar behaviour to the moment crack width curves in Figure 6.13. The rotations at the ultimate moments reached to the values of 6 and 7 mrads. for beam 1 and beam 2,

respectively, which is less (32%) than corresponding mean rotation about 9.5 mrad in the test TW1(A). This indicates that the ductility of the connection is a function of the ductility of the reinforcement used as stability tie bars.

The values 0.32 x ultimate moment M_u, 0.68 x ultimate rotation ϕ_u and 0.49 x stiffness J_s in test TW1(A) were achieved in this test using Method 2. These deteriorations can be attributed to the absence of the removed items and the quality of the weld.

7.5 Test series 2

7.5.1 Test TW2

In the case of single sided test TW2 the cracks are more diagonal than in the double sided tests. A transverse flexural crack was first marked at an applied moment of 47.3 kNm being greater than 35.5 kNm in test TW1(A). The measured crack widths (using crack width measurement) at this point were 0.04 and 0.06 mm on either side of the column (see Plate 6.13). The recorded crack width at this moment in Figure 6.20(a)) is 0.26 mm being greater than the above values, because it includes the tensile deformation of the in-situ infill concrete over a distance of 100 mm from the column face. The largest cracks are, as expected, at the column to in-situ interface (Plate 6.14). These initiated at the same load, which coincides with the large reduction in stiffness seen in Figures 6.26(a) to 6.28. Unlike in the double sided test TW1(A) the magnitude of crack opening has increased after the first flexural cracks due to the effect of the slab and the nonsymmetrically loaded connection inducing moment in the

column, hence increasing the cracks. The column in this test was heavily cracked by comparison with all the tests carried out.

Horizontal bursting cracks are a clear indication of unconfined concrete compressive failure in the in-situ concrete infill. A second horizontal crack occurs at the level of the top surface of the solid steel billet, and is possibly indicative of local stress concentrations there as in test TW1(A). Unlike test TW1(A) the damaged zones are not only limited in the beams and joint but also big damage occurred in the column tension up to about 220 mm above slab in-situ infill (Plate 6.14) and compression zones 160 mm from the top level of the edge beam to downward (Plate 6.17 left) and about joint size 100 mm below the joint (Plate 6.16).

Surprisingly, it seems that the interface has no affect on the compressive strain or deformation in the joint zone in this test. Also, it should be noticed that the SG1 recorded more strain than the others at a moment value of between 115.15 and M_u = 156.43 kNm due to the extent of the damaged zone in the beam. The compressive concrete strain obtained from the strain gauge in the beam near to the joint zone at failure was 0.00328. After the concrete in the tension zone failed to take any more tensile force, these were then taken by the tie bars in two stages; firstly in the cranked part of the bars, and secondly in the part of the bars nearest to the main and edge beams. That the strains did not, in general, reach their uniaxial yield value which indicates that the full plastic moment for the connection was not attained. Although the full plastic moment of the connection was not attained, it was mentioned earlier that the column in this test was heavily cracked by comparison with all the tests carried out. This suggests, structurally speaking, that the flexural continuity of the connection was being maintained to the extent that it weakened the column. This requires a strong

column to be used at the connection between the beam and external column. The ultimate moment M_u = 156.43 kNm was about 2/3 of M_u in test TW1(A).

The moment-relative rotation $M_{con} - \phi$ results in Figure 6.26 show very small variations in the Method 1 up to about ultimate moment, which was not the case in test TW1(A). By comparing Figure 6.26(a) and Figure 6.27(a) it is seen that there is no rotation obtained using the Method 2 up to the M_{cr} = 34.84 kNm (which is about $0.22 M_u$) because there was almost no crack opening (see Figure 6.20), which is the key parameter in using Method 2, up to this value. It seems that the Method 1 is more reliable because of being independent of the horizontal deformations than the Method 2. The largest rotation was once again obtained using *Eq*.6.1(d) as ϕ_u = 38 mrad which is 3.75 x ϕ_u in the test TW1(A). This large difference is due mainly to the contribution of the bending stiffness of the column to the flexibility of the connection. In the test TW1(A) there was no moment in the column being symmetrically loaded. However, in this single sided test M_u was distributed into the column at the top and bottom level of the joint producing a double curvature in the column as in a real frame environment.

It was found that no matter the type of the subframe. (double sided or single sided). Method 1 V4 gives the lowest stiffness and largest rotation, which can be seen in Figure 6.28 in each cycle.

Overall, the values 0.66 x ultimate moment M_u, 3.75 x ultimate rotation ϕ_u and 0.18 x stiffness J_s in test TW1(A) were achieved in this test using Method 1.

7.6 Test series 3

This test series 3 included three tests on double sided slab-beam-column full scale (internal) subframe SF1 assemblage TB1(A), and double sided in-situ-beam-column subframes TB1(B) and TB1(C) incorporating two way billet connection. In the test TB1(C) the RHS billet in the column and beam end plate (Figure 5.9) were not incorporated. The aim of the tests TB1(B) and TB1(C) where smaller length beams were tested was an attempt to simplify even further the full scale tests.

7.6.1 Test TB1(A)

Figures 7.3 and 7.4 present comparison of moment versus crack opening of the tests on double and single sided slab-in-situ/beam-to-column subframes incorporating billet connection. These figures show that tests TB1(B) and TB1(C), which were based on smaller length beams and in-situ infill concrete only, were terminated due to the bond failure of the joint. They exhibited much less ductile failure than the tests TB1(A) and TB2 which were based on the double and single sided long span beams with floor slabs. Test TB2 was terminated due to the sudden failure of the joint. Figures 7.5 and 7.6 present the comparison of moment versus crack opening at top of slabs and beams in four main tests using welded plate and billet connections.

Examination of the joint after the test ended revealed that failure in test TB1(A) was due to the significant tensile yield failure of the longitudinal 2T25 tie bars rather than the fracture of the tie rod at the top level of the beam. The strength of the joint was mainly dominated by the fully effective stability tie bars.

Also, in this full scale test a transverse flexural crack was first observed at an applied bending moment of 35.5 kNm (see Plate 6.18), at the same load and location as in the test TW1(A). The measured crack widths at this point were 0.01 mm on either corner of the column on one side, and 0.4 mm (being the largest crack) and 0.2 mm at slab to slab joints, respectively on beams 1 and 2 sides and 0.05 at the column to joint interface. These initiated at the same load, which coincides with the large reduction in stiffness seen in Figure 6.37 and were interpreted as the point at which the section is cracked flexurally.

The compressive deformations δ_B (Figure 6.30) at failure was 0.57 mm for beam 1 (not available for beam 2) measured over the same distance of 180 mm in the test TW1(A). The concrete + grout strain calculated from these value is 0.0032, and being less than 0.0035 ultimate strain at which concrete is normally assumed to fail. The compressive concrete strain obtained from the strain gauges in the beams near to the joint zone at failure were 0.0018 and 0.0011, respectively for beams 1 and 2 (Figure 6.31) < 0.0032 (includes two interfaces). It once again tells us the affect of the interface. Generally, the strains in the grout were greater than those in the concrete. It is hard to find a reason to explain that the maximum concrete strain (should not be confused with strain at M_u) in beam 2, measured at the same distance from the column face as the strain in the grout reached a value of 8080 με. This was not the case for beam 1 (1800 με). Comparison of moment versus compressive strains in beams in the four main tests is presented in Figure 7.9. Steel strains increased to more than 18600 με (A SG2 in Figure 6.32) and 20500 με in Figure 6.33, indicating significant yielding of the bars. Ultimate failure was due to significant yielding of the

bars, and crushing failure of the grout and concrete in the joints and beams, although it was not as badly damaged as in test TW1(A).

The moment-relative rotation $M_{con} - \phi$ results in Figures 6.35 and 6.36 show small variations in the different methods of measurement up to about M_{con} = 60 kNm.

Figure 6.37 shows the tangent and unloading stiffnesses of the connections. There is no significant change in stiffnesses in cycle 3. The stiffnesses decreased in cycles 4 and 5 because of the repeated loading and unloading damaging the components. The slab rotations are less than those obtained from the beam rotations in the cycles 1-4, unlike in the cycles 5 as a result of more cracks far from the column faces giving less crack opening at column/slab (in-situ) boundaries. By comparing the results of the two Methods it is once again found that the Method 1 gives the lower tangent stiffnesses than the Method 2 in each cycle.

The mean values of 189.78 kNm ultimate moment M_u, 15.36 and 7.66 mrad ultimate rotation ϕ_u and 12990 and 27440 kNm/rad secant stiffness J_s were achieved in this test using Methods 1 and 2, respectively.

Comparing the two tests TW1(A) and TB1(A) the values 0.80 x ultimate moment M_u, 1.5 and 0.81 x ultimate rotation ϕ_u and 0.50 and 1.0 x stiffness J_s in test TW1(A) were achieved in this test using Methods 1 and 2, respectively.

7.6.2 Test TB1(B)

First transverse flexural cracks were marked at an applied bending moment of 24.0 kNm at the locations in Plates 6.21 and 6.22. This is same as in the test TB1(A) and suggests that the slabs being replaced with in-situ infill concrete only do the same job

when the section is uncracked flexurally. The measured crack widths at this point were not more than 0.15 mm on either of the column then increased to 0.2 mm at 75 kN in cycle 3.

Large flexural cracks initiated at 76.5 kNm in cycle 4 at the top middle of the in-situ infill concrete are extended down to and stopped by the top of the projecting billet from the column. The largest cracks were expected to be a continuation of the first cracks at the column to joint interface. These would have been transferred to their right locations (column to joint interface) if the slabs were used, even the absence of slabs has no effect on the first cracks.

The compressive deformations δ_B (Figure 6.39) at failure were 0.3 mm for both beams measured over the same distance of 180 mm in the test TW1(A). The concrete + grout strain calculated from these value is 0.00167 (was 0.0032 in TB1(A)) The compressive concrete strain measured from the strain gauges in the beams near to the joint zone at failure were 0.000531 and 0.000648, respectively for beams 1 and 2 (Figure 6.40) < 0.00167 (includes two interfaces). It is once again found that the maximum concrete strain in beam 2 at the same distance for joint centre from the column face (60 mm) reached a value of 1800 με. Steel strains in Figures 6.41 and 6.42 increased to more than 2560 με and 2435 με, being much less when compared with 18600 με and 20500 με, in TB1(A), indicating possible yielding of the bars. Ultimate failure was due to the in-situ infill concrete flexural (bond) failure above the mid-span of the beams.

The moment-relative rotation $M_{con} - \phi$ results in Figure 6.43 show small variations in the different methods of measurement up to about M_{con} = 60 kNm and very good agreement between M_{con} = 60 and 107 kNm, except M2 B1. The rotations

obtained using M2 B1&B2 come close as M_{con} approaches to ultimate value. The results also show that the relative rotation $\phi_u = 6$ mrad for M2 B1 and $\phi_u = 7$ mrad for M2 B2. They are quite small but need to be compared the values in test TB1(A) obtained using the Method 2. This has been done and it was found that the ratio of these rotations to the corresponding (available) rotation in test TB1(A) is 0.76 and 0.92. It indicates that the use of this test arrangement to replace full tests with slabs would not make difference more than 24% as far as the ductility of the connection is concerned. This also indicates that it would be possible to obtain the full strength and ductility of the test TB1(A) by employing longer beam length to prevent bond failure.

Figure 6.44 shows the tangent and unloading stiffnesses of the connections. There is an increase in slab 1 stiffness in cycle 3 as a result of more cracks far from the column face giving less crack opening at in-situ/column boundary.

Comparing tests TB1(A) and TB1(B) the values 0.97 x ultimate moment M_u, 0.84 x ultimate rotation ϕ_u and 1.07 x stiffness J_s in test TB1(A) were achieved in this test.

7.6.3 Test TB1(C)

In this test the RHS billet in the column and beam end plate (Figure 5.9) were not incorporated. First transverse flexural cracks were observed at an applied bending moment of 15 kNm, being less than the applied moment at which the first cracks were marked in TB1(B) by 7.7 kNm, at the locations in Plates 6.23 and 6.24. This reduction in moment is due possibly to the absence of the above items (RHS billet and beam end

plate), and may be accepted as the second finding that the items have influence on bending load or moment bya factor of 1.5 at which the section is cracked flexurally.

The compressive deformations δ_B (0.41 mm and 0.37 mm) in Figure 6.46 and concrete strains (0.000873 and 0.000697) in Figure 6.47 measured near to the joint zone at failure were greater than the values in the test TB1(B), respectively for beams 1 and 2. Steel strains in Figures 6.48 and 6.49 increased to more than 2900 με and 2830 με being also greater than the values in the test TB1(B). This does not necessarily mean that this connection is stronger, because the stability tie bars used in this test were weaker than the bars used in the test TB1(B). (Full information about the stability tie bars used in all the test carried out is presented in Table A5.4.1 in Appendix 5.4.) Ultimate failure was due to the in-situ infill concrete flexural failure above the mid-span of the beams similar to the test TB1(B). The ratio of the ultimate failure moment of test TB1(C) / TB1(B) is = 0.97.

The moment-relative rotation $M_{con} - \phi$ results in Figure 6.50 show very good agreement up to about M_{con} = 75 kNm. The above mentioned horizontal cracks cause less slab (in-situ) rotations than the beams thereafter. At M_u the relative rotation ϕ_u = 6.2 mrad for M2 B1 and ϕ_u = 7.4 mrad for M2 B2. These are close to 6 and 7 mrad in test TB1(B). The ratio of these rotations to the corresponding rotation in test TB1(A) is 0.81 and 0.97. This shows that the use of this test arrangement to replace full tests with slabs is even better than the test TB1(B) by improving the above 24% difference in rotation to 19% as far as the ductility of the connection is concerned. This improvement in the ductility was not the case for the strength of the connection where a value of 0.93 x the ultimate strength of the test TB1(A) was

achieved in this test. This test gives approximately the same secant flexural stiffness as in test TB1(A).

Figure 6.51 shows the tangent and unloading stiffnesses of the connections. The increase in slabs stiffness in cycle 5 is also due to the horizontal cracks being exception to the observations in the test TB1(B) values.

Comparison of the two tests TB1(A) and TB1(C) indicated that the values 0.93 x ultimate moment M_u, 0.89 x ultimate rotation ϕ_u and 1.02 x stiffness J_s in test TB1(A) were achieved in this test.

7.7 Test series 4

7.7.1 Test TB2

The joints in test TB2 showed different patterns of cracking from those of the test TB1(A) as the first cracks are more diagonal starting from the corners of the column and spreading into the slabs with 45°. In this single sided full scale test, cracks were first marked at an applied bending moment of 29.6 kNm being the lowest value test series (TW1(A), TW2, TB1(A)). The measured crack widths at this moment were 0.1 mm on either internal corner of the column (see Plates 6.25 to 6.27). The recorded crack opening at this moment was 0.18 mm, even there was no crack at the face of the column where crack opening was recorded. This explains that the recorded crack opening should not be interpreted as the surface cracks. They are only the tensile deformation of the in-situ infill concrete, over the top of the beams, up to where the first cracks appear at the face of the column passing between the measuring points. The recorded crack opening is a quantity that is used in conjunction with compressive

deformation to derive the relative rotation of the beam to column using Method 2. The cracks are also, unlike the test TW2, observed at the column to edge beams (Plate 6.28) and at the column to in-situ interfaces (Plate 6.29). This may be attributed to the rotation of the edge beams due to the dowel action of the tie rods. These cracks initiated at the same moment, which coincides with the large reduction in stiffness seen in Figures 6.60(a) to 6.60(b). At a moment value of 38.83 kNm a horizontal crack was observed from the joint grout to the main beam at the mid-height of the billet due to the overstressing of the concrete in compression in the beam that cover the billet. This became a point from which the behaviour of all curves in each graph entered into a new region with large increase in the magnitude of the deformations and strains.

The compressive concrete strain measured from the strain gauges in the beam near to the joint zone at failure was 0.0015. The grout strain (0.0051) in the joint was greater than the concrete strain in the beam. The maximum concrete strain in the beam at the same distance from the column face as the grout strain reached a value of 10100 με (Figure 6.54). Minimum and maximum steel strains were about 670 and 2600 (Figures 6.55 and 6.56) when failure of the connection occurred due to bond slip in the tie bars and extensive cracking in the tops of the floor slab and concrete crushing failure in the beam surrounding the billet. This large difference is due mainly to the geometry of the bars and location of the strain gauges in single sided tests. The failure moment in this test relied on the shear capacity of the tie rod. This test was terminated due to the sudden failure of the joint indicating that the tie rod is the key parameter for ensuring continuity of load transfer to the column and therefore it is the controlling parameter in the design of the single sided connection as the floor slab and stability tie bars are not fully effective. In a real frame environment this would give rise to a

dangerous failure, therefore it must not be employed at the beam to external column locations as semi-rigid partial strength connection. Appendix A5.4 reports an average ultimate shear capacity of the tie rod of 89.07 kN that induces a predicted moment value of 26.25 kNm in the joint without slabs. The test results without slabs and tie bars are not available for the billet connections. The contribution of the less effective slabs and tie bars, based on the measured strength, increased the strength of the joint by 120% whereas this increase was 625% in the double sided test TB1(A) to compare with their predicted values.

The moment-relative rotation $M_{con} - \phi$ results in Figure 6.58 show excellent agreement using Method 1 up to about M_{con} = 40 kNm and this limit falls to about M_{con} = 25 kNm for the Method 2 in Figure 6.59. By comparing the above figures it is seen that the Method 1 gives greater relative rotation. The largest rotation was once again obtained using *Eq*.6.1(d) as ϕ_u = 33 mrad (was 38 mrad in TW2) which is 2.16 x ϕ_u in the test TB1(A). This large difference is due mainly to the contribution of the column to the flexibility of the connection, although it was not as badly damaged as in test TB2.

It was found that no matter the type of the subframe or connection studied, it is the Method 1 V4 which gives the lowest stiffness and largest rotation. The validity of the above observation can clearly be seen in Figure 6.60 for the tangent and unloading stiffnesses of the connection in each cycle.

Comparing the two tests TB1(A) and TB2 the values 0.31 x ultimate moment M_u, 2.16 and 2.45 x ultimate rotation ϕ_u and 0.30 and 0.38 x stiffness J_s in test TB1(A) were achieved in this test using Methods 1 and 2, respectively.

7.8 Summing up

In this section, the performance of the connections have been compared based on their flexural strength, relative rotation and flexural stiffness. Most of the subframes were subjected to the same beam end vertical bending load distance to the face of the column to facilitate comparison of test results. The measured and predicted ultimate moments of the connections are listed in Table 6.1. It is clear that the predicted flexural strengths of the connections are greater than those measured. This was mainly due to the variable strength of contiguous materials being much greater than each other, uncertainties of the contribution of the each individual component, simplifications made in the calculations and most likely the geometry of the subframes. The ratio of the measured experimental flexural strengths of the connections to those of the predicted M_u/M_{pred} varied from 0.84 to 0.95 in the double sided subframes but to between 0.29 (TB2) and 0.65 (TW2) for the single sided subframe tests.

Comparing the ultimate strength of the connections in the four main full scale tests in Figures 7.10 to 7.13, it is clear that the flexural strengths of the welded plate connections were greater than those of their billet counterparts. This was mainly due to the ultimate tensile resistance F_{wt} in the weld being much greater than the horizontal shear resistance P_s in the M16 tie rods used in the bolted billet connection tests. The lever arm of these forces also helped to increase the bending strength of the connections. The measured experimental flexural strength M_u = 238.78 kNm of the double sided welded plate connection TW1(A) is greater than the billet connection TB1(A) M_u = 191.34 kNm by 25%. This should be interpreted as the reduction due

mainly to the type of the connection. The reduction from 238.78 kNm to 76.34 kNm in TW1(C) by 68% is due to removal of the contribution of the fully effective stability tie bars and floor slabs, being greater than 162.44/76.34 = 2.13 x connection capacity itself. Finally, the large difference from 238.78 kNm to 156.43 kNm in single sided test TW2 is due mainly to geometry of the subframe.

By comparing the results of the single sided tests TW2 and TB2 it is found that the ratio of the ultimate moments TB2/TW2 = 58.02/156.43 = 0.37 is less than this ratio in corresponding double sided tests TB1(A)/TW1(A) = 191.34/238.78 = 0.80. It is very interesting to note that this ratio of the predicted ultimate moment values is also 0.80 = 201.89/252.58. This clearly indicates that it is possible to predict the ultimate strength of the connections with tie bars and slabs in double sided subframes. However the ultimate strength capacity ratio TB2/TB1(A) = 58.02/191.34 = 0.30 is much less than the ratio TW2/TW1(A) = 156.43/238.78 = 0.66. This indicates that the single sided connections are mainly limited by the strength of the connection itself as the tie steel is not fully effective. The incorporation of the slabs and especially the tie bars in these tests is less dominant on the real behaviour of the connections than in the double sided tests, but on the other hand it must be considered that the connections alone are not used in a real frame environment. They are always accompanied by the tie bars, slabs and in-situ infill concrete or grout to fulfil their function in the completed structure during the service life.

The values 0.97 and 0.93 x the ultimate strength of the test TB1(A) were achieved in the further simplified short beam length tests TB1(B) and TB1(C), respectively. This confirms that the use of these tests arrangements to replace full tests with slabs would not make a greater difference than 7% as far as the strength of the

connection is concerned. This shows that, within the normal scatter in experimental work of this type, either test, TB1(B) or TB1(C), may be used to generate strength data, and is the first step towards the validation of the further simplified short beam length tests.

The joints generally exhibited a remarkable strength (except TB2) particularly with floor slabs. Values of the ultimate moment capacity M_u of 0.46 up to 0.70 of the actual ultimate moment capacity of the composite beam M_{beam} were attained. These satisfy the limits of $0.25M_{beam} \leq M_u \leq M_{beam}$ in the classification of partial-strength steel beam-to-column connections in Eurocode 3: Part 1.1: ENV 1993-1.1: 1992. (There is no classification system for precast concrete beam-to-column connections in the literature yet). However the resulting $M_{u\,\text{connection}}/M_{u\,beam}$ of 0.18 in the single sided test TB2 is unlikely to give sufficient connection strength to resist the applied loads for use in a typical semi-rigid frame design and must therefore continue to be classified as nominally pinned $M_u \leq 0.25M_{beam}$

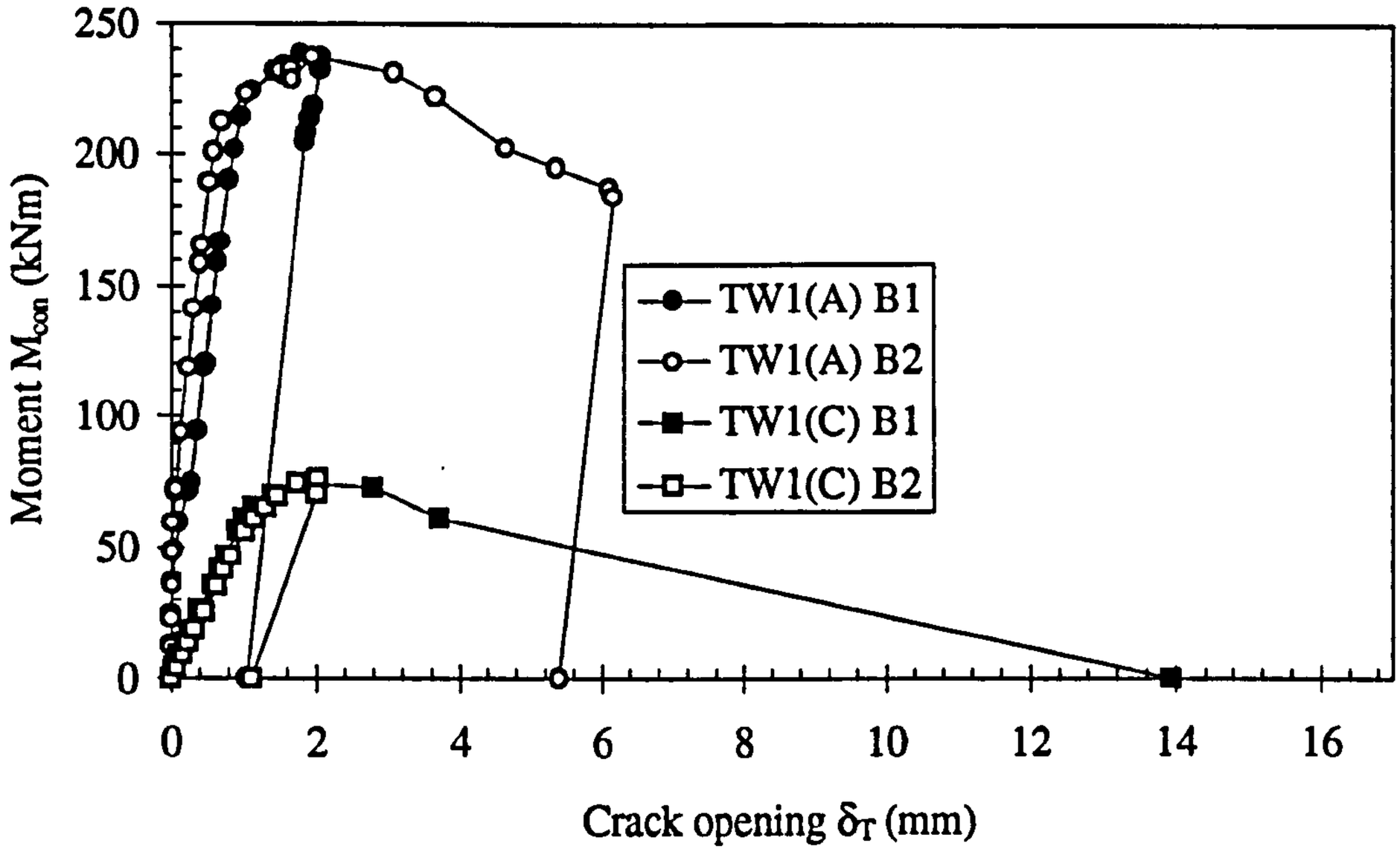

Figure 7.1: Moment versus crack opening at top of beams in tests using welded plate connection

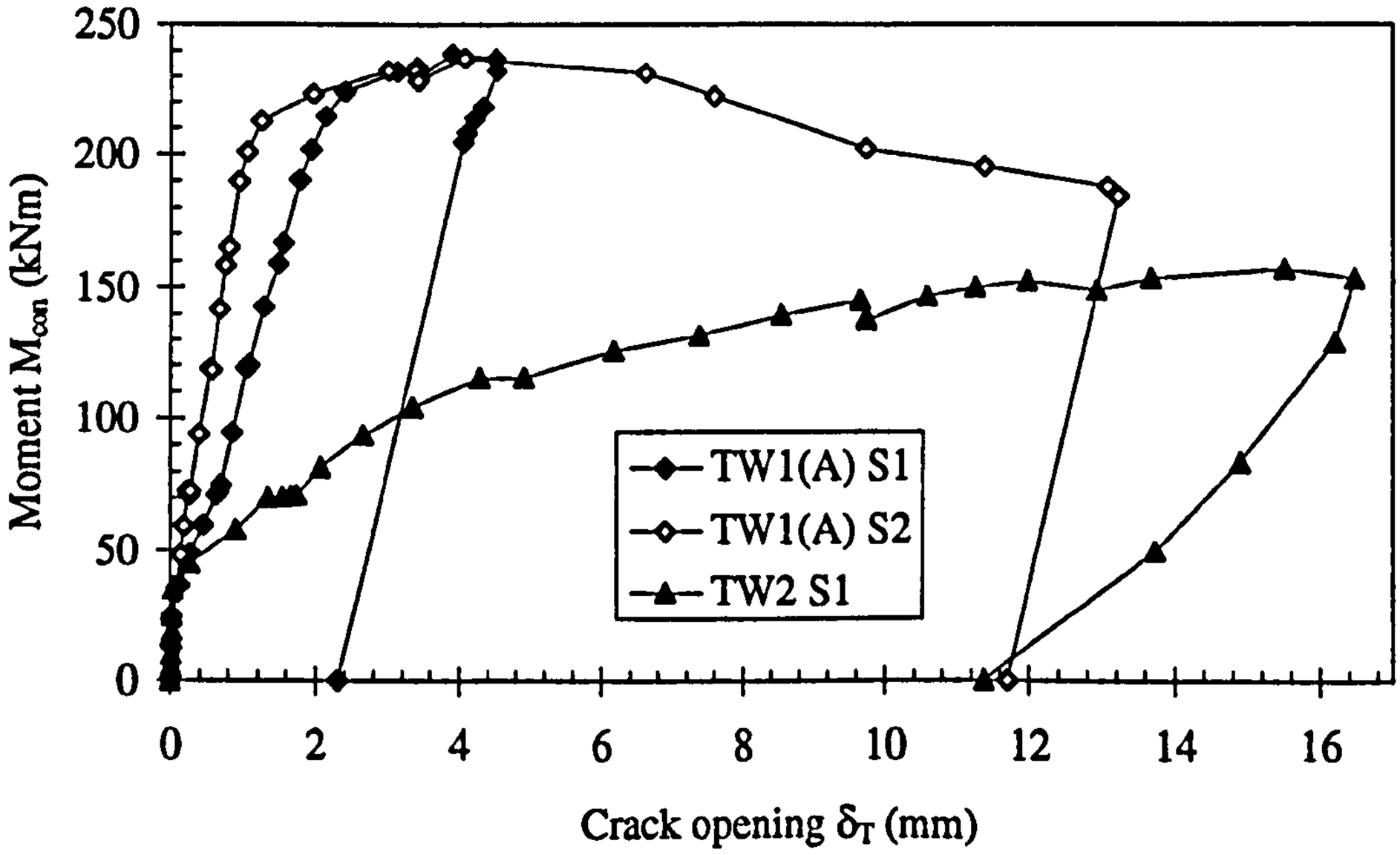

Figure 7.2: Moment versus crack opening at top of slabs in tests using welded plate connection

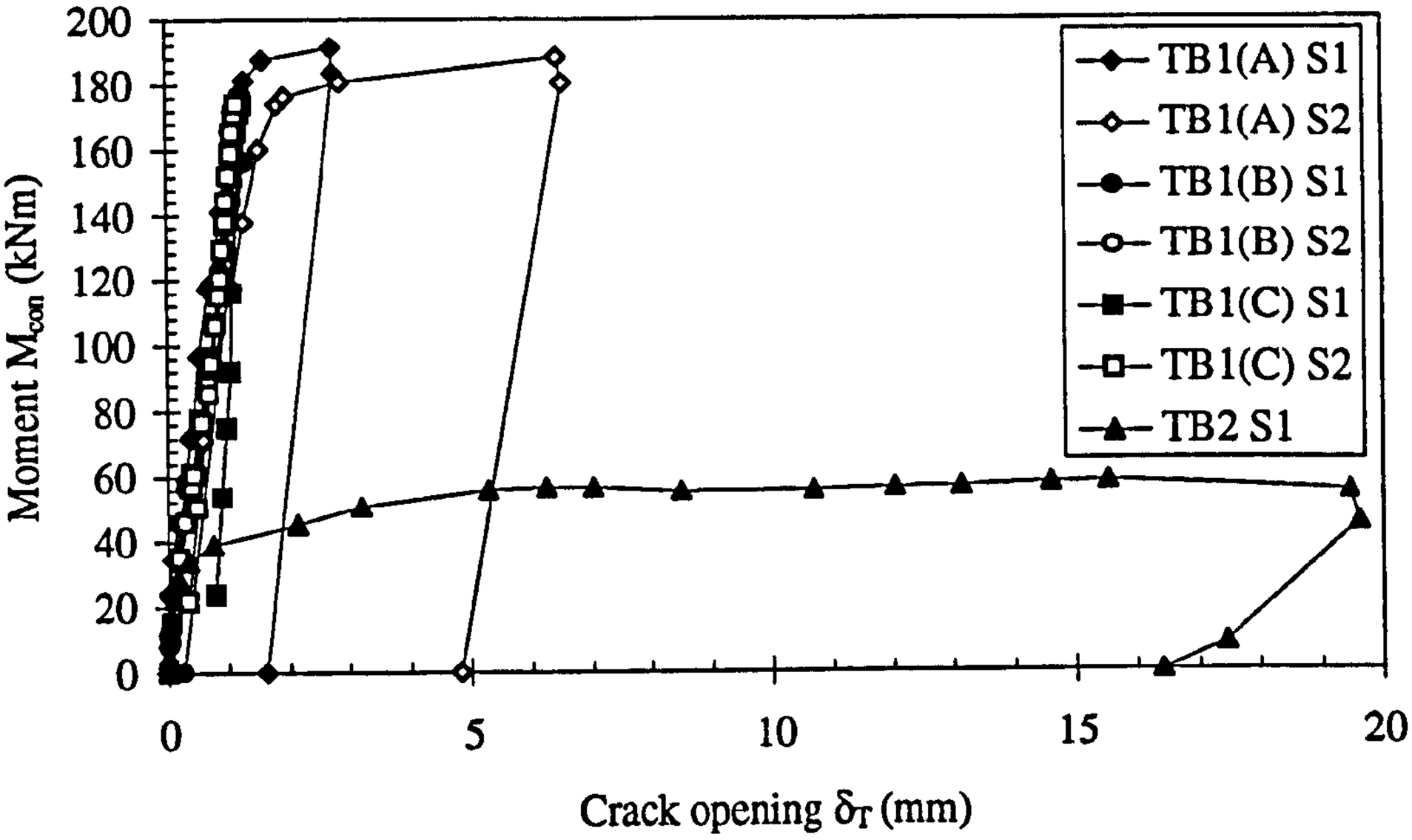

Figure 7.3: Moment versus crack opening at top of slabs in tests using billet connection

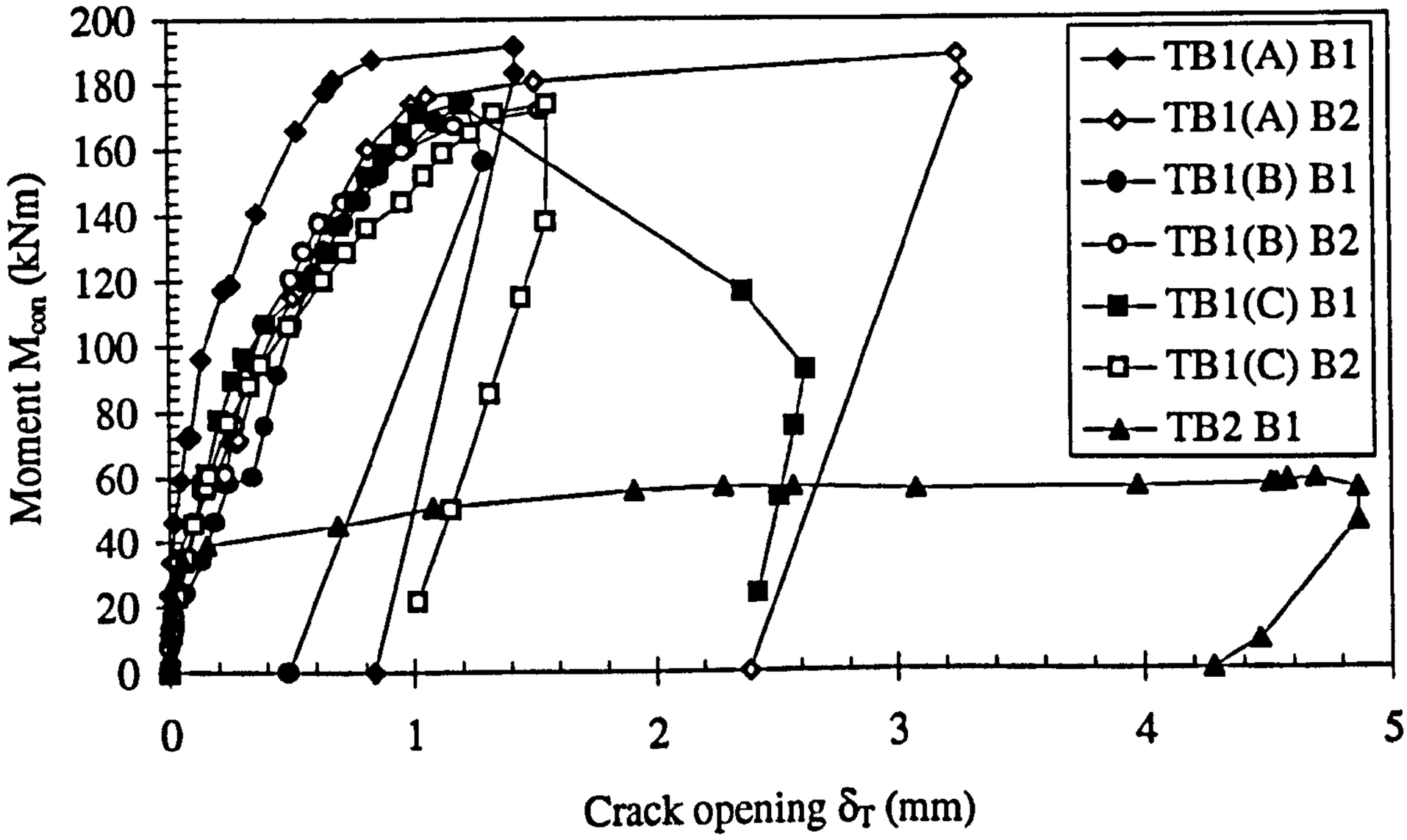

Figure 7.4: Moment versus crack opening at top of beams in tests using billet connection

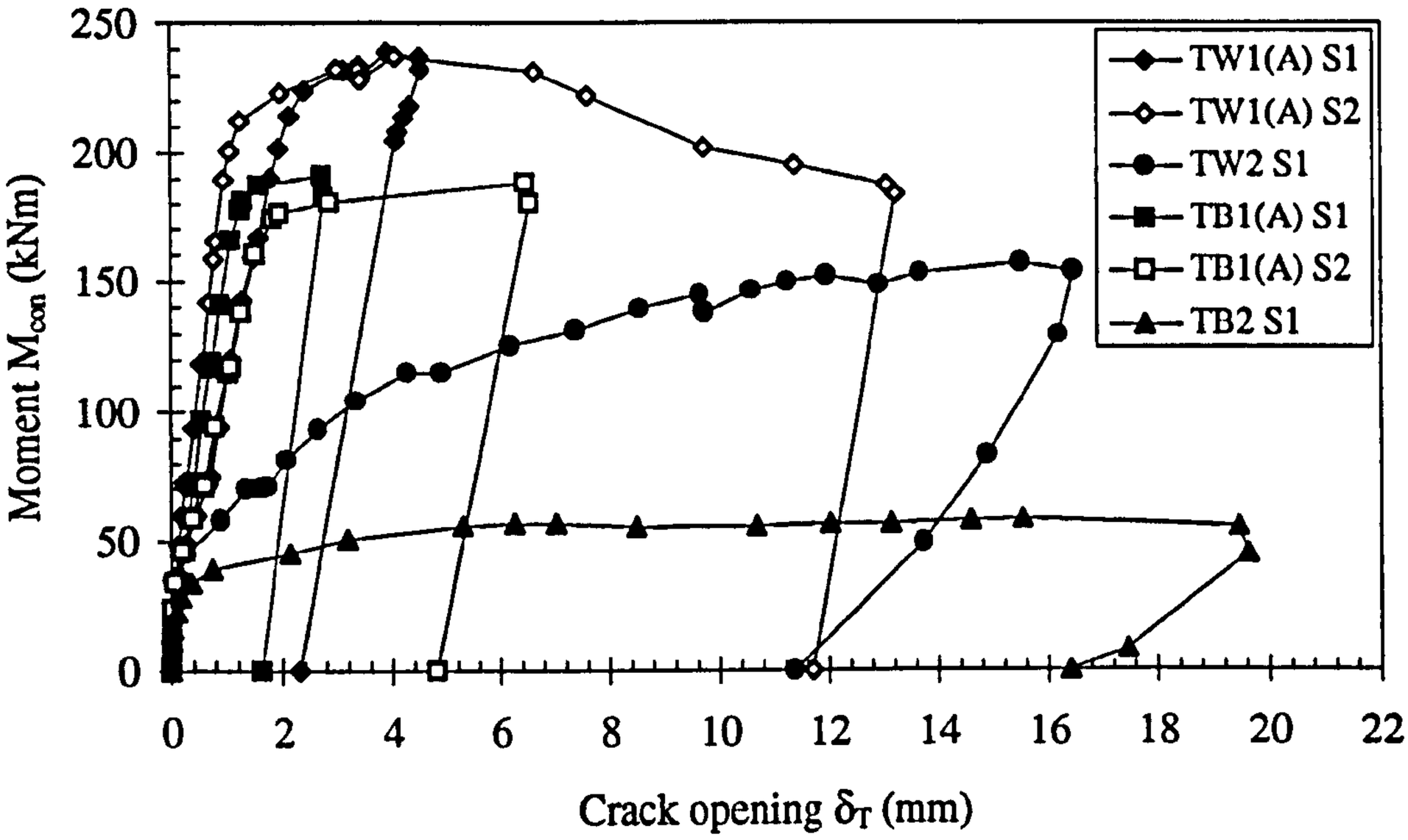

Figure 7.5: Comparison of moment versus crack opening at top of slabs in four main tests using welded plate and billet connections

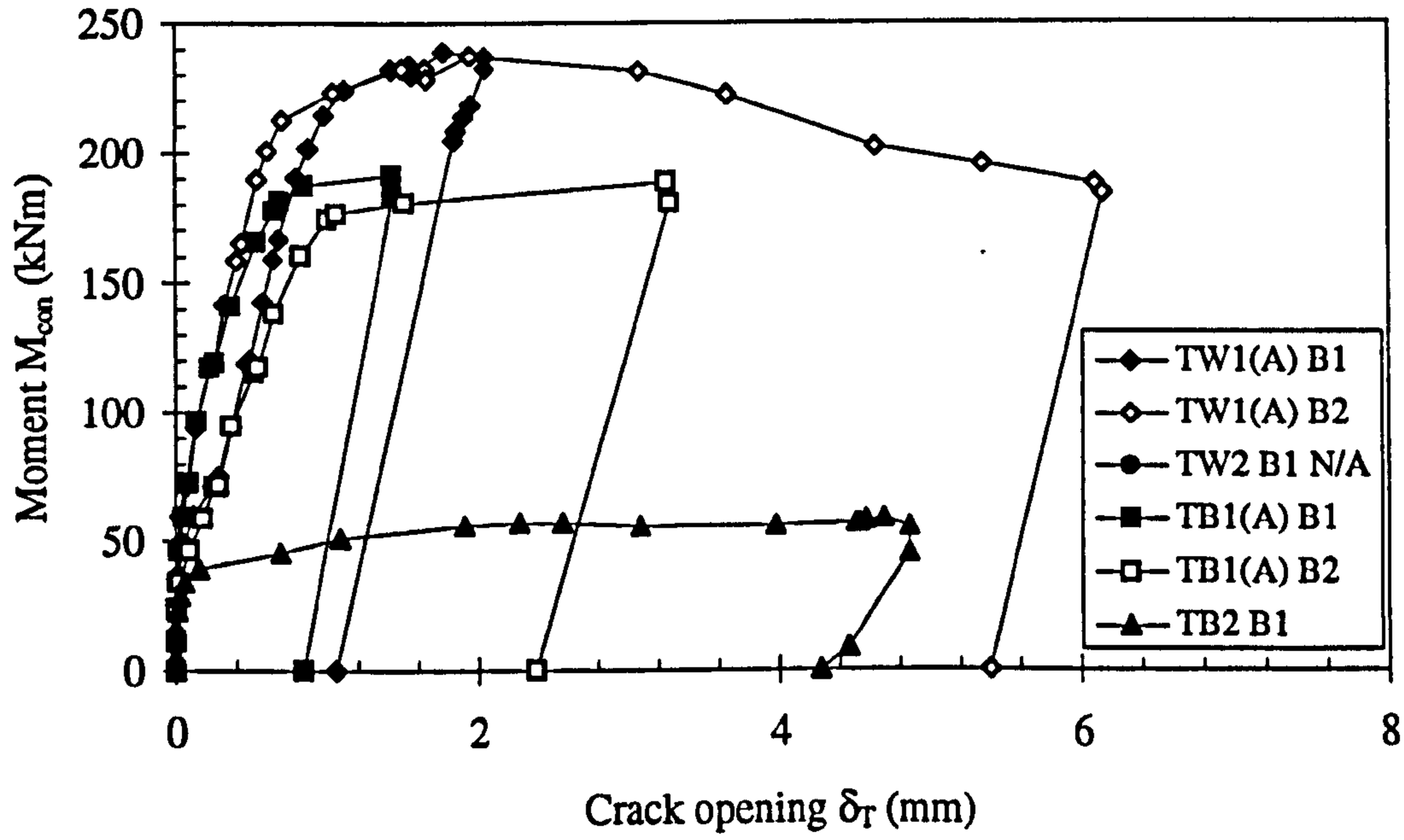

Figure 7.6: Comparison of moment versus crack opening at top of beams in four main tests using welded plate and billet connections

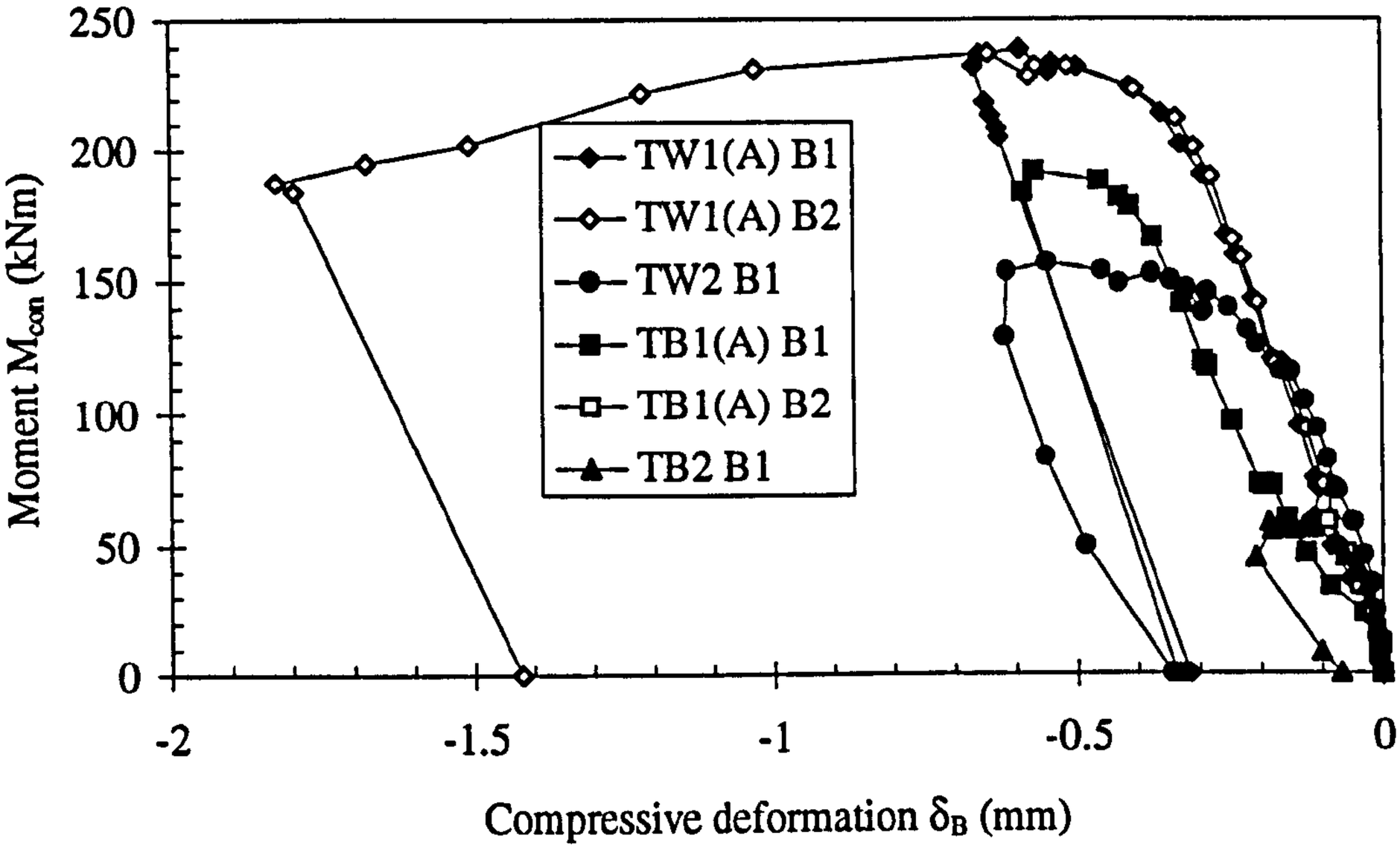

Figure 7.7: Comparison of moment versus compressive deformation in beams in four main tests using welded plate and billet connections

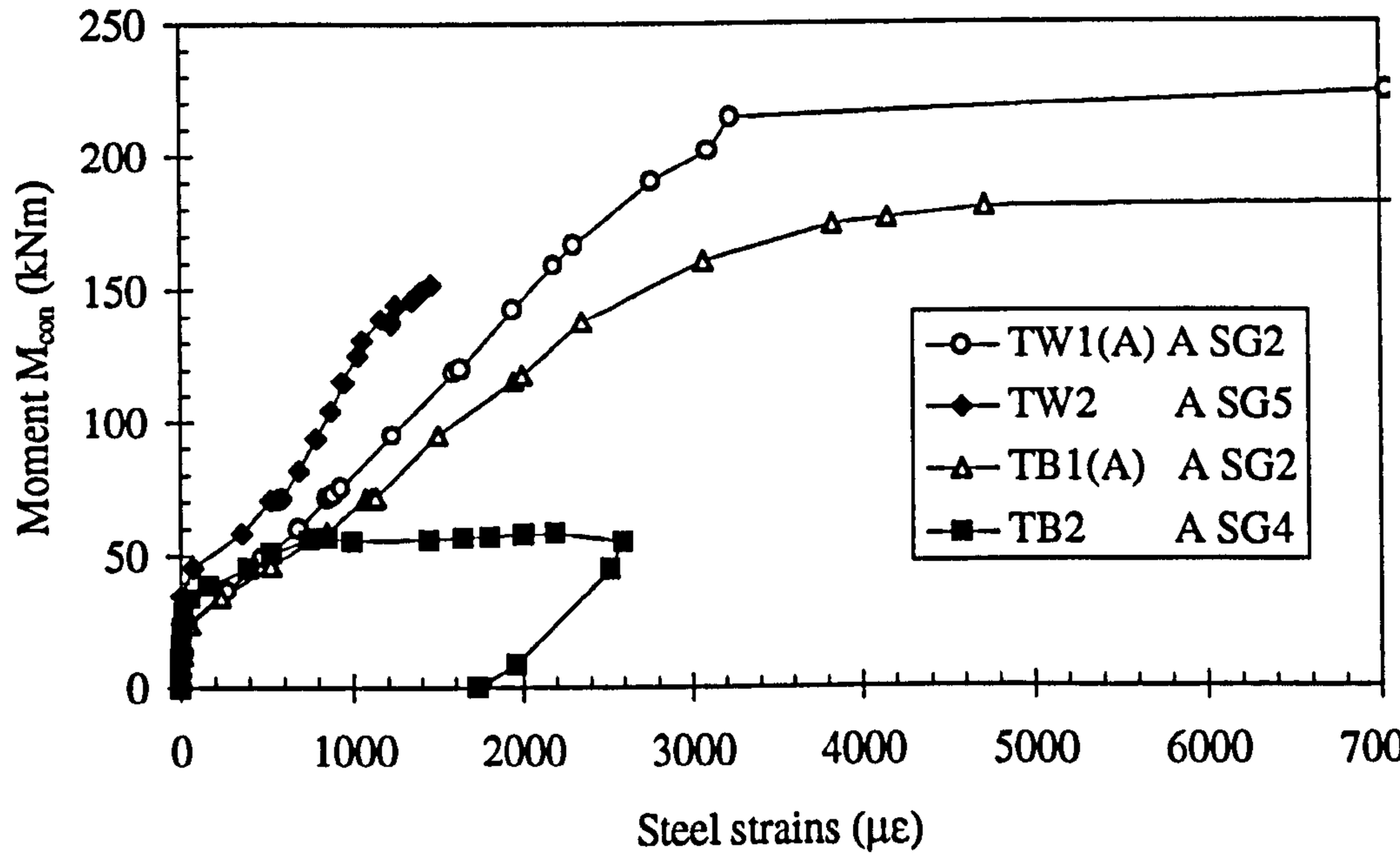

Figure 7.8: Moment versus maximum steel strains in stability tie bars in four main tests

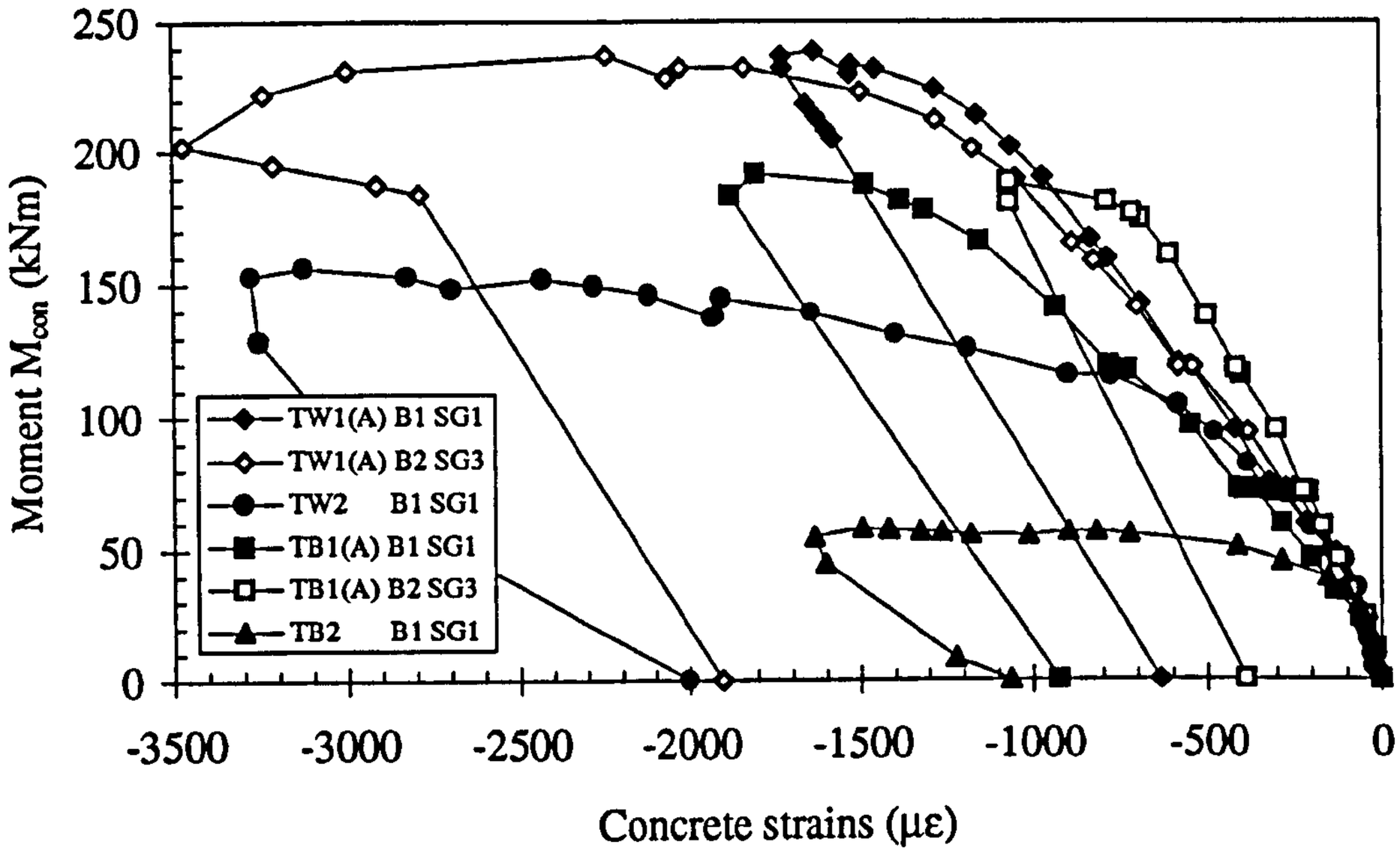

Figure 7.9: Comparison of moment versus compressive strains in beams in four main tests using welded plate and billet connections

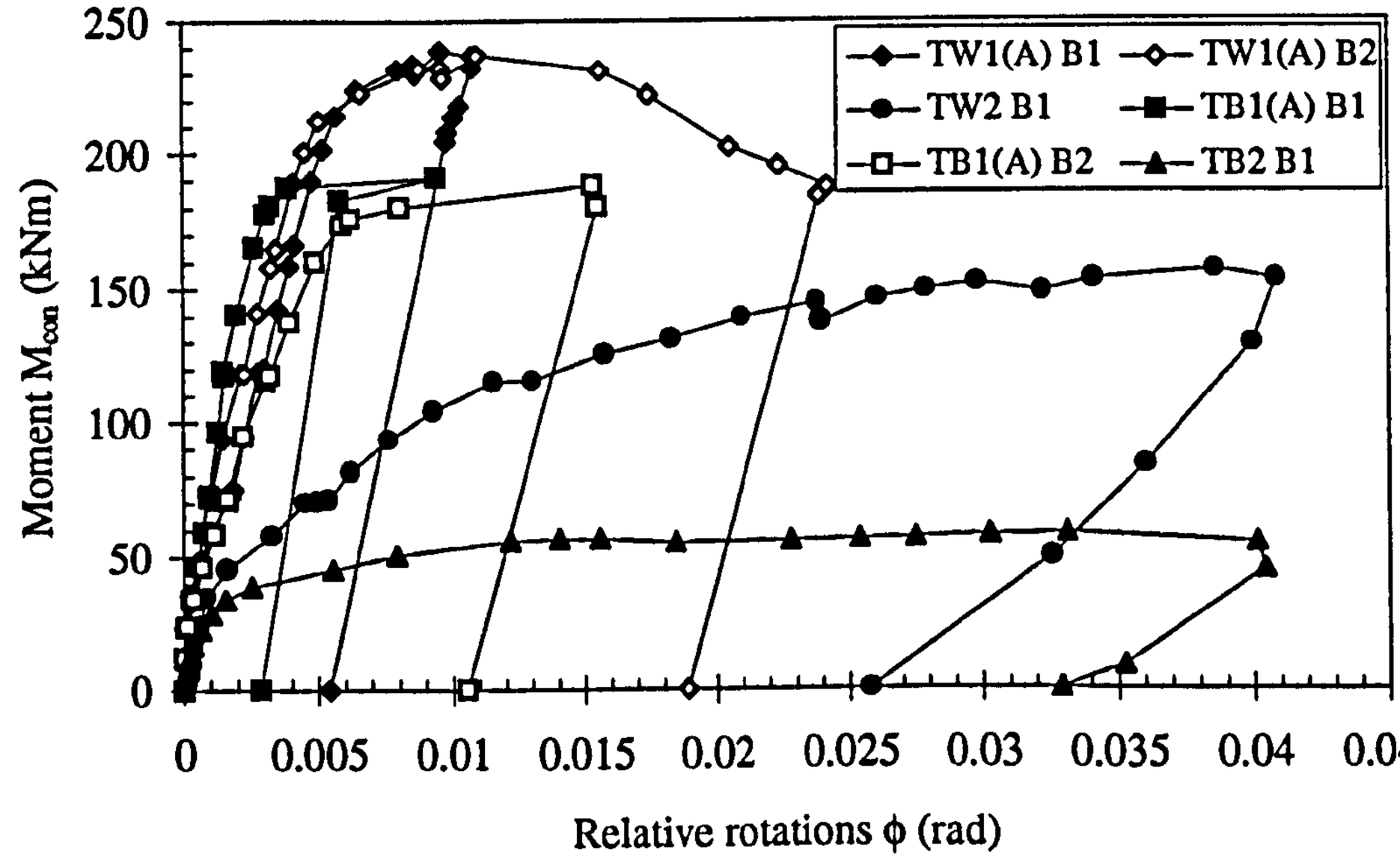

Figure 7.10: Moment versus relative rotations in beams in four main tests using Method 1 (see Figure 6.7(a) for derivation of the relative rotation M1 B1 V4)

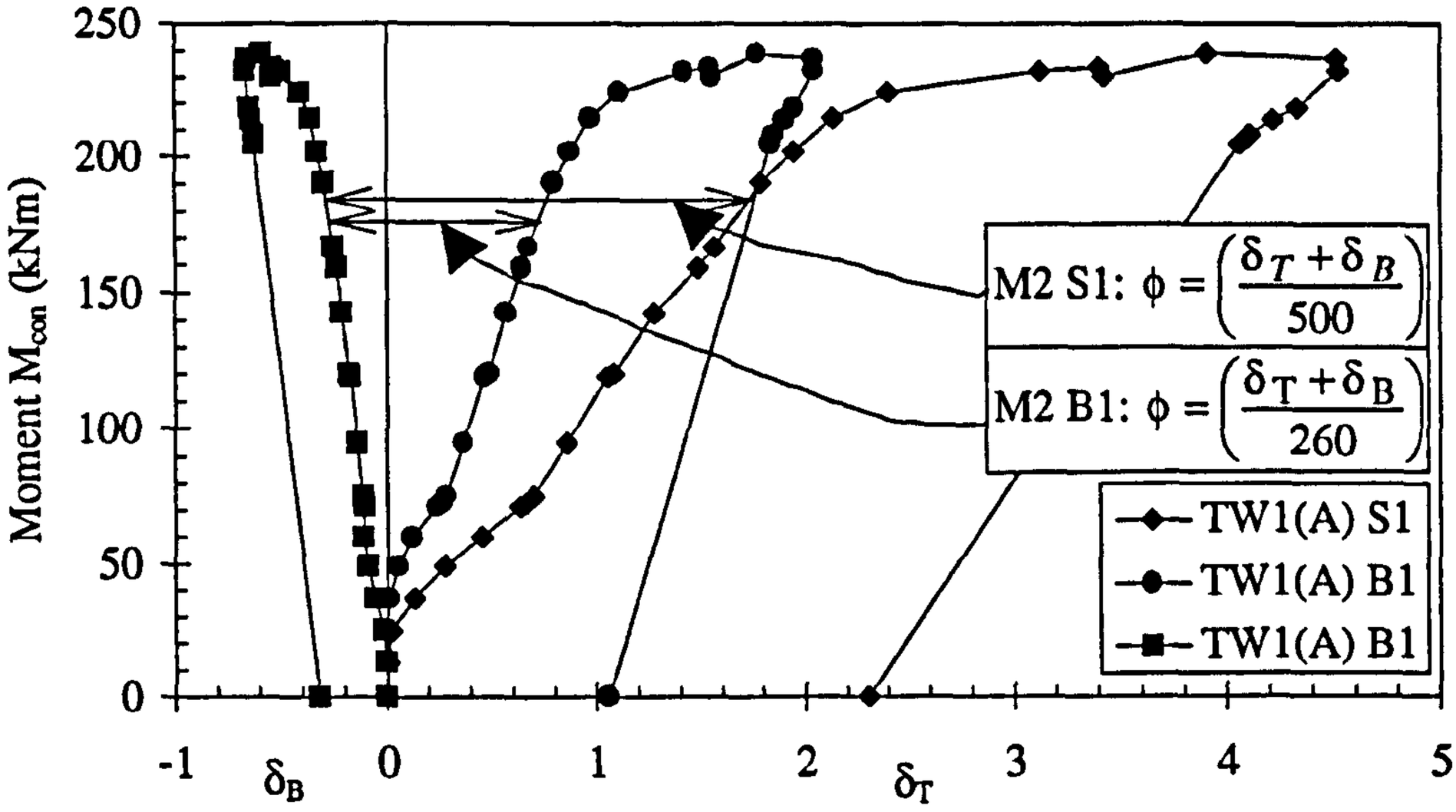

Figure 7.11: Moment versus compressive deformation and crack width in test TW1(A) beam 1 side showing derivation of the relative rotation using Methiod 2

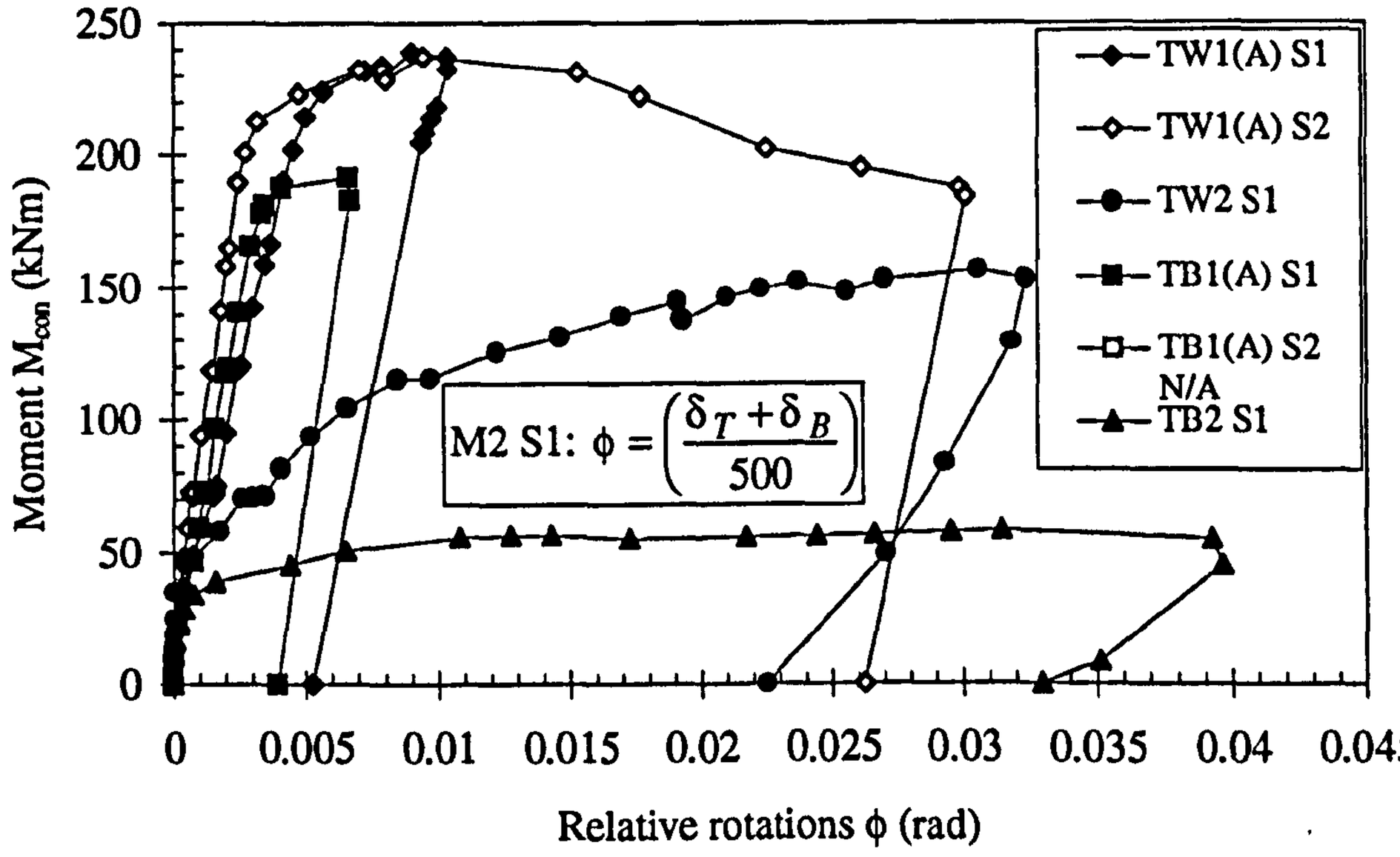

Figure 7.12: Moment versus relative rotations in slabs in four main tests using Method 2

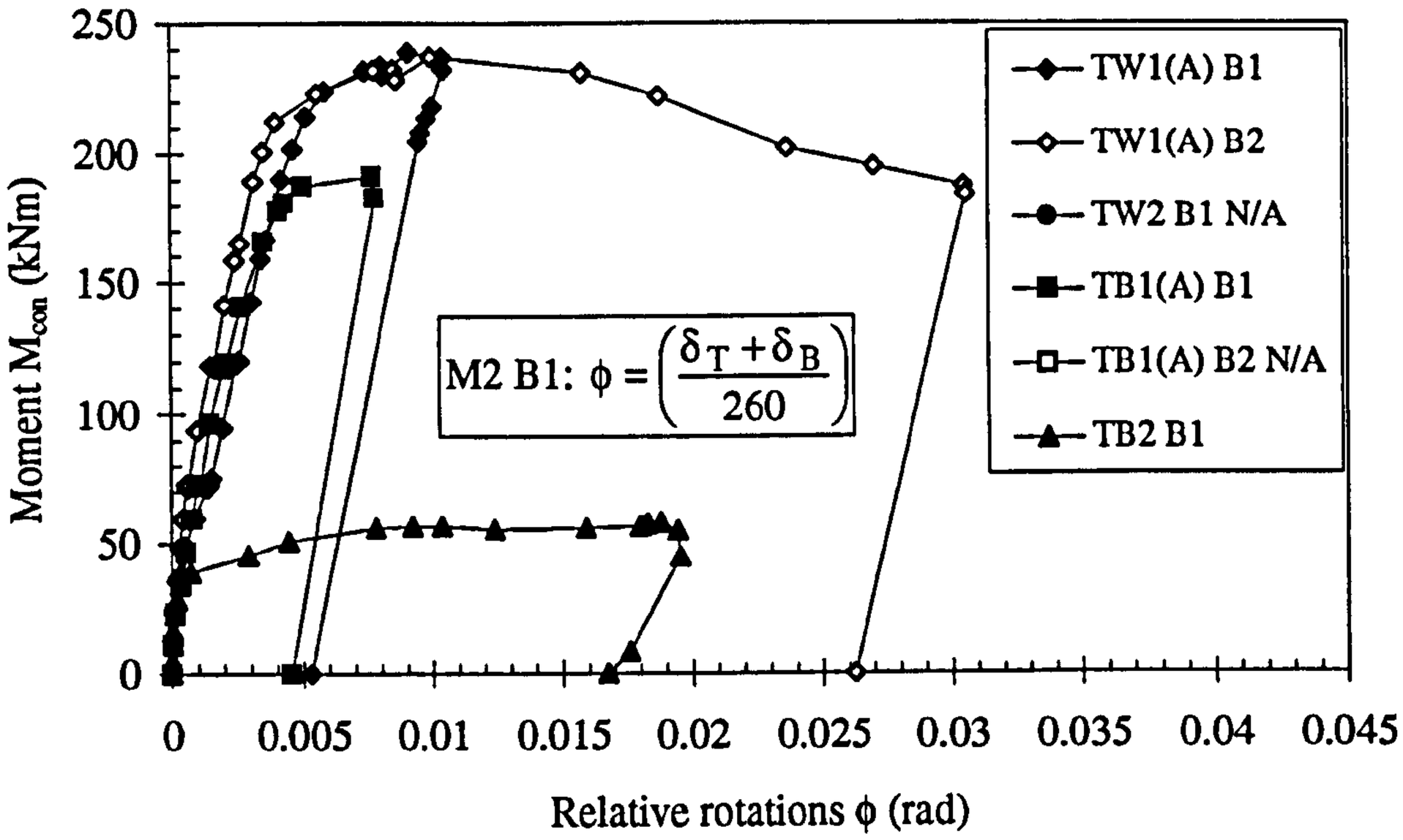

Figure 7.13: Moment versus relative rotations in beams in four main tests using

Method 2

CHAPTER 8

ISOLATED JOINT TESTS

8.1 Objective of the precast-in-situ-precast interfaces tests

The history of precast concrete structures shows that where failures have occurred they are usually associated with the joints and their influence on the overall and local action of the structures, both during and after construction. Because joints tend to relate to small areas of structural members, it is important to appreciate that the design calculations must be related to the localised stresses that can occur since these can be materially different from the stresses that are used in designing the member as a whole.

Local stresses under a bearing should not be added directly to the overall stresses in the member; usually they can be treated separately. The local and overall stresses should be checked separately, and only if the overall stresses are close to the relevant maximum allowable stresses need the interaction of the two be assessed. Where a local load represents a small part of the total loading its influence can be neglected. It is difficult to provide clear guidance to cover all cases but local effects can be evaluated experimentally.

The main objective of the isolated tests is to obtain information in areas confined by precast members and/or reinforced in-situ concrete or grout. This information is necessary in order to be able to interpret the effects of localised under or over strengthening in connections, where the behaviour is often disguised in a single

result. The information is also required to validate finite element work (using computer programs such as SWANSA) and assist in the prediction of joints stiffness and strength. The results for all of the isolated tests are reported on and discussed in Chapter 9.

8.2 Identification of isolated joint tests

The experimental work has been carried out in two main areas :-

(a) frame connection tests

(b) isolated joint tests on parts of the connections tested in (a)

The data collected from (b) will be used to assist in the separation of the various components found in a full connection test; for example, local cracking in the tension zone, and crushing in the compression zone of a moment resisting connection. Being able to characterise the behaviour of a full frame connection by simplifying it into a number of isolated components will enable a larger range of connection types and sizes to be studied as shown in Figure 8.1.

When connections such as these are subjected to hogging bending moments and shears, the extreme fibres in the soffit of the joint are subjected to compression. Concrete material non-linearities will proceed from the positions of the maximum stress. The situation is complicated by the fact that the site concreted or grouted infill is bound on two faces by smooth (ex - mould) precast faces. The precast-in-situ interfaces are a major source of deformation and must be included in any investigation. Thus, the total deformation δ_B in the concrete is the sum of the elastic deformation in the precast δ_{cp} and in-situ δ_{ci} concretes, plus the two precast-in-situ interfaces 2λ,

where λ is the normal deformation of each interface across a concrete joint subjected to uniaxial compression or flexure, or both. In this work x is defined as the gauge length (or centre-to-centre distance) between deflection transducers and their targets over which the total deformation δ_B is measured as shown in Figure 8.1.

If the depth of the section (i.e. beam only or beam plus floor slab) is large in comparison to the depth of the infill, say 2 to 3 times the infill depth, the stress across the precast-in-situ interface is approximately axial (see Plates 6.3 and 6.4 in full scale frame connection test). This situation, which is represented by position "1" in Figure 8.1, has been studied in the isolated test series 1 to 5. If the depth of the section is small, say 1.5 times the infill, bending stresses will predominate across the section and the response may be different to the axial case, and this has been studied in test series 6. It is therefore possible to isolate the regions identified in Figure 8.1 and to construct small prismatic specimens to represent the precast and in-situ concretes or grout, inclusive of the two interfaces, as shown in Figure 8.2.

The extreme fibres in the top of the joint are subjected to tension. Cracks in the column to slab or beam interface will cause the transfer of tensile force from the concrete to the long tie steel positioned over the tops of the beams. The force in the tie bar is axial. This situation, which is represented by position "2" in Figure 8.1, has been studied in series 7.

8.3 Compression tests

In the compression zone the concrete in the precast elements will be confined to varying degrees by the reinforcing stirrups in the beam and column members. Concrete is usually C40. However lateral splitting in the in-situ concrete in the joint can only be

restrained by frictional contact across the interfaces. In-situ infill is C20. These tests were carried out to evaluate the deformability in the joint between concretes having different strength. It was not possible to include the steel billet (shown dotted in Figure 8.1) in these specimens. This could have an effect on the result and is to be suggested as further research.

Cubes and prisms were made using mix proportions for each test. They were stored in a water tank until one day before filling the in-situ infill concrete. Mix proportions (see Section 5.5 Concrete Mixes) and, specified and average compressive cube strength of tests series 1 to 7 at the test days are presented in Tables 8.1 and 8.2, respectively.

The cubes and prisms were taken out from the water tank one day before filling the specimens and were dried using a towel. Two cubes or prisms were placed in the end of a mould shown in Figure 8.2, with ex-steel mould surfaces towards the centre, and gap was filled for each of the specimens using fresh concrete or grout. The precast faces were dry (i.e. were not dampened). The specimens were stored in the water tank.

Demec pips (or POTs) were attached to sides of the specimens shown in Figure 8.4. Plate 8.1 shows typical test assembly of test series 1, 2 and 3. Plates 8.2 and 8.3 show typical test assembly of test series 4 and 5, respectively.

In this test series the important measurements were:

i) ultimate load capacities of the specimens

ii) deformability in the joint between concretes having different strength

The loading was applied incrementally until failure. The failure was defined by sudden specimen failure in compression. The specimens were tested in Dennison M/C testing

machine. Certificate for calibration was checked before using the machine for each test series.

Test series 1:

The purpose of the tests was to find out the compressive strength of the specimens and the compressive deformations of the joints with a varying thickness of in-situ infill concrete as shown in Figure 8.3. The main geometric variable considered was the thickness of the in-situ infill (t) which as shown in Figure 8.3 varied from t = 50 to 100 mm. The strength of the precast concrete = in-situ infill. Fifteen cubes were made using mix 1 concrete, a further mix was cast using mix 2 concrete for repeatability purposes.

The test specimens were placed upright and crushed. For t = 50 and 75 mm infill gap, 4 inches gauge length and for t =100 mm infill gap 8 inches gauge length were used.

Test series 2:

These tests were carried out to evaluate the deformability in the joint between concretes having different thickness AND strength. Five specimens, as shown in Figure 8.5, were tested.

In this test the thickness of the in-situ infill was varied from 25 mm, 50 mm and 100 mm, and the tests were carried out when the compressive cube strength of the in-situ infill concrete reached 21.5 N/mm^2. The precast concrete = 40.9 N/mm^2. A dry jointed precast prism 200 mm (using 2 no 100x100x100 mm cubes) long was tested to give the value for t = 0. A solid 200 mm long prism was also tested to give a datum

strength for the precast concrete. In one additional experiment a thin sheet of polythene was placed between the precast cubes and in-situ infill. A thickness of t = 50 mm was suggested for this. Two of these were made just to be sure of measuring real effect.

Test series 3:

This test series is similar to test series 2 with the following differences :-

1. To keep the height of all specimens the same to obtain maximum compressive strength, and to observe the effect of the thickness t on the deformability of the joint.

2. To use the same length gauge (8 inches) to measure strain for all specimens used in these test series, and to compare compressive deformability and strain over the same distance.

In this test series six specimens were tested as shown in Figure 8.6. The height of the specimens is 300 mm. The distance between demec pips is 200 mm, and t was varied from 0, 25, 50 to 100 mm. Two solid prism 300 mm long x 100 x 100 mm were cast in grade C40 and C20 concrete to provide datum strengths for the precast and in-situ concrete, respectively. The casting sequence and instrumentation was the same as in test series 1.

Test series 4:

This test series is similar to test series 2 and 3 with the following differences :-

1. To use nominal grade C50 and C25 for the precast and in-situ concrete, respectively. (Although the mix designs were the same as in the C40 and C20 concrete, the strengths achieved here were greater).

2. To measure compressive deformability on four vertical faces of specimens to find out the effect of the bending moment due, possibly, to the eccentricity of the applied uniaxial compressive load. This might, due to a small imperfection, affect the results.

In this test series deformations were recorded using linear potentiometers instead of demec pips. It was experimentally convenient. The specimens were placed upright and linear potentiometers were attached in clockwise and symmetrically in vertical direction. See Plate 8.2.

In this test series five specimens were tested as shown in Figure 8.7. The height of the specimens was varied from 225 mm to 300 mm, and t was varied from 25, 50, to 100 mm. Two reference prisms were also cast using wholly precast and wholly in-situ infill mixes.

Test series 5:

Although the foregoing tests gave information on the behaviour of precast-in-situ interfaces, no account was made of the presence of two sections (see Section B-B in Figure 5.6) having different joint grout thickness t = 10 mm at the outer sections and 110 mm at the centre section at the end of the beam incorporating the billet connection found in real full scale frame connection test. It was felt that the introduction of these sections might influence the deformability at the interface, and for this reason a set of prisms were cast as shown in Figure 8.8 at the same day using the same concretes and

grout used in the column, beam 1 and joint grout in full scale tests TB1(A). As before, three reference prisms representing column, beam and joint grout were cast to provide datum points.

The main aim of these tests was to observe the difference between compressive deformation in the joint with grout thickness t = 10 mm and 110 mm. The strength of the precast and in-situ infill were nominally identical.

8.4 Bending tests

8.4.1 Small scale bending tests

Test series 6:

These tests were used to study joint deformation in flexure, as shown in Figure 8.9.

Two modes of failure were of interest:-

i) tension cracking at the bottom shown in Figure 8.10

ii) compression deformability at the top shown in Figure 8.11

For these experiments 500x100x100 mm prisms shown in Figure 8.12 were used. The loading details are shown in Figure 8.13 respectively. Plate 8.4 shows test assembly for test series 6.

For the tensile cracking tests the modulus of rupture was calculated when the separation occurred and therefore no instrumentation was required. For the compression test high tensile reinforcement was used in the bottom of the prism as shown in Figure 8.12. The area of steel bars was calculated as follows:-

$F_{cc} = 0.67 f_{cu} b\ 0.603\ d$ for a balanced section

$$F_{cc} = (0.67)(20)(100)(0.603)(80) = 64.642 \text{ kNm}$$

$$A_s = \frac{F_{cc}}{f_y} = \frac{64.642 \times 10^3}{460} = 141 \text{ mm}^2$$

$\therefore$ Use 2 no T10 bars $\left(157 \text{ mm}^2\right)$ shown in Figure 8.12.

Using two linear potentiometers across two targets, the deformation δ was measured over a distance x = 118 mm as shown in Figure 8.14.

To determine the modulus of elasticity of precast concrete E_{cp} and in-situ infill concrete E_{ci}, 2 no 500x100x100 mm prisms made from the two mixes separately were tested. Before carrying out any of the flexural tests, ultrasonic pulse velocity (UPV) methods were used to find E_c for the standard and composite specimens. The UPV test gives the dynamic modulus E_{cq} from which the static modulus may be derived (according to BS 8110) as follows:-

$$E_c\left(\text{kN/mm}^2\right) = 1.25E_{cq}\left(\text{kN/mm}^2\right) - 19$$

where

$$E_{cq} = \rho V^2(1+\mu)(1-2\mu)/(1-\mu)10^{-3}$$

V = pulse velocity (m/s)

ρ = density (kg/m^3)

μ = dynamic value for Poisson's ratio 0.25 (assumed)

The predicted collapse load was calculated as in Section 5.10 in Chapter 5. The maximum bending moment of the specimens was predicted at the centre of the specimens from the internal forces as:-

$$x = \frac{F_{st}}{0.67 f_{cu} b} \times 10^3 = \frac{79.6}{0.67 x 19.8 x 100} 10^3 = 60 \text{ mm}$$

x is the depth of the stress block (mm), from the condition of internal forces to be in equilibrium.

where

F_{st} = 79.6 kN is the total tensile yield load in the 2T10 reinforcement bars tested

f_{cu} =19.8 is the actual compressive cube strength of in-situ concrete at test day (N/mm^2). See Table 8.2

b is breath of the section = 100 mm

The predicted moment was found as:-

$$M_{pred} = F_{st}\left(85 - \frac{1}{2}x\right)10^{-3} = 79.6\left(85 - \frac{1}{2}60\right)10^{-3} = 4.38 \text{ kNm}$$

where 85 is the measured effective depth from the top of the specimens to the centre of the bars.

The predicted collapse load was found as:-

$$W = \frac{M_{pred}}{0.5h} 10^3 = \frac{4.38}{05x100} 10^3 = 87.6 \text{ kN}$$ (see Figure 8.13) for wholly infill specimen

Similarly, by replacing f_{cu} =39.4 N/mm^2 in the above equation the moment and applied load were found as M_{pred} = 5.57 kNm and W = 111.3 kN for wholly precast specimen. The M_{pred} will be between the range 4.38 - 5.57 kNm for the specimens having in-situ infill concrete.

The loading was applied in one step to the tension and incrementally (5 kN) to the compression specimens until failure. The flexure failure was defined by sudden specimen failure in rupture for the tension and concrete crushing for the compression specimens. These specimens were also tested in the Dennison M/C testing machine.

8.4.2 Isolated tension test

Test series 7:

The test was carried to evaluate crack width opening and the compression deformability in the joint at the top and bottom of the specimen, and strains in 2T25 bars used in the top of the specimen (see Figure 8.15).

Section A, representing a precast column, was cast using mix 1 concrete. Mix proportions used in this test are presented in Table 8.1 for mix 1, mix 2 and mix infill. Reinforcement details of the sections are presented in Figure 8.16. Four 10 mm strain gauges were attached to the 2T25 bars 100 mm c/c as shown in Fig 8.15. (Two of

them can be seen in this figure, the other two were attached to the other bar.) The reinforcement of section B, representing a precast beam, was placed in the same mould. A 20x300x400 mm polystyrene plate was used between section A and B. Section B was then cast using mix 1 concrete. The polystyrene plate was removed and section C was cast using infill concrete.

Using 2M16 bolts, a 250x300x25 thick plate was bolted to the section A and B at the bottom of the joint to act as a load spreader in order to distribute the point reaction.

A test rig was designed as in full-scale frame connection tests in Chapter 5 to accommodate the test specimen. The rig consists of two parallel steel frames perpendicular to the specimen. The frames are capable of carrying 400 kN (right) and, used to apply a vertical bending load, and 600 kN (left), used to clamp the Section A, as shown in Plate 8.5 at the centre of the horizontal 250x150x16 RHS cross beam between two 152x76x10 channel-stanchions. This was calculated on the basis of the available number of the holding down bolts. The vertical bending load at the free end (right) of the cantilever beam of the test specimen was applied incrementally (5 kN) through a hand operated hydraulic jack and measured using a 200 kN capacity electrical resistance load cell. The jack was clamped to the cross beam as shown in Plate 8.5. The beam is loaded so as to bend in plane only and to keep the Section A in a horizontal plane. This induces the correct bending moments and shear forces in the joint by keeping the lever arm constant.

One semi roller load spreader was used underneath the load cell to make sure that the position of the applied load is kept constant.

Using 4M16 bolts, two lifting channels were bolted to the section A and B at the bottom of the joint to act as a load spreader in order to distribute the point reaction. The specimen was lifted using the lifting channels and carried by crane from casting to testing place. It was placed on to a permanent roller and temporary supports on the laboratory strong floor.

The Section A was permanently braced against in and out of plane movements, which might be caused during the loading.

Trestles and timber shims were provided to support the test specimen temporarily. The specimen was then seated at the joint on to the permanent roller support at the free (right) end on to the timber shims that were placed on the top of the trestles (see Plate 8.5). The horizontal position of the specimen was adjusted using small timber packs.

The entire concrete units were then painted white to detect the cracks. The testing date was dictated by the compressive cube strength of the in-situ infill concrete.

The important measurements were:-

(a) crack width δ_T at boundary of the column and in-situ concrete

(b) compressive deformation δ_B in the compression zone

(c) strain in the tie bars in the tension zone

For the test four deflection transducers were attached to sides of the specimen as shown in Fig 8.15 to measure the crack width and compressive deformation. (Two of them can be seen in this figure, the other two were attached to other side of the specimens.) Plate 8.5 shows test assembly for test series 7. All of the offsets were measured at the beginning of test after the attachments of the POTs were completed.

Four 10 mm steel strain gauges (type: FLA - 10-11, gauge resist: 120 ± 3 Ω, gauge factor: 2.11) as shown in Figures 8.15 were used to record the strains on the bars.

All signals from the sensors were automatically recorded using a AXIS SOFTWARE 3465 data logger. The signals were than linearized by inputting the respective calibration factors (the load cells were calibrated before carrying out the tests) for the various sensors into the data logger and the results were displayed directly in the units of millimetre for POTs and kN for the load cells. The data logger was linked to an PC and operated using the proprietary software. The logged data in the hard disk was transferred into a floppy disk and the data was processed as in full-scale frame connection tests in Chapter 5 using the software package Excel (version 5.0) through Windows.

The predicted collapse load was calculated as in Section 5.10 in Chapter 5. The maximum hogging bending moment of the joint was predicted at the column face from the internal forces as:-

$$x = \frac{T}{0.67 f_{cu} b} \times 10^3 = \frac{502}{0.67 x 20.2 x 300} 10^3 = 123.6 \text{ mm}$$

x is the depth of the stress block (mm), from the condition of internal forces to be in equilibrium.

where

T = 502 kN is the total tensile yield load in the 2T25 longitudinal tie bars tested

f_{cu} =20.2 is the actual compressive cube strength of in-situ concrete at test day (N/mm^2) - Table 8.2.

b is breath of the section = 300 mm

The predicted moment was found as:-

$$M_{pred} = T\left(321.5 - \frac{1}{2}x\right)10^{-3} = 502\left(321.5 - \frac{1}{2}123.6\right)10^{-3} = 130.37 \text{ kNm}$$

where 321.5 is the measured effective depth from the bottom of the joint to the centre of the bars.

The predicted collapse load was found as:-

$$P = \frac{M_{pred}}{0.715} = \frac{130.37}{0.715} = 182.3 \text{ kN (ignoring self weight of test specimens)}$$

where 0.715 is the lever arm distance from the face of the column to the centre of the applied load.

The loading scheme was aimed at simulating the action of the axial tensile force in bars in a precast concrete skeletal frame connection. This action causes hogging bending moment to the beam-to-column joint.

The bending load was applied monotonically to failure in increments of 5 kN. Between any two successive increments a visible check was carried out on cracks in the critical zones of the joint, and the stroke of the POTs and jack.

The test procedure was to apply load increments until the joints were not capable of supporting any further load.

	Isolated joint tests																
Test no	Test series 1			Test series 2		Test series 3		Test series 4		Test series 5			Test series 6		Test series 7		
Mix no	1	infill	2	1	infill	1	infill	1	infill	1	grout*	2	1	infill	1	infill	2
Agg.	3.40	3.00	3.00	3.00	4.30	3.00	4.00	3.00	4.30	3.00	N/A	3.00	3.00	4.30	3.00	4.30	3.00
Sand	2.60	2.25	2.25	2.25	3.20	2.25	3.00	2.25	3.20	2.25	2.00	2.25	2.25	3.20	2.25	3.20	2.25
Cem. OPC	1.00	1.00	1.00	1.00	1.00	1.00	1.00	1.00	1.00	1.00	1.00	1.00	1.00	1.00	1.00	1.00	1.00
Water	0.64	0.57	0.57	0.57	0.80	0.55	0.74	0.52	0.75	0.55	0.45	0.55	0.57	0.57	0.53	0.75	0.53
Slump mm	70	60	65	80	70	65	40	80	75	70	N/A	100	150	55	80	60	70

Table 8.1: Mix proportions by weight in test series 1 - 7 of isolated joint tests (*Admixture, Tricosal, 1% of cement weight was used)

	Isolated joint tests																
Test no	Test series 1			Test series 2		Test series 3		Test series 4		Test series 5			Test series 6		Test series 7		
Mix no	1	infill	2	1	infill	1	infill	1	infill	1	grout*	2	1	infill	1	infill	2
Specified	40.0	40.0	40.0	40.0	20.0	40.0	20.0	40.0	20.0	40.0	40.0	40.0	40.0	20.0	40.0	20.0	40.0
Actual	42.4	40.7	46.6	40.9	21.4	41.2	19.0	52.7	26.7	38.3	46.4	50.3	39.4	19.8	40.6	20.2	39.1

Table 8.2: Specified and actual (average) compressive cube strength (N/mm^2) in test series 1 - 7 of isolated joint tests (*Admixture, Tricosal, 1% of cement weight was used)

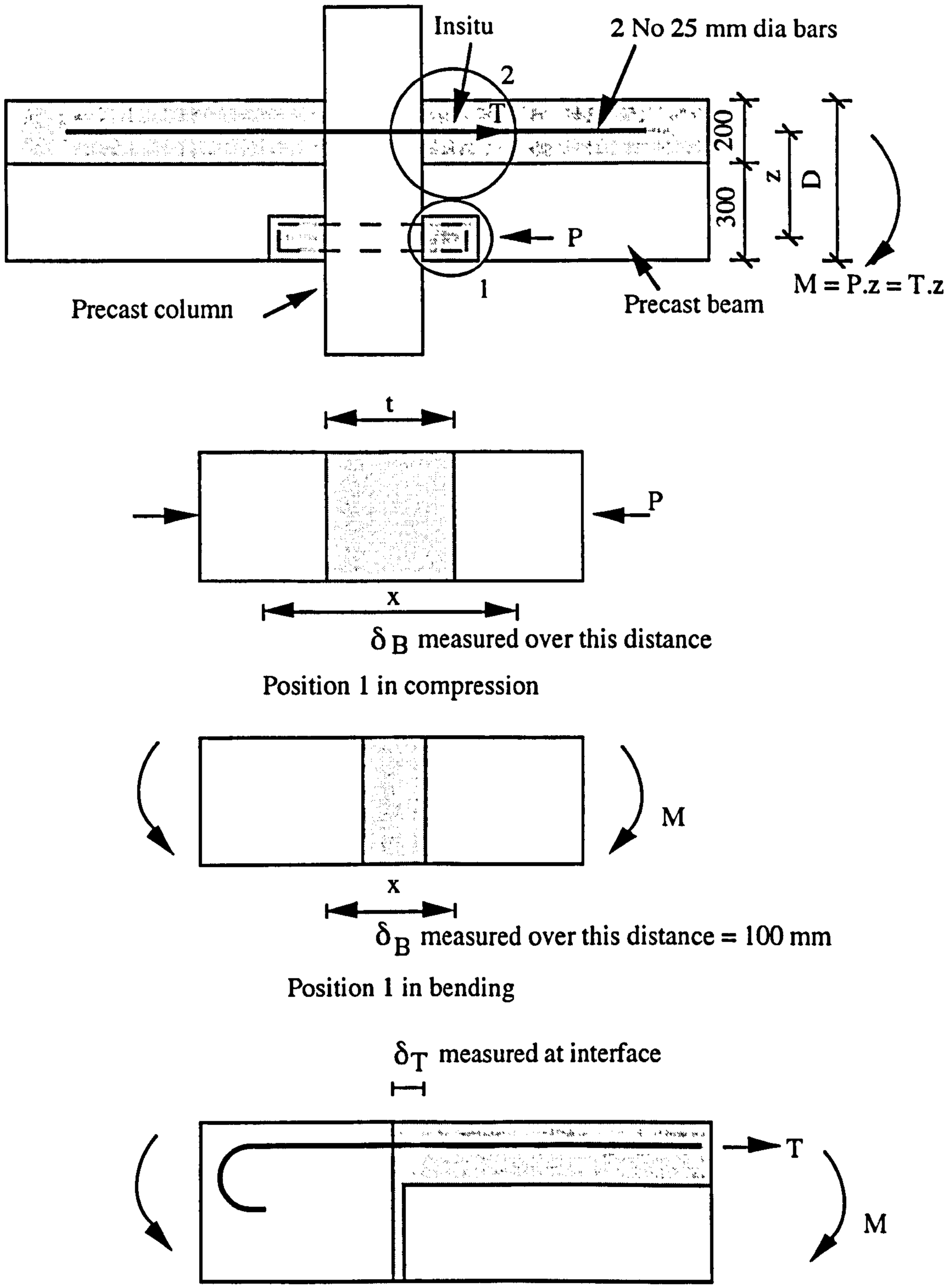

Figure 8.1 Sub-sections of beam-column connection used in simplified model

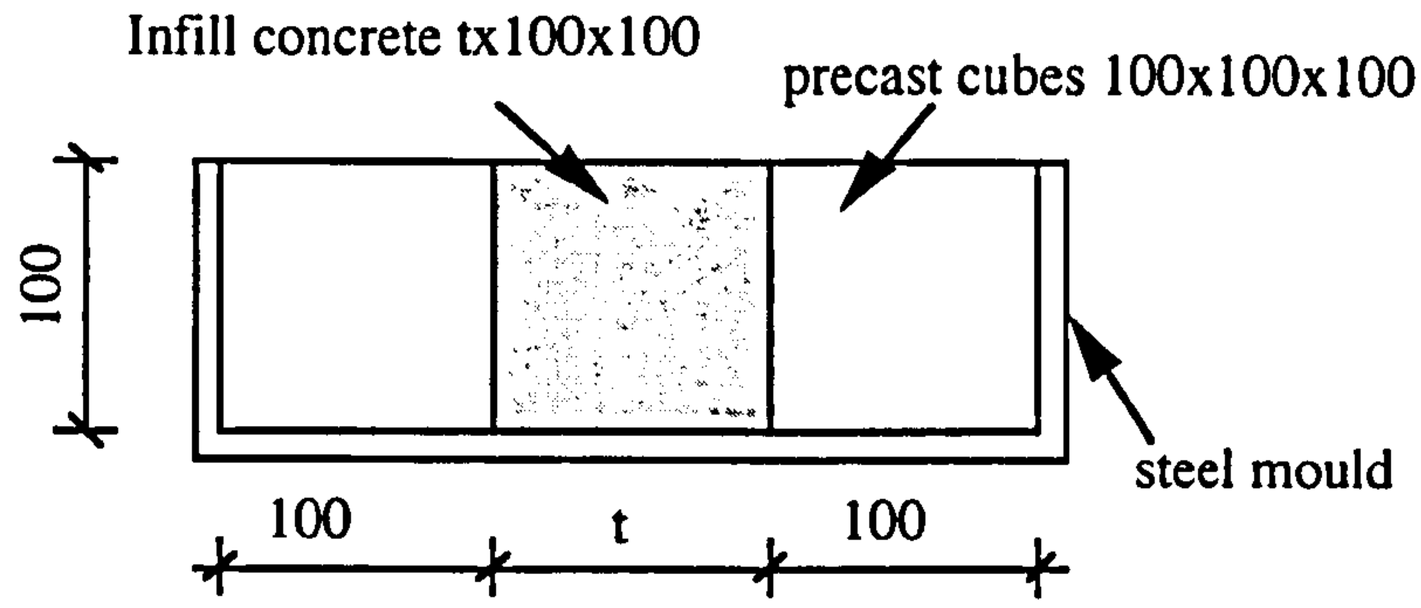

Figure 8.2 Filling the gap using fresh concrete

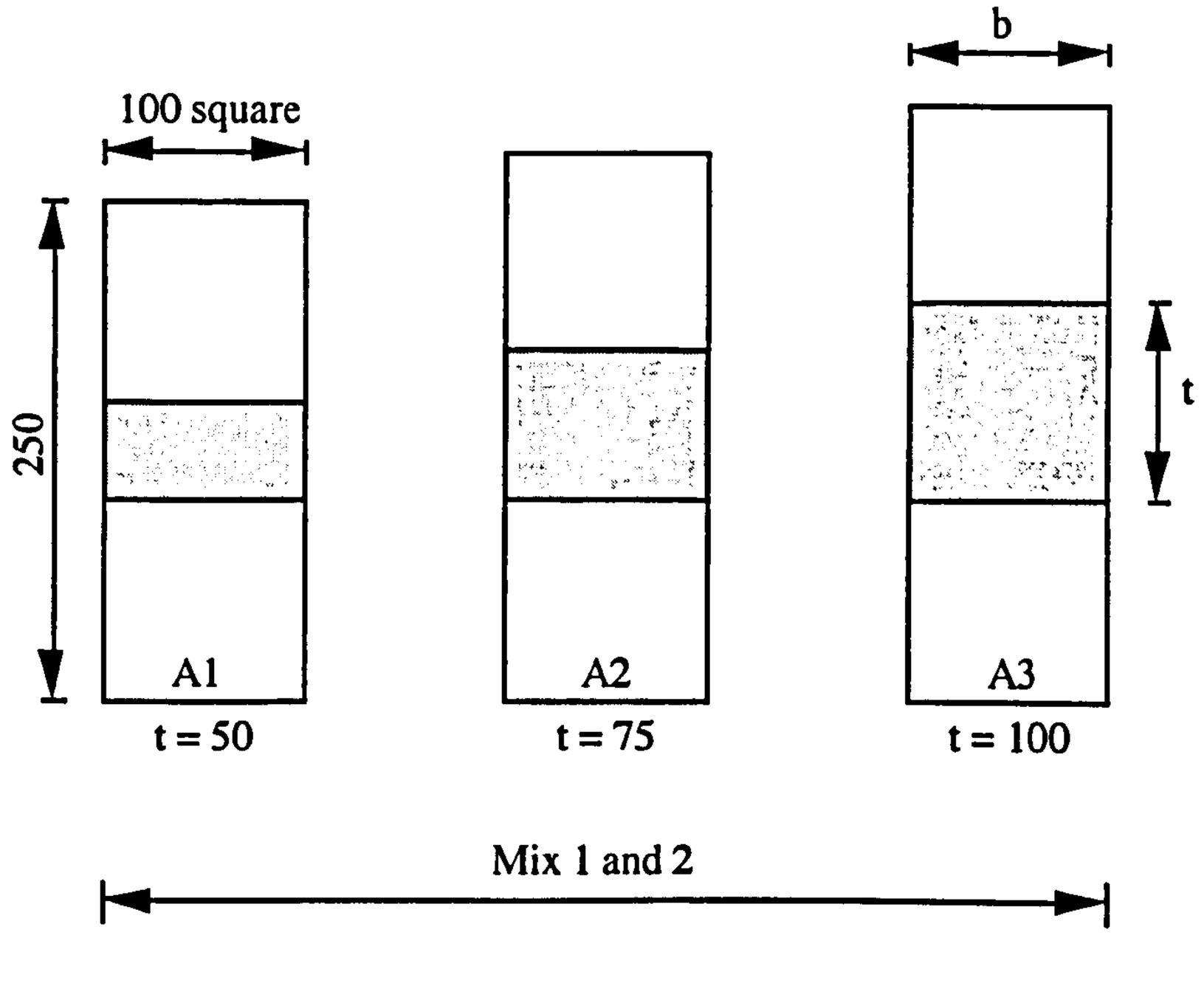

Figure 8.3: Compressive specimens type A used in test series 1

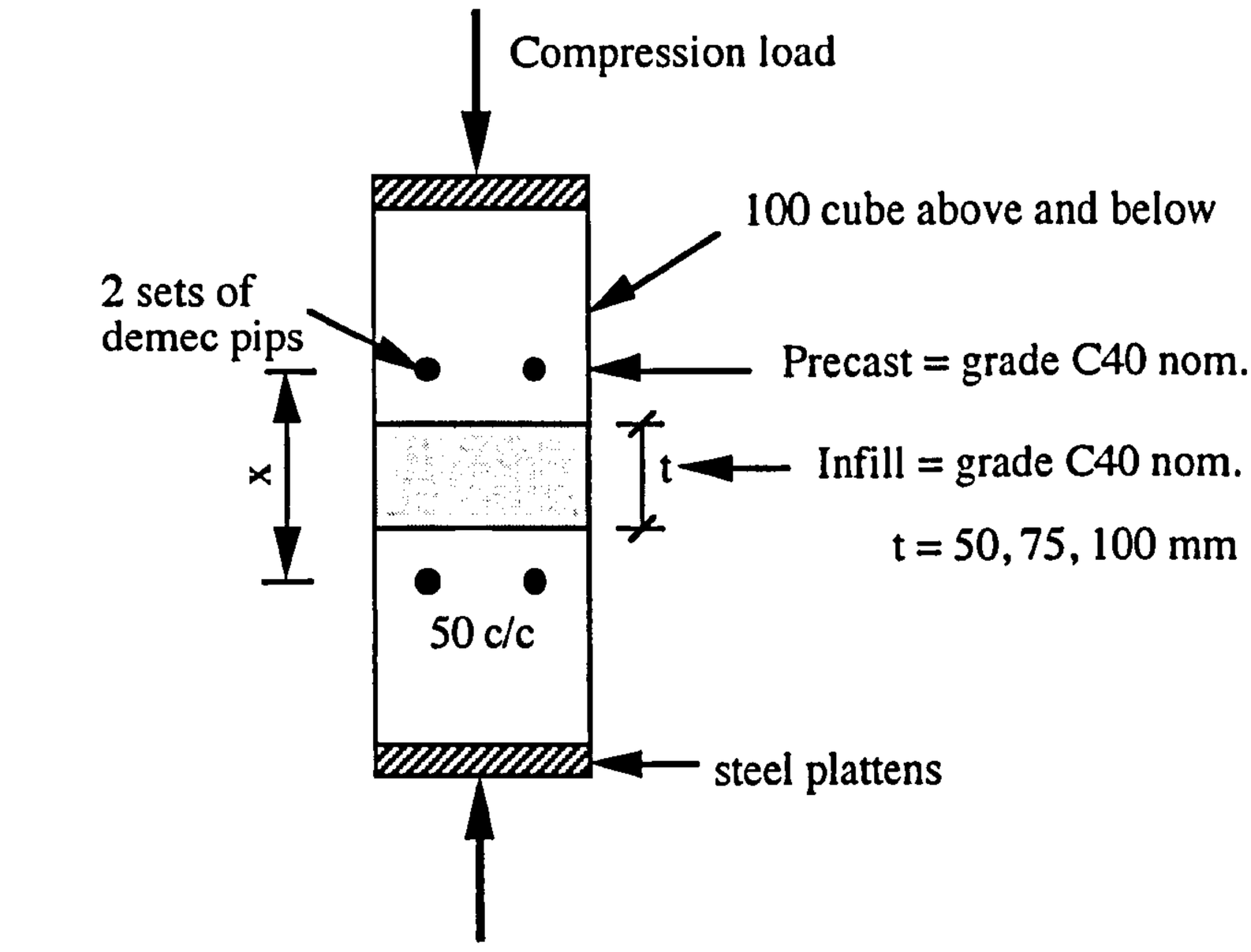

Figure 8.4 Location of demec pips

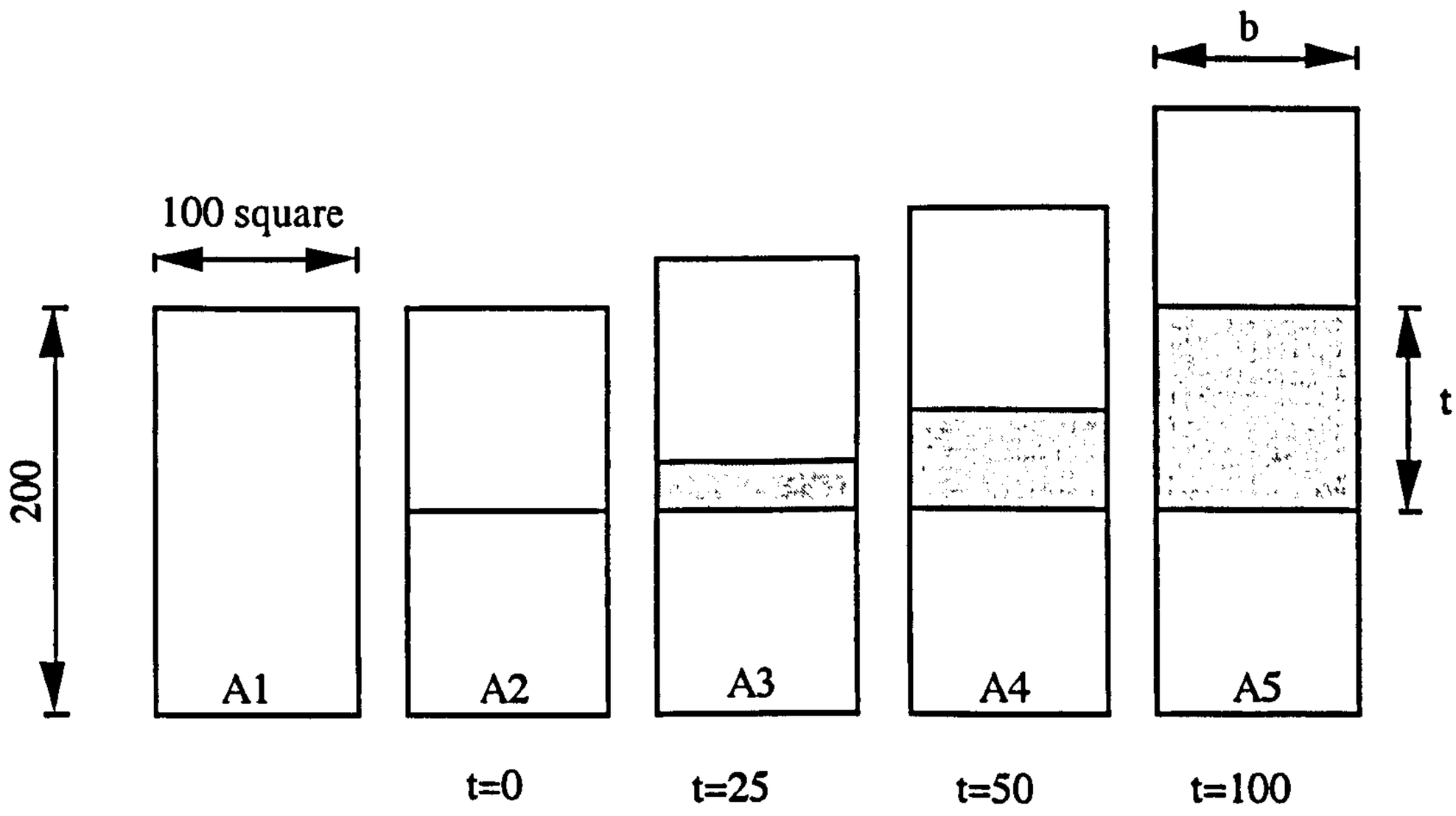

Figure 8.5: Compressive specimens type A used in test series 2

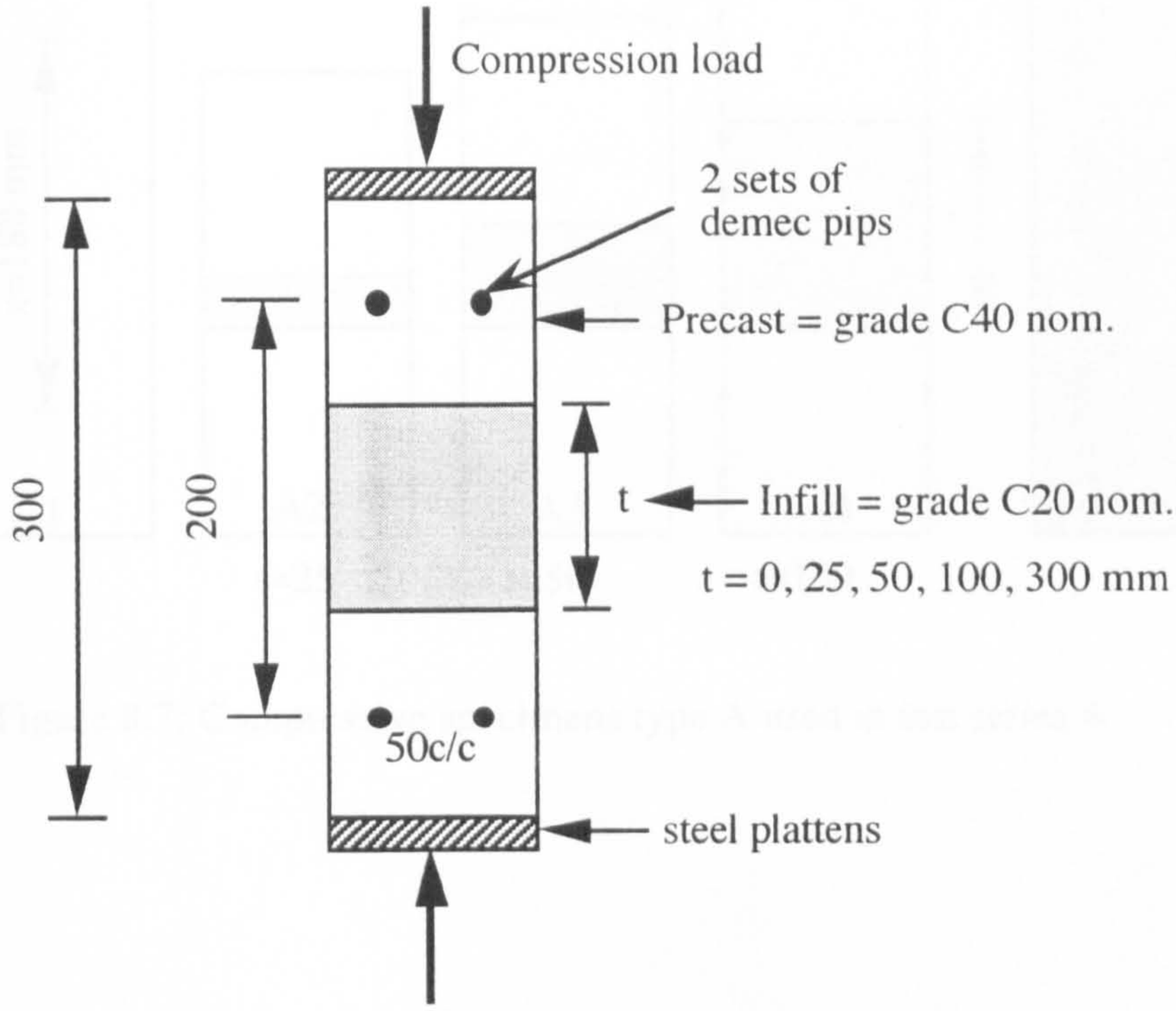

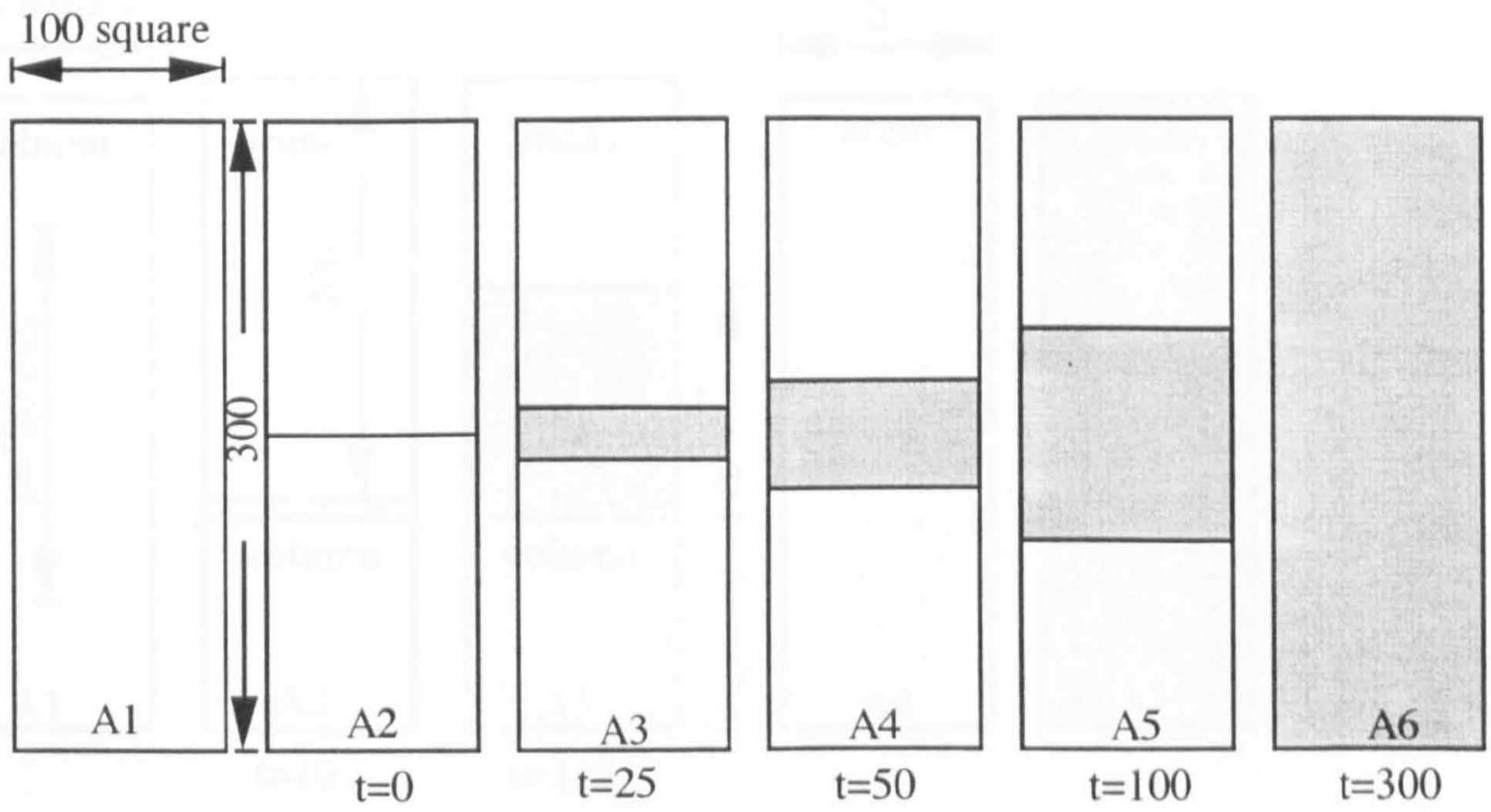

Figure 8.6 Compressive specimens type A used in test series 3

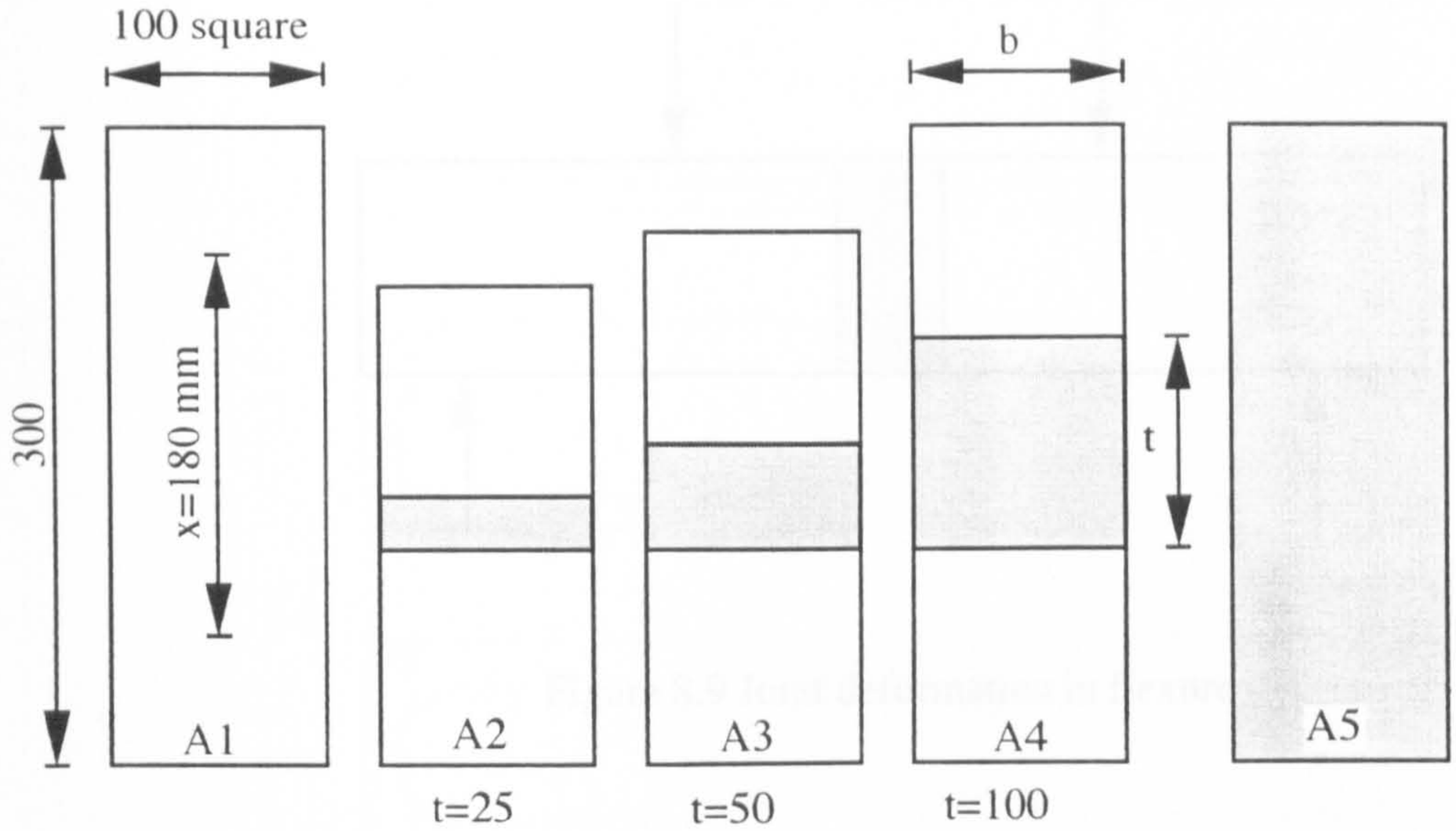

Figure 8.7: Compressive specimens type A used in test series 4

Figure 8.8: Compressive specimens type A used in test series 5

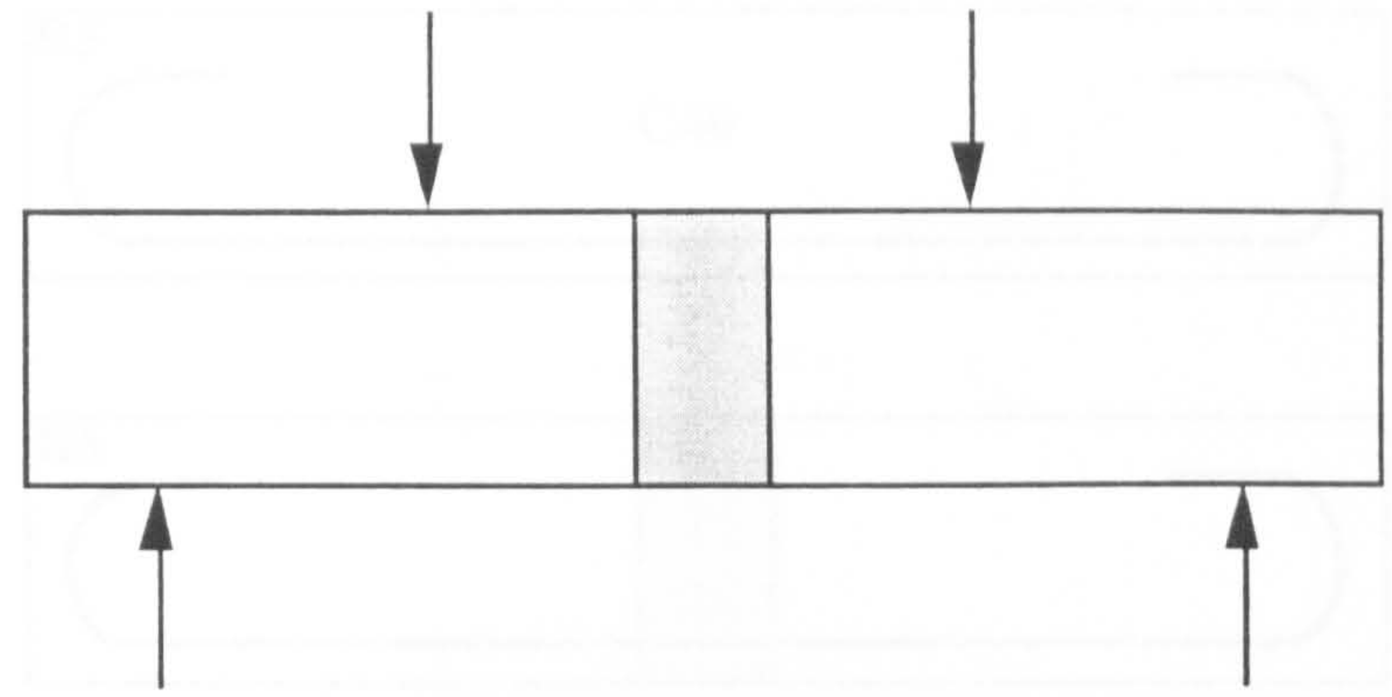

Figure 8.9 Joint deformation in flexure

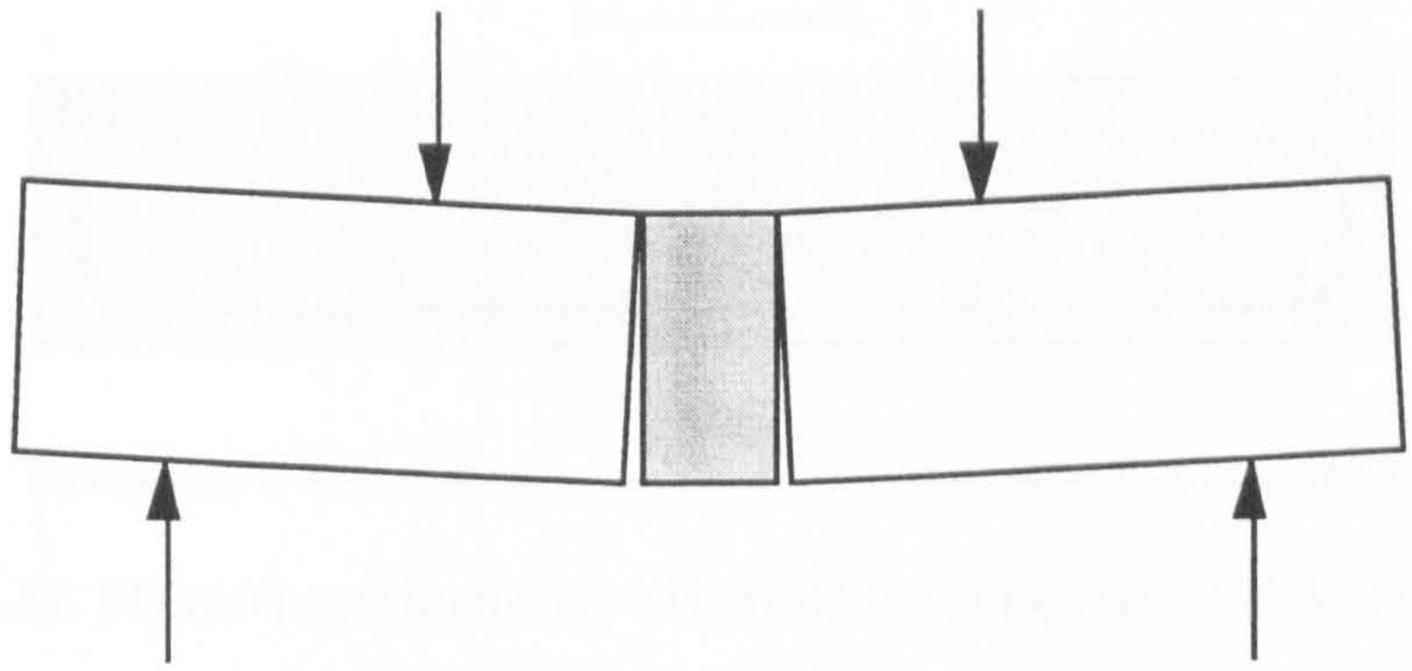

Figure 8.10 Tension cracking at the bottom

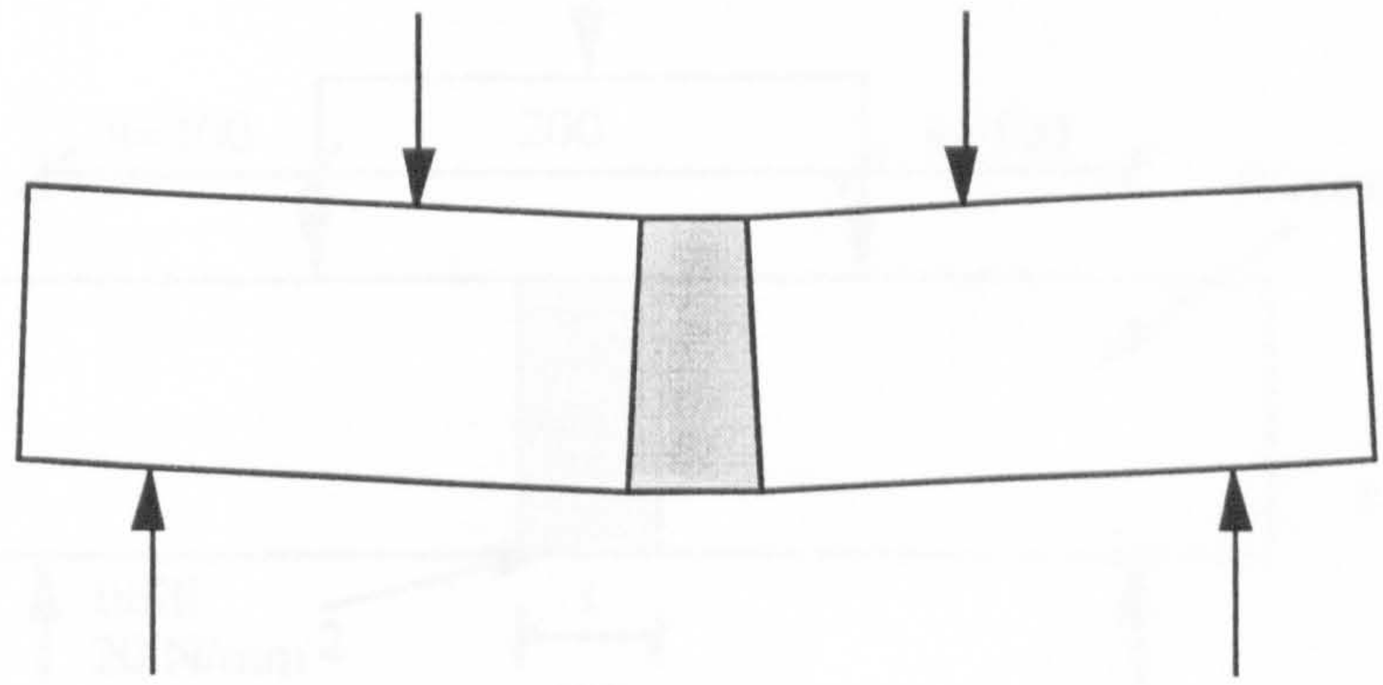

Figure 8.11 Compression deformability at the top

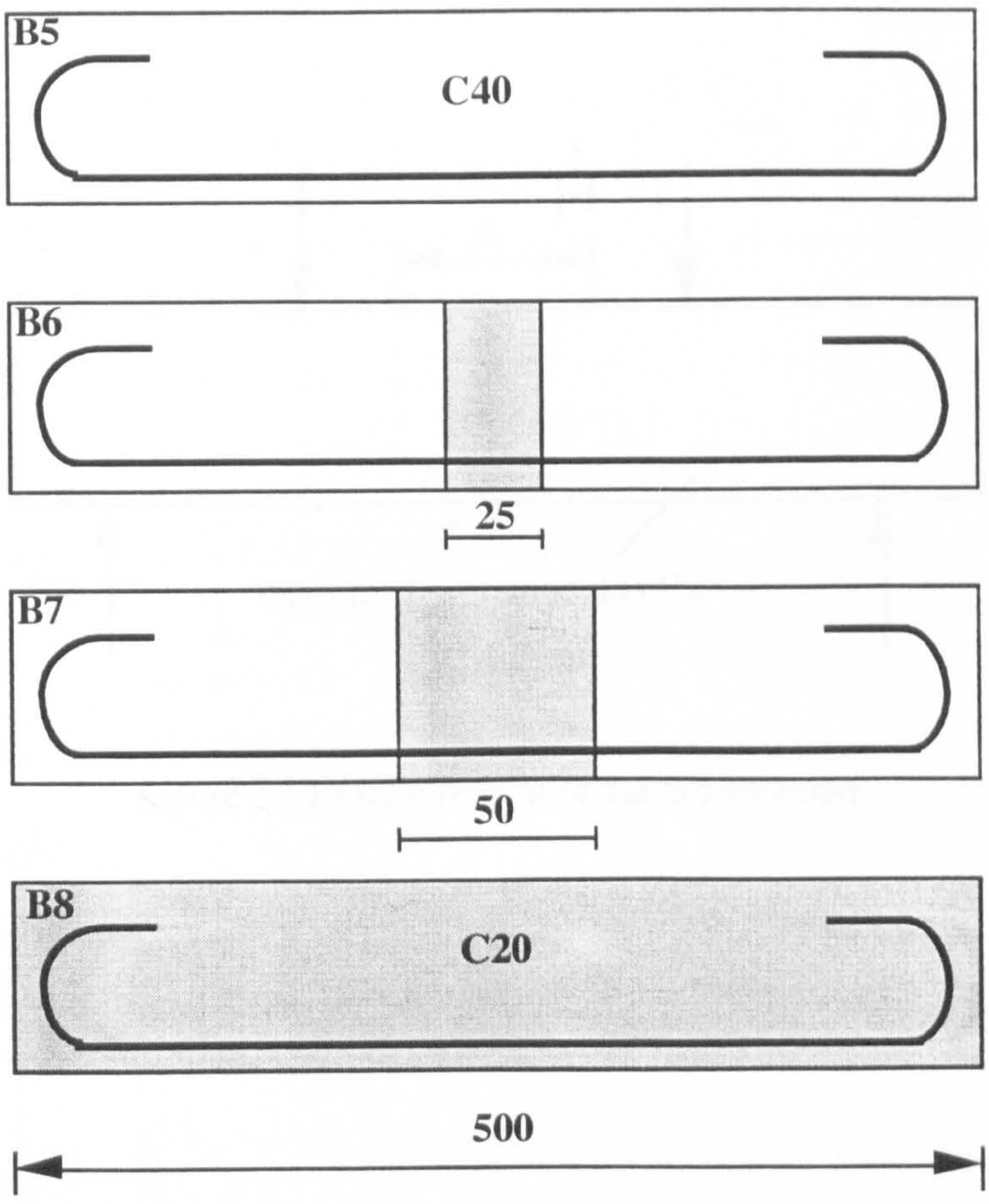

Figure 8.12. Flexural specimens type B tested for compression deformability in test series 6

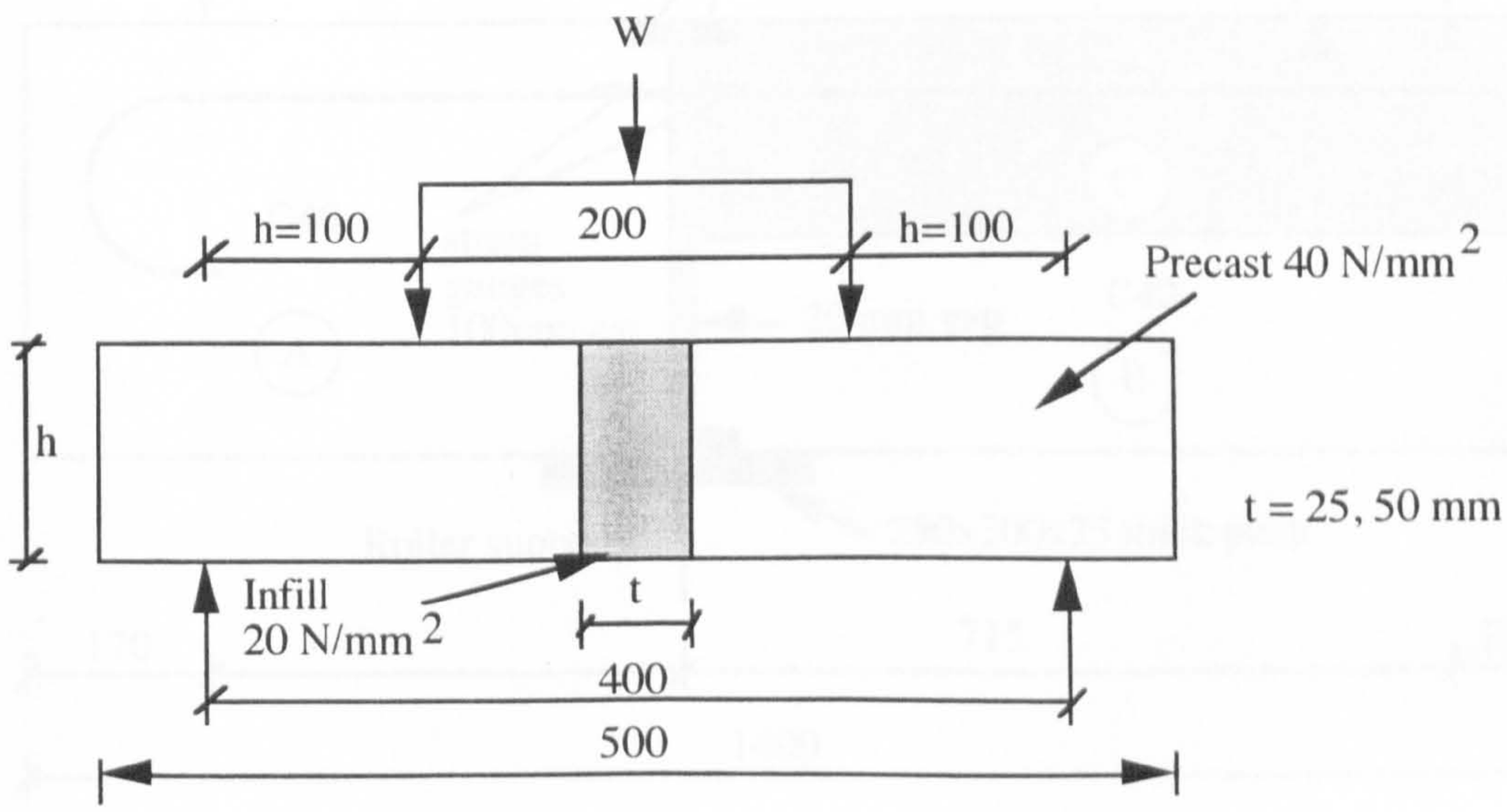

Figure 8.13 The loading of the flexural specimens type B

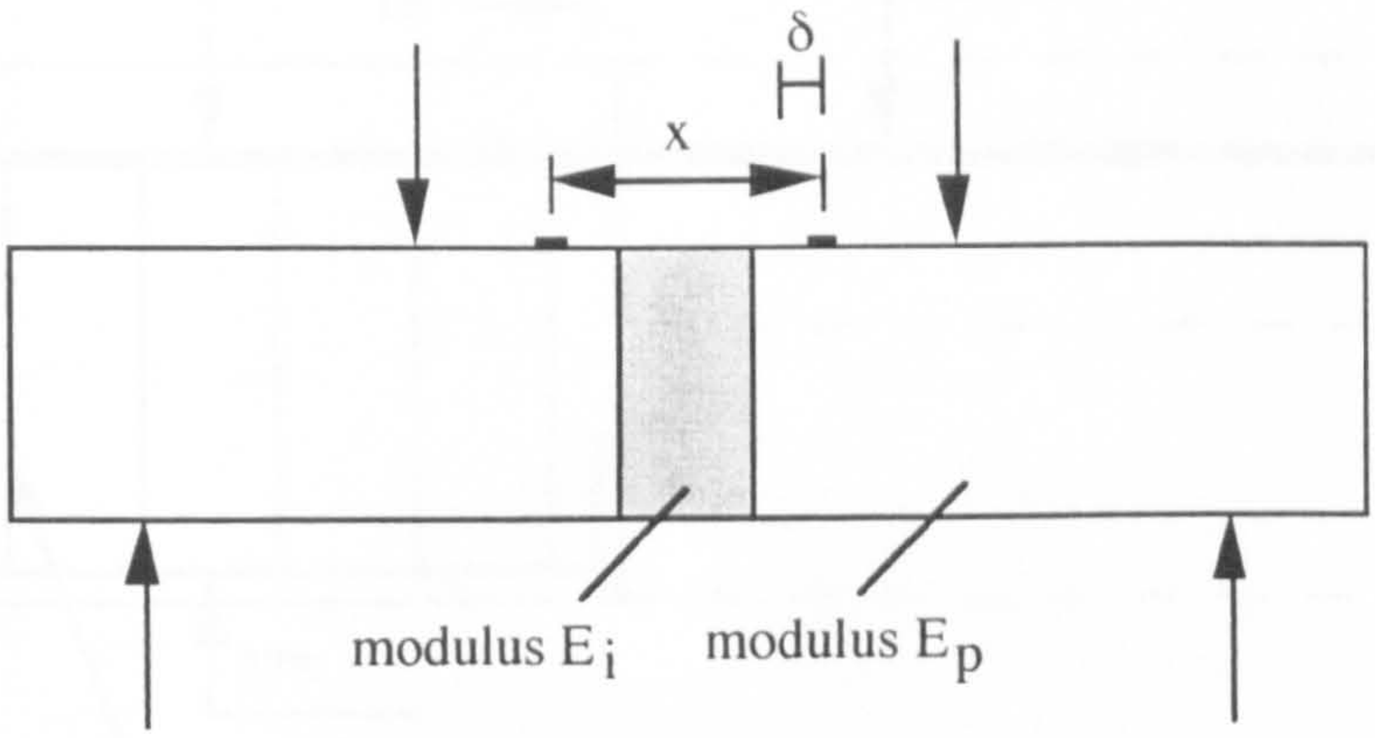

Figure 8.14 Measurement of the deformation

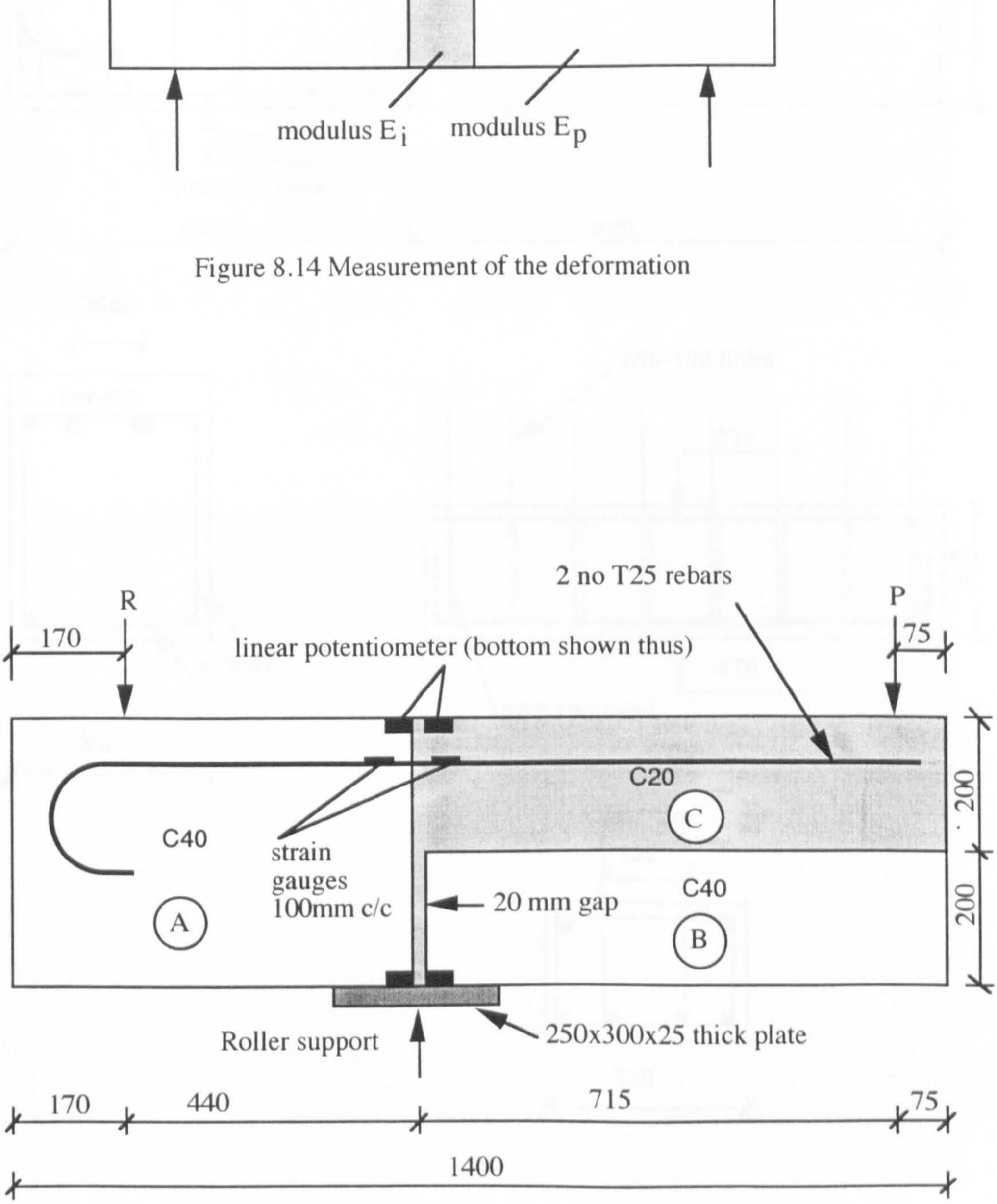

Figure 8.15 General arrangement for flexural joint test

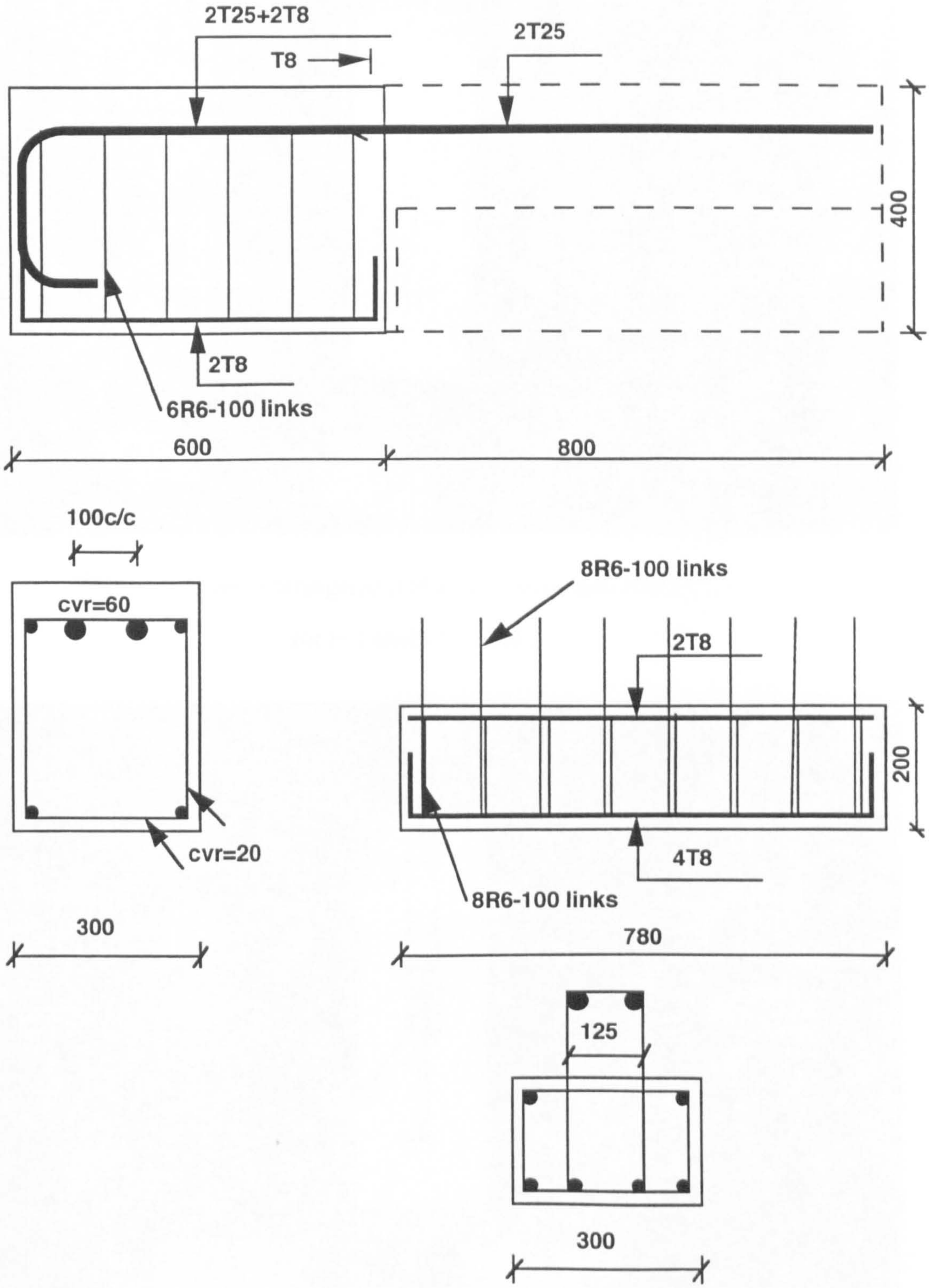

Figure 8.16 Reinforcement used in the test series 7

Plate 8.1: General arrangement of compression specimens type A

for test series 1, 2 and 3

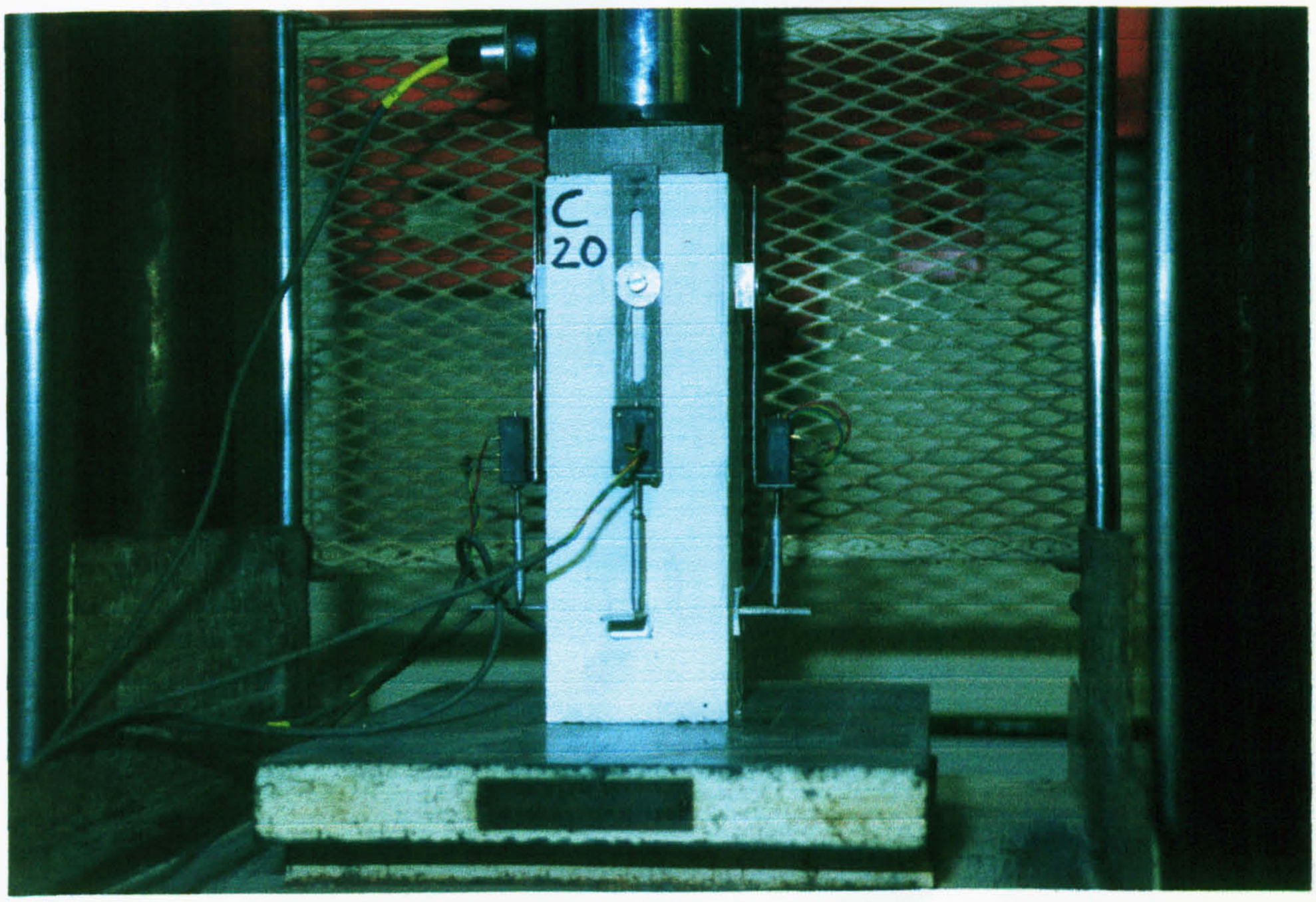

Plate 8.2: General arrangement of compression specimens type A

for test series 4

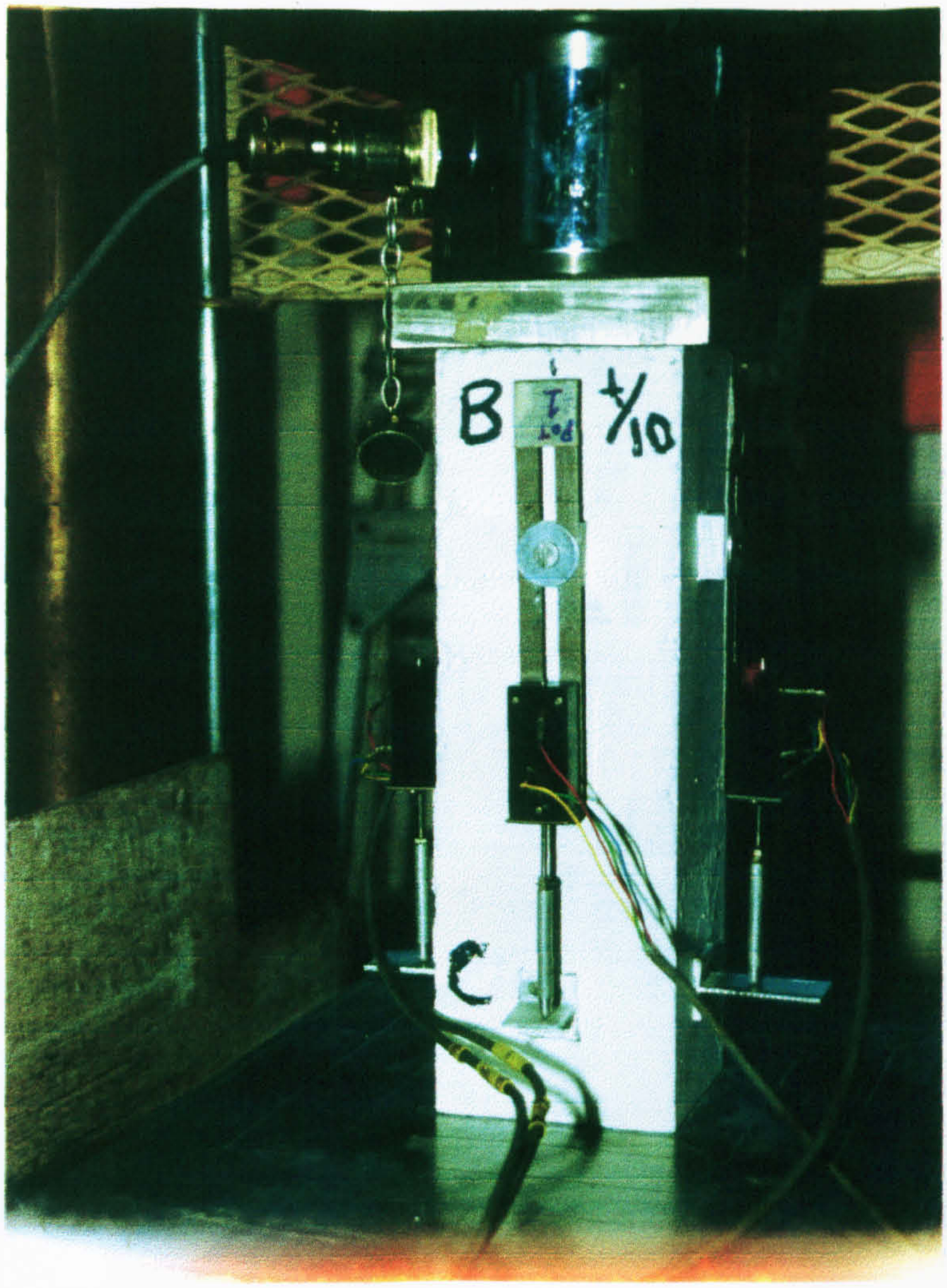

Plate 8.3: General arrangement of compression specimens type A

for test series 5

Plate 8.4: General arrangement of flexural specimens type B for test series 6

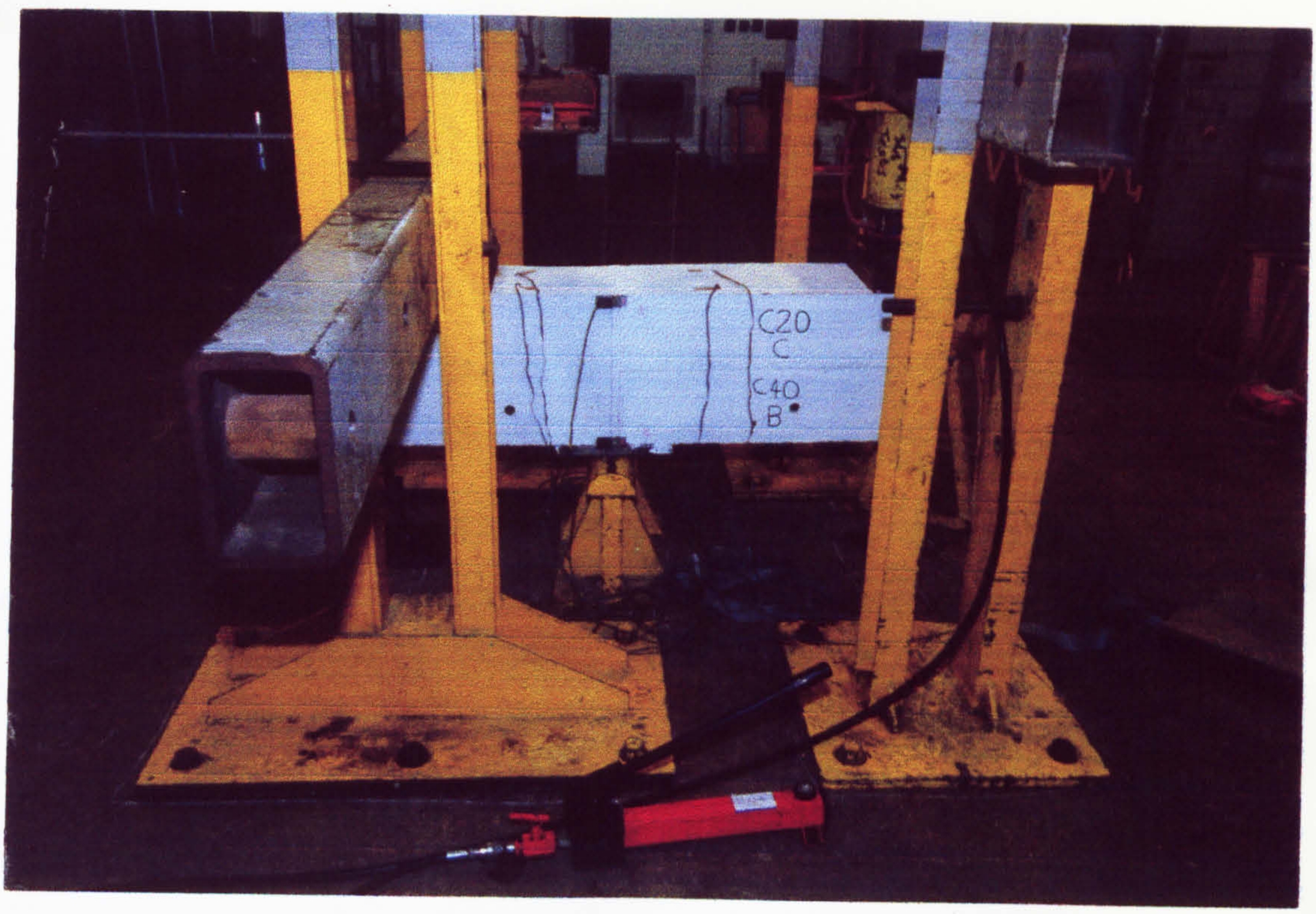

Plate 8.5: General arrangement for bond slip test for test series 7

CHAPTER 9

RESULTS AND DISCUSSION OF COMPONENT METHOD FOR ISOLATED JOINT TESTS

9.1 Results

For test series 1-3 hand calculations were carried out and graphs were plotted using Excel in PC.

AXIS SOFTWARE 3465 was used to process and present the test results for series 4-7 in three stages. The first stage was to transfer data from magnetic tape to PC hard disc (C drive). The second stage involved transferring the data from C drive data file to Excel Spreadsheet. The third stage was to use the spreadsheet in the Excel for calculations (see Section 5.8 in Chapter 5 for details).

9.1.1 Compression tests

In test series 1-3 the axial strain was calculated by using Demec extensometers and 2 sets of Demec pips which were attached to one cast side of the specimens and calculated by multiplying the extensometer reading by 1.99×10^{-5} for 4 inches length gauge, and 1.0×10^{-5} for 8 inches length gauge. In test series 4 and 5 linear potentiometers attached to four sides of the specimens were used to take into account the possibility of nonaxial loading. The strain was calculated by dividing the extensometer reading by the gauge length. In all of these tests the uniaxial compressive

stress σ was calculated by dividing the applied compression load by the cross-section of the specimen. The "effective" secant Young's modulus E_{ce} was calculated at $^2/_3$ ultimate uniaxial compressive stress for each specimen using the measured average uniaxial strain.

Figures 9.1(a) and 9.1(b) show the uniaxial compressive stress versus measured average uniaxial strain in the joint for mixes 1 and 2, respectively.

The failure loads, maximum uniaxial compressive stresses and "effective" secant modulii are presented in Table 9.1. Typical damaged zones for test series 1 are presented in Plate 9.1(a) and 9.1(b) for mixes 1 and 2 respectively.

It was necessary to reduce the compressive cube strength of the in-situ infill concrete from 40 N/mm^2 to 20 N/mm^2 and to vary the thickness of the in-situ infill concrete between 25 mm, 50 mm and 100 mm in test series 2 to observe the real effect of the thickness t on the uniaxial compressive deformability of the joint.

Figures 9.2(a) and 9.2(b) show the uniaxial compressive stress versus measured average uniaxial strain and deformation, respectively in the joint in test series 2. The failure loads, maximum uniaxial compressive stresses and "effective" secant modulii are presented in Table 9.2. Typical damaged zones for test series 2 are presented in Plate 9.2.

It was also necessary to keep the height of all the specimens the same to obtain maximum uniaxial compressive strength by eliminating the variation in height of specimen. By measuring the uniaxial strain across a known constant distance it was possible to observe the real effect of the in-situ infill concrete t which was varied from 0 to 100 mm in test series 3.

Figures 9.3(a) and 9.3(b) show the uniaxial compressive stress versus measured average uniaxial strain and deformation, respectively in the joint in test series 3. The failure loads, maximum uniaxial compressive stresses and "effective" secant modulii are presented in Table 9.3. Typical damaged zones for test series 3 are presented in Plate 9.3

Figures 9.4(a) to (e) show the uniaxial compressive stress versus measured uniaxial strain in the joint for each of the specimens tested in test series 4. Each specimen has four stress versus strain curves giving different E_{ce} values. It can be seen from these figures the effect of any unintended eccentricity of the applied load inducing a bending moment, which might be taken into account by using the lowest stress versus strain curve to obtain a conservative value of E_{ce}. Figure 9.4(f) shows the uniaxial compressive stress versus average uniaxial strain obtained from four readings. The variation in the mean value of E_{ce} obtained from the curves in Figure 9.4(f) is not great and at variance with the minimum and maximum values by 14.9 and 15.0%, respectively. The failure loads, maximum uniaxial compressive stresses and "effective" modulii are presented in Table 9.4. Typical damaged zones for this test series are presented in Plate 9.4.

Figures 9.5(a) to (f) show the uniaxial compressive stress versus measured uniaxial strain in the joint for the specimens tested in test series 5.

Because each specimen in this test series has four stress versus strain curves, the strains obtained from the opposite faces were averaged to observe the variation in the mean value of the "effective" modulii E_{ce}. It was found that it is better to use the mean value of the "effective" modulii rather than the average value obtained from the opposite faces. The failure loads, maximum uniaxial compressive stresses and

"effective" modulii are presented in Table 9.5. Typical damaged zones for this test series are presented in Plates 9.5(a) and (b).

9.1.2 Calculation of effective Young's modulus

For the purpose of structural analysis the members are considered homogeneous of equivalent modulus E_{ce}, and the strains in the equivalent material are the same as in the composite one. The deformability of a joint(s) reduces the stiffness of the connection such that the net value for Young's modulus can be derived as follows:-

The total deformation is given by (see Figure 9.13):-

$$\delta = \delta_{cp} + \delta_{ci} + 2\lambda \qquad Eq.9.1$$

where

$$\delta = \frac{\sigma}{E_{ce}} x\,,\ \delta_{cp} = \frac{\sigma}{E_{cp}}(x-t) \text{ and } \delta_{ci} = \frac{\sigma}{E_{ci}} t$$

λ = deformability of each interface

where

$\sigma = \frac{P}{A}$ uniaxial compressive stress for compression specimens

$\sigma = \frac{M}{Z}$ flexural stress for bending specimens (see Figure 9.17)

Thus

$$E_{ce} = \frac{1}{\frac{1}{E_{cp}} + \frac{t}{x}\left(\frac{1}{E_{ci}} - \frac{1}{E_{cp}}\right) + \frac{n\lambda}{x\sigma}} \qquad Eq.9.2$$

where E_{cp} = Young's modulus for the precast concrete, E_{ci} = Young's modulus for the in-situ infill concrete, P = uniaxial compressive load, A cross-sectional area of the compression specimens, n = number of the interfaces in the joint, λ = is the interface deformability (mm) which has been found to be dependant on the infill thickness t, and x = is the gauge length over which the interface deformation is measured.

Variation in the maximum uniaxial compressive stress σ, and "effective" secant modulus E_{ce} (measured at 2/3 ultimate stress) with t is presented in Figures 9.6 to 9.10.

9.1.3 Bending tests

9.1.3.1 Small scale bending tests

Test series 6:

The deformation was calculated by using two linear potentiometers which were mounted on a steel rod and this clamped to the top of the specimen. The deflection of the two linear potentiometers multiplied by 7.5 (1 division = 7.5 mm deflection). The average deflection was then used in the final presentation of the moment deflection graphs.

The bending moment and flexural stresses are calculated as follows:-

$$M = 0.5Wh \qquad Eq.9.3$$

and $Z_{uncr} = I_u / x_u$

$Z_{cr} = I_{cr} / x_{cr}$

Hence $$\sigma = \frac{M}{Z} \qquad Eq.9.4$$

This is the relationship for a flexurally uncracked and cracked equivalent sections (see details in Section 10.2).

To determine the second moment area of the uncracked equivalent section I_u and the cracked I_{cr} the static modulii given in Table 9.6 were used for the modular ratio $\alpha_e = E_s / E_{ce}$. E_s is the modulus of elasticity of the steel taken as 200 kN/mm^2.

Figure 9.16(a) to (c) shows the applied moment versus average compressive deformation in the joint in test series 6, for t = 0, 25 and 50 mm, respectively. Two theoretical curves, based on the section properties derived from the cracked (Z_{cr}) and uncracked (Z_{uncr}) concrete beam, are also plotted in these figures. The failure moments, maximum flexural stresses are presented in Table 9.7. Figure 9.16(d) shows flexural stress vs. average compressive flexural strain in top of specimens for this test series. The zone of interface deformability for the flexural specimens is defined in Figure 9.17. Variation in the interface deformability λ with t is presented in Figure 9.18 and in the ratio E_{ce} / E_{cp} with E_{ci} in Figure 9.19.

Specimens tested for compression deformability failed in shear at 4.32 and 3.75 kNm for C40 and C40/t = 50 mm, respectively. This was an unintended failure and so for C20 and C40/t = 25 mm four plates were used at the bottom and top of the

specimen on the supports and in the bottom of the applied load points to reduce the shear effects and these specimens failed at 4.5 and 5.5 kNm in flexure as expected. Typical damaged zones for this test series 6 are presented in Plates 9.6(a) and (b).

9.1.3.2 Isolated tension test

Test series 7:

Figures 9.20 to 9.26 show the results from the bending test in test series 7.

The strain in the 2T25 high tensile reinforcement bars was calculated using four strain gauges which were attached on the bars (two for each), the distance between the strain gauges was 100 mm c/c. The average strain was used to calculate force in the steel bars. Bending moment was calculated by multiplying the applied load by the lever arm of 715 mm. Crack width and compressive deformations were calculated using four linear potentiometers, shown in Figure 8.17.

In the tension zone an "effective tensile stiffness K_e" is found which relates bond and tensile deformation δ_T to the applied tension forces. Experimental testing has been carried out to measure these values, which may then be validated against the results of full connection assembly tests.

The anchorage bond length L is the length of the reinforcement bar required to develop the steel stress f_s and is given by:-

$$L = \frac{f_s A_s}{\pi \phi \beta \sqrt{f_{cu}}} \qquad Eq.9.5$$

where ϕ is the effective bar size which, for a single bar is equal to the bar size and, for a group of bars in contact is equal to the diameter of a bar of equal total area A_s and β is a bond coefficient dependent on the bar type. Values of β are given by BS 8110 (Clause 3.12.8.4). For deformed bars $\beta = 0.5$ (BS 8110: Table 3.28). The β values already include a partial safety factor γ_m of 1.4.

Effective anchorage length of the bars was calculated from :

$$L_e = \frac{\delta_T}{\varepsilon_{av}} \qquad Eq.9.6$$

where;

δ_T = average crack width (at the level of ε_{av})

ε_{av} = average axial tensile strain in the bars

Typical damaged zones for the test are presented in Plate 9.7.

Referring to Method 2 in full-scale tests in Chapter 6 Section 6.1.2, relative rotation of the specimens representing beam and slab to the specimen representing column was calculated by the crack width plus compressive deformation divided by the distance between the linear potentiometers located at the top and bottom of the specimen.

9.2 Discussion of isolated tests results

9.2.1 Compression tests

In test series 1 it was expected that the compression load for t = 50 mm > t = 75 mm > t = 100 mm for mixes 1 and 2, but it was found not be the case. One of the reasons for this is probably that the compressive strength of the precast and infill concrete were similar, i.e. 40.7 to 46.6 N/mm^2. For this reason the effect of the in-situ infill concrete on the uniaxial compressive strength of the joint and on the "effective" secant modulus of the specimens cannot be observed, as shown in Figures 9.6(a) and 9.6(b), but the effect of the compressive cube strength of the precast concrete can be observed on the ultimate uniaxial compressive stress of the specimens. Specimens made from mix 1 concrete failed at lower loads than specimens made from mix 2 concrete.

The ratio of the failure stress of the specimen to that of the precast concrete varied from 0.71 to 0.79, which is to be expected for specimen of height to breadth ratios of 2.5 to 3.0.

Values for E_{ce} are lower than would be expected from the well established relationships, e.g. $E_c = 5.5\sqrt{f_{cu}}$ (BS 8110, 1985) and $E_c = 9.1 f_{cu}^{1/3}$ (Neville, 1981), which would indicate E_c in the range 28 to 33 kN/mm^2 for the maximum stresses in the tests. Clearly the presence of two interface joints reduces E_c to approximately 2/3 of monolithic values.

In test series 2 both the compressive strength of the infill and the joint thickness were varied to observe the real effect of the thickness t on the uniaxial compressive deformability of the joint. As expected specimens having a larger infill thickness failed at lower loads, as shown in Figures 9.7(a) and 9.7(b). The most likely

reason for this is the large difference in compressive cube strength of the infill and precast concretes (21.4 N/mm^2 and 40.9 N/mm^2, respectively at the test day).

The effect of a single interface joint is to reduce the monolithic strength and elastic modulus by between 6% and 21%. The large change in elastic modulus is probably due to the sudden increase in strain (see Figure 9.2(a)) just prior to the point at which E_{ce} was measured. The specimen also consisted of one "dry" joint, making it susceptible to having a lower stiffness than in the monolithic case.

In test series 3 specimens having large thickness failed at lower load. The trend was also as expected. From these curves shown in Figures 9.3(a) and (b) it can be concluded that:-

i) - solid specimen A1, C40 long prism, and solid specimen A6, C20 long prism might not be compared with the other specimens due to there being no interface in the specimens, but both can be compared to each other to see the effect of the compressive cube strength of the concrete on the evaluation of Young's modulus for the C40 and C20 concretes. This has been done and presented in Figures 9.8(a) and 9.8(b)

ii) - specimen A2, C40/t=0 (2x150 mm prisms), is different to the remainder because of having a single dry interface joint.

iii) - specimens A3, A4 and A5 can be compared, as shown in Figures 9.8(a) and 9.8(b), with each other to see the real effect of the thickness and compressive strength of the in-situ infill concrete on the evaluation of the deformability in the joint between concrete having different strength. C40/t = 50 curve was expected to lie between C40/t = 25 and C40/t = 100 curves as for maximum stress, but it was not. The reason for this is that the specimen separated due to sensitivity of the joint in one

interface during removal from the mould. This and previous flexure tension crack test results show that this kind of joints is very weak in tension and flexure. The broken interface is therefore significant in a compression test because the failure mode is by lateral splitting.

The effect of a single interface joint is to reduce the monolithic strength and elastic modulus by 8% and 44%, respectively. The large change in elastic modulus is probably due to the sudden increase in strain (see Figure 9.3(a)) just prior to the point at which E_{ce} was measured. The specimen also consisted of one "dry" joint, making it susceptible to having a lower stiffness than in the monolithic case as in the test series 2.

In the test series 4 specimens having large thickness failed at lower loads, as shown in Figure 9.4. It is now obvious that the thickness of the in-situ infill concrete does effect the uniaxial compressive strength and Young's modulus of the specimens as shown in Figures 9.9(a) and 9.9(b). It has been reported by Bljuger (1988) that relatively large deformations of mortar and concrete layers are caused by local contact deformations and because of this are independent of layer thickness. It was found, in these compression tests, not to be the case. This might be the case if the strength of the in-situ infill concrete is the same as the strength of the precast members as observed in test series 1.

The main aim of the test series 4 was to observe the compressive deformability measuring on four surfaces of each specimen. This might be different from surface to surface due, possibly, to the bending moment induced by a small eccentricity of the applied compressive load. It has been found that, as it can be seen from Figures 9.4(a) to 9.4(e), this does not significantly effect the deformability of the joint. The most

damaged surface, includes the effect of the bending moment, of each specimen must be used to obtain the deformability of the joint. This surface may be simulated to the joint's compression zone in full scale frame connection test. i.e. concrete crushing. It was suggested to use mean value of deformability measured from four surfaces.

Figures 9.5(a) and (f) show the uniaxial compressive stress versus strain for specimens in test series 5. The ratio of the failure stress to the cube strength of the precast and grout varied from 0.88 to 0.97, which is to be expected for specimen height to breadth ratios of 3.0. The failure was due to specimen crushing failure in the weakest part. This indicates that the compressive continuity of the joint was being maintained to the lowest strength of the concrete. The main aim of this test was to find out the variation in the behaviour of the specimens A2 and A3 incorporating 10 and 110 mm grout thickness, respectively. Although the specimen having 110 mm grout thickness, A3, failed at test stress of 35.0 N/mm^2 being lower than the value 37.3 N/mm^2 of the specimen A2 Figure 9.10(a) it attained approximately the same modulus as shown in Figure 9.10(b). This is because 100 mm in the upper part, simulating beam concrete f_{cu} = 50.3 N/mm^2, of the specimen A2 (see Figure 8.5) was replaced with grout, f_{cu} = 46.4 N/mm^2, in the specimen A3. The wholly grouted specimen A5 gave the lowest modulus in this test series. In a real joint construction as seen in full scale tests in Chapter 5, the specimen A3 incorporates a RHS billet projecting from the column face. This would give a rise to the strength of the specimen bring in line with the specimen A2 or even greater. This indicates that the results of either specimen A2 or A3 may be used to generate the behaviour of the joint.

9.2.2 Effect of infill on Young's modulus of concrete

Figures 9.11 and 9.12(a) show E_{ce}/E_{cp} ratio versus t/x for series 3 and 4 for experimental results and the analytical equation 9.2. There are no E_{cp} and E_{ci} values for series 1 and 2. Figure 9.12(b) shows E_{ce}/E_{cp} versus t/x at various stress levels for series 4. The zone of interface deformability for compressive specimens is defined in Figure 9.13. Figures 9.14 and 9.15 show σ versus λ for series 3 and 4 for experimental and analytical equation.

In Figures 9.11 and 12(a) the difference between analytical and experimental curves is thought to be due to the term $\frac{n\lambda E_{cp}}{x\sigma}$. This term was taken as zero to plot the analytical curves. Because the interface deformability λ is not known in the term, analytically. It is derived after obtaining E_{ce} from the tests. From equation 9.2 the deformability of the joint λ can be derived as follows:-

$$\lambda = \frac{\sigma}{n}\left(\frac{x}{E_{ce}} - \frac{(x-t)}{E_{cp}} - \frac{t}{E_{ci}}\right) \qquad Eq.9.7$$

In the above equation λ is a linear function of the stress σ. At lower stress levels the variation in λ is greater than the upper cases because of the presence of voids between interfaces, cement rich zones giving greater deformation. These voids are closed rapidly at lower stresses (stress concentration leads to local deformation) and give larger λ values, initially, as shown in Figure 9.13. At this stage it is not

possible to find variation in λ with t. In the above equation as t increases, the term $-\frac{t}{E_{ci}}$ decreases the λ values, and the term $\frac{x}{E_{ce}}$ increases the λ values.

Two reduction factors causing a decrease in the E_{ce}/E_{cp} ratio were found as:-

1) Reduction factor due to t :

the term $\frac{t}{x}\left(\frac{E_{cp}}{E_{ci}}-1\right)$ (would be zero if t = 0, hence there would be no reduction in the E_{ce}/E_{cp} ratio)

2) Reduction factor due to the interface deformability λ:

the term $\frac{n\lambda E_{cp}}{x\sigma}$

With t = 0, then $\lambda = 0$ for wholly precast and infill specimens, and equation 9.7 becomes:-

$$\lambda = \sigma x\left(\frac{1}{E_{ce}}-\frac{1}{E_{cp}}\right) \text{ for a single dry interface joint} \qquad Eq.9.8$$

For wholly precast and infill specimens in Figures 9.11 and 12(a) there is no interface hence no reduction in the E_{ce}/E_{cp} ratio, and the analytical and experimental results are the same, but for the specimen having a single dry interface joint the reduction

factor as shown in Figure 9.11, only due to the interface deformability (the term $\frac{n\lambda E_{cp}}{x\sigma}$) is about 44% (in this specimen no reduction due to t). For the specimens with infill concrete the area above the analytical curves shows the reduction factor due to t, and the area between analytical and experimental curves shows the reduction factor due to the term $\frac{n\lambda E_{cp}}{x\sigma}$.

Clearly as t increases the reduction factor due to t increases, and due to λ decreases. Figure 9.12(b) shows the variation in the E_{ce}/E_{cp} ratio between the analytical and the experimental curves with various stress levels at which the E_{ce} values were obtained and used in the curves. The same stress levels were used for each specimen. In this case the reduction factor due to the deformability term increases as t increases as shown in Figure 9.12(b) as the difference between the solid and dashed lines.

Figures 9.14 and 9.15 show the uniaxial stress versus interface deformability λ of the joint in the extreme stress zone as shown in Figure 9.13. There are no values for wholly precast and infill specimens (no interfaces). The data for the curves were calculated on the basis of the relative deflection of each specimen up to 14 and 20 N/mm^2 stress levels where the regular data were available for the specimens, respectively for the test series 3 and 4. It was done by obtaining the gradient of the stress deflection σ - δ curve of each specimen.

Analytical curves were plotted using equation 9.7.

where $\sigma = \frac{P}{A}$

Experimental curves were plotted using the data obtained from:

$$\lambda = \left(\delta - \frac{(x-t)}{x}\delta_{cp} - \frac{t}{x}\delta_{ci} \right) \text{ using the same stress for each specimen} \quad Eq.9.9$$

At each stress level δ, δ_{cp} and δ_{ci} were found from the corresponding specimens, and substituted in above equation to find λ. This caused a "zigzag" pattern to the test curves in Figure 9.14 and 9.15 due to the fact that λ is derived from the algebraic summation of 3 measured terms, and small variations in measurements at each load increment will have drastic effects on the final output value.

From Figure 9.14, analytically and experimentally, the variation in the deformability λ with stress σ is in the increasing order of magnitude :- t = 100, 25, 50 and 0 (dry joint). Initially the specimen with t = 50 mm infill shows similar behaviour to the specimen with t = 0 (dry one) because of the separated interface giving larger λ values at lower stresses. After gaining full contact interfaces, the variation in λ is negligible for the specimens having infill concrete. Gaining the full contact interfaces in a dry joint takes longer (requires greater stresses levels) than the others, and the increase in λ is continuous with the increase in stress σ, because the voids in a precast-infill interface are less than in the dry joint one. Most of the voids in the precast-infill interfaces are filled with fresh concrete making a good contact zone.

The ratio of the total interface deformability 2λ of the specimen with t = 50 mm (two interfaces) to the total joint deformation δ (measured over a distance x = 200 mm) is about 0.51, and 0.78 for the single dry joint one at 14 N/mm^2 stress level. This

was the maximum stress at which the deformations of the wholly infill specimen were recorded.

From Figure 9.15 the variation in the deformability λ is in the increasing order, in magnitude :- t = 100, 25 and 50 mm as in Figure 9.14, analytically. This order was not improved experimentally. Once again the large values of the λ take place at lower stresses. The maximum ratio of the $2\lambda/\delta$ is about 0.14 for specimen with t = 100 mm infill (the δ was measured over a distance x = 180 mm). This effect might be ignored to find flexural stiffness of the connections to compare with those δ_T and δ_B.

9.2.3 Bending tests

9.2.3.1 Small scale bending tests

Test series 6:

In test series 6, the specimens having interfaces tested for tension cracking in flexure failed at the same load of 0.4 kN. The thickness of the infill concrete had no effect on the tension cracking in flexure. Also, these results show that these kind of joints are very weak in tension and there is no need to carry out further experimental tests in this area.

Most of the specimens tested for compression deformability failed in shear. This was an unintended failure as shear links which reduce shear effects were not used. Specimen C40/t = 25 mm failed in flexure as expected.

From Figure 9.16(a) the gradients of the theoretical moment deflection M-δ curves are 43.5 and 27.75 kNm/mm for C40 specimen based on the transformed section properties derived from the flexurally cracked and uncracked concrete beam.

First flexural crack occurred at 1.88 kNm. Up to the first crack the compressive deformation δ is less than the theoretical values, thereafter the experimental values of δ lie between the two theoretical curves. The gradient of the experimental M-δ curve is approximately 133.35 kNm/mm up to a moment M = 1.0 kNm, and 29.17 kNm/mm between M = 1.0 - 2.75 kNm (close to the flexurally cracked curve), and 18.18 kNm/mm thereafter. A shear crack occurred at a moment of 2.5 kNm and propagated from the bottom supports towards the bottom of the applied load points. At 3.5 kNm another flexural crack appeared in the middle of the tension zone extending to the compression zone. The specimen failed at 4.32 kNm in shear. The failure load which was calculated based on the compressive cube strength f_{cu} of the specimen at test day was 5.57 kNm. The ratio of the failure loads was 0.78.

From Figure 9.16(b) the gradient of the theoretical curves is 42.5 and 27.75 kNm/mm. It varies with E_{ce} and Z. The experimental curve lies below the theoretical curves. Because this specimen has two interfaces. Their effect increases the compressive deformation δ reducing the flexural stiffness of the joint. There might be two reasons for this behaviour:-

1) The strength of the in-situ infill concrete

2) The presence of the two interfaces.

The specimens failed at 5.5 kNm in bending. The trend was as expected. The calculated failure moments based on the compressive cube strengths of the concretes at test day were in the range of 4.38 and 5.57 kNm for wholly infill and precast specimens, respectively. It seems that the joint and its interfaces do not reduce the strength of the specimen in flexure. (It does reduce the uniaxial strength of the specimens in compression tests, especially for specimen having large difference

between the compressive cube strengths of the infill and the precast concretes. See test series 2, 3 and 4 in compression). The ratio of the test failure load to the calculated maximum failure load was 0.99. This was the most successful result within the specimens tested in this test series. First flexural crack occurred at 1.63 kNm. The gradient of the moment deflection M-δ curve is 19.36 kNm/mm between 1.0-3.25 kNm moment values. The recorded maximum flexural strain was 0.00518. It was not possible to record the strain at failure load. The ratio of the recorded maximum strain to the ultimate strain, ε_{cu}, of 0.0035 was 1.48. This large difference is due to the two interfaces of the joint.

From Figure 9.16(c) the gradient of the two theoretical curves is 42.65 and 27.35 kNm/mm. The experimental curve is similar to C40/t=25 mm curve, but this specimen failed at 3.75 kNm in shear. The expected range was 4.38 to 5.57 kNm and the ratio of the test failure moment to the calculated failure moments was in the range of 0.67 to 0.86.

Figure 9.16(d) shows the flexural stress strain curves of the specimens. At the same stress level, the strain in the specimens having in-situ infill concrete is greater than the wholly precast one. Unfortunately, linear potentiometers attached to the wholly in-situ specimen did not record deflections up to a moment value of 1.75 kNm. But this specimen failed at 4.5 kNm in bending. First shear crack occurred at 1.88 kNm. The calculated maximum failure moment for this specimen was 4.38 kNm. The test failure moment was greater than the calculated value by 2.7%.

Figure 9.18 shows the flexural stress based on the uncracked section versus interface deformability λ of the joint in the extreme stress zone as shown in Figure 9.17. There are no values for wholly precast and infill specimens. Because of having

no data for the wholly infill specimen up to 1.75 kNm, it was not possible to find interface deformability λ of the joint initially which is very important to evaluate the variation in λ. The data for the curves were calculated on basis of the relative deflection of each specimen between 12.9 - 21.5 N/mm^2 stress levels where the regular data were available for the specimens. It was done by obtaining the gradient of the moment deflection M - δ curve of each specimen.

Analytical curves were plotted using equation 9.7.

where $\sigma = \dfrac{M}{Z_{uncr}}$

Surprisingly, the gradient of the two analytical curves was found to be negative. This is because the derived values for E_{ce} were larger than was expected. Figure 9.19 shows that there is a limiting value for the ratio E_{ce}/E_{cp} which gives a value of $\lambda = 0$. Taking $E_{cp} = 30$ kN/mm^2, x = 118 mm (to be consistent with experiments) and t = 25 mm and 50 mm, if E_{ce}/E_{cp} lies above the lines drawn on Figure 9.19 then λ will be negative. If E_{ce}/E_{cp} falls below the lines then λ will be positive. In the case of test series 6 the ratio of E_{ce}/E_{cp} was 0.98, indicating that λ will be negative in specimen t = 25 mm and positive in specimen t = 50 mm.

Experimental curves were plotted using the data obtained from equation 9.9 using the same flexural stress for each specimen. As in the compression specimens, at each flexural stress level δ, δ_{cp} and δ_{ci} were found from the corresponding specimens, and substituted in above equation to find λ. This also caused a "zigzag" pattern to the test curves in Figure 9.18 due to the fact that λ is derived from the algebraic summation of 3 measured terms, and small variations in measurements at

each load increment will have drastic effects on the final output value. In this test it was found that an increase in t decreases λ, both analytically and experimentally. However, it is possible to draw boundary envelopes to these results which give :-

$$\lambda/\sigma = +0.0002 \text{ to } 0.0003 \text{ mm / N / mm}^2 \text{ for t = 25 mm}$$

and

$$\lambda/\sigma = +0.00005 \text{ to } 0.0001 \text{ mm / N / mm}^2 \text{ for t = 50 mm.}$$

The values for t = 25 mm are similar to these obtained for the axial load tests (see Figure 9.15).

9.2.3.2 Isolated tension test

Test series 7:

In the tension zone the linear stiffness of the embedded reinforcement is a function of the axial stiffness of the bars themselves, and the lever arm to the compressive zone. Because the latter may change during the onset of concrete crushing and may not be assumed from the geometry of the connection, it is necessary to measure the actual strains in the bars

From Figure 9.20 the relationship between the average axial tensile strain ε_{av} and the crack width δ_T is approximately linear up to a crack width of 0.5 mm. Where an effective bond exists the strain in the reinforcement may be assumed to be equal to that in the adjacent concrete. Thereafter the strain gradient decreases from 1.84×10^{-3} to 0.82×10^{-3} mm^{-1}. Factors which help to prevent the longitudinal splitting of the concrete along the bars could be expected to increase the usable bond capacity: namely a higher concrete strength, heavier shear links and larger concrete cover to the

reinforcement bars. In this test concrete cover was large enough (60 mm to links) but concrete strength of the in-situ infill was not great enough to extend the linear curve to a larger crack width level, i.e. 1.7 mm where the steel strain is lower than the design yield strain, the strain at $0.87 f_y$ and are hence calculated as $0.87 f_y / E_s = 0.002$ for $f_y = 460\ \text{N/mm}^2$ (Note: $E_s = 200\ \text{kN/mm}^2$).

From Figure 9.21 the anchorage bond stress $f_b = 1.60\ \text{N} / \text{mm}^2$ is lower than the ultimate anchorage bond stress $f_{bu} = 2.25\ \text{N} / \text{mm}^2$ (BS 8110). The calculated anchorage bond length (869 mm) required to develop the stress f_s (437.20 N/mm^2) is greater than the experimental results (779 mm) by 10.4%. A partial safety factor γ_m of 1.56 was obtained

From Figure 9.23 the effective stiffness K of the embedded bar is approximately 180 kN/mm up to a crack width of 0.5 mm, and 100 kN/mm thereafter. The effect of bond slip, tension stiffening etc. are all included in these data.

From Figure 9.26 the flexural stiffness J of the connection is approximately 36200 kNm/rad up to a rotation value of 0.0016 rad, and 16100 kNm/rad thereafter. This data might be used to present a monolithic joint data point to compare with those precast concrete connections tests. (See Chapter 7).

The test procedure was to apply load increments until the joints were not capable of supporting any further bending load.

Steel strains increased to more than 2450 με indicating possible yielding of the bars. Ultimate failure was due to the in-situ infill concrete flexural (bond) failure above the mid-span of the beam as in the tests TB1(B) and TB1(C). The ratio of the

measured experimental flexural strength of the joint to that of the predicted $M_u/M_{pred} = 0.93$.

9.3 Summing up

In this section, the performance of the specimens has been compared based on their uniaxial strength for compression and flexural strength for bending tests only as the relative rotation and flexural stiffness are not applicable.

All the compression specimens were cast in the same cross-sectional area and subjected to the compressive load using the same testing machine to facilitate comparison of test results. The actual cube strengths at test days are listed in Table 8.1 and test strengths in Tables 9.1 to 9.5. It is clear that the test strengths of the specimens are less than those the actual strengths of the weakest cubes in the specimens which is to be expected for specimen of height to breadth ratios of 2.5 to 3.0. This was mainly due to the strength of the different cubes, representing precast and in-situ concretes, being much greater than each other, uncertainties of the contribution of the each individual cube and confinement of the cube representing joint concrete or grout. For the specified grade C40 precast and in-situ concretes, the variations in the test strengths are ignorable and for the specified grade C40 precast and C20 in-situ concretes the variations changed to a decrease with an increase in t indicating the importance of the strength of the in-situ infill concrete. Currently, in design practice this is only used to protect the mechanical connection against fire and corrosion. It was felt that the joint concrete strength that greater than the precast

concrete may cause failure to occur in the member themselves near to the joint attaining the full moment capacity of the connection.

The small bending specimens were subjected to the same beam end vertical reaction bending load distances to the centre of the specimens to facilitate comparison of test results. The measured and predicted ultimate moments of the specimens are listed in Tables 9.6 and 9.7. The ratio of the measured experimental flexural strengths of the compression specimens to those of the predicted M_u/M_{pred} varied from 0.78 up to 1.03 in the wholly precast and in-situ infill specimens.

The joint in the tention test, test series 7, was subjected to the beam end vertical bending load to induce M_{con} at the face of the column to facilitate comparison of test results with those of full scale tests by keeping the same concrete cover to the stability tie bars and meassuring the crack width at the same distamce from the bars. This enables the derivation of the moment-rotation data from the isolated joint test to compare with those of the full scale tests. This has been done and presented in Chapter 10.

	Test Ref	Infill depth t mm	Failure loads kN	Ultimate strength N/mm^2	2/3x Ultimate strength N/mm^2	Effective modulus E_{ce} kN/mm^2
Mix 1	A1	50	300	30.0	20.0	22.8
	A2	75	325	32.5	21.7	22.3
	A3	100	325	32.5	21.7	20.0
Mix 2	A1	50	359	35.9	23.9	19.1
	A2	75	369	36.9	24.6	19.9
	A3	100	357	35.7	23.8	19.8

Table 9.1: Results for axial compression specimens type A used in test series 1

Test Ref	Infill depth t mm	Failure loads kN	Ultimate strength N/mm^2	2/3x Ultimate strength N/mm^2	Effective modulus E_{ce} kN/mm^2
A1	*	318	31.8	21.2	27.9
A2	0	300	30.0	20.0	22.2
A3	25	280	28.0	18.7	21.9
A4	50	200	20.0	13.3	16.0
A5	100	180	18.0	12.0	14.4

Note * Solid precast specimen, i.e. no infill used

Table 9.2: Results for axial compression specimens type A used in test series 2

Test Ref	Infill depth t mm	Failure loads kN	Ultimate strength N/mm^2	2/3x Ultimate strength N/mm^2	Effective modulus E_{ce} kN/mm^2
A1	*	320	32.0	21.3	31.8
A2	0	295	29.5	19.7	17.9
A3	25	260	26.0	17.3	17.5
A4	50	220	22.0	14.7	15.5
A5	100	180	18.0	12.0	15.5
A6	**	160	16.0	10.7	15.3

Note * Solid precast specimen, i.e. no infill used

** Solid infill specimen, i.e. no precast used

Table 9.3: Results for axial compression specimens type A used in test series 3

Test Ref	Infill depth t mm	Failure loads kN	Ultimate strength N/mm^2	2/3x Ultimate strength N/mm^2	Effective modulus E_{ce} kN/mm^2
A1	*	430	43.0	28.7	33.6
A2	25	380	38.0	25.3	27.7
A3	50	310	31.0	20.7	26.2
A4	100	250	25.0	16.7	24.8
A5	**	230	23.0	15.3	23.2

Note * Solid precast specimen, i.e. no infill used

** Solid infill specimen, i.e. no precast used

Table 9.4: Results for axial compression specimens type A used in test series 4

Test Ref	Infill depth t mm	Failure loads kN	Ultimate strength N/mm^2	2/3x Ultimate strength N/mm^2	Effective modulus E_{ce} kN/mm^2
A1	*	338	33.8	22.5	26.7
A2	10	373	37.3	24.9	27.3
A3	110	350	35.0	23.3	26.9
A4	**	453	45.3	30.2	30.4
A5	***	450	45.0	30.0	23.5

Note * Solid precast specimen representing column, i.e. no infill used
** Solid precast specimen representing beam, i.e. no infill used
*** Solid infill specimen, i.e. no precast used

Table 9.5: Results for axial compression specimens type A used in test series 5

Test Ref	Infill depth t mm	Density ρ kg/m^3	Pulse velocity V m/s	E_{cq} kN/mm^2	E_c kN/mm^2
B1	*	2354.8	4.252	38.8	29.5
B2	25	2400.2	4.405	38.2	28.8
B3	50	2385.0	4.386	38.3	28.9
B4	**	2386.4	4.390	35.5	25.3

Note * Solid precast specimen, i.e. no infill used
** Solid infill specimen, i.e. no precast used

Table 9.6: Results for flexural specimens type B used in test series 6

Test Ref	Infill depth t mm	Failure loads kN	Ultimate strength N/mm^2
B5	*	86.3	24.8
B6	25	110.0	31.6
B7	50	75.0	21.5
B8	**	90.0	25.7

Note * Solid precast specimen, i.e. no infill used
** Solid infill specimen, i.e. no precast used

Table 9.7: Results for flexural specimens type B used in test series 6

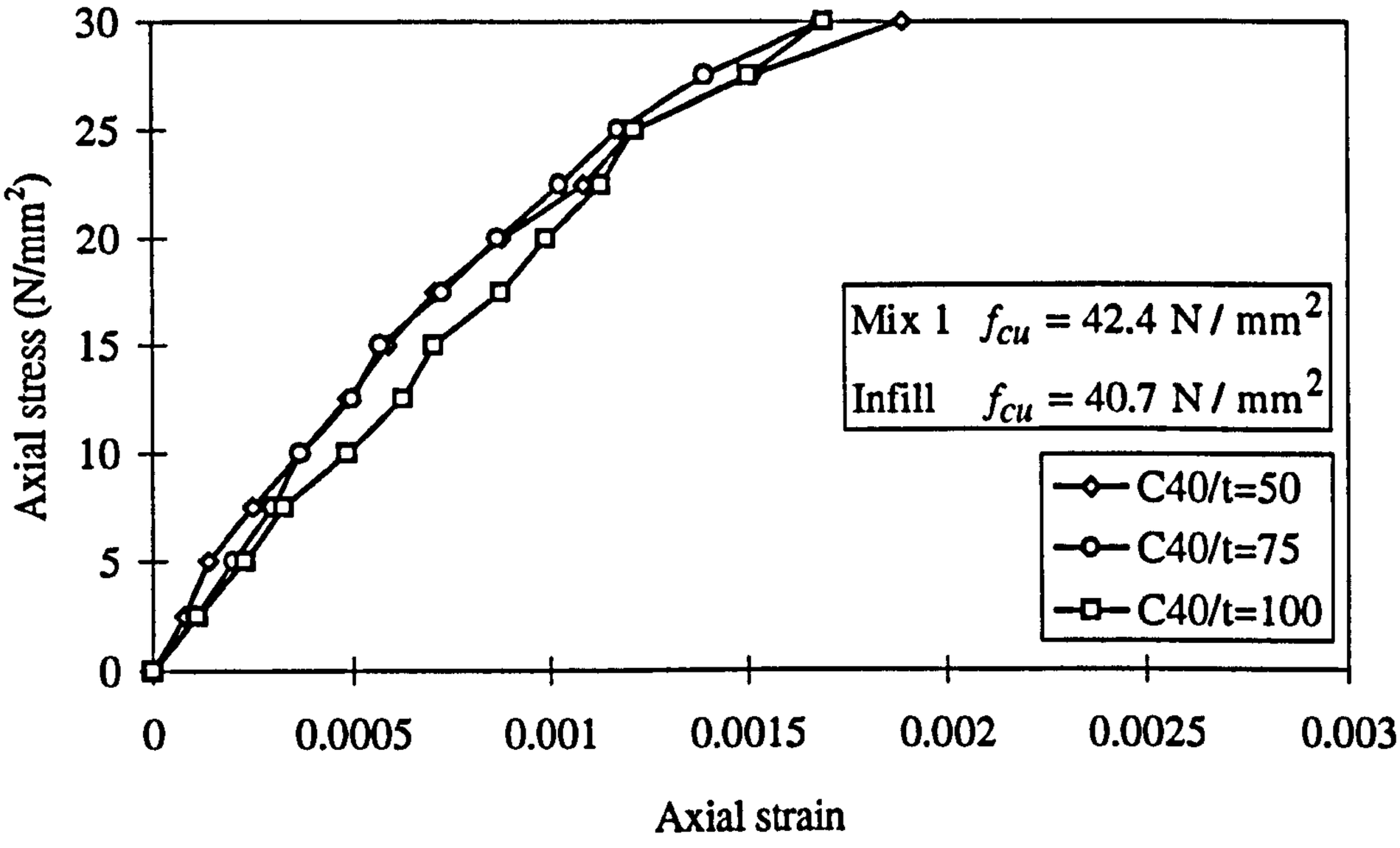

Figure 9.1(a): Axial stress strain data for compressive specimens type A for mix 1 in test series 1 for varying thickness t of insitu concrete

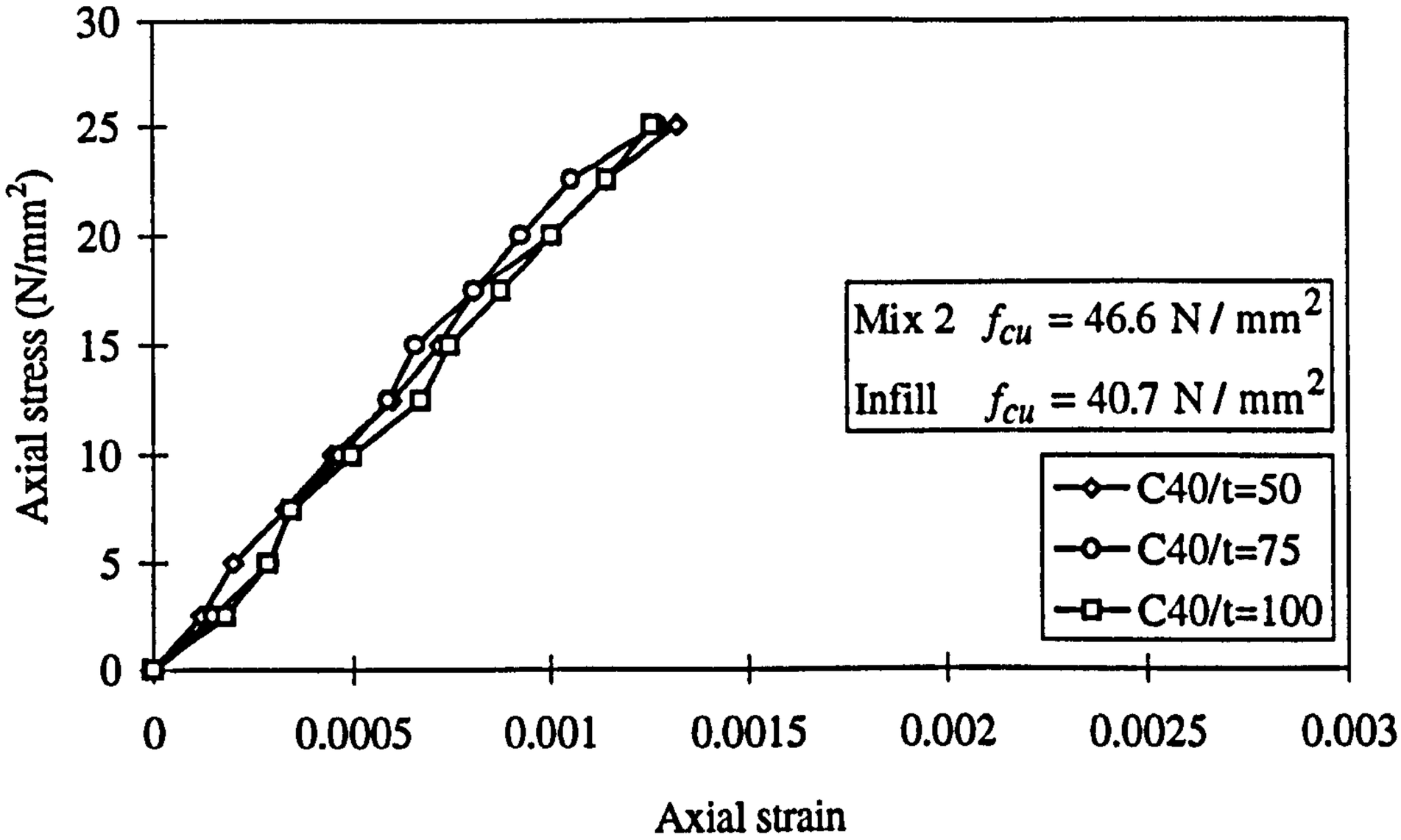

Figure 9.1(b): Axial stress strain data for compressive specimens type A for mix 2 in test series 1 for varying thickness t of insitu concrete

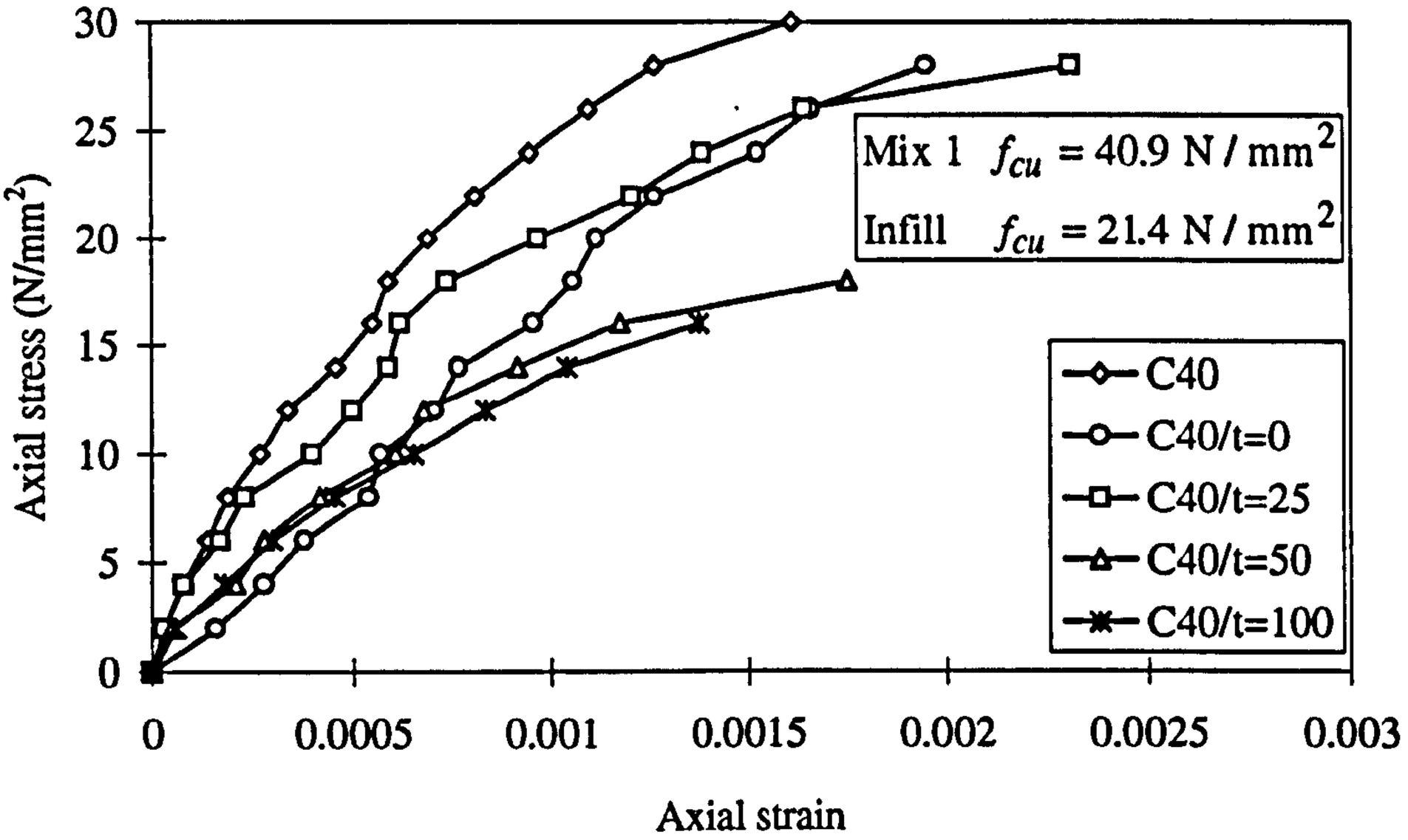

Figure 9.2(a): Axial stress strain data for compressive specimens type A in test series 2 for varying thickness t of insitu concrete

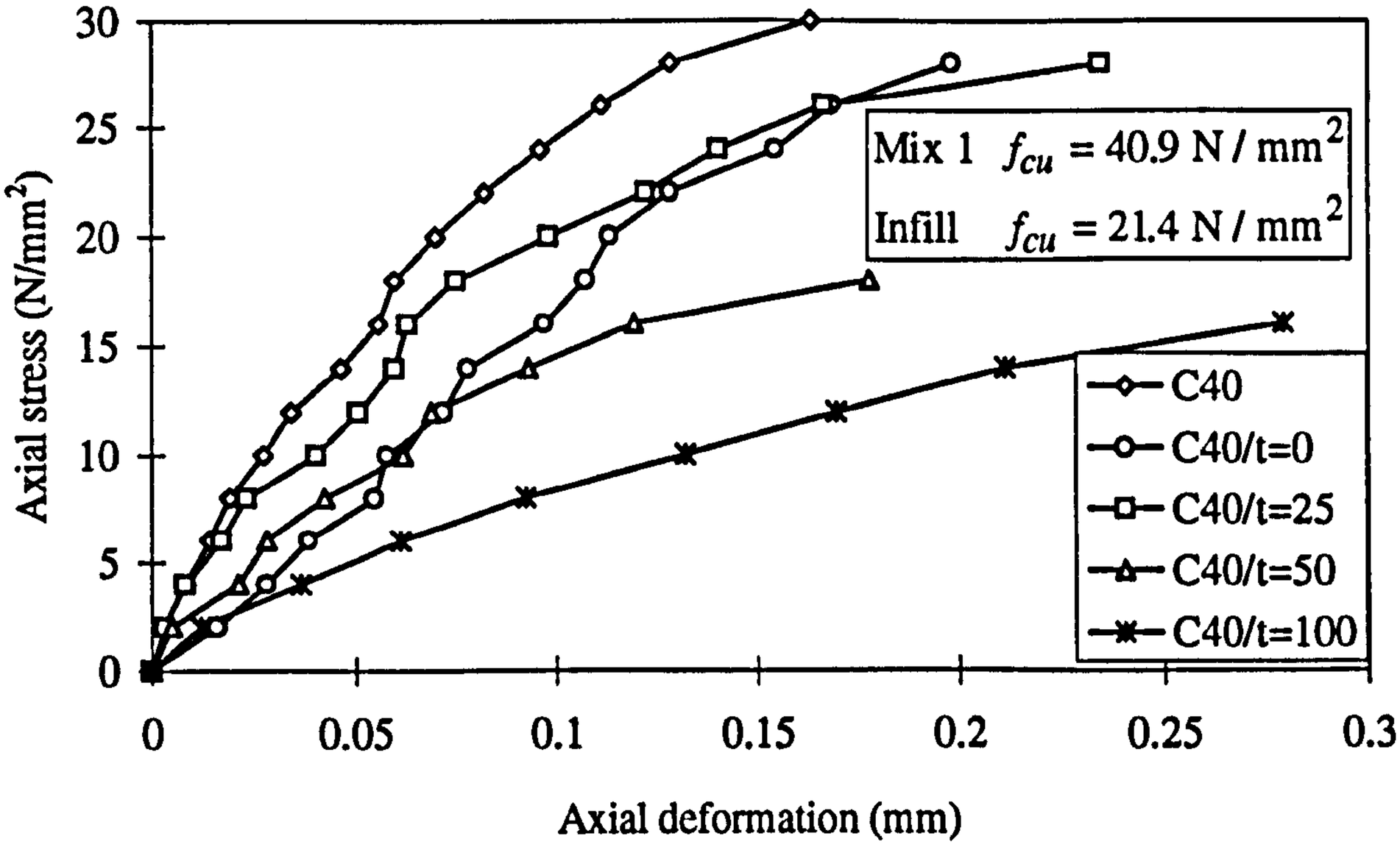

Figure 9.2(b): Axial stress deformation data for compressive specimens type A in test series 2 for varying thickness t of insitu concrete

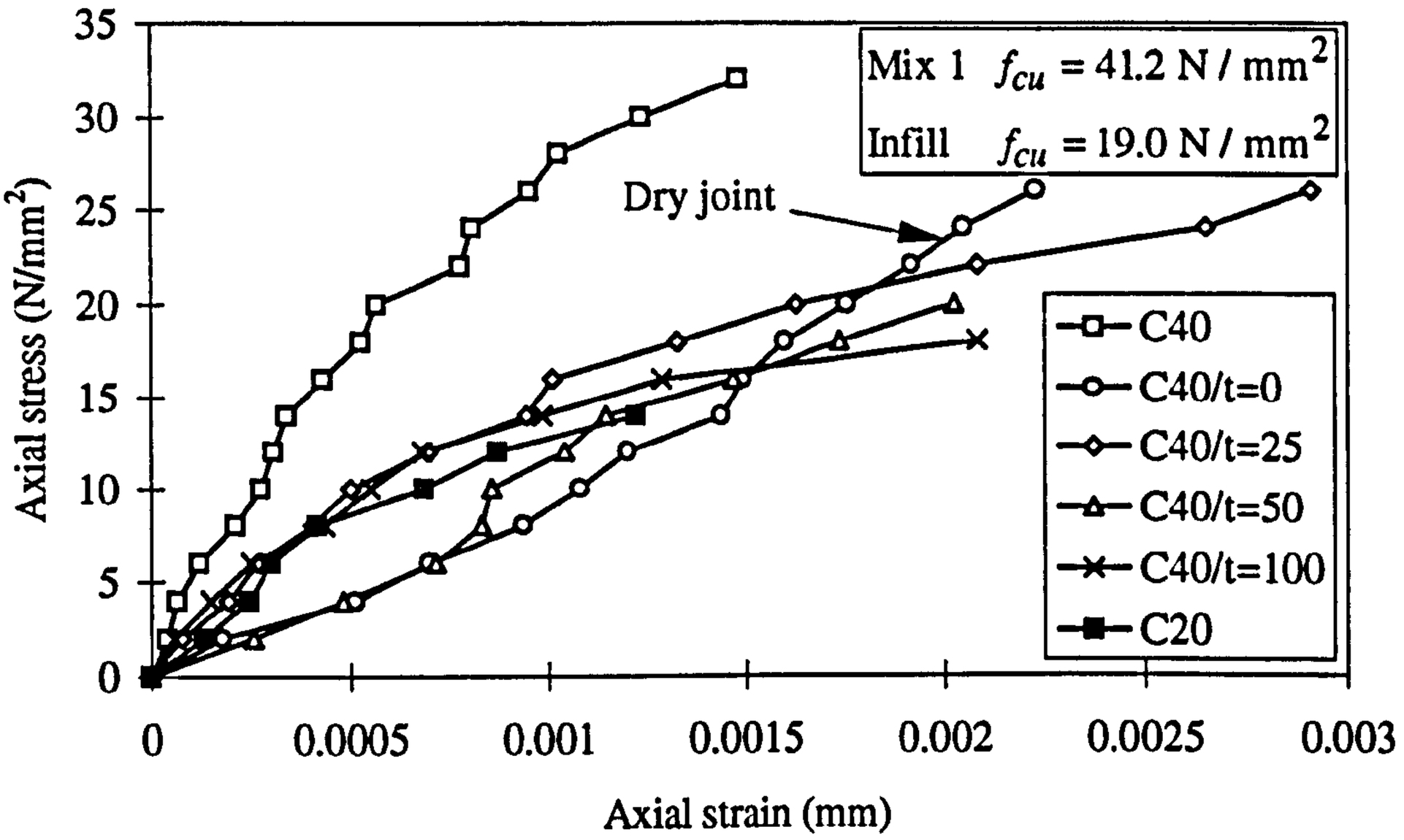

Figure 9.3(a): Axial stress strain data for compressive specimens type A in test series 3 for varying thickness t of insitu concrete

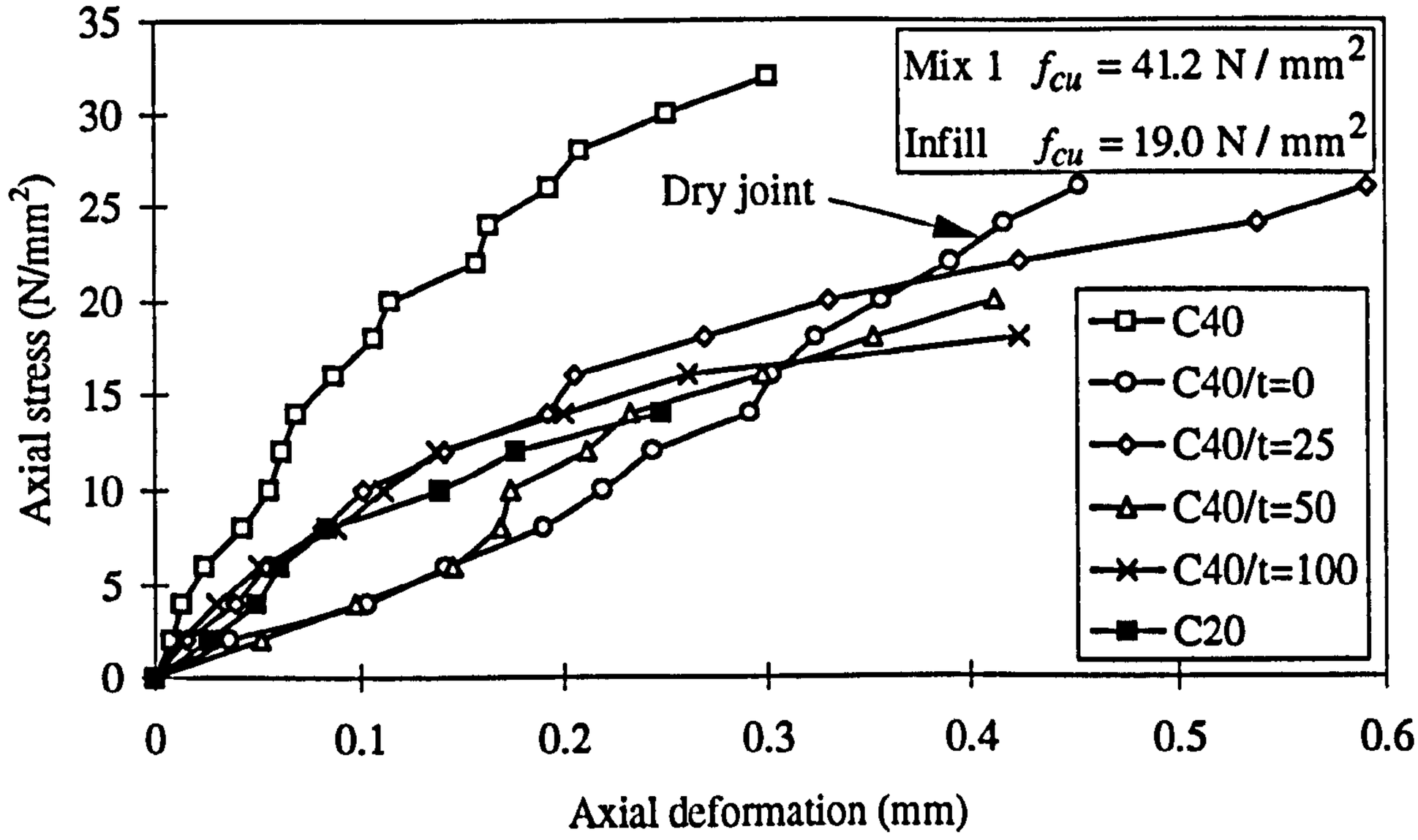

Figure 9.3(b): Axial stress deformation data for compressive specimens type A in test series 3 for varying thickness t of insitu concrete

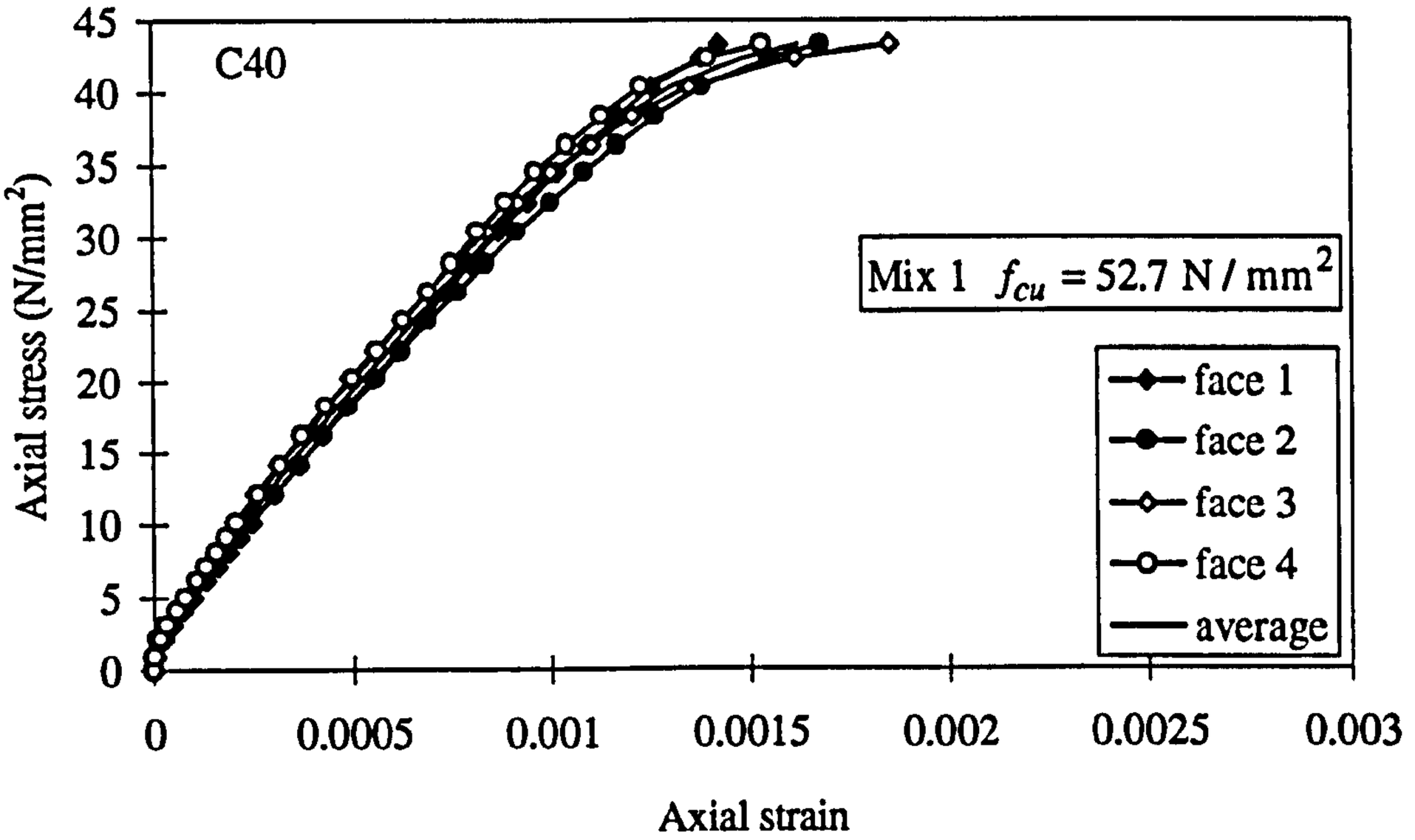

Figure 9.4(a): Axial stress strain data for compressive specimen type A in test series 4 for C40 concrete

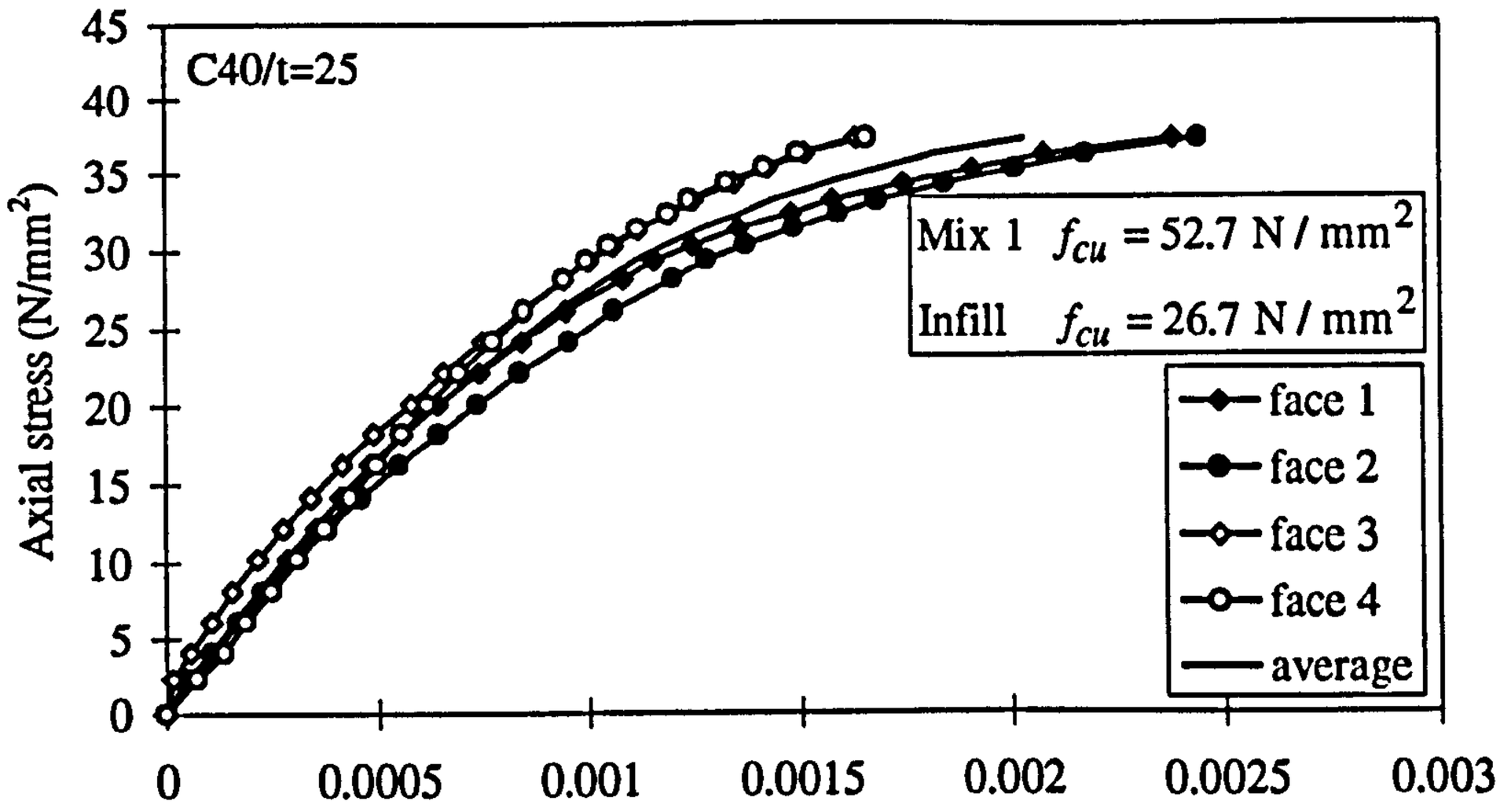

Figure 9.4(b): Axial stress strain data for compressive specimen type A in test series 4 for C40/t=25 mm infill concrete

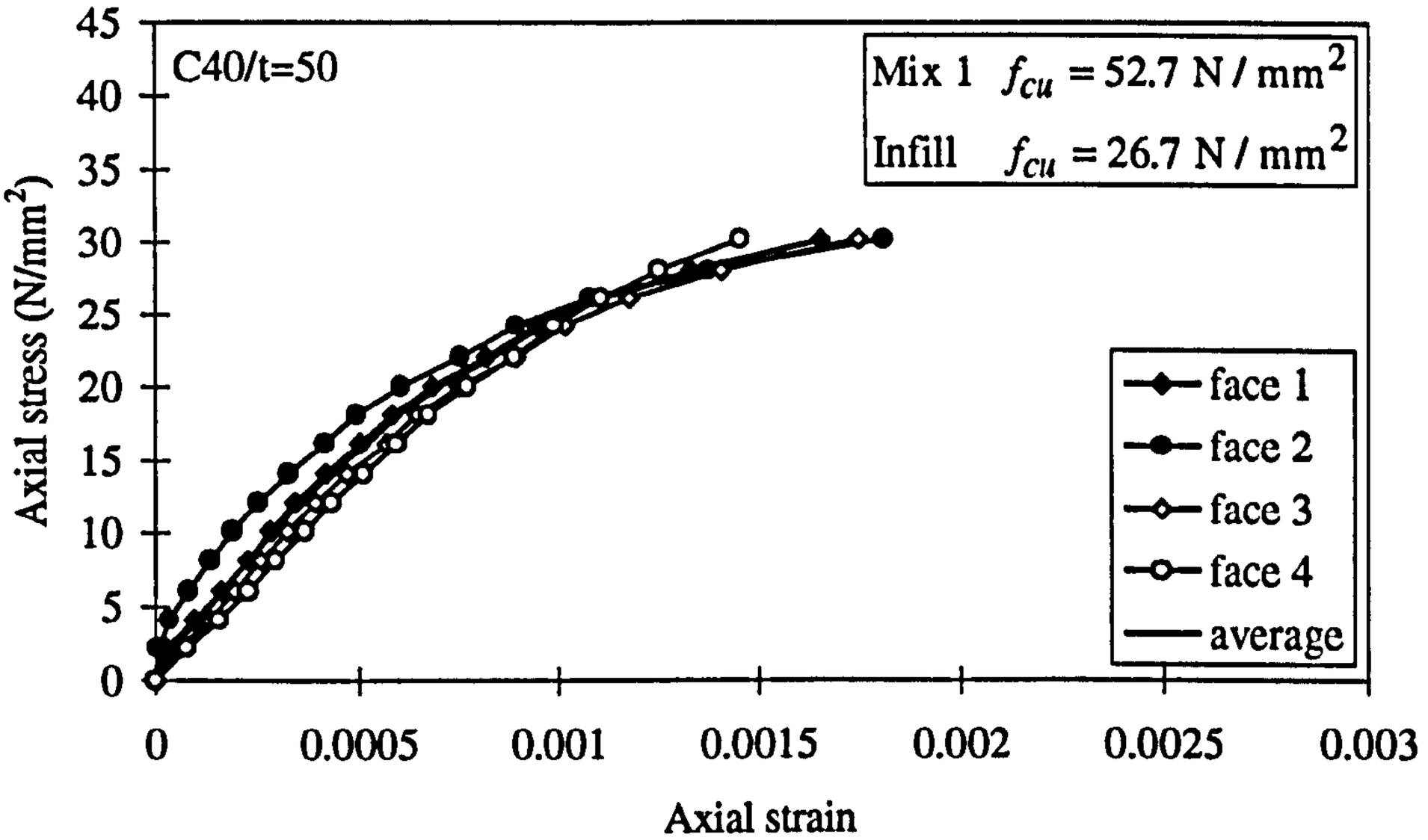

Figure 9.4(c): Axial stress strain data for compressive specimen type A in test series 4 for C40/t=50 mm infill concrete

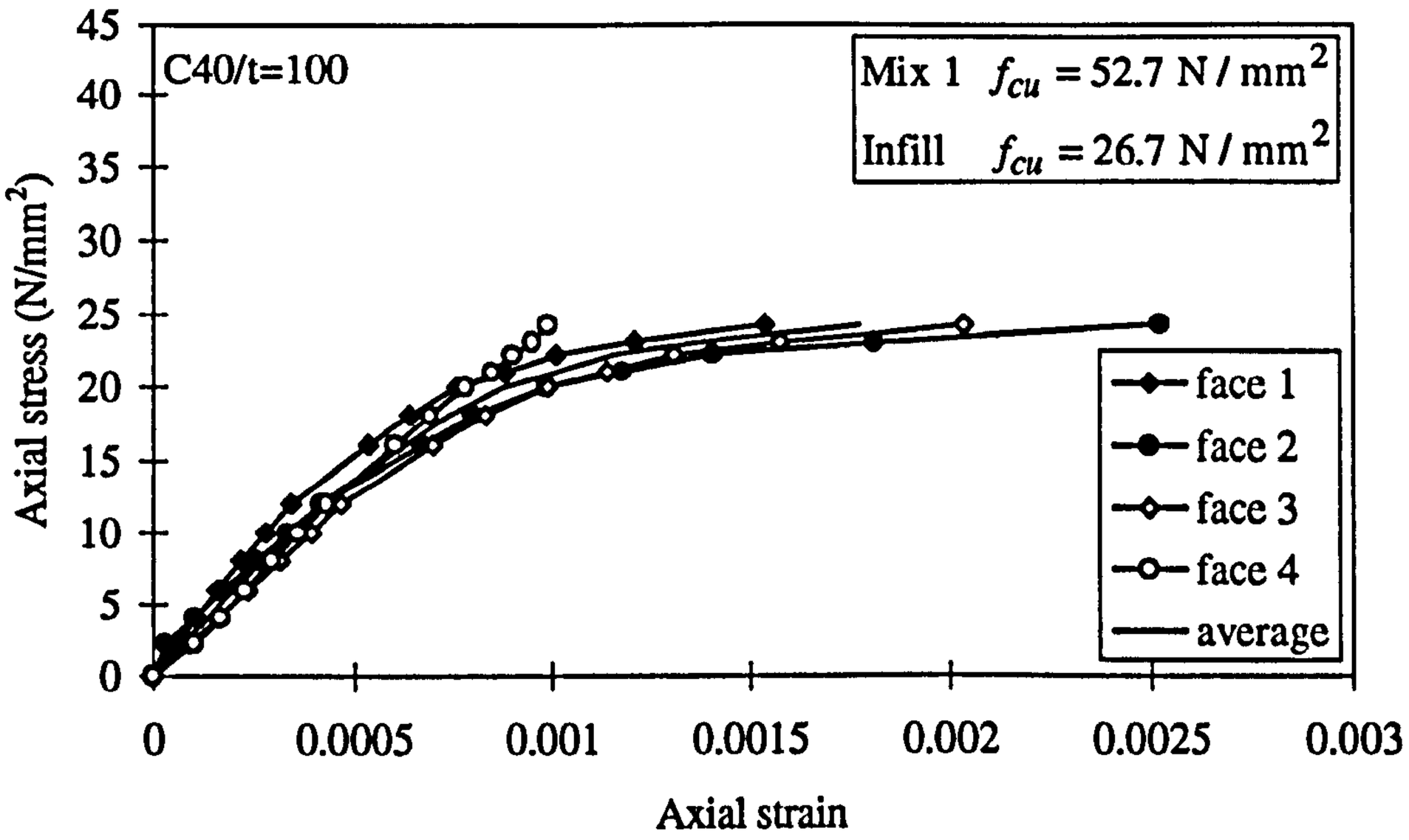

Figure 9.4(d): Axial stress strain data for compressive specimen type A in test series 4 for C40/t=100 mm infill concrete

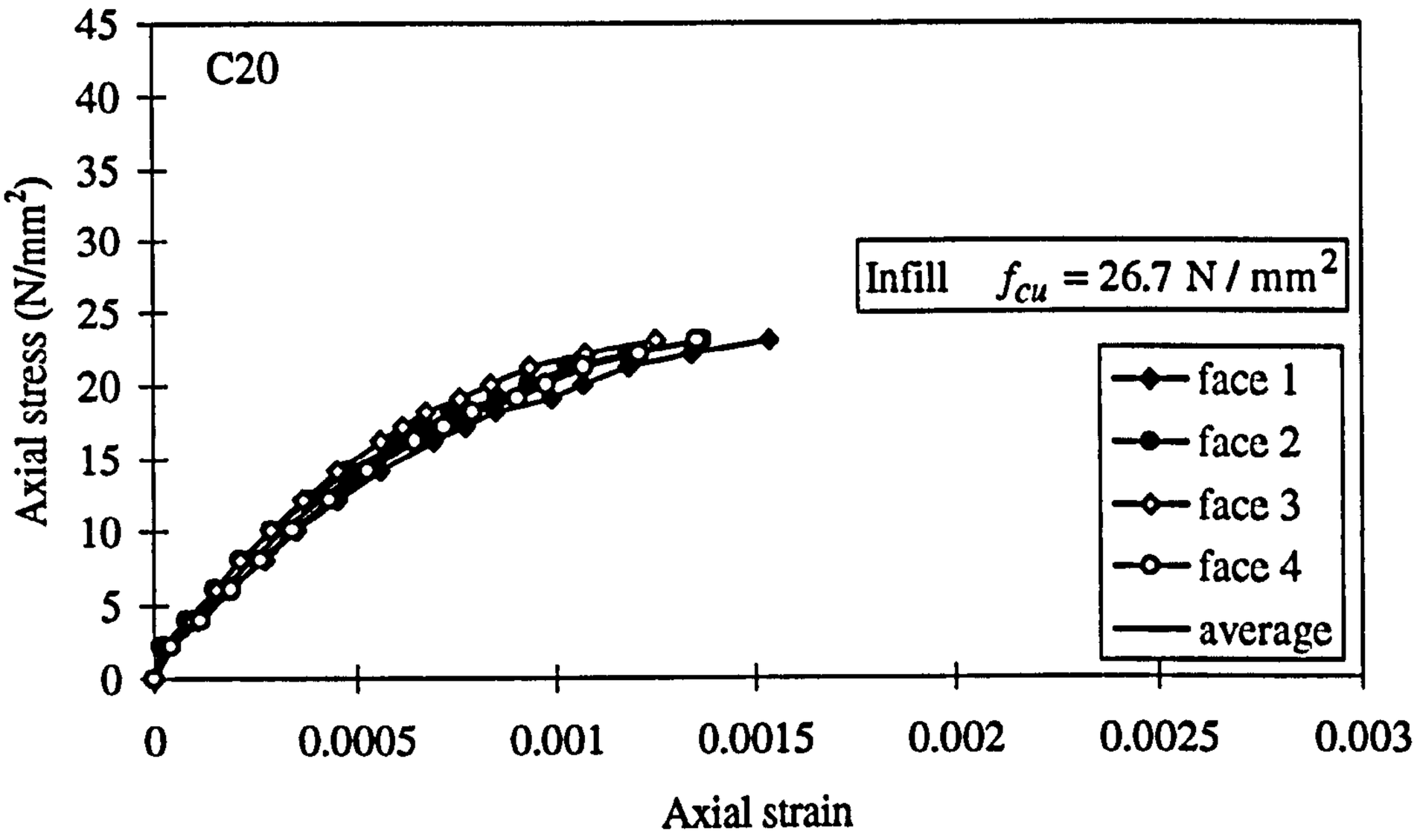

Figure 9.4(e): Axial stress strain data for compressive specimen type A in test series 4 for C20 concrete

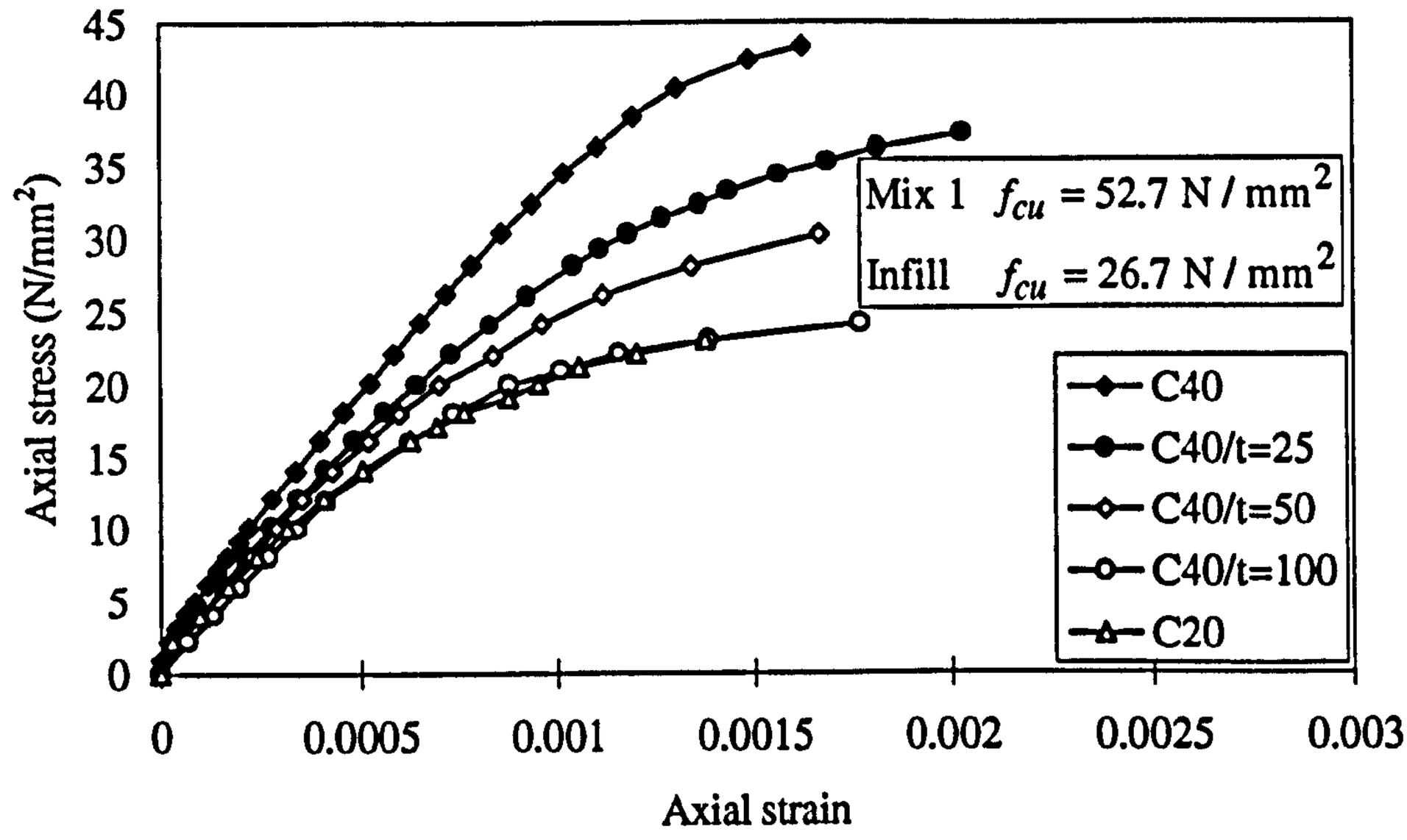

Figure 9.4(f): Mean axial stress strain data for compressive specimens type A in test series 4 for varying thickness t of insitu concrete

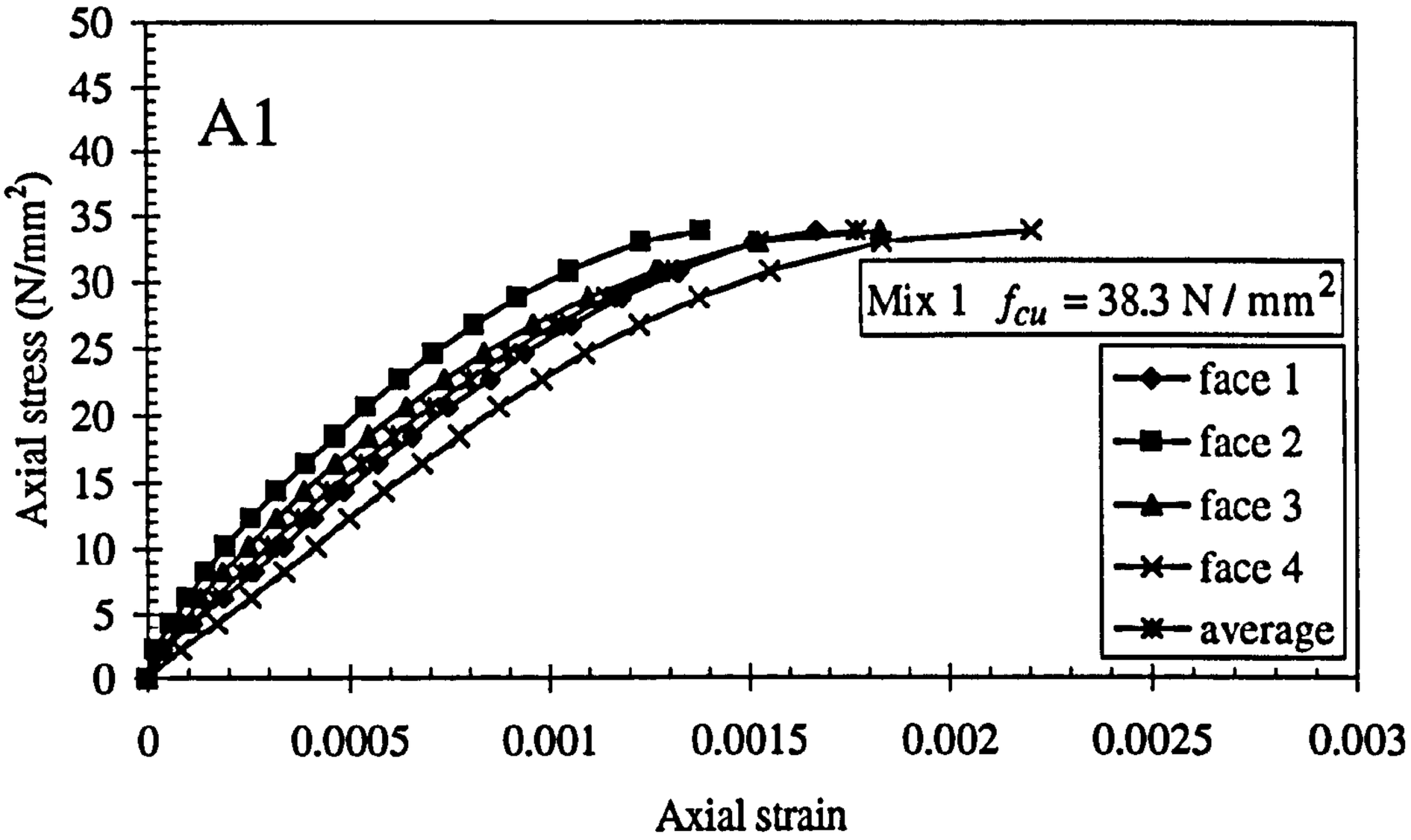

Figure 9.5(a): Axial stress strain data for compressive specimen type A in test series 5 for specimen A1

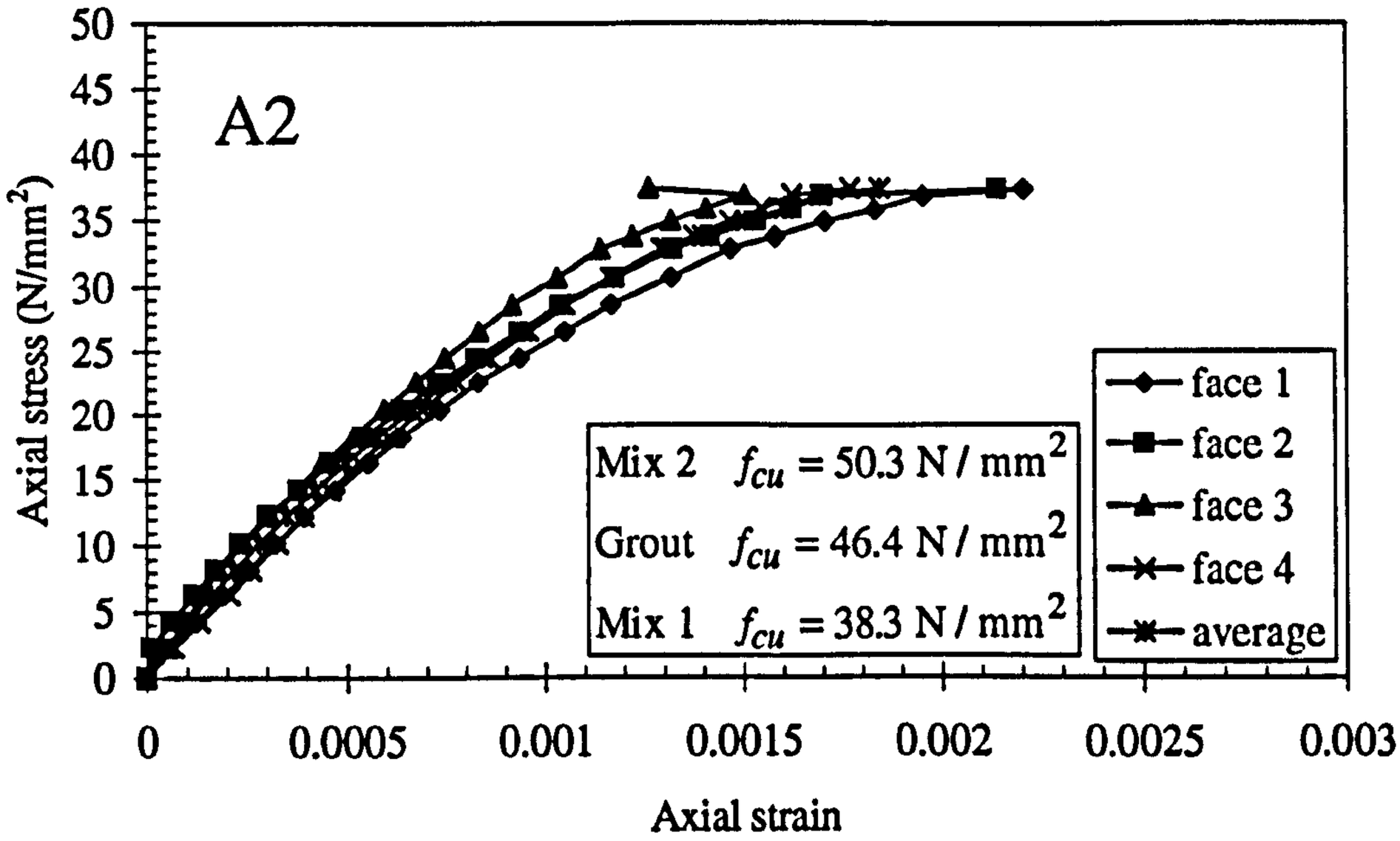

Figure 9.5(b): Mean axial stress strain data for compressive specimen type A in test series 5 for specimen A2

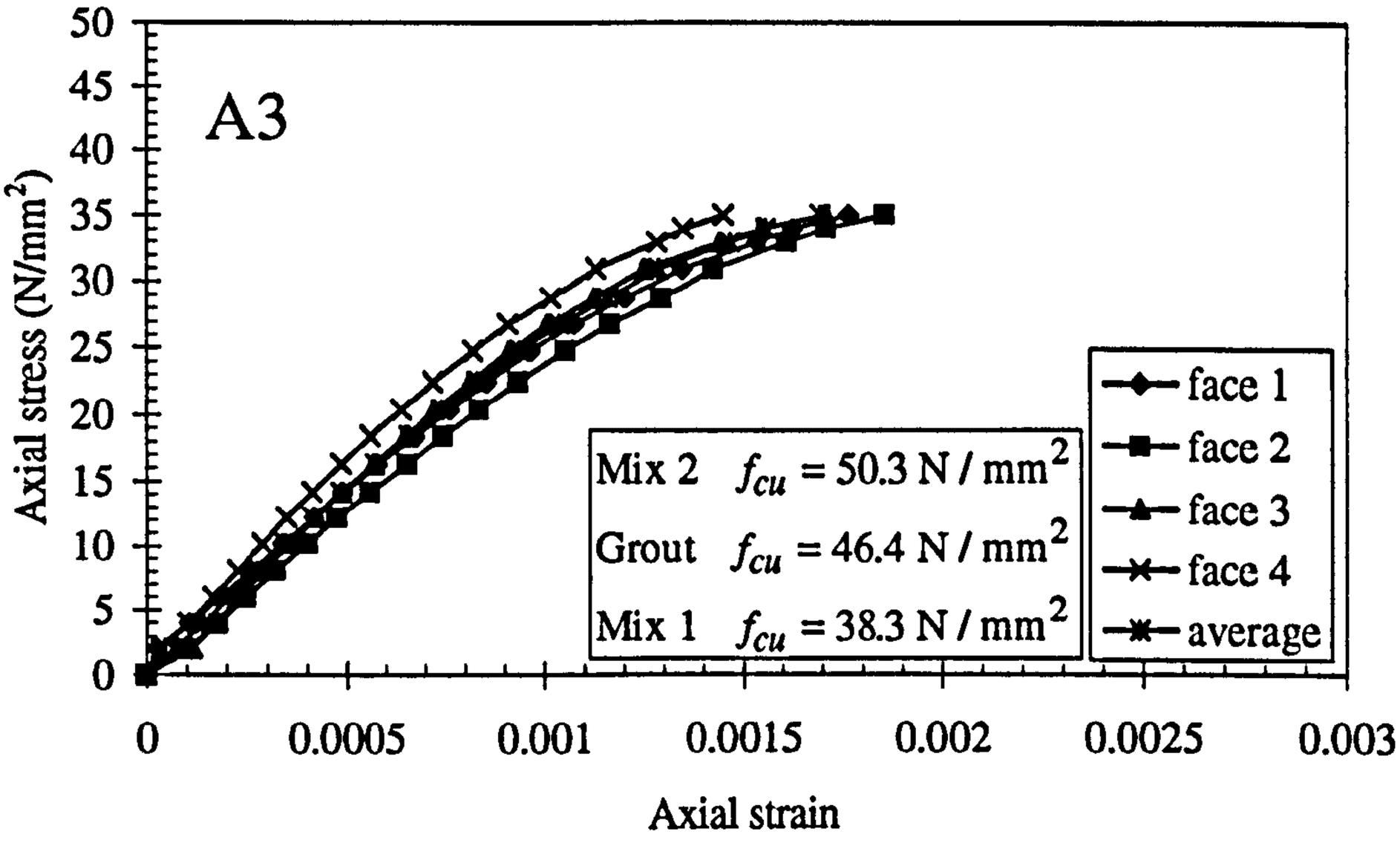

Figure 9.5(c): Axial stress strain data for compressive specimen type A in test series 5 for specimen A3

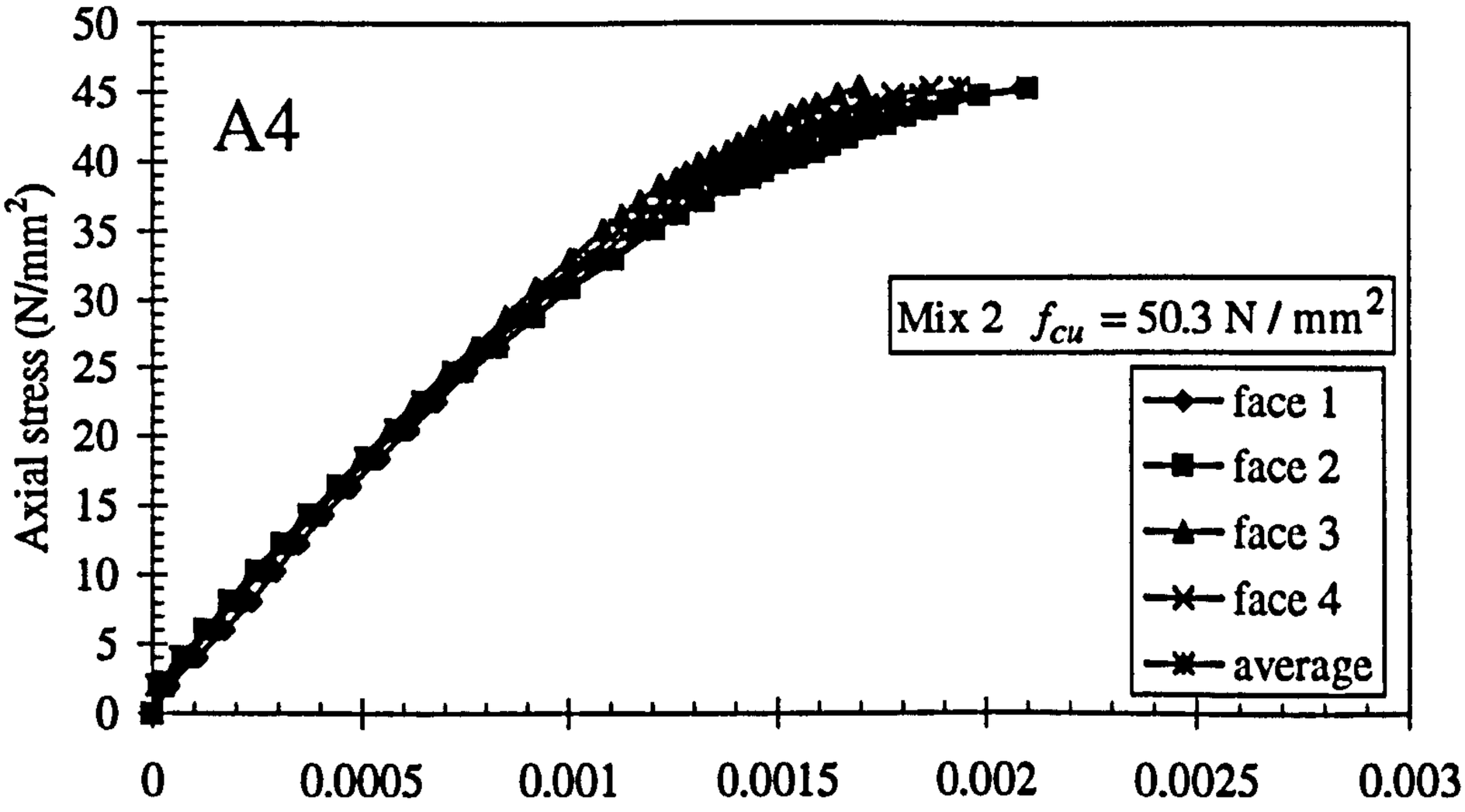

Figure 9.5(d): Mean axial stress strain data for compressive specimen type A in test series 5 for specimen A4

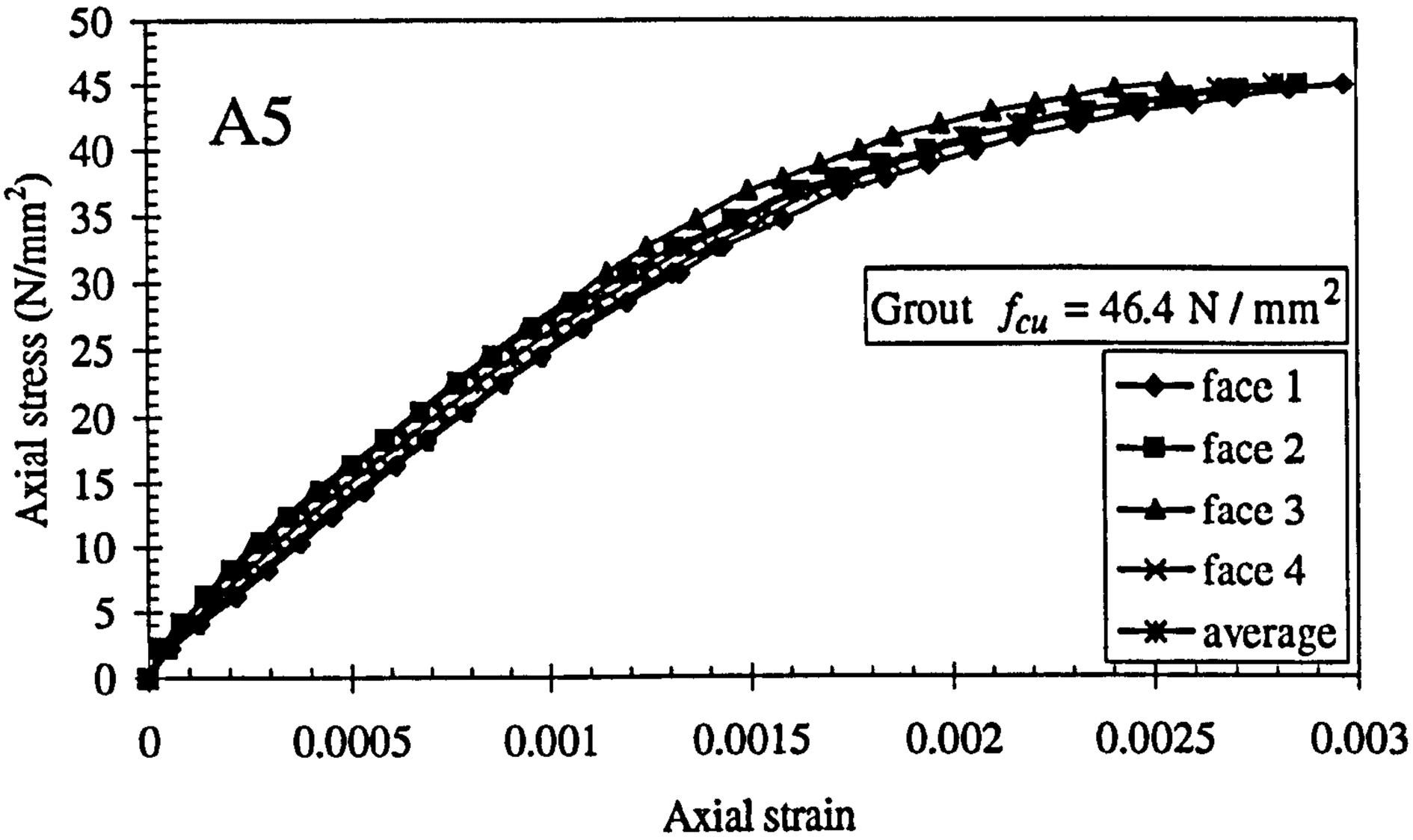

Figure 9.5(e): Axial stress strain data for compressive specimen type A in test series 5 for specimen A5

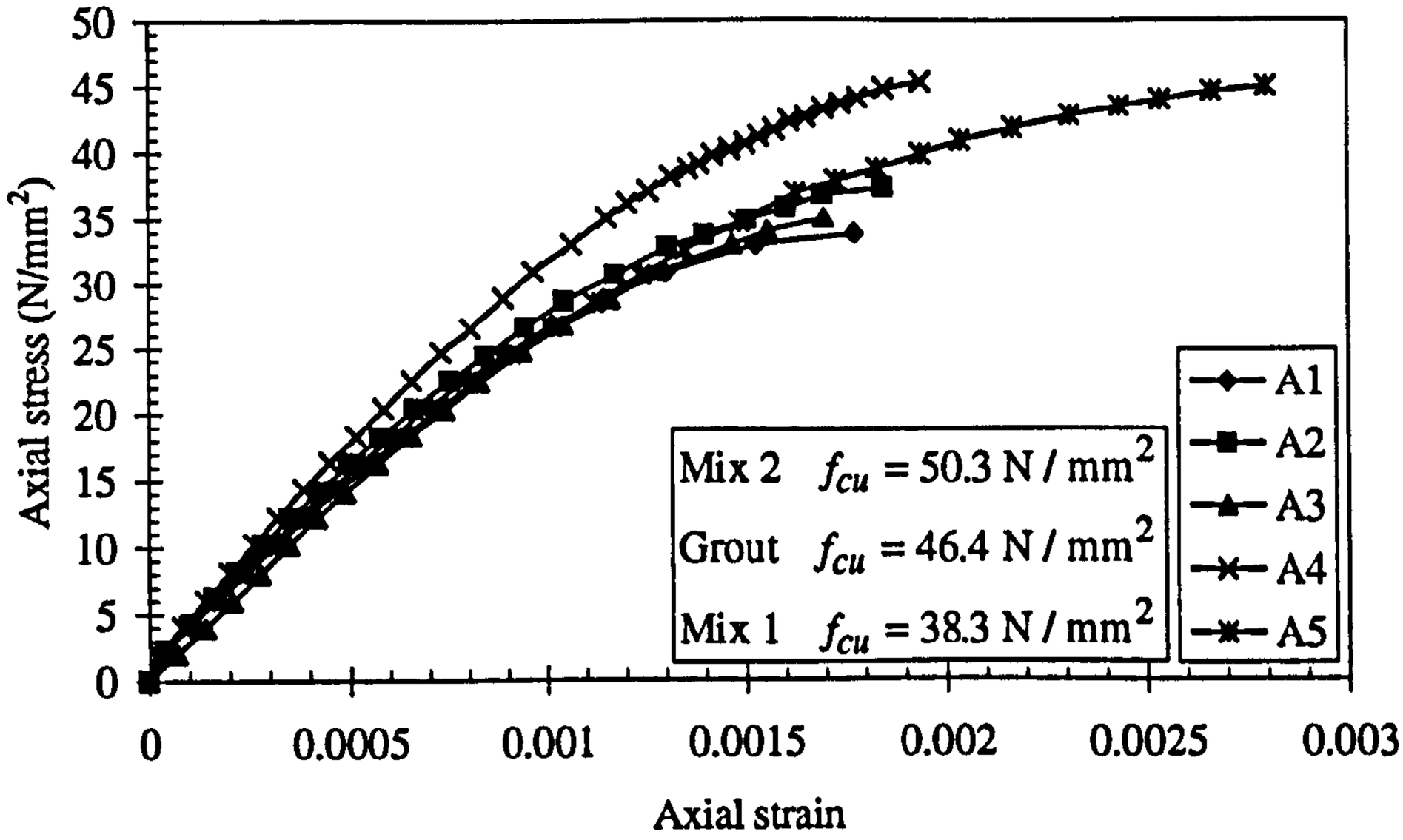

Figure 9.5(f): Mean axial stress strain data for compressive specimens type A in test series 5

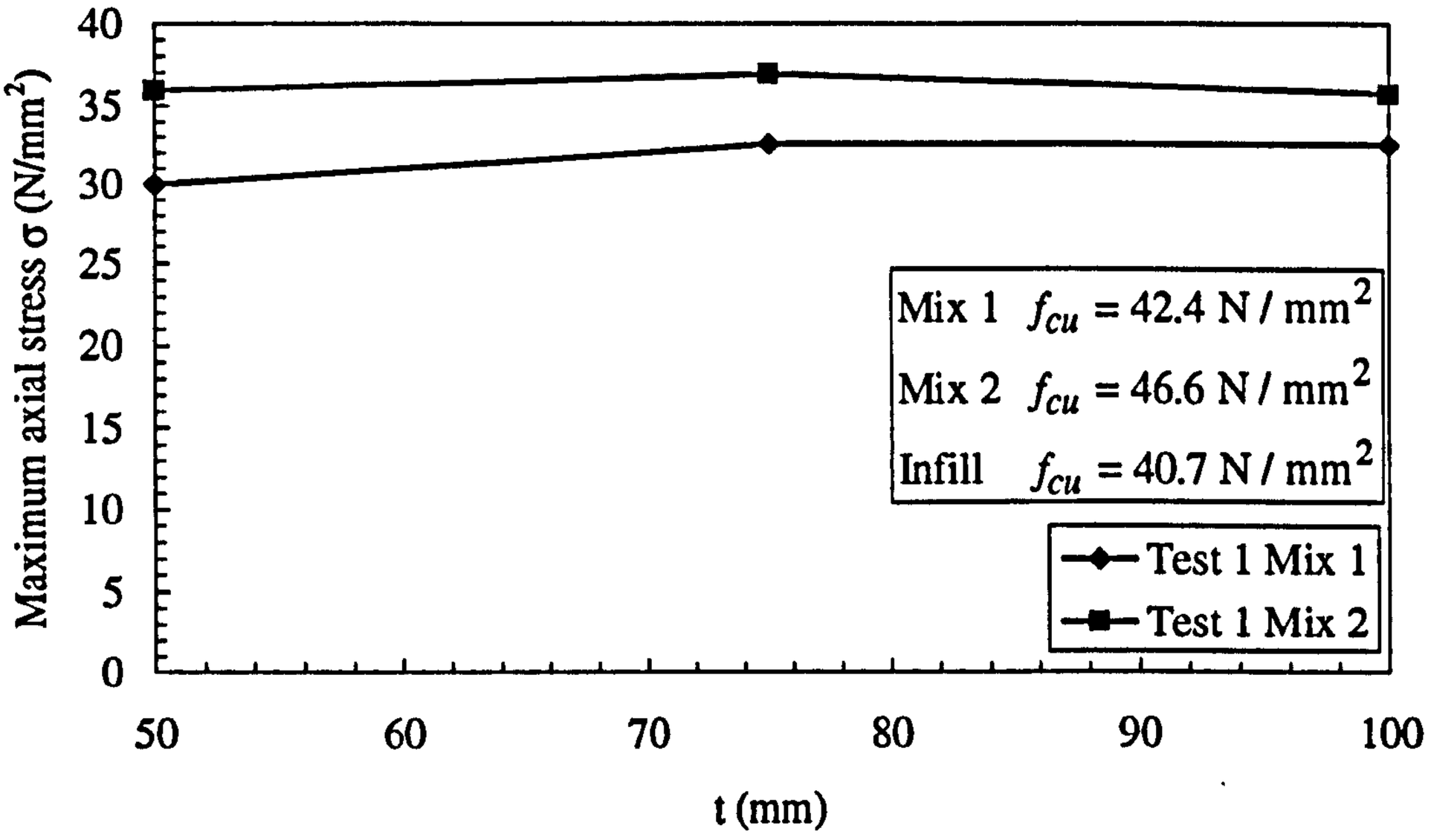

Figure 9.6(a): Variation in maximum axial compressive stress for compressive specimens type A in test series 1 for varying thickness t of infill concrete

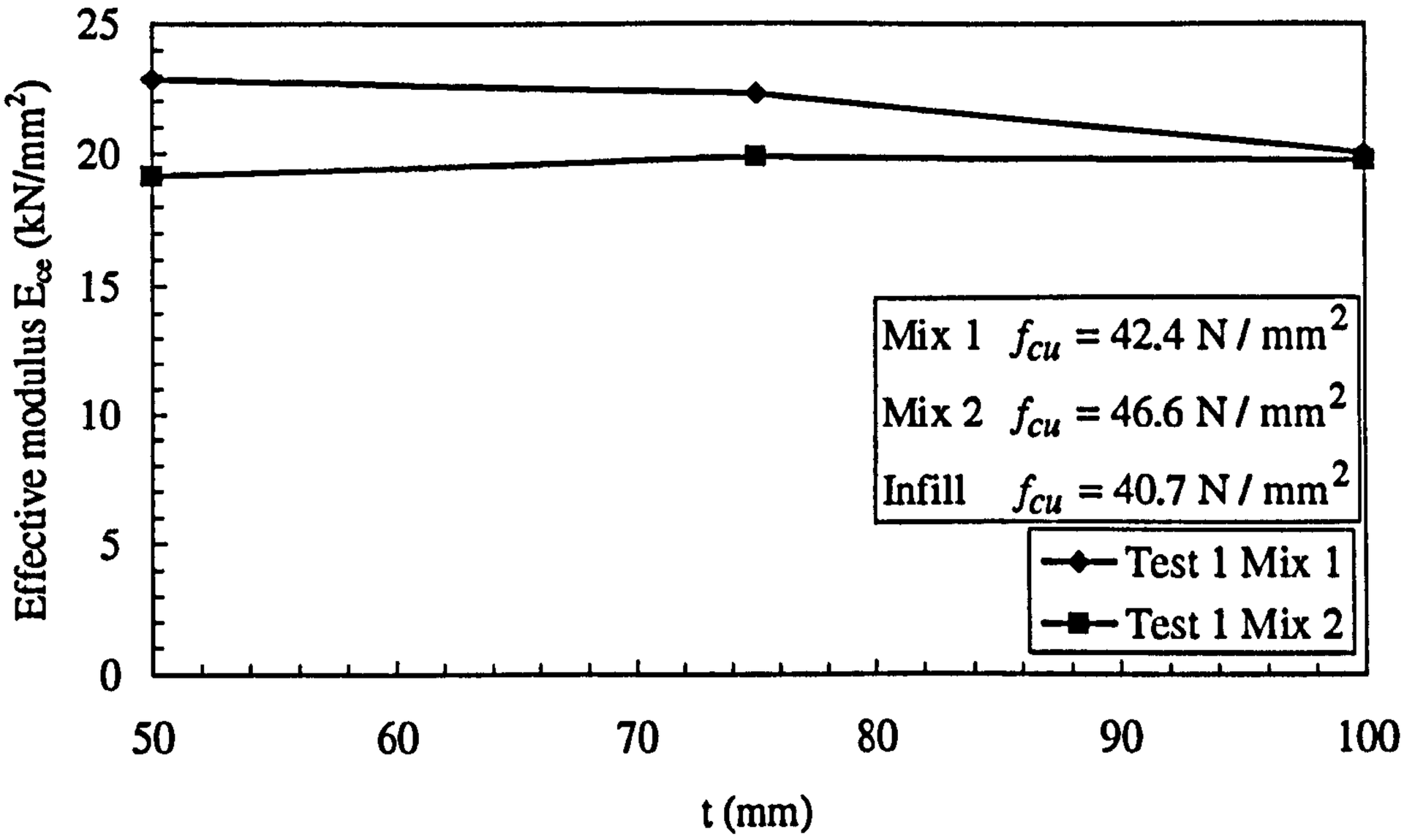

Figure 9.6(b): Variation in effective modulus for compressive specimens type A in test series 1 for varying thickness t of infill concrete

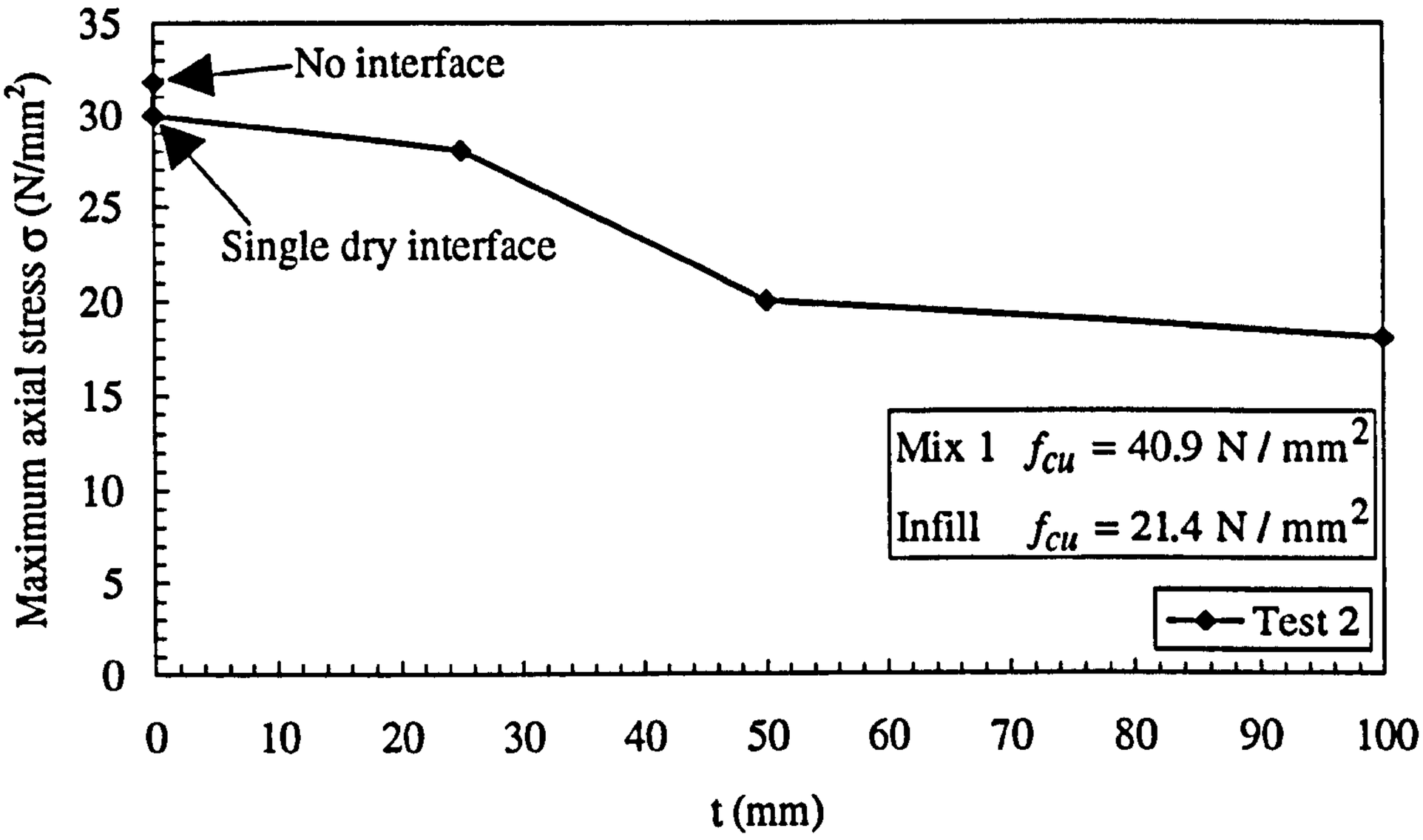

Figure 9.7(a): Variation in maximum axial compressive stress for compressive specimens type A in test series 2 for varying thickness t of infill concrete

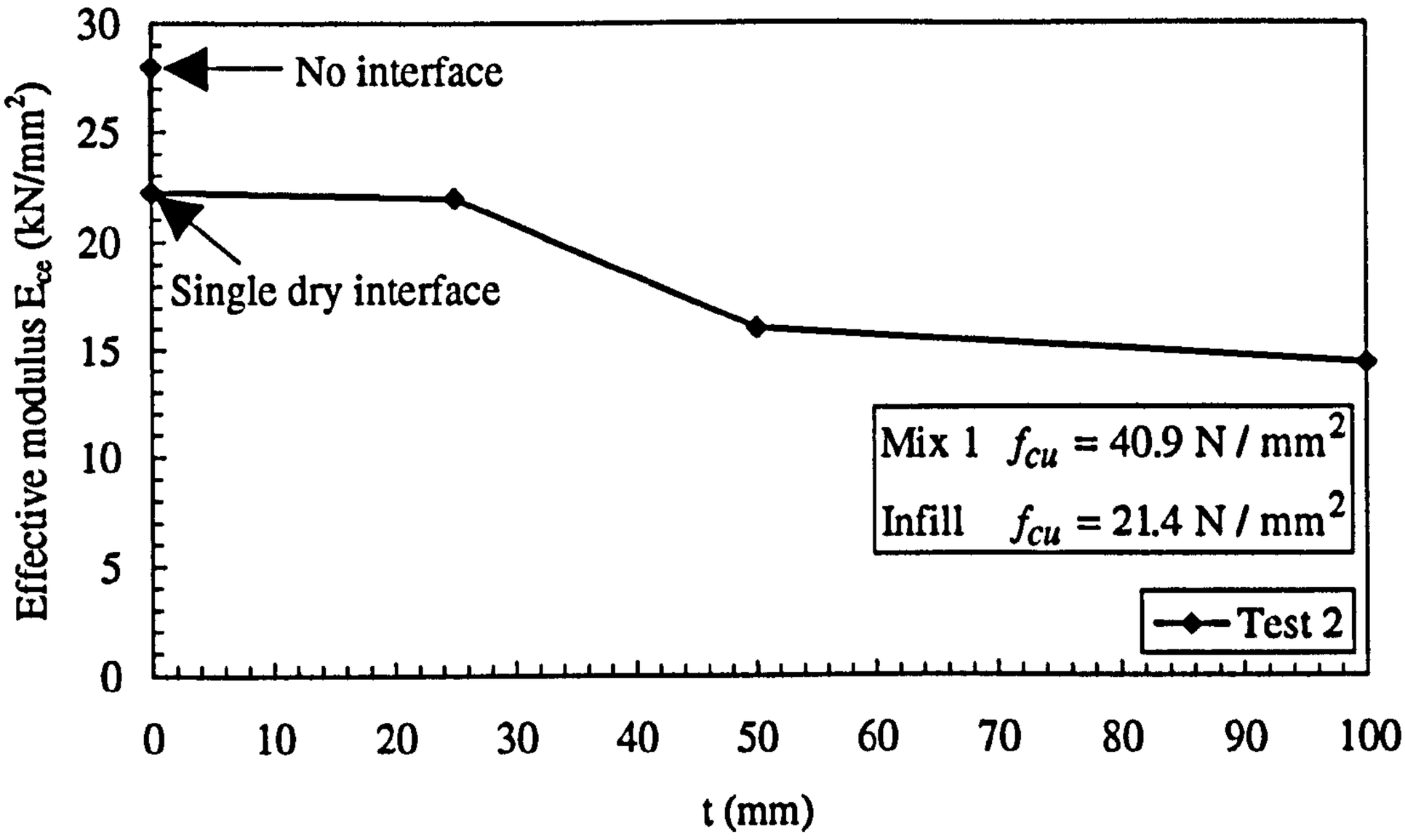

Figure 9.7(b): Variation in effective modulus for compressive specimens type A in test series 2 for varying thickness t of infill concrete

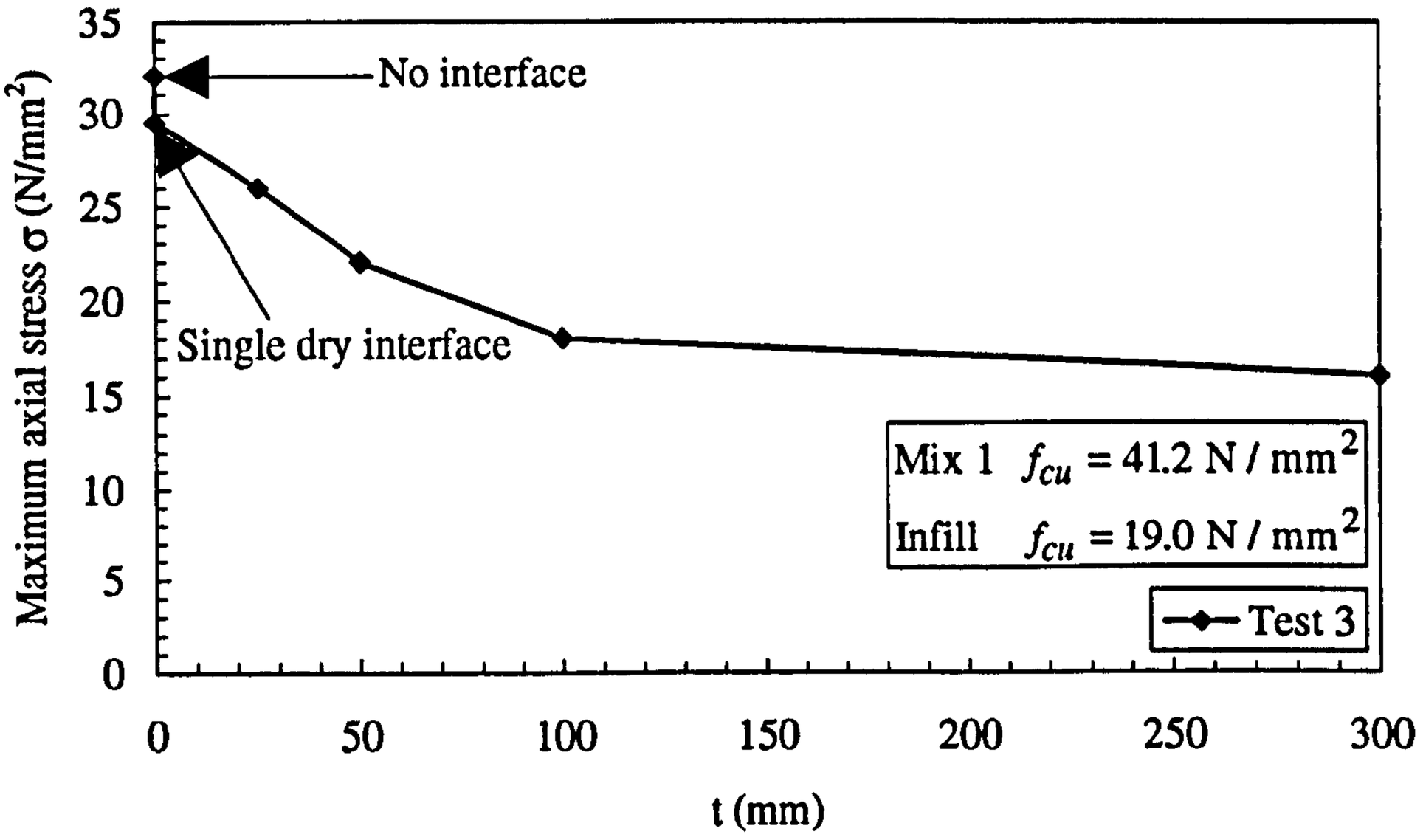

Figure 9.8(a): Variation in maximum axial compressive stress for compressive specimens type A in test series 3 for varying thickness t of infill concrete

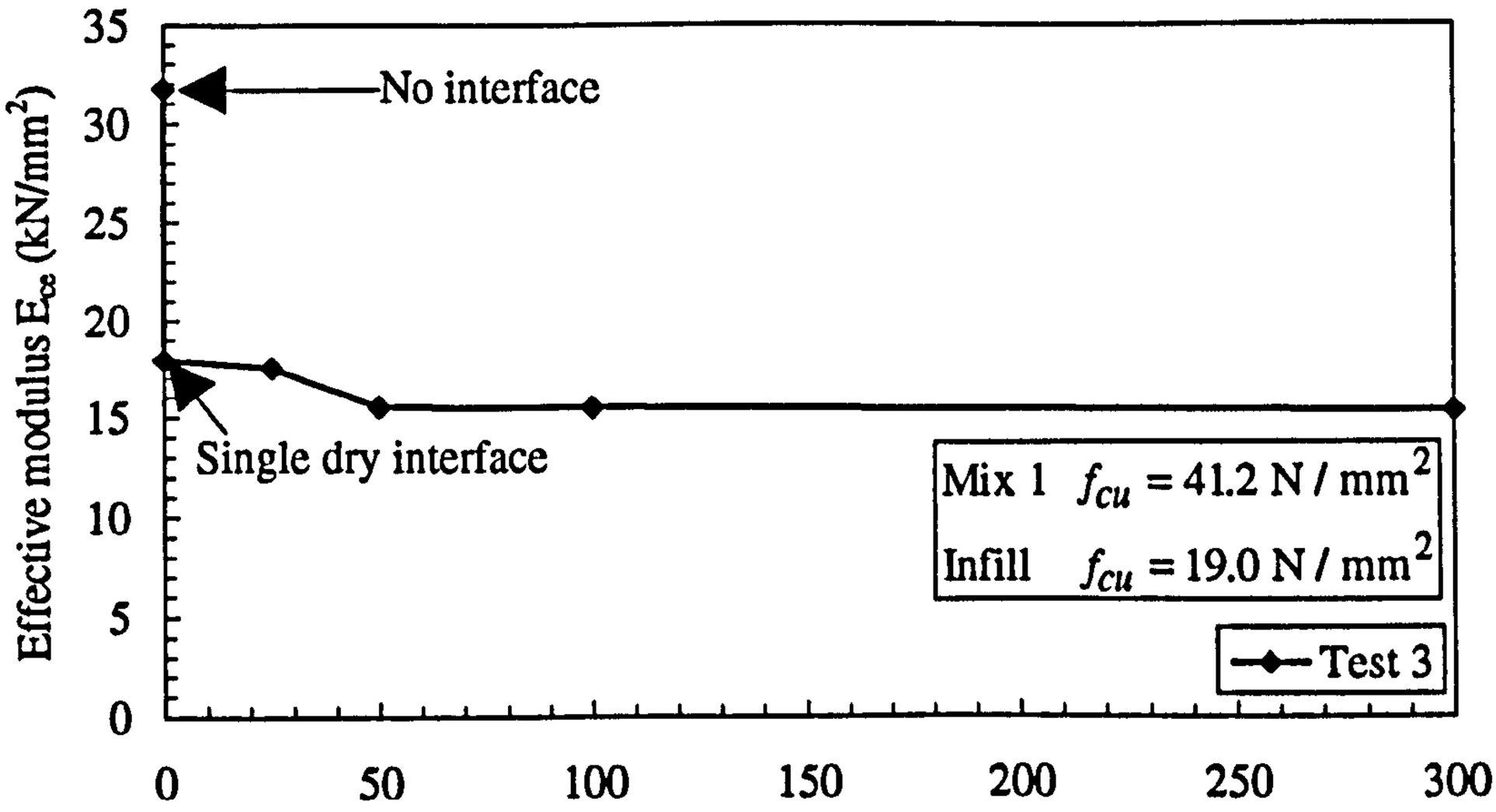

Figure 9.8(b): Variation in effective modulus for compressive specimens type A in test series 3 for varying thickness t of infill concrete

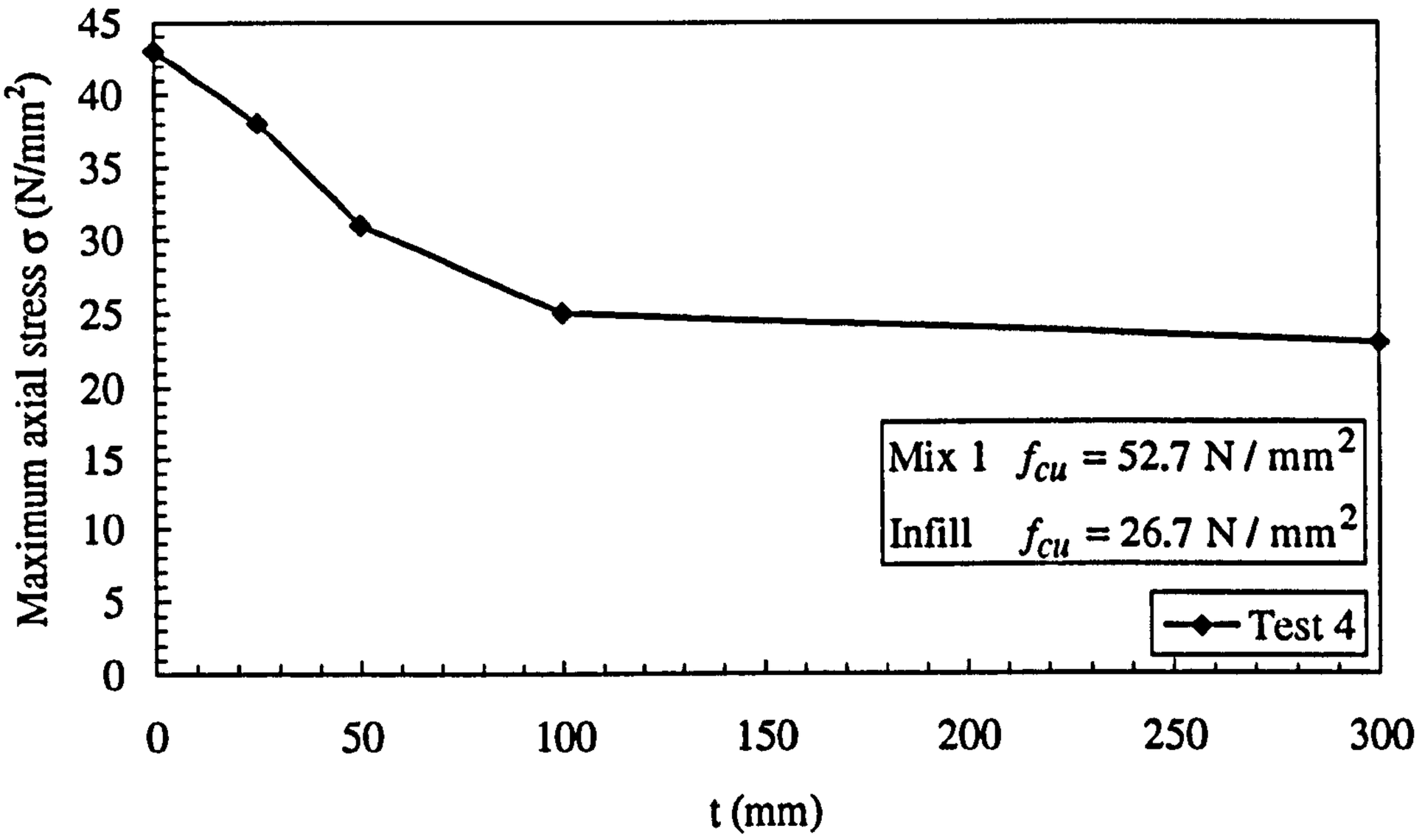

Figure 9.9(a): Variation in maximum axial compressive stress for compressive specimens type A in test series 4 for varying thickness t of infill concrete

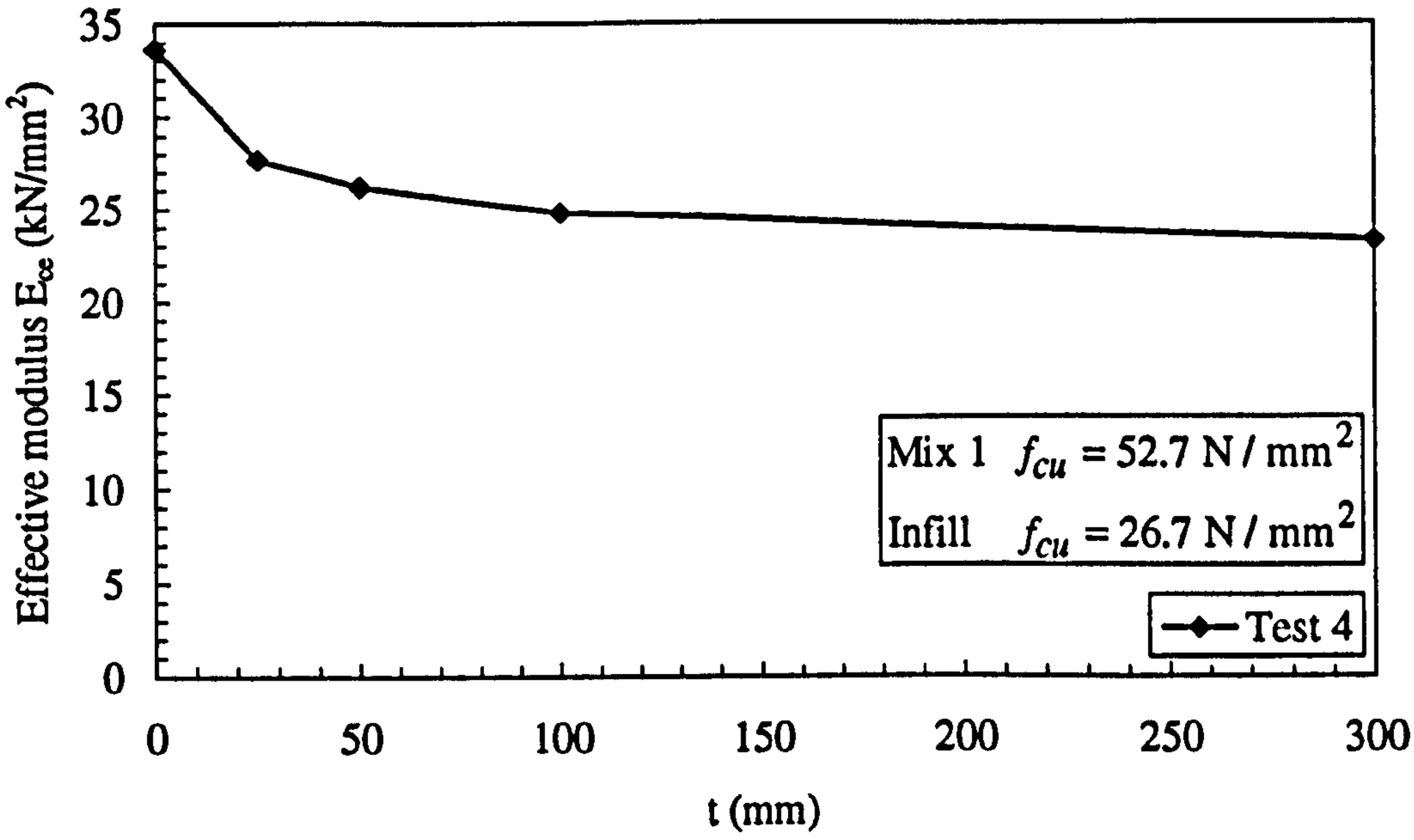

Figure 9.9(b): Variation in effective modulus for compressive specimens type A in test series 4 for varying thickness t of infill concrete

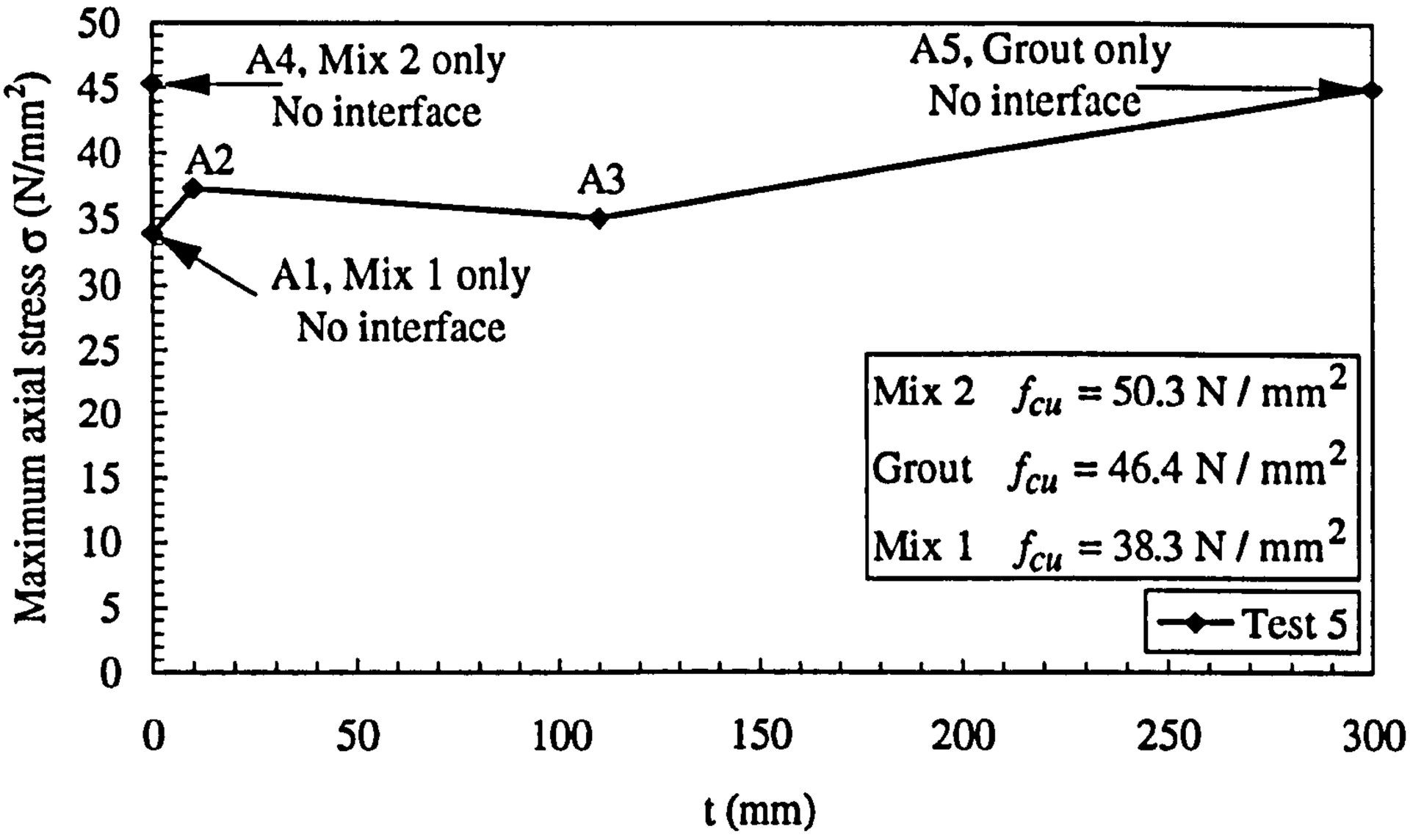

Figure 9.10(a): Variation in maximum axial compressive stress for compressive specimens type A in test series 5 for varying thickness t of infill grout

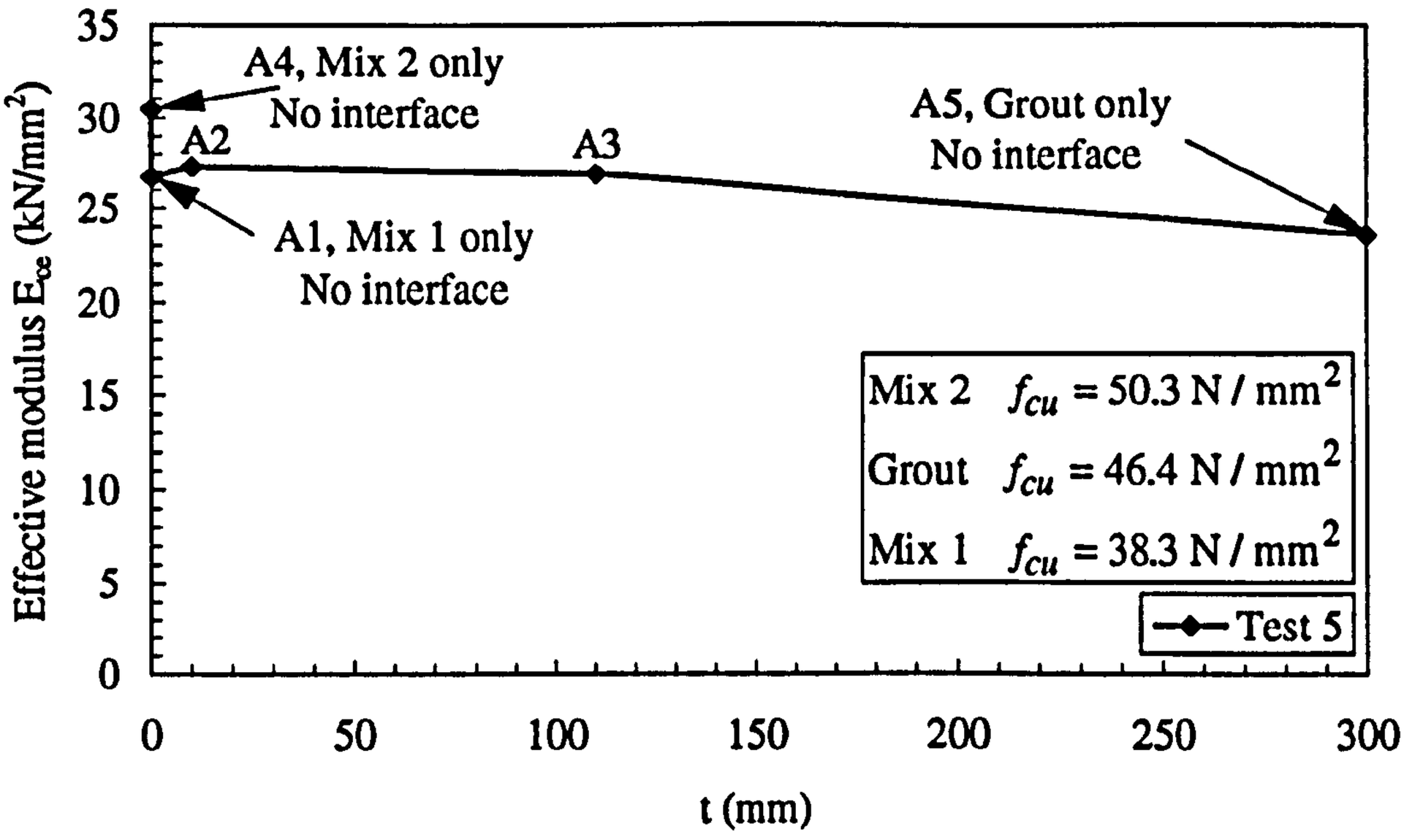

Figure 9.10(b): Variation in effective modulus for compressive specimens type A in test series 5 for varying thickness t of infill grout

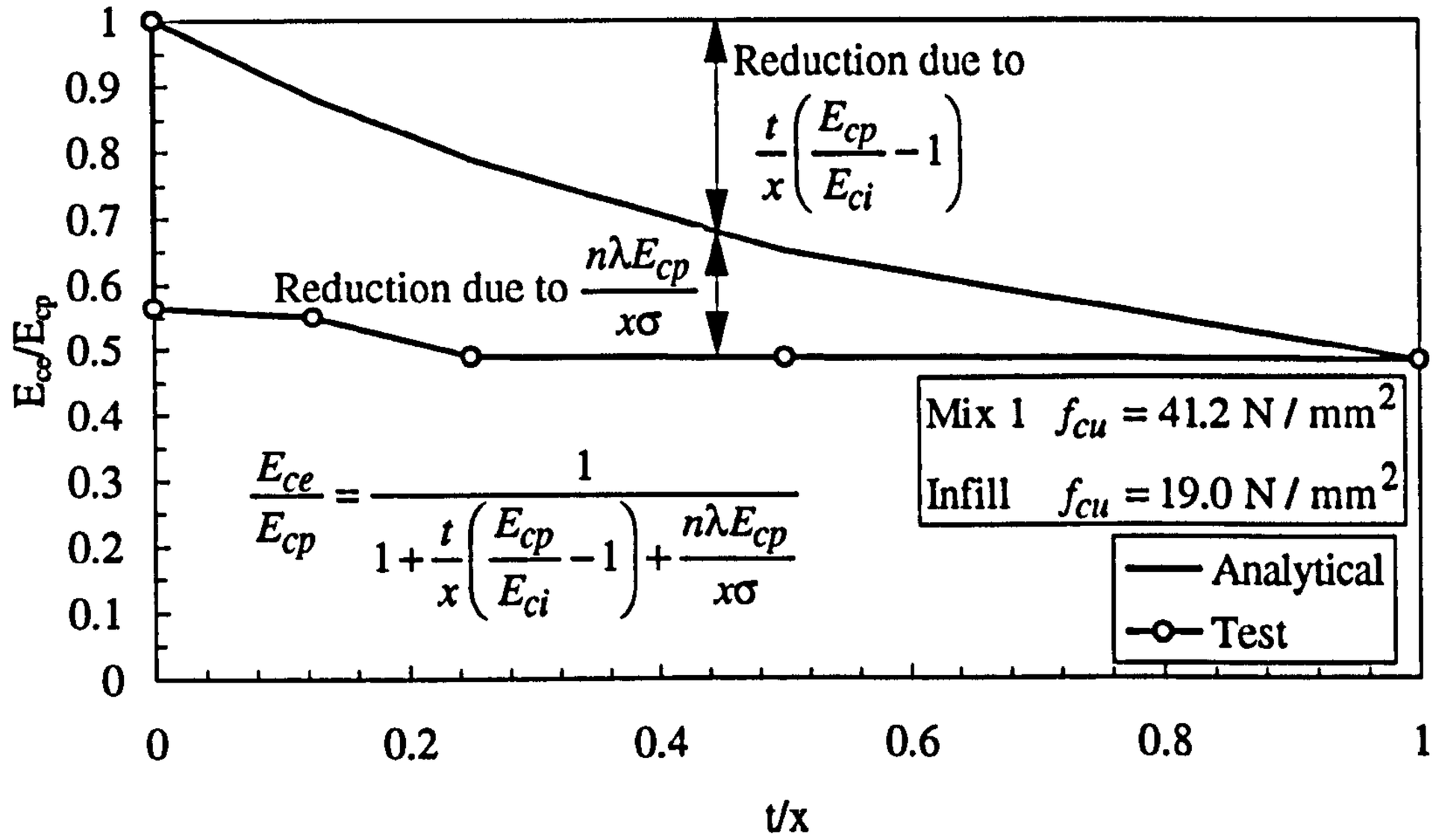

Figure 9.11: Variation in effective modulus for compressive specimens type A in test series 3 for varying thickness t of infill concrete

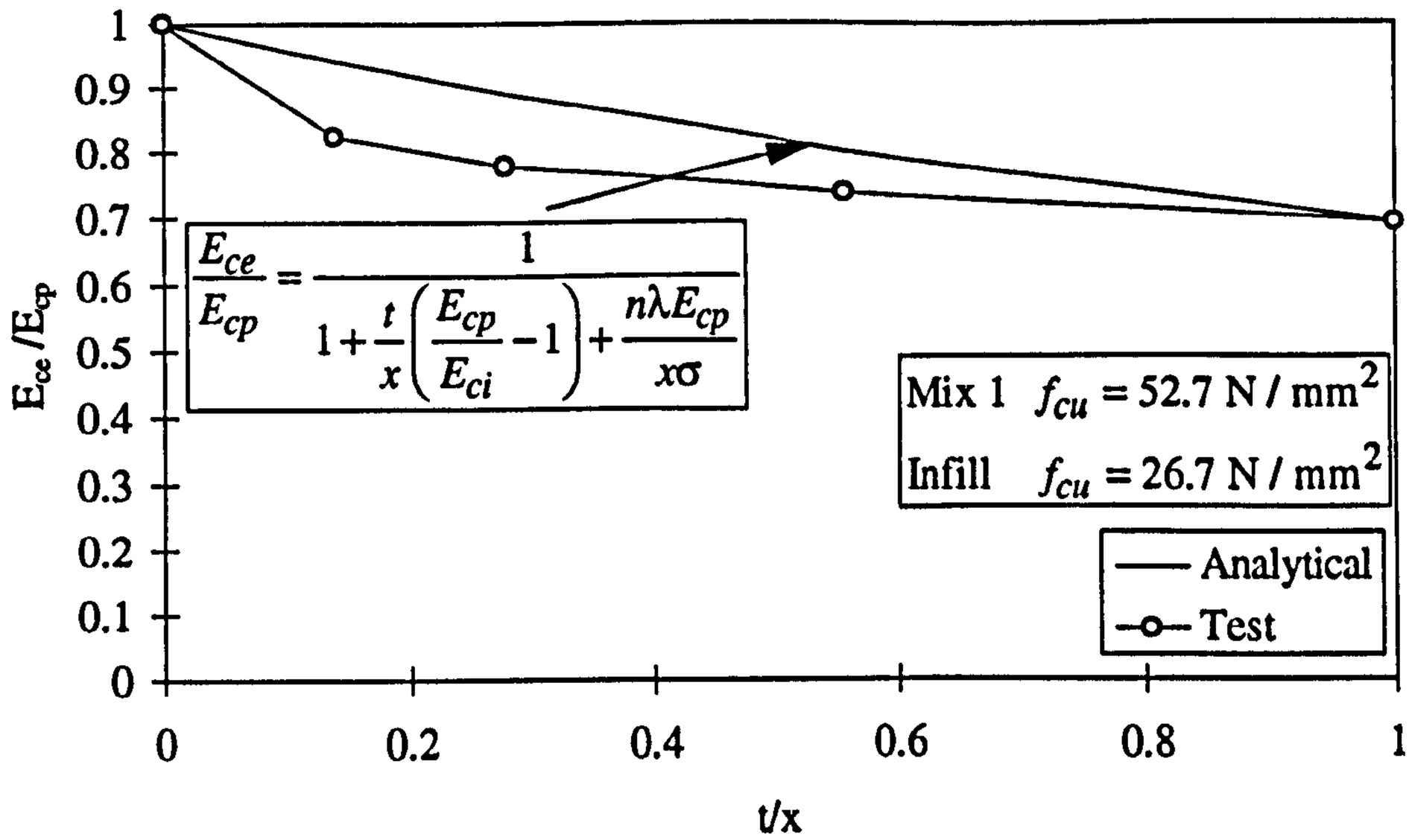

Figure 9.12(a): Variation in effective modulus for compressive specimens type A in test series 4 for varying thickness t of infill concrete

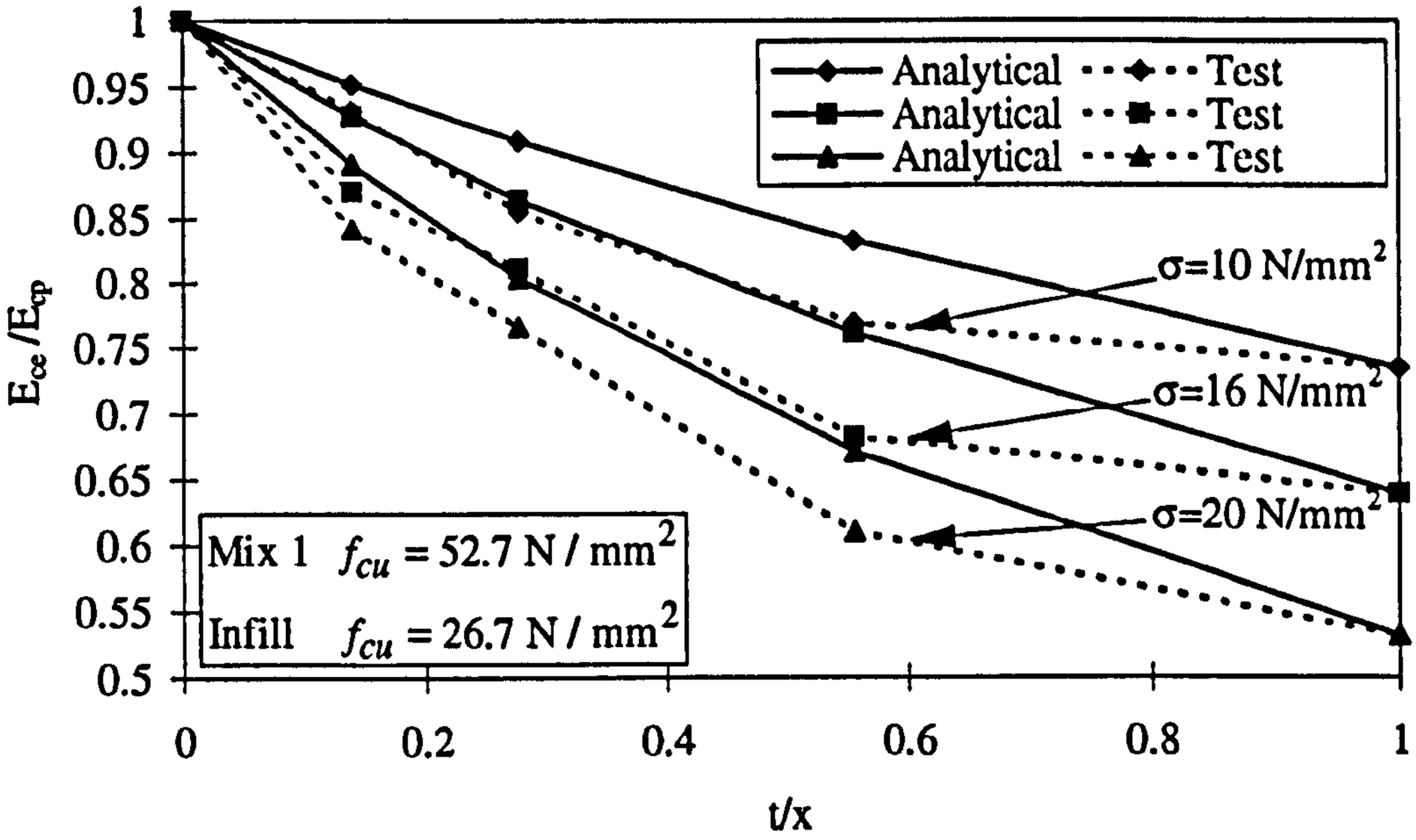

Figure 9.12(b): Variation in effective modulus for compressive specimens type A in test series 4 for varying thickness t of infill concrete and axial compressive stress

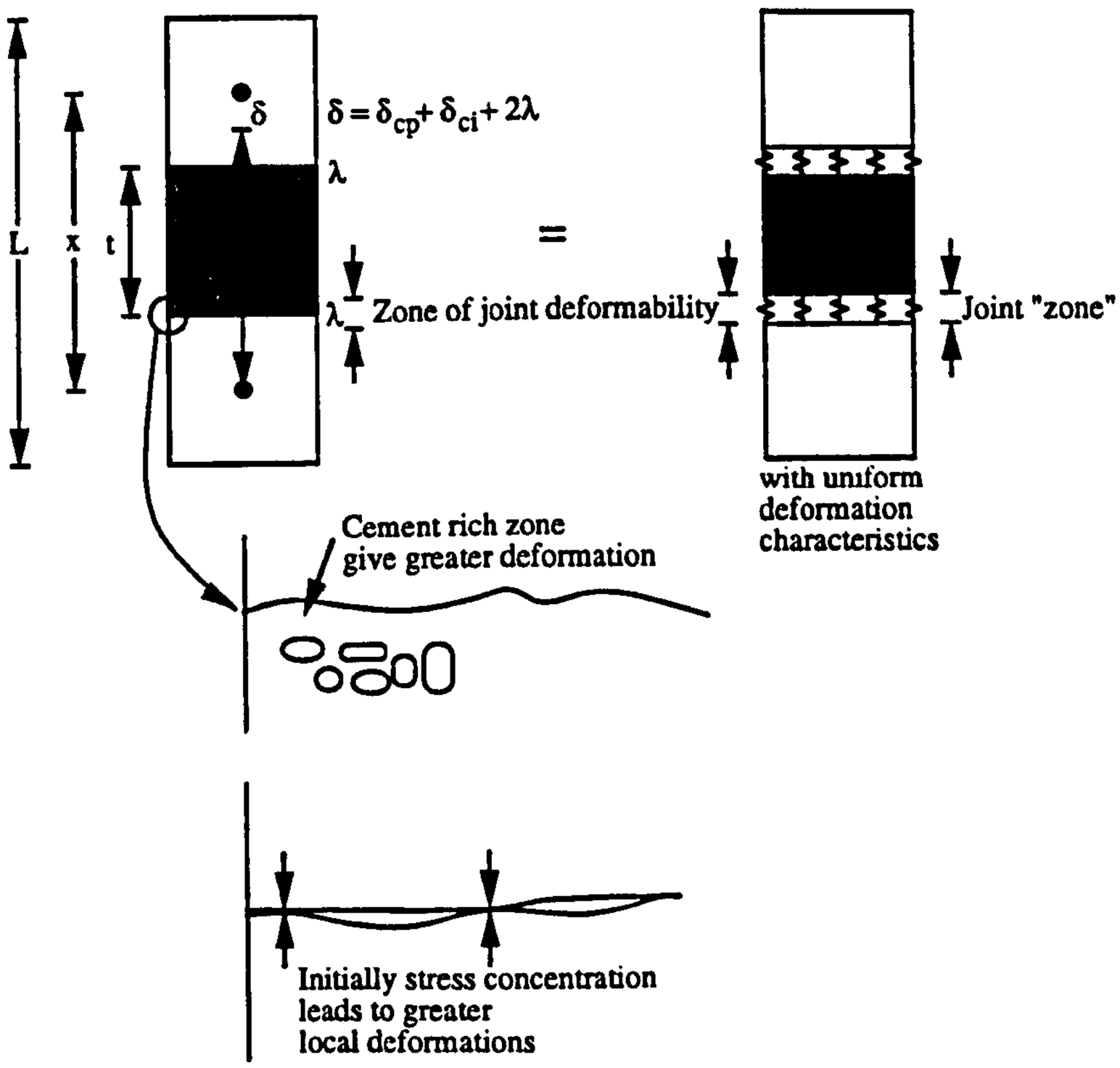

Figure 9.13: Zone of interface deformability for compressive specimens

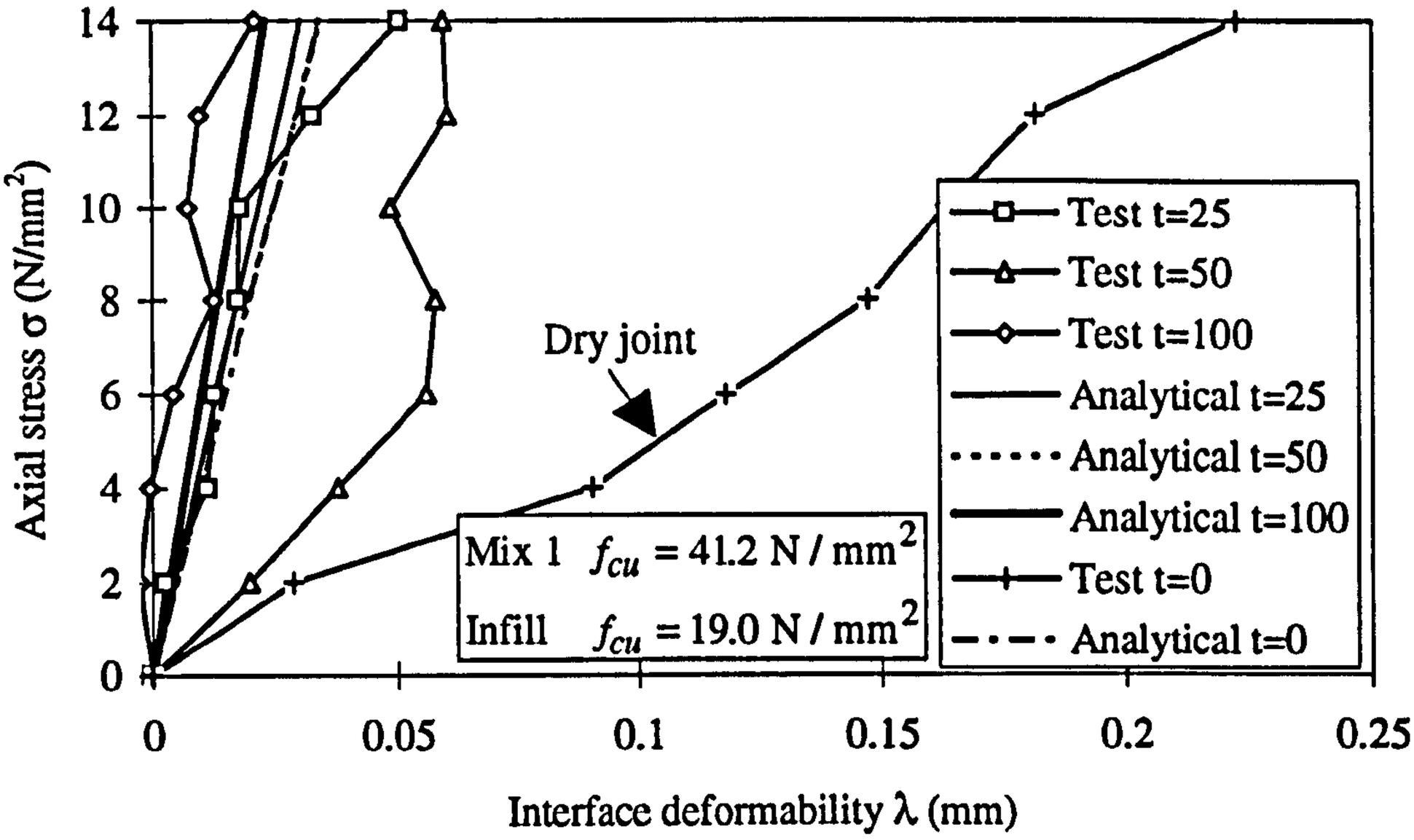

Figure 9.14: Axial stress interface deformability for compressive specimens type A in test series 3 for varying thickness t of infill concrete

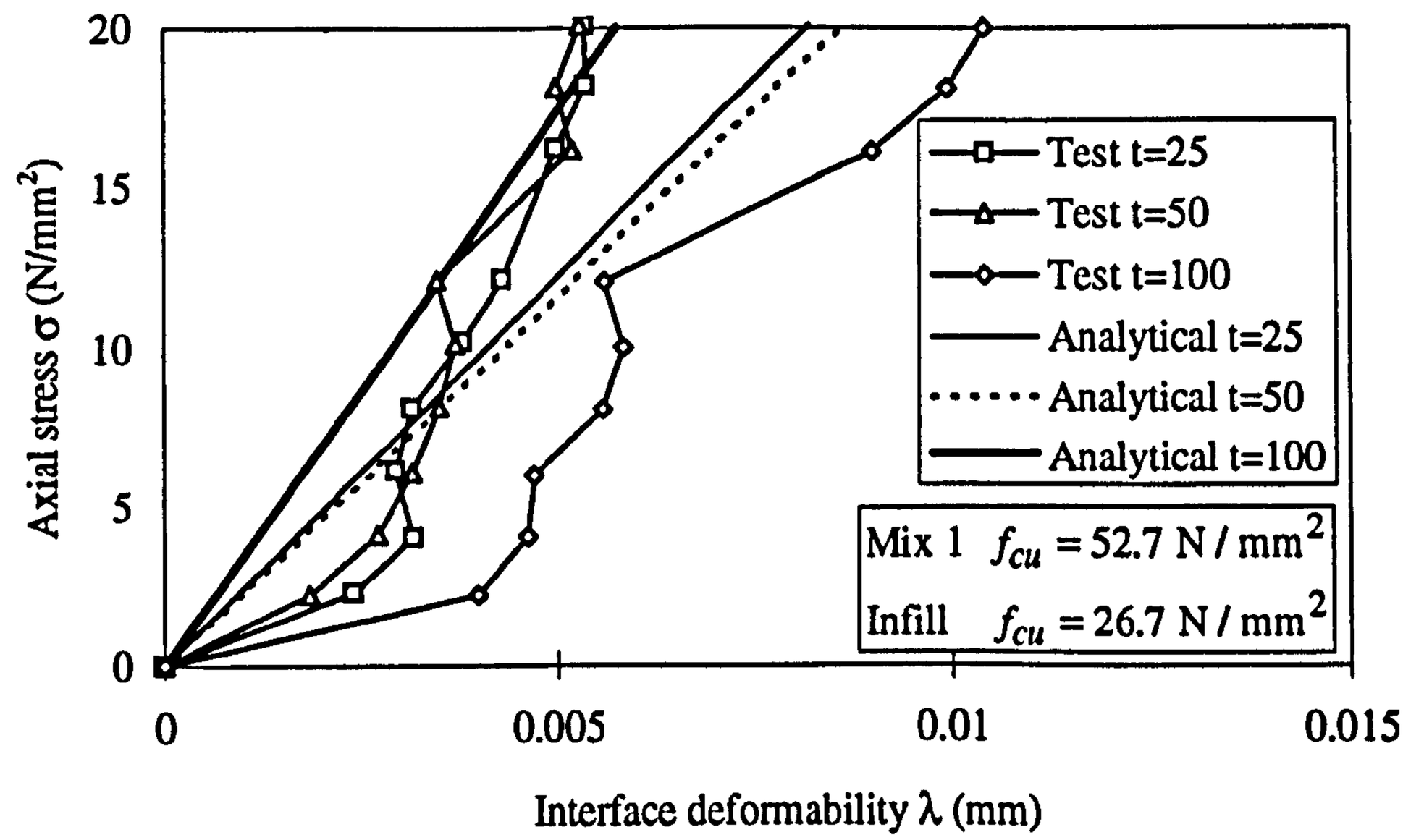

Figure 9.15: Axial stress interface deformability for compressive specimens type A in test series 4 for varying thickness t of infill concrete

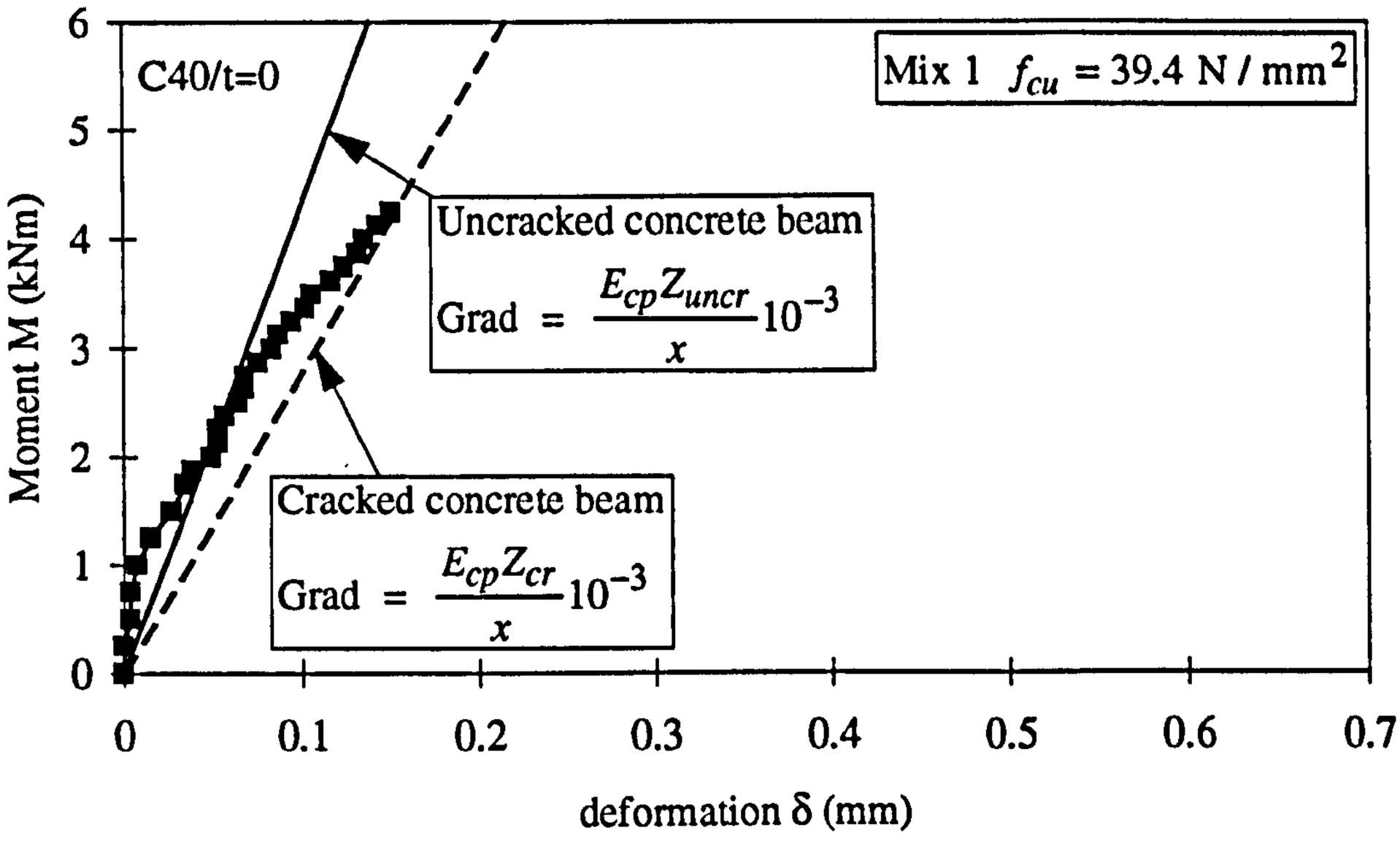

Figure 9.16(a): Load compressive deformation at top of specimen for t = 0 in test series 6

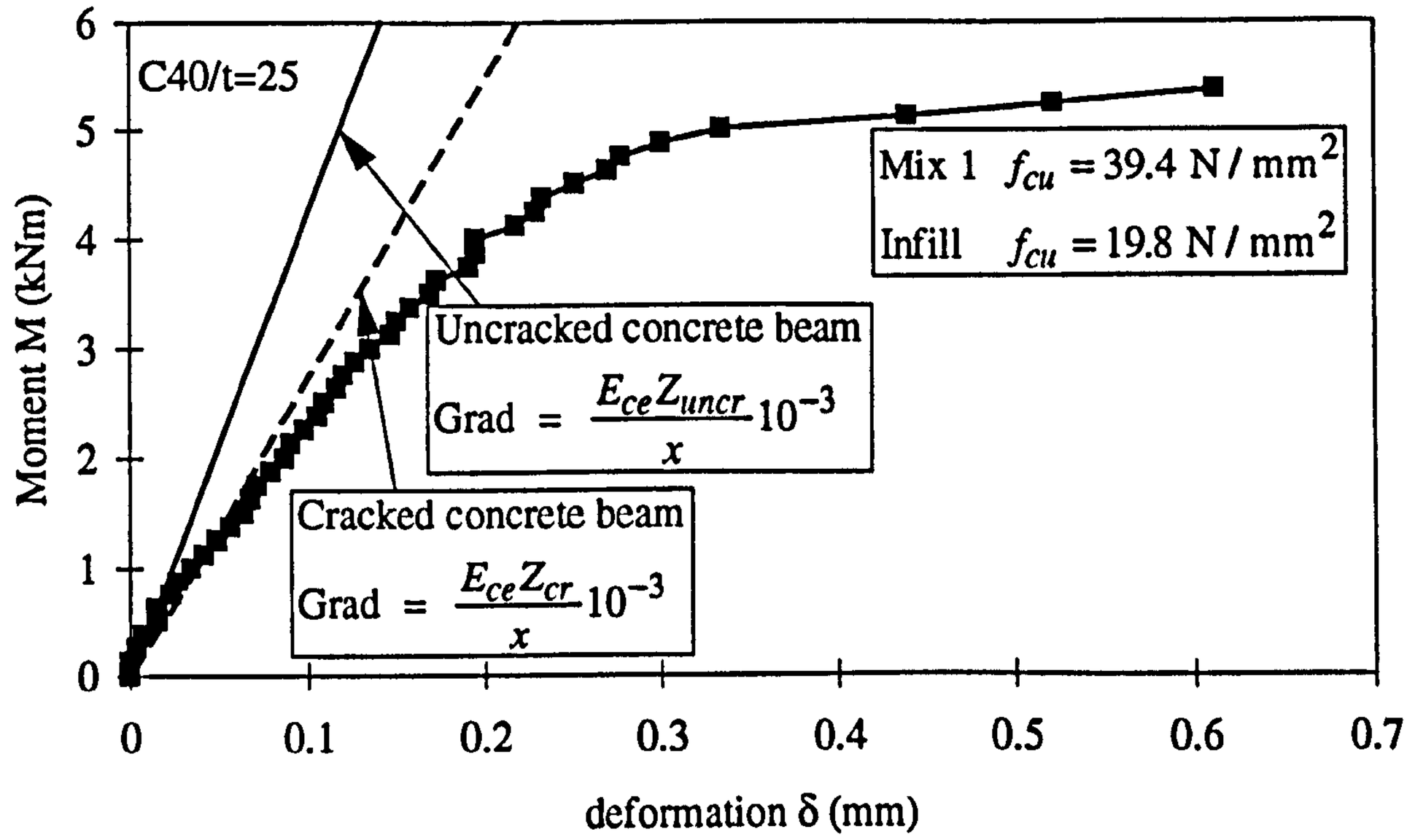

Figure 9.16(b): Load compressive deformation at top of specimen for t = 25 in test series 6

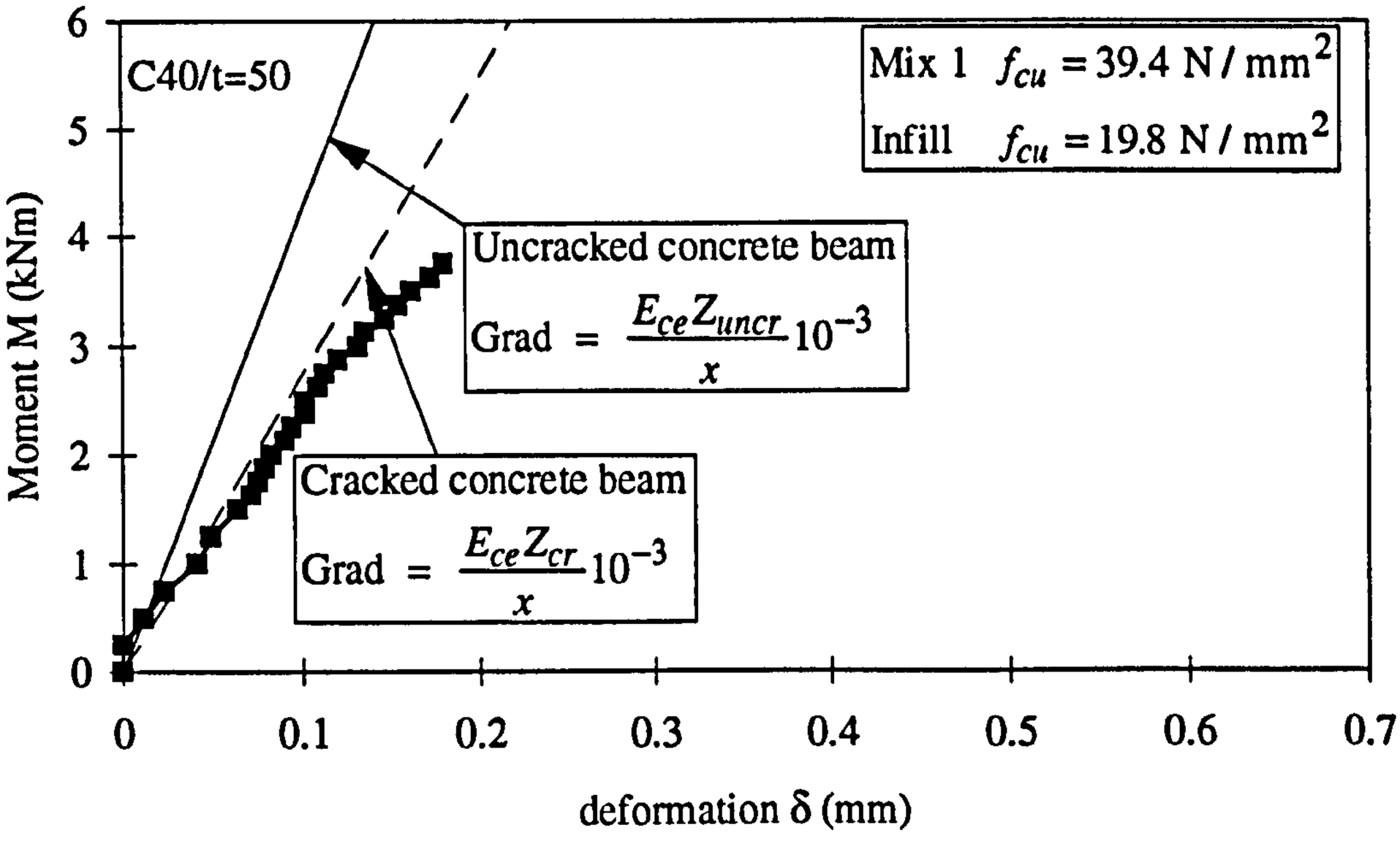

Figure 9.16(c): Load compressive deformation at top of specimen for t = 50 in test series 6

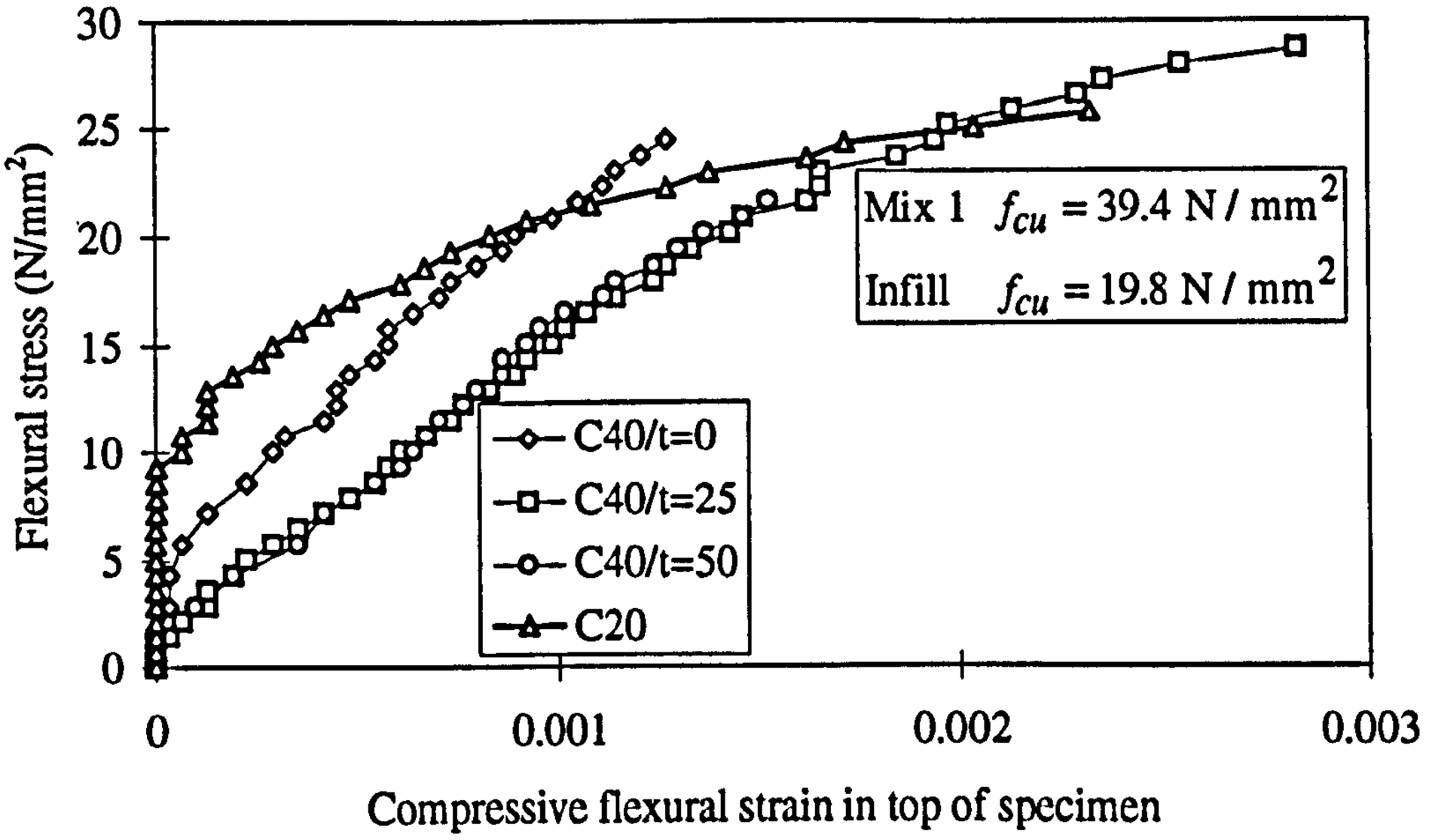

Figure 9.16(d): Flexural stress vs strain data for flexural specimens type B in test series 6

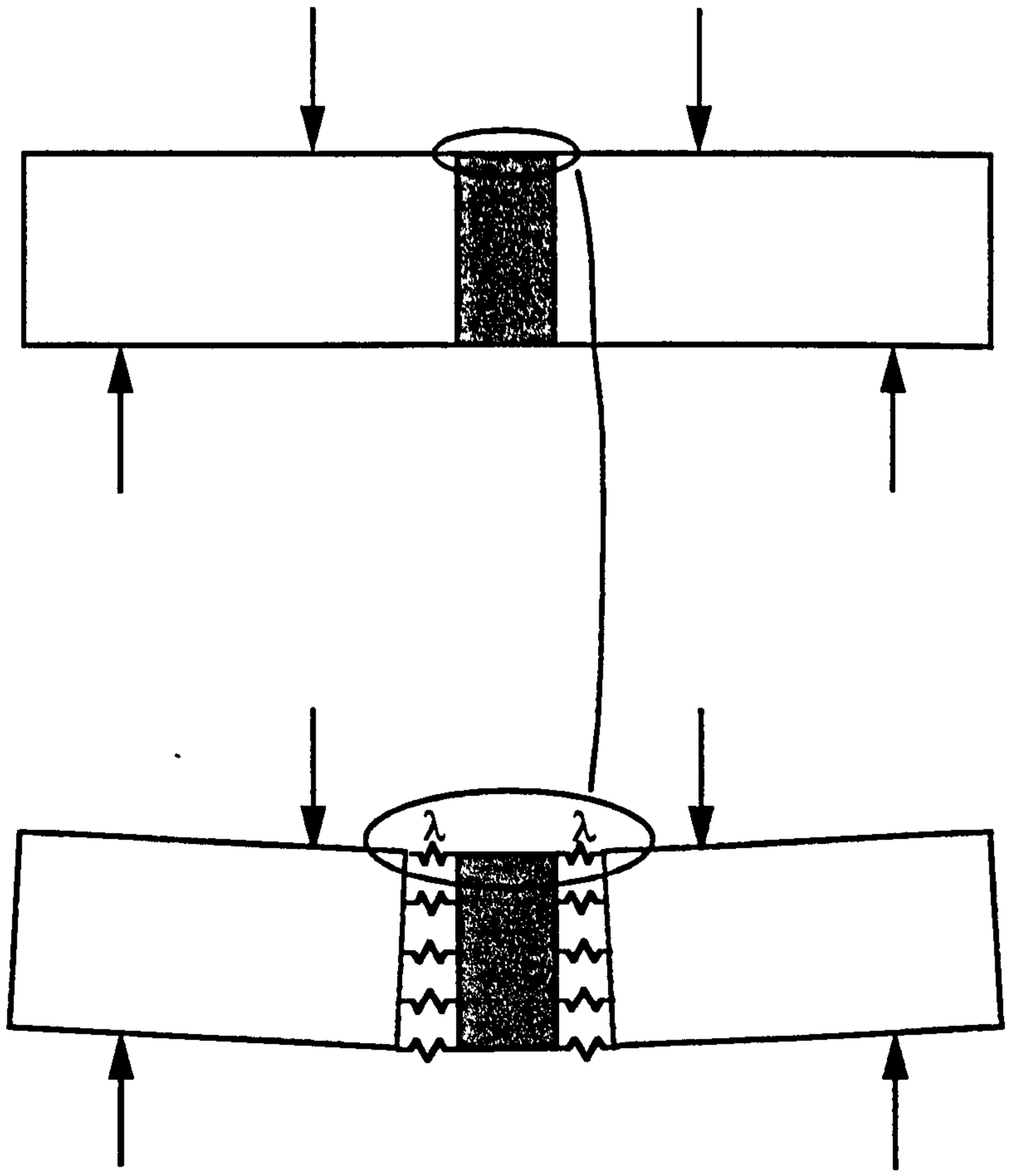

Figure 9.17: Zone of interface deformability for flexural specimens type B in test series 6 for varying thickness t of insitu concrete

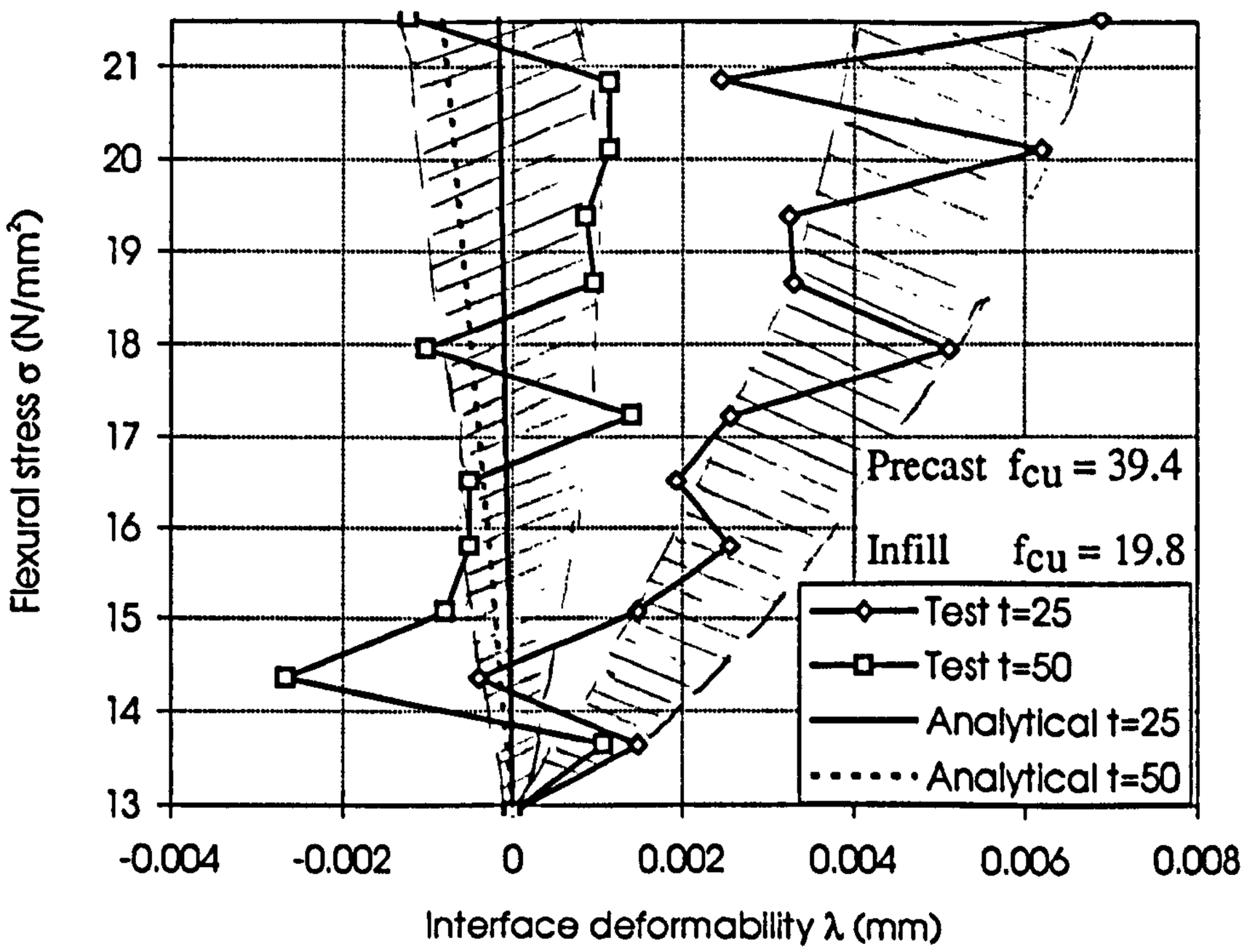

Figure 9.18: Load interface deformability for flexural specimens type B in test series 6 for varying thickness t of insitu concrete

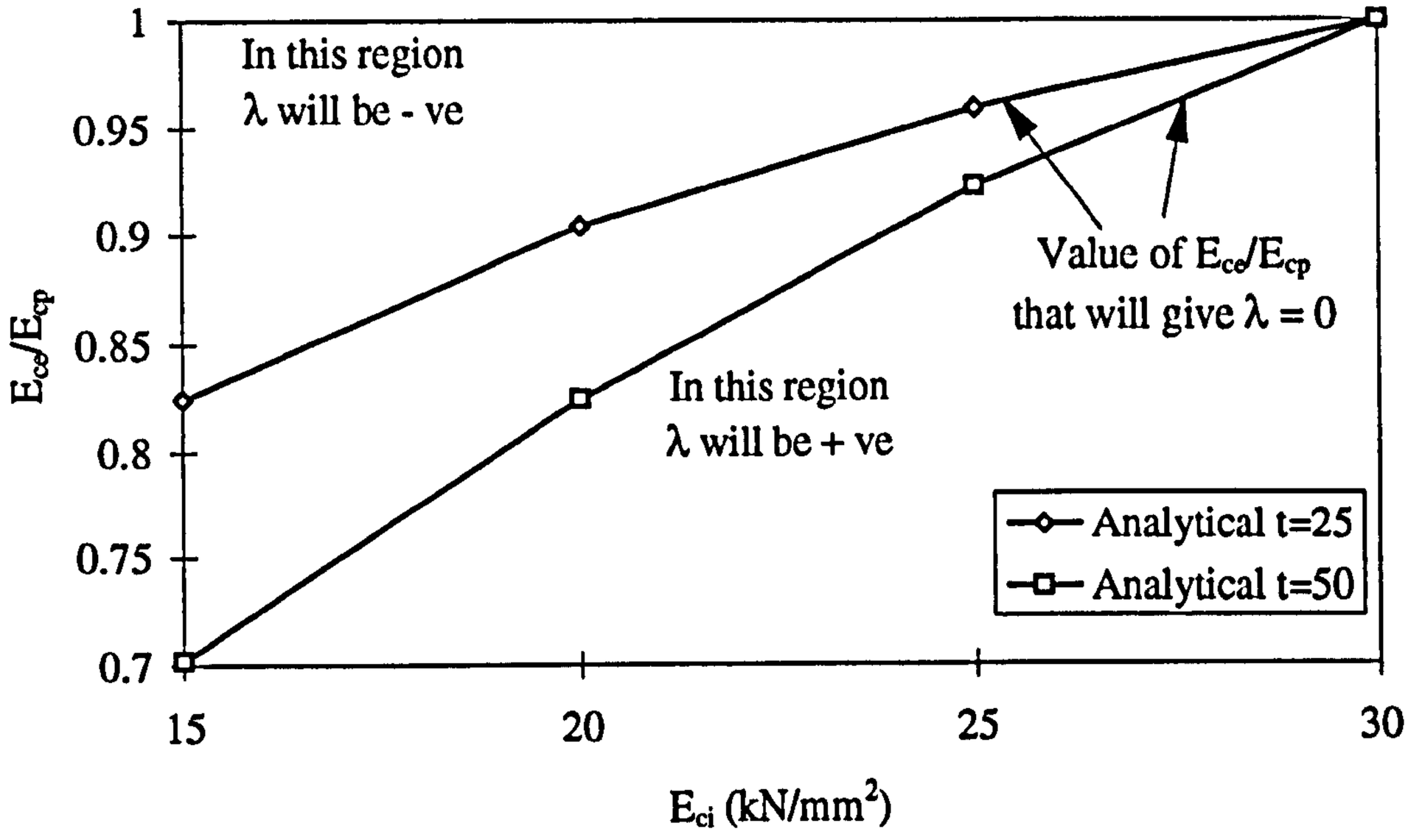

Figure 9.19: Variation in E_{ce}/E_{cp} ratio with E_{ci} for flexural specimens type B in test series 6 for varying thickness t of insitu concrete

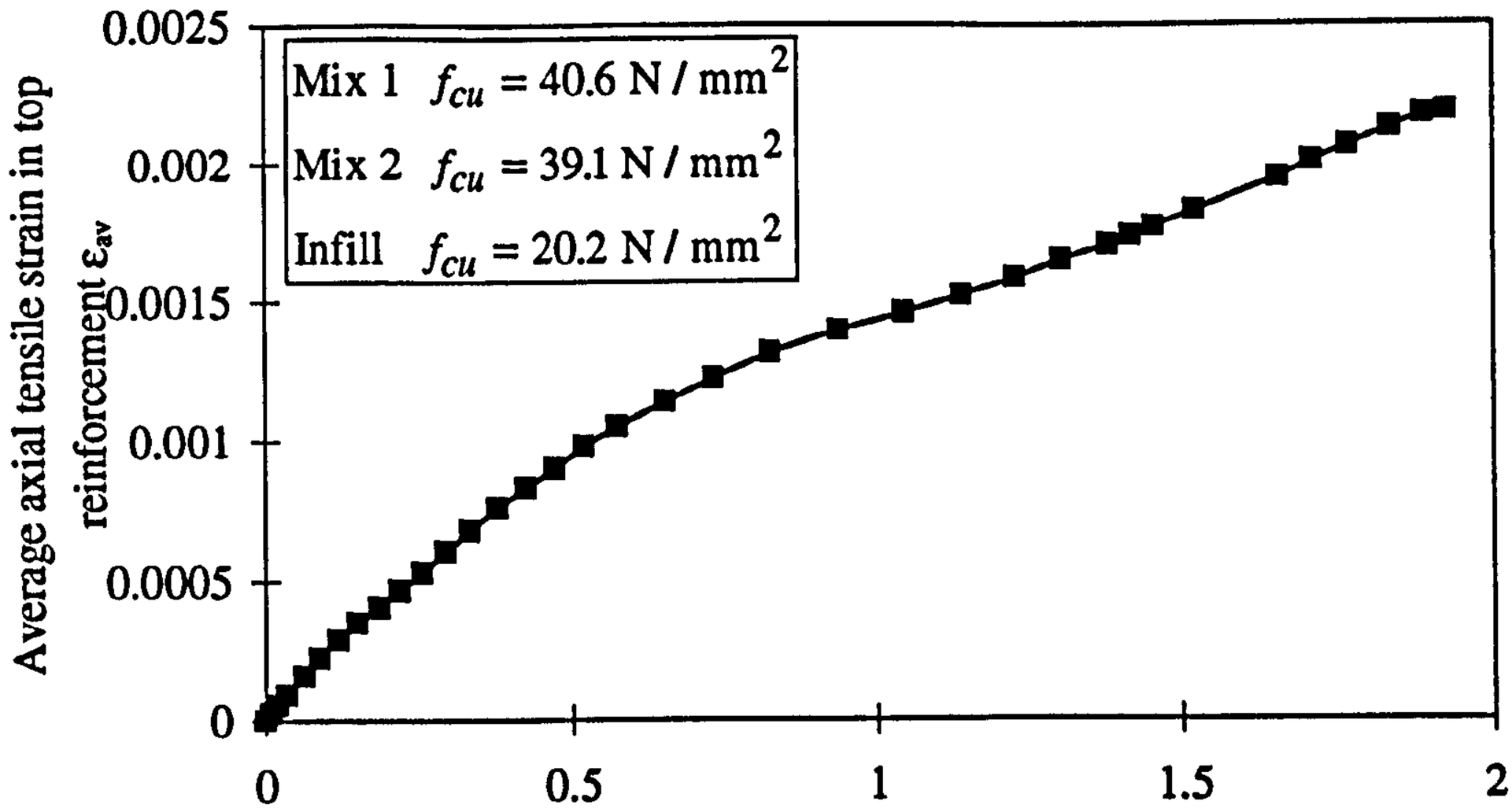

Figure 9.20: Crack width opening vs axial strain in bars in bond slip test in test series 7

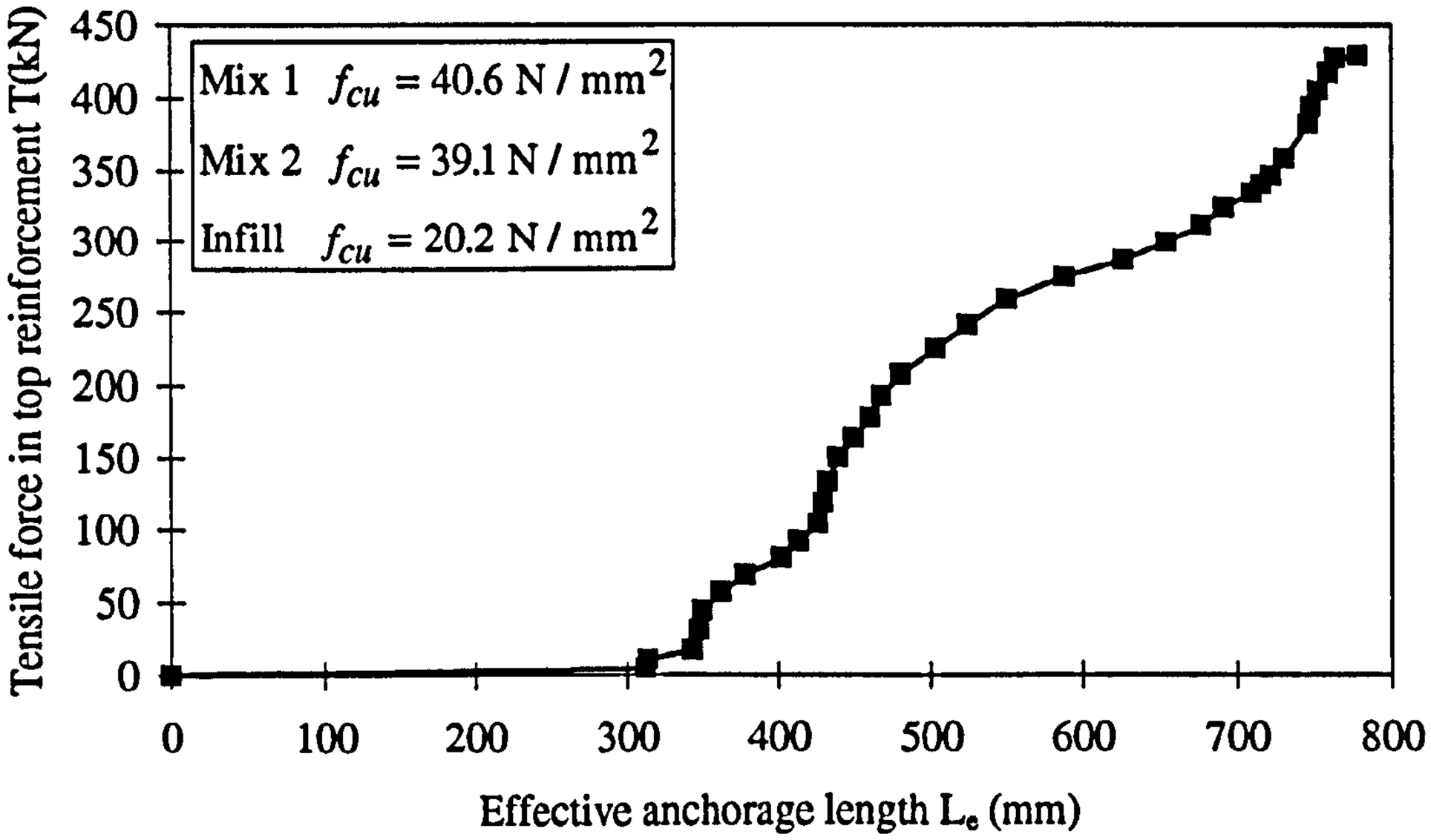

Figure 9.21: Tensile force in bars vs effective anchorage length of bars in bond slip test in test series 7

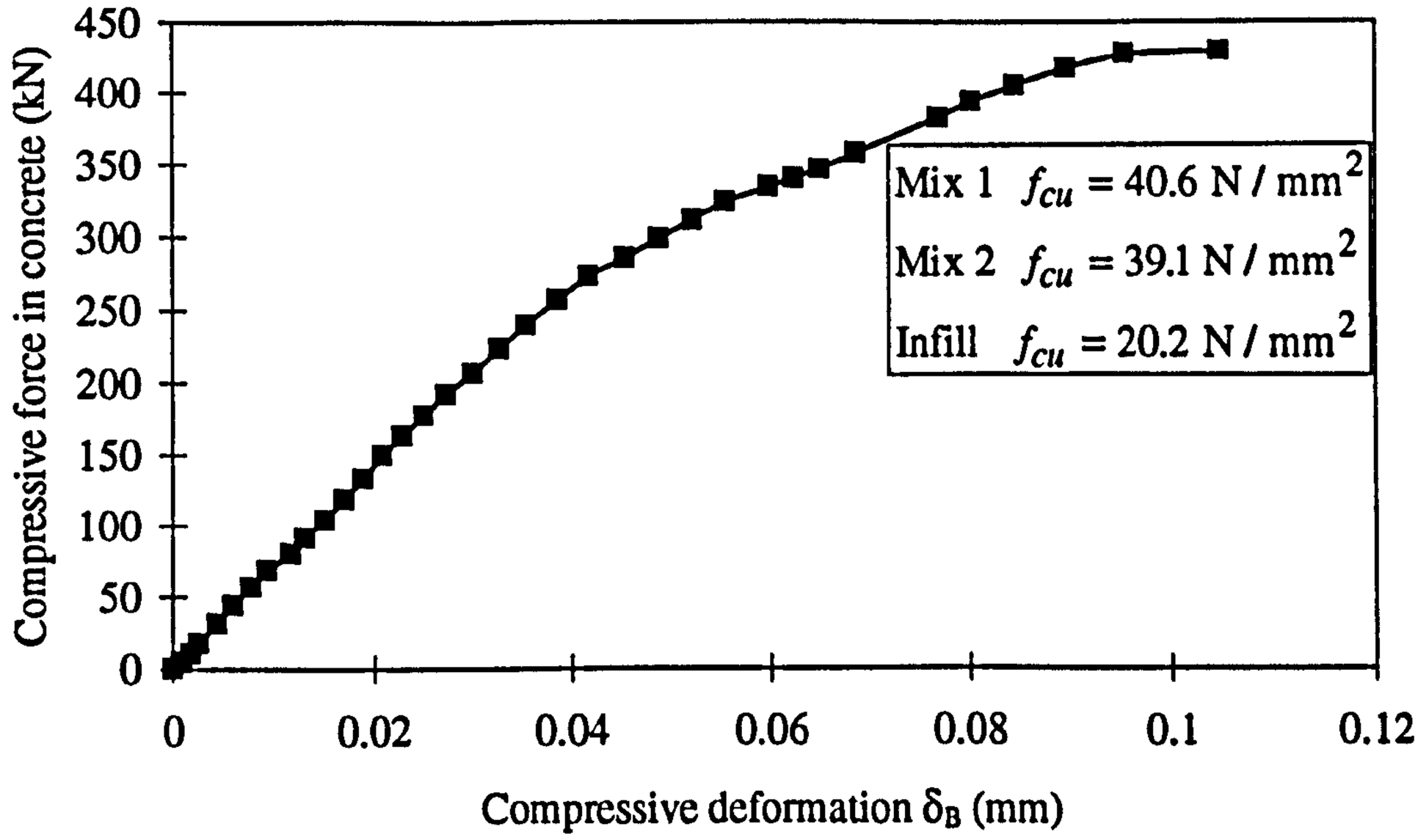

Figure 9.22: Compressive force in concrete vs compressive deformation at bottom of specimen in bond slip test in test series 7

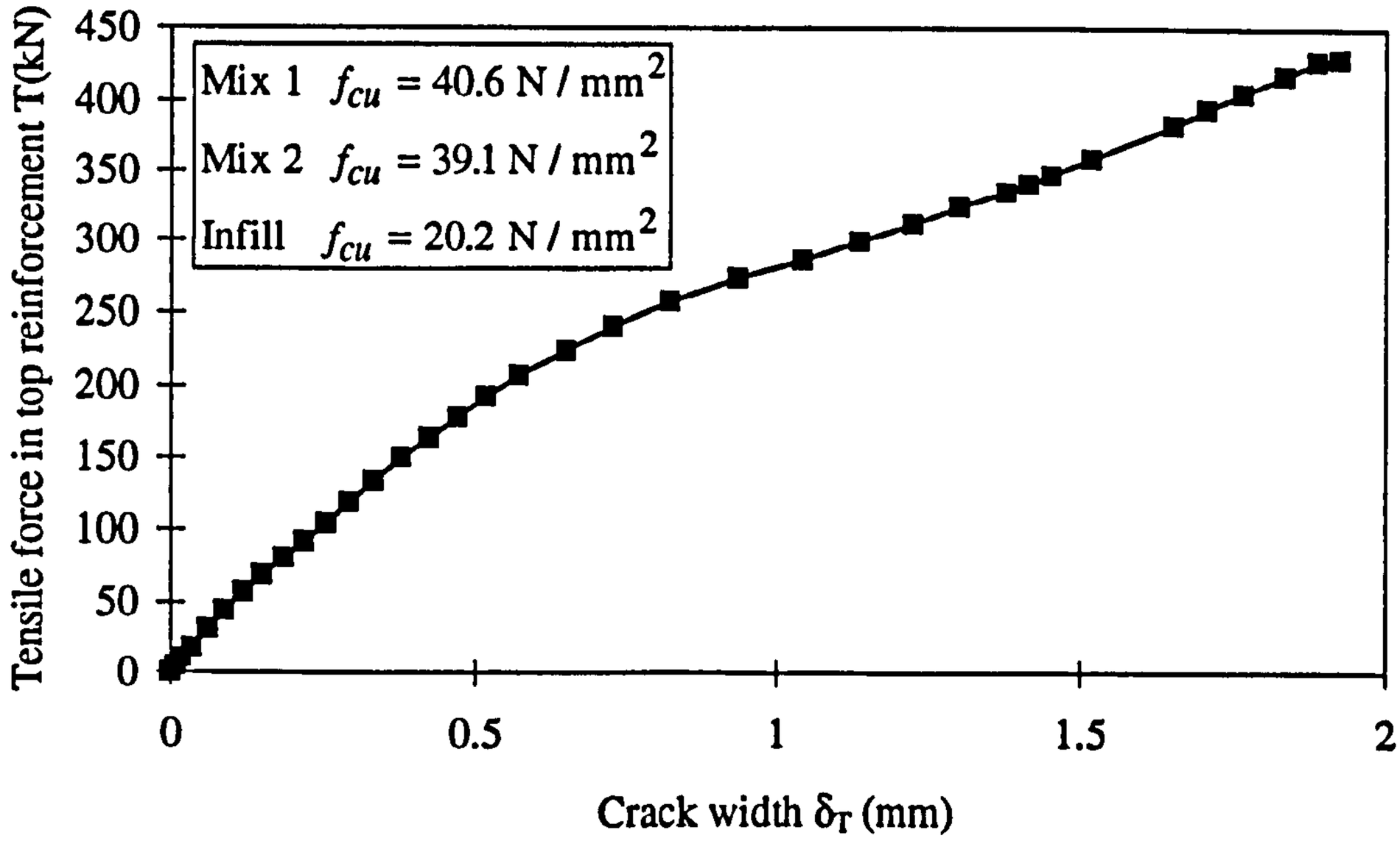

Figure 9.23: Tensile force in bars vs crack width opening at top of specimen in bond slip test in test series 7

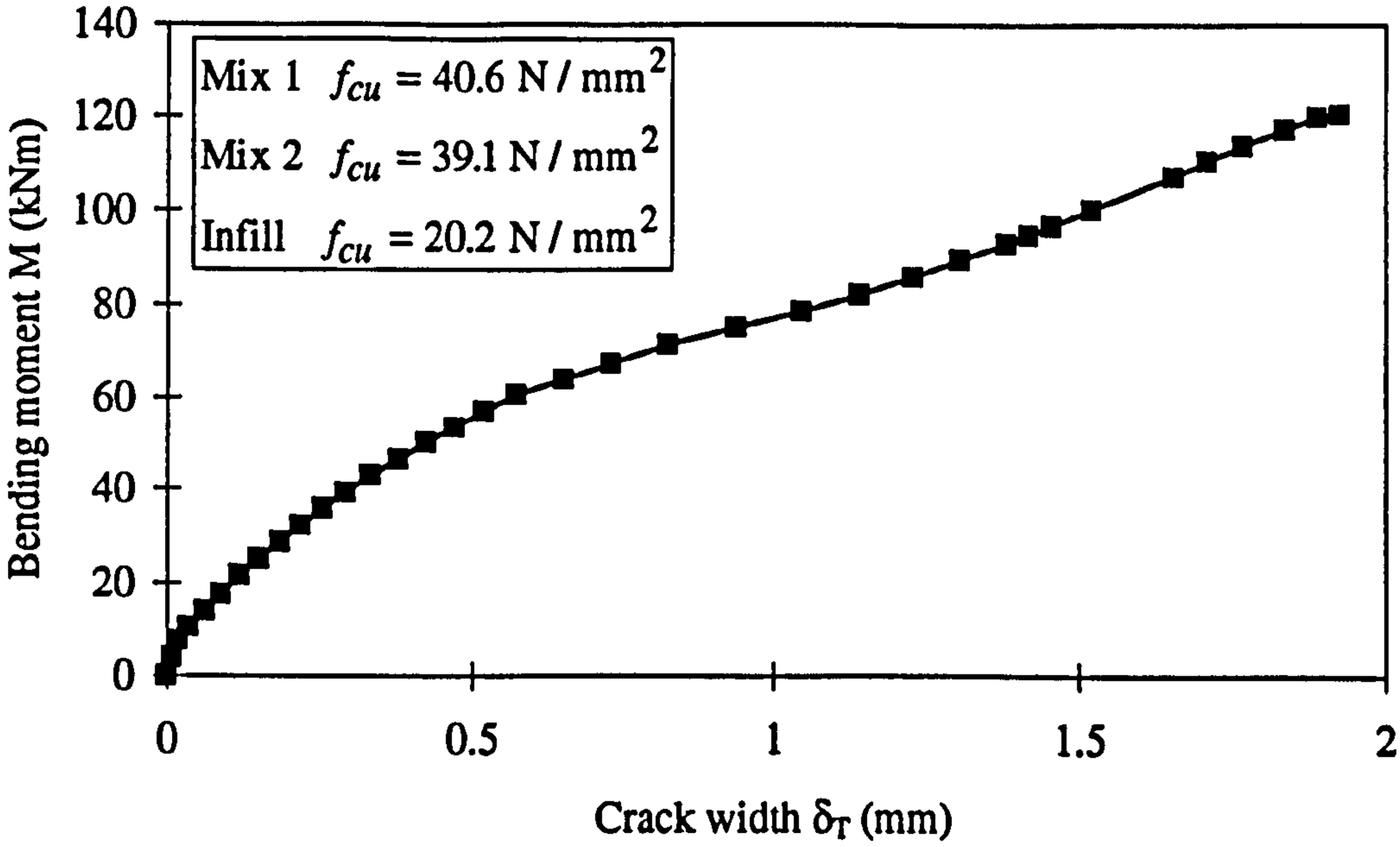

Figure 9.24: Bending moment vs crack width opening at top of specimen in bond slip test in test series 7

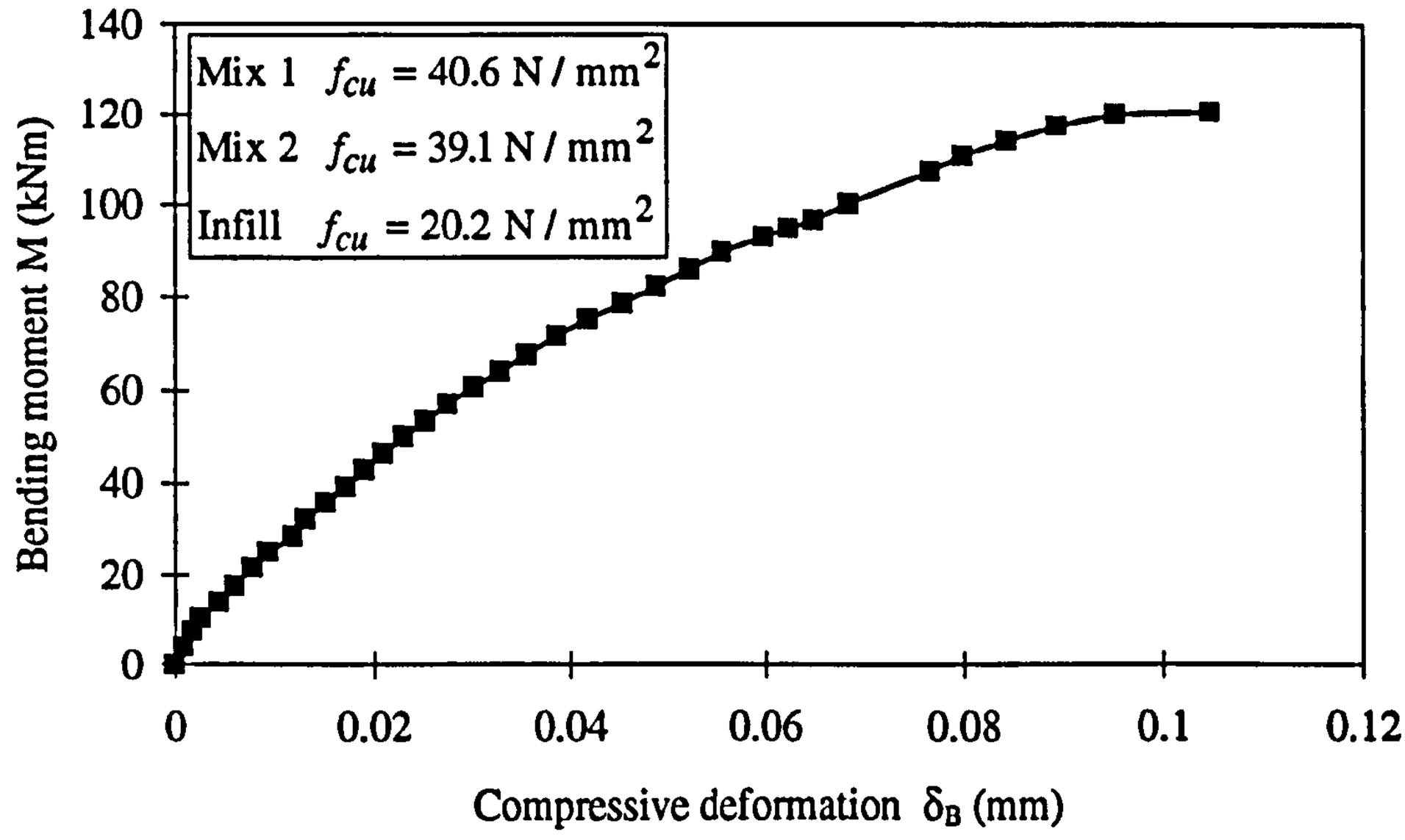

Figure 9.25: Bending moment vs compressive deformation at bottom of specimen in bond slip test in test series 7

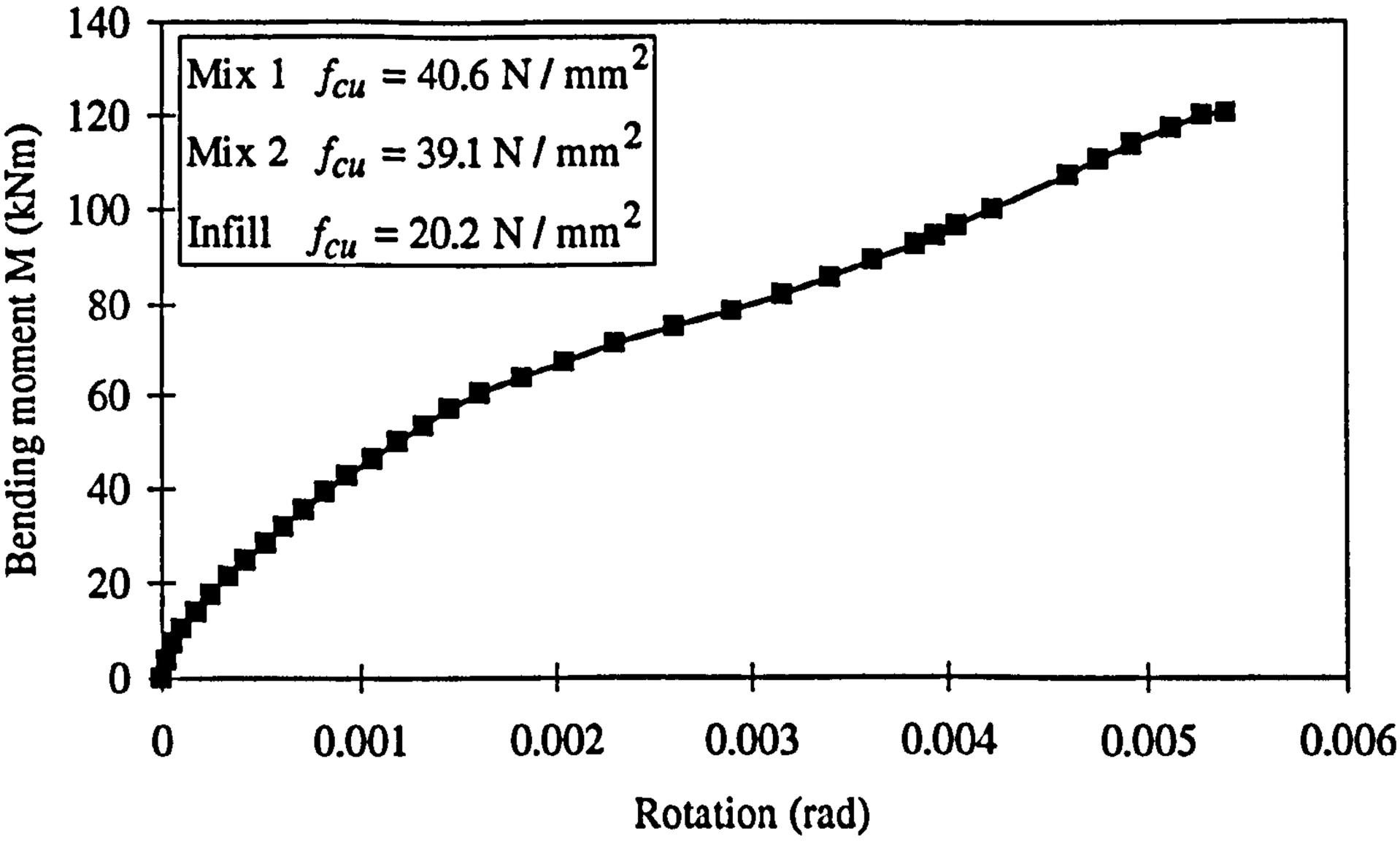

Figure 9.26: Bending moment - rotation behaviour of specimen in bond slip test in test series 7

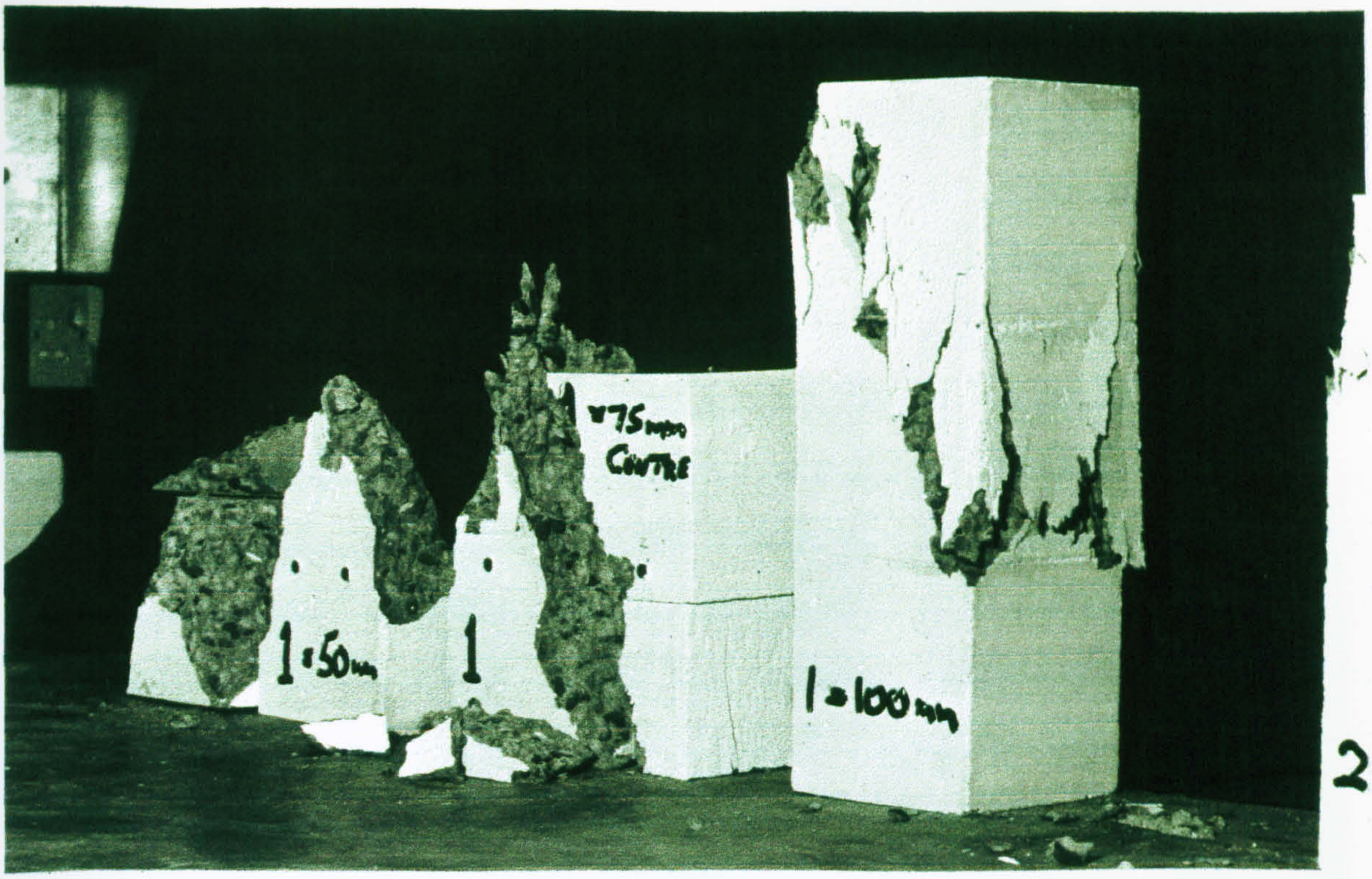

Plate 9.1(a) : Failure regions of test series 1 for mix 1 specimens

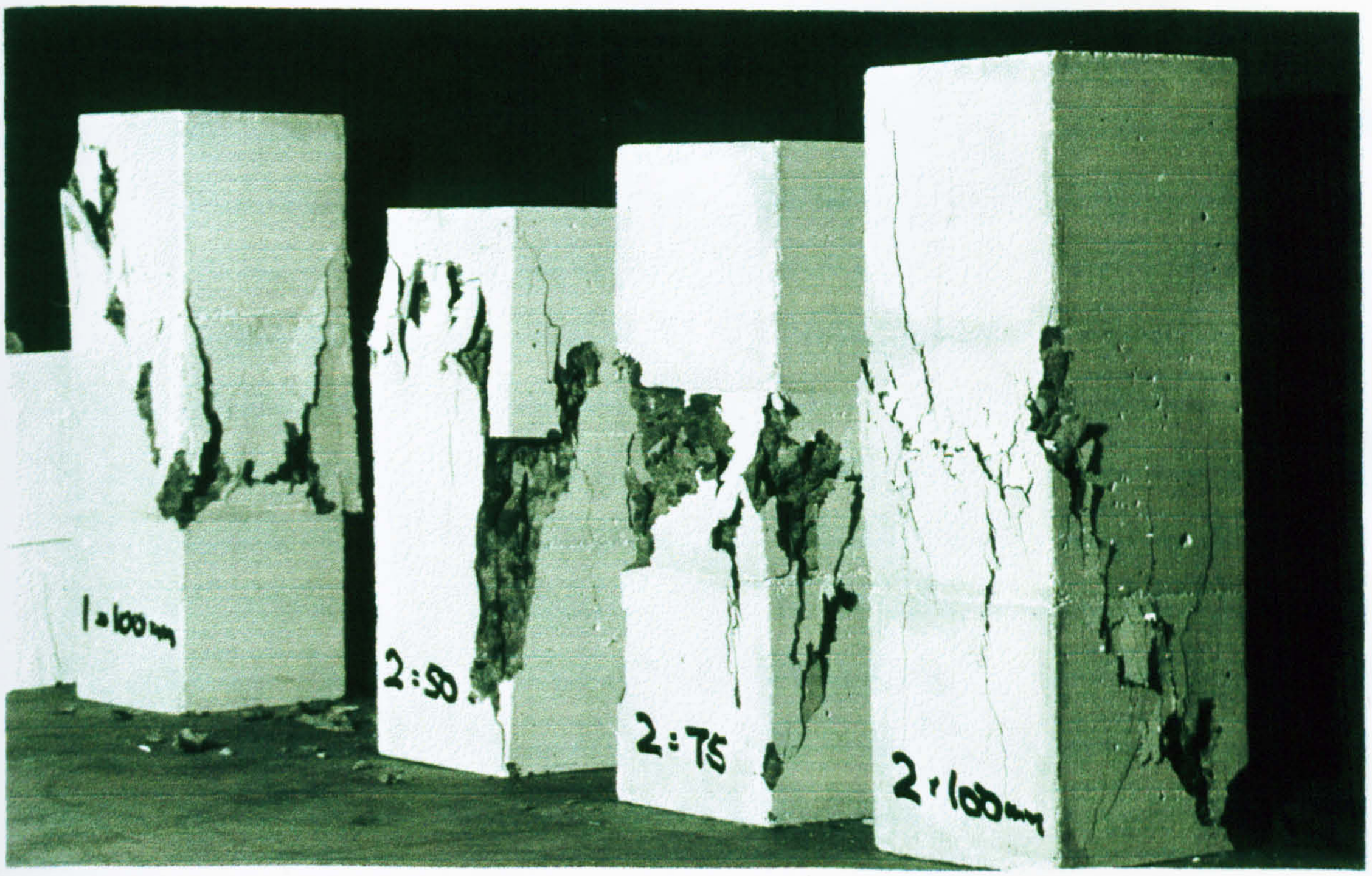

Plate 9.1(b) : Failure regions of test series 1 for mix 2 specimens

Plate 9.2 : Failure regions of test series 2

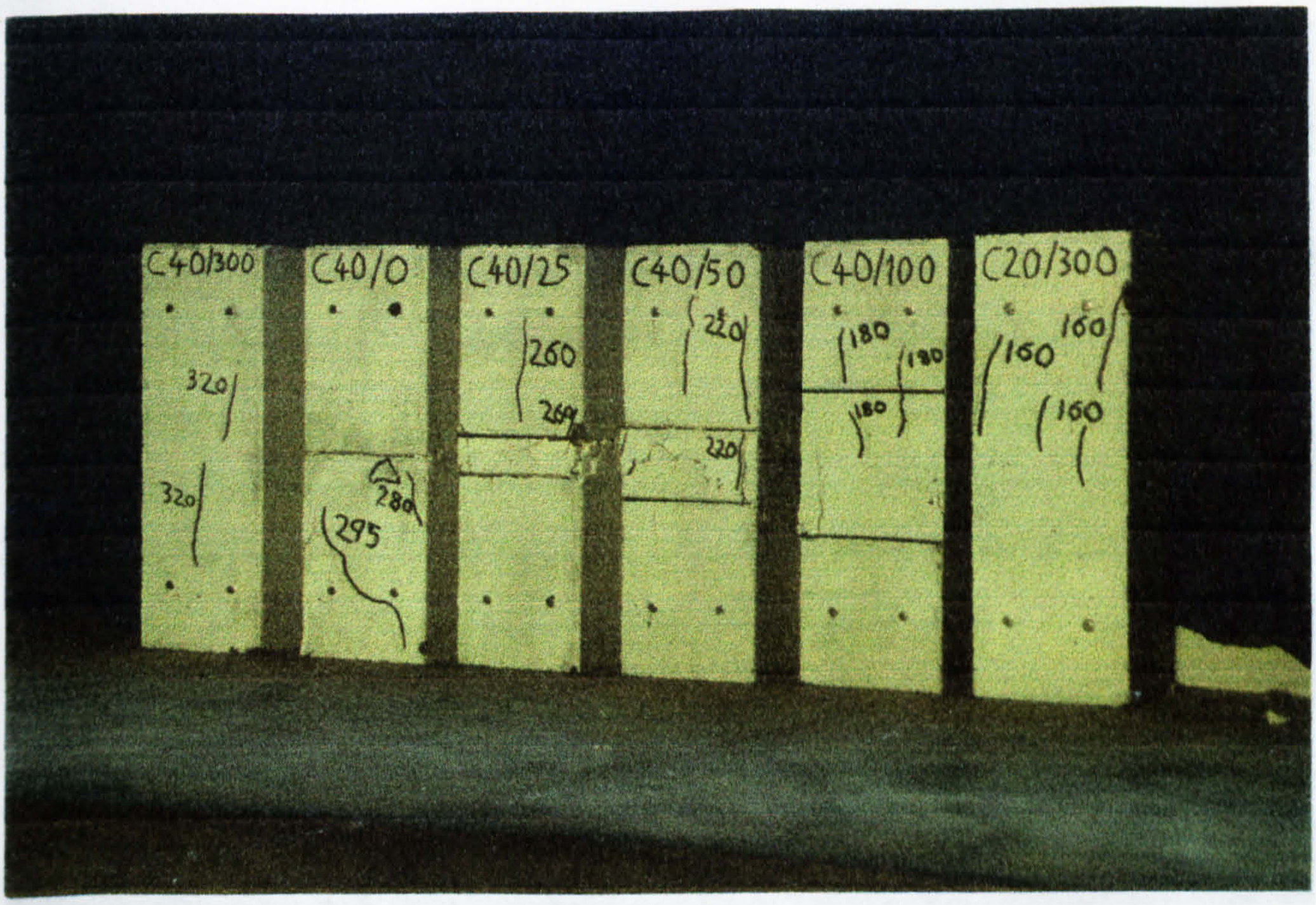

Plate 9.3 : Failure regions of test series 3

Plate 6.4(a): Failure regions of test series 4 (front face)

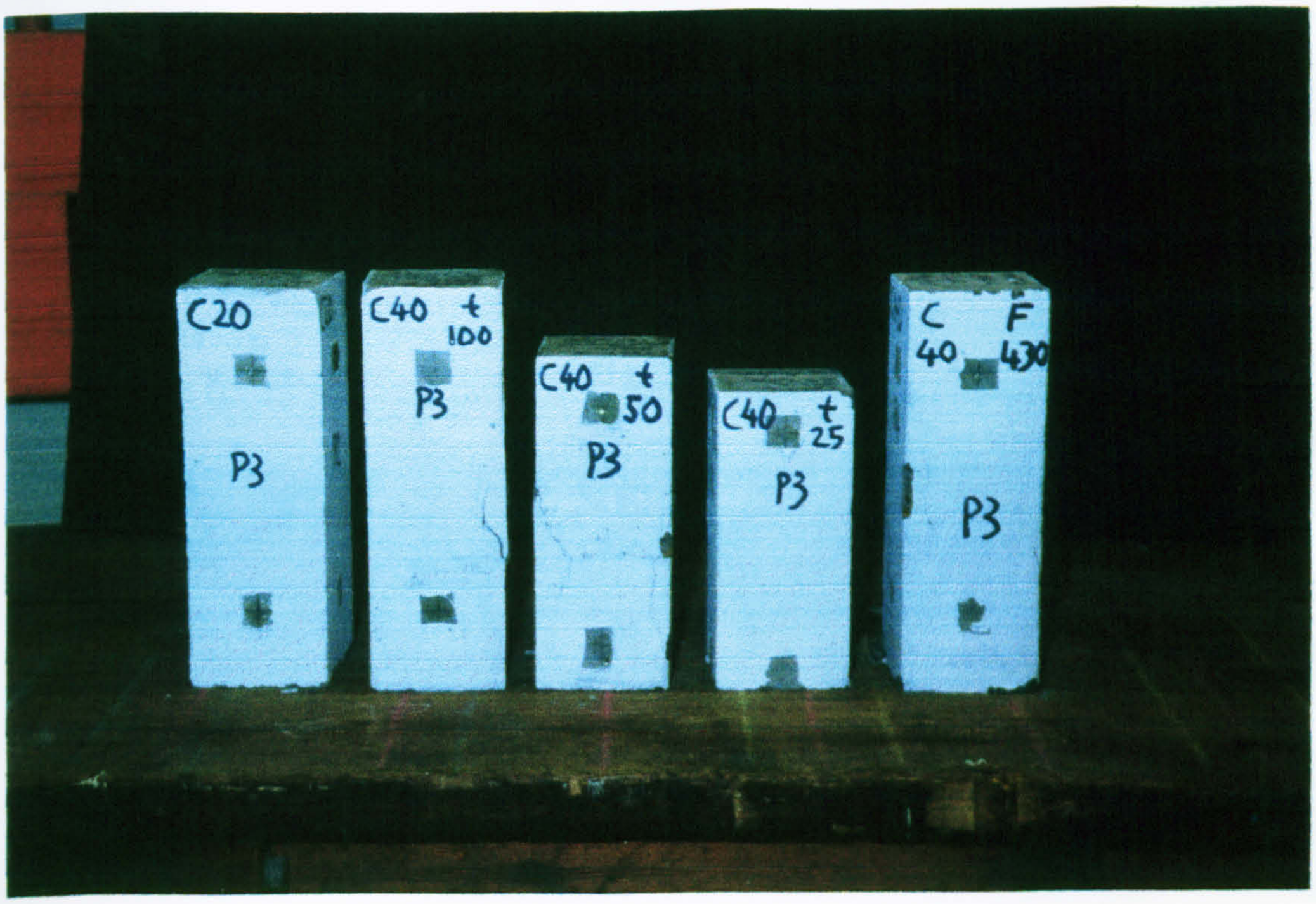

Plate 9.4(b) : Failure regions of test series 4 (back face)

Plate 9.5(a) : Failure regions of test series 5 (front face)

Plate 9.5(b) : Failure regions of test series 5 (the most damaged faces)

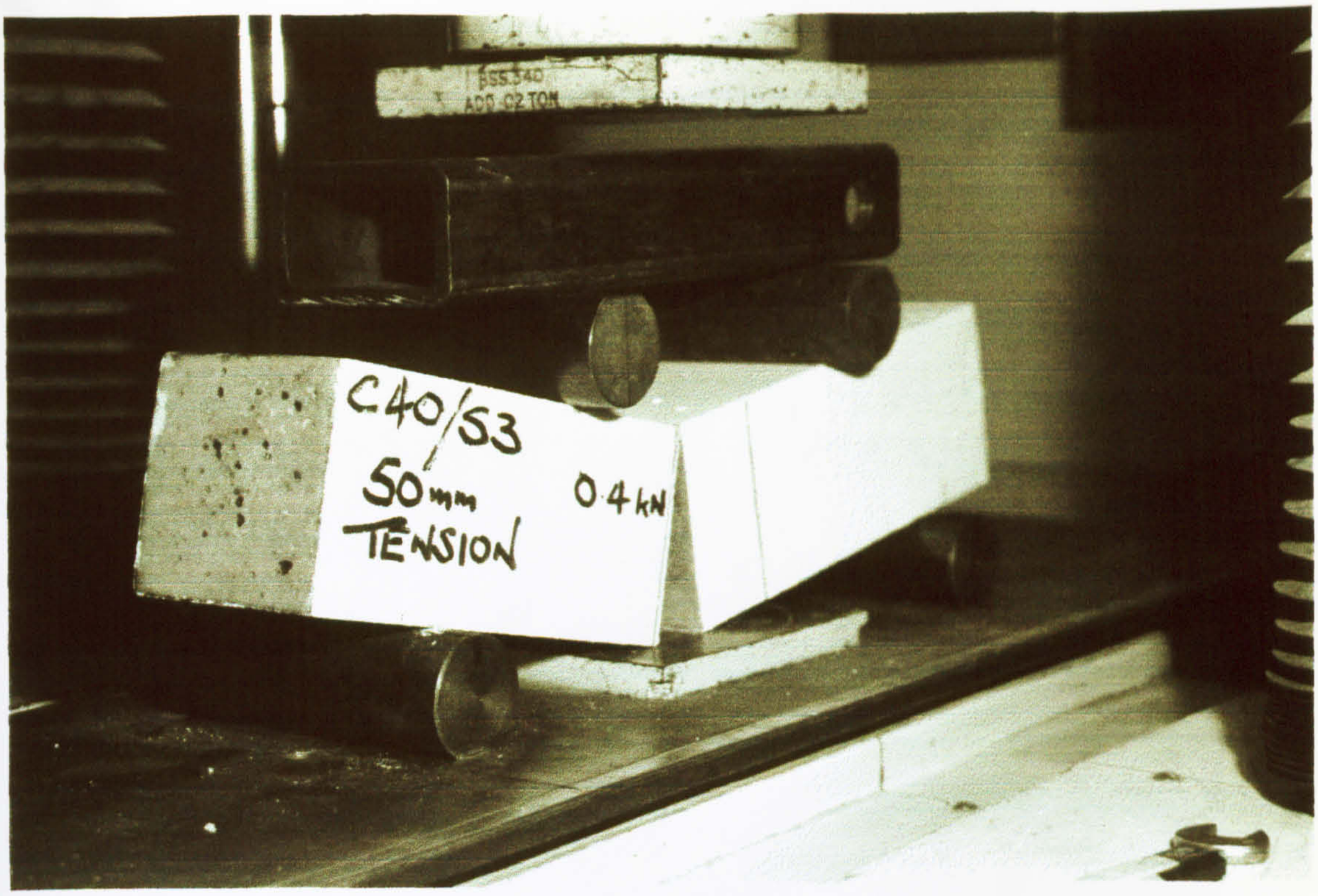

Plate 9.6(a) : Failure region of test series 6 for tension cracking

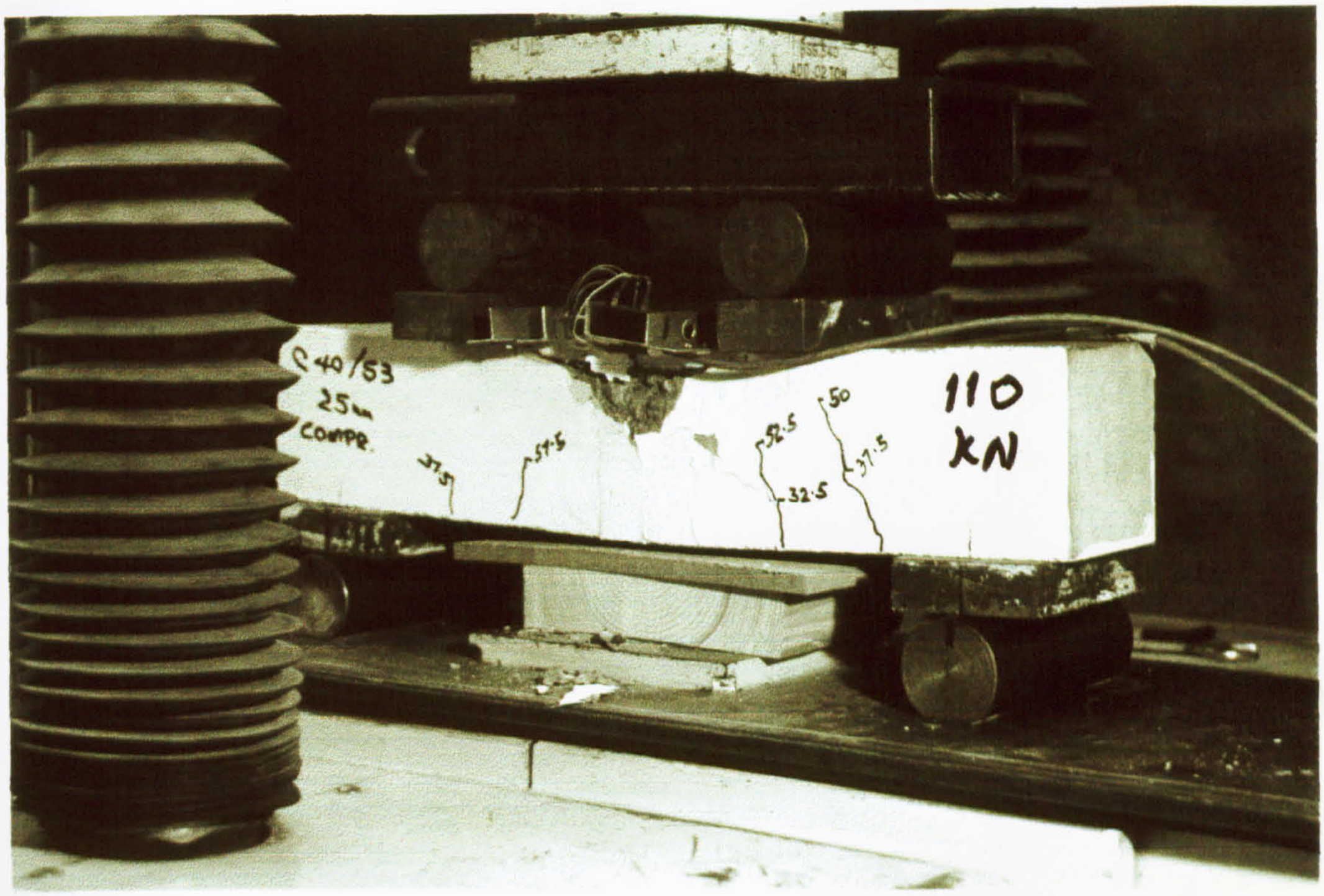

Plate 9.6(b) : Failure region of test series 6 for compression deformability

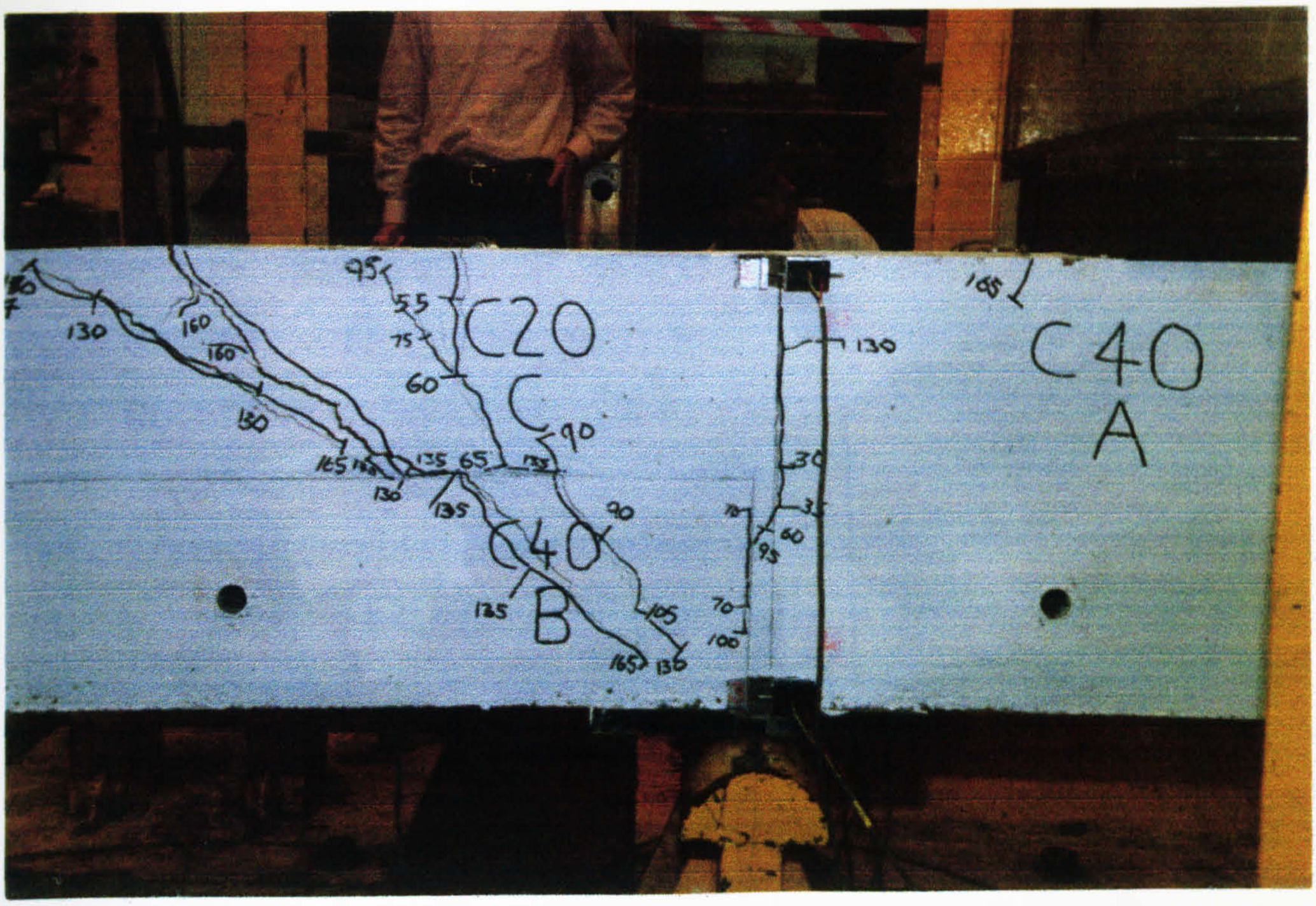

Plate 9.7 : Failure regions of test series 7

CHAPTER 10

VALIDITY OF COMPONENT METHOD

10.1 Simulating joint behaviour from sub-section tests

The experimental work on full scale frame connection tests established that the most common types of connections exhibit some degree of in-plane flexural semi-rigidity. Values of strength, stiffness and ($M_{con} - \phi$) data have been given previously (Chapter 6 Section 6.2). Of course, it rests with the design engineer to decide whether this information justifies a semi-rigid frame design. However, the need to provide further $M_{con} - \phi$ data, without incurring the additional expense of testing, has led to the development of the so called *component method* (Elliott et al, 1994b). Here $M_{con} - \phi$ data are generated by superposition of individual (and combined) actions within the connection. The component method is accepted in semi-rigid steel connection analysis, and previous work by the authors (Elliott et al, 1994b) suggested that it might also be feasible in precast concrete connections.

The main objective of the experimental work of the component method has been to reproduce the moment-rotation characteristics of the connections found in full scale subframe tests, from smaller isolated joint components tests. This has been achieved by studying the influence of the strength and thickness t of in-situ infill concrete on stress-strain behaviour in compression and flexural specimens.

If the crack opening plus other linear displacements in the top of the slab or beam δ_T and the compressive deformation in the concrete at the bottom of the joint δ_B can be computed separately for given loading and expressed in terms of material and geometric properties, a simple method to determine ϕ is possible. In this method an "effective tensile stiffness" is found which relates bond and tensile deformation δ_T to the applied tension forces. Similarly, in the compression zone an "effective concrete modulus" E_{ce} is found by experimentation and the associated strains, and hence deformations δ_B are determined from the appropriate state of stress. They were obtained using the E_{ce} values calculated from the compression tests. It should be noted that this is an application of the component method to the subframe by using the effective modulus of the compression specimens, consisting of precast and in-situ infill concrete, and that it was experimentally found that it is always greater than the infill and less than the precast concretes modulus.

This present work takes the above a further step forward by determining the $M_{con} - \phi$ curves for double sided connections, subjected to equal hogging moments and shear forces, by three methods:

1. Direct measurement using vertical deflections from full scale testing (called 'Method 1 (M1)' defined in Section 6.1.2);
2. Direct measurement using horizontal deformation from full scale testing (called 'Method 2 (M2)' defined in Section 6.1.2);
3. Joint rotations computed from isolated test results based on the 'Component Method' defined in Section 1..4.3 for comparison with 2 above.

10.2 Calculation of moment-rotation in the component method

The elastic theory for reinforced concrete for two types of joint sections, the cracked section (Case 1) and the uncracked section (Case 2) was used to obtain moment-rotation $M_{con}-\phi$ behaviour of the connection from the component method for isolated joint tests. Case 1 is the classical elastic theory for reinforced concrete. It is used in crack-width calculations.

Figure 10.1(a) shows the cross-section of the joint at the column face, subjected to a incremental hogging bending moment M_{con}. The following simplifying assumptions are made (Kong & Evans, 1990):-

(a) Plane sections remain plane after bending. In other words, the strains vary linearly with distances from the neutral axis.

(b) Stresses in the steel and concrete are proportional to the strains.

(c) The concrete is cracked down to the neutral axis, and no tensile stress exist in the concrete above it.

When M_{con} is small enough for the maximum concrete tensile stress not to exceed the tensile strength of the concrete (before the joint starts cracking), an analysis based on an uncracked section becomes relevant. The effective concrete section is then the full section bh, as shown in Figure 10.1(b) and the equivalent section is as in Figure 10.1(c).

The neutral axis of the uncracked section passes through the centroid of the equivalent section, the neutral axis depth x_u is therefore given by:-

$$A_c\left(x_u-\frac{h}{2}\right)=\alpha_e A_s(d-x_u) \qquad Eq.10.1$$

where A_c is the entire concrete area bh and A_s is the area of the tension steel (2T25 stability tie bars) and α_e is the modular ratio E_s/E_{ce}, E_s is the modulus of elasticity of the steel taken as 200 kN/mm^2 and E_{ce} is the effective modulus of elasticity of the concrete as mentioned above. It is necessary to convert the steel to an "equivalent area of concrete by multiplying A_s by α_e. Referring to Figure 10.1(c), the second moment area of the uncracked equivalent section of the joint I_u may be determined using the parallel axis theorem as follows:-

$$I_u = \frac{bh^3}{12} + bh\left(x_u - \frac{h}{2}\right)^2 + \alpha_e A_s (d - x_u)^2 \qquad Eq.10.2$$

At any distance x_i from the neutral axis, the concrete stress f_{ci} and the steel stress f_{si} are given by:-

$$f_{ci} = \frac{M_{con}}{I_u} x_i; \qquad f_{si} = \alpha_e \frac{M_{con}}{I_u} x_i \qquad Eq.10.3$$

The section properties of the joints at the column face change as the joint cracks. Cracking begins in the region where tensile stresses are greatest, and as shown in Figure 6.2(a) and (b) for full scale frame connection test TW1(A), this will occur at the slab-column or beam-column boundaries where the bending moment is maximum.

After cracking the cross sectional properties of the section will change and it is first necessary to determine the depth to the neutral axis, x_{cr}, using first moments of area. Referring to Figure 10.1(d); taking moments about the bottom of the joint:-

$$(bx_{cr} + \alpha_e A_s)x_{cr} = \frac{bx_{cr}^2}{2} + \alpha_e A_s d \qquad Eq.10.4$$

hence x_{cr} may be obtained by solving the resulting quadratic equation.

The second moment of area of the flexurally cracked section I_{cr} is given by:-

$$I_{cr} = \frac{bx_{cr}^3}{3} + \alpha_e A_s (d - x_{cr})^2 \qquad Eq.10.5$$

The compressive bending stress was then found from the bending formula as:-

$$f_{ci} = \frac{M_{con}}{I_{cr}} x_{cr} \qquad Eq.10.6$$

For each value of moment M_{con} at the section, the concrete stress f_c on the compression face was calculated. It was assumed f_c in Figure 10.1(g) is just equal to the uniaxial compressive stress σ of the compression specimens (specimen C40/t=100 mm infill in test series 4 for welded plate and C40/t=110 mm grout in test series 5 for billet connection). Then, the compressive deformation δ_B in each relevent

compression specimen was calculated from the stress versus compressive deformation curve, for example in Figure 10.2, using the above stress values.

From the condition of equilibrium of forces (see Figure 10.1(g)), tensile force T in the bars was calculated as:-

$$T = \frac{M_{con}}{z} \qquad Eq.10.7$$

where z is lever arm, $z = d - x_{cr}/3$, and d is effective depth.

Crack width opening δ_T corresponding to the above T values was obtained from the tensile force in bars versus crack width opening at top of specimen in bond slip test in test series 7 as for example shown in Figure 10.3. Finally, $M_{con} - \phi$ data is derived from the component method, using the Method 2, as follows:-

1. Using the flexurally uncracked section properties Z_u of the joint (at the column face) and floor slab (neglecting the welded plate or billet connection), the compressive flexural stress σ in the joint is determined for a given bending moment M_{con}, i.e. $\sigma = M_{con}/Z_u$.

2. The compressive strain in the joint $\varepsilon = \sigma/E_{ce}$, where E_{ce} is given in Figures 9.9(b) and 9.10(b). Compressive deformation δ_B is determined over a gauge length of 180 mm.

3. The tie force in the top steel is equated to the total compression force in the beam. δ_T being determined directly from the aforementioned crack width test data.

4. Rotation $\phi = \frac{\delta_T + \delta_B}{h}$ *Eq.*10.8

5. Repeat steps 1 to 4 using the flexurally cracked section properties where the flexural tensile stress in the concrete exceeded the limiting value. This point coincided with the commencement of the first crack in the test series 7, i.e at $M_{con} = 30$ kNm.

10.3 Comparison of $M_{con} - \phi$ derived from full tests and the component method

Figure 10.4 shows a comparison of the results obtained from the above work with those obtained in the full scale subframe connection test, test TW1(A). Figure 10.4 shows the two methods are in excellent agreement for $M_{con} < 75$ kNm, and within 14 per cent of one another thereafter as far as the rotation of the connection is concerned. This shows that, within the normal scatter in experimental work of this type, either method may be used to generate $M_{con} - \phi$ data, and is the first step towards the validation of the component method.

The agreement with the full scale results varies between -12 and +14 per cent of the rotation. However, the maximum moment M_u achieved is only 160 kNm, i.e. two-thirds of the full scale double sided test TW1(A) result being greater than the ultimate moment achieved in single sided test TW2 (see Figure 10.5), and the maximum rotation is 4.5 mrad, (less than half of that achieved) in the full scale test. The post-cracking tangent stiffness J_c (in cycle 1) of the connection in the full scale

test varies from 29.7 to 35.7 kNm/mrad, whereas in the component method it is approximately 29.0 kNm/mrad.

The connection initial tangent flexural stiffness in the simplified test may be approximated from the data in Figure 10.4 as follows:-

$$J_u = 485.0 \text{ kNm/mrad}$$

This value was calculated at the first crack level (M_{cr} = 30 kNm) as shown in Figure 10.4. The initial connection stiffnesses in the full scale subframe test are presented in Table A6.1.1 for each cycle for test TW1(A) for Beam 1 side.

Figure 10.5 shows a comparison of the results of the component and the subframe tests with those obtained by Mahdi (1992) in a full scale 3-dimensional test which incorporated 300 x 300 mm beams and columns and a 200 mm deep hollow cored floor slab. In Mahdi's test 2T25 high tensile bars were positioned in the narrow gap between the ends of the slabs. The beam-column connections in the full scale test was subjected to a simultaneous bending moment and vertical shear force. The details of which are given in Chapter 2 Section 2.2.2. The stiffness of the sidesway connection (up to M_{con} = 75 kNm) carried out by Mahdi (1992) as shown in Figure 10.5, may be approximated as follows:-

$$J_c = 20.3 \text{ kNm/mrad.}$$

Neither the ultimate strengths (as far as double sided connections are concerned) nor the ultimate rotations in the full size connections could be reproduced in the simple tests due the sudden failure of the compression specimens and test series 7. It has been reported (Mahdi, 1992) and it was also observed in this study that this did not occur in the full scale test due to the under reinforced nature of the connection and the capability of the connection to redistribute moments in the frame. It should be

noted that the contribution to the strength of connection of the 100 x 100 mm section solid steel billet in the column which was welded to a steel bearing plate in the beam was not included in the simplified models. The contribution of the welded plate connection would provide additional horizontal tensile force at the level of the weld and this would bring the $M_{con} - \phi$ curve of the simplified component method into better agreement with full scale subframe experimental results.

The results of the above exercise for billet connection are shown in Figure 10.6. The agreement with the full scale results is very good up to M_{con} = 100 kNm. However, the maximum moment M_u = 160 kNm is 0.84 of the full scale double sided test TB1(A) result being much greater than the ultimate moment achieved in single sided test TB2 (see Figure 10.6), and the maximum rotation is 4.2 mrad, less than 1/3 of that achieved in the full scale test. The post-cracking tangent stiffness J_c (in cycle 1) of the connection in the full scale test varies from 48.0 kNm/mrad, whereas in the component method it is approximately 30.7 kNm/mrad.

The connection initial tangent flexural stiffness in the simplified test may be approximated from the data in Figure 10.6 as follows:-

$$J_u = 456.0 \text{ kNm/mrad}$$

The initial connection stiffnesses in the full scale subframe test are presented in Table A6.1.11 for each cycle for test TB1(A) for Beam 1 side.

10.4 Summing up

In making comparisons between the $M_{con} - \phi$ results obtained from the different methods there are a number of important features in the behaviour of the full scale test

worthy of further discussion. These points were/are discussed in the context of gaining confidence in using the component method, and to qualify some of the (inevitable) assumptions (in italics) made.

In generating the $M_{con} - \phi$ data using the component method it is assumed that the strains are transferred to the steel tie bars in the isolated joint test in the same manner as in the full scale tests, even though the presence of the hollow core slabs will have an influence on this.

In the isolated tests it is impossible for strains to exceed the uniaxial limit and therefore no redistribution of stress is possible in the component method.

In using the component method it is assumed that plane sections remain plane, and that full horizontal interface shear interaction between the beam and slabs is possible. It is not necessary to include for the effects of the welded joint between the steel billet and narrow plate as this point coincides with the neutral axis.

The comparisons between full scale tests and the component method for the symmetrical gravity loading case for hogging moment have been encouraging for both uncracked and cracked regions of the connection. No attempt has been made in this work to make comparisons with either sagging moments or sidesway situations, or to estimate failure moments.

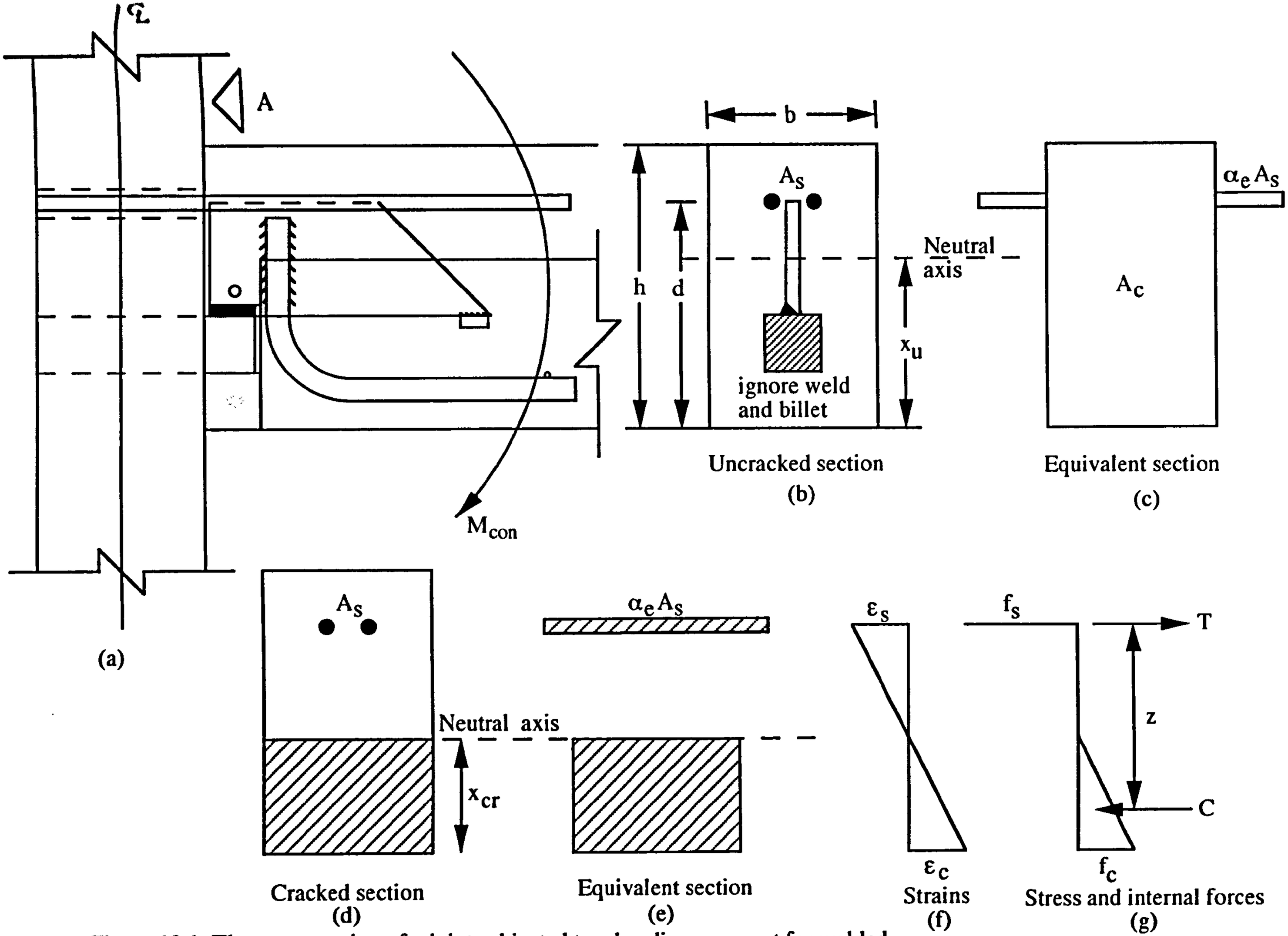

Figure 10.1: The cross-section of a joint subjected to a bending moment for welded plate and billet beam-to-column connection (two way connection)

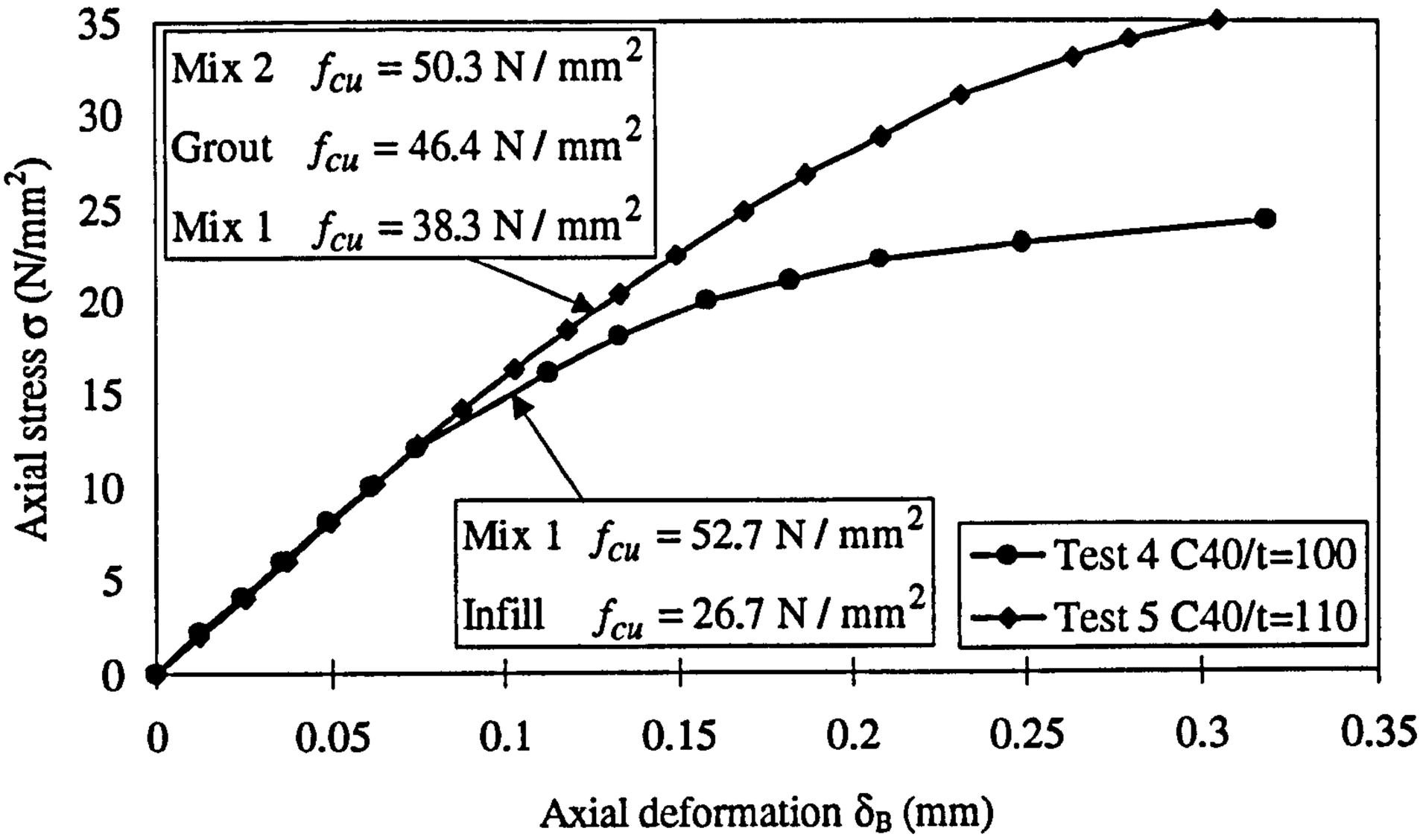

Figure 10.2: Axial stress deformation data for compressive specimens type A in test series 4 and 5 for C40/t=100 mm infill and C40/t=110 mm grout (Section 8.3)

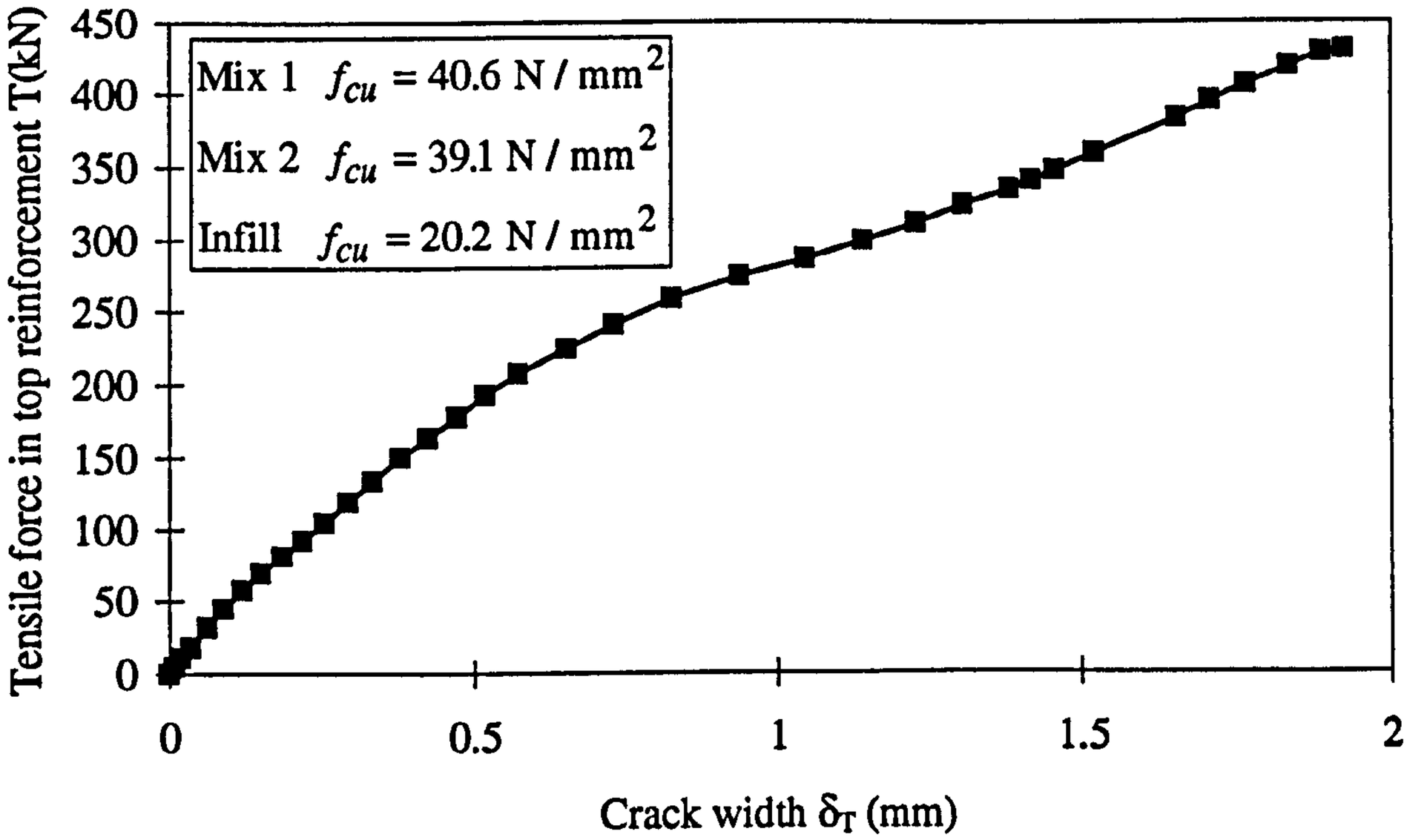

Figure 10.3: Tensile force in bars vs crack width opening at top of specimen in bond slip test in test series 7 (Section 8.4.2)

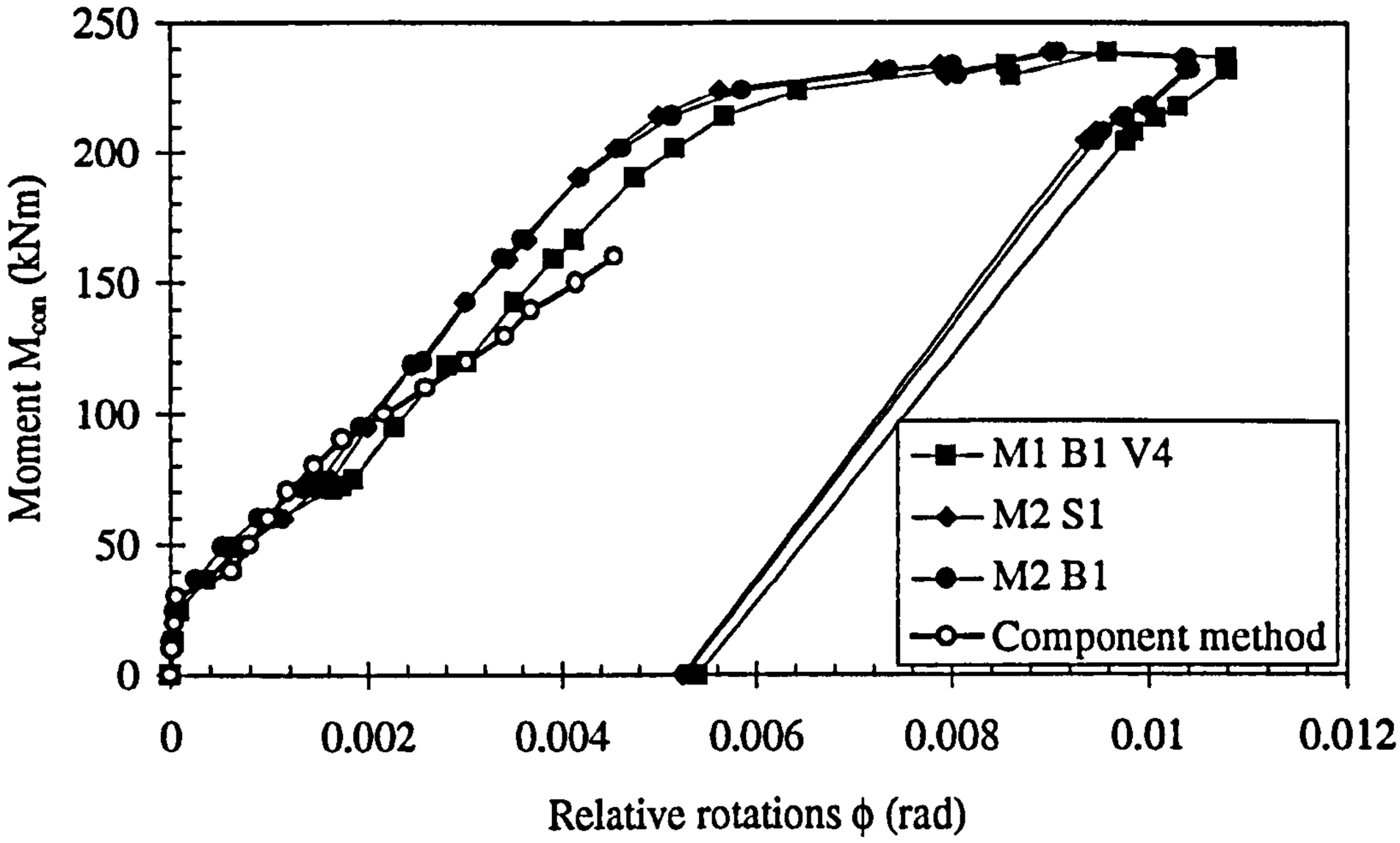

Figure 10.4: Moment-rotation data obtained using three different measurement methods for test TW1(A) compared with component method

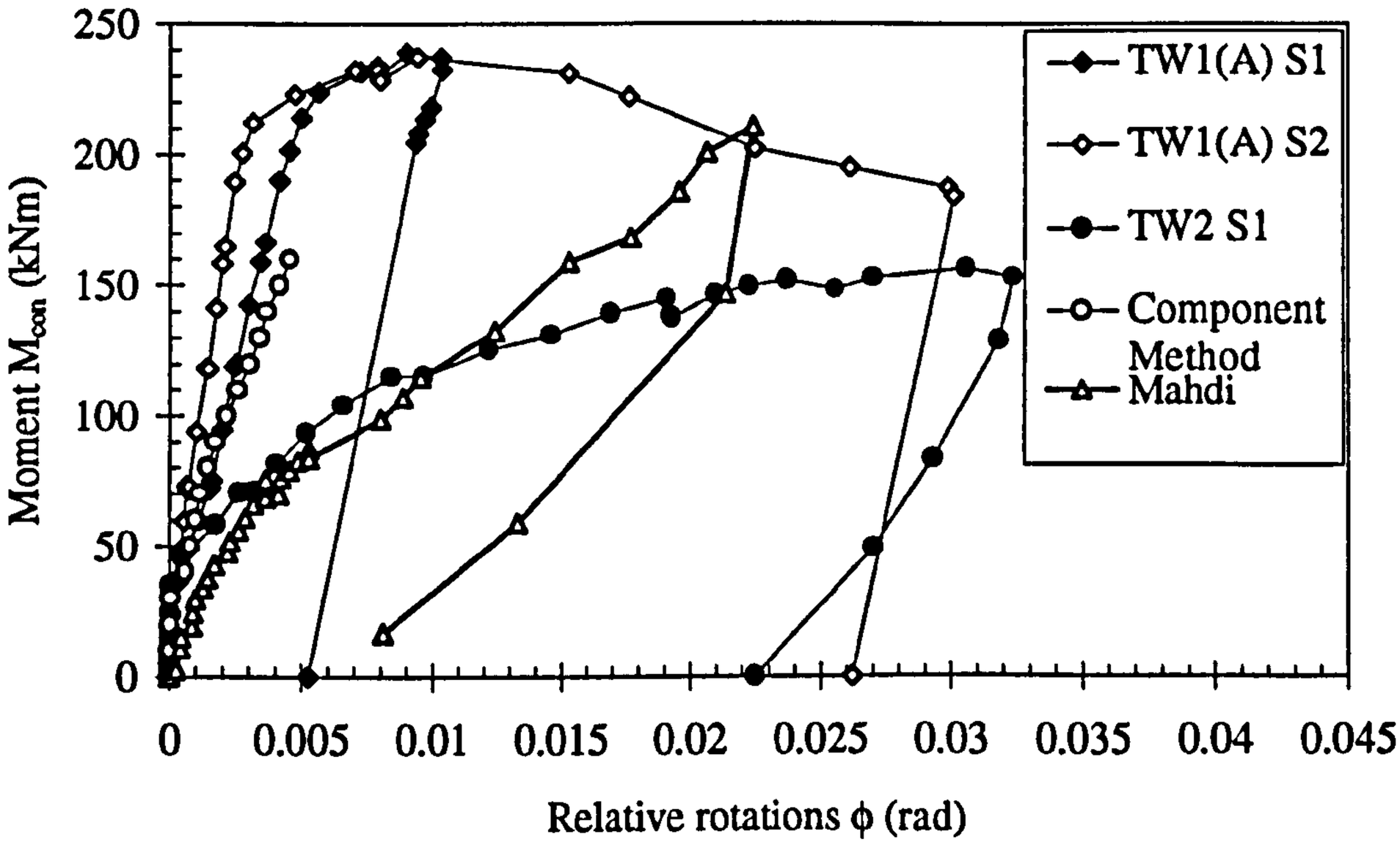

Figure 10.5: Comparision of moment-rotation data with Mahdi's work for welded plate connections

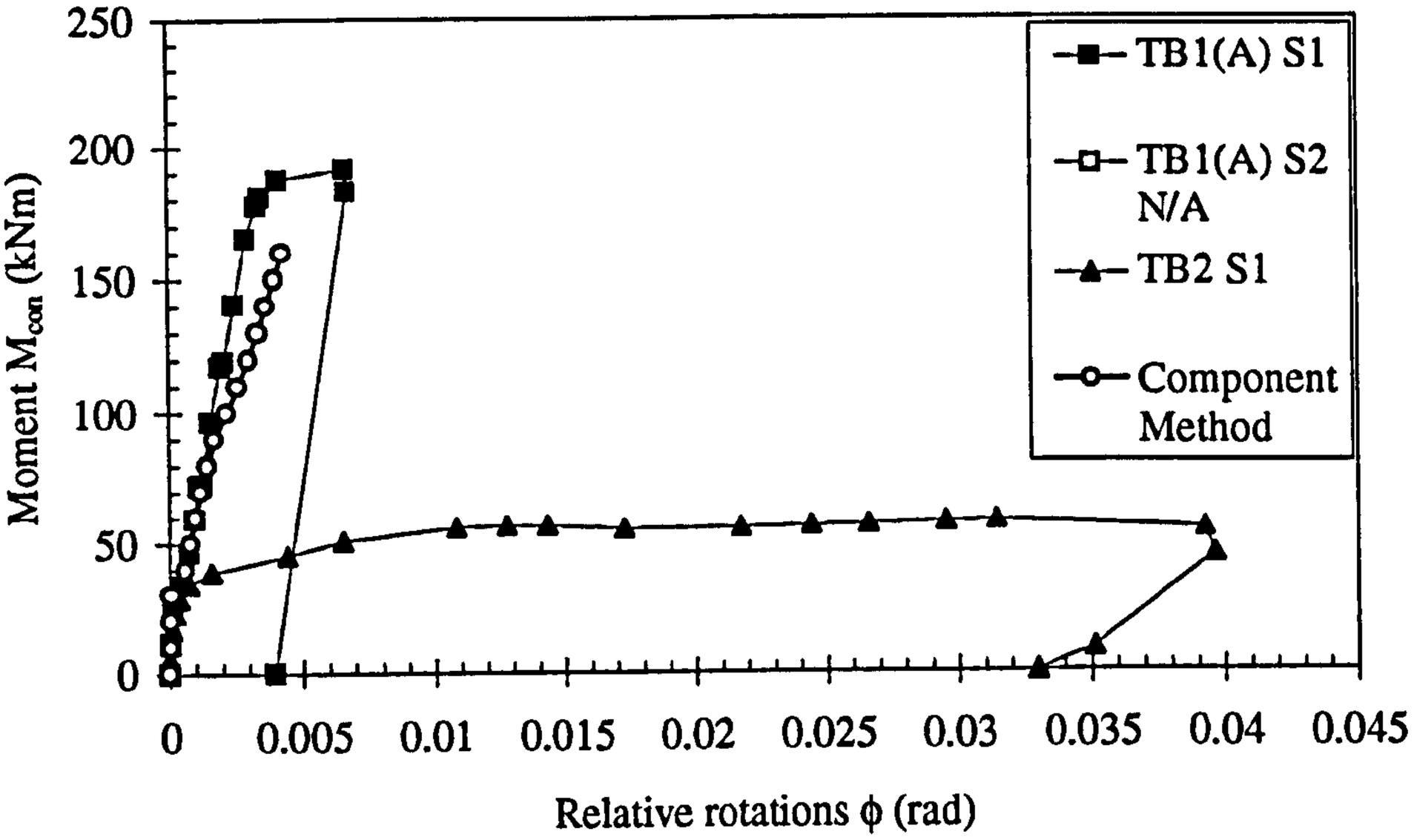

Figure 10.6: Comparision of moment-rotation data with component method for billet connections

CHAPTER 11

DESIGN CONSIDERATIONS

11.1 Introduction

Full scale testing of precast concrete beam-column connections has been carried out to generate practical semi-rigid moment-rotation ($M_{con} - \phi$) data. The tests included 200 mm deep precast hollow cored floor slabs and stability tie reinforcements as used in practice. The results show that connections at internal columns may be considered as full strength and semi-rigid, whereas edge connections should be better classified as pinned-jointed because of their limited strength. Designers may use these results as input data in a frame analysis by adopting the 'beam-line' approach to determine the stiffness and strength of the connection.

Column effective length factors β have been computed in a number of sway sub-frames in unbraced and partially braced precast concrete frames, by varying the frame stiffness ratio and the connection/beam stiffness ratio. Parametric equations have been presented which enable designers to determine β factors for situations currently not catered for in design codes.

11.2 Objectives

Precast concrete skeletal frames are designed as braced, unbraced or partially braced structures, in which the columns are continuous at the floor level. The majority of

connections are either single sided (at the edges of buildings) or double sided (at interior columns), and these have formed the basis of all the experimental tests carried out in this thesis. Precast connections also distinguish between those which include floor slabs (usually hollow cored units) and those which do not. In the former, the tie steel positioned over the top of the beams at the ends of the floor slabs form an integral part of the stability ties required by most Codes of Practice, and act as a vital component in the connection.

Present design methods consider all precast connections as pinned jointed such that continuity between beams at internal connections is not allowed, and column moments, due to sway loads etc., may not be distributed into beams. Although Mahdi (1992), Lindberg et al (1992) and Comair et al (1992) have established that the most commonly used connections do exhibit some degree of in-plane flexural semi-rigidity, it rests with the design engineer to decide whether this information justifies its use in a semi-rigid frame design. To achieve this aim, two sets of data are required.

(a) design equations for column effective length factors β presented in terms of frame AND connection stiffness, which enable column sway deflections and $P-\Delta$ moments to be determined.

(b) moment-rotation ($M_{con}-\phi$) data collected from experimental tests on actual precast concrete beam - column connections. These results provide the connection stiffness used in (a) defined by J_{es}, the lowest secant stiffness, in Figure 11.1(d).

Chapter 4 presented the results of a parametric study of β factors in unbraced and partially braced frames (item (a)), and Chapter 6 presented the $M_{con}-\phi$ data of full scale beam-column-slab sub-frames (item (b)). A method for a semi-rigid approach

to the design of a multi-storey precast frame is proposed and a worked example is presented in this Chapter.

Typical $M_{con} - \phi$ graphs are presented to define the beam-line and to determine various rotational secant stiffnesses, defined by J_s and J_e in Figure 11.1(c) for cycle 5, and J_{us} and J_{es} in Figure 11.1(d) for the corresponding results to failure, of the joints at the ultimate moment M_u, and moment M_e at intersection of the (dashed) beam-line with the $M_{con} - \phi$ curves. A summary of all the values for K_s are presented in Tables 11.1 to 11.7, and for the rotations and measured stiffnesses in Tables 11.8 and 11.9.

11.3 Beam-line concept and experimental tests to determine connection stiffness

For a simply supported beam acted on by a uniformly distributed load q and equal moments at its ends, a formula can be derived for the rotation of the ends of the beam (see Figure 1.7 in Chapter 1). This formula is a linear relationship between the moments and the rotation at the ends of the beam, and this relationship has been plotted in Figures 11.1 to 11.8 for a uniformly distributed load (but can be done in the same way for any type of loading). The beam - line intersects the vertical axis at a moment value equal to the end moment of a fully fixed beam, and the horizontal axis at a rotation value equal to the rotation at the end of a simply supported beam. The point of intersection between the beam - line and the actual moment - rotation characteristic gives the moment and rotation of the connection for a given loading.

When the actual moment - rotation characteristic of the connection is known, it is possible to investigate the moment and rotation of the connection for the various loading conditions on the beam. This has been done for the moment - rotation characteristics of relevant figures in Chapter 6, and is shown in Figures 11.1 to 11.8.

The beam - line is drawn corresponding to a loading and a certain beam span - to - height ratio l/h. The moment - rotation characteristic has to intersect the beam - line, otherwise there will be insufficient rotation capacity available for use in design.

The solid beam - lines in Figures 11.1 to 11.8 give the hogging bending moment of resistance of the composite (or beam only) section M_{beam} for the actual material properties measured in the tests, i.e. actual compressive cube strength of concrete and yield strength of rebar. The rotation capacity ϕ_{bo} is calculated for a typical span of $l = 6$ m (beam span - to - height ratio $l/h = 6000/500 = 12$ inclusive of floor slab, and 6000/300 = 20 without slabs) using the flexurally cracked second moment area of the composite section I_c and a Young's Modulus for the concrete $E_c = 32$ kN/mm^2. The solid beam - lines do not intersect (see detail in Figure 11.1(a)) some of the $M_{con} - \phi$ plots in Figures 11.2 to 11.8 or intersects at critical points (see detail in Figure 11.1(b)). The fact that the beam-line did not intersect is not a convincing argument for use of other more favourable beam lines. This can be avoided by choosing a lower load level or a shorter beam span. For this reason it was decided to use a beam-line (dashed) assuming the beam end moments equal to the moment capacities of the connections ($M_{beam} = M_u$, see Figures 11.1(c) and (d)) to ensure it intersects the $M_{con} - \phi$ plots before attained M_u to obtain reasonable characteristics (e.g. sufficient rotational capacity) of the connection for use in design.

It is desirable for the intersection point to be within the linear elastic part of the $M_{con} - \phi$ plot so that a linear elastic stability analysis may be used. This method has also been used by Zoetemeijer (1989).

When the beam - line approximation is adopted, the lowest secant stiffness J_{es} of the connection is used in calculating the Euler buckling load of the frame. According to Zoetemeijer (1989) this is a safe approximation to the connection behaviour in calculating the stability of the frame. The secant stiffness has also been recommended by Ioannides (1988) for the following reasons:

a) the factored loads will be applied in one step,

b) the secant stiffness provides an integrated average of how the connection arrived at the present level of loading,

c) regardless of the mode of loading and unloading at one time in the life of the structure the actual moment - rotation was followed to arrive at the present state of load.

d) if an initial stiffness is used the deflections derived will be erroneous

It is further proposed that factored loads be utilized in the analysis, otherwise due to the non - linear nature of moment - rotation curves an incorrect factor of safety may be assumed to exist. Using unfactored loads and allowable stress design leads to false factor of safety, underestimates total deflections, and thus underestimates the $P - \Delta$ effects.

11.4 Test series 1

11.4.1 Test TW1(A)

Beam-lines are drawn in Figures 11.2(a) and (b). Although the solid beam-line in Figure 11.2(a) does not intersect the $M_{con}-\phi$ plots for beam 1, it intersects the $M_{con}-\phi$ plots in Figure 11.2(b) at a moment value of 235 kNm, and at a rotation value of 12 mrad., which is greater than the ϕ_u due to the ductility of the connection.

However the intersections of the $M_{con}-\phi$ plots with the dashed beam-lines give the lowest M_e values as 195.60 kNm and 198.40 kNm respectively, for beams 1 and 2 (see Tables A11.1.1&2). Both values were obtained from the intersection of the $M_{con}-\phi$ plot of V4. The lowest secant flexural stiffnesses J_{es} at these moments were calculated as 39.5 kNm/mrad and 44.9 kNm/mrad, respectively. By comparison, the flexural stiffness of the composite section $\frac{4E_cI_c}{l}$ (for l =6 m) is 17.4 kNm/mrad, so that the corresponding values of K_s determined from the various measurements of stiffness defined in Figures 11.1(c) and (d) are given in Table 11.1. It was found that J_{es} is about $81\%\,J_e$, whilst $J_s = 41\%\,J_e$ and $J_{us} = 38\%\,J_e$. This indicates the reduction in the stiffness of the joints at the ultimate moment M_u. Due to the four reversed cycles prior to the fifth cycle, J_s and J_e are greater than J_{us} and J_{es}. Designers adopting the 'beam-line' approach may use J_{es}, the lowest secant stiffness, as input data in a frame analysis to determine strength of the connection. It is safer to use J_{es} as it would have been the secant stiffness value if the joints were loaded in one

cycle to failure. A check is required to ensure that the strength of the connection does not exceed the M_e.

11.4.2 Test TW1(C)

The intersections of the dashed beam-line with the $M_{con} - \phi$ plots in Figure 11.3 give M_e = 64.00 kNm and 62.50 kNm respectively, for beams 1 and 2 (see Table A11.1.3). Both values were obtained from the intersection of the $M_{con} - \phi$ plot of M2. The secant flexural stiffnesses J_{es} at these moments were calculated as 18.3 kNm/mrad and 15.6 kNm/mrad, respectively. The flexural stiffness of the beam section alone $\frac{4E_cI_c}{l}$ (for l =6 m) is 6.1 kNm/mrad. The corresponding values of K_s determined from the various measurements of stiffness are given in Table 11.2. J_{es} = 79% J_e, and J_s = 62% J_e and J_{us} = 54% J_e. In comparison with test TW1(A) the proportion of maximum value is approximately the same at M_e, these proportions are greater at M_u, because the failure was due to weld breaking failure in the joint, whereas ultimate failure was due to significant yielding of the bars and concrete crushing failure in the joints in test TW1(A). Ratios of K_s determined from J_e and J_{es} to corresponding K_s in test TW1(A) are 1.01 and 0.97, respectively, whilst these ratios increase to 1.39 and 1.32 for J_s and J_{us}. It is important not to confuse the ratio 0.97 of K_s determined from J_{es} to the corresponding K_s in test TW1(A) as input data in a frame analysis will approximately give the same strength for the connection. This is because the input data is not only limited to the K_s value, but also the properties of each member in the frame.

11.5 Test series 2

11.5.1 Test TW2

The beam-lines drawn for comparison with the experimental results for the beam and slab are presented in Figure 11.4. The solid beam - line does intersect the $M_{con}-\phi$ plots obtained using the Methods 1 and 2, it intersects the $M_{con}-\phi$ plots before attained M_u due to the ductility of the connection. The intersections of the $M_{con}-\phi$ plots with the dashed beam-line give the same lowest value of M_e as 91.75 kNm for beam 1 for V1, V2, V3 and V4 (see Table A11.1.4). The lowest secant flexural stiffnesses J_{es} at these moments were calculated as 12.2 kNm/mrad. By comparison, the flexural stiffness of the composite section $\frac{4E_cI_c}{l}$ (for l =6 m) is 17.2 kNm/mrad. The values of K_s are given in Table 11.3. $J_{es} = 68\% J_e$, and $J_s = 26\% J_e$ and $J_{us} = 23\% J_e$ being much less than to the corresponding values in test TW1(A). Ratios of K_s determined from J_e and J_{es} to corresponding K_s in test TW1(A) are 0.33 and 0.29, respectively, whilst these ratios decrease to 0.22 and 0.20 for J_s and J_{us} due to the flexibility of the column as mentioned in the discussion of this test.

11.6 Test series 3

11.6.1 Test TB1(A)

Similarly, in Figures 11.5(a) and (b) the intersections of the $M_{con}-\phi$ plots with the dashed beam-lines give the lowest M_e values as 162.20 kNm and 149.75 kNm

respectively, for beams 1 and 2 (see Table A11.1.5 & 6). The lowest secant flexural stiffnesses J_{es} at these moments were calculated as 48.42 kNm/mrad and 33.73 kNm/mrad, respectively. By comparison, the flexural stiffness of the composite section $\frac{4E_cI_c}{l}$ (for l =6 m) is 17.35 kNm/mrad. The values of K_s are given in Table 11.4. In this test $J_{es} > 75\% J_e$, whilst $J_s = 31\% J_e$ and $J_{us} = 29\% J_e$. This indicates the reduction in the stiffness of the joints at the M_u is a function of the greater ductility of the joints.

11.6.2 Test TB1(B)

In Figure 11.6 the intersections of the $M_{con} - \phi$ plots with the dashed beam-lines give the lowest M_e values as 148.5 kNm and 150 kNm respectively, for beams 1 and 2 (see Table A11.1.7). The lowest secant flexural stiffnesses J_{es} at these moments were calculated as 37.1 kNm/mrad and 38.96 kNm/mrad, respectively. By comparison, the flexural stiffness of the composite section $\frac{4E_cI_c}{l}$ (for l =6 m) is 17.5 kNm/mrad. The values of K_s are given in Table 11.5. In this test $J_{es} = 90\% J_e$, whilst $J_s = 68\% J_e$ and $J_{us} = 64\% J_e$ indicating that the M_u is not attained in this test compared to the corresponding values in the test TB1(A).

11.6.3 Test TB1(C)

In Figure 11.7 the intersections of the $M_{con} - \phi$ plots with the dashed beam-lines give the lowest M_e values as 142 kNm and 139.5 kNm respectively, for beams 1 and 2

(see Table A11.1.8). The lowest secant flexural stiffnesses J_{es} at these moments were calculated as 35.06 kNm/mrad and 32.07 kNm/mrad, respectively. By comparison, the flexural stiffness of the composite section $\frac{4E_cI_c}{l}$ (for l =6 m) is 17.4 kNm/mrad. The values of K_s are given in Table 11.6. Ratios of K_s to the corresponding K_s in the test TB1(B) varies from 0.89 to 0.96. These may be regarded as good correlation between the two tests.

11.7 Test series 4

11.7.1 Test TB2

The intersections of the $M_{con} - \phi$ plots with the dashed beam-line in Figure 11.8 give the lowest M_e values as 37.75 kNm for M1 B1 V4, and 40 kNm for M2 S1 and 42.0 kNm for M2 B1 (see Table A11.1.9). The lowest secant flexural stiffnesses J_{es} at these moments were calculated as 16.27, 19.23 and 22.95 kNm/mrad. By comparison, the flexural stiffness of the composite section $\frac{4E_cI_c}{l}$ (for l =6 m) is 17.4 kNm/mrad. The values of K_s are given in Table 11.7.

11.8 Significance to designers

Precast concrete frames are currently designed assuming that beam-column connections are pin jointed, and that column bending moments may not be distributed into the beams. This implies that deflection induced moments must be conservatively summed at the foundation over the **full height** of the structure. Secondly, columns in

unbraced frames must be considered as full height cantilevers where $\beta = 2.3$ (BS 8110, 1985). If the beam-column connection is shown to possess strength, stiffness and ductility, which the internal connections tested in this work clearly do, then columns may be designed for each storey height providing that the total moment in the beam-to-column connection is less than the moment capacity M_{beam} which corresponds the moment-rotational limit of the beam. The designer must therefore select the following:

(a) the type of connection, *welded plate* or *billet*,

(b) the column-beam geometry, i.e. internal or external,

(c) position in frame, i.e. ground floor, upper floor, and

(d) the appropriate $M-\phi$ curve for the connection, and *beam-lines* for all beams in the frame.

The intersection point of the beam-line with the joint experimental $M_{con}-\phi$ curve gives the secant stiffnesses defined by J_e and J_{es}, the connection design strength M_e and the necessary rotation capacities ϕ_e in Figures 11.1(a) and (b). Design values will of course incorporate a partial safety factor to the test results. The resulting connection/beam stiffness ratio is used in frame analysis programs to determine column load, M_{add} and sway deflections. Column β factors may be determined from equation 4.3(a) for example, which may then replace those in BS 8110, Part 2, clause 2.5.6, and EC2, Part 1, clause 4.3.5.3.5.

11.9 Design example

The section describes the analysis and design of a 4 bay x 2 bay x 3 storey precast concrete skeletal sway frame using both linear-elastic and non-linear analytical techniques taking into account the semi-rigid behaviour of the beam-to-column connections. The geometry and loadings were determined in consultation with members of the Precast Concrete Frames Association (Elliott et al, 1994a).

The work was divided into two parts:

I) frame analysis using linear-elastic semi-rigid connections with non-linear elastic components. This work was carried out at Nottingham University.

II) frame analysis using the computer program SWANSA which takes into account material and geometric non-linearities in the reinforced concrete components together with actual non-linear behaviour of the connections. This work was carried out at City University.

In part I a single load combination of dead, imposed and wind loading was used. Member moments and forces were found for pinned, semi-rigid and fully rigid joints with linear and non-linear elastic components. Then, using a linear-elastic analysis, column effective length factors β in the single-storey sub-frames were found. Finally, beams and columns were designed using member moments found in the previous steps and β factors for pinned and semi-rigid joints.

The variation of β with K_s and α has been examined and presented in Chapter 4 Section 4.1.2 both graphically and in the form of design equations similar to those currently used in BS 8110. For the semi-rigid connection a value of $K_s = 0.6$

was used. This was determined from the initial stiffness measured in previous full scale experimental testing on specimens of equal size (Mahdi, 1992) and specification to those used in the frame analysis. Variation in the column and beam moments with K_s is also given.

In Part II, the program *SWANSA* considers both material and geometric nonlinearities in the members. The connections were characterised by tri-linear moment-rotation data which closely approximated the measured experimental data mentioned above. Four different loading combinations were used. Beam and column members were designed from the direct output, which takes into account second-order deflection effects. The computer program is described in detail in Virdi and Ragupathy (1992a) (see Section 2.2.2).

11.10 Frame Design Exercise

10.10.1 Geometry and loading

The design exercise aimed at analysing a 3-storey x 4 bay x 2 bay unbraced structure shown in Figure 11.9. The frame consisted of continuous 300 x 300 mm columns, 300 x 300 mm beams spanning in the x-direction, 200 mm deep hollow core floor slabs and 150 mm deep hollow core roof slabs spanning at right angles to the beams. The columns and beams are reinforced as shown in Figure 11.10. The in-situ concrete infill placed over the top of the beams gives a composite floor beam section 500 mm deep. The compressive cube strength for the precast beam and the insitu infill was taken as 40 N/mm^2, and for the precast column as 50 N/mm^2. See Figure 11.11. (It was not

possible to separate the in-situ infill from the precast beam material in the analysis.) The foundations were considered encastre.

Referring to Figure 11.12, the structure may be considered in two planes:-

(i) in-plane, Figure 11.12(a), where the main flexural strength and stiffness derives from beam and column bending and shear, and beam-column connection in bending and shear.

(ii) out-of-plane, Figure 11.12(b), where the flexural behaviour derives from flexure and shear in the slab and the beam-slab connection, and the torsion in the beam-column connection.

Insufficient experimental data presently exist for case (ii) to be considered further.

The in-plane structure case (i) was analysed as a 2-d plane frame (ignoring the lateral stiffness of the slabs) along the centre of the building.

The floor and roof loading was as follows:-

	Superimposed	Dead	
		Self weight	Finishes*
Floor loads (kN/m^2)	4.00	3.00	3.00
Roof loads (kN/m^2)	1.50	2.30	0.70
Floor beam load (kN/m)**	30.00	47.00	
Roof beam load (kN/m)**	11.25	24.50	

* Partitions, floor or roof finishes, services and ceiling.

** Allow 2 kN/m self weight

Wind loads

Basic wind speed = 40 m/s Building height = 12 m

Class B structure, S1 = S3 = 1.0

S2 = 0.83 (ground roughness = 3)

Horizontal design wind pressure = 0.676 kN/m^2

Horizontal wind point loads at each floor level are

	kN
Roof level	8.11
Second floor	17.75
First floor	18.51

The loading case that produced maximum bending moments in the columns was combined dead, live and wind, with $\gamma_f = 1.20$.

11.10.2 Method of analysis

The frame was analysed using the computer program (Görgün, 1992) (See Chapter 3 Section 3.3) with the rotational and axial stiffness of the beams and columns calculated for the uncracked section. The rotational stiffness of the beam-column connections was specified as follows:-

(a) $K_s = 0$; to simulate a pinned-joint.

(b) $K_s = 0.6$; to simulate the semi-rigid joint stiffness found in previous full-scale experimental testing by Mahdi on components of equal dimensions as in this study. See Figure 1(a).

(c) $K_s = 1 \times 10^9$; to simulate a fully rigid joint, and to serve as a comparison for case (b).

The connection used is assumed to be of welded steel plate type. The moment rotation data used in the analysis is based on tests carried out at Nottingham University (Mahdi, 1992) as given in Table 11.10.

The point of action of the moment and shear force from the beam through the connection is assumed to be at a distance of 50 mm from the face of the column, as shown in Figure 11.13.

11.11 Part I results using linear connections

11.11.1 Pin-jointed connections

In this situation the horizontal loading is shared equally between the columns (because all $E_c I_u$ values are equal). The resulting bending moment diagram for each column and beam is shown in Figure 11.14. The beams, being simply supported, have a maximum bending moments of $wL^2 / 8$ at mid-span, and zero at the support.

i) Column design

Column bending moments due to sway deflection were assessed using two methods. Firstly, by a full computer analysis of the 2-dimension frame with elastic non-linear beam and column components. The computer program (Görgün, 1992) induces sway deflections and iterates towards the maximum column load, at which point the sway deflection increase is unlimited. The resulting bending moments, shown in Figure 11.14(a), are clearly due to the flexibility of a 3-storey pin-jointed frame. The size of

column required to cope with this behaviour is approximately 450 x 450 mm requiring 4 T32 bars.

In the second method, according to BS 8110, second order deflections are assessed for each floor level in turn, using effective length factors of 2.3. This is because $\alpha_c = 10$ for pinned connections (BS 8110, Part 2, clause 2.5). The resulting values for M_{add} are summed over the full height of the frame because no moment may be transferred into the beam through the pinned connection.

External column

Considering the external column ref. 1 (Figure 11.12(a)), the bending moment at the foundation is due to (a) frame action in resisting wind loads, M_w, (b) connection eccentricity, M_e and (c) sway deflections, M_{add}..

(a) The results from the frame analysis give $M_w = 70$ kNm (Figure 11.14(b)).

(b) Moments due to connection eccentricity derive from out of balance beam loads, acting at e = h / 2 + 50 mm as shown in Figure 11.13. The out of balance load at the first floor is due to the ultimate shear force, i.e.

V = 1.2 x 77 x 6.0 / 2 = 277.2 kN for 1st and 2nd floor

V = 1.2 x 35.75 x 6.0 / 2 = 128.7 kN for 3rd floor

e = (300 / 2) + 50 = 200 mm

$\therefore$ M = 55.5 kNm at first and second floor

$\therefore$ M = 25.8 kNm at roof

This moment is distributed in the column according to the flexibility of the column above and below each floor level. See Figure 11.15. The flexibility coefficient for the first floor to ground column is 0.49. Thus M = 0.49 x 55.5 = 27.3 kNm, and the moment at the foundation (using 50% carry over) is M_e = 50% x 27.3 = 13.7 kNm

(c) Sway deflection induced moments are calculated as follows (using BS 8110 notation) :-

$$L_e = 2.3L_o$$

$$a_u = (L_e/b)^2 Kh / 2000$$

$$M_{add} = Na_u$$

where N is the ultimate axial load at each floor level (given above, excluding column self weight), and are given in Table 11.11.

Thus $M_{design} = 322.7K + 83.7$ kNm

If $N = 687$ kN, then $\frac{N}{bh} = \frac{687x10^3}{300x300} = 7.63$

Using BS 8110, Part 3, Chart 47 gives $K = 1.0$

and $M = 406.4$ kNm, then $\frac{M}{bh^2} = 15.05$

$\therefore$ The column may NOT be designed using b = h = 300 mm

Redesigning the column using b = h = 350 mm gives

$$M_{design} = 276.4\ K + 15.4 + 70.0 = 276.4\ K + 85.4 \text{ kNm}$$

Now $\frac{N}{bh} = 5.7 \therefore\ K = 1.0$ $\frac{M}{bh^2} = 8.44$ for which $\frac{A_{sc}}{bh} = 5.5\ \%$

$\therefore$ Use 350 x 350 mm external column with 6 T40 bars

ii) Beam design

The beam moments obtained from the computer program are for spans between column centres, i.e. axis distances. In reality the beam is simply supported between pinned connections at e = 200 mm. Thus, the effective span of the beams = 6000 - (2 x 200) = 5600 mm.

$M_{beam} = 93 \times 5.6^2 / 8 = 364.6$ kNm for the floor beams.

The moment at the end of the beam is zero.

11.11.2 Semi-rigid connections

The 2-d frame was analysed using a beam to column connection having a stiffness of $K_s = 0.6$, but with a limiting strength of $M_{con} = +125$ kNm in the sagging mode

(bottom of connection in tension) and -210 kNm in the hogging mode. These values are the ultimate strengths obtained in the experimental test indicated in Figure 2.8 in Chapter 2.

As before with the pinned-jointed analysis, two methods were used to determine column bending moments. In the first case a full computer analysis (Görgün, 1992) using non-linear frame components gave bending moments which would include for the effects of deflection, i.e. contain M_{add} implicitly. The bending moments in the external columns (ref. 1 and 5) and internal columns (ref. 2, 3 and 4), and in the beams are shown in Figure 11.16.

One notices immediately the effects of moment distribution in the columns where a reduction in the foundation moment from 1080.4 kNm to 47.4 kNm has taken place. The maximum moment of -170 kNm at the floor beam connections is less than hogging connection moment M_{con} = -210 kNm (from Figure 2.8 and Table 11.10).

i) Column design using non-linear analysis

External column (Figure 11.12)

The moment at the foundation = M_w + M_e, where M_w = 47.4 kNm from frame action, and M_e = 13.7 kNm as before. Total = 61.1 kNm.

The moment at the 1st floor M_w = 71.7 kNm plus M_e = 28.5 kNm = 100.2 kNm

The moment at the 2nd floor is either M_w = 59.1 kNm plus M_e = 26.2 kNm = 85.3 kNm, or M_w = 72.3 kNm plus M_e = 29.6 kNm = 101.9 kNm

The column may be designed using b = h = 300 mm with 4 T 25 bars

ii) Beam design

The effect of the semi-rigid connection is to induce a hogging moment in the end of the beam, and to reduce the mid-span sagging moment as shown in Figure 11.16. Now that the connection is capable of carrying beam end moments, the beam moments are based on a 6 m effective span rather than a 5.6 m centre to centre span in the pinned condition. Whether there is a gradual transition in the effective span from 5.6 m to 6.0 m as the connection stiffness increases has not been ascertained at present.

The maximum bending moments are:-

M_{hog} = - 170.3 kNm < -210 kNm (Figure 2.8 and Table 11.10)

M_{sag} = + 283.2 kNm, i.e. a reduction of 81 kNm from the pinned condition

iii) Column design using linear-elastic analysis

In this case a linear-elastic analysis was carried out to determine β factors in the single-storey sub-frames shown in Figure 11.17. The following β factors were also determined from equations *Eq.* 4.1(*a*) and *Eq.* 4.2(*a*) for the upper and ground floor sub-frames using $K_s = 0.6$.

Floor Level	α	β from analysis	β from equations
3	0.405	1.44	1.49 (*Eq.* 4.1(*a*))
2	0.341	1.37	1.44 (*Eq.* 4.1(*a*))
1	0.328	1.18	1.29 (*Eq.* 4.2(*a*))

The design method uses second order elastic deflections assessed at each floor level using the β values (from analysis) given above. If the sum of $M_{add} + M_w + M_e <$ M_{con} the bending moments are assumed to be distributed into the beams and M_{add} is assessed **floor-by-floor,** and not summed over the **total height** of the structure as in the pinned-jointed situation. **This is the crux of this design exercise.** The frame moments for the columns and beams are shown in Figure 11.18. The connection eccentricity moments M_e are as before.

External column

The maximum bending moments are given in Table 11.12.

In all cases the design moment M_{design} is less than the smaller connection moment of resistance M_{con} = 125 kNm, and therefore may be distributed in the beams. The table shows that the column moment is maximum at the 1st floor level, where M = 117.9 kNm and N = 395 kN. At the 2nd floor level where M = 89.9 kNm and N = 126 kN.

The column may be designed using b = h = 300 mm with 4 T 25 bars

11.11.3 Fully rigid connections

The 2-d frame was analysed using rigid connections of stiffness $K_s = 1 \times 10^9$. The strength of the connection was equal to that of the column. Using non-linear frame (Görgün, 1992) components the bending moments in the columns and beams are shown in Figure 11.19. The major differences compared with the semi-rigid analysis occur (as expected) at the ends of the beams, where due to its increased stiffness the beam attracts a greater bending moment.

The frame analysis gives the design forces and moments directly. At the first floor level $N = 376$ kN and $M = 92.4$ kNm.

The column may be designed using b = h = 300 mm with 4 T 25 bars

The maximum beam moments are M_{hog} = -317.4 kNm, and M_{sag} = + 187.8 kNm.

11.12 Part II results using non-linear connections (SWANSA)

11.12.1 Summary of results

Starting with an assumed member geometry and reinforcement, the structure was analysed for the Ultimate Limit State conditions for all four of the above load combination cases. After redesign, the process resulted in the reinforcement shown in Figure 11.10. With this reinforcement, the structure was able to support all the above load combinations safely, with only a small spare capacity.

The results are presented as tabulated values of the axial loads, mid span and end bending moments, and shear forces, in Report to PCFA (Elliott et al, 1994a). The labels for beams and columns are identified in Figure 11.20. It should be noted that the

column moments are taken as beam end moments plus a correction for the eccentricity of the beam and shear force. The maximum beam and connection moment at the FACE of the column is = Beam End Moment + End Shear x 50 mm. A summary of the results for serviceability cases is shown in Table 11.13.

i) Column design using SWANSA output

External column ref C1 - C3, and C13 - C15.

The maximum moment at the foundation = 81 kNm (Bottom of column C13 for Load Case 3) and N = 681 kN. The moment at the 1st floor M_w = 101 kNm (Top of column C1 for Load Case 2) and N = 683 kN. The worst condition at the 2nd floor is M = 84 kNm (Bottom of column C15) and N = 98 kN.

The column may be designed using b = h = 300 mm with 4 T 25 bars

ii) Beam design

The maximum bending moments are found :-

$$M_{hog} = -(140 + 345 \times 0.050) = -157.3 \text{ kNm}$$

$$M_{sag} = +389 \text{ kNm.}$$

11.13 Joint behaviour

As an indication of the joint rotations obtained at the Ultimate Limit State, the values are given in Table 11.14. It will be noted that the maximum relative rotation in the

frame is 0.014.2 mradian, and that this value is well within the failure rotation obtained in tests for this type of joint.

11.14 Discussion

11.14.1 Effect of connection stiffness on column and beam frame moments

These are shown in Figures 11.21 to 11.23 for the beam end and mid-span moments, and the column foundation moments, respectively. Again, the largest changes take place over the range $0 < K_s < 1.5$. The large differences in the moments in columns ref. 1 and 5 are due to the non-symmetrical wind loading combined with the beam loads. A reversal in the moment in the edge column 1 takes place (coincidentally) when $K_s = 0.6$, and shows that the column is in single curvature with the foundation effectively "pinned". The first - second floor column is in double curvature and therefore an effective length factor of about 1.5 could be imagined for this column.

Large changes in moments at the first floor also take place when $K_s < 1$, for example the beam end moment has increased by 2/3 of the total increase at this point. The hogging moment capacity of the connection (-210 kNm) would have been exceeded when $K_s > 2$. Therefore, for this particular frame geometry and loading, using a connector stiffness K_s greater than 2 would require greater connection strength in order for the connection to behave semi-rigidly at the ultimate limit state.

The large end hogging moments can easily be resisted by the compression in the bottom of the beam and the tension in the stability tie steel placed along the top of the beam in the in-situ infill at the ends of the slabs. In many cases no extra reinforcement will need to be provided. The only danger here is in the use of

prestressed beams where the combined stresses due to pretension and frame moments need to be checked.

11.14.2 Comparison of column bending moments for the semi-rigid analysis

Position in edge column	Linear elastic members with BS8110 M_{add}	(Görgün, 1992) Non linear members with linear connection	SWANSA Non linear members and connections
Roof	81	81	82
2nd - Roof	90	85	71
2nd - 1st floor	101	102	84
1st - 2nd floor	118	100	77
1st - Foundation	86	87	86
Foundation	82	61	81

Thus, using the SWANSA results as the basis for comparison, the linear elastic solution with addition M_{add} moments appears to over predict moments at the bottom ends of the columns at the 2nd and 1st floors. The non-linear member analysis is in reasonable agreement with SWANSA except at the foundation where the former under estimates the moment by 20 kNm.

11.15 Conclusions

This exercise set out to design a 3 storey precast concrete frame consisting of 300 x 300 mm beams and columns supporting 200 mm deep hollow cored floor slabs. The

main objective of the exercise was to show that when the connections between the beams and columns are considered as semi-rigid joints, then:-

1. it is possible for the columns to be designed 300 mm square;
2. the negative steel at the end of the beam is catered for by the stability tie steel in the in-situ concrete infill;
3. the mid-span reinforcement in the beam is reduced.

For the semi-rigid connection a value of $K_s = 0.6$ was used. This was determined from the results of some previous full scale experimental testing on specimens of equal size and specification to those used in the frame analysis. Variation in the column and beam moments with K_s has also been given.

The main conclusion is that it is **not** possible to design this frame for 300 mm x 300 mm columns using pin-jointed connections ($K_s = 0$). The required size of column to cope with second-order bending moments of more than 1000 kNm at the foundation is at least 450 mm square.

When the connection is considered semi-rigid ($K_s = 0.6$) the column foundation moment reduces to 61 kNm, and the moment at the first floor to 100 kNm. In both cases it is possible to design the column 300 mm square using 4 T25 bars. Fully rigid connections have a minimal effect in changing the semi-rigid values, reducing the maximum column moment to 92 kNm.

Reductions in beam moments at mid span for the pinned and semi-rigid conditions were in the order of 80 kNm, whilst the negative moment at the end of the beam increased from zero to -170 kNm, respectively.

Thus a semi-rigid design is a practical and economical approach.

Method of measurement		K_s determined from stiffness:			
		J_e	J_{es}	J_s	J_{us}
M1 B V4	Beam 1	2.83	2.27	1.59	1.43
	Beam 2	3.13	2.57	1.33	1.24
	Mean	2.98	2.42	1.46	1.34
	Proportion of maximum value	100 %	81 %	49 %	45 %
M2 S	Slab 1	3.08	2.56	1.66	1.52
	Slab 2	4.70	3.88	1.53	1.44
	Mean	3.89	3.22	1.60	1.48
	Proportion of maximum value	100 %	83 %	41 %	38 %
M2 B	Beam 1	3.06	2.52	1.65	1.51
	Beam 2	3.90	3.23	1.46	1.37
	Mean	3.48	2.88	1.56	1.44
	Proportion of maximum value	100 %	83 %	45 %	41 %

Table 11.1: The values of K_s determined from the various measurements of stiffness in test TW1(A)

Method of measurement		K_s determined from stiffness:			
		J_e	J_{es}	J_s	J_{us}
M2 B	Beam 1	3.75	3.00	2.29	2.00
	Beam 2	3.29	2.55	2.05	1.80
	Mean	3.52	2.78	2.17	1.90
	Proportion of maximum value	100 %	79 %	62 %	54 %
	Ratio of K_s to corresponding K_s in TW1(A)	1.01	0.97	1.39	1.32

Table 11.2: The values of K_s determined from the various measurements of stiffness in test TW1(C)

Method of measurement		K_s determined from stiffness:			
		J_e	J_{es}	J_s	J_{us}
M1 B V4	Mean=Beam 1	1.05	0.71	0.27	0.24
	Proportion of maximum value	100 %	68 %	26 %	23 %
	Ratio of K_s to corresponding K_s in TW1(A)	0.35	0.29	0.18	0.18
M2 S	Mean=Slab 1	1.30	0.94	0.35	0.30
	Proportion of maximum value	100 %	72 %	27 %	23 %
	Ratio of K_s to corresponding K_s in TW1(A)	0.33	0.29	0.22	0.20

Table 11.3: The values of K_s determined from the various measurements of stiffness in test TW2

Method of measurement		K_s determined from stiffness:			
		J_e	J_{es}	J_s	J_{us}
M1 B V4	Beam 1 Beam 2	- 2.41	- 1.94	- 0.75	- 0.70
	Mean=Beam 2	2.41	1.94	0.75	0.70
	Proportion of maximum value	100 %	80 %	31 %	29 %
M2 S	Slab 1 Slab 2	4.29 -	3.28 -	1.86 -	1.67 -
	Mean=Slab 1	4.29	3.28	1.86	1.67
	Proportion of maximum value	100 %	76 %	43 %	39 %
M2 B	Beam 1 Beam 2	3.67 -	2.78 -	1.58 -	1.44 -
	Mean=Beam 1	3.67	2.78	1.58	1.44
	Proportion of maximum value	100 %	76 %	43 %	39 %

Table 11.4: The values of K_s determined from the various measurements of stiffness in test TB1(A)

Method of measurement		K_s determined from stiffness:			
		J_e	J_{es}	J_s	J_{us}
M2 S	Slab 1 Slab 2	3.58 3.80	3.31 3.31	3.49 3.85	3.28 3.41
	Mean	3.69	3.31	3.67	3.35
	Proportion of maximum value	100 %	90 %	99 %	91 %
M2 B	Beam 1 Beam 2	2.43 2.46	2.12 2.23	1.87 1.47	1.72 1.39
	Mean	2.45	2.18	1.67	1.56
	Proportion of maximum value	100 %	89 %	68 %	64 %

Table 11.5: The values of K_s determined from the various measurements of stiffness in test TB1(B)

Method of measurement		K_s determined from stiffness:			
		J_e	J_{es}	J_s	J_{us}
M2 S	Slab 1 Slab 2	3.60 3.73	3.01 3.28	3.45 3.63	2.97 3.24
	Mean	3.67	3.15	3.54	3.11
	Proportion of maximum value	100 %	86 %	96 %	85 %
	Ratio of K_s to corresponding K_s in TB1(B)	0.99	0.95	0.96	0.93
M2 B	Beam 1 Beam 2	2.33 2.08	2.02 1.84	1.76 1.45	1.61 1.35
	Mean	2.21	1.93	1.61	1.48
	Proportion of maximum value	100 %	87 %	73 %	67 %
	Ratio of K_s to corresponding K_s in TB1(B)	0.90	0.89	0.96	0.95

Table 11.6: The values of K_s determined from the various measurements of stiffness in test TB1(C)

Method of measurement		K_s determined from stiffness:			
		J_e	J_{es}	J_s	J_{us}
M1 B V4	Mean=Beam 1	N/A	0.94	0.22	0.08
	Ratio of K_s to corresponding K_s in TB1(A)	N/A	0.48	0.29	0.11
M2 S	Mean=Slab 1	N/A	1.11	0.23	0.08
	Ratio of K_s to corresponding K_s in TB1(A)	N/A	0.34	0.12	0.05
M2 B	Mean=Beam 1	N/A	1.32	0.60	0.16
	Ratio of K_s to corresponding K_s in TB1(A)	N/A	0.47	0.38	0.11

Table 11.7: The values of K_s determined from the various measurements of stiffness in test TB2

Test Ref.	ϕ_{cr}			ϕ_u			ϕ_f			ϕ_{end}		
	M1 B V4	M2 S	M2 B	M1 B V4	M2 S	M2 B	M1 B V4	M2 S	M2 B	M1 B V4	M2 S	M2 B
TW1(A)	0.086	0.070	0.054	9.58	9.00	9.09	10.80	10.38	10.43	5.40	5.24	5.27
	0.043	0.067	0.055	10.99	9.43	9.94	24.21	30.05	30.55	18.89	26.24	26.25
TW1(B)	N/A	N/A	N/A	N/A	N/A	N/A	N/A	N/A	N/A	N/A	N/A	N/A
TW1(C)	0.045	N/A	0.29	0.72	N/A	6.06	1.46	N/A	12.84	3.95	N/A	53.26
	0.07	N/A	0.54	0.75	N/A	6.97	0.75	N/A	6.93	0.49	N/A	4.05
TW2	0.86	0.042	*	38.59	30.55	*	40.85	32.36	*	25.80	22.51	*
TB1(A)	-	0.122	0.115	-	6.59	7.66	-	6.68	7.75	-	3.91	4.52
	0.12	0.073	0.063	15.36	-	-	15.51	-	-	10.55	-	-
TB1(B)	-	0.27	0.32	-	3.05	5.81	-	3.19	6.18	-	0.86	2.50
	-	0.20	0.21	-	2.87	7.03	-	2.87	9.43	-	2.13	28.38
TB1(C)	-	0.26	0.24	-	3.37	6.21	-	3.37	11.39	-	N/A	N/A
	-	0.16	0.14	-	3.08	7.41	-	3.08	7.41	-	N/A	N/A
TB2	1.02	0.40	0.19	33.11	31.45	18.78	40.44	39.67	19.52	32.90	32.96	16.73

Table 11.8: Summary of the relative rotations ϕ_{cr}, ϕ_u, ϕ_f and ϕ_{end} values in mrad. * M2 B not available for test TW2

Test Ref.	J_e			J_{es}			J_s			J_{us}		
	M1 B V4	M2 S	M2 B	M1 B V4	M2 S	M2 B	M1 B V4	M2 S	M2 B	M1 B V4	M2 S	M2 B
TW1(A)	49300	53700	53400	39500	44600	44000	27700	29000	28800	24900	26500	26300
	54600	81900	68000	44900	67700	56300	23200	26700	25400	21600	25100	23800
TW1(B)	N/A	N/A	N/A	N/A	N/A	N/A	N/A	N/A	N/A	N/A	N/A	N/A
TW1(C)	-	N/A	22900	-	N/A	18300	115500	N/A	13990	103400	N/A	12300
	-	N/A	20100	-	N/A	15600	119000	N/A	12500	101300	N/A	11000
TW2	18100	22300	*	12200	16200	*	4700	6000	*	4100	5100	*
TB1(A)	-	74710	63900	-	57040	48420	-	32400	27440	-	29020	24970
	41970	-	-	33730	-	-	12990	-	-	12250	-	-
TB1(B)	-	62620	42470	-	58000	37125	-	61080	32770	-	57370	30100
	-	66470	43110	-	58000	38960	-	67360	25680	-	59720	24400
TB1(C)	-	62710	40510	-	52410	35060	-	60050	30660	-	51600	27980
	-	64930	36210	-	57040	32070	-	63080	25160	-	56380	23470
TB2	-	-	-	16270	19230	22950	3780	4040	10490	1370	1400	2830

Table 11.9: Summary of the flexural stiffnesses J_e, J_{es}, J_s and J_{us} values in kNm/rad. * M2 B not available for test TW2

Rotation (Rad)	Moment (kNm)
-0.0220	-140.0
-0.0150	-130.0
-0.0001	-20.0
0.0000	0.0
0.0020	50.0
0.0220	210.0
0.0230	220.0

Table 11.10: Moment rotation data for the joint (Mahdi, 1992)

Floor Level	L_o	L_e	$\frac{L_e}{b}$	a_u	M_{add}	M_w	M_e
2 - 3	10.95	25.18	83.95	$1.057K$	$136.3K$	-	-
1 - 2	7.75	17.83	59.42	$0.530K$	$147.8K$	-	-
G - 1	3.95	9.09	30.28	$0.138K$	$38.5K$	-	-
Total	-	-	-	-	$322.7K$	70.0	13.7

Table 11.11: Calculation of design moments at foundations for $K_s = 0$

Floor Level	L_o	L_e	$\frac{L_e}{b}$	a_u	M_{add}	M_w	M_e	M_{design}
3 - 2				0	0	55.3	25.8	81.1
2 - 3	3.20	4.61	15.36	$0.035K$	$4.38K$	59.3	26.2	89.9
2 - 1				0	0	71.4	29.6	101.0
1 - 2	3.80	5.23	17.43	$0.046K$	$18.17K$	71.2	28.5	117.9
1 - G				0	0	58.8	27.3	86.1
G - 1	3.95	4.66	15.54	$0.036K$	$23.78K$	44.9	13.7	82.4

Table 11.12: Calculation of design moments at each floor level $K_s = 0.6$

Item	Load Case 1 mm	Load Case 2 mm	Load Case 3 mm	Load Case 4 mm
Maximum Beam Deflection	17.0	17.5	16.9	9.5
Roof Level Sway	-2.7	-2.2	20.3	17.0
Second Floor Level Sway	-2.7	-2.1	17.1	14.2
First Floor Level Sway	-2.7	-2.1	9.5	7.6

Table 11.13: Deflection of beams and storey level sway (SWANSA)

Beam Number	Left Joint	Right Joint
B1	10.30	14.2
B2	9.95	13.09
B3	3.50	7.33
B4	12.57	12.22
B5	30.09	12.22
B6	7.16	7.16
B7	12.22	0.72
B8	12.22	12.57
B9	4.54	4.36
B10	14.2	10.30
B11	13.09	9.95
B12	7.33	3.50

Table 11.14: Rotation in the joint (mrads) (SWANSA)

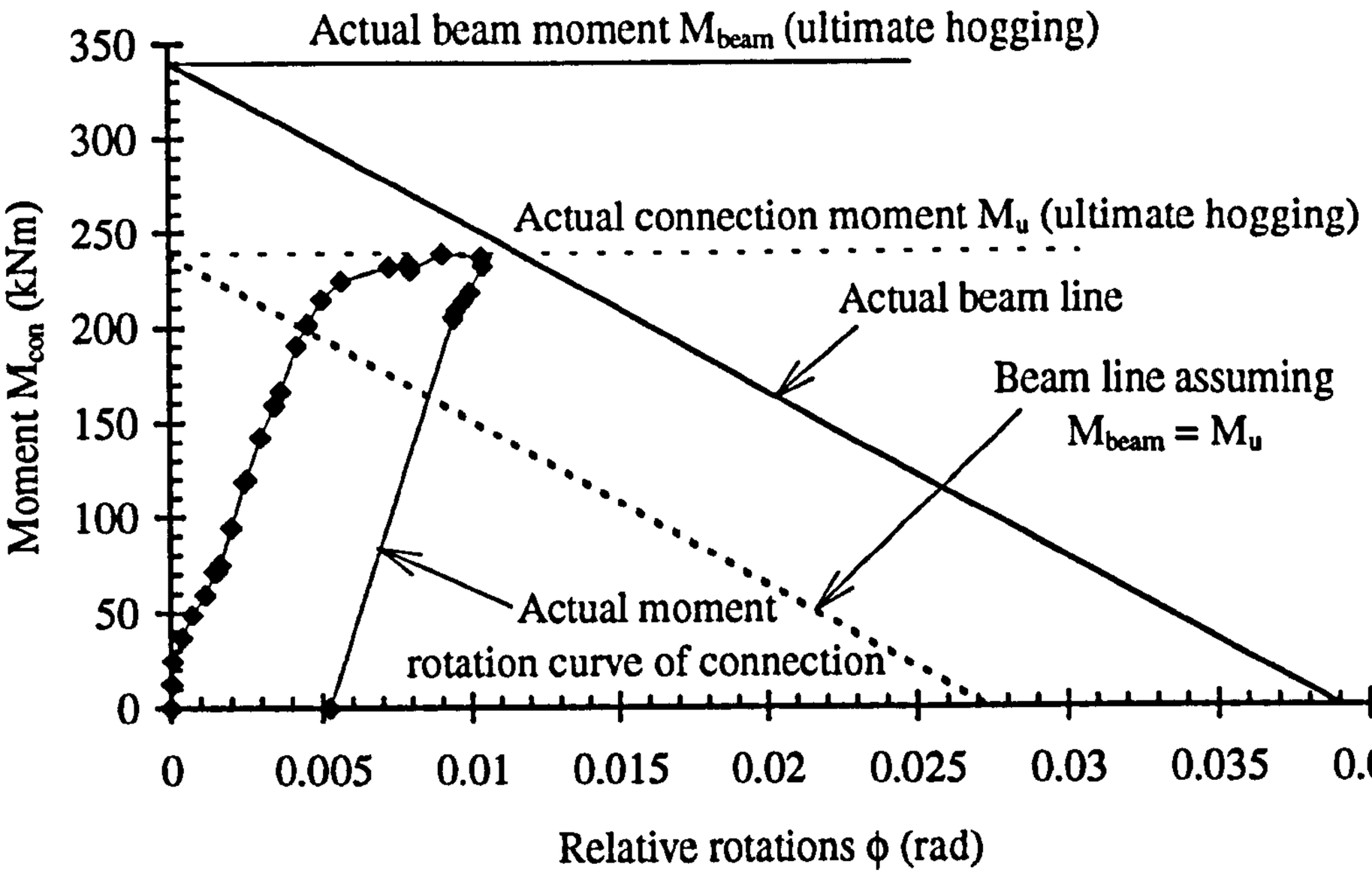

Figure 11.1(a): Actual moment versus relative rotation curve with beam-lines

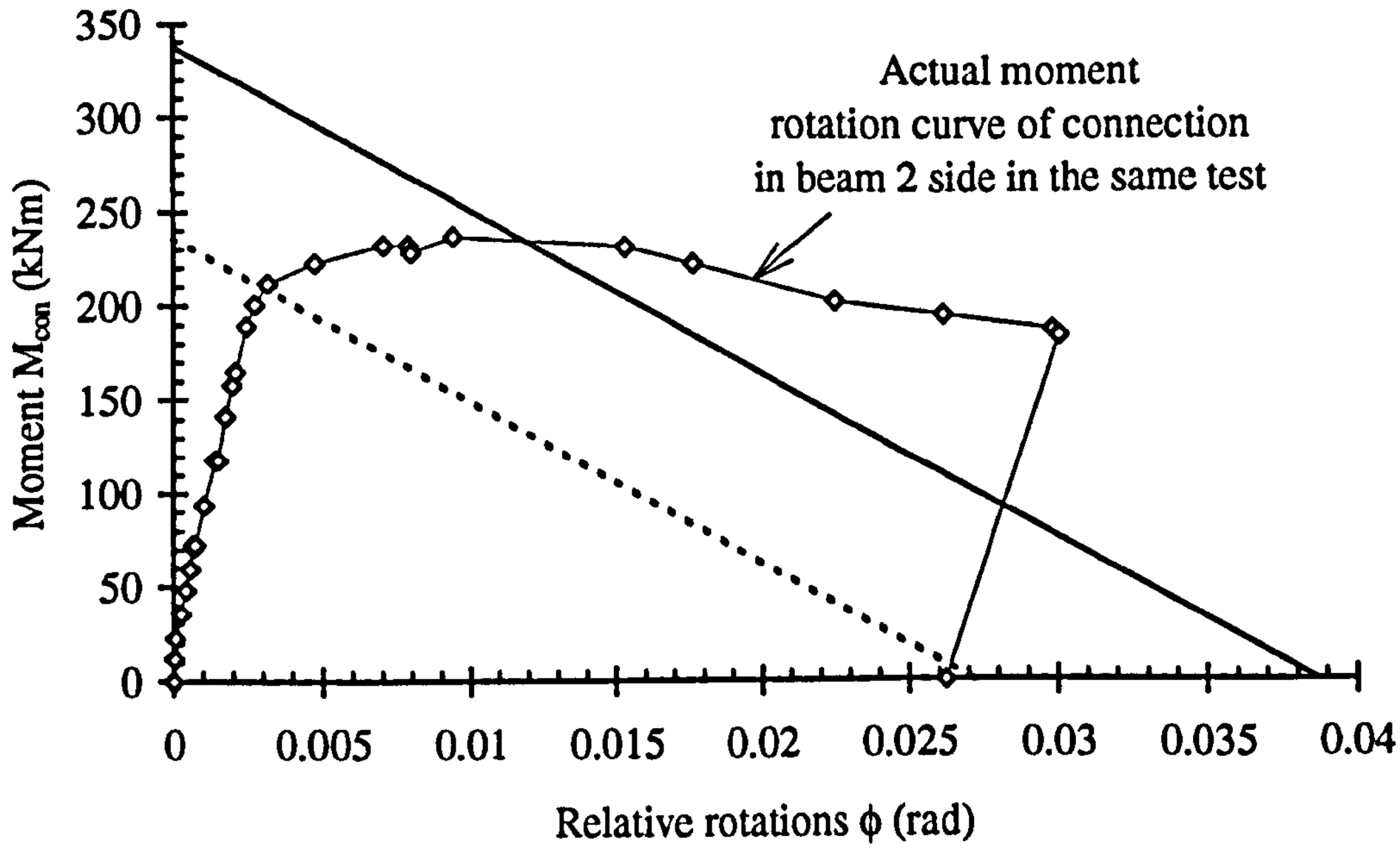

Figure 11.1(b): Actual moment versus relative rotation curve with beam-lines

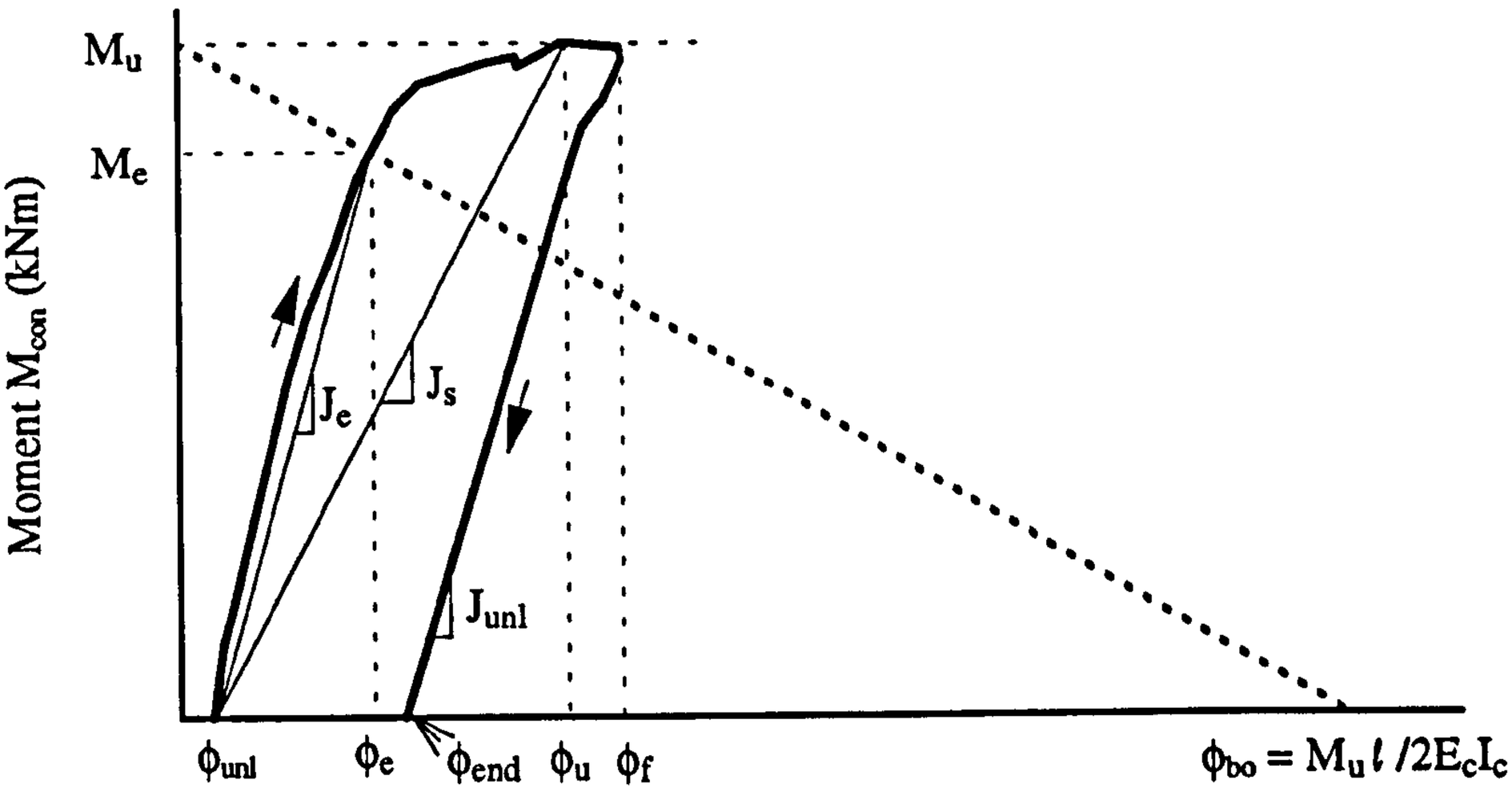

Figure 11.1(c): Actual moment versus relative rotation curve at which flexural stiffnesses were defined for cycle 5

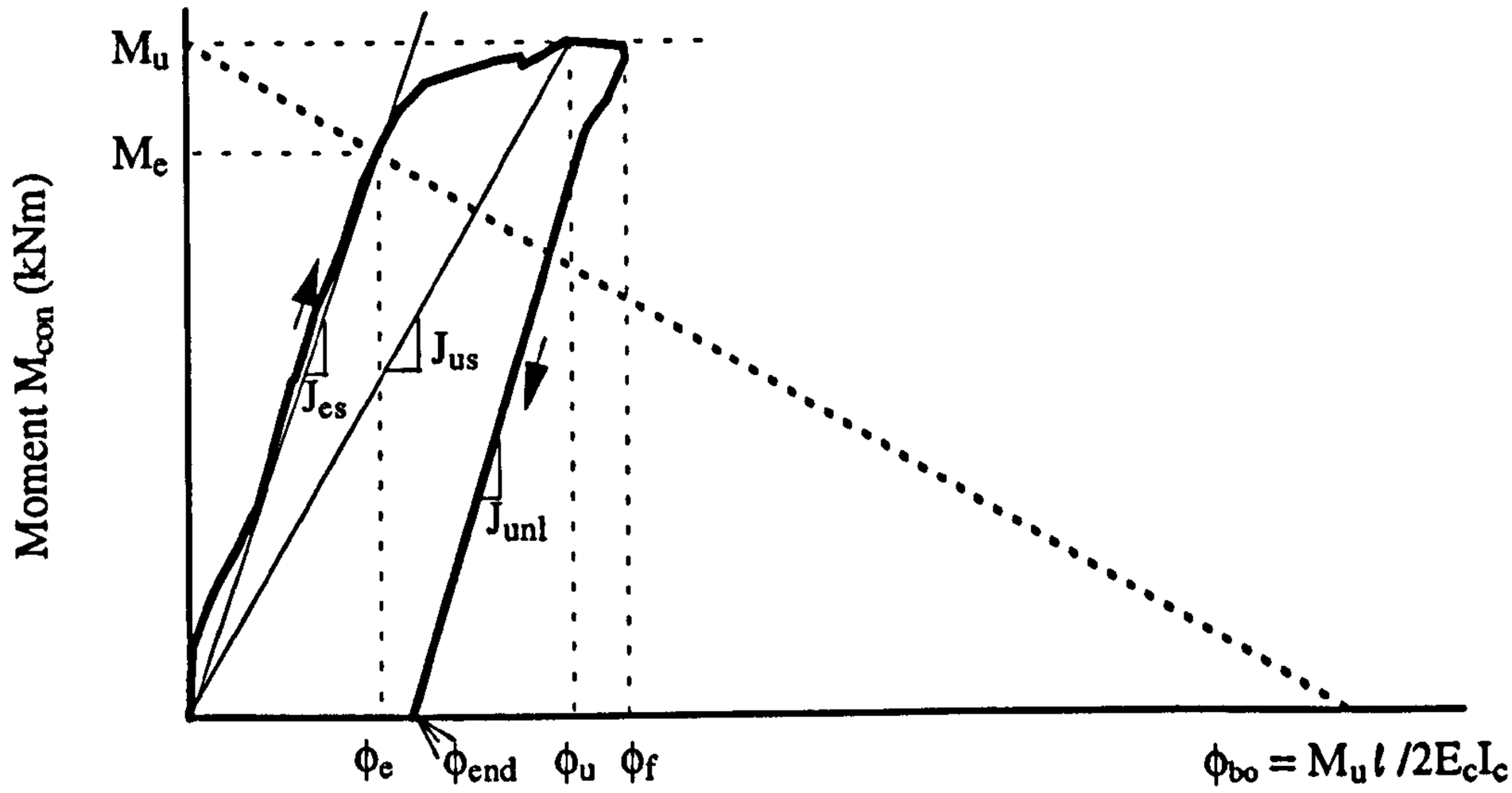

Figure 11.1(d): Actual moment versus relative rotation curve at which flexural stiffnesses were defined for full cycle

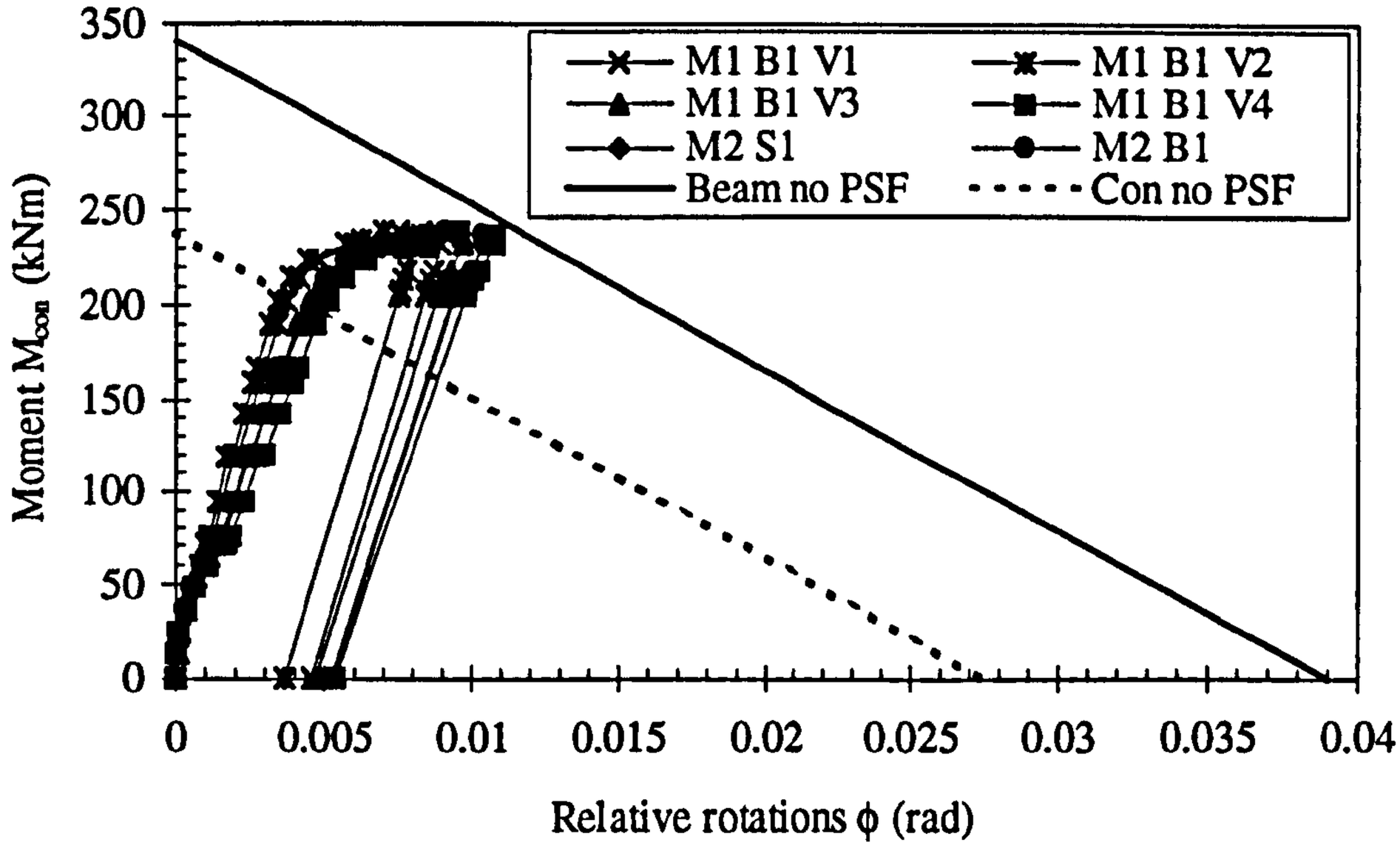

Figure 11.2(a): Moment versus relative rotations in beam 1 and slab 1 in TW1(A) using Methods 1 and 2 with beam lines

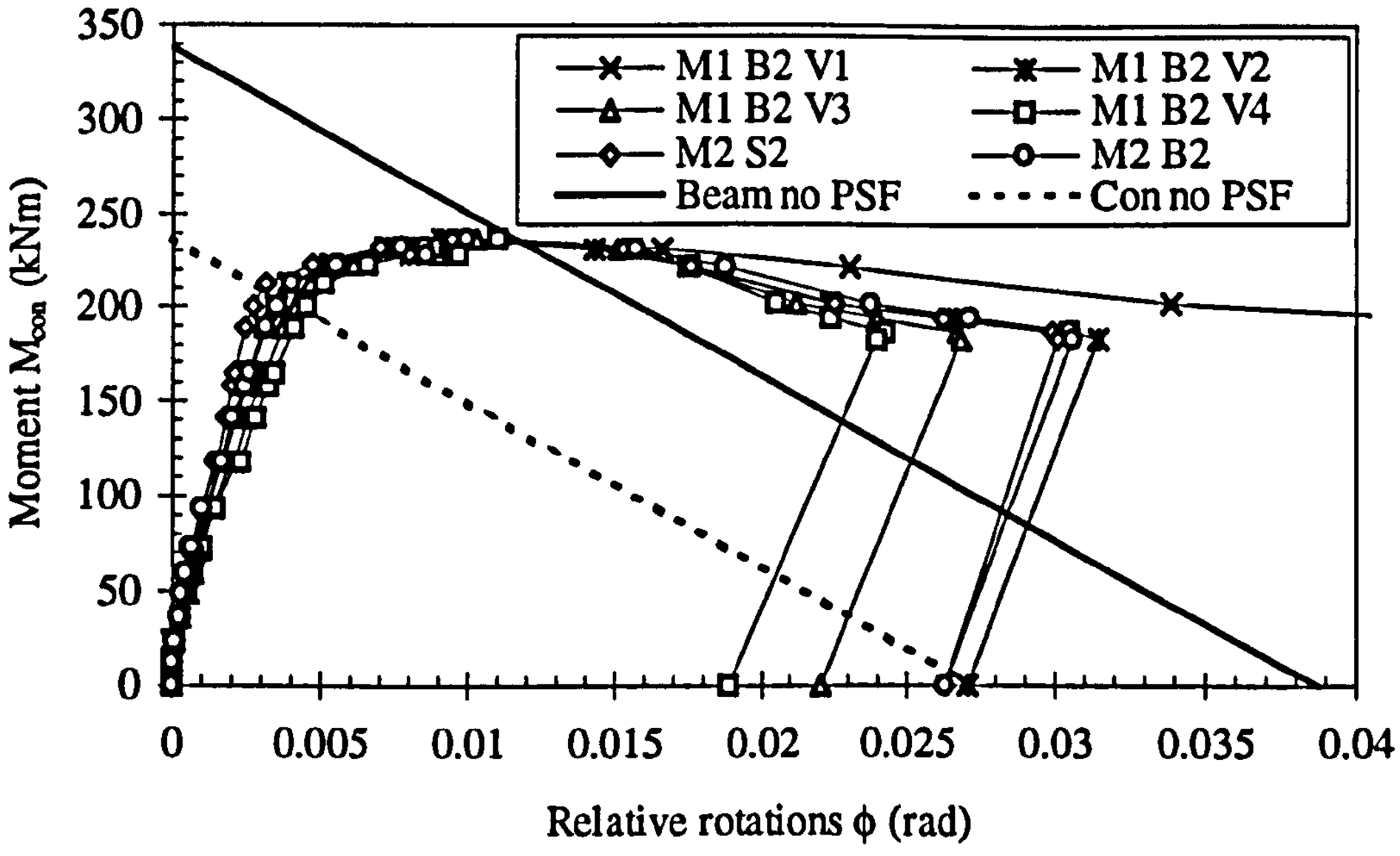

Figure 11.2(b): Moment versus relative rotations in beam 2 and slab 2 in TW1(A) using Methods 1 and 2 with beam lines

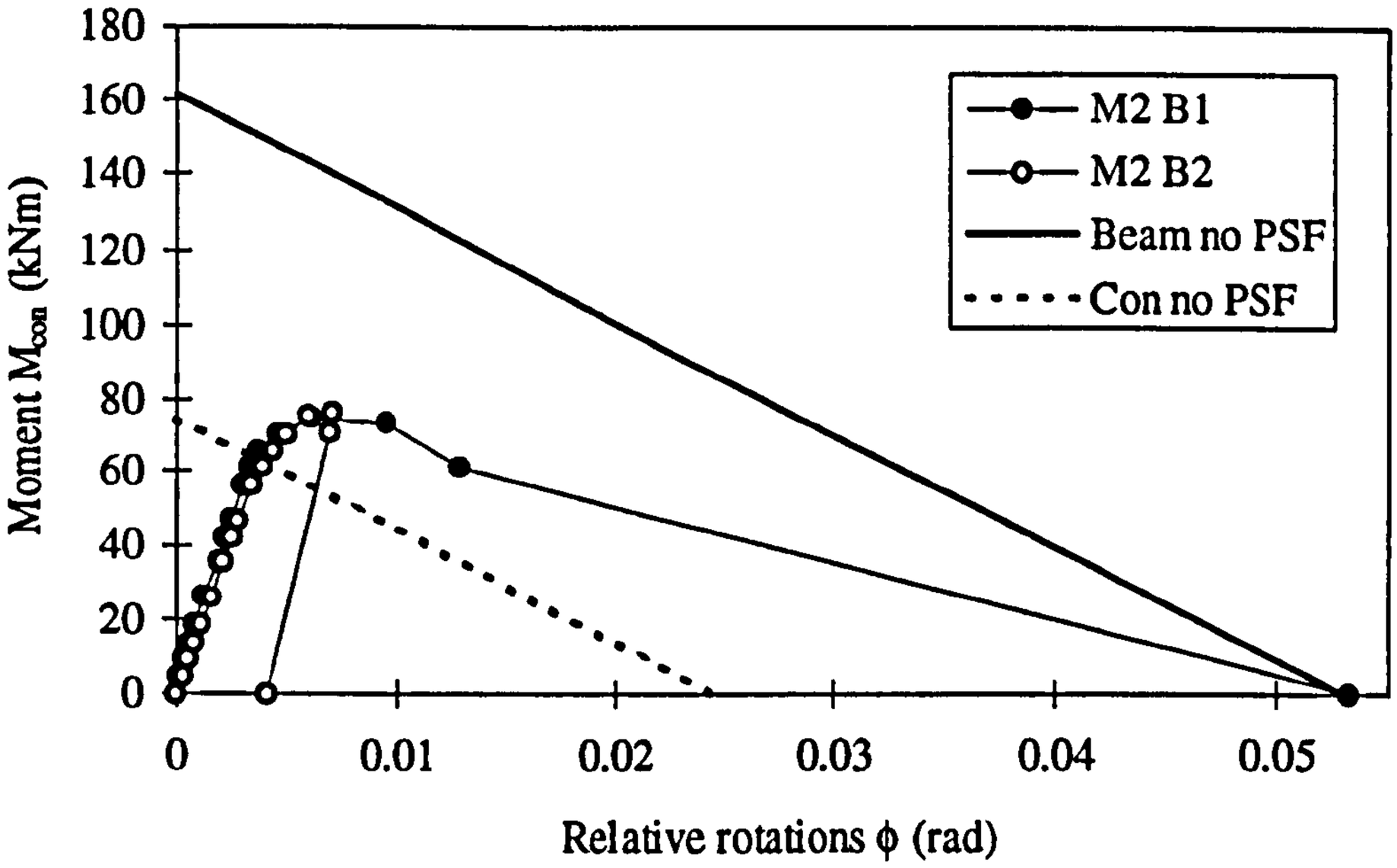

Figure 11.3: Moment versus relative rotations for both beams 1 and 2 in TW1(C) using Method 2 with beam lines (no slabs, and Method 1 is not applicable)

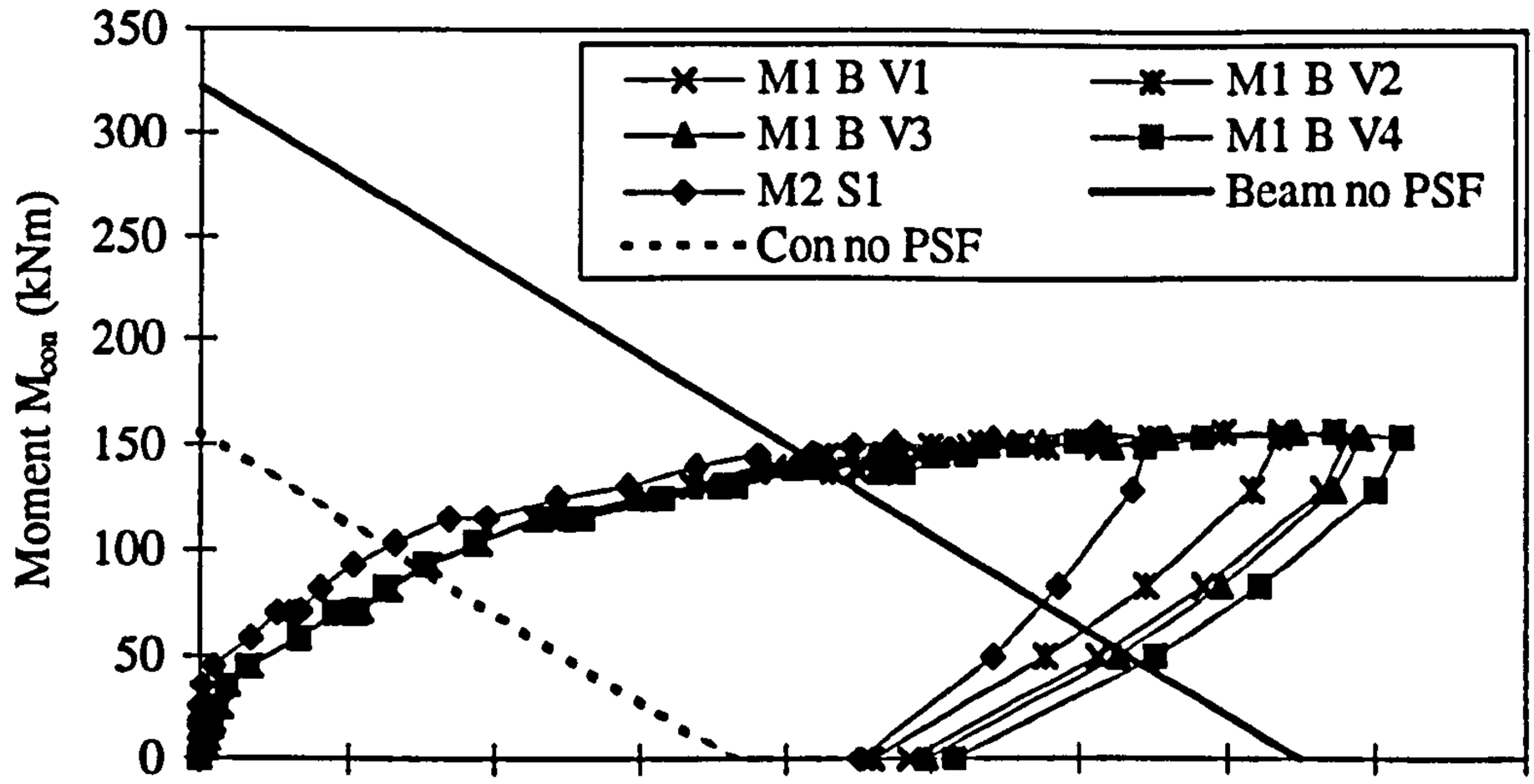

Figure 11.4: Moment versus relative rotations in beam 1 and slab 1 in TW2 using Methods 1 and 2 with beam lines (no slab 2 and beam 2, single sided test)

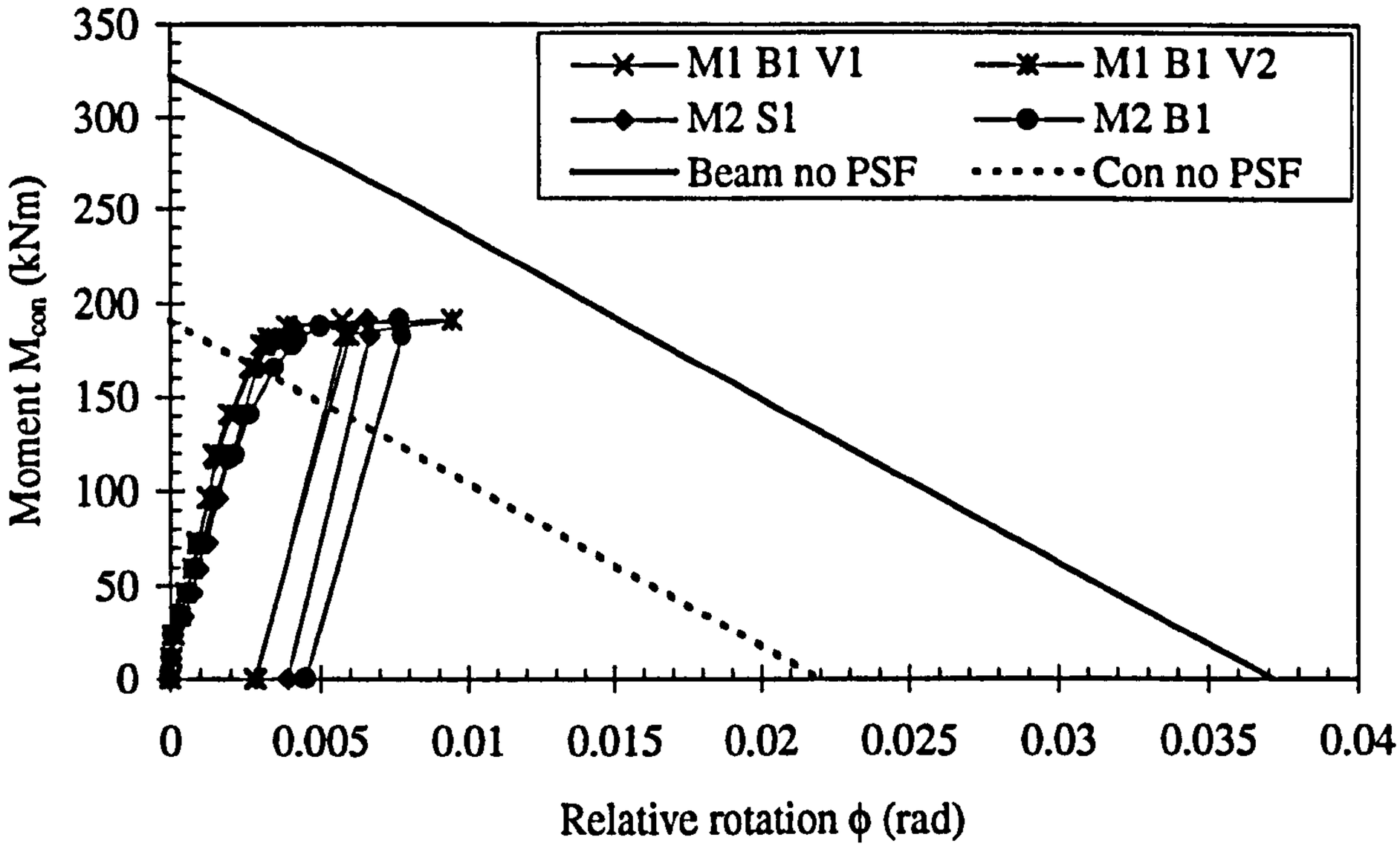

Figure 11.5(a): Moment versus relative rotations in beam 1 and slab 1 in TB1(A) using Methods 1 and 2 with beam lines (no V3 and V4 due to a fault in POT18)

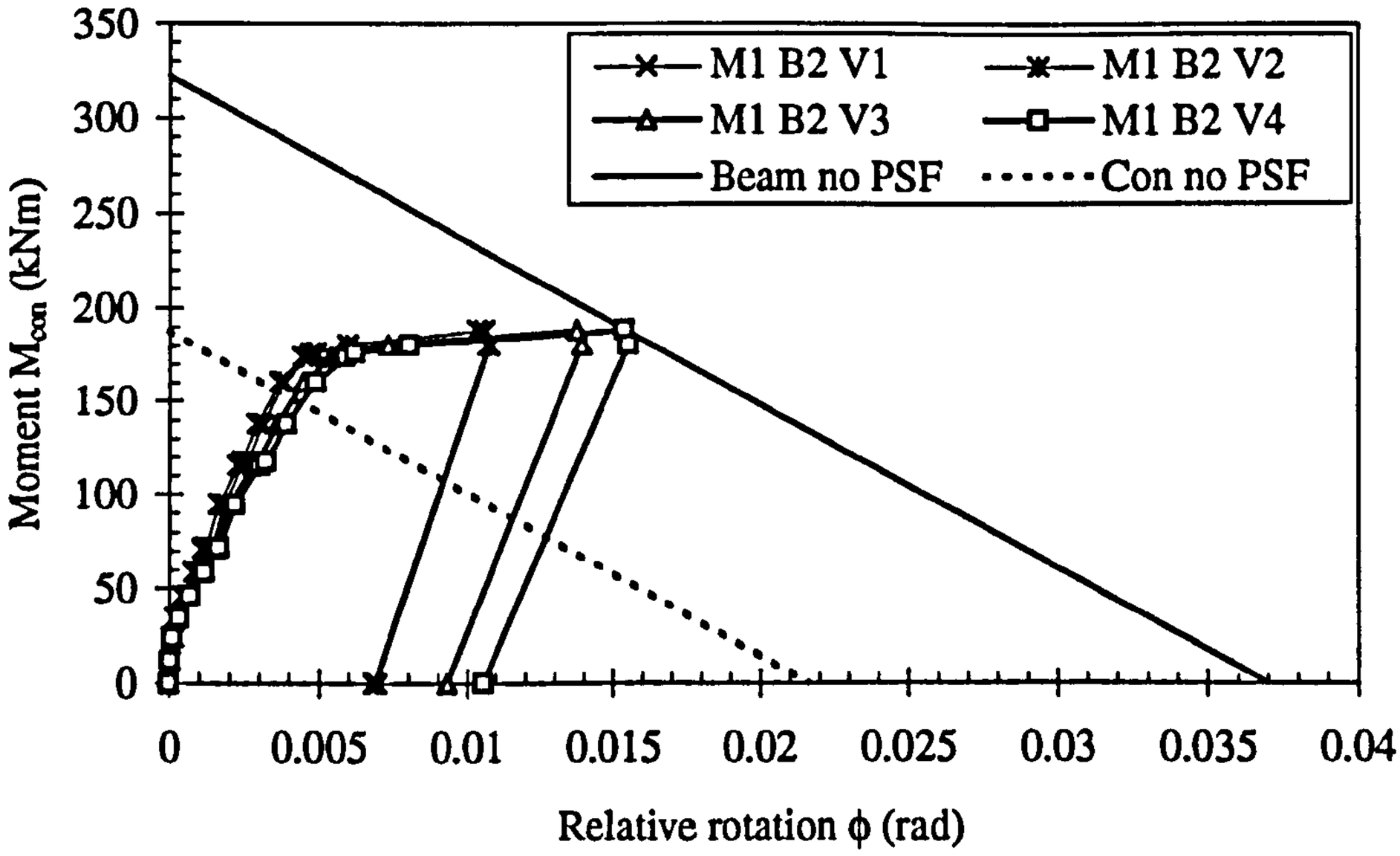

Figure 11.5(b): Moment versus relative rotations in beam 2 in TB1(A) using Methods 1 and 2 with beam lines (no slab 2 due to a fault in POT9)

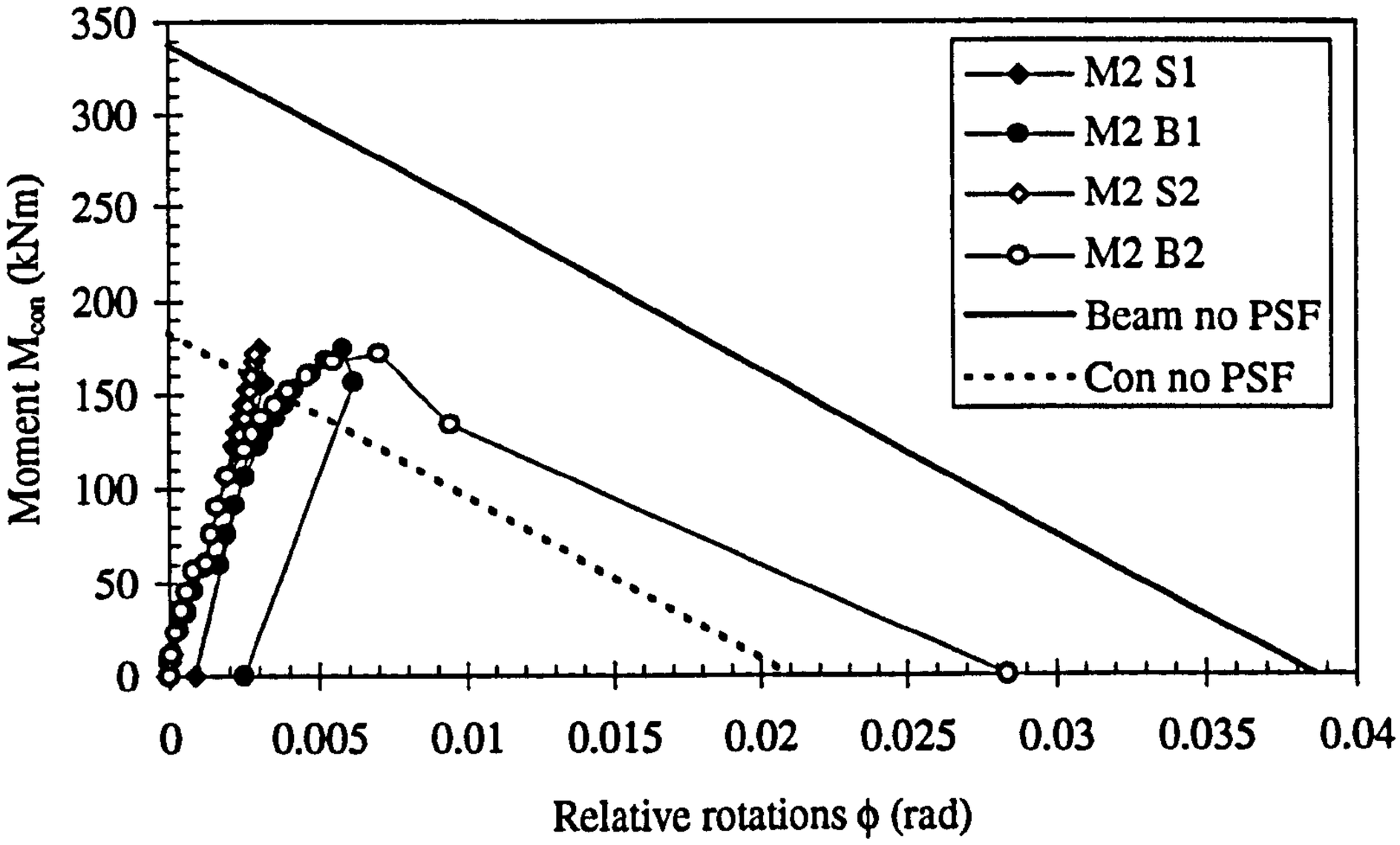

Figure 11.6: Moment versus relative rotations in slabs (in situ) and beams in TB1(B) using Method 2 with beam lines (Method 1 is not applicable)

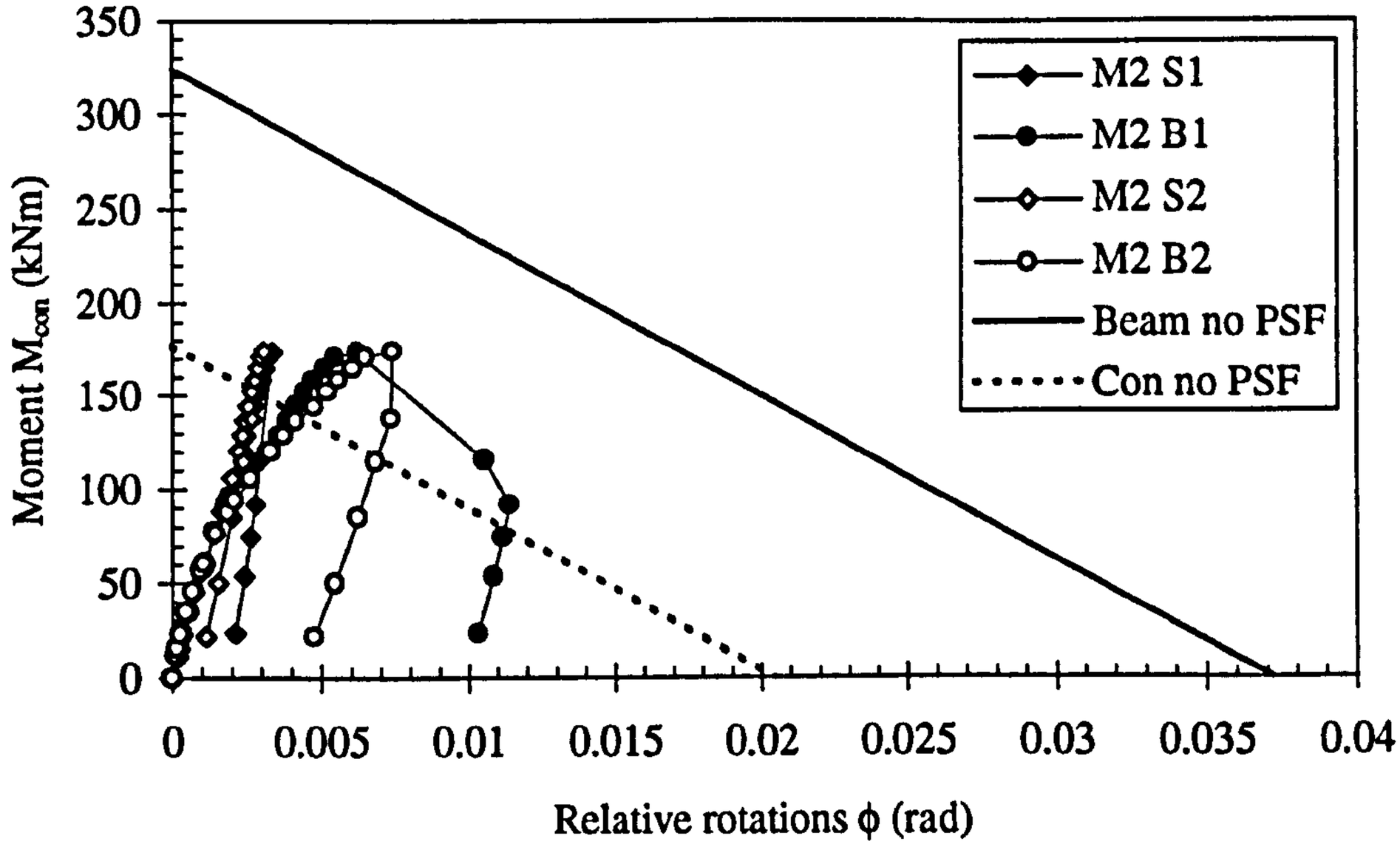

Figure 11.7: Moment versus relative rotations in slabs (in situ) and beams in TB1(C) using Method 2 with beam lines (Method 1 is not applicable)

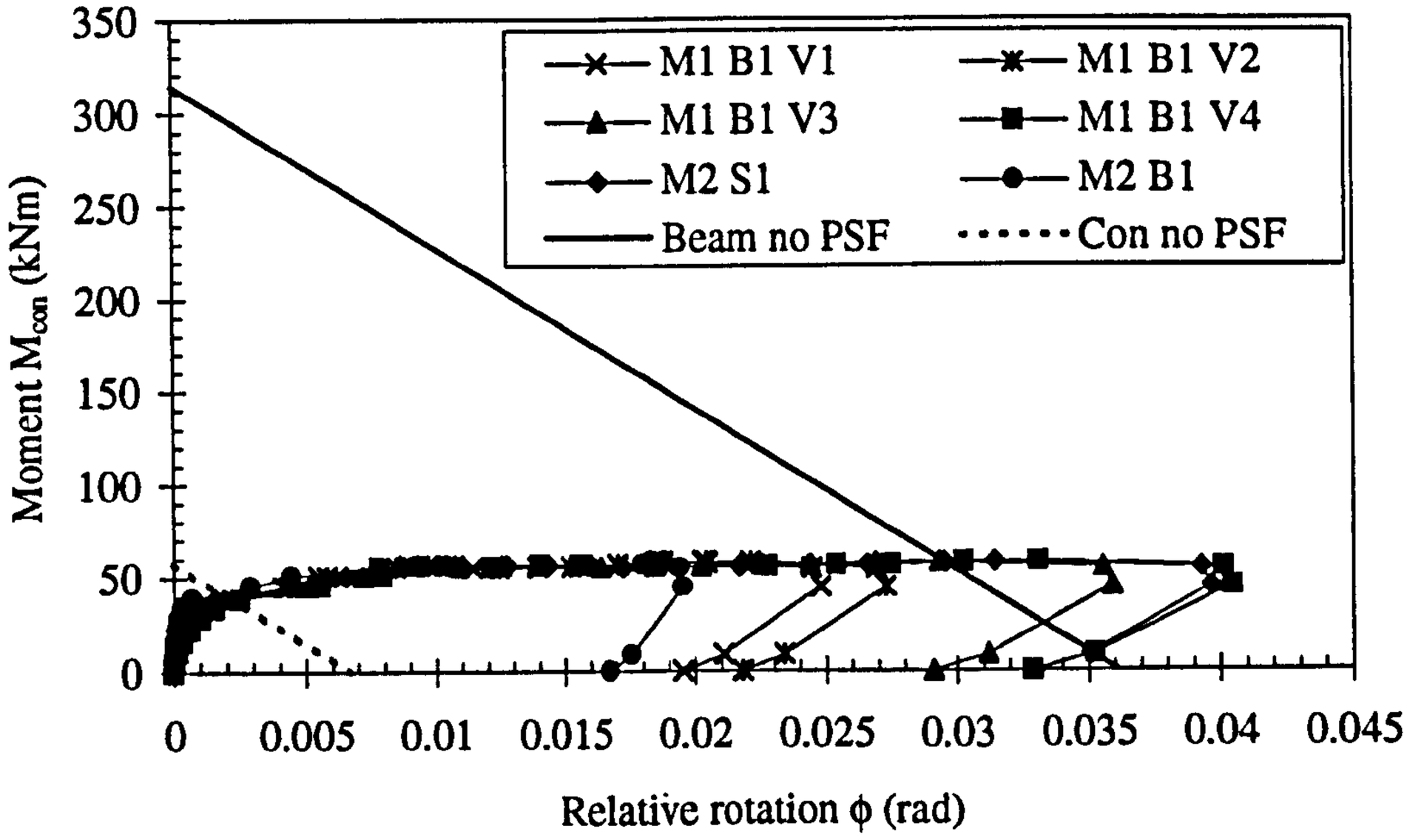

Figure 11.8: Moment versus relative rotations in slab 1 and beam 1 in TB2 using Methods 1 and 2 with beam lines (no slab 2 and beam 2, single sided test)

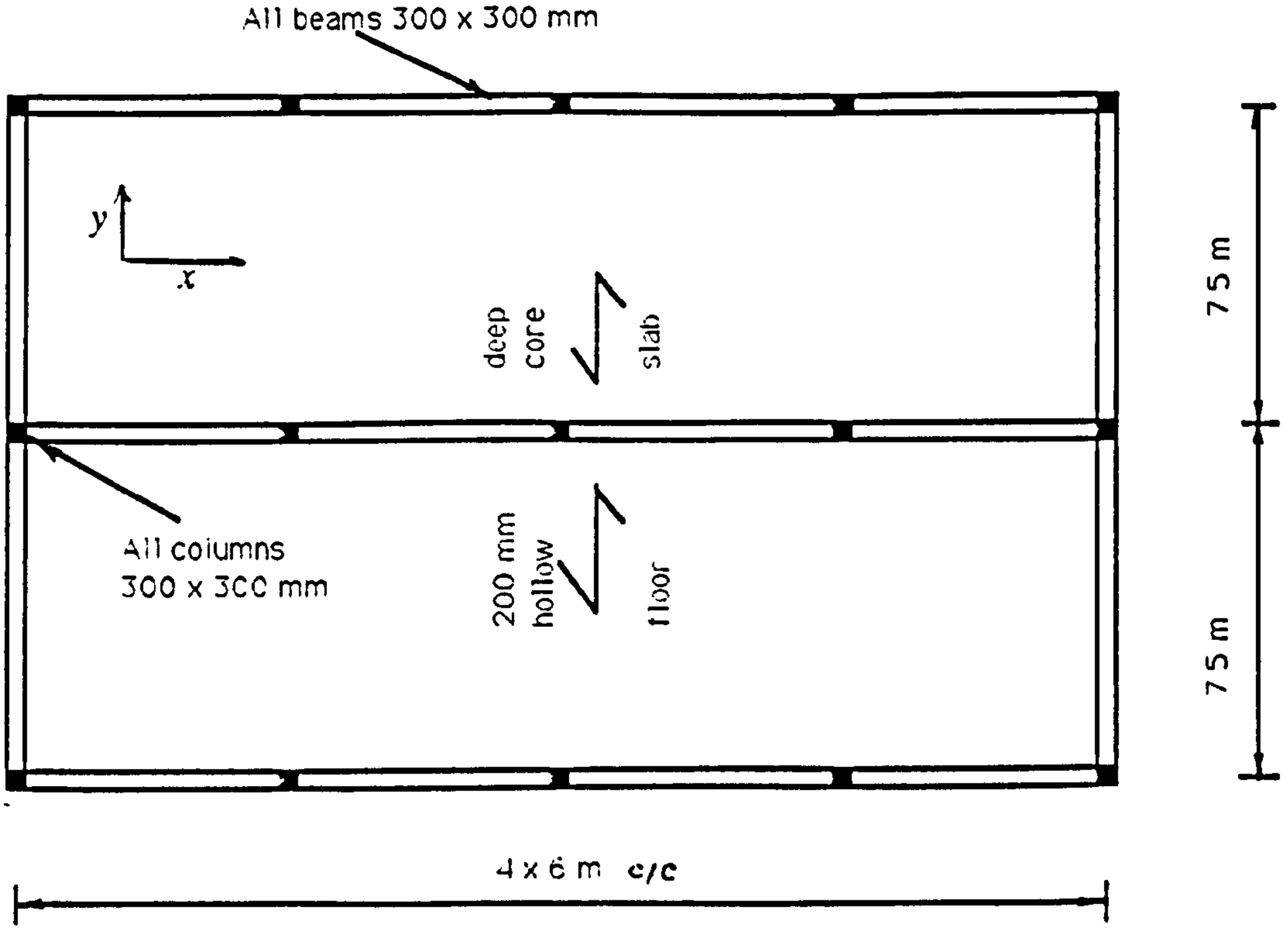

Figure 11.9: Plan of 3-storey frame considered in this design analysis

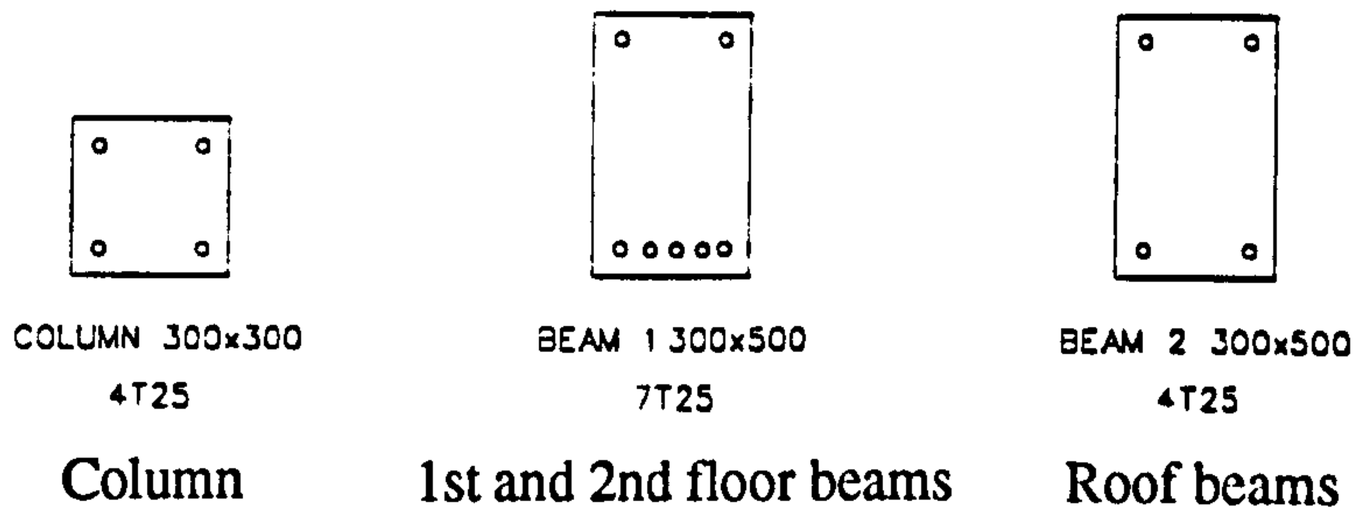

Figure 11.10: Beam and column reinforcement details

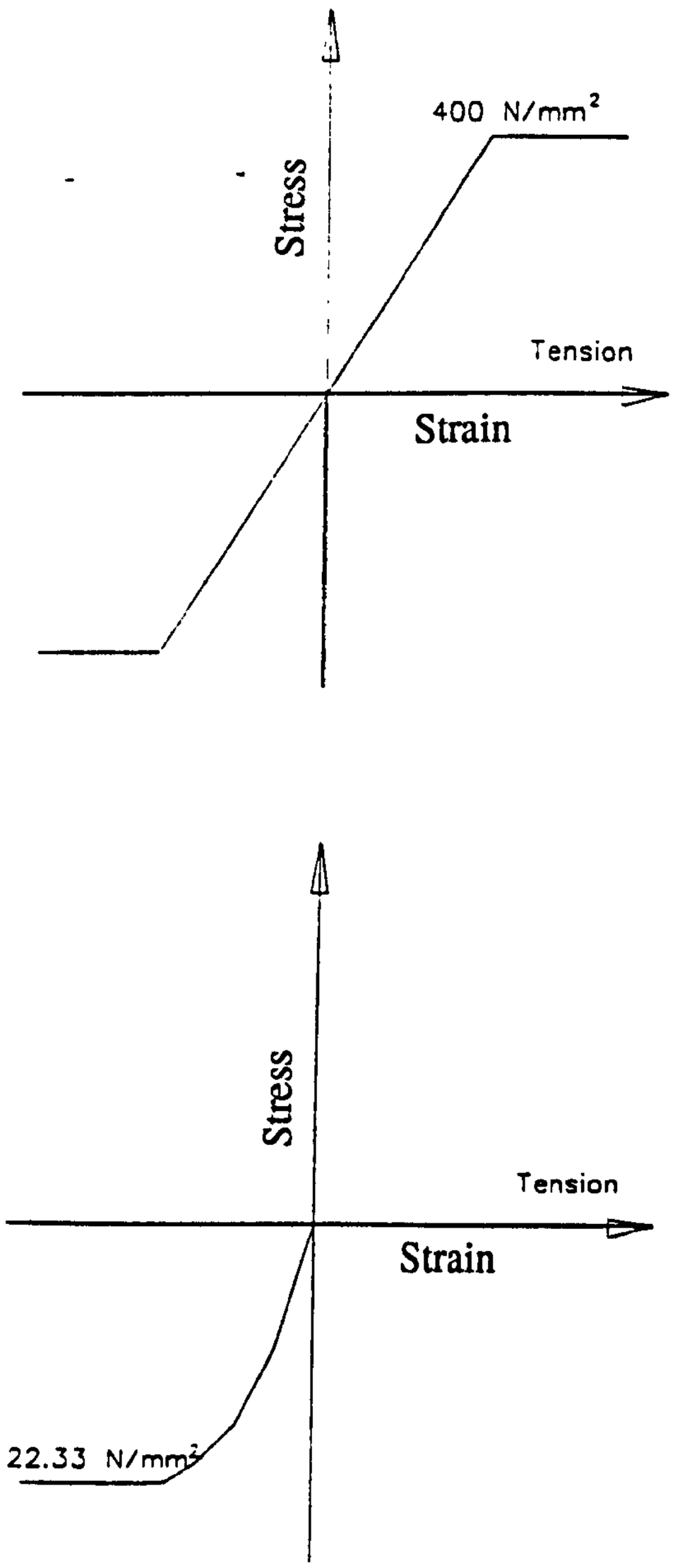

Figure 11.11: Stress vs strain data for steel and concrete used in analysis

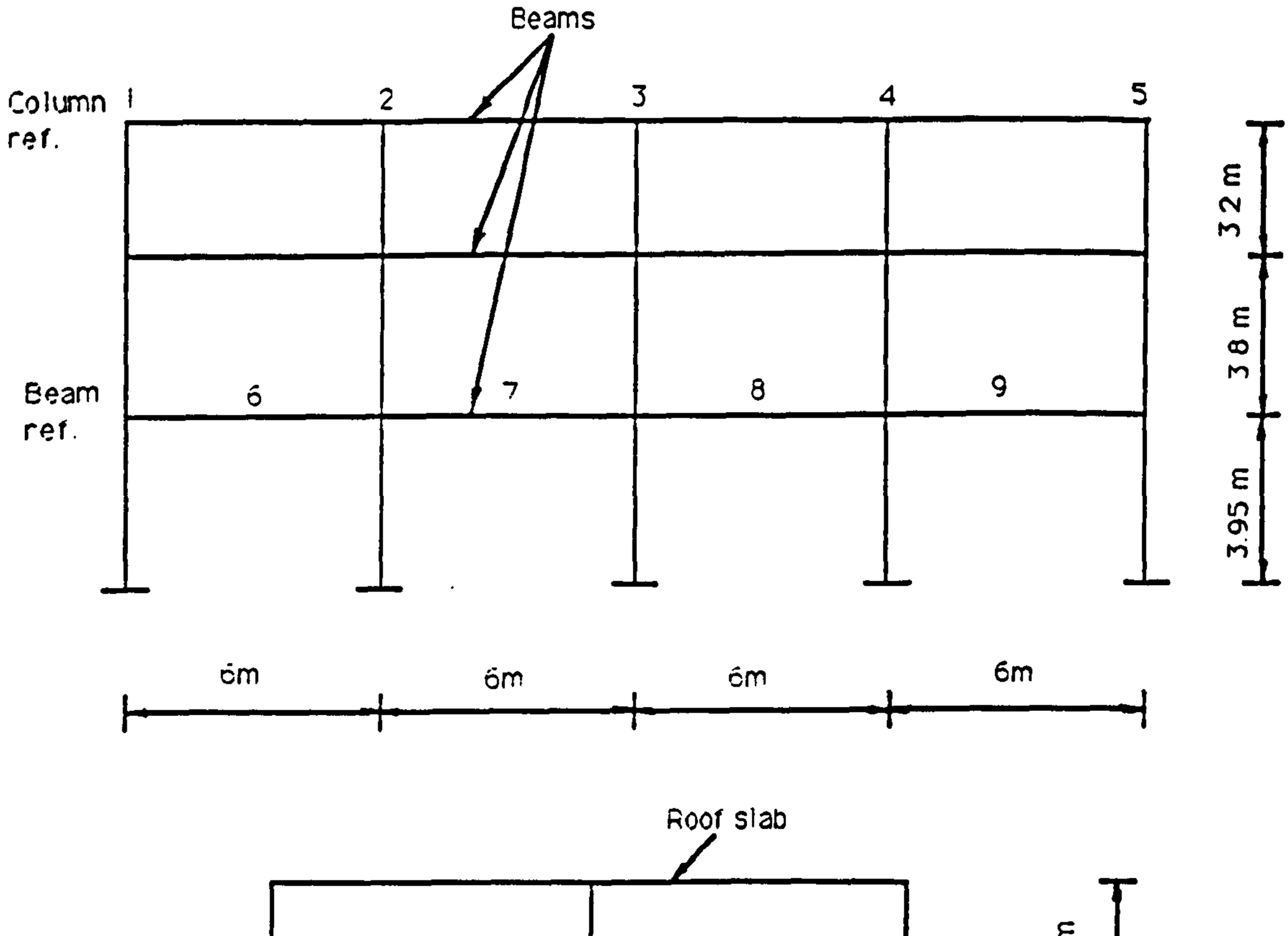

Figure 11.12: Simplified 2-d frames

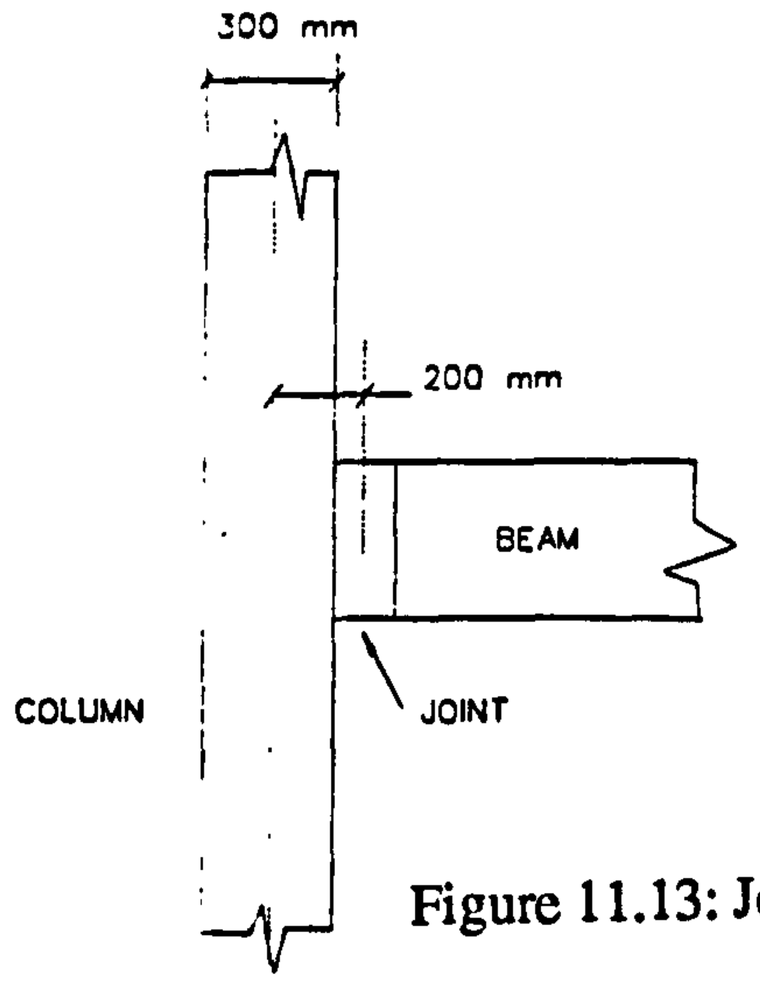

Figure 11.13: Joint eccentricity

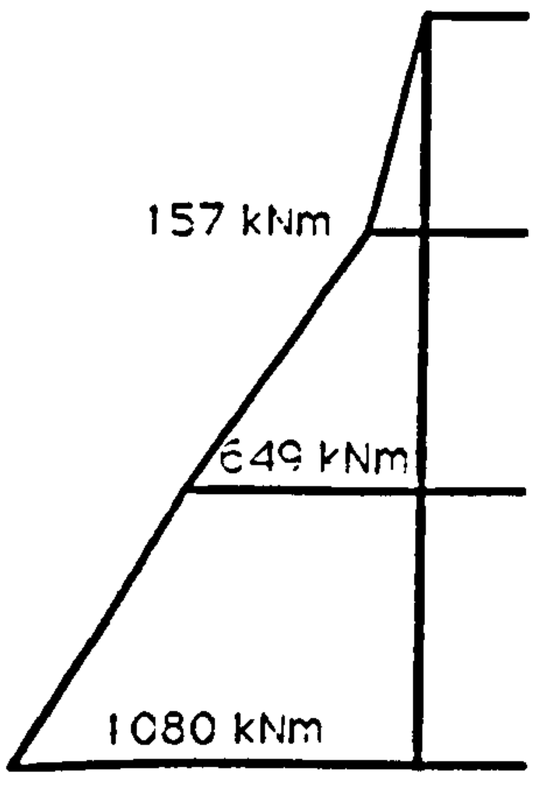

Total moment

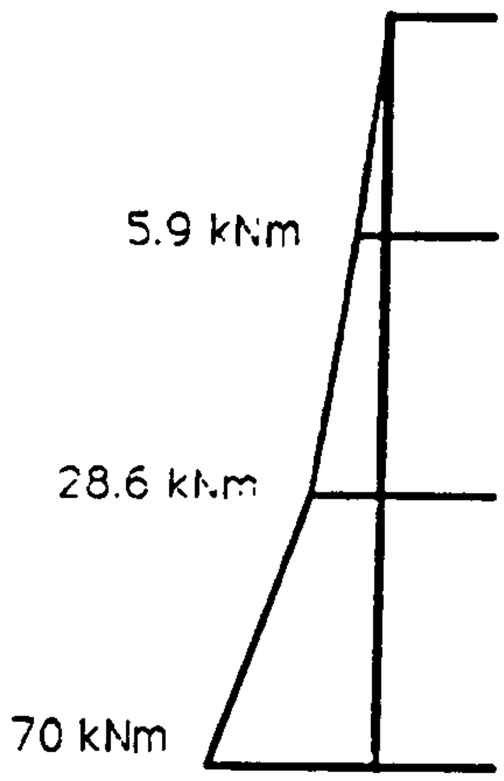

Linear components

Figure 11.14: Bending moments for pin jointed frame

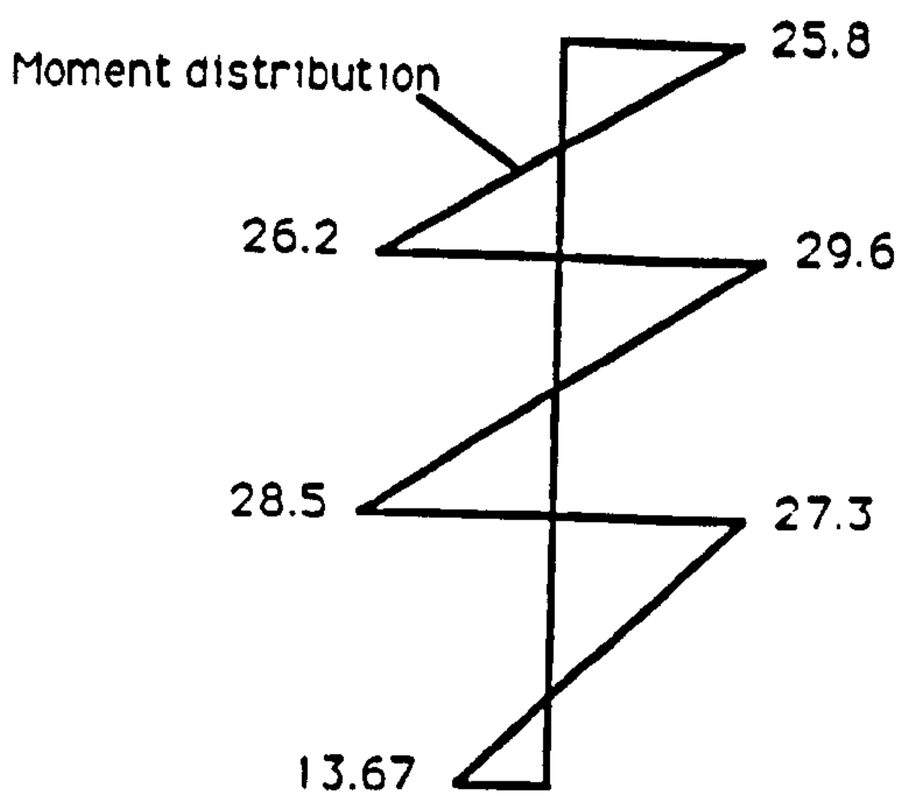

Figure 11.15: Distribution of moments in edge column due to connector eccentricity

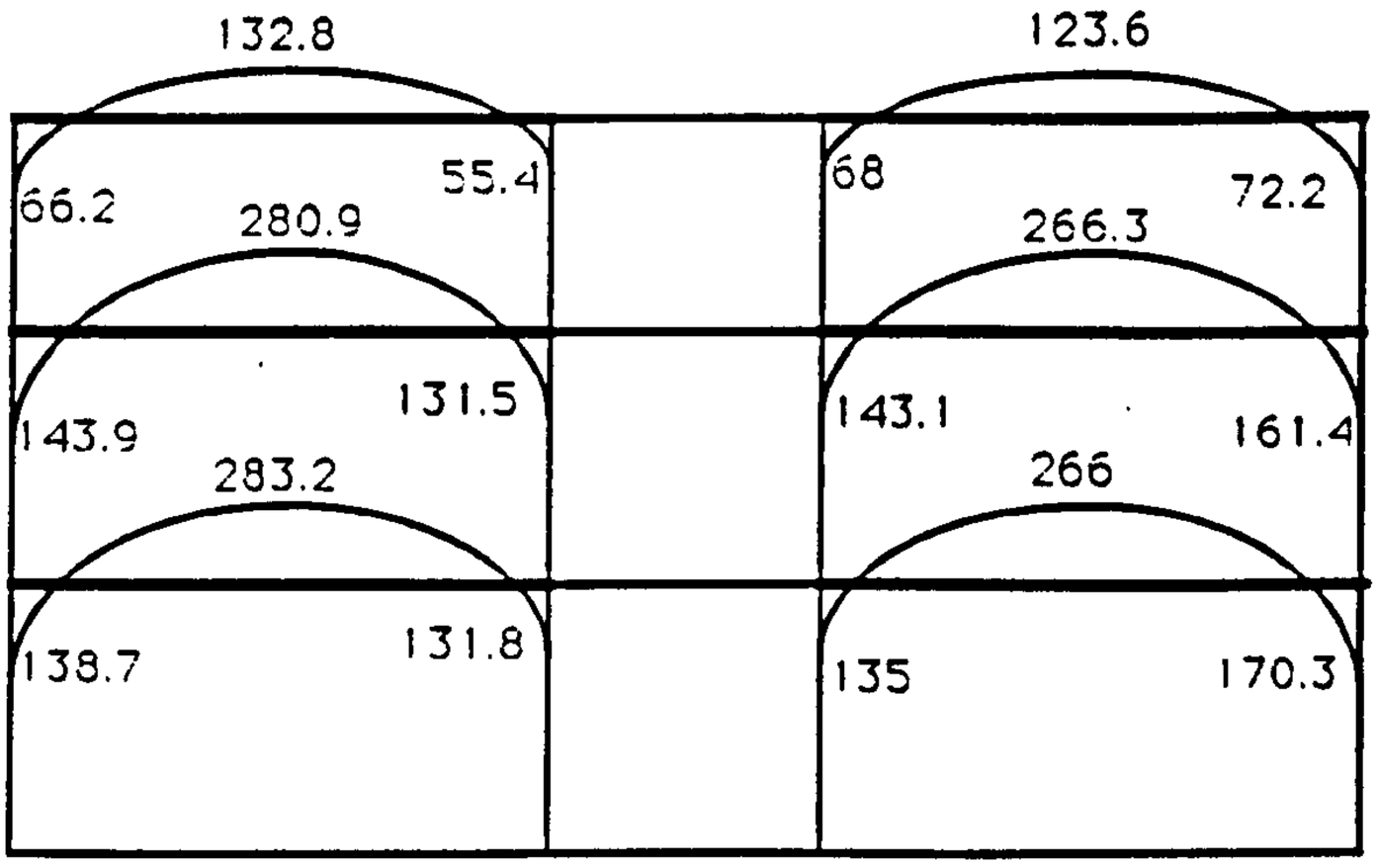

Beam ref. 6,9

Beam ref 7,8

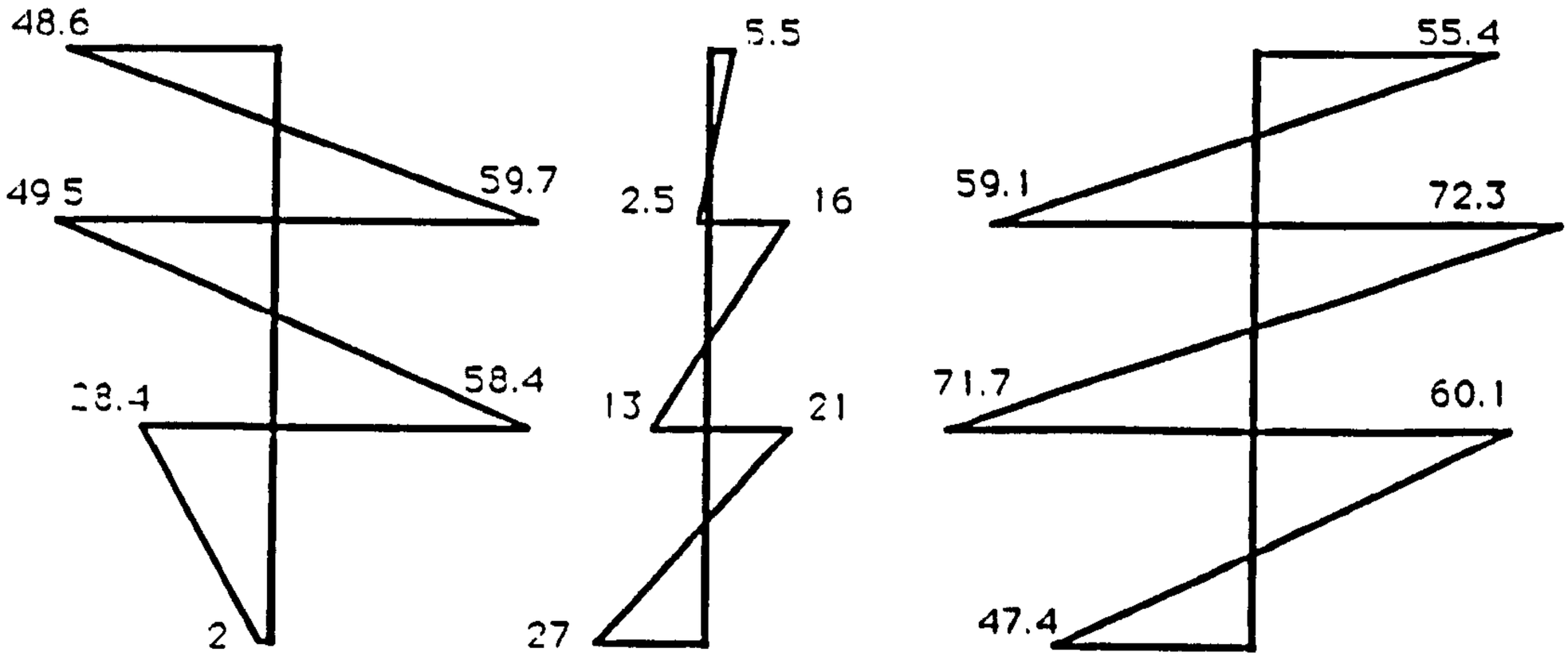

External column ref. 1

Internal 2,3,4

External 5

Figure 11.16: Bending moments using non-linear components and $K_s = 0.6$

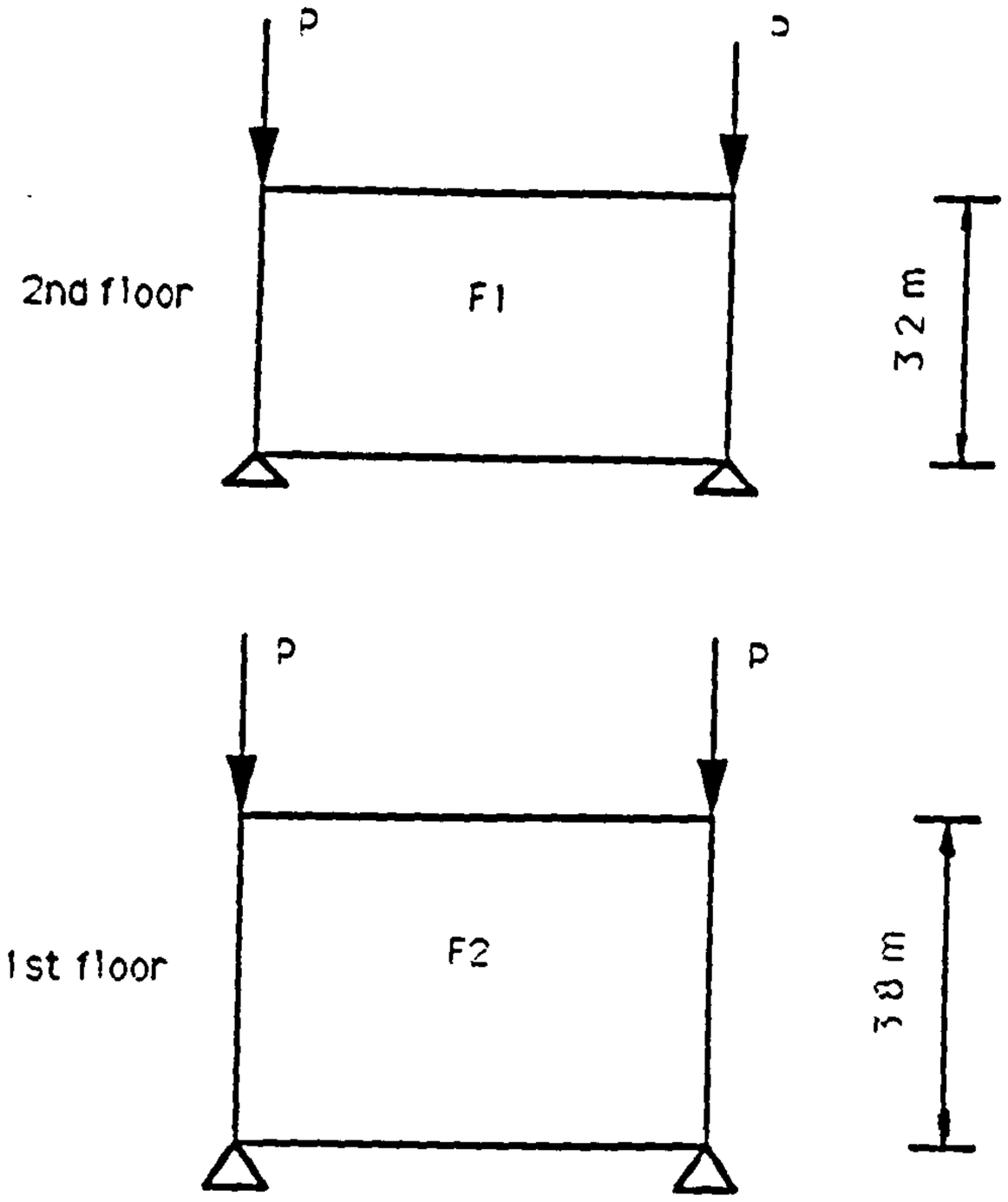

Figure 11.17: Sub-frames considered for 2nd, 1st and ground floor

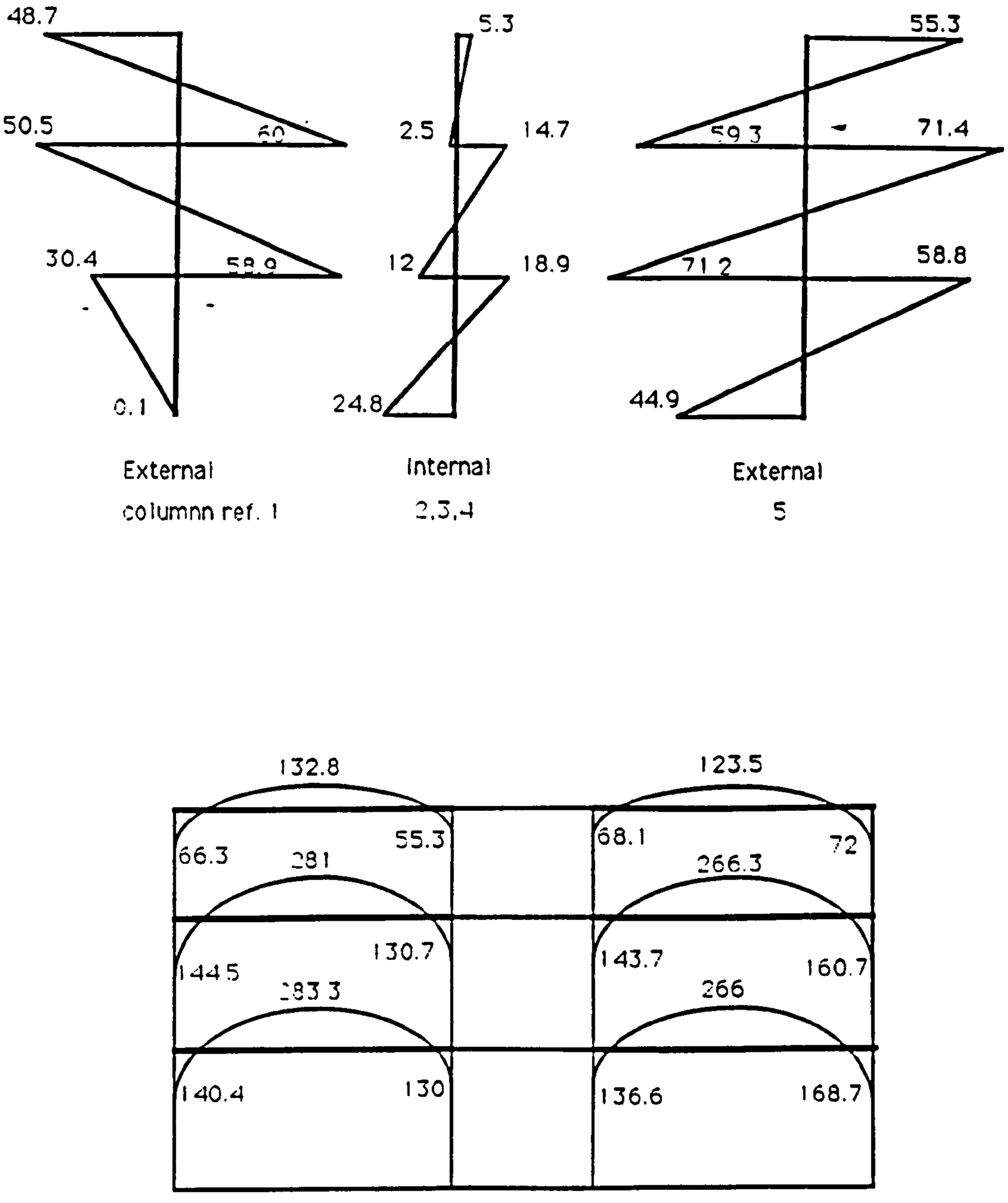

Figure 11.18: Bending moments using linear-elastic components and $K_s = 0.6$

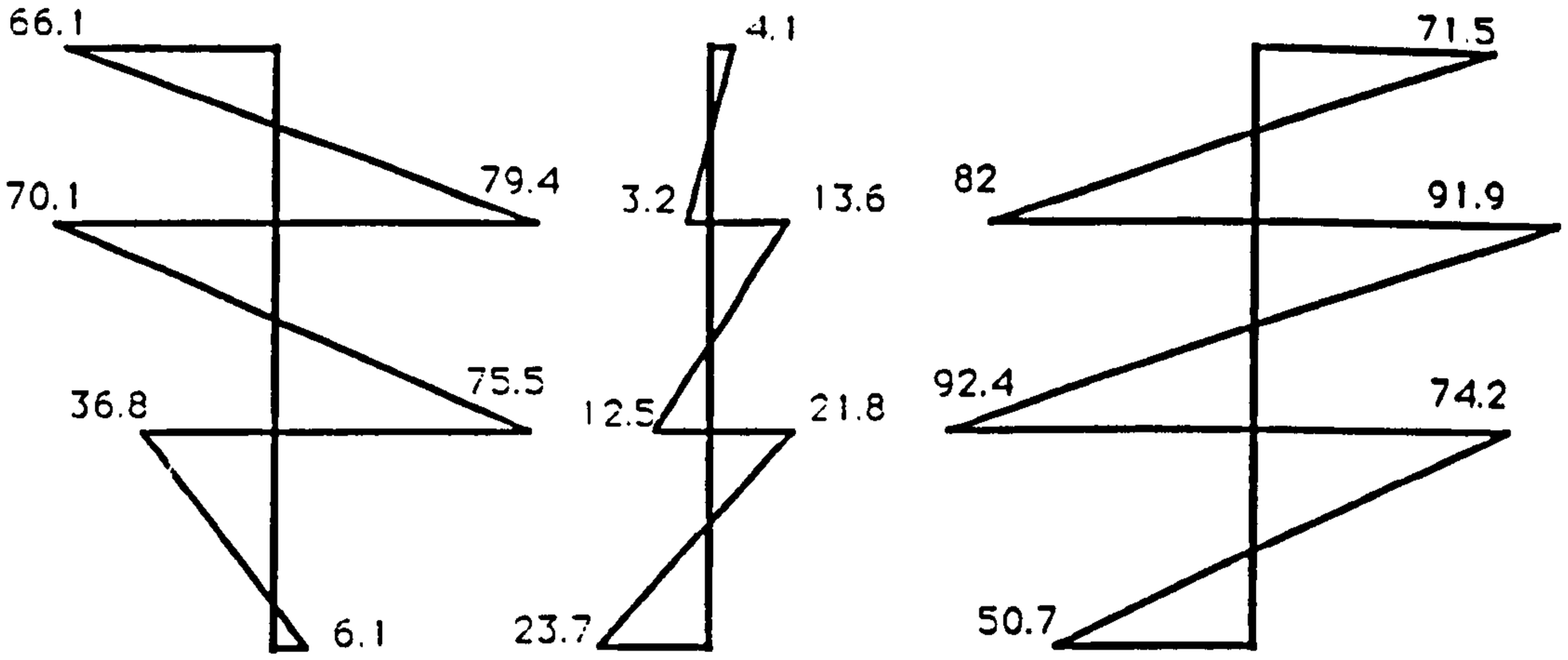

External | Internal | External

columnn ref. 1 | 2,3,4 | 5

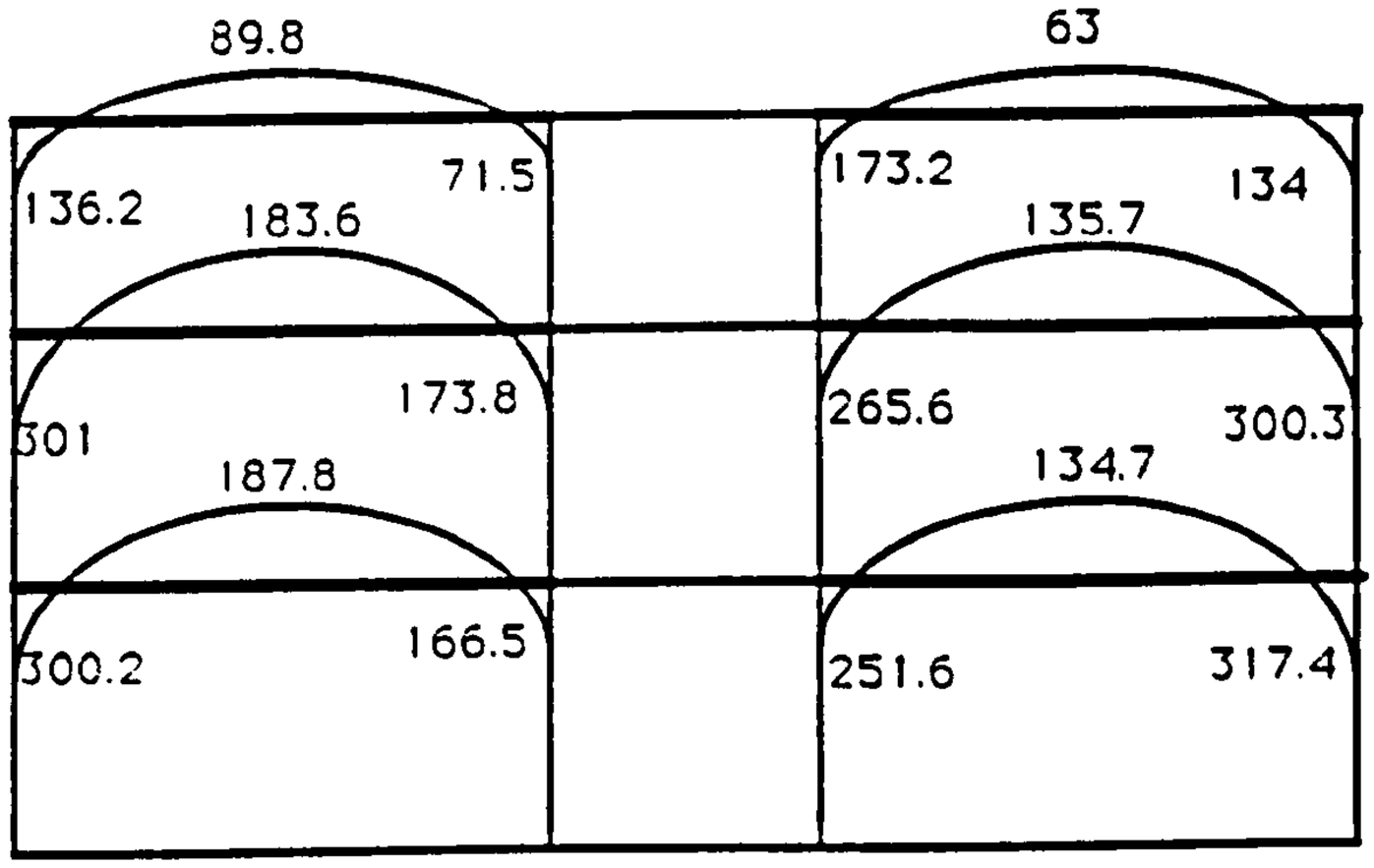

Beam ref. 6,9 Beam ref. 7,8

Figure 11.19: Bending moments using non-linear components and $K_s = 1 \times 10^9$

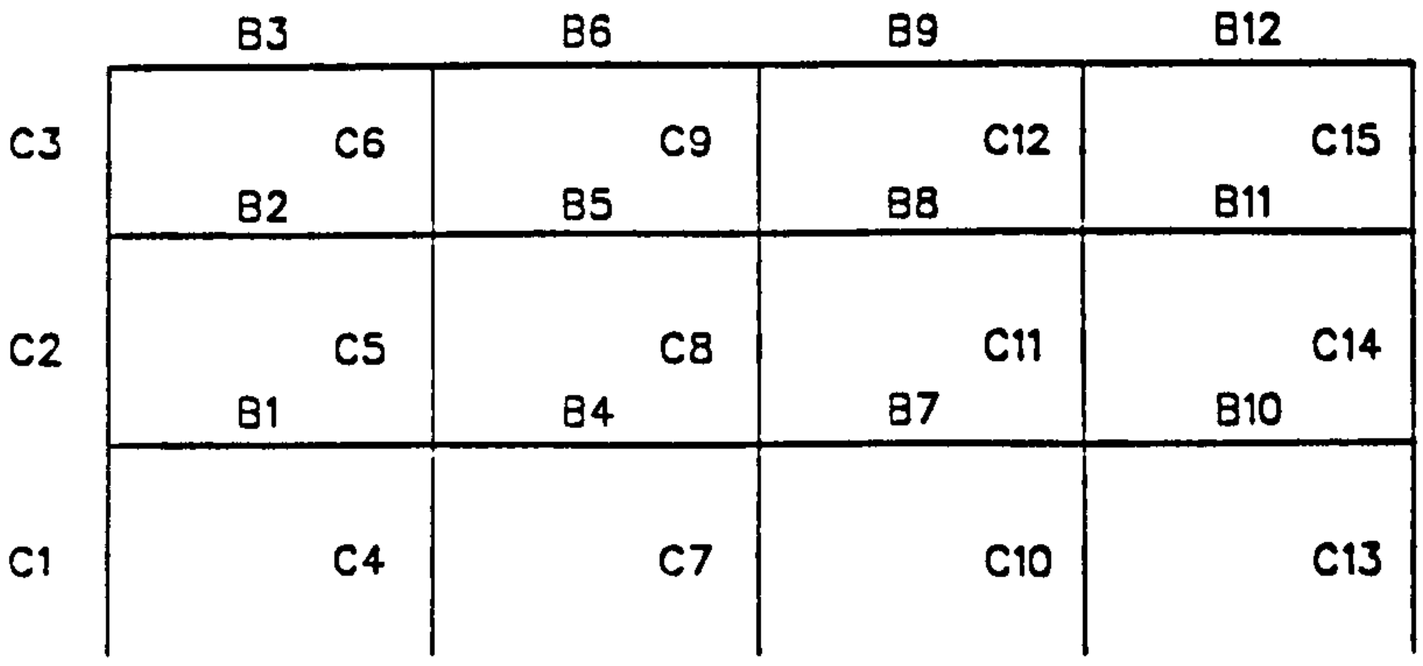

Figure 11.20: Identification for beam and column members used in SWANSA analysis

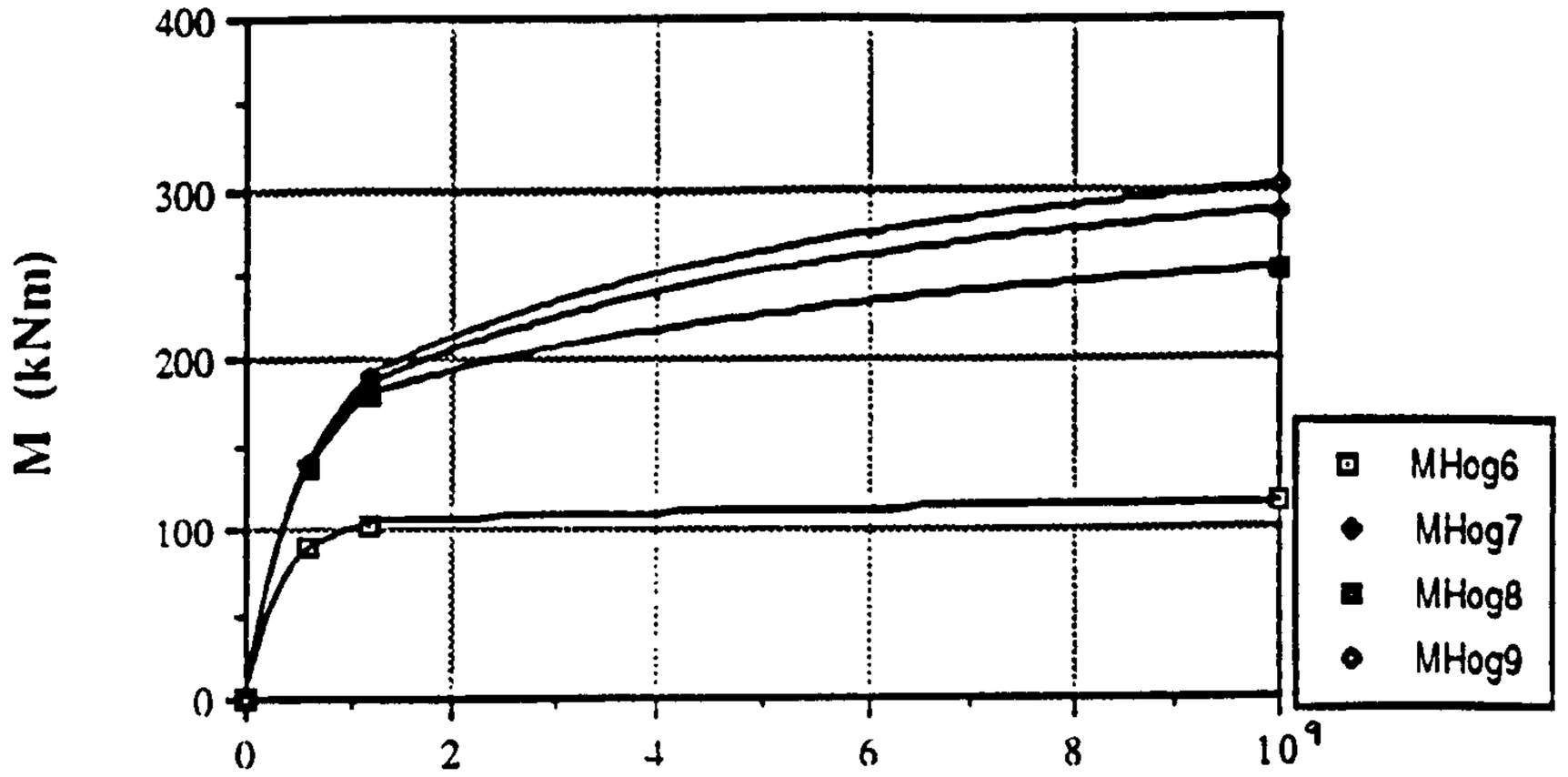

Figure 11.21: Variation in hogging moment in first floor beam with K_s

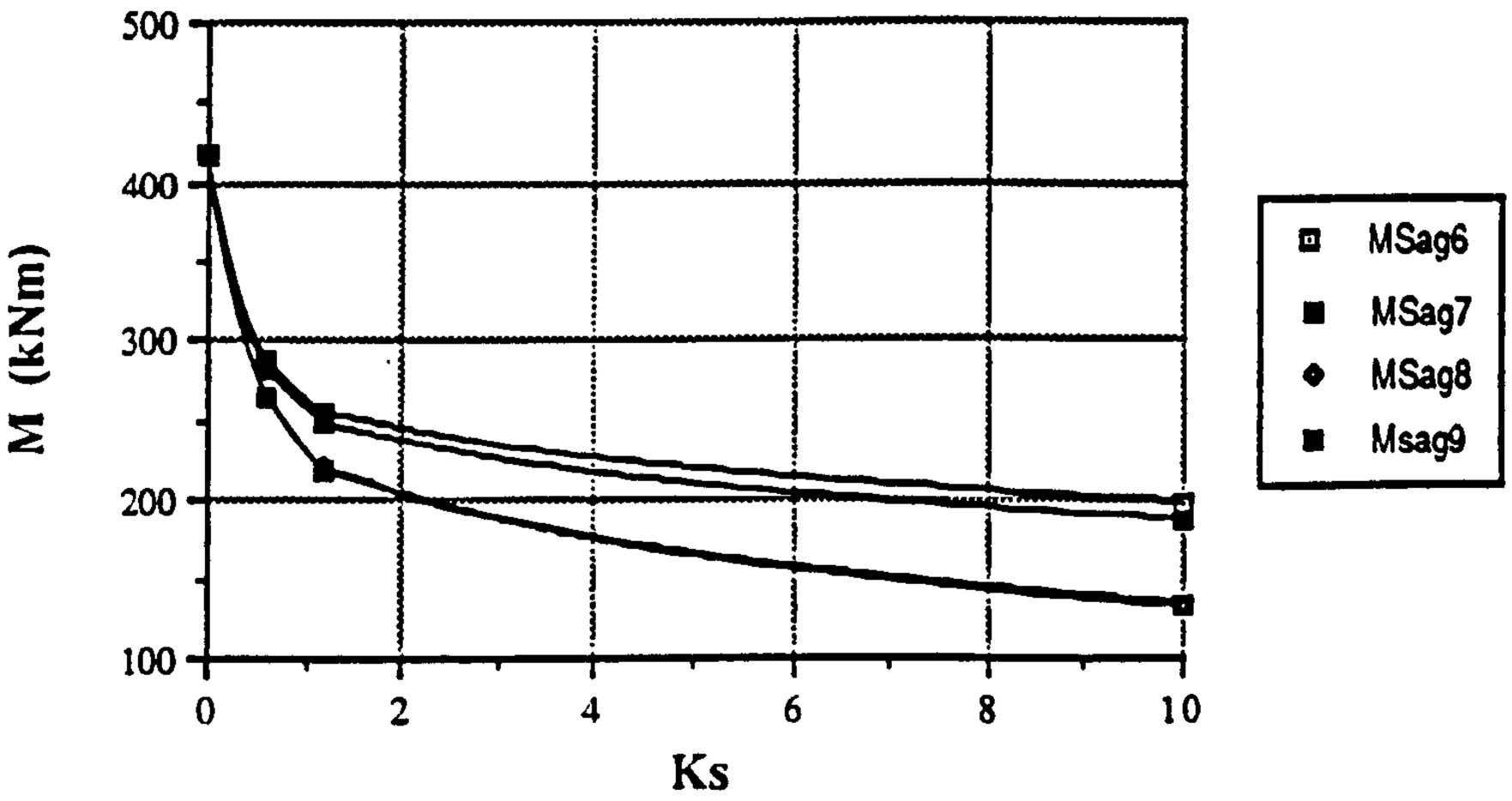

Figure 11.22: Variation in sagging moment in first floor beam with K_s

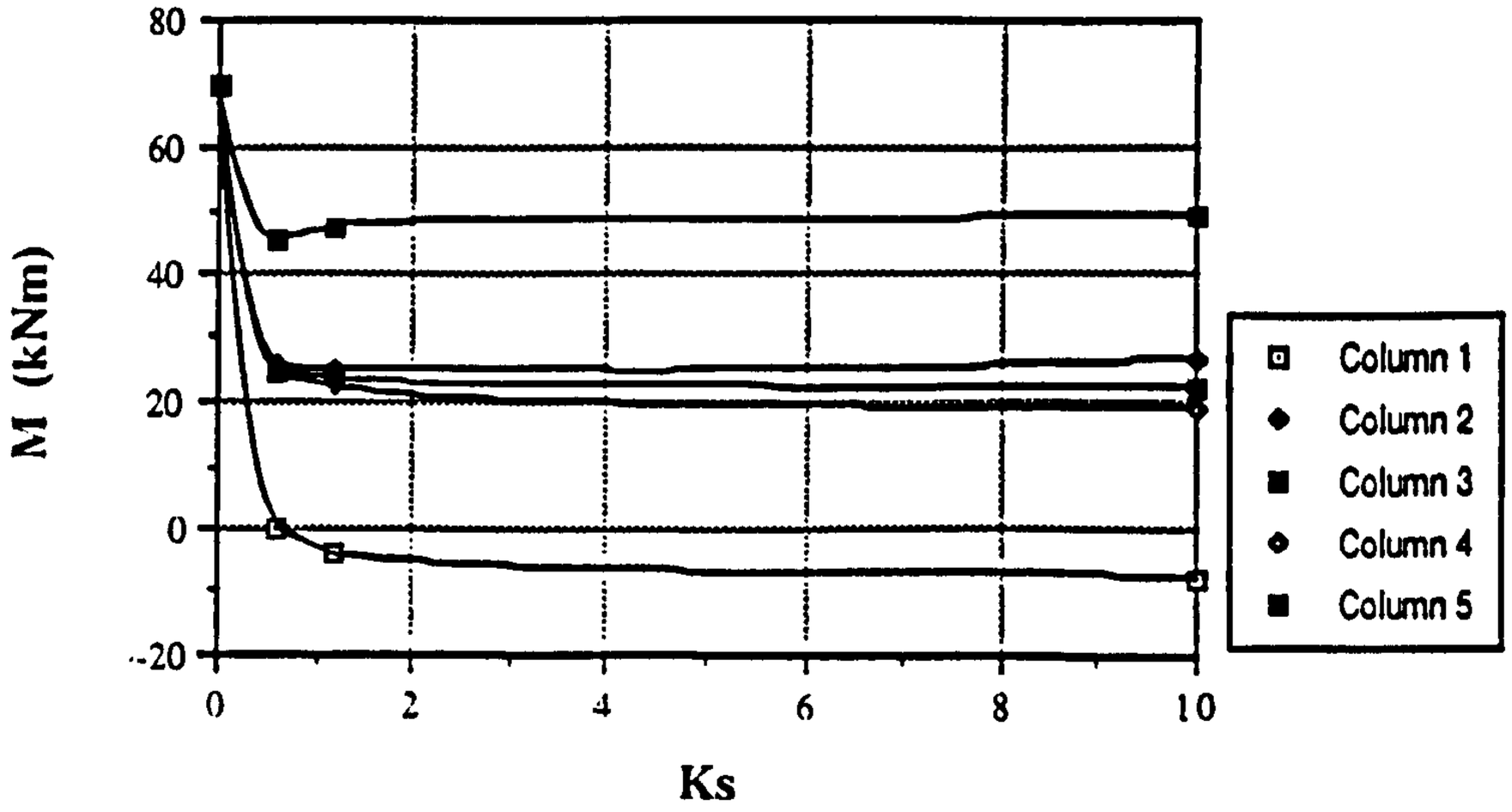

Figure 11.23: Variation in column foundation moment with K_s

CHAPTER 12

CONCLUSIONS AND FUTURE WORK

12.1 Introduction

The current practice in the design of precast concrete frames is to ignore any inherent strength, stiffness and ductility existing in the connections between the beams and columns, and to design both beams and columns on the assumption of pinned joints. The effect of this on the design of sway frame columns results in impracticable and uneconomical selections for frames above three storeys. This is because the column is assumed to behave as a vertical cantilever from the foundation transferring all the beam reaction moments and wind moments in an additive manner fully to the base without involving frame action. For larger columns the additional moments due to $P-\Delta$ and instability effects become prohibitive.

The presence of concrete as grout filled joints is ignored in design except to protect the mechanical connection from corrosion and fire danger. Similarly the presence of longitudinal reinforcing bars interconnecting the beam and column at floor level for frame integrity purposes is not utilised in other ways in current design procedures. However it is clear that the presence of such existing materials together with that of the mechanical connection, must provide the joint with existing residual strength, stiffness and ductility properties which are at present untapped.

The work developed in this thesis builds on the previous promising work in the field at Nottingham University which indicated the positive design and behavioural advantages of utilising the existing semi-rigid joint properties which allow for the safe design of such structures in the form of small slender columns for taller structures.

The present work advances the knowledge base in the following ways :-

1. Full scale of testing of two types of joint, the welded plate and the billet connections, has showed that the essential $M-\phi$ relation could be assessed in several independent ways. This has been done for the beam/column alone, beam and floor slab/column composite behaviour for both double sided and single sided beam arrangements. This has given a more complete data base of the semi-rigid joint behaviour, including various elastic stiffnesses which could be incorporated into design. See Section 12.2.1.

2. A fundamental appraisal of the behaviour of in-situ joint concrete surrounded by stirrups precast concrete, resulting in a new estimate of strength and stiffness, depending on the relative thickness of the in-situ bond has been established, which can be used to simulate concrete compression joint behaviour. Similarly a basic test approach to asses concrete crack widths for concrete unformed with frame integrity bars. The results of these tests have been used to form the basis of the "component method" for estimating $M-\phi$ relations for the joint. See Section 12.2.2.

3. The effect of joint stiffness in the presence of beams and columns has been expanded and re-appraised for these basic subframes, which are suitable for use with sway frames and partially braced sway frames. Column effective length factors have been derived to allow for instability effects, and presented in the form of curves and formulae. See Section 12.3.

4. A semi-rigid design approach has been prepared for precast concrete frames, which incorporates the essentials of the present approach for rigidly connected in-situ frames (BS 8110) with limited modifications and safeguards, but providing designers with the same basic approach.

It has been tested carefully for a three storey three bay structures against an advanced non-linear analysis programme, and the author's elastic large deflection analysis programme, and found to perform well.

12.2 Experimental work

12.2.1 Frame connection tests

The frame connection test showed that damage to the precast subframe occurred mainly at the bottom of the connections in the compression zone whilst the members had suffered little damage beyond the connections. The only exceptions to this were in the welded plate connection test where the floor slabs and tie bars were omitted so that the failure was due to exceeding the strength of the weld, and in the single sided connections where the failure was due to exceeding the strength of the column. The initial tangent flexural stiffness of the connection was maintained up to 0.10 to 0.13 of the ultimate moment capacity of the connection M_u in the double sided connections and between 0.22 and 0.49 in the single sided tests. At failure M_u was approximately 0.84 to 0.95 of the predicted ultimate moment of resistance of the connections in double sided tests and 0.29 to 0.65 in the single sided tests. The effect of the floor slab and the tie bars was to increase the ultimate moment (by 215%), rotation (by 46%) and stiffness (by 105%) compared to the basic connection. Currently, in practice this

remarkable contribution of the floor strength and stiffness to the flexural capacity of the joint is neglected in design.

A beam-line assuming $M_{beam} = M_u$ of each connection is proposed which intersects the $M_{con} - \phi$ plots before attained M_u to obtain reasonable characteristics of the connection for use in design. The beam - line is drawn corresponding to a loading and a certain beam span - to - height ratio. The moment - rotation characteristic has to intersect the beam - line, otherwise there will be insufficient rotation capacity available for use in design.

12.2.2 Interface tests

If the relative rotation ϕ of a beam to column can be assumed to take place wholly at the face of the column then ϕ may be computed from the rigid body displacements at the top and bottom of the section, leading to the aforementioned component method of analysis.

$M_{con} - \phi$ connection data obtained from full scale tests were compared with similar data generated using the component method. A two stage approach was used to validate the component method.

Stage 1. True $M_{con} - \phi$ data were obtained from vertical beam deflections measured within 300 mm of the face of the column. These values were within 10 per cent of those obtained by summating extreme fibre horizontal deformations.

Stage 2. $M_{con}-\phi$ data were generated by summating horizontal deformations obtained from isolated, small scale compression and tension joint tests.

In comparing the results obtained in one of the full scale tests and the component method, it is noted that both concrete and tie steel uni-axial yield strains are exceeded in the former, whereas this is not possible in the isolated tests. For this reason the full scale ultimate test moment of 238.78 kNm and rotation capacity of 10 mrad are not achieved; the values being 160 kNm and 4.4 mrad, respectively. This is because no redistribution of stress is possible in isolated tests, and cracking is affected by the presence of floor slabs in the full scale tests. However, the points where the stiffness of the full scale connection changes, i.e. after the first flexural crack at 30 kNm moment, and the magnitude of the stiffness are both faithfully reproduced in the component method.

In conclusion it is such that, within the limitations described, the component method provides a reasonable tool to generate $M_{con}-\phi$ data, and needs to be developed further.

12.3 Analytical parametric studies

The variation in the effective length factors β with joint and member stiffness parameters K_s and α are presented both graphically and in the form of design equations similar to these currently used in BS 8110. It is found that the change in the response of a structure is greatest when $K_s < 1.5$, and β factors increase due to :-

i) an increasing number of total degrees of freedom in the sub-frame;

ii) an increase in α, the relative stiffness of the columns to the beam members;

iii) a decrease in K_s, the relative stiffness of the connection to a fully encastre beam member.

The results enable designers to determine β factors for situations currently not catered for in codes of practice, in particular the upper storey in a partially braced frame.

12.4 Summing up

- The bending strength of precast concrete beam-column connections depends on the type of connection and its location in the frame. Double sided connections achieved full capacity because the tie steel embedded within in-situ concrete in the precast floor slab is fully effective, whilst the use of single sided connections are limited by the strength of the connection itself as the tie steel is not fully effective.

- The secant stiffness of the connections in all the tests varies from 0.7 to 3.9 times the flexural stiffness ($4E_cI_c / l$) of the beam to which it is attached. Thus some connections may not be suitable in a semi-rigid frame analysis, because the suitability of each type of connection for use in a semi-rigid design must be related to the stiffness and strength of the frame for which it is a part.

- A simplified method to generate moment-rotation data is presented and validated against the results of full scale 3-dimensional tests.

- Design equations for column effective length factors are given in terms of frame and connection stiffness.

- A design method is proposed which supplements the existing methods of BS 8110 and EC2 for concrete column design, whereby the strength and stiffness of the connection enables column moments to be shared with the connected beams, making possible a more economical and practical approach to the design of precast concrete frames.

12.5 Recommendations for future work

The work should be divided into two main parts:

12.5.1 Experimental work

Cyclic loading frame connection tests (including floor slabs) and several smaller interface tests to include the following:-

a) Frame connection tests

In plane tests on double sided internal connections (internal beams). Build precast concrete sub-frames for the most popular types of connections i.e. cleat and corbel and test as nonsway structures in order to realise the true response of the connections.

In plane tests on single sided connections. These tests may be used to determine the differences between single and double sided situations, with the aim of finding equivalent symmetrical arrangements, and/or the influence of the 3rd dimension. This is the essential information required by the 3-d computer frame analysis programs.

b) Interface tests

1. Precast-in-situ-precast concrete joints tests in compression and flexure using the same concrete mixes in the above frame connection tests and carry out the tests on the same day with them using the same load cells and instrumentation for consistency.

2. Crack width opening and bond pull-out tests in areas confined by precast members and/or reinforced in-situ concrete.

This information is necessary in order to be able to interpret the effects of localised under or over strengthening in connections, where the behaviour is often disguised in a single result.

12.5.2 Analytical work

Carry out frame stability analyses using available programs to develop the design equations for column effective length factors in multi-storeys x multi-bays frames in *unbraced* and *partially braced* precast concrete skeletal frames in terms of frame and connection stiffness.

Appendix 5.1

Grading of aggregate

Sieve size (mm)	Retained (gms)	% Retained	% Passing	Grading limits BS 882/1992 Table 3
14	NIL	NIL	100	100
10	374	9.4	90.6	85 - 100
6.3	3416	85.9	4.7	-
5	155	3.9	0.8	0 - 25
2.36	18	0.5	0.3	0 - 5

Table A5.1.1: Grading of coarse aggregate (10 mm single sized gravel aggregate)

(Civil Engineering-Concrete Laboratory, Material stocks, August 1994)

Sieve size (mm)	Retained (gms)	% Retained	% Passing	Grading limits BS 882/1992 Table 4	
				Overall	Grade M
10	NIL	NIL	100	100	-
5	10	0.4	99.6	89 - 100	-
2.36	389	14.1	85.5	60 - 100	65 - 100
1.18	227	8.3	77.2	30 - 100	45 - 100
600 µmm	489	17.8	59.4	15 - 100	25 - 80
300 µmm	14.63	53.3	6.1	5 - 70	5 - 48
150 µmm	1.65	6.0	0.1	0 - 15	-

Table A5.1.2: Grading of fine aggregate (sand)

Appendix 5.2

Design mixes

	Test series 1													
Comp.	Column			Beam 1			Beam 2			Joints		Slab-beam in situ		
Mix no	1	2	3	1	2	3	1	2	3	1	2*	1	2	3
Agg.	3.00	3.00	3.00	3.00	3.00	3.00	3.00	3.00	3.00	3.00	3.00	3.55	3.55	3.55
Sand	2.25	2.25	2.25	2.25	2.25	2.25	2.25	2.25	2.25	2.25	2.25	2.70	2.70	2.70
Cem. OPC	1.00	1.00	1.00	1.00	1.00	1.00	1.00	1.00	1.00	1.00	1.00	1.00	1.00	1.00
Water	0.55	0.54	0.52	0.55	0.52	0.52	0.53	0.523	0.515	0.53	0.55	0.65	0.62	0.63
Slump mm	75	130	75	150	65	65	65	90	70	65	75	100	50	50

Table A5.2.1: Mix proportions by weight in test series 1 (* Re-concrete the joints for TW1(C))

	Test series 2									
Comp.	Column			Beam 1	L Beams			Joints	Slab-beam in situ		
Mix no	1	2	3	Ready mixed	1	2	3*	1	1	2	3
Agg.	3.00	3.00	3.00	3.00	3.00	3.00	3.00	3.00	3.55	3.55	3.55
Sand	2.25	2.25	2.25	2.25	2.25	2.25	2.25	2.25	2.70	2.70	2.70
Cem. OPC	1.00	1.00	1.00	1.00	1.00	1.00	1.00	1.00	1.00	1.00	1.00
Water	0.55	0.52	0.52	0.55	0.55	0.55	0.545	0.54	0.55	0.53	0.53
Slump mm	85	75	80	65	-	-	-	65	90	80	80

Table A5.2.2: Mix proportions by weight in test series 2 (* Upstand for L beams)

	Test series 3				
Comp.	Columns	Beam 1&Beams in TB1(B)	Beam 2&Beams in TB1(C)	Joints*	Slab-beam in situ
Mix no	Ready mixed	Ready mixed	Ready mixed	1	Ready mixed
Agg.	3.00	3.00	3.00	N/A	3.55
Sand	2.25	2.25	2.25	2.00	2.70
Cem. OPC	1.00	1.00	1.00	1.00	1.00
Water	0.55	0.55	0.55	0.45	0.55
Slump mm	70	100	50	N/A	140

Table A5.2.3: Mix proportions by weight in test series 3 (*Admixture, Tricosal, 1% of cement weight was used)

	Test series 4					
Comp.	Column			Beam 1 & L Beams	Joints*	Slab-beam in situ
Mix no	1	2	3	Ready mixed	1	Ready mixed
Agg.	3.00	3.00	3.00	3.00	N/A	3.55
Sand	2.25	2.25	2.25	2.25	2.00	2.70
Cem. OPC	1.00	1.00	1.00	1.00	1.00	1.00
Water	0.55	0.53	0.53	0.55	0.45	0.55
Slump mm	85	65	70	90	N/A	50

Table A5.2.4: Mix proportions by weight in test series 4 (*Admixture, Tricosal, 1% of cement weight was used)

Appendix 5.3

Functions of sensors in the experimental work

POTs	Function
1	records crack opening between the column and insitu infill at the top of beam 2
2	records crack opening between the column and insitu infill at the top of beam 1
3	records horizontal deflection between the slab and the top of beam 2
4	records horizontal deflection between the slab and the top of beam 1
5	records crack opening between the column and the beam 2 at the top of joint
6	records crack opening between the column and the beam 1 at the top of joint
7	records tensile deflection at the top of beam 2
8	records tensile deflection at the top of beam 1
9	records horizontal deflection between the column and the beam 2 at the bottom of joint
10	records horizontal deflection between the column and the beam 1 at the bottom of joint
11	records vertical deflection of the joint at the column face on the beam 2 side
12	records vertical deflection of the joint at the column face on the beam 1 side
13	records vertical deflection of the joint at the end of the beam 2
14	records vertical deflection of the joint at the end of the beam 1
15	records vertical deflection of the beam 2 at the joint face

Table A5.3.1: Function of the linear potentiometers

16	records vertical deflection of the beam 1 at the joint face
17	records vertical deflection of the beam 2 at 200 mm from the joint face
18	records vertical deflection of the beam 1 at 200 mm from the joint face
19	records vertical deflection of the beam 2 at the free end
20	records vertical deflection of the beam 1 at the free end

Table A5.3.1: Function of the linear potentiometers (continued)

Steel strains	Function
A SG1	records strain in bar A at 200 mm distance from face of the column on beam 2 side
A SG2	records strain in bar A at 50 mm distance from face of the column on beam 2 side
A SG3	records strain in bar A at center of the column
A SG4	records strain in bar A at 50 mm distance from face of the column on beam 1 side
A SG5	records strain in bar A at 200 mm distance from face of the column on beam 1 side

Table A5.3.2: Function of the steel strain gauges on bar A

Steel strains	Function
B SG1	records strain in bar B at 200 mm distance from face of the column on beam 2 side
B SG2	records strain in bar B at 50 mm distance from face of the column on beam 2 side
B SG3	records strain in bar B at center of the column
B SG4	records strain in bar B at 50 mm distance from face of the column on beam 1 side
B SG5	records strain in bar B at 200 mm distance from face of the column on beam 1 side

Table A5.3.3: Function of the steel strain gauges on bar B

Concrete strains	Function
SG1	records compressive strain at the bottom of the beam 1
SG2	records tension strain at the top of the beam 1
SG3	records tension strain at the top of the in situ infill concrete on beam 1 side
SG4	records compressive strain at the bottom of the beam 2
SG5	records tension strain at the top of the beam 2
SG6	records tension strain at the top of the in situ infill concrete on beam 2 side

Table A5.3.4: Function of the concrete strain gauges

Load cells	Function
1	records magnitude of applied load at the top of beam 1
2	records magnitude of applied load at the top of beam 2
3	records magnitude of self weight at the bottom of beam 1
4	records magnitude of self weight at the bottom of beam 2

Table A5.3.5: Function of the load cells

Appendix 5.4

Predicted ultimate hogging bending moment capacity of the connections

A5.4.1 Total tensile yield load F_t' in 2T25 stability tie bars

Figures A5.4.1 and A5.4.2 show the internal forces induced in the connections at the sections in the vicinity of the column faces, respectively for the welded plate and billet, and bolted billet beam-to-column connnections. F_t' is the total tensile yield load in the 2T25 stability tie bars used in tests carried out. In all the tests require stability tie bars, two T25 x 1000 mm long hot-rolled deformed high tensile bars were cut at the random from the lengths used in the tests. They were tested in accordance with the requirements of BS EN 10 002-1: 1990 for the yield stress and elastic modulus in the 2000 kN INSTRON 8500 testing machine. Results are presented in Table A5.4.1. The yield load P_y was obtained from load extension plot at 0.43% strains for each bar. Thus,

$$F_t' = P_{y(bar\ A)} + P_{y(bar\ B)}$$

e.g.

$F_t' = 526.91$ kN for test TW1(A)

A5.4.2 Total fillet weld tensile yield load F_{wt} :

The ultimate tensile forces in the weld were calculated by measuring the weld lengths and throat thicknesses after welding was completed. It is not possible to find the tensile force before welding. Because the required weld dimensions might not be achieved in practice depends on welder. It is vital to measure the actual dimmensions of weld after completion. It was done on three regions as shown in Figure A5.4.1

The strength of fillet weld is calculated using the throat thickness. For the 90 degree fillet weld the throat thickness is taken as 0.7 times the size or leg length.

Strength of weld = 0.7 leg length p_w / 10^3 kN / mm

where p_w is the design strength of fillet weld taken as $p_w = 215$ N / mm^2, Table 36, Clause 6.6.5.1. BS 5950: Part 1.

Weld lengths were measured as 80 mm

The weld strength factor $\gamma_m = 1.2$

Thus, the calculated shear tensile capacity in each weld (See Figure A5.4.1) :-

$$F_{wt1} = 1.2 \times 14 \times 215 \times 80 / 10^3 = 288.96 \text{ kN}$$

$$F_{wt2} = 1.2 \times 6 \times 215 \times 80 / 10^3 = 123.84 \text{ kN}$$

$$F_{wt3} = 1.2 \times 4 \times 215 \times 80 / 10^3 = 82.56 \text{ kN}$$

$$F_{wt} = F_{wt1} + F_{wt2} + F_{wt3} = 495.36 \text{ kN}$$

A5.4.3 The shear capacity P_s of M16 tie rods

P_s is the shear force in the M16 tie rods used in the bolted billet connection tests. Two M16 x 400 mm long grade 8.8 tie rods were cut at the random from the lengths used in the tests. They were tested in accordance with the requirements of BS 18: 1987 to estimate the shear strength from the ultimate tensile load. Testing was carried out using a ZWICK 1484 testing machine. The shear capacity P_s was obtained from

average tensile capacity $P_{t(average)}$ of two tie rods at 0.2% proof stress for each rod using tensile stress area A_t=157 mm^2. Thus,

0.2% Proof stress =695.99 N/mm^2 for tie rod 1

0.2% Proof stress =665.51 N/mm^2 for tie rod 2

$$P_{t(average)} = \frac{(695.99 + 665.51))}{2} \times 157 = 106.88 \text{ kN}$$

$$P_s = \frac{P_{t(average)}}{1.2} = \frac{106.88}{1.2} = 89.07$$

A5.4.4 Concrete compression force F_{cc} :

F_{cc} = force in the concrete in compression

The concrete stress = $0.67 f_{cu}$

$$F_{cc} = 0.67 f_{cu} bx$$

where

b is breath of the section = 300 mm

x is the depth of the stress block and

f_{cu} is the concrete compressive cube strength in N/mm^2

A5.4.5 Moment capacity of the welded plate and billet connection

Total tensile force in the connection inTW1(A) (See Figure A5.4.1) :-

$$F_t' + F_{wt} = 526.91 + 495.36 = 1022.27 \text{ kN}$$

For internal forces to be in equilibrium:

$$F_{cc} = F_t' + F_{wt}$$

$$0.67 f_{cu} bx = 1022.27 x 10^3$$

$$x = 5085.9 \frac{1}{f_{cu}} = \text{depth of the stress block (mm)},$$

Because the internal forces are equal, the moments of resistance with respect to the steel + weld and concrete are equal. Taking moment about concrete compressive force F_{cc}, the predicted ultimate hogging bending moment capacity of the connection M_{pred}:-

$$M_{pred} = F_t' \left(400 - \frac{1}{2} x\right) 10^{-3} + F_{wt} \left(200 - \frac{1}{2} x\right) 10^{-3}$$

by substituting above F_t', F_{wt} and x values, the equation becomes

$$M_{pred} = \left(309.84 - 2599.59 \frac{1}{f_{cu}}\right)$$

This force F_{wt} is difficult to measure, beacuse the weld cannot be tested and the identical weld cannot be applied. This might change the predicted moment capacity of the connection.

Based on above assumption the predicted ultimate hogging bending moment capacity of the welded plate connectionr for $f_{cu} = 40\,\mathrm{N/mm^2}$:

$$x = 5085.9\frac{1}{40} = 127 \text{ mm and}$$

$$M_{pred} = 526.91\left(400 - \frac{1}{2}127\right)10^{-3} + 495.36\left(200 - \frac{1}{2}127\right)10^{-3} = 244.92 \text{ kNm}$$

or

$$M_{pred} = \left(309.84 - 2599.59\frac{1}{40}\right) = 244.92 \text{ kNm}$$

Thus, the predicted collapse load:

$$P = \frac{M_{pred}}{2.365} = 103.56 \text{ kN}$$

where

2.365 is the lever arm from the face of the column to the centre of the applied load P to the free end of the cantilever beams (see Figure 5.2 for details).

100 kN was used to carry out the test due to self weight of the test specimens were ignored.

At test day $f_{cu} = 45.4\,\mathrm{N/mm^2}$ was obtained by crushing the cubes made of the same mix for ***beam-to-column joint concrete*** to find out a new x value based on above equation to calculate the actual ultimate moment capacity of the connection. In this case

$x = 112$ mm

$$M_{pred} = 526.91\left(400 - \frac{1}{2}112\right)10^{-3} + 495.36\left(200 - \frac{1}{2}112\right)10^{-3} = 252.59\ \mathrm{kNm}$$

A5.4.6 Moment capacity of the bolted billet connection

Similarly, total tensile force in the connection in test TB1(A):

$$F_t' + P_s = 481.56 + 89.07 = 570.63\ \mathrm{kN}$$

For internal forces to be in equilibrium:

$$F_{cc} = F_t' + P_s$$

$$0.67 f_{cu} bx = 570.63 x 10^3$$

$$x = 2838.9 \frac{1}{f_{cu}}$$

The predicted ultimate hogging bending moment capacity of the connection M_{pred} :-

$$M_{pred} = F_t'\left(400 - \frac{1}{2}x\right)10^{-3} + P_s\left(300 - \frac{1}{2}x\right)10^{-3}$$

by substituting above F_t', P_s and x values

the equation becomes

$$M_{pred} = \left(219.34 - 809.98\frac{1}{f_{cu}}\right)$$

At test day $f_{cu} = 46.4\,\mathrm{N/mm^2}$ was obtained by crushing the cubes made of the same mix for ***beam-to-column joint grout*** to calculate the actual ultimate moment capacity of the connection. In this case

$$M_{pred} = \left(219.34 - 809.98\frac{1}{46.4}\right) = 201.89\ \mathrm{kNm}$$

The predicted moments were calculated in this way by substituting corresponding F_t', F_{wt} and P_s values in the relevant equation above for each test reducing to a function of f_{cu}. The calculated predicted moments are presented in Tables 5.5 to 5.8. with F_t', F_{wt}, P_s and f_{cu} values.

Test reference	25 mm bar reference	Length of bar L (m)	Weight of bar M (gm)	area of bar A (mm^2)	E_s (kN/mm^2)	Yield load P_y (kN)	Yield stress f_y (N/mm^2)	Tensile load T (kN)	Tensile str. f_t (N/mm^2)
TW1(A)	A	1.000	3777	481	197.966	263.007	546.792	312.199	649.062
	B	1.000	3792	483	202.936	263.904	546.385	314.472	651.080
TW2	A	1.000	3633	463	195.779	231.047	499.023	279.872	604.476
	B	1.000	3748	477	203.838	256.263	537.239	308.488	646.724
TB1(A)	A	1.001	3774	480	203.802	239.236	498.408	295.391	615.397
	B	0.993	3741	480	196.726	242.323	504.840	296.621	617.942
TB1(B)	A	0.997	3796	485	199.712	262.028	540.265	314.478	648.402
	B	0.997	3796	485	199.712	262.028	540.265	314.478	648.402
TB1(C)	A	0.997	3758	480	198.750	243.123	506.507	298.831	622.565
	B	0.997	3758	480	198.750	243.123	506.507	298.831	622.565
TB2	A	1.004	3783	480	198.012	243.597	507.485	298.846	622.596
	B	1.001	3771	480	201.427	240.739	501.539	295.450	615.521

Table A5.4.1: Test results of the 25 mm stability tie bars used in the tests carried out

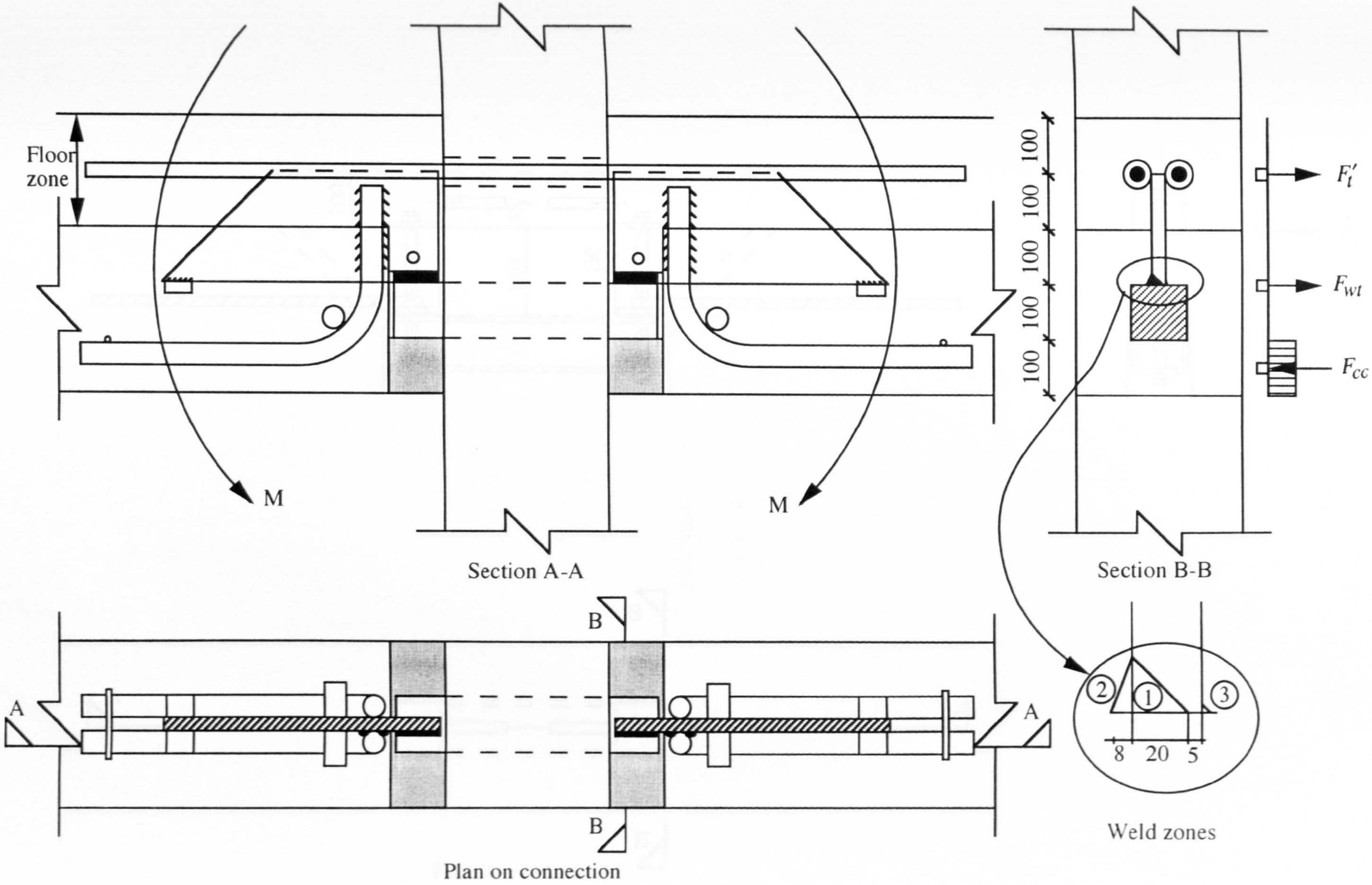

Figure A5.4.1: Internal forces acting on the welded plate connection

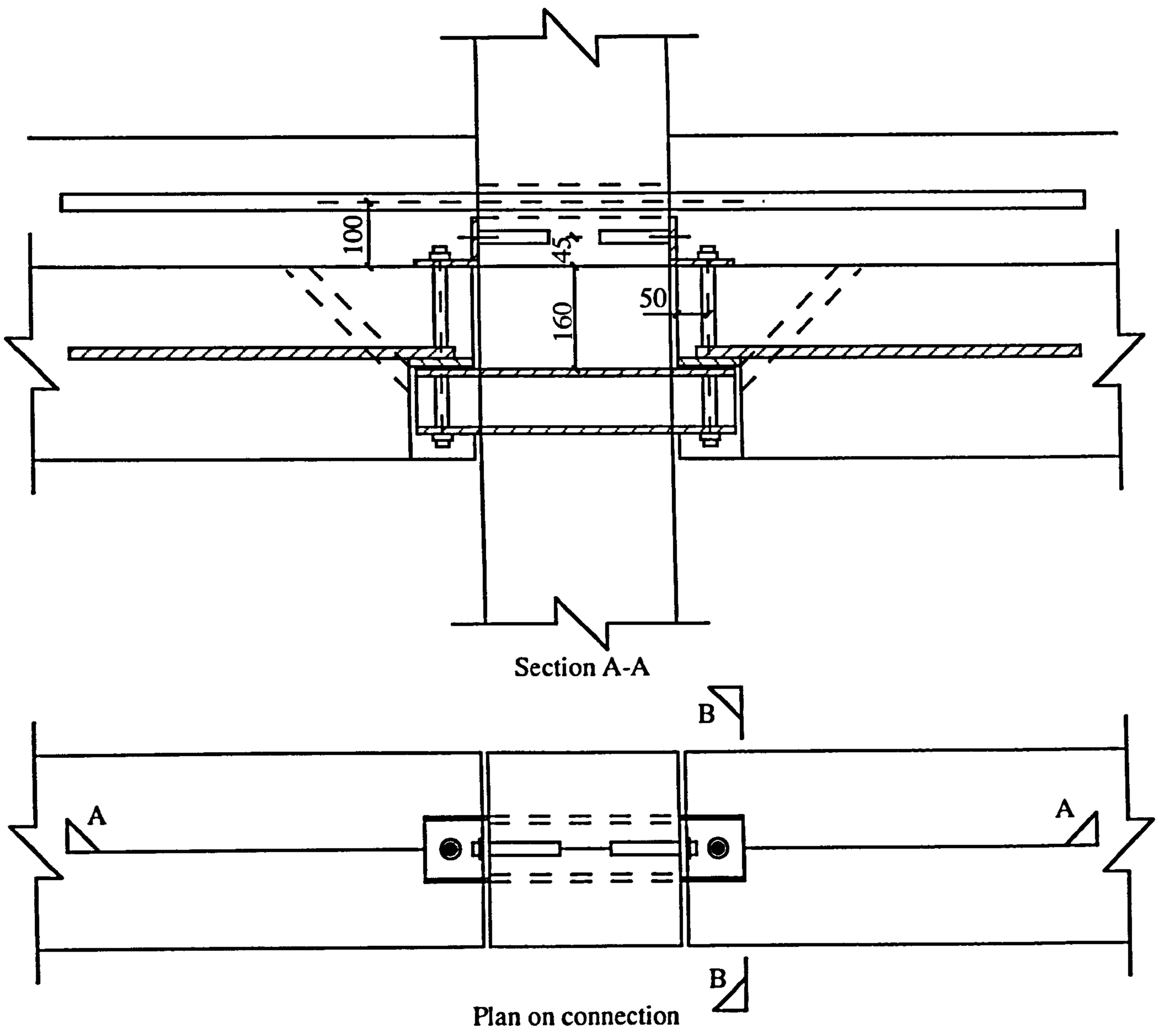

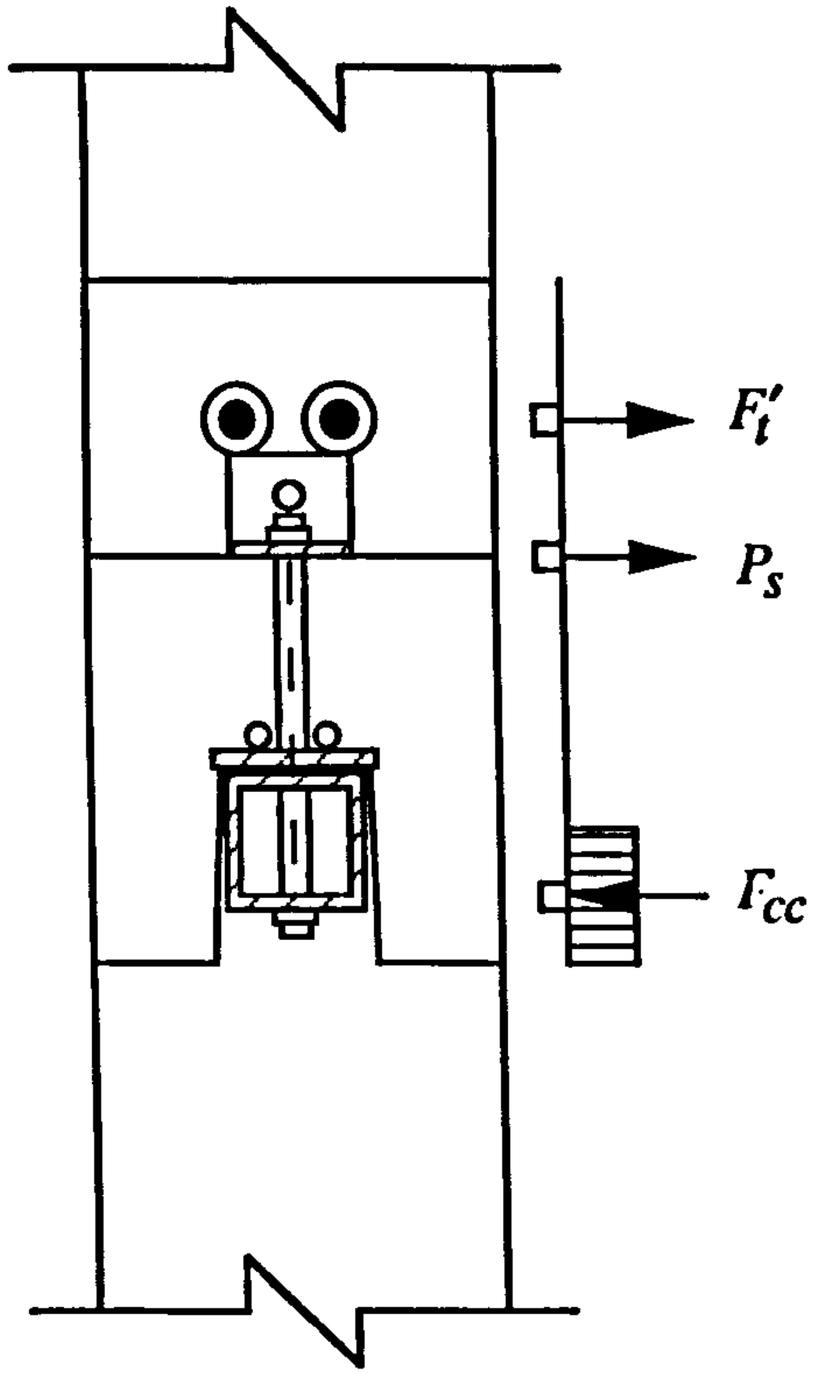

Figure A5.4.2: Internal forces acting on the billet connection

Appendix 6.1

Flexural stiffnesses

Cycle	Stiffness	Tangent flexural stiffnesses of connection (kNm/rad) from the slope of the $M_{con} - \phi$ curves					
Ref.	Ref.	M1 B1 V1	M1 B1 V2	M1 B1 V3	M1 B1 V4	M2 S1	M2 B1
C1	J_u	172100	183800	233900	280400	323400	409100
	J_c	47800	53300	36500	29700	32400	35700
	J_{unl}	89500	93000	79300	72300	81900	91300
C2	J_c	84000	80700	67700	61200	68300	71600
	J_{unl}	91300	89500	76500	69700	77500	84800
C3	J_c	79900	76900	65350	59400	66800	69900
	J_{unl}	79600	79700	69500	64075	74100	81000
C4	J_c	76600	78000	60400	52500	60300	57400
	J_{unl}	95800	87200	72400	65100	70400	72000
C5	J_c	61200	62100	51200	45800	50000	49500
	J_{unl}	53300	53300	49200	46800	49500	48800

Table A6.1.1: Tangent flexural stiffnesses of connection for each cycle in TW1(A) for beam 1 side

Cycle	Stiffness	Tangent flexural stiffnesses of connection (kNm/rad) from the slope of the $M_{con} - \phi$ curves					
Ref.	Ref.	M1 B2 V1	M1 B2 V2	M1 B2 V3	M1 B2 V4	M2 S2	M2 B2
C1	J_u	652900	767500	562500	482300	341100	418500
	J_c	56300	59200	57100	55700	82100	98100
	J_{unl}	138400	148100	148900	149400	208200	249600
C2	J_c	125300	121500	111200	105500	152200	170100
	J_{unl}	143800	149500	134400	126500	188800	220500
C3	J_c	117800	118400	108900	103700	153300	176900
	J_{unl}	150300	156200	135500	125300	179700	209000
C4	J_c	75900	73900	63000	57600	92900	80000
	J_{unl}	113200	110800	95400	87900	134500	136100
C5	J_c	63500	61500	52800	48600	81900	61600
	J_{unl}	51800	42400	38800	36800	48300	42800

Table A6.1.2: Tangent flexural stiffnesses of connection for each cycle in TW1(A) for beam 2 side

Cycle Ref.	Rot. & Stiffness Ref.	Secant flexural stiffnesses of connection (kNm/rad) from the chord of the $M_{con} - \phi$ curves					
		M1 B1 V1	M1 B1 V2	M1 B1 V3	M1 B1 V4	M2 S1	M2 B1
C1	ϕ_{cr}	0.00014	0.000133	0.000105	8.61E-05	7.02E-05	5.42E-05
	ϕ_{peak}	0.001132	0.000973	0.001367	0.001629	0.001472	0.001327
	ϕ_{unl}	0.000338	0.000208	0.00047	0.000645	0.000603	0.000548
	J_{is}	175600	184400	234200	285500	350200	453400
	J_s	62800	73100	52000	43700	48300	53600
C2	ϕ_{peak}	0.001196	0.001063	0.001462	0.001727	0.001542	0.001419
	ϕ_{unl}	0.000403	0.000255	0.000515	0.000689	0.000608	0.000565
	J_s	84300	84600	73000	66900	77100	83100
C3	ϕ_{peak}	0.001288	0.00116	0.00157	0.001844	0.001625	0.001507
	ϕ_{unl}	0.000346	0.000219	0.000492	0.000673	0.000614	0.00058
	J_s	84800	82900	71100	64900	73700	79700

Table A6.1.3: Secant flexural stiffnesses of connection for each cycle in TW1(A) with rotations and K_s values for beam 1 side

Cycle Ref.	Rot. & Stiffness Ref.	Secant flexural stiffnesses of connection (kNm/rad) from the chord of the $M_{con} - \phi$ curves					
		M1 B1 V1	M1 B1 V2	M1 B1 V3	M1 B1 V4	M2 S1	M2 B1
C4	ϕ_{peak}	0.001907	0.001734	0.002375	0.002803	0.002446	0.002446
	ϕ_{unl}	0.000668	0.000373	0.000736	0.000979	0.00076	0.000796
	J_s	76000	78400	63000	55750	64800	63600
C5	ϕ_u	0.007482	0.007018	0.008557	0.009584	0.008999	0.009086
	ϕ_f	0.008964	0.008147	0.009737	0.010797	0.010377	0.010428
	ϕ_{end}	0.004606	0.003658	0.004703	0.005399	0.005244	0.005273
	J_s	35000	35900	30500	27700	29000	28800
	J_{us}	31900	34000	27900	24900	26500	26300
$K_s = \frac{J_s l}{4E_c I_c}$		2.007	2.058	1.749	1.588	1.663	1.651
$K_s = \frac{J_{us} l}{4E_c I_c}$		1.829	1.949	1.600	1.428	1.519	1.508

Table A6.1.3: Secant flexural stiffnesses of connection for each cycle in TW1(A) with rotations and K_s values for beam 1 side (continued)

Cycle Ref.	Stiffness Ref.	Secant flexural stiffnesses of connection (kNm/rad) from the chord of the $M_{con} - \phi$ curves					
		M1 B2 V1	M1 B2 V2	M1 B2 V3	M1 B2 V4	M2 S2	M2 B2
C1	ϕ_{cr}	3.29E-05	2.7E-05	0.000037	4.32E-05	6.66E-05	0.000055
	ϕ_{peak}	0.000892	0.000853	0.000891	0.000915	0.000658	0.000566
	ϕ_{unl}	0.000366	0.000362	0.000403	0.000428	0.000308	0.000275
	J_{is}	699600	854900	622800	532900	346000	419000
	J_s	81600	85300	81600	79500	110600	128500
C2	ϕ_{peak}	0.000812	0.000798	0.000909	0.000977	0.000701	0.000618
	ϕ_{unl}	0.000316	0.000322	0.000379	0.000414	0.000324	0.000295
	J_s	87800	89200	78400	72900	181400	207400
C3	ϕ_{peak}	0.000832	0.000817	0.000939	0.001016	0.000743	0.000654
	ϕ_{unl}	0.000348	0.000351	0.000403	0.000436	0.000338	0.000306
	J_s	87300	89000	77300	71500	173300	202500

Table A6.1.4: Secant flexural stiffnesses of connection for each cycle in TW1(A) with rotations and K_s values for beam 2 side

Cycle Ref.	Rot. & Stiffness Ref.	Secant flexural stiffnesses of connection (kNm/rad) from the chord of the $M_{con} - \phi$ curves					
		M1 B2 V1	M1 B2 V2	M1 B2 V3	M1 B2 V4	M2 S2	M2 B2
C4	ϕ_{peak}	0.001652	0.001651	0.00195	0.002135	0.001416	0.001495
	ϕ_{unl}	0.000606	0.000583	0.000709	0.000788	0.000536	0.000625
	J_s	71700	71700	60700	55400	109800	99600
C5	ϕ_u	0.009274	0.009117	0.010273	0.010991	0.009425	0.009939
	ϕ_f	0.051222	0.031393	0.026764	0.024206	0.03005	0.030547
	ϕ_{end}	0.047672	0.027061	0.022021	0.018889	0.026244	0.02625
	J_s	27300	27800	24800	23200	26700	25400
	J_{us}	25600	26000	23100	21600	25100	23800
$K_s = \frac{J_s l}{4E_c I_c}$		1.565	1.594	1.422	1.330	1.531	1.456
$K_s = \frac{J_{us} l}{4E_c I_c}$		1.468	1.491	1.324	1.238	1.439	1.365

Table A6.1.4: Secant flexural stiffnesses of connection for each cycle in TW1(A) with rotations and K_s values for beam 2 side (continued)

Cycle	Stiffness	Tangent flexural stiffnesses of connection (kNm/rad) from the slope of the $M_{con} - \phi$ curves				
Ref.	Ref.	M1 B1 V1	M1 B1 V2	M1 B1 V3	M1 B1 V4	M2 B1
C1	J_u	474500	391500	251000	205000	31800
	J_c	164200	154500	137100	127900	19000
	J_{unl}	279900	327500	272500	246700	30500
C2	J_c	382100	327500	272500	246700	35000
	J_{unl}	409100	330100	272200	245500	36900
C3	J_c	377100	330100	272200	245500	35100
	J_{unl}	442600	191800	179100	171500	37700
C4	J_c	375300	335000	276700	249700	36000
	J_{unl}	249300	310100	258600	233000	27700
C5	J_c	219600	195700	177400	167600	22500
	J_{unl}	N/A	N/A	N/A	N/A	N/A

Table A6.1.5: Tangent flexural stiffnesses of connection for each cycle in TW1(C) for beam 1 side

Cycle	Stiffness	Tangent flexural stiffnesses of connection (kNm/rad) from the slope of the $M_{con} - \phi$ curves				
Ref.	Ref.	M1 B2 V1	M1 B2 V2	M1 B2 V3	M1 B2 V4	M2 B2
C1	J_u	200200	205100	149400	127800	16800
	J_c	224100	220700	147300	122100	16500
	J_{unl}	286700	300400	218700	186700	24500
C2	J_c	282300	288400	221900	193800	26100
	J_{unl}	288300	304800	232300	202300	26500
C3	J_c	270400	281600	220300	193800	26300
	J_{unl}	270400	272400	213200	187700	27300
C4	J_c	261900	268400	215600	192100	26300
	J_{unl}	290800	306100	238600	209800	26400
C5	J_c	199800	205700	181500	168800	19500
	J_{unl}	293600	293000	293000	293000	24600

Table A6.1.6: Tangent flexural stiffnesses of connection for each cycle in TW1(C) for beam 2 side

Cycle Ref.	Rot. & Stiffness Ref.	Secant flexural stiffnesses of connection (kNm/rad) from the chord of the $M_{con} - \phi$ curves				
		M1 B1 V1	M1 B1 V2	M1 B1 V3	M1 B1 V4	M2 B1
C1	ϕ_{cr}	1.96E-05	2.37E-05	3.69E-05	4.51E-05	0.000288
	ϕ_{peak}	0.000122	0.000133	0.000161	0.000179	0.001192
	ϕ_{unl}	4.18E-05	4.25E-05	5.39E-05	6.1E-05	0.000487
	J_{is}	475300	391500	251900	206200	32200
	J_s	213900	196300	162100	146300	22000
C2	ϕ_{peak}	9.79E-05	0.000111	0.00014	0.000158	0.001172
	ϕ_{unl}	4.03E-05	4.21E-05	5.34E-05	6.04E-05	0.000495
	J_s	460900	375500	300500	267300	22100
C3	ϕ_{peak}	9.9E-05	0.000112	0.000141	0.000159	0.001192
	ϕ_{unl}	4E-05	4.17E-05	5.33E-05	6.05E-05	0.000500
	J_s	435500	363600	290700	258500	21400

Table A6.1.7: Secant flexural stiffnesses of connection for each cycle in TW1(C) with rotations and K_s values for beam 1 side

Cycle Ref.	Rot. & Stiffness Ref.	Secant flexural stiffnesses of connection (kNm/rad) from the chord of the $M_{con} - \phi$ curves				
		M1 B1 V1	M1 B1 V2	M1 B1 V3	M1 B1 V4	M2 B1
C4	ϕ_{peak}	0.000208	0.000236	0.00027	0.000291	0.002149
	ϕ_{unl}	5.71E-05	6.35E-05	7.11E-05	7.58E-05	0.000711
	J_s	249100	216200	193900	182200	19500
C5	ϕ_u	0.000547	0.000613	0.000681	0.000723	0.006056
	ϕ_f	0.001012	0.00112	0.001329	0.001458	0.012839
	ϕ_{end}	0.001629	0.001804	0.003129	0.003953	0.053263
	J_s	152700	136000	122600	115500	13990
	J_{us}	136700	122000	109800	103400	12300
$K_s = \frac{J_s l}{4E_c I_c}$		25.000	22.266	20.073	18.910	2.290
$K_s = \frac{J_{us} l}{4E_c I_c}$		22.381	19.974	17.977	16.929	2.014

Table A6.1.7: Secant flexural stiffnesses of connection for each cycle in TW1(C) with rotations and K_s values for beam 1 side (continued)

Cycle Ref.	Rot. & Stiffness Ref.	Secant flexural stiffnesses of connection (kNm/rad) from the chord of the $M_{con} - \phi$ curves				
		M1 B2 V1	M1 B2 V2	M1 B2 V3	M1 B2 V4	M2 B2
C1	ϕ_{cr}	4.47E-05	4.37E-05	6.02E-05	7.05E-05	0.000539
	ϕ_{peak}	0.000117	0.000117	0.000171	0.000205	0.001544
	ϕ_{unl}	4.77E-05	4.93E-05	7.27E-05	8.72E-05	0.000667
	J_{is}	202900	207700	150600	128600	16800
	J_s	218600	218900	149600	125000	16600
C2	ϕ_{peak}	0.000135	0.00013	0.00018	0.000211	0.001608
	ϕ_{unl}	4.83E-05	4.82E-05	7.23E-05	8.73E-05	0.000675
	J_s	293600	316900	238400	206600	15900
C3	ϕ_{peak}	0.000138	0.000131	0.000182	0.000213	0.001622
	ϕ_{unl}	4.88E-05	4.6E-05	7.29E-05	8.97E-05	0.000682
	J_s	286000	309900	233600	202500	15700

Table A6.1.8: Secant flexural stiffnesses of connection for each cycle in TW1(C) with rotations and K_s values for beam 2 side

Cycle Ref.	Rot. & Stiffness Ref.	Secant flexural stiffnesses of connection (kNm/rad) from the chord of the $M_{con} - \phi$ curves				
		M1 B2 V1	M1 B2 V2	M1 B2 V3	M1 B2 V4	M2 B2
C4	ϕ_{peak}	0.000206	0.0002	0.000267	0.000309	0.002430
	ϕ_{unl}	6.8E-05	6.03E-05	9.23E-05	0.000112	0.000883
	J_s	264300	271000	214600	190000	17100
C5	ϕ_u	0.000605	0.000586	0.00069	0.000754	0.006968
	ϕ_f	0.00061	0.000593	0.00069	0.000754	0.006932
	ϕ_{end}	0.000454	0.000422	0.000463	0.000488	0.004047
	J_s	142100	145200	127800	119000	12500
	J_{us}	126200	130300	110700	101300	11000
$K_s = \frac{J_s l}{4E_c I_c}$		23.265	23.773	20.924	19.483	2.047
$K_s = \frac{J_{us} l}{4E_c I_c}$		20.662	21.333	18.124	16.585	1.801

Table A6.1.8: Secant flexural stiffnesses of connection for each cycle in TW1(C) with rotations and K_s values for beam 2 side (continued)

Cyc. Ref.	Stiff. Ref.	Tangent flexural stiffnesses of connection (kNm/rad) from the slope of the $M_{con} - \phi$ curves				
		M1 B1 V1	M1 B1 V2	M1 B1 V3	M1 B1 V4	M2 S1
C1	J_u	55000	57000	59500	60800	1190500
	J_c	9400	9300	9300	9300	12900
	J_{unl}	28400	28200	28700	28900	56400
C2	J_c	22300	22200	22600	22800	38800
	J_{unl}	24500	24500	25000	25300	46100
C3	J_c	22000	21800	22100	22200	38400
	J_{unl}	23400	23300	23700	24000	42700
C4	J_c	21300	21100	21300	21500	36700
	J_{unl}	14700	14700	14500	14400	20600
C5	J_c	14100	14300	14000	13800	19400
	J_{unl}	10000	10800	10100	9900	15000

Table A6.1.9: Tangent flexural stiffnesses of connection for each cycle in TW2

Cyc	Rot. & Stiffness	Secant flexural stiffnesses of connection (kNm/rad) from the chord of the $M_{con}-\phi$ curves				
Ref	Ref.	M1 B1 V1	M1 B1 V2	M1 B1 V3	M1 B1 V4	M2 S1
C1	ϕ_{cr}	0.000994	0.000953	0.000894	0.000864	4.2449E-05
	ϕ_{peak}	0.004609	0.004583	0.004535	0.00451	0.00260653
	ϕ_{unl}	0.002203	0.002167	0.002164	0.002162	0.00143347
	J_{is}	35100	36600	39000	40300	820800
	J_s	15200	15300	15500	15600	26900
C2	ϕ_{peak}	0.005062	0.005045	0.004978	0.004944	0.00300837
	ϕ_{unl}	0.002349	0.002338	0.00234	0.002342	0.00162306
	J_s	24700	24500	25100	25400	44800
C3	ϕ_{peak}	0.005308	0.005305	0.005243	0.00521	0.0032451
	ϕ_{unl}	0.002431	0.002421	0.00242	0.002419	0.00171633
	J_s	23900	23900	24400	24700	43600

Table A6.1.10: Secant flexural stiffnesses of connection for each cycle in TW2 with rotations and K_s values

Cyc Ref	Rot. & Stiffness Ref.	Secant flexural stiffnesses of connection (kNm/rad) from the chord of the $M_{con} - \phi$ curves				
		M1 B1 V1	M1 B1 V2	M1 B1 V3	M1 B1 V4	M2 S1
C4	ϕ_{peak}	0.011457	0.011392	0.011506	0.011565	0.0084351
	ϕ_{unl}	0.005149	0.004798	0.005135	0.005309	0.00429571
	J_s	12800	12800	12700	12600	17100
C5	ϕ_u	0.036843	0.034839	0.037318	0.03859	0.03054551
	ϕ_f	0.039077	0.036729	0.039454	0.040854	0.03236408
	ϕ_{end}	0.024272	0.022973	0.024844	0.025804	0.02251306
	J_s	4900	5200	4900	4700	6000
	J_{us}	4200	4500	4200	4100	5100
$K_s = \frac{J_s l}{4E_c I_c}$		0.285	0.303	0.285	0.273	0.349
$K_s = \frac{J_{us} l}{4E_c I_c}$		0.244	0.262	0.244	0.239	0.297

Table A6.1.10: Secant flexural stiffnesses of connection for each cycle in TW2 with rotations and K_s values (continued)

Cycle	Stiffness	Tangent flexural stiffnesses of connection (kNm/rad) from the slope of the $M_{con} - \phi$ curves					
Ref.	Ref.	M1 B1 V1	M1 B1 V2	M1 B1 V3	M1 B1 V4	M2 S1	M2 B1
C1	J_u	171920	247310	POT18 faulty		171230	189250
	J_c	62660	58190			48010	57780
	J_{unl}	111500	111670			100280	128200
C2	J_c	114020	110330			96300	131070
	J_{unl}	99090	100150			104330	133630
C3	J_c	115820	115420			96590	129230
	J_{unl}	105150	119040			104040	132730
C4	J_c	92740	95470			87320	93200
	J_{unl}	75530	77470			94570	103650
C5	J_c	55600	56370			66110	49820
	J_{unl}	57410	62480			66260	56750

Table A6.1.11: Tangent flexural stiffnesses of connection for each cycle in TB1(A) for beam 1 side

Cycle	Stiffness	Tangent flexural stiffnesses of connection (kNm/rad) from the slope of the $M_{con} - \phi$ curves					
Ref.	Ref.	M1 B2 V1	M1 B2 V2	M1 B2 V3	M1 B2 V4	M2 S2	M2 B2
C1	J_u	145830	271000	204120	178930	292010	334270
	J_c	43030	43470	35600	32510	37680	34520
	J_{unl}	91660	77180	65350	60370	POT9 faulty	POT9 faulty
C2	J_c	85090	81840	68220	62790		
	J_{unl}	85900	90830	75060	68660		
C3	J_c	88310	82300	68340	62780		
	J_{unl}	75120	78250	66950	62020		
C4	J_c	68630	67140	53770	48730		
	J_{unl}	70340	70260	57980	53010		
C5	J_c	44000	43440	35450	32400		
	J_{unl}	46620	47080	39400	36330		

Table A6.1.12: Tangent flexural stiffnesses of connection for each cycle in TB1(A) for beam 2 side

Cycle Ref.	Rot. & Stiffness Ref.	Secant flexural stiffnesses of connection (kNm/rad) from the chord of the $M_{con} - \phi$ curves					
		M1 B1 V1	M1 B1 V2	M1 B1 V3	M1 B1 V4	M2 S1	M2 B1
C1	ϕ_{cr}	0.000135	0.0000916	POT18 faulty		0.000122	0.000115
	ϕ_{peak}	0.000914	0.000922			0.001128	0.000965
	ϕ_{unl}	0.000302	0.000362			0.000508	0.000527
	J_{is}	172850	254625			191180	202140
	J_s	78800	78120			63840	74590
C2	ϕ_{peak}	0.000934	0.000977			0.001192	0.001042
	ϕ_{unl}	0.000328	0.000375			0.000508	0.000531
	J_s	114710	118050			106040	140730
C3	ϕ_{peak}	0.000915	0.000957			0.001204	0.001062
	ϕ_{unl}	0.000268	0.000360			0.000522	0.000542
	J_s	122430	123560			103410	135600

Table A6.1.13: Secant flexural stiffnesses of connection for each cycle in TB1(A) with rotations and K_s values for beam 1 side

Cycle Ref.	Rot. & Stiffness Ref.	Secant flexural stiffnesses of connection (kNm/rad) from the chord of the $M_{con} - \phi$ curves					
		M1 B1 V1	M1 B1 V2	M1 B1 V3	M1 B1 V4	M2 S1	M2 B1
C4	ϕ_{peak}	0.001531	0.001503	POT18 faulty		0.001946	0.001958
	ϕ_{unl}	0.000197	0.000150			0.000688	0.000812
	J_s	95340	97600			87190	91770
C5	ϕ_u	0.005726	0.009443			0.006594	0.007662
	ϕ_f	0.005987	0.009443			0.006678	0.007750
	ϕ_{end}	0.002797	0.002849			0.003914	0.004523
	J_s	34550	20590			32400	27440
	J_{us}	33360	20260			29020	24970
$K_s = \frac{J_s l}{4E_c I_c}$		1.986	1.183			1.862	1.577
$K_s = \frac{J_{us} l}{4E_c I_c}$		1.917	1.165			1.668	1.435

Table A6.1.13: Secant flexural stiffnesses of connection for each cycle in TB1(A) with rotations and K_s values for beam 1 side (continued)

Cycle Ref.	Stiffness Ref.	Secant flexural stiffnesses of connection (kNm/rad) from the chord of the $M_{con} - \phi$ curves					
		M1 B2 V1	M1 B2 V2	M1 B2 V3	M1 B2 V4	M2 S2	M2 B2
C1	ϕ_{cr}	0.000161	0.0000876	0.000111	0.000123	0.0000726	0.0000627
	ϕ_{peak}	0.001193	0.001109	0.001383	0.001525	POT9 Faulty	
	ϕ_{unl}	0.000588	0.000355	0.000488	0.000557		
	J_{is}	148320	272680	215660	194630	329150	381160
	J_s	59490	63980	51300	46530		
C2	ϕ_{peak}	0.001370	0.001158	0.001454	0.001607		
	ϕ_{unl}	0.000549	0.000389	0.000507	0.000568		
	J_s	90910	88540	73590	67690		
C3	ϕ_{peak}	0.001396	0.001192	0.001487	0.001640		
	ϕ_{unl}	0.000563	0.000407	0.000510	0.000563		
	J_s	83620	88220	72260	66080		

Table A6.1.14: Secant flexural stiffnesses of connection for each cycle in TB1(A) with rotations and K_s values for beam 2 side

Cycle Ref.	Rot. & Stiffness Ref.	Secant flexural stiffnesses of connection (kNm/rad) from the chord of the $M_{con} - \phi$ curves					
		M1 B2 V1	M1 B2 V2	M1 B2 V3	M1 B2 V4	M2 S2	M2 B2
C4	ϕ_{peak}	0.002453	0.002296	0.002790	0.003046	POT9 Faulty	
	ϕ_{unl}	0.000894	0.000717	0.000819	0.000872		
	J_s	66680	65820	53130	48320		
C5	ϕ_u	0.010344	0.010592	0.013736	0.015361		
	ϕ_f	0.010696	0.010780	0.013897	0.015508		
	ϕ_{end}	0.006829	0.006951	0.009321	0.010546		
	J_s	19920	19060	14570	12990		
	J_{us}	18200	17770	13700	12250		
$K_s = \frac{J_s l}{4E_c I_c}$		1.145	1.095	0.837	0.747		
$K_s = \frac{J_{us} l}{4E_c I_c}$		1.046	1.021	0.787	0.704		

Table A6.1.14: Secant flexural stiffnesses of connection for each cycle in TB1(A) with rotations and K_s values for beam 2 side (continued)

Cycle Ref.	Stiffness Ref.	Tangent flexural stiffnesses of connection (kNm/rad) from the slope of the $M_{con} - \phi$ curves			
		M2 S1	M2 B1	M2 S2	M2 B2
C1	J_u	83260	66830	99210	94000
	J_c	50580	43020	59880	60640
	J_{unl}	70000	65400	91520	91350
C2	J_c	65450	62850	84900	87310
	J_{unl}	66160	64100	85930	86850
C3	J_c	67440	59540	82500	82530
	J_{unl}	69160	62100	86960	87470
C4	J_c	65300	48160	65980	64900
	J_{unl}	70720	55420	76730	74740
C5	J_c	62240	33650	63340	26620
	J_{unl}	67130	42430	N/A	N/A

Table A6.1.15: Tangent flexural stiffnesses of connection for each cycle in TB1(B) for both beams

Cycle Ref.	Rot. & Stiffness Ref.	Secant flexural stiffnesses of connection (kNm/rad) from the chord of the $M_{con} - \phi$ curves			
		M2 S1	M2 B1	M2 S2	M2 B2
C1	ϕ_{cr}	0.000266	0.000318	0.0002	0.000207
	ϕ_{peak}	0.000938	0.001113	0.000759	0.000761
	ϕ_{unl}	0.00012	0.000243	0.000156	0.00017
	J_{is}	91040	76280	114860	111030
	J_s	61850	52150	74400	74240
C2	ϕ_{peak}	0.000981	0.001133	0.000803	0.000795
	ϕ_{unl}	0.000129	0.000272	0.000163	0.000177
	J_s	67400	65170	87790	90880
C3	ϕ_{peak}	0.000977	0.001234	0.000828	0.000831
	ϕ_{unl}	0.000123	0.000274	0.000168	0.000181
	J_s	68940	60450	85740	87010

Table A6.1.16: Secant flexural stiffnesses of connection for each cycle in TB1(B) with rotations and K_s values for both beams

Cycle Ref.	Rot. & Stiffness Ref.	Secant flexural stiffnesses of connection (kNm/rad) from the chord of the $M_{con} - \phi$ curves			
		M2 S1	M2 B1	M2 S2	M2 B2
C4	ϕ_{peak}	0.001576	0.002248	0.001594	0.001637
	ϕ_{unl}	0.000203	0.000503	0.00035	0.00037
	J_s	66410	48890	66680	65300
C5	ϕ_u	0.003046	0.005805	0.002874	0.007034
	ϕ_f	0.00319	0.006184	0.002874	0.009431
	ϕ_{end}	0.000861	0.0025	0.002126	0.028378
	J_s	61080	32770	67360	25680
	J_{us}	57370	30100	59720	24400
$K_s = \frac{J_s l}{4E_c I_c}$		3.490	1.872	3.849	1.467
$K_s = \frac{J_{us} l}{4E_c I_c}$		3.278	1.720	3.412	1.394

Table A6.1.16: Secant flexural stiffnesses of connection for each cycle in TB1(B) with rotations and K_s values for both beams (continued)

Cycle Ref.	Stiffness Ref.	Tangent flexural stiffnesses of connection (kNm/rad) from the slope of the $M_{con} - \phi$ curves			
		M2 S1	M2 B1	M2 S2	M2 B2
C1	J_u	59740	63240	98290	117270
	J_c	55890	55060	49000	50660
	J_{unl}	97550	109090	76830	82830
C2	J_c	73060	80450	67440	73810
	J_{unl}	93930	107990	75000	80810
C3	J_c	71020	78020	65520	70900
	J_{unl}	93000	105920	74320	80510
C4	J_c	61220	61130	58980	49600
	J_{unl}	88120	87990	71770	63910
C5	J_c	63360	33240	64830	26820
	J_{unl}	109350	63640	75620	45590

Table A6.1.17: Tangent flexural stiffnesses of connection for each cycle in TB1(C) for both beams

Cycle Ref.	Rot. & Stiffness Ref.	Secant flexural stiffnesses of connection (kNm/rad) from the chord of the $M_{con} - \phi$ curves			
		M2 S1	M2 B1	M2 S2	M2 B2
C1	ϕ_{cr}	0.000257	0.000242	0.000161	0.000135
	ϕ_{peak}	0.000999	0.000999	0.000988	0.000941
	ϕ_{unl}	0.000238	0.000305	0.000204	0.000228
	J_{is}	60040	63630	96440	115290
	J_s	57050	57070	57060	59950
C2	ϕ_{peak}	0.001043	0.001032	0.001033	0.000977
	ϕ_{unl}	0.000239	0.000317	0.000189	0.000208
	J_s	71720	79440	69230	76820
C3	ϕ_{peak}	0.001058	0.001057	0.001037	0.000982
	ϕ_{unl}	0.000241	0.000315	0.000196	0.000216
	J_s	30480	33650	29660	32460

Table A6.1.18: Secant flexural stiffnesses of connection for each cycle in TB1(C) with rotations and K_s values for both beams

Cycle Ref.	Rot. & Stiffness Ref.	Secant flexural stiffnesses of connection (kNm/rad) from the chord of the $M_{con} - \phi$ curves			
		M2 S1	M2 B1	M2 S2	M2 B2
C4	ϕ_{peak}	0.001881	0.001958	0.001804	0.002101
	ϕ_{unl}	0.000476	0.000545	0.000328	0.000497
	J_s	58790	58660	58700	50030
C5	ϕ_u	0.003367	0.006208	0.003084	0.007407
	ϕ_f	0.003367	0.011394	0.003084	0.007407
	ϕ_{end}	N/A	N/A	N/A	N/A
	J_s	60050	30660	63080	25160
	J_{us}	51600	27980	56380	23470
$K_s = \frac{J_s l}{4E_c I_c}$		3.452	1.762	3.625	1.446
$K_s = \frac{J_{us} l}{4E_c I_c}$		2.965	1.608	3.241	1.349

Table A6.1.18: Secant flexural stiffnesses of connection for each cycle in TB1(C) with rotations and K_s values for both beams (continued)

Cyc. Ref.	Stiff. Ref.	Tangent flexural stiffnesses of connection (kNm/rad) from the slope of the $M_{con} - \phi$ curves					
		M1 B1 V1	M1 B1 V2	M1 B1 V3	M1 B1 V4	M2 S1	M2 B1
C1	J_u	28330	28390	27270	26670	64000	136010
	J_c	3030	2720	1990	1750	1820	2380
	J_{unl}	18480	17250	13800	12490	15570	21020
C2	J_c	15510	14270	11390	10300	12190	16260
	J_{unl}	153200	14660	11920	10850	12770	17250
C3	J_c	14290	13230	10510	9490	10950	14730
	J_{unl}	15320	14210	11690	10700	12450	16610
C4	J_c	13540	12330	9970	9060	10240	13700
	J_{unl}	10900	10340	8480	7750	8770	12610
C5	J_c	8310	7860	6250	5640	6030	11240
	J_{unl}	9830	9420	7690	7020	8000	18640

Table A6.1.19: Tangent flexural stiffnesses of connection for each cycle in TB2

Cyc	Rot. & Stiffness	Secant flexural stiffnesses of connection (kNm/rad) from the chord of the $M_{con} - \phi$ curves					
Ref	Ref.	M1 B1 V1	M1 B1 V2	M1 B1 V3	M1 B1 V4	M2 S1	M2 B1
C1	ϕ_{cr}	0.000956	0.000894	0.000975	0.001017	0.000399	0.000187
	ϕ_{peak}	0.007808	0.008445	0.010887	0.012162	0.010824	0.007785
	ϕ_{unl}	0.005096	0.005571	0.007306	0.008211	0.00766	0.005508
	J_{is}	29780	31870	29230	28020	71350	152370
	J_s	7120	6580	5100	4570	5130	7140
C2	ϕ_{peak}	0.00892	0.009685	0.012542	0.014033	0.012731	0.009213
	ϕ_{unl}	0.005689	0.006244	0.008316	0.009397	0.008831	0.006369
	J_s	14340	13550	10480	9370	10780	14760
C3	ϕ_{peak}	0.009793	0.010702	0.013905	0.015576	0.014303	0.010364
	ϕ_{unl}	0.006368	0.007011	0.009383	0.01062	0.010085	0.007255
	J_s	13540	12510	9950	8990	10150	13890

Table A6.1.20: Secant flexural stiffnesses of connection for each cycle in TB2 with rotations and K_s values

Cyc Ref	Rot. & Stiffness Ref.	Secant flexural stiffnesses of connection (kNm/rad) from the chord of the $M_{con} - \phi$ curves					
		M1 B1 V1	M1 B1 V2	M1 B1 V3	M1 B1 V4	M2 S1	M2 B1
C4	ϕ_{peak}	0.02029	0.022119	0.02934	0.033108	0.031449	0.018778
	ϕ_{unl}	0.02023	0.022161	0.029349	0.033099	0.032543	0.018757
	J_s	4150	3820	2890	2570	2700	5010
C5	ϕ_u	0.024473	0.026915	0.035599	0.04013	0.039281	0.019418
	ϕ_f	0.02479	0.0273	0.035936	0.040441	0.039672	0.019521
	ϕ_{end}	0.019546	0.021824	0.029099	0.032895	0.032956	0.016725
	J_s	5860	5420	4220	3780	4040	10490
	J_{us}	2240	2040	1540	1370	1400	2830
$K_s = \frac{J_s l}{4E_c I_c}$		0.337	0.311	0.242	0.217	0.232	0.603
$K_s = \frac{J_{us} l}{4E_c I_c}$		0.129	0.117	0.089	0.079	0.080	0.163

Table A6.1.20: Secant flexural stiffnesses of connection for each cycle in TB2 with rotations and K_s values (continued)

Appendix 11.1

Secant flexural stiffnesses

Cycle Ref.	Rot. & Stiffness Ref.	Secant flexural stiffnesses of connection (kNm/rad) from the chord of the $M_{con} - \phi$ curves					
		M1 B1 V1	M1 B1 V2	M1 B1 V3	M1 B1 V4	M2 S1	M2 B1
C5	M_e	205.00	207.00	200.10	195.60	199.7	199.3
	ϕ_e	0.00387	0.00364	0.00444	0.00495	0.00448	0.00453
	J_e	64000	63400	54000	49300	53700	53400
	J_{es}	53000	56900	45100	39500	44600	44000
$K_s = \frac{J_e l}{4E_c I_c}$		4.000	3.635	3.096	2.827	3.079	3.062
$K_s = \frac{J_{es} l}{4E_c I_c}$		3.039	3.262	2.586	2.265	2.557	2.523

Table A11.1.1: Secant flexural stiffnesses of connection at intersection with beam-line in TW1(A) with rotations and K_s values for beam 1 side

Cycle Ref.	Stiffness Ref.	Secant flexural stiffnesses of connection (kNm/rad) from the chord of the $M_{con} - \phi$ curves					
		M1 B2 V1	M1 B2 V2	M1 B2 V3	M1 B2 V4	M2 S2	M2 B2
C5	M_e	205.40	205.00	200.80	198.40	210	205
	ϕ_e	0.00361	0.00364	0.00415	0.00442	0.0031	0.00364
	J_e	68400	67100	58400	54600	81900	68000
	J_{es}	56900	56300	48400	44900	67700	56300
$K_s = \frac{J_e l}{4E_c I_c}$		3.922	3.847	3.348	3.131	4.696	3.899
$K_s = \frac{J_{es} l}{4E_c I_c}$		3.262	3.228	2.775	2.574	3.882	3.228

Table A11.1.2: Secant flexural stiffnesses of connection at intersection with beam-line in TW1(A) with rotations and K_s values for beam 2 side

Cycle Ref.	Rot. & Stiffness Ref.	Secant flexural stiffnesses of connection (kNm/rad) from the chord of the $M_{con} - \phi$ curves	
		M2 B1	M2 B2
C5	M_e	64.00	62.5
	ϕ_e	0.0035	0.0040
	J_e	22900	20100
	J_{es}	18300	15600
$K_s = \frac{J_e l}{4E_c I_c}$		3.749	3.291
$K_s = \frac{J_{es} l}{4E_c I_c}$		2.996	2.554

Table A11.1.3: Secant flexural stiffnesses of connection at intersection with beam-line in TW1(C) with rotations and K_s values for both beams

Cyc Ref	Rot. & Stiffness Ref.	Secant flexural stiffnesses of connection (kNm/rad) from the chord of the $M_{con} - \phi$ curves				
		M1 B1 V1	M1 B1 V2	M1 B1 V3	M1 B1 V4	M2 S1
C4	M_e	91.75	91.75	91.75	91.75	102.20
	ϕ_e	0.0075	0.0075	0.0075	0.0075	0.0063
	J_e	18100	18100	18100	18100	22300
	J_{es}	12200	12200	12200	12200	16200
$K_s = \frac{J_e l}{4E_c I_c}$		1.053	1.053	1.053	1.053	1.297
$K_s = \frac{J_{es} l}{4E_c I_c}$		0.710	0.710	0.710	0.710	0.940

Table A11.1.4: Secant flexural stiffnesses of connection at intersection with beam-line in TW2 with rotations and K_s values

Cycle Ref.	Rot. & Stiffness Ref.	Secant flexural stiffnesses of connection (kNm/rad) from the chord of the $M_{con}-\phi$ curves					
		M1 B1 V1	M1 B1 V2	M1 B1 V3	M1 B1 V4	M2 S1	M2 B1
C5	M_e	167.20	167.80	POT18 Faulty		166.00	162.20
	ϕ_e	0.002775	0.0027			0.00291	0.00335
	J_e	64860	65810			74710	63900
	J_{es}	60250	62150			57040	48420
$K_s = \frac{J_e\, l}{4E_c I_c}$		3.728	3.782			4.294	3.672
$K_s = \frac{J_{es}\, l}{4E_c I_c}$		3.463	3.572			3.279	2.783

Table A11.1.5: Secant flexural stiffnesses of connection at intersection with beam-line in TB1(A) with rotations and K_s values for beam 1 side

Cycle Ref.	Stiffness Ref.	Secant flexural stiffnesses of connection (kNm/rad) from the chord of the $M_{con}-\phi$ curves					
		M1 B2 V1	M1 B2 V2	M1 B2 V3	M1 B2 V4	M2 S2	M2 B2
C5	M_e	156	157	152	149.75	POT9 Faulty	
	ϕ_e	0.0037	0.00358	0.00415	0.00444		
	J_e	55590	54840	45640	41970		
	J_{es}	42160	43850	36630	33730		
$K_s = \frac{J_e\, l}{4E_c I_c}$		3.195	3.152	2.623	2.412		
$K_s = \frac{J_{es}\, l}{4E_c I_c}$		2.423	2.521	2.105	1.938		

Table A11.1.6: Secant flexural stiffnesses of connection at intersection with beam-line in TB1(A) with rotations and K_s values for beam 2 side

Cycle Ref.	Rot. & Stiffness Ref.	Secant flexural stiffnesses of connection (kNm/rad) from the chord of the $M_{con} - \phi$ curves			
		M2 S1	M2 B1	M2 S2	M2 B2
C5	M_e	159.5	148.5	159.5	150
	ϕ_e	0.00275	0.004	0.00275	0.00385
	J_e	62620	42470	66470	43110
	J_{es}	58000	37125	58000	38960
$K_s = \frac{J_e l}{4E_c I_c}$		3.577	2.426	3.797	2.463
$K_s = \frac{J_{es} l}{4E_c I_c}$		3.314	2.121	3.314	2.226

Table A11.1.7: Secant flexural stiffnesses of connection at intersection with beam-line in TB1(B) with rotations and K_s values for both beams

Cycle Ref.	Rot. & Stiffness Ref.	Secant flexural stiffnesses of connection (kNm/rad) from the chord of the $M_{con} - \phi$ curves			
		M2 S1	M2 B1	M2 S2	M2 B2
C5	M_e	152	142	154	139.5
	ϕ_e	0.0029	0.00405	0.0027	0.00435
	J_e	62710	40510	64930	36210
	J_{es}	52410	35060	57040	32070
$K_s = \frac{J_e l}{4E_c I_c}$		3.604	2.328	3.732	2.081
$K_s = \frac{J_{es} l}{4E_c I_c}$		3.012	2.015	3.278	1.843

Table A11.1.8: Secant flexural stiffnesses of connection at intersection with beam-line in TB1(C) with rotations and K_s values for both beams

Cyc	Rot. & Stiffness	Secant flexural stiffnesses of connection (kNm/rad) from the chord of the $M_{con} - \phi$ curves					
Ref	Ref.	M1 B1 V1	M1 B1 V2	M1 B1 V3	M1 B1 V4	M2 S1	M2 B1
C1	M_e	39	39	38	37.75	40	42
	ϕ_e	0.0022	0.0022	0.00228	0.00232	0.00208	0.00183
	J_e	N/A	N/A	N/A	N/A	N/A	N/A
	J_{es}	17730	17730	16670	16270	19230	22950
$K_s = \frac{J_e l}{4E_c I_c}$		N/A	N/A	N/A	N/A	N/A	N/A
$K_s = \frac{J_{es} l}{4E_c I_c}$		1.019	1.019	0.958	0.935	1.105	1.319

Table A11.1.9: Secant flexural stiffnesses of connection at intersection with beam-line in TB2 with rotations and K_s values

REFERENCES

ACI-ASCE Committee 352. Recommendations for design of beam-column joints in monolithic reinforced concrete structures. ACI 352 R-7, American Concrete Institute, Detroit, 1976, 19 pp.

Aksogan, O. and Görgün, H. The non-linear analysis of planar frames composed of flexurally connected members, Cukurova University Journal, Faculty of Engineering and Architecture, Vol. 8, No. 2, December 1993, pp. 117-129.

Anderson, D., Colson, A. and Jaspart, J.P. Connections and frame design for economy. New Steel Construction. October 1993, pp. 30- 33.

Bhatt, P., Kirk, D.W. Tests on an improved beam-column connections for precast concrete. ACI Journal/November-December 1985, pp. 835-843

Bijlaard, F.S.K. and Steenhuis, C.M. Prediction of the influence of connection behaviour on the strength, deformations and stability of frames, by classification of connections. American Institute of Steel Construction, INC. April 1991, pp. 307-318.

Bison Floors Limited. Amington House, Silica Road, Tamworth, Staffordshire B77 4AZ U.K.

Bjorhovde, R., Colson, A. and Brozzetti, J. Classification system for beam-to-column connections. The Journal of Structural Engineering. Vol. 116, No. 11. November 1990, pp. 3059-3070.

Bljuger, F. Design of precast concrete structures. Ellis Horwood Series. John Wiley. 1988, 296 pp.

Briquet, C., Guisse, S., Jaspart, J. P., Lognard, B. and Maquoi, R. Research activities under COST C1 at the Department MSM of the University of Liege, COST

C1 Proceedings of the 2nd Workshop, Semi-rigid Behaviour of Civil Engineering Structural Connections, Prague, October 1994, pp. 75-88.

British Standard Institution, 1983 : BS 12 Specification for ordinary and rapid hardening Portland cement.

British Standard Institution, 1983 : BS 1881 Method of testing concrete.

British Standard Institution 1985: BS 5950 Part 1 Structural use of steelwork in building.

British Standard Institution 1985:

BS 8110: Part 1: Structural use of concrete, Code of practice for design and construction.

BS 8110: Part 2: Code of practice for special circumstances.

BS 8110: Part 3: Design charts for simply reinforced beams.

BS 4449: 1988: British Standard specification for carbon steel bars for the reinforcement of concrete.

British Standard BS EN 10 002-1: 1990: Part 1: Tensile testing of metallic materials, Method of test at ambient temperature

British Standard Institution, 1992 : BS 882 Specification for aggregates from natural sources.

City University. Semi-rigid connections in precast concrete frames, Grant Reference No GR/K20866.

Clarke, J.L. Tests on embedded steel billets for precast concrete beam-to-column connections. Cement and Concrete Association Publication 42.523, August 1978.

Comair, F. and Dardare, J. Investigation on the behaviour of semi-rigid precast beam-to-column connections. Part 1. CERIB DPO FCO/MM 1991/04/09 EX 9102.

Comair, F. and Dardare, J. Model testing of precast semi-rigid beam-column connection. Proceedings of the First State of the Art Workshop, COST C1, Strasbourg, October 1992, pp. 99 -119.

Cranston, W.B. Analysis and design of reinforced concrete columns, Research Report 20, Cement and Concrete. Association, 52 Grosvenor Gardens, London SW1W OAQ, 1972, 54 pp.

Crendon Structures Ltd. Thame Road, Long Crendon, Aylesbury Bucks, Long Crendon 206481.

Davies, G., Elliott, K.S. and Mahdi, A. A. Progress Report 1 to the Precast Concrete Frames Association, The effect of moment-rotation behaviour of connections on the stability of precast concrete structures, Dept. of Civil Eng. Nottingham University, 28 September 1989.

de Chefdebien, A. and Dardare, J. Experimental investigations on current connections between precast concrete components. COST C1 Proceedings of the 2nd. Workshop, Semi-rigid Behaviour of Civil Engineering Structural Connections, Prague, 26-28 October 1994, pp. 21-30.

Dolan, C.W., Stanton, J.F. and Anderson, R.G. Moment resistant connections and simple connections. Specially Funded R&D Program, PCISFRAD Projects 1 and 4. PCI Journal/March-April 1987, pp. 62-74.

Dolan, C.W., Pessiki, S.P. Model testing of precast concrete connections. PCI Journal/March-April 1989, pp. 85-103.

Durrani, A.J. and Wight, J.K. Behaviour of interior beam-to-column connections under earthquake-type loading. ACI Journal / May-June 1985, pp. 343-349.

Ehsani, M.R. and Wight, J.K. Exterior reinforced concrete beam-to-column connections subjected to earthquake-type loading. ACI Journal / July-August 1985, pp. 492-499.

Elliott, K.S. and Tovey, A.K. Precast concrete frame buildings. Design guide. British Cement Association, Wexham Springs, Slough SL3 6PL, 1992a, 88 pp.

Elliott, K.S., Davies, G. and Mahdi, A. A. Semi-rigid joint behaviour on columns in precast concrete buildings. Proceedings of the First State of the Art Workshop, COST C1, Strasbourg, October 1992b, pp. 282-295.

Elliott, K.S., Görgün, H., Virdi, K.S., and Ragupathy, P. Report to the Precast Concrete Frames Association, on analysis and design of a-3 storey precast concrete sway frame, Dept. of Civil Eng. Nottingham University & Dept. of Civil Eng. City University, August 1994a.

Elliott, K.S., Davies, G. and Görgün, H Determination of moment-rotation in semi rigid precast concrete connections using the component method, COST C1 Proceedings of the 2nd. Workshop, Semi-rigid Behaviour of Civil Engineering Structural Connections, Prague, 26-28 October 1994b, pp. 31-40.

Elliott, K.S. Minutes of 2nd Meeting of Concrete Structures Working Group. COST Project C1 'Semi-rigid Behaviour', 23 May 1994c, pp. 1-7.

Elliott, K.S. Minutes of 4th Concrete Structures Working Group WG1 Meeting. COST Project C1 'Semi-rigid Behaviour', 15 December 1995a, pp. 1-12.

Elliott, K.S. Minutes of 1st Meeting of Concrete Structures WG1-UK Branch. University of Nottingham, 15 February 1995b, pp. 1-6.

Elliott, K.S. Multi-storey precast concrete framed structures, Blackwell Science Ltd. 1996a, Oxford, UK, 624 pp.

Elliott, K.S., Davies, G. and Görgün, H. Component method validation tests in precast concrete semi rigid connections, Semi-rigid Structural Connections, Proc. IABSE Colloquium, Vol. 75, Istanbul, September 1996b, pp. 299-308.

Elliott, K.S., Davies, G. and Görgün, H. Effective length factors in precast concrete frames, Semi-rigid Structural Connections, Proc. IABSE Colloquium, Vol. 75, Istanbul, September 1996c, p349-358.

Elliott, K.S., Davies, G. and Görgün, H. Semi-rigid connections in precast concrete frames. Report to EPSRC. Grand No. GR/K17286. Dept. of Civil Eng. Nottingham University, October 1996d.

Elliott, K.S. The European research effort on the stability of precast concrete structures. The 4th International Symposium on Noteworthy Developments in Prestressing & Precasting, Singapore, 3-4 July 1997a, pp. 69-77.

Elliott, K.S., Davies, G. and Görgün, H. Semi-rigid connections in precast concrete frames. FIP Symposium, Johannesburg, 10-12 March 1997b.

Eurocode 2: Design of concrete structures. General rules and rules for buildings. 1992.

Eurocode 3: Design of steel structures-Part 1.1: General rules and rules for buildings. April 1992.

FIP Commission on Prefabrication, Design of multi-storey precast concrete structures, Thomas Telford Ltd, Telford House, PO Box 101, 26-34 Old Street, London EC1P 1JH, England, 1986.

Görgün, H. Dugum noktalarina donel yaylarla bagli cubuklardan olusan duzlemsel cercevelerin non-linear analizi (in Turkish). M.Sc. Thesis, University of Cukurova, Department of Civil Engineering, July 1992.

Görgün, H., Elliott, K.S. and Davies, G. Semi-rigid behaviour of connections in precast concrete structures. Progress Report 1, No. SR 95 029. Dept. of Civil Eng. Nottingham University, September 1994.

Görgün, H., Elliott, K.E. and Davies, G. Semi-rigid behaviour of connections in precast concrete structures. Progress Report 2, No. SR 95 030. Dept. of Civil Eng. Nottingham University, April 1995.

Görgün, H. Semi-rigid behaviour of connections in precast concrete structures. Dept. of Civil Engineering Report No. SR 96-001, University of Nottingham, February 1996, 344 pp.

Görgün, H. An experimental study of the behaviour of double sided welded plate connection in precast concrete frames. Dept. of Civil Engineering Report No SR 97-001, University of Nottingham, January 1997, 160 pp.

Gregory, M. : Elastic instability: Analysis of buckling modes and loads of frames structures, E&F.N Spon Limited, London 1967, pp. 234-237.

Ioannides, A.S. Frame analysis including semi-rigid connections and P-delta effects. Connections in Steel Structures, Behaviour, Strength and Design. Elsevier Applied Science, London and New York, 1988, pp. 214-221.

Jaspart, J.P. Extending of the Merchant-Tankine formula for the assessment of the ultimate load of frames with semi-rigid joints. J. Construct. Steel Research 11. 1988, pp. 283-312.

Johnson, R.P. and Anderson, D. Designers' handbook to Eurocode 4- Part 1.1 / Design of composite steel and concrete structures. Thomas Telford services Ltd, Thomas Telford House, 1 Heron Quarry, London E14 4JD, 1993, 182 pp.

Kong, F.K. and Evans, R.H. Reinforced and prestressed concrete. 3rd ed., Van Nostrand Reinbold, U.K., 1990.

Lindberg, R., Vinha, J., Myllyvilta, S. and Hellman, H. Beam-to-column connections in storey-height concrete frame. Report 57. Tampere University of Technology, Department of Civil Engineering, Structural Engineering. P.O. Box 600. SF-33101 Tampere, Finland. September 1992, 104 pp.

Loo, Y. C., and Yao, B. Z. Static and repeated load tests on precast concrete beam-to-column connections. PCI JOURNAL March-April 1995, pp. 106-115.

Mahdi, A. A. Critical buckling values of rotational stiffness of connections in precast concrete frames. Internal Report No. SR 91003. Dept. of Civil Eng. Nottingham University, January 1991.

Mahdi, A. A. Moment-rotation behaviour of connections in precast concrete structures. PhD Thesis, University of Nottingham, Department of Civil Engineering, July 1992.

Mohamed, S.A.M. and Jolly, C.K. An experimental study of the behaviour of sleeved bolt connections in precast concrete frames. Magazine of Concrete Research, 1995, 47, No. 171, June, pp. 119-127.

Neville, A.M. Properties of concrete. Longman Group Limited, Longman House, Burnt Mill, Harlow Essex CM20 2JE, England, 1981.

Nethercot, D.A. Joint action and the design of steel frames. The Structural Engineer, Volume 63A/No.12. December 1985, pp. 371-379.

Nethercot, D.A. The influence of semi-rigid joint action on the behaviour of steel frame structures. Development in Structural Engineering, Vol 2, ed. B V H Topping, Spon, August 1990, pp. 696-721.

Nethercot, D.A. Behaviour of semi-rigid connections and implementation in frame design. American Institute of Steel Construction, INC. April 1991, pp. 360-369

Notes on ACI 318-89: Building code requirement for reinforced concrete with design applications. Edited by Ghosh S.K and Basil G. Rabbat Portland Cement Association 1990, pp. 13-1, 13-11.

Pillai, S.U. and Kirk, D.W. Ductile beam-column connection in precast concrete. ACI Journal / November-December 1981. pp. 480-487.

Southampton University. Finite element analysis of precast concrete connections.

Stanton, J. F., Anderson, R. G., Dolan, C. W. and Mc Cleary, D. E. Moment resistant connections and simple connections. PCI Specially Funded Research and Development Program, Research Project 1/4 Prestressed Concrete Institute, Chicago, Illinois 1986, 436 pp.

The Institution of Structural Engineers. Structural joints in precast concrete: Manual. 11 Upper Belgrave Street, London SW1X 8BH, August 1978, 56 pp.

Tschemmernegg, F. and Huter, M. Classification of beam-to-column joints. COST C1 Working Group 2 on "Steel and Composite", doc. C1/WD2/93-16, June 1993.

Vambersky, J.N.J.A. Mortar joints loaded in compression. Delft University of Technology / Corsmit Consulting Engineers The Netherlands. Prefabrication of concrete structures. Proceedings of the international seminar Delft, October 1990, pp. 25-26.

Virdi, K.S. and Ragupathy, P. Analysis of precast concrete frames with semi-rigid joints. Proceedings of the First State of the Art Workshop, COST C1, Strasbourg, October 1992a, pp. 296-307.

Virdi, K.S. and Ragupathy, P. Tests on precast concrete subframes with semi-rigid joints. Proceedings of the First State of the Art Workshop, COST C1, Strasbourg, October 1992b, pp. 120 -131

Wood, R.H. Effective lengths of columns in multi-storey buildings, Part 1: Effective lengths of single columns and allowances for continuity. The Structural Engineer, Vol. 52. No.7, July 1974, pp. 235-244.

Wood, R.H. Effective lengths of columns in multi-storey buildings, Part 2: Effective lengths of multiple columns in tall buildings with sidesway. The Structural Engineer, Vol. 52. No.8, August 1974, pp. 295-302.

Wood, R.H. Effective lengths of columns in multi-storey buildings, Part 3: Features which increase the stiffness of tall frames against sway collapse, and recommendations for designers. The Structural Engineer, Vol. 52. No.9, September 1974, pp. 341-346.

Zoetemeijer, P. Influence of joint characteristics on structural response of frames. Structural connections, Stability and strength (ed R Narayanan), Elsevier Applied Science Publishers Ltd, 1989, pp. 121-151.

BIBLIOGRAPHY

Bass, A.J. and Mottram, J.T. Behaviour of connections in frames of fibre-reinforced-polymer section. The Structural Engineer / Volume 72 / No 17 / 6 September 1994.

Bazant, P. Initial post-critical analysis of asymmetric bifurcation in frames, Journal of Structural Engineering. Vol.115, No.11, November 1989, pp. 2845-2855.

Bernuzzi, C. and Zandonini, R. Connection response and stability of steel frames. American Institute of Steel Construction, INC. April 1991, pp. 295 306.

Bruggeling, A.S.G. and Huyge, G.F. Prefabrication with concrete, A.A. Balkema, Rotterdam, Netherlands, 1991.

Chan, L.S. and Ho, G.W.M. Non-linear vibration analysis of steel frames with semi-rigid connections. ASCE. Vol. 120, No. 4, April 1994, pp. 1075-1087.

Chen, W.F. and Lui, E.M. Structural stability theory and implementation. Elseiver, 1988, pp. 5-12, 253.

Chen, W.F. Design analysis of semi-rigid frames with lrfd. American Institute of Steel Construction, INC. April 1991, pp. 370-379.

Coates, R.C., Coutie, M.G. and Konk, F.K. Structural Analysis. 3rd ed., Chapman & Hall, 2-6 Boundary Row, London SE1 8HN, 1988.

Concise Eurocode, For the design of concrete buildings, British Cement Association, Century House, Telford Avenue, Crowthome, Berkshire RG11 GYS, July 1993.

El-Ghazaly, H.A. and Al-Zamel, H.S. An innovative detail for precast concrete beam-column moment connections. Can. J. Civ. Eng. Vol. 18. 1991, pp. 690-710.

EL-Metwally, S.E. and Chen, W.F. Moment-rotation modelling of reinforced concrete beam-column connections. ACI Structural Journal / July-August 1988, pp. 384-394.

Engstrom, B. Anchorage of ribbed bars in the post yield stage. Proceedings of the First State of the Art Workshop, COST C1, Strasbourg, October 1992, pp. 65-76.

French, C.W., Amu, O. and Tarzikhan, C. Connections between precast elements-failure outside connection region. ASCE, Jnl of Structural Engg, Vol 115, No. 2, February 1989, pp. 316-340.

French, C.W., Hafner, M. and Jayashankar, V. Connections between precast elements-failure within connection region. ASCE, Jnl of Structural Engg, Vol. 115. No. 12, December 1989, pp. 3171-3193.

Glower, C.W. Structural precast concrete, C.R. Books Ltd, The Adelphi, John Adam Street, London, W.C.2. 1964.

Goto, Y., Miyashita, S. and Chen, W.F. Classification of semi-rigid connections based on the elastic-plastic mechanical behaviour of frames. Structures congress XII, conf. code 20480, 24-28 April 1994, Atlanta, GA, USA. pp. 1191-1196.

Hanson, N. W. and Conner, H. W. Seismic resistance of reinforced concrete beam-column joints. Proceedings, ASCE, V.93, ST5, October 1967, pp. 533-560.

Hanson, N. W. Seismic resistance of concrete frames with grade 60 reinforcement. Proceedings, ASCE, V.97, ST6, June 1971, pp. 1685-1700.

Johnson, B.C : The column research council guide to design criteria for metal compression members. 2nd ed, John Wiley and Sons, Inc. New York 1966.

Lee, D., Wight, J. K. and Hanson, R. D. RC beam-column joints under large load reversals. Proceedings, ASCE, V. 103, ST12, December 1977, pp. 2337-2350.

MacGinley, T.J. and Ang, T.C. Structural steelwork design to limit state theory. Butterworth & Co (Publishers) Ltd, 1987.

MacGinley, T.J. and Choo, B.S. Reinforced concrete design theory and examples. 2nd ed. E & FN Spon, an imprint of Chapman & Hall, 2-6 Boundary Row, London SE1 8HN, 1990.

Moore, D.B., Nethercot, D.A. and Kirby, P.A. Testing steel frames at full scale. The Structural Engineer/Volume 71/Nos 23 & 24 / 7 December 1993, pp. 418-427.

Mosley, W.H. and Bungey, J.H. Reinforced concrete design. 3rd ed., Macmillan Education Ltd. Houndmills, Basingstoke, Hampshire RG21 2XS, 1987.

Nakata, S. Tests of reinforced concrete beam-column subassemblages for US-Japan Co-operative Research Program. Building Research Institute, Ministry of construction, Ibaraki pref, October 1980, 112 pp.

Plaut, R.H., Requirements for lateral bracing of columns with two spans. Journal of Structural Engineering. Vol.119, Number 10, October 1993, pp. 2913-2931.

Priestley, N. M. J. Overview of PRESS research program, PCI JOURNAL, July-August 1991, pp. 50-57.

Richard, R.M., Hsia, W.K., and Chmielowiee, M. Moment-rotation curves for double framing angles, Proceedings of the Structures Congress. Material and member behaviour, ASCE. August 1987.

Richard, R.M., Hsia, W.K., and Chmielowiee, M. Derived moment-rotation curves for double framing angles. International Journal of Computers and Structures, Vol 30. No 3. pp. 485-494, 1988.

Richardson, J.G. Precast concrete production. Cement and Concrete Association, 52 Grosvenor Gardens, London SW1W OAQ, 1973.

Seckin, M. and Fu, H.C. Beam-column connections in precast reinforced concrete construction. ACI Structural Journal, V. 87, No. 3, May-June 1990, pp. 252-261.

Smyrell, A.G. Approximate formulas for determining the effective length of steel columns to BS 5950. The Structural Engineer / Volume 71 No. 5/2 March 1993.

Smyrell, A.G. Approximate formulas for effective length of steel columns ASCE. Vol. 120, No. 9, September 1994, pp. 2793-2801.

Stefano, M.D., Luca, A.D. and Astaneh-Asl, A. Modeling of cyclic moment-rotation response of double-angle connections. ASCE. Vol. 120, No. 1, January 1994, pp. 212-229.

Timoshenko, S. and Gere, J.M.: Theory of elastic stability, McGraw-Hill, 2nd ed, 1961, pp. 65-67.

Uzumeri, S. M. and Seckin, M. Behavior of reinforced concrete beam-column joints subjected to slow load reversals. Publication No. 74-05, Department of Civil Engineering, University of Toronto, March 1974, 84 pp.

Vassilev, T.V. Semi-rigid behaviour of concrete structures, Report of activities 1993. Department of Civil Engineering. Inst. of Architecture and Civ. Engng. VIAS-Sofia 1 Chr. Smirnenski str. 1421 Sofia, Bulgaria.

Wang, P.C. Numerical and matrix methods in structural mechanics. John Wiley & Sons, Inc. New York, 1966, pp. 182-194.

Yau, C.Y. and Chan, S.L. Inelastic and stability analysis of flexibly connected steel frames by springs-in-series model. ASCE, Vol. 120, No. 10, October 1994, pp. 2803-2819.